

Involvement of the prefrontal cortex- limbic pathway in the development of food addiction

Pablo Calvé Pérez

DOCTORAL THESIS UPF 2022

Thesis Directors:

Dr. María Victoria Puig Velasco

Dr. Elena Martín García

Prof. Rafael Maldonado López

Department of Experimental and Health Sciences

Hospital del Mar Medical Research Institute



A mis padres y a Verónica,

Abstract

Food addiction is closely associated with eating disorders including obesity and binge eating. However, the neural alterations underlying this disorder have not been yet clarified. We have trained mice in an operant model to develop food addiction and we recorded neural activities in the medial prefrontal cortex (mPFC) and the nucleus accumbens (NAc) to identify the dynamic neural abnormalities underlying the development of this behavioral disorder. Interestingly mPFC-to-NAc signaling was disrupted at high frequencies during lever-press decision-making for reinforcement in addicted animals. Moreover, addicted mice exhibited reduced low gamma oscillations and theta-gamma coupling in the NAc during reward expectancy. Disrupted mPFC-to-NAc connectivity and gamma synchrony in the NAc correlated with increased reinforcement levels, underlying the functional relevance of these abnormalities. The CB1 antagonist rimonabant rescued both neural alterations. These findings suggest that abnormal mPFC-NAc circuit dynamics are candidate mechanisms underlying specific behavioral alterations during food addiction. This thesis unravels new neurophysiological signatures involved in food addictive-like behaviors that will shed light in novel treatments to food addiction and related eating disorders.

Resumen

La adicción a la comida está estrechamente relacionada con los trastornos alimentarios, como la obesidad y los atracones. Sin embargo, aún no se han esclarecido las alteraciones neuronales que subyacen a este trastorno. Hemos entrenado ratones en un modelo operante para desarrollar adicción a la comida y registramos actividades neuronales en la corteza prefrontal medial (mPFC) y el núcleo accumbens (NAc) para identificar las anomalías en dinámicas neuronales que subyacen al desarrollo de este trastorno del comportamiento. Curiosamente, la señalización de mPFC a NAc se interrumpió a altas frecuencias durante la toma de decisiones de presión de palanca para el refuerzo en animales adictos. Además, los ratones adictos exhibieron oscilaciones gamma baja reducidas y acoplamiento theta-gamma en el NAc durante la expectativa de recompensa. La conectividad interrumpida de mPFC a NAc y la sincronía gamma en el NAc correlacionaron con mayores niveles de refuerzo, lo que subyace a la relevancia funcional de estas anomalías. El antagonista de CB₁ rimonabant rescató ambas alteraciones neurales. Estos hallazgos sugieren que las dinámicas anormales del circuito mPFC-NAc son mecanismos candidatos que subyacen a alteraciones conductuales específicas durante la adicción a la comida. Esta tesis descifra nuevas firmas neurofisiológicas involucradas en comportamientos similares a los de la adicción a comida que ayudarán en la búsqueda de tratamientos novedosos para la adicción a comida y los trastornos alimentarios relacionados.

Abbreviations

2-AG	2-arachidonoylglycerol
A	Addicted
AC	Adenylyl cyclase
AEA	N-arachidonylethanolamide
AgRP	Agouti-related peptide
AP	Active period
ARC	Arcuate nucleus
BDNF	Brain-derived neurotrophic factor
BED	Bing eating disorder
BMI	Body mass index
BR	Archaerhodopsin
CART	Cocaine and amphetamine regulated transcript
CB1R	Cannabinoid type-1 receptor
CB2R	Cannabinoid type-2 receptor
CCK	Cholecystokinin
ChR2	Channelrhodopsin-2
CNS	Central nervous system
CNO	Clozapine-N-oxide
CpG	Cytosine-phosphoguanine
D2R	Dopamine receptors type 2
DA	Dopamine
DAT	Dopamine transporter
DBS	Deep brain stimulation
dIPFC	Dorsolateral prefrontal cortex

dmPFC	Dorsal component of the medial prefrontal cortex
DMS	Dorsomedial nucleus
DREADDs	Designer receptors exclusively activated by designer drugs
DSE	Depolarization-induced suppression of excitation
DSI	Depolarization-induced suppression of inhibition
DSM	Statistical manual of mental disorders
DSM-5	Statistical manual of mental disorders v5
dsRNA	Duplex RNA
eCB-LTD	Endocannabinoid-mediated long-term depression
eCBs	Endocannabinoids
eCB-STD	Endocannabinoid-mediated short-term depression
EEG	Electroencephalography
ENA	Extreme non-addicted
ERK	Extracellular signal-regulated kinases
FDA	Food and drug administration
FR	Fixed ratio
GIRKs	G protein-coupled inwardly rectifying potassium channels
GPCRs	G protein-coupled receptors
Gpe	External part of the globus pallidus
Gpi	Internal part of the globus pallidus
ICD-11	International statistical classification of diseases and related health problems
IL	Infralimbic
IP3	Inositol triphosphate
JNK	c-Jun N-terminal kinase
Kir3	Inwardly rectifying K ⁺ channels
L	Laminar

LFP	Local field potential
LH	Lateral hypothalamic
mAChRs	Muscarinic acetylcholine receptors
mGluRs	Metabotropic glutamate receptors
MI	Modulation index
miRNAs	MicroRNAs
MOR	μ -opioid receptor
mPFC	Medial prefrontal cortex
MSN	Medium spiny neurons
MUA	Multi-unit activity
mYFAS	Modified Yale Food Addiction Scale
NA	Non-addicted
NAc	Nucleus accumbens
NMDA	N-methyl-D-aspartate
NpHR	Halorhodopsin
NPY	Neuropeptide Y
NTS	Nucleus of the solitary tract
OA	Overeaters anonymous
PAC	Phase amplitude coupling
PBN	Parabrachial nucleus
PC	Principal component
PCA	Principal component analysis
PET	Positron emission tomography
PFC	Prefrontal Cortex
PKA	Protein kinase A
PL	Prelimbic
PLC	Phospholipase C

POMC	Peptides pro-opiomelanocortin
PR	Progressive ratio
PSI	Phase slope index
PVN	Paraventricular nucleus
RISC	RNA-induced silencing complex
RNAi	RNA interference
rTMS	Repetitive transcranial magnetic stimulation
SNpr	Substantia nigra pars reticulata
STN	Subthalamic nucleus
SUA	Single-unit activity
tDCS	Transcranial direct current stimulation
VMH	Ventromedial nucleus
vmPFC	Ventral component of the medial prefrontal cortex
VP	Ventral pallidum
VTA	Ventral tegmental area
YFAS	Yale Food Addiction Scale
Δ^9 -THC	Δ^9 -tetrahydrocannabinol

Index

Introduction	1
1. Eating disorders and obesity.....	1
1.1. Eating disorders.....	1
1.1.1. Diagnosis of eating disorders.....	2
1.1.1.1. Anorexia nervosa and bulimia nervosa.....	2
1.1.1.2. Binge eating disorder	3
1.2. Obesity	5
2. Food addiction: the concept.....	9
2.1. Food addiction: development and refinement over the years	10
2.2. Food addiction diagnostic tool: Yale Food Addiction Scale	14
2.3. Food addiction and its linkage with comorbid diseases	17
2.4. Food addiction: a controversial construct	21
3. Neurobiology of food addiction and eating disorders	25
3.1. Food intake control.....	25
3.1.1. Homeostatic regulation of food intake.....	26
3.1.1.1. Food intake cycle	27
3.1.1.2. Central regulation.....	28
3.1.1.3. Peripheral regulation	31

3.1.2.	Hedonic regulation of food intake	35
3.1.2.1.	The brain executive system and the decision to eat.....	35
3.1.2.2.	The brain reward system and the desire and pleasure to eat	36
3.2.	The brain's reward circuitry	39
3.2.1.	Ventral tegmental area	41
3.2.2.	Nucleus accumbens.....	44
3.2.3.	Prefrontal cortex	53
3.3.	Modulation of the reward circuitry	59
3.3.1.	Opioid signaling.....	60
3.3.2.	Dopaminergic signaling.....	61
3.3.2.1.	Dopaminergic neurons	61
3.3.2.2.	Dopamine receptors	63
3.3.2.3.	Dopaminergic system in food addiction and eating disorders	69
3.3.3.	Endocannabinoid signaling.....	70
3.3.3.1.	Cannabinoid receptors.....	70
3.3.3.2.	Endocannabinoid ligands	74
3.3.3.3.	Cannabinoid type-1 receptor signaling	75
3.3.3.4.	Endocannabinoid modulation of brain reward system.....	77

3.3.3.5. The endocannabinoid system in food addiction and eating disorders	80
4. Dynamics in the transition to addiction: stages of the food addiction cycle	82
4.1. Habitual overeating: maladaptive habit formation.....	83
4.2. Overeating to relieve a negative emotional state: the emergence of a negative affect	85
4.3. Overeating despite aversive consequences: failure of inhibitory control	88
5. Complex multifactorial nature of food addiction and eating disorders: gene and environment interaction.....	89
5.1. Genetic mechanisms of food addiction and eating disorders	90
5.2. Epigenetic mechanisms of food addiction and eating disorders	95
5.2.1. Histones modifications	97
5.2.2. DNA methylation.....	99
5.2.3. Non-coding RNA: microRNA.....	101
6. Animal models of food addiction and eating disorders....	106
6.1. Food addiction mouse model	107
6.2. Innovative technological approaches	112
6.2.1. Chemogenetics.....	113
6.2.2. Calcium imaging.....	115

6.2.3. Optogenetics	116
7. Electrophysiological approaches	118
7.1. Electroencephalography recordings	119
7.2. In vivo extracellular recordings.....	122
8. Therapeutics for food addiction and eating disorders	126
8.1. Non-pharmacological treatments	127
8.1.1. Behavioral therapies	127
8.1.2. Brain stimulation therapeutics	128
8.1.3. Neurofeedback strategies.....	131
8.2. Pharmacotherapies	132
Objectives	135
Materials and Methods	139
Results	159
Chapter 1	161
Chapter 2	237
Discussion.....	255
Conclusions	291
Bibliography.....	297
Annex	373

Introduction

1. Eating disorders and obesity

1.1. Eating disorders

Eating disorders are defined as a persistent disturbance of eating or eating-related behavior resulting in the altered consumption or absorption of food and significantly impair physical health or psychological functioning (American Psychiatric Association, 2013). Eating disorders affect millions of people worldwide (around 4.6% of the world population) regardless of age, nationality, or gender, occurring most commonly among late adolescents and young adult women (Mishra *et al.*, 2017; Zipfel *et al.*, 2022). These severe illnesses consider that mental disorders are usually chronic and relapsing, often inducing psychiatric comorbidity (such as anxiety and depression, among others) and medical sequelae that lead to substantial personal, familial, and social costs. Moreover, even though the prevalence of eating disorders has persisted stable in the last years, mortality rates remain very high (3.3 million healthy life per year) and its association with measurable psychological and neurocognitive traits is highly elevated (Schaumberg *et al.*, 2017; van Hoeken and Hoek, 2020). Thus, the combination of these facts with the increased level of consciousness of eating disorders in the general population has sparked the scientific community's interest in understanding the neurobiological mechanisms underlying eating disorders (Smink *et al.*, 2012).

The current understanding of eating disorders etiology is based on family, twin, and adoption studies that have robustly demonstrated

that eating disorders reflect the complex trait inheritance influenced by genetic and environmental factors (Yilmaz *et al.*, 2015). Moreover, evidence have shown that genes and heritability play a major role in increasing the risk of suffering an eating disorder in healthy individuals, although these may also affect individuals without a hereditary history of eating disorders. Thus, epigenetic mechanisms offer an additional layer of gene regulation, which connects external and internal environmental stimuli and non-coding genetic variation with transcriptional consequences that alter downstream phenotypes (Hübel *et al.*, 2019).

1.1.1. Diagnosis of eating disorders

From a diagnostic perspective, the Diagnostic and Statistical Manual of Mental Disorders (DSM) is the main psychiatry manual used to diagnose mental disorders by the American Psychiatric Association. In the fifth version of the manual (DSM-5), the eating disorders section is named “Feeding and Eating Disorders” and the diagnostic criteria are provided for three feeding disorders: pica, rumination, and avoidant/restrictive food intake disorders. In addition, three different types of eating disorders are described: **anorexia nervosa**, **bulimia nervosa**, and **binge eating disorder**.

1.1.1.1. Anorexia nervosa and bulimia nervosa

Anorexia nervosa and bulimia nervosa are the most classical forms of eating disorders, reporting similar symptoms based on distorted

body image and self-perception of weight or shape. Notwithstanding, essential differences subsist between both eating disorders. **Anorexia nervosa** is characterized by a persistent restriction of energy intake, an intense fear of gaining weight or becoming fat, persistent behavior that interferes with weight gain, and a disturbance in self-perceived weight or shape. The 12-month prevalence of anorexia nervosa is 0.4% among young females (American Psychiatric Association, 2013). On the other hand, **bulimia nervosa** is characterized by recurrent episodes of binge eating followed by inappropriate compensatory behaviors to prevent weight gain, such as self-induced vomiting, diuretics use, and fasting or excessive exercise. The 12-month prevalence of bulimia nervosa is 1-1.5% among young females (American Psychiatric Association, 2013).

According to the DSM-5, some eating disorder symptoms coincide with those manifested in substance use disorders, such as craving and compulsive use. These resemblances may reflect the participation of similar neurobiological systems, including those involved in the regulatory self-control and reward processing. Therefore, in the highly obesogenic environment in which our Western society is involved, much attention has been paid to eating disorders characterized by compulsive behaviors and abnormal overeating, such as **binge eating disorders**.

1.1.1.2. Binge eating disorder

Binge eating disorder (BED) is a severe, life-threatening, but treatable eating disorder characterized by recurrent episodes of binge eating

(consuming large amounts of food in short periods) accompanied by a sense of lack of control, indicated by the inability to abstain from eating or stop eating once started, without compensatory behavior such as self-induced vomiting or excessive exercise. According to the DSM-5, an “episode of binge eating” is defined as eating in a discrete period of time (within 2 hours period) an amount of food that is definitely larger than most people would eat in a similar period of time under similar circumstances. Remarkably, to consider an episode of binge eating, occurrences of excessive food consumption must be accompanied by a sense of lack of control (American Psychiatric Association, 2013).

Furthermore, binge episodes are commonly associated with eating more rapidly than usual, eating until feeling uncomfortably full, eating large amounts of food when not feeling physically hungry, eating alone because of being embarrassed by how much one is eating, and feeling disgusted with oneself, depressed, or very guilty after overeating. For the diagnosis of binge eating disorder, individuals must experience at least three of the behavioral control indicators previously mentioned. In addition, the type of food consumed during binges varies across individuals and episodes. Thus, binge eating disorder appears to be characterized more by an anomaly in the amount of food consumed than by a craving for a specific nutrient (American Psychiatric Association, 2013).

Both binge eating disorder and bulimia nervosa have recurrent episodes of binge eating. However, binge eating is not associated with the recurrent use of inappropriate compensatory behavior as in

bulimia nervosa. Moreover, binge eating disorder typically does not present sustained dietary restrictions designed to influence body weight and shape (American Psychiatric Association, 2013).

Epidemiological studies report that 1.6-2.0% of worldwide people suffer from binge eating disorder, considering this disease the most prevalent with around 2.8 million affected people. Binge eating disorder diagnosis is three times more common than anorexia and bulimia being the most extended in terms of age, race, gender (1.6% women and 0.8% men), and income levels (Kessler *et al.*, 2013; Cossrow *et al.*, 2016). It is diagnosed in normal-weight, overweight and obese individuals, revealing independence with the body weight. However, studies have revealed a positive association between recurrent binge eating and weight gain, reporting a strong relationship between binge eating disorder degree and obesity degree in patients. Remarkably, it is important to highlight that not all individuals suffering from binge eating disorders are obese. Thus, binge eating disorder and obesity are disparate concepts (Wonderlich *et al.*, 2009; Wildes *et al.*, 2012).

1.2. Obesity

Obesity is a chronic disease defined as abnormal or excessive fat accumulation that may impair health. It is considered the 21st-century epidemic and COVID-19, reaching epidemic proportions with over 4 million dying people per year (WHO, 2017). Obesity is associated with profound medical consequences which are linked with an increased risk of cardiovascular pathologies, diabetes, and

cancer, among other diseases (Bray, 2004). The body mass index (BMI) is the current tool employed to classify overweight and obesity in adults. BMI is a ratio of weight to a height calculated by dividing a person's weight in kilograms (kg) by the square of his height in meters (kg/m^2). BMI is closely associated with obesity and obesity-related comorbidities (González-Muniesa *et al.*, 2017), defining the following classification: BMI < 18.5 – underweight; BMI = 18.5 – 24.9 – average weight; BMI = 25 – 29.9 – overweight; and BMI > 30 – obese (WHO, 2017).

Obesity is one side of the double burden of malnutrition, and nowadays, the number of obese individuals surpasses underweight individuals in every region of the world except sub-Saharan Africa and Asia (WHO, 2017). Thus, overweight and obesity dramatically increase in low, middle, and high-income countries, especially in urban areas. Since the middle of the 20th century, the prevalence of overweight and obesity has dramatically escalated, affecting more than 1.9 billion adults, representing 39% of the world population (40% of women and 39% of men). Over 650 million adults were obese in 2016, representing 13% of the world's adult population (15% of women and 11% of men) (WHO, 2017). Moreover, overweight and obesity prevalence among young people has radically risen from 4% in 1975 to 18% in 2016 (18% of girls and 19% of boys). This increased prevalence translates into a global health cost of approximately US\$ 2 trillion, equivalent to 2.8% of the world's gross domestic product (WHO, 2017).

Obesity is induced by an imbalance between energy intake and energy expenditure, resulting in the storage of non-essential lipids in adipose cells. Therefore, obesity at a population level may result from high energy foods overconsumption and low physical activity. However, the etiology of obesity is much more complex. The responsible factors that prompt obesity are heterogeneous and involve interactions among genetic, individual, environmental, and social elements (Sellayah *et al.*, 2014). Thus, obesity is a multifactorial disease that results from diverse alterations of complex internal and environmental factors that lead to a variety of **obese phenotypes**.

Specific obese phenotypes are characterized by an excessive desire for food, compulsive consumption, and the inability to restrain oneself despite the desire to eat. These symptoms are similar to those presented by individuals addicted to drug abuse and are described in the DSM for substance use disorders (Volkow and O'Brien, 2007). Preclinical and clinical investigations have provided multiple evidence suggesting similar neurobiological substrates involved in the dopamine (DA)-modulated circuits that are disrupted in obese and drug-dependent individuals (Volkow *et al.*, 2011a, 2013; Volkow and Baler, 2015). These similar neuroadaptations in the reward system consisted of reductions of striatal dopamine type-2 receptors activity levels (Nora D. Volkow *et al.*, 2008), as well as a lack of the classic increase in releases of DA during food or drug consumption (Gene-Jack Wang *et al.*, 2014) in both drug-addicted and obese subjects. The attenuation of the DA response to the reinforcer in the reward system pathway provokes a mismatch

between the experiences of the expected and the actual reinforcer, which may lead to a compulsive behavior for the desired substance (Nora D. Volkow *et al.*, 2008; Volkow *et al.*, 2011a). However, the understanding of the essential neurobiological mechanisms involved in obesity still remain poor.

Although important progressions in research and metabolic treatments related to obesity have been performed across the years, the prevalence rates of obesity continue to augment, and no effective treatment is still available. Moreover, a lack of success is present in behavioral treatments focused on sustaining weight loss. Therefore, considering the previous observations mentioned, it is crucial to consider that some forms of obesity should not be diagnosed exclusively as a metabolic disorder. At least some forms of comorbidity must be considered with a mental disorder (Volkow and O'Brien, 2007; Lerma-Cabrera *et al.*, 2016). However, although several authors claimed obesity as a mental disorder due to its addictive dimensionality, obesity is not currently included in the DSM-5, neither in the feeding and eating disorders nor in the substance use disorders sections. In this framework, certain foods, mainly highly caloric and palatable foods, seem to possess addictive properties, contributing to excessive consumption and an elevated risk of developing obesity and eating disorders.

Additionally, it has been affirmed that gut microbiota interacts with several organs, including the brain among others. Intestinal microbiota and their metabolites might target the brain directly via vagal stimulation or indirectly through immune-neuroendocrine

mechanisms. Microbiota and metabolites might regulate metabolism, adiposity, homeostasis and energy balance, and central appetite and food reward signaling, which together have crucial roles in obesity (Asadi *et al.*, 2022). Nonetheless, there is still much to investigate about the physiological mechanism of obesity and gut-brain axis and its effect on appetite, eating behaviors, and other physiological mechanisms of the body.

2. Food addiction: the concept

In 1956, Theron Randolph was the first to introduce the term **food addiction**, describing it as “a specific adaptation to one or more regularly consumed foods to which a person is highly sensitive, which produces a common pattern of symptoms descriptively similar to those of other addictive processes”. Despite not having a specific food that was always consumed, Theron Randolph noticed that this adaptation occurred with certain types of foods such as corn, wheat, coffee, milk, eggs, and potatoes (Randolph, 1956). However, nowadays, the point of view of this concept shifts to the potentially addictive properties of processed food containing added fats and refined carbohydrates. In this sense, the current concept of food addiction includes the idea that some specific foods; especially highly processed, highly palatable and highly caloric foods; possess an addictive potential that might contribute to the addictive behavior of overeating.

2.1. Food addiction: development and refinement over the years

In the last years, as a consequence of the global obesity problem, the concept of food addiction has become increasingly popular. This augmented popularity is reflected in a high number of media reports and lay literature and a substantial increase in the number of scientific publications. Most of these studies have focused on both animal models and human studies (Figure 1) (Meule, 2015; Fernandez-Aranda *et al.*, 2018).

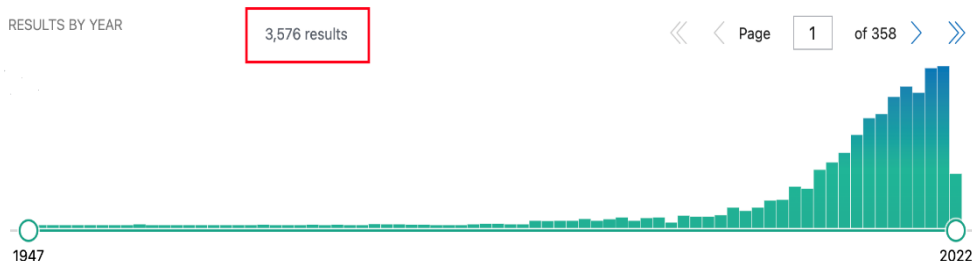


Figure 1. Number of animal and human studies published on food addiction from 1947 to 2022.

The first beginnings of the association between food and addiction started in the 19th century. Concretely, in 1880, the *Journal of Inebriety* used the term addiction in reference to chocolate (Weiner and White, 2007). Years later, in 1959, food addiction was widely used among scientists and laypeople. Moreover the term was also employed by Overeaters Anonymous (OA), a self-help organization founded in 1960 based on the 12-step program of Alcoholics Anonymous to decrease overeating (Russell-Mayhew *et al.*, 2010). In the 1980s, researchers attempted to describe the food pathology

displayed by patients suffering from anorexia nervosa and bulimia nervosa as an addictive behavior (Feldman and Eysenck, 1986; De Silva and Eysenck, 1987). The studies on addictive personality in bulimia nervosa patients were accompanied by a case study in which substance abuse was found to be a useful metaphor in the treatment of bulimia nervosa and the evolution of the “Foodaholics Group Treatment Program” (Stoltz, 1984).

After these first attempts to describe eating disorders as an addiction, research interests changed in the 1990s to a new research focus: chocolate. It was already noticed that chocolate is a food that people most often have problems controlling its consumption, and it was described that chocolate possesses a combination of high fat and sugar content, which makes it a “hedonically ideal substance” (Max, 1989). Few studies were performed in which so-called “chocoholics” or “chocolate addicts” were investigated. These studies compared consumption patterns and the physiological response to chocolate exposure between “chocoholics” and controls (Hetherington and MacDiarmid, 1993; Bruinsma and Taren, 1999). Nevertheless, these studies had major shortcomings because the term food addiction was poorly defined and the participants were recruited based on non-standardized self-identification reports (Greenberg; Rozin and Stoess, 1993).

In the early 2000s, the objectives of the scientific studies were focused on the examination of neural mechanisms underlying overeating and obesity that may parallel findings from substance dependence (Nora D Volkow *et al.*, 2008). These investigations were

performed using neuroimaging techniques in humans and reported that a “reward deficiency syndrome” correlated with lower D₂R availability in obese individuals, similar to what was found in substance dependence (Wang *et al.*, 2001). Other studies using animal models revealed that similar brain areas are activated during the experience of food and drug craving. Moreover, investigations in which neural activation to high-calorie food stimuli as studied found that individuals with bulimia nervosa and binge eating disorder exhibit higher activation in reward-related brain areas than the control group. These results were nearly similar to those observed in individuals with substance dependence who show higher reward-related activity in response to substance-related cues (Pelchat *et al.*, 2004; Schienle *et al.*, 2009) (Figure 2).

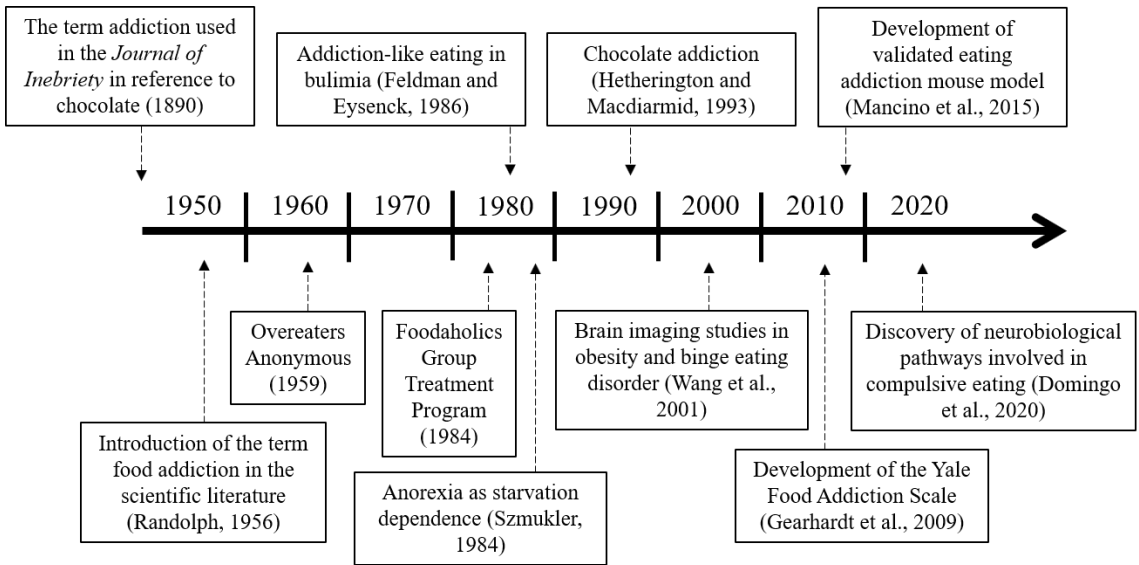


Figure 2. Some focus areas with selected references in the topic of food addiction research (Adapted from Meule, 2015).

In the 2010s, a new approach was developed to diagnose food addiction in individuals: the Yale Food Addiction Scale (Gearhardt *et al.*, 2009). Due to the development of this validated tool to diagnose food addiction high interest in this field drove investigations in animals and humans studying the neurobiological mechanisms involved in food addiction and the development of potential therapeutic targets (Lindgren *et al.*, 2018). For instance, recent studies using rodents have validated an animal model of food addiction in which addictive-like behaviors and phenotypic traits can be investigated (Mancino *et al.*, 2015). Using this model of food addiction, studies revealed essential neurobiological pathways between different brain areas that are crucial in developing addictive-like behaviors (Domingo-Rodriguez *et al.*, 2020). However, although

the term addiction was already used in reference to food by the end of the 19th century and has been debated in the scientific community for decades with a particular focus on whether the phenotype should instead be considered as a behavioral addiction (Schulte *et al.*, 2016), it is still a controversial subject. Indeed, comprehensive reviews of the literature on food addiction conclude that a large body of investigations now supports food addiction's validity and clinical utility (Schulte *et al.*, 2020; Horsager *et al.*, 2021). Specifically, empirical support for critical aspects such as literature with more than 50 scientific studies over the past decade and differentiation, among other conditions. Moreover, many authors have partial support for the occurring symptoms of food addiction and its diagnostic criteria. On the other hand, other authors still prefer to debate its validity and applicability by discussing the pros and cons of the food addiction construct (Fletcher and Kenny, 2018), making food addiction an exciting field for developing research (Figure 2).

2.2. Food addiction diagnostic tool: Yale Food Addiction Scale

The concept of food addiction is still a disputed topic as its recognition as a mental disorder is not included in any of the versions of the DSM. However, the need for a precise tool to capture the symptomatology of addiction led to the development of the **Yale Food Addiction Scale (YFAS)** (Gearhardt *et al.*, 2009). This validated tool was accepted by the scientific community and measured the presence of food addiction symptoms. It consisted of a 25-item self-report instrument based primarily on the diagnostic

criteria for substance dependence in the DSM-IV-TR but adapted to the context of food, with added elements to assess the significance of distress or impairment caused by the symptoms. The YFAS had well internal consistency, convergent validity with related measures of the substance of eating behavior, and discriminant validity with measures of substance use (Gearhardt *et al.*, 2009).

In 2014, an abbreviated version of the YFAS, the modified YFAS (**mYFAS**), was developed. In comparison with the YFAS, the mYFAS consisted of 9 self-report questions, of which 7 of them assessed the 7 DSM-IV-TR substance use disorder criteria and 2 additional questions that evaluated clinically significant impairment and distress. The mYFAS was employed to study epidemiologic cohorts with food addiction symptomatology (Flint *et al.*, 2014). Elevated scores on the mYFAS report were associated with obesity, binge eating, impulsivity, craving, an attentional bias for food cues, adverse bariatric surgery outcomes, and medical conditions (Kirrilly M. Pursey *et al.*, 2014; Meule and Gearhardt, 2014).

Two years later, a newer version of the YFAS, called the **YFAS 2.0**, was developed to reflect the updated changes in substance use disorder diagnostic criteria published in the latest version of the DSM (DSM-5) (Gearhardt *et al.*, 2016). The DSM-5 combined what was previously conceptualized in the DSM-IV as 2 separate and hierarchical disorders (substance abuse and substance dependence) into one new construct that defines substance use disorders on a range from mild to moderate to severe, with the severity of addiction depending on how many of the established criteria apply. Severity is

measured on a continuous scale from mild (2-3 symptoms endorsed), moderate (4-5 symptoms endorsed), and severe (6 or more symptoms endorsed) out of 11 total symptoms (versus the previous 7 in the DSM-IV) (American Psychiatric Association, 2013). In addition, in this newest classification of the DSM, the term addiction is synonym with severe substance use disorder (Volkow *et al.*, 2016).

To maintain consistency with the current diagnostic understanding of addiction, the YFAS 2.0 consisted of a 35-item which assesses the 11 substance use disorder symptoms included in the DSM-5. As in the DSM-5, the YFAS 2.0 uses mild, moderate and severe symptoms for the diagnostic threshold (Gearhardt *et al.*, 2016). Compared to the original YFAS, the YFAS 2.0 diagnosed food addiction in more individuals that met the diagnostic criteria (6% more). A possible reason for this increase in the number of diagnosed individuals could be that the original YFAS evaluated the dependence criteria exclusively, whereas the YFAS 2.0 assesses dependence and abuse criteria (Gearhardt *et al.*, 2016).

Finally, in 2017, a shortened **mYFAS 2.0** version was then derived from the YFAS 2.0 by selecting 1 item for each of the 11 diagnostic criteria plus 2 items to assess clinically significant impairment and distress. This abbreviated version is currently employed as a brief screening measure in extensive epidemiological studies (Schulte and Gearhardt, 2017).

2.2.1. Food addiction prevalence based on the YFAS

According to the YFAS scale, the weighted mean prevalence of food addiction is 19.9% in the adult population (Kirrilly M. Pursey *et al.*, 2014). This prevalence affects from 2 to 12% of healthy BMI individuals (Schulte and Gearhardt, 2018) and doubles in individuals suffering from obesity with ranges from 18 to 24%. Moreover, the prevalence of food addiction is even higher in individuals with eating disorders ranging from 50 to 85%, particularly in binge eating disorder and bulimia nervosa respectively (Hilker *et al.*, 2016; Burrows *et al.*, 2017). In terms of gender, food addiction seems to be more prevalent in females than males in healthy BMI (11.1% and 6.4%, respectively) and obese population (24.9% and 12.2%, respectively) (Kirrilly M. Pursey *et al.*, 2014).

2.3. **Food addiction and its linkage with comorbid diseases**

Based on the increased degree of comorbidity between mental disorders with substance use disorders and addiction-like eating (Volkow *et al.*, 2013; Volkow and Baler, 2015; Lindgren *et al.*, 2018), it seems acceptable to assume that food addiction is also prevalent among individuals suffering mental disorders. Indeed, investigations have demonstrated substantial comorbidity between food addiction and eating disorders. For instance, clinical studies with adults suffering from binge eating disorder revealed that at least 50% of obese adults diagnosed with binge eating disorder also met the criteria for food addiction (Davis *et al.*, 2011; Gearhardt *et al.*, 2012). However, it is worth mentioning that not all the individuals

who accomplished the food addiction criteria (30%) were clinically diagnosed as binge eaters. These results suggest that food addiction and binge eating disorder are two independent disorders (Davis *et al.*, 2011). Different authors defend this fact with two hypotheses.

The presence of food addiction in the absence of binge eating disorder may be supported by the hypothesis that food addiction could be developed after an extensive, severe and compulsive form of binge eating disorder, being food addiction a more acute and pathologically-dense form of binge-eating disorder (Davis, 2013; Gordon *et al.*, 2018). In that sense, it is postulated that there is occasional overeating at the beginning stages that displays no behavioral pathology or psychiatric disruptions. Then, mild and intermittent “loss of control” towards eating starts to appear, manifested as episodic binges that tend to become more compulsive and frequent in some individuals over time. When these behavioral alterations become severe, a diagnosis of binge-eating disorder may be warranted, suggesting that chronic binge-eating disorder develops into a more severe syndrome that displays significant psychopathology and strong addictive tendencies towards food. Therefore, it seems more appropriate to describe this condition as food addiction (Figure 3) (Davis, 2013, 2017).

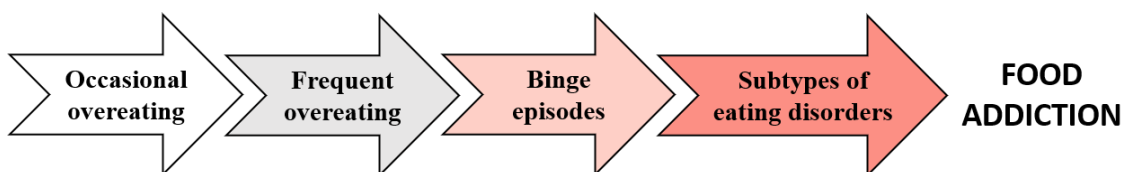


Figure 3. Schematic representation of ascending dimension reflecting the increase in severity and compulsivity, from occasional overeating to food addiction. Adapted from (Davis, 2013).

Although this point of view explaining the absence of binge eating disorder in food addiction might be a hypothesis, another explanation is described by the different patterns of consumption contributing to a feeling of loss of control. For instance, substance-use disorder patients could consume abnormal amounts of addictive substances in short periods (binge consumption) or consume the same amount over the day. The addictive-like eating present in food addiction can be equally characterized by binge eating or “grazing” (Davis, 2017). “Grazing” is an abnormal eating behavior characterized by repetitive eating of small amounts of food in an unplanned manner, without the ability to resist such repeated eats despite intentions to stop. This aberrant behavior in food intake has been associated with weight regain in obese patients who cannot stop snacking during their weight loss schedule (Conceição *et al.*, 2014) (Figure 4).

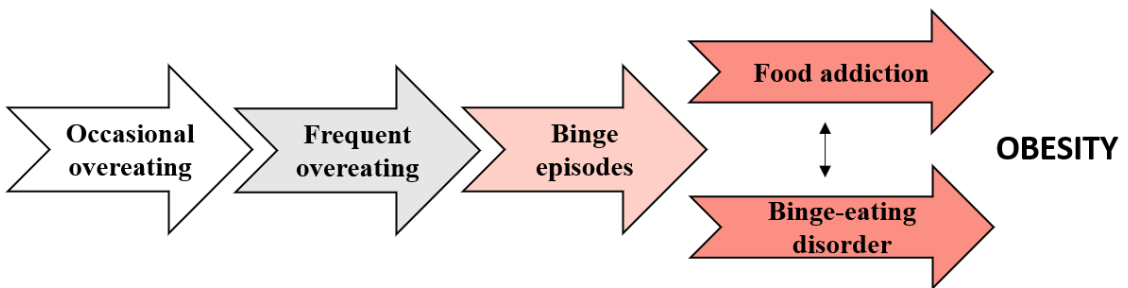


Figure 4. Schematic representation of the ascending dimension reflecting increased severity and compulsivity in a non-linear way from occasional overeating to food addiction and binge-eating disorder.

Taking all these together, these hypotheses suggest that although a considerable linking pattern exists between compulsive overeating, such as binge eating and grazing, and the putative psychopathological condition of food addiction, there are theoretical and behavioral

features that differentiate both pathologies, describing food addiction as an identifiable clinical syndrome.

Furthermore, numerous heterogeneous results about the effect of food addiction on body weight have demonstrated the association of this disorder with overweight and obesity. For example, clinical studies of meta-analysis in humans revealed that the symptoms of food addiction are more prevalent among adults in the overweight and obese BMI category (24.9%) than adults in the normal BMI category (11.1%) (Kirrilly M. Pursey *et al.*, 2014). Moreover, prevalence rates of food addiction in adults with BED range from 40% to 50%, while in individuals suffering from bulimia nervosa, the prevalence increases by over 80% (Gearhardt *et al.*, 2014; De Vries and Meule, 2016). Numerous studies also reported that obese patients who meet the criteria for food addiction present higher levels of eating disorder psychopathology, poorer life quality, more significant depressive symptoms, and augmented scores on impulsivity and self-control measures (Ivezaj *et al.*, 2016). Additionally, a correlation between food addiction severity levels and impairments in decision-making and attentional capacity was observed in obese individuals (Steward *et al.*, 2018).

Overall, these findings highlight the fact that the high comorbidity may be because compulsive eating, obesity, and food addiction share common mechanisms such as binge eating and reward dysfunction, leading to an overlap of food addiction with both eating anomalies (Gearhardt *et al.*, 2014; Meule and Gearhardt, 2014; Burrows *et al.*, 2018; Meule, 2019). Thus, this overlapping underscores the

importance of studying the relationship between food addiction, obesity, and compulsive eating as a potential transdiagnostic construct across eating-related disorders, although these are not included in the DSM-5 and the 11th version of the International Statistical Classification of Diseases and Related Health Problems (ICD-11) (Fernandez-Aranda *et al.*, 2018; Cassin *et al.*, 2019; Gearhardt and Hebebrand, 2021; Hebebrand and Gearhardt, 2021).

2.4. Food addiction: a controversial construct

The diagnostic construct of food addiction is nowadays a highly controversial subject among the scientific community. This concept is currently divided into three prevailing views.

At first glance, investigations and evidence suggest that although highly caloric and processed foods appear to differ from traditionally addictive substances, these foods containing refined carbohydrates and fat are highly reinforcing, mood-altering, and some individuals (but not all) will consume them compulsively, being these types of foods associated with behavioral indicators of addiction, such as diminished control over consumption, strong cravings, continued use despite adverse consequences, and repeated failed attempts to quit the food. Thus, highly caloric and processed foods can be viewed as addictive, producing a similar behavioral alteration to drugs of abuse (Ifland *et al.*, 2015; Gearhardt and Hebebrand, 2021).

Another point of view is that food addiction is not a valid concept because addiction results from the “exposure to a single chemical agent or compound that is effective in engaging the central nervous

system,” and this specific addictive substance has not been identified in foods. Therefore, it may be the act of eating rather than the food itself which is addictive, suggesting that the correct term for representing a behavioral addiction may be “eating addiction” (Hebebrand *et al.*, 2014; Hebebrand and Gearhardt, 2021).

Finally, another perspective of the food addiction construct is that neither food nor eating addiction may reflect valid concepts questioning the existence of underlying addictive processes when considering eating disorders and obesity (Finlayson, 2017; Rogers, 2017; Hebebrand and Gearhardt, 2021).

Several studies have revealed that food addiction may be a statement representing substance use disorders. These studies have demonstrated biological and behavioral changes in response to highly palatable foods, similar to what occurs in drug addiction (Ifland *et al.*, 2015; Mancino *et al.*, 2015; Schulte *et al.*, 2016). Multiple reviews suggest that exposure to highly palatable foods engages the reward system and leads to DA release in the mesolimbic pathway (Volkow *et al.*, 2011a; Smith and Robbins, 2013; Lindgren *et al.*, 2018; Ribeiro and Oliveira-Maia, 2021). For instance, a recent systematic review examining the validity of food addiction deduced that many identified studies (52 studies in 35 articles) support food addiction as a diagnostic construct consistent with the criteria for other substance use disorders. Among these studies, brain reward dysfunction and impaired control were sustained by the most significant number of studies ($n = 21$ and $n = 12$, respectively). In contrast, risky use was supported by the fewest ($n = 1$), followed by

evidence consistent with addiction, such as genetic susceptibility, substance sensitization and impulsivity (Gordon *et al.*, 2018).

Indeed, it must be considered that not all foods are equally implicated in the addictive process. Highly processed foods such as pizza, ice cream, white bread, cookies, or potato chips are more effective than minimally processed foods such as fruits, vegetables, and legumes at activating the reward-mesolimbic pathway and releasing DA in the Nucleus accumbens (Small and DiFeliceantonio, 2019; De Araujo *et al.*, 2020). Moreover, highly processed foods containing refined carbohydrates and fat, but not minimally processed foods, have been associated with addictive manners such as loss of control over consumption, intensive craving, and inability to quit the food (Erica M. Schulte *et al.*, 2015; Gordon *et al.*, 2018). Thus, highly processed foods can be viewed as having addictive potential. It has been suggested that individuals will addictively consume foods containing high quantities of sugar but little or no fat due to the ability of refined carbohydrates to quickly increase glucose in the blood vessels (Erica M Schulte *et al.*, 2015; Lennerz and Lennerz, 2018).

Moreover, sugar could be regulated as a substance of abuse due to the adverse health outcomes, similar to the ones reported in alcohol use disorder (Lustig *et al.*, 2012). Conversely, other studies with humans suggest that the combination of sugar and fat is more associated with addictive symptoms than sugar itself (Markus *et al.*, 2017; Pursey *et al.*, 2017). Many studies have also focused on studying the role of other ingredients in combination with sugar. For instance, removing fiber increases the addictive potential of highly

processed food by augmenting the rapid ingestion of reinforcing ingredients (Erica M. Schulte *et al.*, 2015; Lennerz and Lennerz, 2018). Furthermore, sodium is a common ingredient of highly processed foods that enhances the addictive value of sugar and fat foods (Morris *et al.*, 2008; Fazzino *et al.*, 2019). Thus, a single macronutrient is not necessary for maladaptive eating but rather the combination of ingredients and macronutrients in highly palatable and highly caloric food. This mixture of nutrients may physiologically activate the mesolimbic pathway of the brain reward circuitry, modifying reward optimization and, consequently, eating behaviors (Fletcher and Kenny, 2018).

On the other hand, several authors do not support the idea of "sugar addiction", arguing that the evidence obtained in highly processed food addiction studies is unconvincing (Westwater *et al.*, 2016; Wiss *et al.*, 2018). Moreover, some researchers argue that it should be more appropriate to mention this condition as eating addiction, classifying it as a behavioral disorder that involves dependence on a behavior or substance (Hebebrand *et al.*, 2014; Hebebrand and Gearhardt, 2021). However, the addictive-like consumption of highly processed food requires both a behavior and a substance (eating and food, respectively), being this substance-behavioral pattern is also frequently observed in individuals addicted to tobacco (smoking and tobacco) and alcohol (drinking and alcohol). Thus, there are striking parallels between the classification of other addictive substances and the current debate about the addictiveness of high palatable caloric foods, which involve both behavioral and substance-related symptoms (Gordon *et al.*, 2018).

According to the controversial evidence previously commented, critics and proponents agree that more research is needed to elucidate the fundamental construct of food addiction and identify the characteristics of food ingredients that may have addictive effects (Pursey *et al.*, 2017). The present work intends to provide new neurobiological evidence confirming the validity of food addiction as a substance use disorder by discovering innovative therapeutic targets that may play crucial roles in preventing and treating eating disorders and obesity.

3. Neurobiology of food addiction and eating disorders

3.1. Food intake control

Behaviors such as eating, drinking and copulating are natural stimuli that begin with a motivation to initiate the behavior. The motivational drive and the behaviors that consequently follow are influenced by past and present experience with the reinforcing stimuli that augment the likelihood and/or strength of the behavioral response (Nora D. Volkow *et al.*, 2017). With respect to eating behavior, the regulation of food intake involves close relationships between **homeostatic** and **non-homeostatic hedonic** factors that are balanced to ensure the initiation and maintenance of eating behavior (Onaolapo and Onaolapo, 2018; Cifuentes and Acosta, 2021) These complementary factors are activated in all feeding situations to maintain the balance control regulation on energy intake and energy expenditure that maintain body weight and metabolic functions. However, the degree

to which each regulative process is activated may depend on the type of food and the individual's physiological state (Rossi and Stuber, 2018; Parmar and Can, 2022). Remarkably, highly processed palatable foods rich in refined carbohydrates and fat are massively craved among several individuals not only to satiate their hunger but for sensation of pleasure (Alonso-Alonso *et al.*, 2015; Blanco-Gandia *et al.*, 2021), prevailing reward-related signals over homeostatic control that lead to an excessive food intake which surpass body energy requirements (Caron and Richard, 2017).

3.1.1. Homeostatic regulation of food intake

The maintenance of the energy balance is managed by a complex physiological control system that contains afferent signals from the periphery and efferent signals from the brain. Afferent signals coming from the gastrointestinal tract and the adipose tissue inform about energy storage states, whereas efferent signals coming from the central nervous system (CNS) affect the energy intake and expenditure (Sandoval, 2008). This control is integrated by multiple interactions between the mentioned organs to maintain an appropriate energy balance through **short-term** and **long-term** regulating processes (Abdalla, 2017).

Appetite control comprises short-term and long-term regulation. Short-term signals control hunger, satiation and satiety determining the beginning and the end of a meal, and the interval between meals. On the other hand, long-term signals coming from the adipose tissue

regulate body energy depots coordinating the eating behavior (Abdalla, 2017).

3.1.1.1. Food intake cycle

After ingestion of a meal, the chemo- and mechano- receptors of the gastrointestinal tract send afferent signals to the brain via sensory input, from the vagus nerve to the nucleus of the solitary tract, informing about the amount of food ingested and its nutrient content. This information is driven by short-term signals that provide “satiety signals” which determine the initial and ending timings of the meal. After digestion, once nutrients have been metabolized in peripheral tissues or have directly crossed the blood-brain barrier, long-term signals coming from the adipose tissue are sent to the arcuate nucleus of the hypothalamus. At the same time, a large amount of products from digestion and components responsible for metabolism are integrated and assembled in the brain informing about the metabolic state resulting from food intake (Hopkins *et al.*, 2000; Hopkins and Blundell, 2016). After information processing in the brain, efferent signals are triggered to modify energy intake and expenditure (Sandoval *et al.*, 2008) (Figure 5).

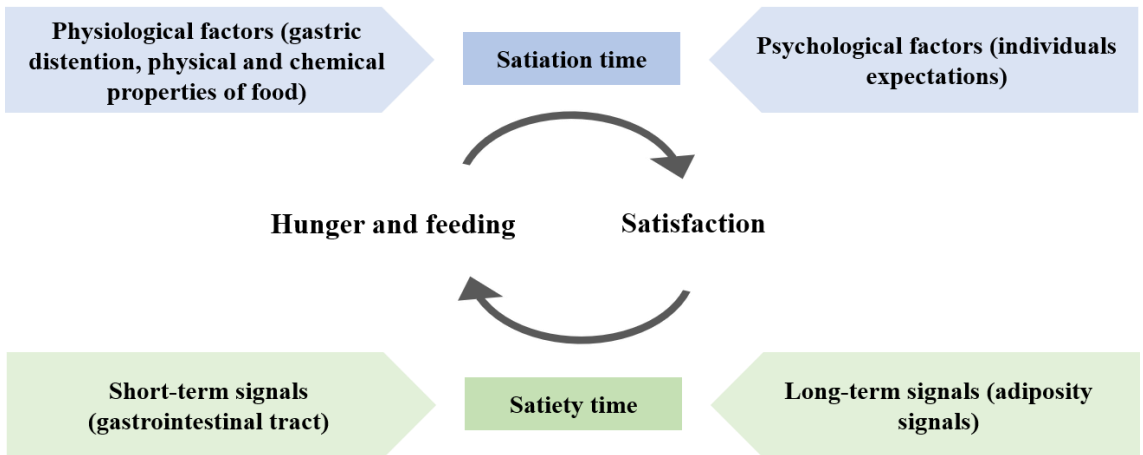


Figure 5. Food intake cycle and its components (Adapted and modified from Abdalla 2017).

3.1.1.2. Central regulation

The essential parts in the central regulation of homeostatic energy balance are the **hypothalamus** which plays a major role in the appetite control, and the **brainstem** which has a crucial role in regulating the amounts of food ingested (Schneeberger *et al.*, 2014; MacDonald *et al.*, 2020).

The hypothalamus receives sensory information from mechanical receptors in the stomach that inform about its filling, chemical satiety signals from nutrients in the blood, signals from gastrointestinal hormones, hormonal signals from the adipose tissue, and signals from the cerebral cortex, such as taste, smell and sight of the food (Figure 6). All this information is processed by the hypothalamus and consequently efferent signals are sent for the food intake control. The hypothalamus is composed of several interconnected nuclei that

regulate appetitive control such as the **arcuate nucleus (ARC)**, the paraventricular nucleus (PVN), the dorsomedial nucleus (DMN), the ventromedial nucleus (VMH), and the **lateral hypothalamic area (LH)** (Timper and Brüning, 2017). Specifically, the ARC and the LH are two essential areas of the hypothalamus that play crucial roles in the homeostatic regulation

In the **ARC**, many hormones released from the gastrointestinal tract and adipose tissue assemble to control food intake and energy expenditure. Two types of neurons are present in the ARC that project to other hypothalamic areas involved in appetite control: orexigenic neurons that co-express anabolic peptides such as neuropeptide Y (NPY) and agouti-related peptide (AgRP), and anorexigenic neurons that co-express the catabolic peptides pro-opiomelanocortin (POMC) (melanocyte peptide-stimulating hormone α -, β -, γ -MSH precursor), and the cocaine and amphetamine regulated transcript (CART). The NPY/AgRP positive neurons stimulate food intake whereas the POMC/CART positive neurons represses feeding (Abdalla, 2017) (Figure 6).

The **LH** performs the role of feeding center by triggering motor drives for food searching in situations of energy deficit (Rossi *et al.*, 2019). As previously mentioned, regulation of food intake requires the information integration from both homeostatic and hedonic mechanisms. In this context, the activity of LH modulates the hedonic quality of gustatory stimuli impacting on conditioned taste preference and aversion (Ferssiwi *et al.*, 1987; Touzani and Sclafani, 2002). The LH receives through the parabrachial nucleus (PBN)

gustatory sensory information via the nucleus of the solitary tract (NTS) that is coupled to the reinforcing qualities of LH perturbation, reflecting the importance of the LH role in promoting the consumption of palatable foods (Wiepkema, 1971; Tokita *et al.*, 2014).

On the other hand, the PVN, VMH and DMN have a crucial role in the satiety center (Mishra *et al.*, 2017). Precisely, the VMH receives POMC neuronal projections from the ARC that play an important role in activating BDNF neurons in the VMH with the goal of decreasing food intake. Finally, the PVN also encloses an increased level of neuropeptide Y and α -MSH terminals that originate in the ARC, and whose destruction may result in hyperphagia and obesity (Abdalla, 2017) (Figure 6).

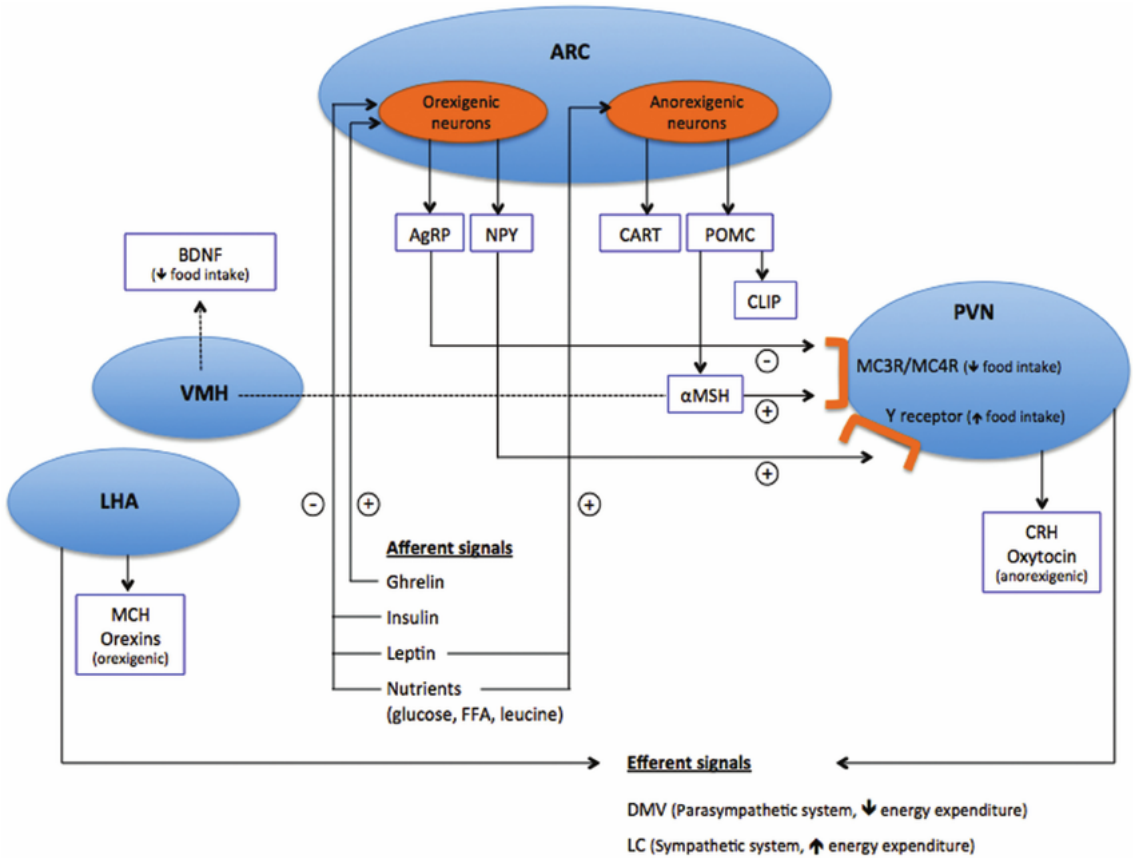


Figure 6. Simplified scheme of regulation of energy homeostasis by the hypothalamus. ARC, arcuate nucleus; PVN, paraventricular nucleus; VMH, ventromedial hypothalamus; LHA, lateral hypothalamic area; AgRP, agoutirelated peptide; NPY, neuropeptide Y; CART, cocaine-amphetamine-related transcript; POMC, proopiomelanocortin; α -MSH, alpha-melatonin stimulating hormone; BDNF, brain-derived neurotrophic factor; MCH, melanin-concentrating hormone; CRH, corticotropin-releasing hormone; DMV, dorsal motor nucleus of the vagus (Haliloglu and Bereket, 2015).

3.1.1.3. Peripheral regulation

Peripheral control of appetite is primarily regulated by peptide neurotransmitters and hormones released by the gastrointestinal tract and the adipose tissue, which provide information to the CNS about the energy status of the body (Mishra *et al.*, 2017). These

neurotransmitters are classified as **orexigenic** and **anorexigenic** substances (summarized in table 1); and their receptors are highly expressed in the hypothalamic feeding and satiety centers.

Table 1. Orexigenic and anorexigenic substances release from peripheral organs. Adapted from (Mishra *et al.*, 2017).

Orexigenic substances	Anorexigenic substances
Neuropeptide Y	α -MSH
Agouti-Related Protein (AgRP)	Leptin
Melatonin concentrating hormone	Serotonin
Orexin A	Corticotropin releasing hormone (CRH)
Orexin B	Norepinephrine
Endorphins	Insulin
Ghrelin	Glucagon-like peptide
Cortisol	Cholecystokinin (CCK)
	Cocaine- and amphetamine-regulated transcript (CART)
	Peptide YY

Energy homeostasis depends on brain reliability to process and trigger an adequate response to these peripheral hormonal and nutritional chemicals, being the perception of satiety after food intake reported by different sensors. Initially, the vagal stretch and tension sensors perceive the nutrients stored in the stomach, triggering the synthetization of neurotrophic factors that inform about meal-taking. Among these neurotrophic factors, the brain-derived neurotrophic factor and neurotrophin-3 regulate long-term repercussions on

energy balance (Fox *et al.*, 2006). As a consequence, **ghrelin** hormone is quickly repressed once food has been ingested, as it is the primarily signal secreted by oxyntic gland cells in the mucosa of the empty stomach (Cummings *et al.*, 2001; Cummings, 2006). The hunger or satiety signal induced by the presence or absence of ghrelin, respectively, is detected by the ghrelin receptor expressed on a subpopulation of vagal afferent innervating neurons in the nodose ganglia (Burdyga *et al.*, 2006).

Chemical signals informing about levels of ingestion are also sent from the intestine. Among many others, **Cholecystokinin (CCK)** appears to be the most relevant signal in the upper small intestine in food intake control. This hormone is released from enteroendocrine cells acting on a paracrine manner on CCK₁ receptors expressed on vagal sensory nerve terminals in the mucosal lamina with the objective of reducing food intake (Raybould *et al.*, 2006). Moreover, CCK is also synthesized within the brain followed by a post-translational process that generates an 8 amino acid peptide (CCK-8) which acts as an anorexigenic neuropeptide reducing food intake (Blevins *et al.*, 2000; Blevins and Baskin, 2010).

The presence of glucose in the lumen may be communicated to the brain via a wide variety of cotransporters and receptors expressed in the intestine. In addition, pancreatic β -cells are characterized by their glucose sensing capabilities, signaling glucose availability to the brain by their secretory products insulin and amylin. **Insulin** circulates in the bloodstream in proportion to white fat deposits, serving as a sensor of body fat content to the hypothalamus and other

brain areas (Kolaczynski *et al.*, 1996). On the other hand, **amylin** plays a major role in decreasing food intake and slowing gastric emptying through the activation of receptors expressed in postrema area and ascending pathways to the hypothalamus and limbic structures (Lutz *et al.*, 2001).

Finally, **leptin** is a peptide secreted mainly by the adipose tissue having a key role in energy homeostasis. Leptin levels in the bloodstream positively correlated with the amount of body fat, being its secretion increased after periods of food intake (Friedman, 2004). This anorexigenic substance acts directly in the ARC inhibiting NPY and AgRP neurons and enhancing POMC/CART neurons to decrease food intake and consequently augment signals of energy expenditure (Abdalla, 2017).

Disruptions in sensing of metabolic signals due to the inability to detect energy-storage fluctuations have been associated with obesity (Caron and Richard, 2017). Multiple investigations have demonstrated that obesity causes profound changes to the energy balance centers of the hypothalamus which lead to loss of central leptin (Volkow *et al.*, 2013) and insulin sensitivity (Williams, 2012). Furthermore, recent studies revealed that obesity induces central ghrelin resistance in neural circuits involved in behavioral regulation, and altered secretion of ghrelin from the stomach (Zigman *et al.*, 2016).

3.1.2. Hedonic regulation of food intake

As previously commented, the brain integrates information about the availability of nutrients ingestion and storage, consequently responding with behavioral, autonomic and endocrine outputs. However, the decision to eat is not uniquely regulated by internal homeostatic signals but also by hedonic signals which contribute feeding, such as food palatability and environmental cues (Volkow *et al.*, 2013; Kure Liu *et al.*, 2019). In the **hedonic regulation**, the cortical and subcortical limbic areas of the CNS play a crucial role triggering a pleasure signal together with learning and memory processes to ensure feeding. These communicated areas form an essential network constituted of an executive system and a reward system that exert a decisional control on food intake (Caron and Richard, 2017)

3.1.2.1. The brain executive system and the decision to eat

The brain executive system interacts with adjacent cortical areas which are essential for executive functions, such as voluntary eating. The prefrontal cortex (PFC) is a system influenced by adjacent somatosensory, gustatory and olfactory cortices that collect sensory inputs from the oral cavity and digestive tract, being these sensory inputs associated with the organoleptic properties of food. Thus, dysfunction of the PFC may contribute to the development of craving, compulsive eating, and may confer vulnerability for developing food addiction (Goldstein and Volkow, 2011; Caron and Richard, 2017).

3.1.2.2. The brain reward system and the desire and pleasure to eat

The brain executive system interacts with both adjacent cortical areas and with subcortical limbic structures establishing the motivational and the pleasure value of food. Palatable food has reinforcing effects that are mediated, in part, by abrupt DA increases in the brain reward system, mediating the pleasure sensation of eating (Volkow *et al.*, 2011a).

The **ventral tegmental area (VTA)** and the **nucleus accumbens (NAc)** are two interconnected components of the limbic circuit that have a crucial role in the brain reward system. Experiments in animals have demonstrated that, upon a first exposure to a palatable food, the firing activity of DA neurons in the VTA increases with a consequently augment in DA release in the NAc (Norgren *et al.*, 2006). Furthermore, existing evidence suggest that peripheral signals that modulate food intake exert their effects in part by hypothalamic signaling to VTA, and also by their direct actions on the the VTA DA meso-accumbens and meso-limbic pathways. When exposed to food stimuli, orexigenic hormones induce an increased activity of VTA DA cells and trigger dopamine release in the NAc (Opland *et al.*, 2010). Moreover, neurons present in the VTA and NAc express peptides and hormonal peripheral receptors, such as glucagon-like peptide 1, ghrelin, leptin, insulin, orexin and melanocortin receptors (Volkow *et al.*, 2013). Thus, several hormones and neuropeptides involved in energy homeostasis directly modulate the DA reward

system, indicating an important cross-talk between the homeostatic and hedonic systems.

In the reward system, the NAc DA signaling integrates the incentive salience of food-related stimuli (“wanting”) and the hedonic sensation (“liking”) aspects of the rewarding process associated with food intake. Remarkably, the implicated circuits in food wanting and liking are identical as those implicated in drug intake (Nora D. Volkow *et al.*, 2017). The modulation of endogenous signaling systems is suggested to be associated with “liking” responses, while the DA pathway from the VTA to NAc is linked with “wanting” or the motivation towards the pleasure of food consumption (Caron and Richard, 2017). This distinction in “liking” and “wanting” concepts emerged mainly from previous research on drug addiction, where stimuli that are often no longer “liked” are still intensely “wanted” (Berridge, 1996; Robinson and Berridge, 2003), being this conceptual differentiation helpful to better understand the neurobiological disorder of food addiction.

In the context of food intake, “liking” a food is typically followed by “wanting” it and consequently ingesting it without adverse effects. However, highly palatable foods may magnify the natural rewarding effects generated during food intake, leading to abnormal food and energy consumption even during periods of energy abundance (Kure Liu *et al.*, 2019). Indeed, “liking” and “wanting” seem to possess distinct roles in promoting food overconsumption. In “liking” processes, some individuals experience an overstated hedonic response to palatable foods, consequently enjoying more the food and

consuming beyond homeostatic needs. By contrast, “wanting” processes may enhance the vulnerability to compulsive overeating through augmented reactivity towards cues signaling craved foods' availability, causing damage in self-control. Therefore, “liking” seems to play an important role in establishing the motivational properties of food. However, once these properties are retained, the up-regulation of “wanting” promotes overconsumption in an obesogenic environment, leading to insensitivity of homeostatic signals and over-reactivity to external cues linked to the craved food (Hopkins and Blundell, 2016).

Therefore, the NAc receives complex inputs and outputs from multiple brain regions, such as the VTA, the PFC, and the hypothalamus having a crucial role in the desire and pleasure to eat. This critical brain node integrates information from the PFC and gustatory circuits and signals emerging from peripheral regions. Furthermore, the NAc sends reward-related information to the lateral hypothalamus and receives learning-related inputs from the hippocampus and amygdala, being the NAc a crucial key modulator of the mesocorticolimbic dopaminergic pathway (Figure 7).

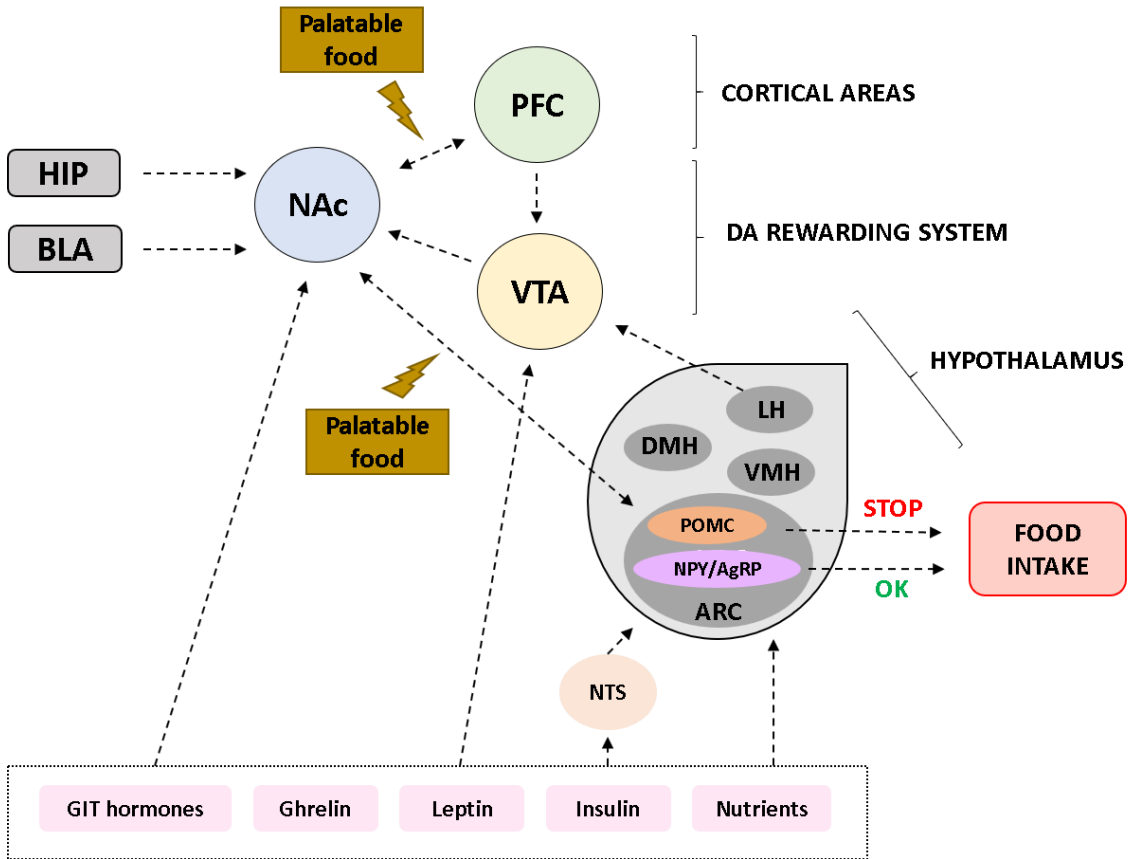


Figure 7. Schematic representation of the interconnected systems affecting food intake. It includes food-responsive peptides and hormones, energy homeostatic structures in the hypothalamus, the core of the dopamine (DA) rewarding system in the nucleus accumbens and ventral tegmental area, and various cortical areas in charge of processing affect, motor, and cognitive information. NTS, solitary nucleus tract; ARC, arcuate nucleus; DMH, dorsomedial nucleus; VMH, ventromedial nucleus; LH, lateral hypothalamic area; NAc, nucleus accumbens; PFC, prefrontal cortex; VTA, ventral tegmental area; HIP, hippocampus; BLA, basolateral amygdala; GIT, gastrointestinal tract. Adapted from (Volkow *et al.*, 2013; Caron and Richard, 2017).

3.2. The brain's reward circuitry

Food, water, and sex are essential needs that trigger a natural rewarding effect due to their action in the brain reward system. The

mesolimbic and mesocortical pathways within this system comprise dopaminergic neurons projecting from the VTA to limbic and cortical areas, respectively (Koob and Le Moal, 2008). Notwithstanding, these principal pathways are strongly overlapped and are collectively referred to as the **mesocorticolimbic system** (Wise, 2005).

The mesocorticolimbic circuit regulates perception and evaluation of rewarding and aversive stimuli in the environment. When exposed to **positive reinforcement**, the release of DA from the VTA to the NAc promotes the pleasure feeling, triggering the activation of other brain areas, such as the amygdala and the hippocampus, involved in emotional states and reward-related memories. In return, DA release in the NAc promotes a goal-directed behavior for reward acquisition mediated by frontal cortical areas, regions involved in executive function control (Koob and Volkow, 2016; Moore *et al.*, 2017). On the other hand, **aversive stimuli** may also modulate the mesocorticolimbic circuit by decreasing DA concentration at synaptic levels, contributing to negative reinforcement induced by aversive emotional states (Koob, 2017). Thus, the fluctuation of DA levels coming from the VTA may critically contribute to the motivational or silencing encoding of a given stimulus, in addition to the complex interconnected network of related brain areas that involve glutamatergic, GABAergic, cholinergic, and dopaminergic transmission (Bromberg-Martin *et al.*, 2010) (Figure 8).

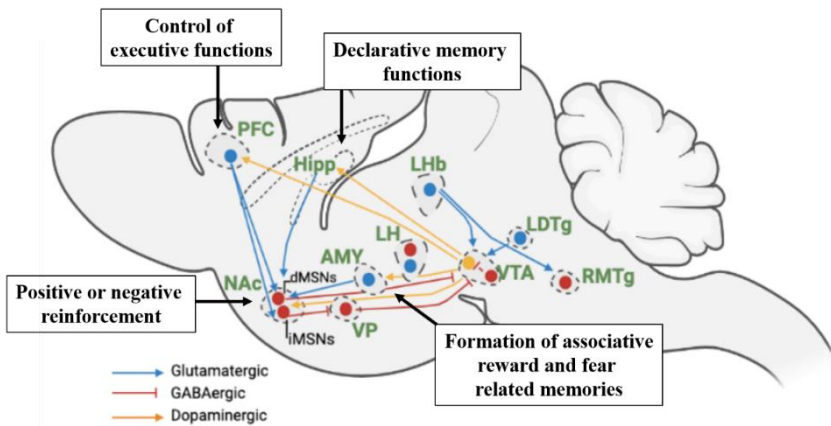


Figure 8. The mesocorticolimbic circuitry. A simplified schematic diagram of the mesocorticolimbic circuitry in rodent brain highlighting the major dopaminergic, glutamatergic and GABAergic connection to and from the ventral tegmental area (VTA) and nucleus accumbens (NAc). Amy, amygdala; Hipp, hippocampus; LH, lateral hypothalamus; mPFC, medial prefrontal cortex; LHb, lateral habenula; LDTg, lateral dorsal tegmentum; RMTg, rostromedial tegmentum. Adapted from (Russo and Nestler, 2013).

3.2.1. Ventral tegmental area

The VTA is a heterogeneous brain area constituted of dopaminergic projecting neurons (~60%), GABAergic interneurons, and GABAergic projecting neurons (~30-35%). Moreover, a smaller proportion of glutamatergic neurons (~2-3%) have been found in the VTA (Margolis *et al.*, 2012; Morales and Margolis, 2017). Although the majority of VTA neurons exclusively release DA, GABA, or glutamate, some specific VTA neurons co-release different combinations of neurotransmitters, such as DA and glutamate (TH-VGLUT2), dopamine, and GABA (TH-VGAT), or glutamate and GABA (VGLUT-VGAT). Moreover, peptides and neurotransmitters, such as CCK and BDNF, may also be released by particular VTA neurons (Seroogy *et al.*, 1988, 1994). These findings

highlight the complexity of VTA cytoarchitecture and local connectivity that are still poorly known.

In an overall view, the VTA has two principal DA output pathways to coordinate reward-seeking behavior, one projecting to the NAc (mesolimbic pathway) and the other projecting to the PFC (mesocortical) and additional areas, including the amygdala and hippocampus (Figure 9). Most studies have focused on both pathways since the stimulation of VTA neurons projecting to the NAc, PFC, and other areas may be critical in motivation, emotion, and cognitive control of palatable food.

Reinforcement is caused by the stimulation of the mesolimbic pathway that leads to an increase of DA release in the NAc, which is associated with the intensity of pleasure sensation (Volkow *et al.*, 2011a; Oleson and Cheer, 2012). Moreover, it is known that reinforcement is modulated by GABAergic projections from VTA to NAc and lateral habenula (Stamatakis *et al.*, 2013). Previous studies have revealed that the activation of VTA DA neurons diminishes GABA release in the NAc, consequently leading to an increased motivational drive (Berrios *et al.*, 2016). By contrast, optogenetic studies demonstrated that the selective activation of VTA glutamatergic neurons projecting to the NAc triggered a GABA release onto medium spiny neurons of the NAc that promoted aversion (Qi *et al.*, 2016). Thus, it is evident that the different VTA neurons projecting to the NAc critically regulate DA neuron function inducing reinforcement or aversion.

The activation of the mesocortical pathway is critical for cognitive control, motivation, and emotional response regulation (Nora D. Volkow *et al.*, 2017). Previous studies demonstrated the importance of the mesocortical pathway in cognitive control by the inhibition of VTA DA neurons projecting to the mPFC. This DA elimination resulted in a loss of cortical inhibition mediated by mesocortical DA and glutamate-releasing neurons (Kabanova *et al.*, 2015). However, other brain areas also receive DA projections from the VTA, including the amygdala and hippocampus, where aversive states and contextual relations of drug-related cues are processed, respectively (George F Koob and Volkow, 2010).

Finally, the VTA also receives excitatory inputs from diverse brain regions, including glutamatergic projections from the laterodorsal tegmental nucleus, the lateral habenula, and the PFC. Projections coming from the laterodorsal tegmental nucleus preferentially synapse on DA VTA neurons projecting to the NAc, consequently leading to reward activation. By contrast, enhancing glutamatergic lateral habenula neurons that innervate DA VTA neurons projecting to PFC produces aversion (Lammel *et al.*, 2012). Furthermore, GABAergic inhibitory inputs from the rostromedial tegmental nucleus are sent to the VTA inducing a repressive control over DA VTA neurons projecting to the NAc (Cooper *et al.*, 2017). However, the VTA receives projections from other brain regions, such as the NAc, amygdala, ventral pallidum, and lateral hypothalamus. Thus, the explained afferent and efferent projections to the VTA form a complex local microcircuit inside the mesocorticolimbic system.

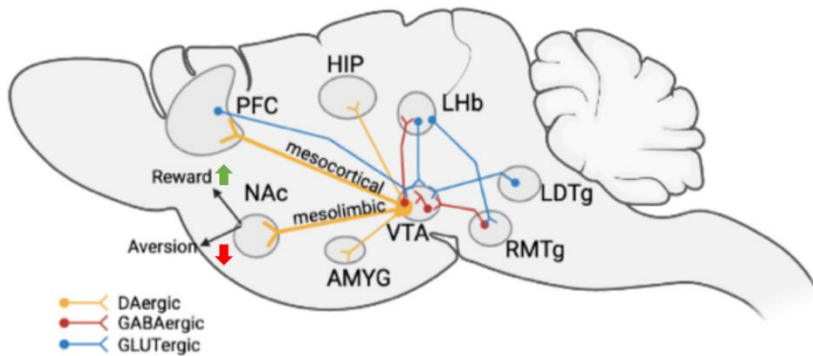


Figure 9. Schematic representation of the complex VTA microcircuitry showing the main outputs and inputs of this area. PFC, prefrontal cortex; HIP, hippocampus; LHB, lateral habenula; LDTg, laterodorsal tegmental nucleus; RMTg, rostromedial tegmental nucleus; VTA, ventral tegmental area; AMG, amygdala; NAC, nucleus accumbens. Adapted from (Cooper *et al.*, 2017).

3.2.2. Nucleus accumbens

The striatum is a central connectivity hub situated in the forebrain with a particular role in processing motivation, affection, cognition, and sensorimotor information. It arises from diverse systems to exert a behavioral action output. However, the striatum is divided into the **dorsal striatum** and the **ventral striatum** according to morphological and functional differences. These subregions are highly heterogeneous regions differentiated primarily by the diverse range of neuron types and neuromodulators (Gerfen *et al.*, 1987; Brimblecombe and Cragg, 2017).

Concretely, the ventral striatum consists of the **nucleus accumbens** and the olfactory tubercle. The NAc is the major component of the ventral striatum, being a crucial hub of communication-processing involved in motivation and reward-related behaviors (Hyman *et al.*,

2006; Volkow *et al.*, 2011a; Nora D. Volkow *et al.*, 2017). This key node targets natural rewards and drug reinforcing effects by stimulating DA transmission across functional connections between limbic system structures, such as the amygdala, hippocampus, and basal ganglia (Mogenson *et al.*, 1980; Di Chiara and Imperato, 1988; Volkow *et al.*, 2011b). The NAc is divided into two functional subregions known as the core (central part) and the shell (surrounding medially, ventrally and laterally the core) with different anatomical connectivity and presumed behavioral roles (Figure 10). The **core** is assumed to integrate learning reward-cue associations, responses to motivational stimuli, impulsive choices, and initiation of motor actions. On the other hand, the **shell** is involved in reward prediction, affective processing, and drug relapse (Di Chiara, 2002; Nora D. Volkow *et al.*, 2017).

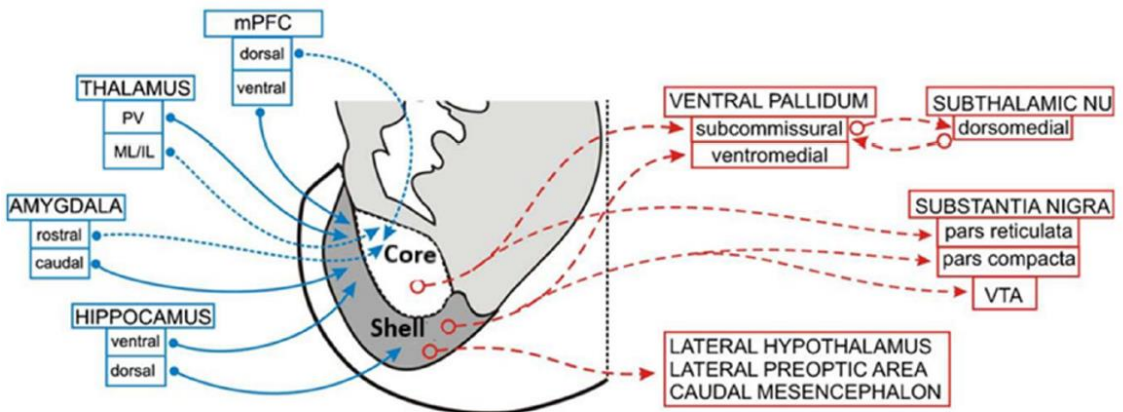


Figure 10. Schematic diagram of the inputs and outputs of the core and shell of the nucleus accumbens. Dopaminergic, serotonergic, and noradrenergic inputs have been omitted from the drawing. ML/IL, midline and intralaminar thalamic nuclei; mPFC, medial prefrontal cortex; PV, paraventricular thalamic nucleus; VTA, ventral tegmental area (Basar *et al.*, 2010).

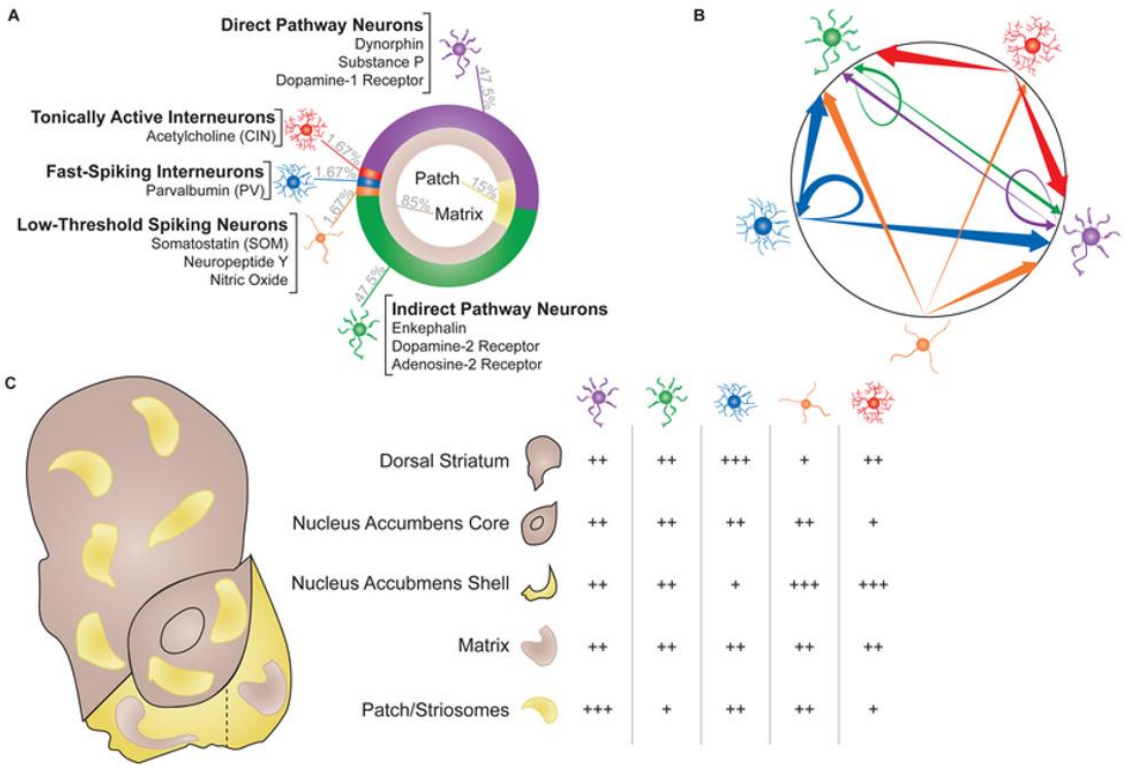


Figure 11. Basic structural anatomy of the striatum. **A.** Ring charts showing relative expression (% , gray text) of cell types (outer ring) or patch/matrix (inner ring). Cell types labeled with known and exclusive markers for each population. **B.** Intra-striatal connectivity schematic showing preferential connections between cell types. Arrows signify projection target, circled arrows signify synapses onto other neurons of the same type. Cell populations: purple, direct pathway; green, indirect pathway; blue, fast-spiking interneuron; orange, low-threshold spiking interneurons; red, tonicly active interneurons. Arrow thickness: thin, low connectivity; medium, moderate connectivity; thick, strong connectivity. (**C,** bottom, left) Schematic of rodent striatum, dividing dorsal, core, and shell into separable subregions (lateral and medial divided by dashed line). Matrix (brown) and patch (yellow) shaped and distributed to show relative expression in each subregion. (right) Table showing relative distribution of different cell types within each region of the striatum. Direct pathway neurons, purple; indirect pathway neurons, green; tonicly active interneurons, red; fast-spiking interneurons, blue; low-threshold spiking interneurons, orange. +, low relative expression; ++, average relative expression; +++ high relative expression (Castro and Bruchas, 2019).

The principal population of neurons in the NAc is GABAergic medium spiny neurons (MSNs) (~95%), whereas the remaining neuron population (~5%) consists of GABAergic and cholinergic interneurons. MSNs are extensively subdivided into two subtypes based on their output projecting areas, neurochemical content, and receptor markers. MSNs of the “direct pathway” express DA receptor type-1, dynorphin, and substance P, whereas MSNs of the “indirect pathway” express DA receptor type-2, adenosine 2A receptors, and enkephalin (Castro and Bruchas, 2019) (Figure 11).

In the “**direct pathway**”, MSNs extend their axonal projections to the internal part of the globus pallidus (GPi), and the substantia nigra pars reticulata (SNpr), inducing the inhibition of GABAergic neurons in both areas. As a consequence of SNpr inhibition, thalamic glutamatergic neurons projecting to the cortex that receive SNpr input are disinhibited, promoting movement. By contrast, MSNs of the “**indirect pathway**” indirectly innervate the SNpr via the outer part of the globus pallidus (GPe) and the subthalamic nucleus (STN). The inhibition of GABAergic projections to the STN from GPe leads to glutamatergic projections disinhibition from STN to the SNpr/GPi output nuclei. Ultimately, the activation of GABAergic neurons in the SNpr and GPi represses the thalamus, consequently reducing movement (Kreitzer and Malenka, 2008; Gerfen and Surmeier, 2011). This is the traditional model widely studied in the dorsal and ventral striatum (Figure 12). However, recent studies have proposed a newer model in which the direct and indirect pathways are functionally and structurally interlaced by intrastriatal connections (Calabresi *et al.*, 2014).

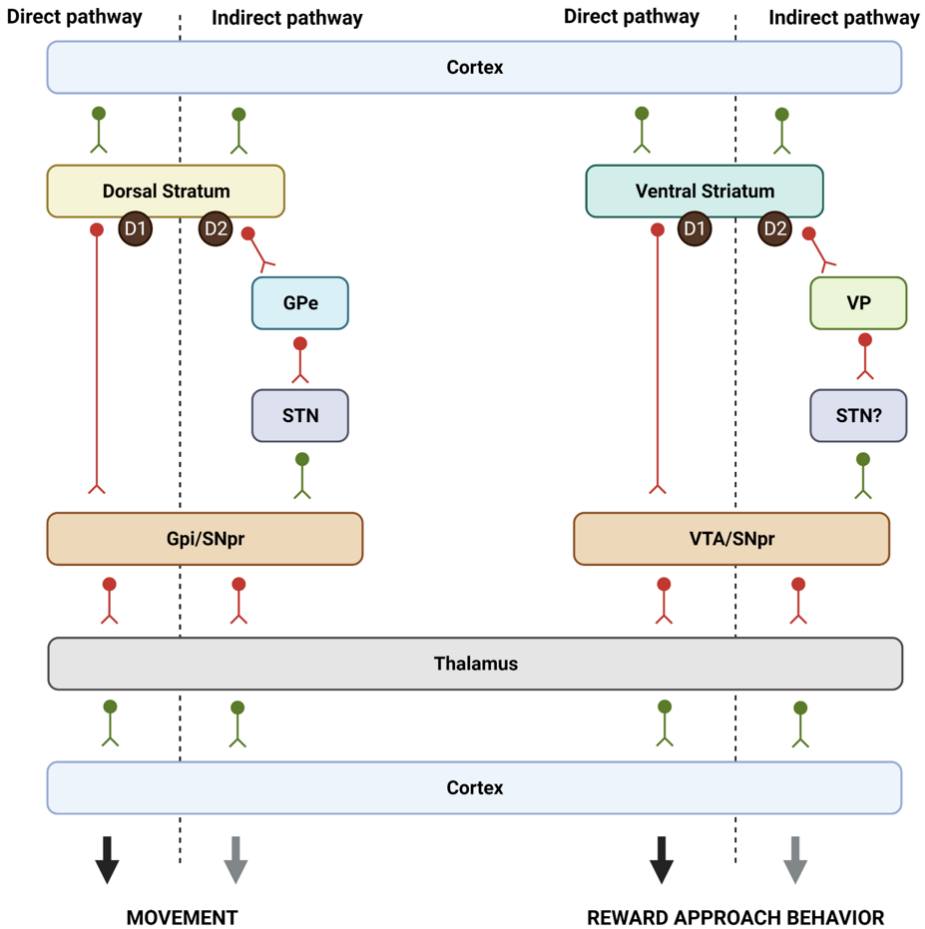


Figure 12. Schematic representation of the traditional view for direct and indirect pathways in the dorsal striatum and ventral striatum. GPe and GPi, external and internal globus pallidus; VP, ventral pallidum; SNpr, substantia nigra pars reticulata; STN, subthalamic nucleus; D1 and D2 dopaminergic receptors. Excitatory glutamatergic projections in green and inhibitory GABAergic responses in red. Adapted from (Gerfen and Surmeier, 2011; Mannella *et al.*, 2013).

Accordingly, optogenetic and tracing tools studies have demonstrated that a significant proportion of “direct pathway” MSNs also project to the ventral pallidum (VP), whereas some “indirect pathway” MSNs directly innervate the thalamus. These recent

findings reconstruct the classical model highlighting the VP as an essential target in reward circuitry. Classical “direct pathway” MSNs expressing DA receptor type-1 may be involved in a novel indirect pathway that innervates the VP. On the other hand, classical “indirect pathway” MSNs expressing DA receptor type-2 may contribute in the direct pathway regulation (Kupchik *et al.*, 2015; Kupchik and Kalivas, 2017; Klawonn and Malenka, 2018) (Figure 13).

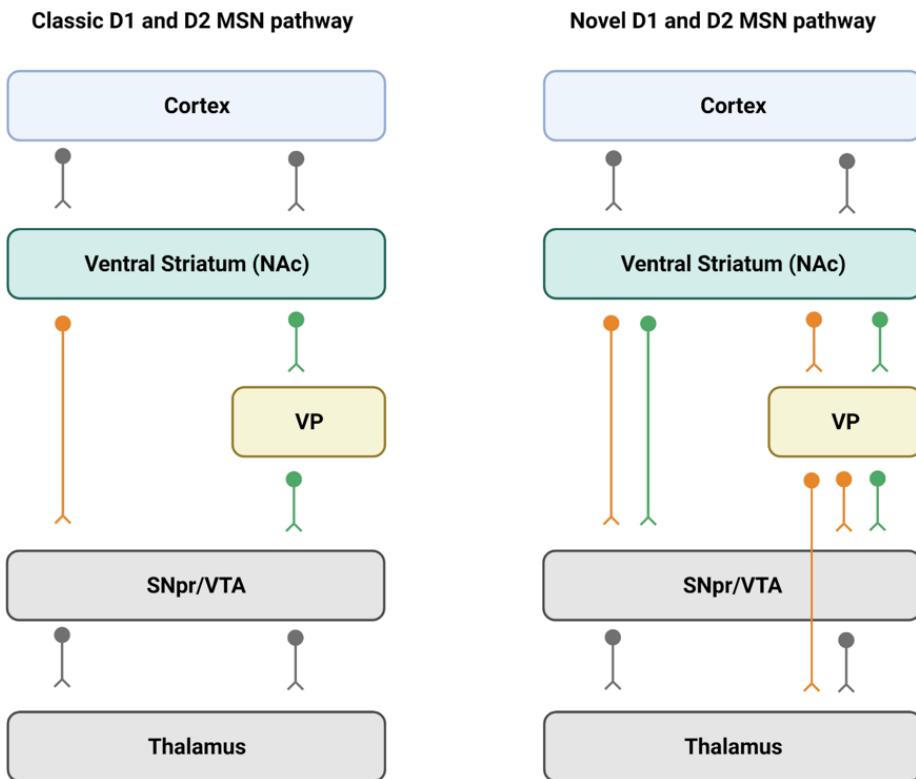


Figure 13. Schematic diagram of NAc D1 and D2 MSN anatomical connectivity emphasizing the differences between the classic conceptualization of indirect and direct pathways and the novel view. D1 MSNs are marked in orange whereas D2 MSNs are represented in green. NAc, nucleus accumbens; VP, ventral pallidum; SNr, substantia nigra pars reticulata; VTA, ventral tegmental area; D1 and D2 dopaminergic receptors. Adapted from (Kupchik *et al.*, 2015; Klawonn and Malenka, 2018).

The major efferent projections of the NAc innervate the VP and other brain areas, such as substantia nigra, VTA, hypothalamus, and brainstem. Recent studies have revealed the presence of two distinct DA NAc-VP circuits based on the NAc topography. From one side, DA NAc core projections innervate primarily the dorsolateral portion of the VP, which projects to the subthalamic nucleus and SNpr. From the other side, DA NAc projections from the shell mainly extend their axons to the ventromedial VP division, which contains a reciprocal connection with the PFC and the VTA (Salgado and Kaplitt, 2015) (Figure 14). Thus, recent studies on addictive-like behaviors have paid particular attention to the connection between the NAc and the VP. Function restoration of DA receptor type-1 NAc-VP synapses removed cocaine locomotor sensitization, whereas function recovery of DA receptor type-2 NAc-VP synapses corrected cocaine withdrawal-induced anhedonia (Creed *et al.*, 2016). These evidences suggest that VP projections from NAc MSNs DA receptor type-1 and NAc MSNs DA receptor type-2 regulate various behavioral features associated with cocaine addiction. Moreover, the VP is also involved in eating behaviors as the activation and inhibition of GABA receptors of the VP repressed and increased food intake, respectively (Shimura *et al.*, 2006; Taha *et al.*, 2009; Covelo *et al.*, 2014).

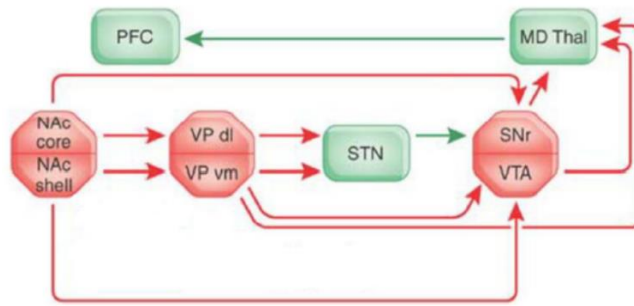


Figure 14. Distinct dopaminergic nucleus accumbens-ventral pallidum circuits based on NAc topography. Only major projections are shown. COLOR indicates inhibitory structures and pathways, whereas COLOR indicates excitatory connections. MD Thal, mediodorsal thalamic nucleus; NAc, nucleus accumbens; PFC, prefrontal cortex; SNr, substantia nigra pars reticulata; STN, subthalamic nucleus; VP dl/vm, ventral pallidum, dorsolateral, and ventromedial; VTA, ventral tegmental area. Adapted from (Sesack and Grace, 2010).

Finally, anatomical and functional evidence suggests that NAc projections to the VTA may also mediate feeding behavior, the strongest response effect produced by NAc inactivation observed in the NAc shell (Reynolds and Berridge, 2001). The VTA receives NAc shell projections that create long-loop feedback that controls DA neuron's activity in a bidirectional sense (Carr and Sesack, 2000; Yang *et al.*, 2018). Previous investigations have revealed that NAc neurons synapse onto both DA VTA and GABA VTA neurons, forming a direct and indirect feedback loop. In the **direct loop**, MSNs of the medial part of the NAc directly suppress the activation of DA VTA neurons, leading to a repressed behavioral output. By contrast, in the **indirect loop**, MSNs of the lateral part of the NAc shell synapse with GABAergic VTA neurons inducing the disinhibition of DA VTA neurons that project back to the lateral part of the NAc shell

(Figure 15). The activation of the indirect pathway triggers an increasing activity in DA VTA neurons that enhance reward-related outbreaks (Yang *et al.*, 2018). Additionally, other brain areas from cortical and subcortical structures, such as the PFC, amygdala, hippocampus, and thalamus, send information to MSNs of the NAc and VTA that consequently project to essential cellular targets in the NAc subregions (Sesack and Grace, 2010). Altogether, these evidences suggest that the NAc is a crucial circuitry hub that translates motivation into action. However, further studies are needed to understand the specific neurobiological signatures underlying this addictive-like behavior.

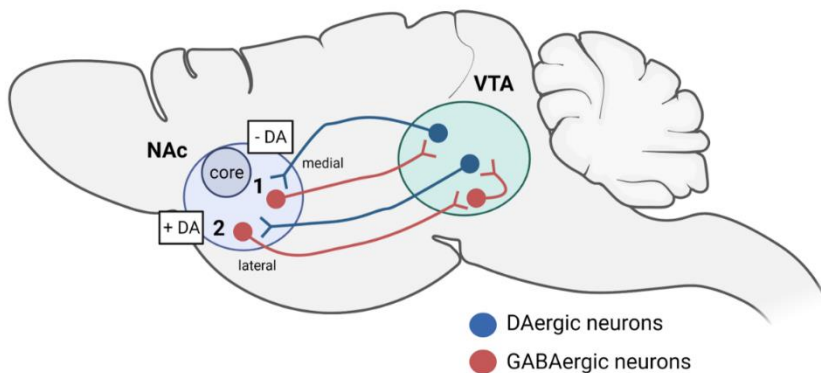


Figure 15. Simplified diagram of the feedback connectivity between NAc and VTA. (1). The direct feedback loop in which medial shell NAc D1 MSNs synapse on medial VTA DA neurons that project back to the medial NAc suppressing behavioral output. (2) The indirect feedback loop in which lateral shell NAc DIMSNs synapse on VTA GABAergic neurons, which exert inhibitory influence over NAc lateral-projecting DA neurons. These neurons project back to the lateral NAc, promoting reward-related behaviors. NAc, nucleus accumbens; VTA, ventral tegmental area. Based on (Yang *et al.*, 2018).

3.2.3. Prefrontal cortex

The PFC is a brain area involved in several executive functions, including the regulation of cognitive, emotional, and motivational processes. These functions are associated with control behavior such as response inhibition, planning, attention, and decision-making (Miller and Cohen, 2001). Dysregulation of these functions has been associated with a loss of self-behavioral control driving compulsive food intake, drug use, and addiction (Goldstein and Volkow, 2011). The two major prefrontal regions implicated in the regulation of DA system function are the medial prefrontal cortex (mPFC) and the orbitofrontal cortex (OFC), regions that carry out independent but complementary forms of cognitive processing (George F Koob and Volkow, 2010).

The cytoarchitecture of the **mPFC** consists principally of excitatory glutamatergic pyramidal projecting neurons (~80%), and GABAergic inhibitory interneurons (~20%) (Pistillo *et al.*, 2015). Similar to other cortical areas, the mPFC presents a laminar (L) organization that establishes intracortical circuits between the superficial layers' excitatory pyramidal neurons (L2/3) and other pyramidal and GABAergic neurons. These excitatory projections from deeper layers (L5/6) also innervate subcortical areas, including the VTA and NAc. Moreover, deep pyramidal neurons located in L5 and 6 receive projections from DA VTA neurons, while pyramidal neurons in L2, 3, and 5 receive inputs from other cortical regions, the thalamus, basolateral amygdala (BLA), and hippocampus. Thus, the communication between the VTA and PFC that forms part of the mesocortical circuit evaluates the salience motivational significances

associated with context and stimuli, such as drug and food associated context (Douglas and Martin, 2004) (Figure 16).

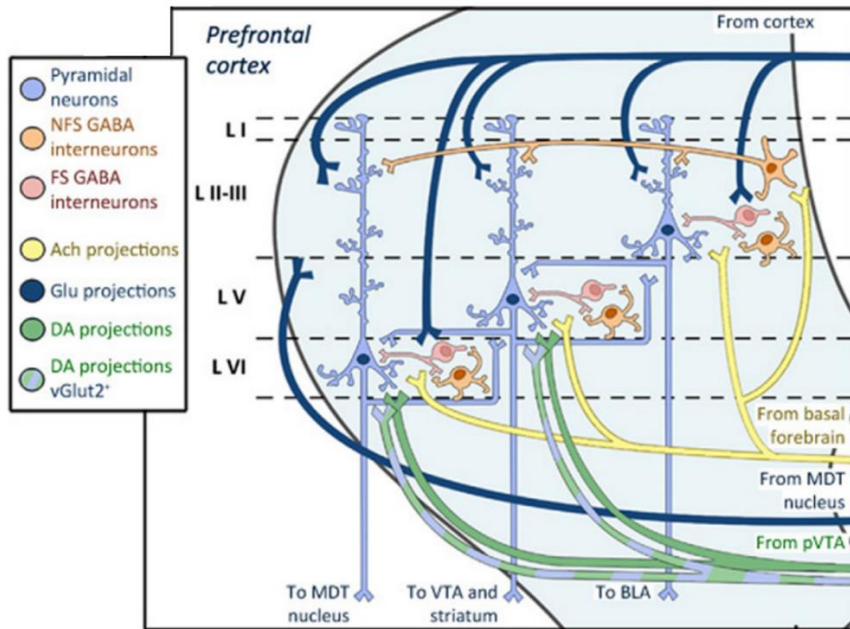


Figure 16. Simplified diagram of the connectivity in the rodent mPFC. The pyramidal neurons in superficial layers (L2/3) are mainly cortico-cortical neurons. The pyramidal neurons in deep layers (L5/6) are cortico-subcortical neurons mainly projecting to VTA and NAc. Pyramidal neurons in L5 and 6 receive projections from DA VTA neurons while pyramidal neurons in L2, 3 and 5 receive functional inputs from other cortical areas, thalamus, BLA and hippocampus. NAc, Nucleus accumbens; VTA, ventral tegmental area; BLA, basolateral amygdala; FS, fast-spiking; NFS, non-fast spiking (Pistillo *et al.*, 2015).

Within the rodent mPFC, several areas are defined along a dorsal to the ventral axis that seems to play distinct functional roles. These subregions are the medial precentral, anterior cingulate, prelimbic (PL), and infralimbic (IL) cortex. They are usually grouped in a dorsal component (dmPFC), including the anterior cingulate cortex

and PL, and in a ventral component (vmPFC) encompassing the IL and ventral orbital cortex (Heidbreder and Groenewegen, 2003). Indeed, all these regions forming the dmPFC and vmPFC have been widely related to addictive processes. Previous studies have revealed that the anterior cingulate is mainly engaged in attentional selectivity, discrimination learning, and impulsive actions (Perry *et al.*, 2015).

Moreover, drug addiction investigations reported that PL and IL areas have dissociable roles in cocaine-seeking behavior, suggesting that cocaine-seeking was promoted and repressed by the PL and IL, respectively (Moorman *et al.*, 2015). Thus, the canonical functional dichotomy between PL and IL postulates that PL promotes natural reward and drug-seeking, whereas the IL suppresses it. Several studies support this model as it has been demonstrated that the pharmacological inactivation of PL effectually blocks drug-priming and cue-induced reinstatement of cocaine-seeking (McFarland and Kalivas, 2001). Additionally, the optogenetic inhibition of PL neurons attenuated cocaine reinstatement and decreased induced relapse of food-seeking (Calu *et al.*, 2013; Stefanik *et al.*, 2013). Further studies have also focused on understanding IL's involvement in addictive-like behaviors. For instance, experiments in trained rodents to self-administer cocaine revealed that the inhibition of IL enhanced lever pressing in the late extinction of cocaine self-administration (Peters *et al.*, 2008a). By contrast, the activation of IL using glutamate agonists repressed cocaine-induced reinstatement (Peters *et al.*, 2008b).

However, the established PL and IL behavioral roles model represents an overly simplistic framework as opposite PL and IL effects were observed with different substances and behavioral environments. Studies using GABA receptor agonists that induced PL inactivation demonstrated a decreased ability of a footshock-associated conditioned stimulus to diminish cocaine responding (Limpens *et al.*, 2015). Moreover, prolonged cocaine self-administration with punishment-conditioning in rats reduced the excitability of PL pyramidal neurons. On the other hand, photostimulation of PL pyramidal neurons decreased cocaine compulsive behavior (Chen *et al.*, 2013). Finally, studies of food addiction revealed that the inhibition of IL reduced food pellet seeking without affecting the expression of extinction (Sangha *et al.*, 2014).

These conflicting and contradictory findings have been partially clarified with essential clues obtained from human investigations. Although the homology between human and rodent PFC is still not completely understood, the mPFC is relatively comparable across species due to the similarities in functions and connections (Jasinska *et al.*, 2015). From a translational perspective, the human dorsolateral PFC (dlPFC) is parallel to the rodent PL area and the vmPFC is equivalent to the rodent IL area (Koob and Volkow, 2016) (Figure 17).

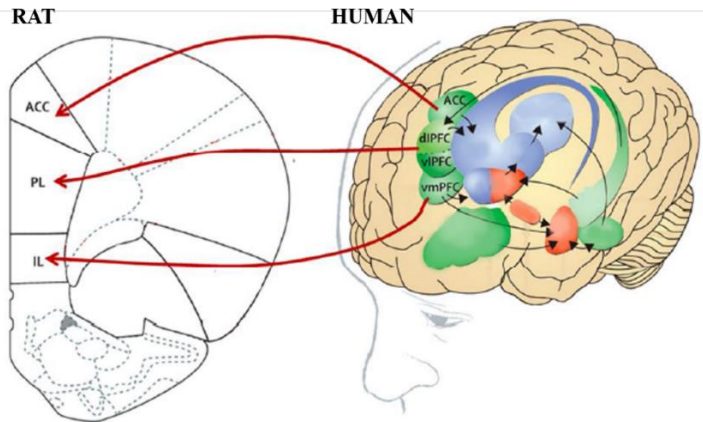


Figure 17. Correspondence between rat and human medial frontal regions. ACC, anterior cingulate cortex; PL, prelimbic cortex; IL, infralimbic cortex; dlPFC, dorsolateral prefrontal cortex; vlPFC, ventrolateral prefrontal cortex; vmPFC, ventromedial prefrontal cortex. Adapted from (Koob and Volkow, 2016).

Neuroimaging studies in humans demonstrated that dlPFC activity increased in response to specific cocaine-related cues being this key brain area linked to risks of drug relapse (Wexler *et al.*, 2001; Marhe *et al.*, 2013). Moreover, cocaine users showed a decreased activation of the dlPFC when responding to inhibition tasks (Crunelle *et al.*, 2012). Remarkably, all this evidence were reflected in animal models of cocaine addiction that showed learned associations between drug cues, drug-seeking, and punishment conditioning, establishing an essential determining role of the PL in the expression of conditioned fear-related behaviors (Burgos-Robles *et al.*, 2009). Thus, the aggravation of cocaine-seeking by an altered dorsal mPFC could be explained by governance of inhibitory control processes over the dorsal mPFC circuitry, suggesting that the PL has a crucial role in

associative learning, both associating the environmental cue or the reward associated punishment (Jasinska *et al.*, 2015).

Altogether, the mPFC and rest of the frontal areas have a complex role involved in reward-seeking, associative learning, and inhibitory control. Other brain areas such as the basal ganglia and extended amygdala are regulated by frontal regions, which send top-down glutamatergic projections to the VTA, NAc, dorsal striatum, hippocampus, and amygdala (Parsons and Hurd, 2015). Specific “Go circuits” and “stop circuits” have been identified based on whether their recruitment facilitates or hinders the transition to addictive behavior (Bock *et al.*, 2013; Picciotto and Kenny, 2013). Neurons in the orbitofrontal cortex that directly link to the NAc and the medial wall of the dorsal striatum are activated by the “Go circuit” (Pascoli *et al.*, 2018; Hu *et al.*, 2019). On the other hand, excitatory synaptic transmission in PL mPFC neurons that project to the NAc are stimulated by the “Stop circuit”, which inhibits compulsive-like behavior (Hu *et al.*, 2019; Domingo-Rodriguez *et al.*, 2020). Thus, “Go circuit” and “Stop circuit” are crucial in controlling reward sensitivity. An alteration in the regulation of both circuits may lead to the transition to addiction and compulsive-like behaviors (Figure 18).

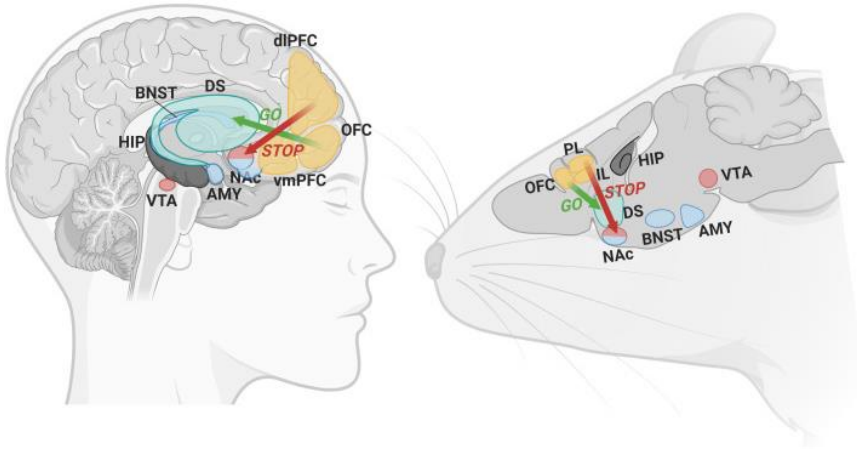


Figure 18. Schematic representation of mouse brain areas involved in reward sensitivity, conditioning, emotional processing, and inhibitory control circuits. The loss of control or compulsivity seems to result from an imbalance between the “Stop” and “Go” top-down cortical circuits with a hypofunction of the PL-ventral striatum network and hyperactivity of the OFC-dorsal striatum networks. VTA, ventral tegmental area; NAc, nucleus accumbens; DS, dorsal striatum; AMY, amygdala; BNST, bed nucleus of the stria terminalis; HIP, hippocampus; dlPFC, dorsolateral prefrontal cortex; vmPFC, ventromedial prefrontal cortex; OFC, orbitofrontal cortex; PL, prelimbic; IL, infralimbic. Adapted from (R. Maldonado *et al.*, 2021).

3.3. Modulation of the reward circuitry

The circuitry of the brain reward system is modulated by dopaminergic and endocannabinoid signaling and by the opioid system, among others. These three main endogenous signaling systems interact to integrate the hedonic values of natural, pleasurable stimuli.

The rewarding properties of a natural compound, such as food, are divided into hedonic components (pleasure and palatability) and incentive motivation (appetite) that are regulated and measured independently. Essential neurotransmitters process and integrate these functional components. Opioid and GABA/benzodiazepine

systems regulate the hedonic factors related to food, whereas, the dopaminergic system controls incentive motivation. Remarkably, the endocannabinoid system seems to influence both the motivation to feed and the hedonic values of foods, probably by modifying palatability (Berridge, 1996; Jager and Witkamp, 2014).

3.3.1. Opioid signaling

The endogenous opioid system is composed of endogenous opioids such as endorphins, enkephalins, and dynorphins that activate opioid receptors. This system assigns hedonic values to rewards, and integrating reward-related information to guide decision-making and goal-directed behavior execution (Volkow *et al.*, 2019). Several studies have focused on understanding the relationship between opioid receptors and the hedonic properties of food.

The activation of the μ -opioid receptor (MOR) either by injection of morphine in the mesolimbic reward system or by receptor stimulation in the NAc leads to a pleasure increase in food which promotes feeding (Bozarth and Wise, 1983; Peciña and Berridge, 2005). Moreover, opioid agonists increase food intake and hedonic reactions to food, whereas MOR antagonists and inverse agonists reduce food consumption and hedonic responses (Glass *et al.*, 1999; Yeomans and Gray, 2002; Giuliano *et al.*, 2012; Nathan *et al.*, 2012). This evidence is supported by imaging studies in humans that demonstrate that food intake leads to endogenous opioids release in the brain reward circuitry, which possibly contributes to obesity (Burghardt *et al.*, 2015; Tuulari *et al.*, 2017). In addition, neurological mechanisms

have been suggested to support overeating and compulsive food intake. For instance, the repeated overstimulation of MOR after prolonged consumption of high palatable food may result in a long-term downregulation of MOR and the subsequent requirement of more significant amounts of food to produce the equivalent hedonic effect (Davis *et al.*, 2009).

3.3.2. Dopaminergic signaling

DA is a neurotransmitter with crucial influences on behavioral and neuronal circuits. In addition, DA signaling plays an essential role in multiple CNS functions, such as voluntary movement, feeding, affect, decision making, attention, learning, working memory, and reward. Thus, given the breadth of DA vital tasks, it is not surprising that multiple human disorders have been linked to dopaminergic dysfunctions, including Parkinson's disease, Tourette's syndrome, schizophrenia, obsessive-compulsive disorder, and addiction (Tritsch and Sabatini, 2012).

3.3.2.1. Dopaminergic neurons

DA neurons are located in the mammalian CNS and in several peripheral tissues. The major dopaminergic networks identified within the brain are the nigrostriatal, mesolimbic and mesocortical, and tuberoinfundibular pathways. The **nigrostriatal pathway** is conferred by DA neurons projecting from substantia nigra pars compacta to the dorsal striatum, mainly involved in movement

control and habits. The **mesolimbic** and **mesocortical pathways** are formed by DA neurons projecting from the VTA to NAc and PFC, respectively. These DA neurons are involved in the reward system modulating reinforcement, reward-related learning, and motivation. Finally, the **tuberoinfundibular pathway** is constituted of DA neurons that arise in the arcuate nucleus and end in the median eminence of the hypothalamus. This pathway is involved in the release and synthesis of pituitary neurons, primarily prolactin (Beaulieu and Gainetdinov, 2011; Baik, 2013) (Figure 19).

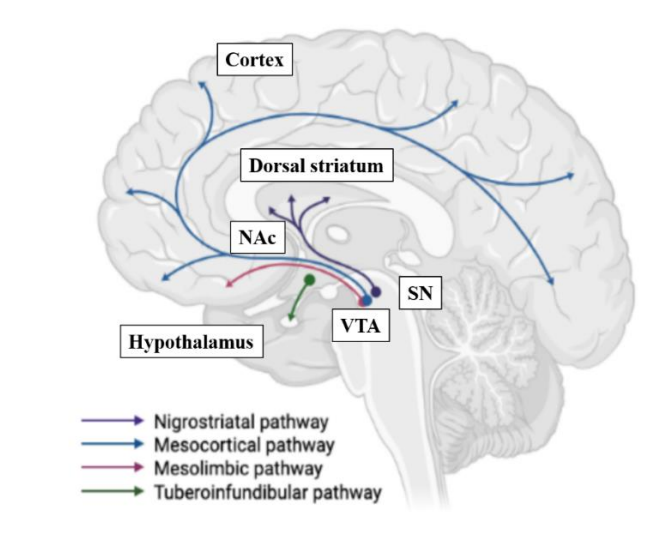


Figure 19. Dopaminergic pathways in the human brain. Major four dopaminergic pathways are presented: the nigrostriatal pathway, mesolimbic pathway, mesocortical pathway, and tuberoinfundibular pathway. VTA, ventral tegmental area; SN, substantia nigra; NAc, nucleus accumbens.

DA neurons are observed in two different activity states the active (firing states) state or the silent (non-firing) state. When DA neurons

are firing, they can fire in a stable irregular **tonic mode** (low frequency, 1-8 Hz) or a transitory (500 msec) **phasic mode** (high frequency, >15 Hz) with bursts of the action potential. The spontaneously firing activity at low frequencies suggests that each neuron provides a basal DA tone to several target neurons. Exposure to salient (reinforcing, novel, unexpected or aversive) stimuli induces changes in firing activity from low frequencies to burst phasic firing at high frequencies associated with reinforcement learning (Nora D Volkow *et al.*, 2017). Firing in the tonic mode is generated by intrinsic pace-maker membrane properties of DA neurons and results in DA release (in the range of nM) from extrasynaptic release sites. These low DA concentrations are sufficient to activate high-affinity DA receptors, which determine arousal of motivation (Ford, 2014). On the other hand, phasic spiking is dependent on glutamate receptor activation and voltage-gated ionic channels and results in an augmented extracellular DA release (in the range of μM) in the synaptic cleft, which stimulates the low-affinity postsynaptic DA receptors that lead to behaviorally salient stimuli (Dreyer *et al.*, 2010). Subsequently, DA is rapidly removed from the synapse by the DA transporter (DAT) that ends the signal.

3.3.2.2. Dopamine receptors

DA mediates its physiological activity by interacting with DA receptors that belong to the extensive family of G protein-coupled receptors (GPCRs). This class of receptors is characterized by seven hydrophobic transmembrane sections and a vital third

intracytoplasmic loop that interacts with a high amount of G-proteins types and effector molecules (Missale *et al.*, 1998; Beaulieu and Gainetdinov, 2011). Based on their structural, pharmacological, and signaling properties, these DA receptors are commonly subdivided into the **D₁-like DA receptors** subfamily, which comprises D₁ and D₅ receptors, and the **D₂-like DA receptors** subfamily which involves D₂, D₃, and D₄ receptors (Jaber *et al.*, 1996). Common structural characteristics are shared with the individual receptors within the same subfamily. However, different sequence variations are detected between them, playing a unique role in determining their specific affinity for ligands and coupling to transduction pathways. The affinity of D₂-like receptors is generally reported to be 10- to 100- fold higher than D₁-like receptors, with D₃ and D₄ receptors exhibiting the highest sensitivity for DA and D₁ receptors the shortest. Nevertheless, D₁ and D₂ receptors can be found in both high and low-affinity states, having analogous nanomolar affinities for DA in their affinity states (Beaulieu and Gainetdinov, 2011) (Table 2).

Regarding the distribution of DA receptors, these receptors are highly expressed in the CNS and periphery. D₁ and D₂ receptors are the most abundant receptor subtypes expressed in the brain, with D₁R being the most expressed and widely distributed. Both receptors are most prominently found in areas where DA fibers innervate, such as the dorsal striatum, NAc, olfactory tubercle, and cortex, among other structures. Inside the cell, D₁ and D₂ receptors are localized in the presynaptic sites of nerve terminals and axonal varicosities; and the

postsynaptic sites of dendritic shafts and spines (Tritsch and Sabatini, 2012).

The genetic differences between D₁- and D₂-like receptors concern the absence and presence of introns in their coding sequence, respectively. Whereas the D₁-like subfamily genes do not contain introns, the genes that encode for the D₂-like subfamily comprise several introns. The D₂R gene (DRD2) contains exons that generate two splicing variants termed D₂S and D₂L. These two alternatively spliced isoforms differ in the presence of an additional 29 amino acids in the third intracellular loop (Khan *et al.*, 1998). Moreover, expression levels are different between these two variants of the D₂R, with the D₂L mRNA being highly expressed compared to the shorter variant (Usiello *et al.*, 2000). Additionally, D₂S is mainly expressed presynaptically, playing a role in autoreceptor functions, whereas D₂L seems to be predominant postsynaptically (Beaulieu and Gainetdinov, 2011) (Table 2).

Table 2. Basic characteristics of DA receptors. Modified from (Tritsch and Sabatini, 2012).

	D ₁ -LIKE FAMILY		D ₂ -LIKE FAMILY		
<i>DA receptor subtype</i>	D ₁ R	D ₅ R	D ₂ R	D ₃ R	D ₄ R
<i>Gene</i>	<i>Drd1</i>	<i>Drd5</i>	<i>Drd2</i>	<i>Drd3</i>	<i>Drd4</i>
<i>Number of introns</i>	0	0	6	5	3
<i>Splice variants</i>	No	No	Yes (D ₂ S, D ₂ L)	Yes	Yes
<i>Affinity for DA (μM)</i>	1.0-5.0	0.2-2.0	0.2-2.0	0.02-0.2	0.01-0.1
<i>G protein coupling</i>	Gα _s , Gα _{olf}	Gα _s , Gα _q	Gα _i , Gα _o	Gα _i , Gα _o	Gα _i , Gα _o

D₁- and D₂-like receptor subfamilies differ functionally concerning the intracellular signaling pathways. Although DA receptors enhance the activation of heterotrimeric G proteins, the roles of the second messenger pathways and effector proteins activated by both receptors interpose opposite effects. D₁-like DA receptors (D₁ and D₂) activate G_{s/olf} family of G proteins to enhance cAMP production by adenylyl cyclase (AC) enzymes. On the other hand, D₂-like DA receptors (D₂, D₃, and D₄) couple with G proteins' Gi/o family, leading to AC enzymes inhibition. In the absence of DA, DA receptors constitute an inactive trimeric complex form by the combination of the βγ-complex with the α-subunit which is bounded to GDP. By contrast, in the presence of DA, GDP releases and leads to the binding of GTP with the α-subunit, which consequently drives the dissociation of the trimeric complex. Then, the α-subunit and βγ-complex transduce the signal to activate some effector systems. For instance, G_s protein activation enhances AC, whereas G_{as} protein activation inhibits the production of cAMP. The formation of cAMP triggers a signaling cascade by enhancing protein kinase A (PKA) (Pierce *et al.*, 2002; Beaulieu and Gainetdinov, 2011). PKA has a variety of substrates such as voltage-gated potassium (K⁺), sodium (Na⁺), and calcium (Ca²⁺) channels, ionotropic glutamate, GABA receptors, and transcription factors that mediate the effects of DA receptor stimulation. One of the major targets of PKA is the DA and cAMP-regulated phosphoprotein (DARPP-32), a multifunctional protein highly expressed in the striatum and cortical areas that modulate downstream signal transduction pathways in response to multiple neurotransmitters, including DA. The phosphorylation of DARPP-32

in response to activation of D₁R triggers the amplification of PKA signaling by inhibiting protein phosphatase-1. On the other hand, dephosphorylation of DARPP-32 by the calmodulin-dependent protein phosphatase 2B upon D₂R stimulation converts DARPP-32 into a potent inhibitor of PKA signaling (Beaulieu and Gainetdinov, 2011; Tritsch and Sabatini, 2012) (Figure 20).

In addition to cAMPA/PKA-regulated signaling, DA receptors modulate intracellular levels of Ca²⁺ by acting on ion channels. Specifically, βγ-subunits activate phospholipase C (PLC) after D₂R stimulation. The activation of PLC results in the formation of inositol triphosphate (IP₃), diacylglycerol, and enhanced intracellular Ca²⁺ mobilization in response to IP₃. Moreover, D₂R βγ-subunits are involved in the regulation of N-type Ca²⁺ channels and G protein-coupled inwardly rectifying potassium channels (GIRKs), leading to a repressive firing activity in neurons (Lüscher and Slesinger, 2010) (Figure 20).

On the other hand, DA receptors do not exclusively signal through heterotrimeric G proteins and may also engage in G protein-independent signaling events. Thus, D₁R and D₂R alter membrane trafficking of Ca²⁺ channels, N-methyl-D-aspartate (NMDA), and GABA receptors through direct protein-protein interactions or downstream of tyrosine kinase activation (Beaulieu and Gainetdinov, 2011) (Figure 20).

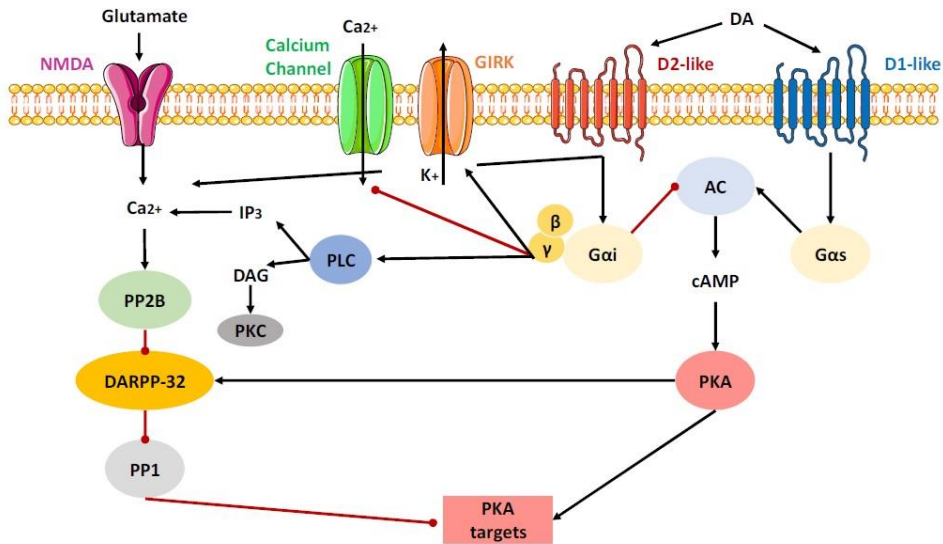


Figure 20. Intracellular DA signaling pathways. Schematic of signaling networks cAMP/PKA-dependent and G $\beta\gamma$ -dependent regulated by D1- and D2-like receptor responding neurons. Black and red arrows indicate activation and inhibition, respectively. NMDA, N-methyl-D-aspartate; PP2B, protein phosphatase 2B; DARPP-32, DA and cAMP-regulated phosphoprotein; PP1, protein phosphatase 1; IP3, inositol triphosphate; DAG, diacylglycerol; PLC, phospholipase C; GIRK, G protein-coupled inwardly rectifying potassium channels; AC, adenylyl cyclase; cAMP, cyclic adenosine monophosphate; PKA, protein kinase.

As previously mentioned, DA receptors act through diverse signaling mechanisms. However, DA receptors can undergo desensitization in response to extensive exposure to agonists. Additionally, these receptors can experience resensitization when an agonist does not activate them for a prolonged period. DA receptor desensitization is induced by G protein-coupled receptor kinases phosphorylation, which recruits arrestins, promoting the internalization of the receptor from the cellular membrane (Laporte *et al.*, 2002).

3.3.2.3. Dopaminergic system in food addiction and eating disorders

Alterations in the dopaminergic system have been associated with food addiction and eating disorders due to the crucial involvement of this system in rewarding and eating behaviors. Some types of foods, particularly high palatable foods, may induce neuroadaptations in the DA system, modulating its reinforcing effects. These neuroadaptations are similar to those produced by drugs of abuse that hijack the DA system, amplifying an uncontrolled dopamine effect on neuronal plasticity.

Previous studies in humans demonstrated that visual and olfactory exposure to palatable food augmented extracellular DA in the dorsal striatum of normal-weight healthy controls with food deprivation. Moreover, dopamine release correlated with the increased self-reports of hunger and desire for food, providing evidence of a striatal DA release for a conditioned-cue response (Volkow *et al.*, 2002a). These evidence are consistent with the crucial role of DA in the modulation of food rewarding properties and food intake motivation (Bello and Hajnal, 2010). Preclinical studies using rodents also detected a strong correlation between adaptations in the DA system and compulsive eating behavior (DiFeliceantonio and Small, 2019). Rodents that consumed highly palatable and energy-dense food displayed an increased compulsivity toward food, which was reflected in decreased expression of dorsal striatum DA receptors.

Furthermore, lentivirus-mediated knockdown of striatal D₂R rapidly developed addiction-like reward deficits and compulsive-like food-seeking in rats with extended access to palatable high-fat food

(Johnson and Kenny, 2010). Thus, the participation of the DA system is also supported by the increased reinstatement of food-seeking behavior enhanced by the administration of D₂R agonists (Ball *et al.*, 2011). These results obtained in rodent studies were consistent with reports in humans, revealing that obesity is linked to downregulation of striatal D₂R, which is associated with cortical areas dysfunction (Nora D Volkow *et al.*, 2017). Altogether, these findings highlight the importance of the DA system, specifically the D₂R, in the mesolimbic pathway regulation, being a potential target for pharmacological treatment of eating disorders.

3.3.3. Endocannabinoid signaling

The endocannabinoid system is a neuromodulatory network involved in several physiological roles, including reward-related processes, among many others. The endocannabinoid system is extensively distributed in the central and peripheral nervous system and in other tissues, where it controls different brain functions by acting on diverse cell types and cellular compartments (Katona and Freund, 2012; Piazza *et al.*, 2017). It is composed of endogenous cannabinoid receptors, endocannabinoids (eCBs), and the enzymes involved in their synthesis and degradation (Lutz *et al.*, 2015).

3.3.3.1. Cannabinoid receptors

Endogenous and exogenous cannabinoids act at least in the two canonical receptors of the endocannabinoid system, the cannabinoid

type-1 receptor (CB₁R) and cannabinoid type-2 receptor (CB₂R). These are receptors of the GPCR family mainly coupled to G_{i/o} protein (Childers and Deadwyler, 1996) that regulate diverse brain functions and pathologies, including addictive-related behaviors.

The **CB₁R** is abundantly expressed in the CNS, being the most highly expressed GPCR in the brain (Westlake *et al.*, 1994; Tsou *et al.*, 1998). The brain regions with the highest levels of CB₁R expression include the hippocampus, olfactory bulb, cerebellum, and basal ganglia (Flores *et al.*, 2013). At a cellular level, studies using knockout mice of CB₁R revealed that this receptor is primarily expressed in GABAergic neurons (Monory *et al.*, 2006; Martín-García *et al.*, 2016). Specifically, expression levels of CB₁R are very large in GABAergic synaptic terminals of the cortex and hippocampus (Kawamura *et al.*, 2006; Katona and Freund, 2012; Steindel *et al.*, 2013; Hu and Mackie, 2015; Martín-García *et al.*, 2016), whereas CB₁R expression is low in glutamatergic synapses and astrocytes (Monory *et al.*, 2006; Puente *et al.*, 2011; Ruehle *et al.*, 2013; Gutiérrez-Rodríguez *et al.*, 2018). These findings suggest that CB₁Rs are primarily detected in axon terminals close to presynaptic areas. However, several studies have identified expression levels of CB₁R in neurons mitochondria and astrocytes (Bénard *et al.*, 2012; Koch *et al.*, 2015; Gutiérrez-Rodríguez *et al.*, 2018). Altogether, CB₁R is dispersed in GABAergic (~56%) and glutamatergic (~12%) terminals, astrocytes (~6%), mitochondria (~15%), and other compartments of the hippocampus (~11%) (Gutiérrez-Rodríguez *et al.*, 2018) (Figure 21).

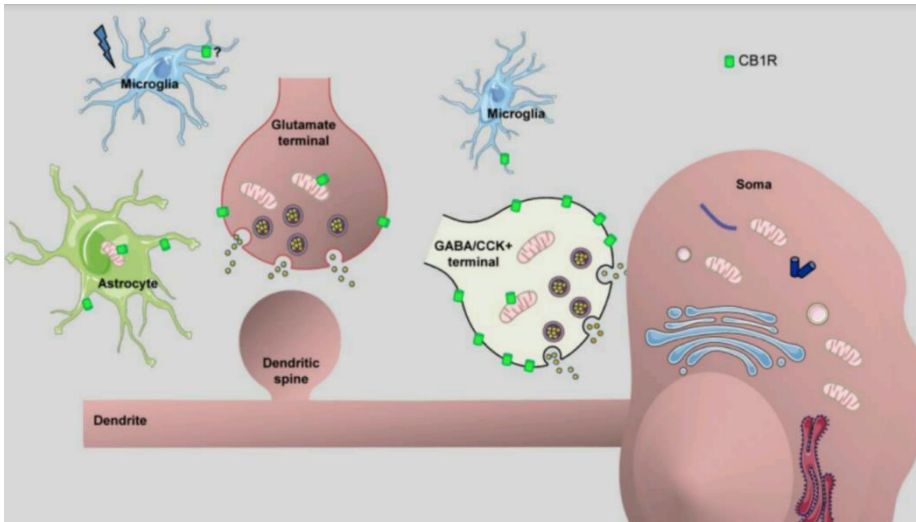


Figure 21. Distribution of CB₁R in the CNS. The accumulation of CB₁R is high in GABAergic synaptic terminals, low in glutamatergic synaptic terminals, and very low in astrocytes. CB₁R is also located in mitochondria of neurons and astrocytes (Manzanares *et al.*, 2018).

On the other hand, levels of **CB₂R** expression are low in the CNS, being this receptor highly expressed in the periphery, particularly in immune cells and tissues such as the spleen, bones, and skin (Atwood and Mackie, 2010). CB₂R was not identified in the CNS under normal (not pathological) conditions until 2005 (Van Sickle *et al.*, 2005). However, nowadays, many studies have detected CB₂R in the brainstem, cortical, hippocampal, frontal cortex, amygdala, striatum, and mesencephalic neurons in normal conditions (Gong *et al.*, 2006; Onaivi, 2006; Brusco *et al.*, 2008; Lanciego *et al.*, 2011). Furthermore, many authors have demonstrated the functional involvement of CB₂R in rewarding processes (Navarrete *et al.*, 2013; Galaj *et al.*, 2020; Zhang *et al.*, 2021).

Both CB₁R and CB₂R participate in the endocannabinoid system by activating the heterotrimeric G_{i/o} proteins. Consequently, AC activity is inhibited, leading to a decrease in cAMP synthesis and PKA activity. Coupling to heterotrimeric G_{i/o} proteins additionally stimulates enzymes of the MAPK family, such as extracellular signal-regulated kinases 1 and 2 (ERK1/2), p38, and c-Jun N-terminal kinase (JNK) (McAllister and Glass, 2002; Bosier *et al.*, 2010). The transcription of genes is regulated downstream as a result of these mechanisms. The activation of G_{i/o} proteins leads to the repression of neurotransmitter release by the inhibition and stimulation of voltage-activated Ca²⁺ channels and inwardly rectifying K⁺ channels (Kir3), respectively (McAllister and Glass, 2002) (Figure 22).

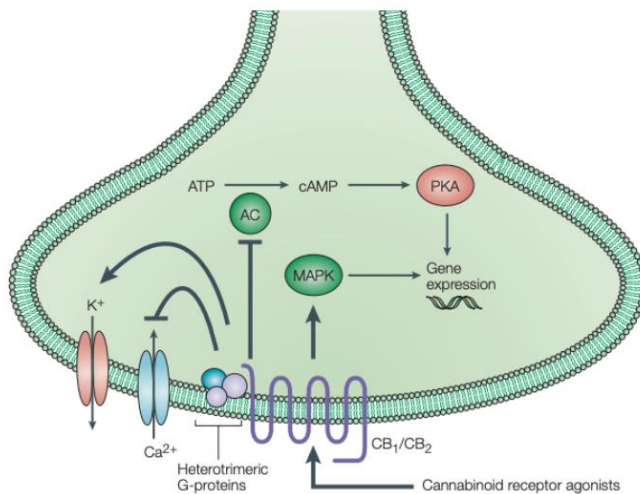


Figure 22. Major signaling pathways of cannabinoids. CB₁, cannabinoid receptor 1; CB₂, cannabinoid receptor 2; AC, adenylyl cyclase; ATP, adenosine triphosphate; cAMP, cyclic adenosine monophosphate; PKA, protein kinase A; MAPK, mitogen-activated protein kinase (Di Marzo *et al.*, 2004).

3.3.3.2. Endocannabinoid ligands

eCBs are lipids acting as messengers that can diffuse across membranes in a paracrine, autocrine, and possibly endocrine manner (Piomelli, 2003; Kano *et al.*, 2009; Katona and Freund, 2012; Zou and Kumar, 2018). The two-best characterized eCBs are N-arachidonylethanolamide (anandamide, AEA) and 2-arachidonoylglycerol (2-AG). These are arachidonic acid derivatives conjugated with ethanolamine to form fatty acid amines or glycerol to form monoacylglycerols. These lipidic derivatives are synthesized “on-demand” by diverse pathways present in cell membranes and are consequently released through Ca^{2+} mechanisms. Thus, endocannabinoid signaling is extremely dependent on the state of synaptic activity (Alger and Kim, 2011).

AEA and 2-AG present varying selectivity for CB_1R , CB_2R , and other targets and various concentration distribution (McAllister and Glass, 2002). **AEA** is a partial agonist of CB_1R and CB_2R , whereas **2-AG** is a full agonist of CB_1R and CB_2R presented at higher concentrations (Sugiura *et al.*, 2006).

Apart from endogenous cannabinoids, existing natural and synthetic compounds have a particular affinity toward cannabinoid receptors. The most abundant **natural cannabinoids** in the *Cannabis sativa* plant are Δ^9 -tetrahydrocannabinol (Δ^9 -THC) and cannabidiol. Δ^9 -THC is the main psychoactive component of marijuana, acting as a partial agonist of CB_1R and CB_2R . On the other hand, cannabidiol does not present psychoactive effects, and its affinity for CB_1R and CB_2R is significantly reduced (Morales *et al.*, 2017). Among

synthetic cannabinoids designed with different selectivity profiles for CB₁R and CB₂R, WIN55,212-2, HU-210 and CP55,940 are the most common agonists with an affinity for both receptors. By contrast, the most common antagonists that block activation of cannabinoid receptors are CB₁R-selective competitive antagonists such as rimonabant (SR141716A), and taranabant (MK-0364), AM281, and LY320135, among others. Notwithstanding, most molecules that inhibit cannabinoid receptors' activity also act as inverse agonists, inducing inverse cannabimimetic effects in the absence of agonists (Martín-García *et al.*, 2010; Pertwee *et al.*, 2010).

3.3.3.3. Cannabinoid type-1 receptor signaling

Upon eCBs ligand binding and receptor activation, CB₁R are primarily coupled to G_{i/o} protein, leading to a rapid decrease in levels of cAMP by inhibiting AC activity. Subsequently, cAMP modulates different types of ion channels and enzymes in a dependent or independent manner. For example, postsynaptic neuronal depolarization induces the opening of Ca²⁺ channels that lead to the synthesis of 2-AG. On the other hand, the activation of group 1 metabotropic glutamate receptors (mGluRs) and M1/M3 muscarinic acetylcholine receptors (mAChRs) triggers endocannabinoids release in a Ca²⁺ independent manner, where the activation of PLC is concerned. Subsequently, the resulting eCBs are liberated in the postsynaptic area and migrate retrogradely to act on CB₁R in the presynaptic area that, finally, inhibit neurotransmitter release (Kano *et al.*, 2009; Lau *et al.*, 2017) (Figure 23). Several studies have

revealed that CB₁R activation represses the release of neurotransmitters (Schlicker and Kathmann, 2001). Thus, the eCB system is involved in several forms of synaptic plasticity at different synapses. Subsequent to activation of CB₁R, the inhibition of neurotransmitter liberation may be transient (seconds), resulting in endocannabinoid-mediated short-term depression (eCB-STD), or persistent (minutes to hours), leading to endocannabinoid-mediated long-term depression (eCB-LTD). Among eCB-STDs, the depolarization-induced suppression of inhibition (DSI) in GABAergic synapses and the depolarization-induced suppression of excitation (DSE) in glutamatergic synapses are two different forms of eCB-STD (Castillo *et al.*, 2012).

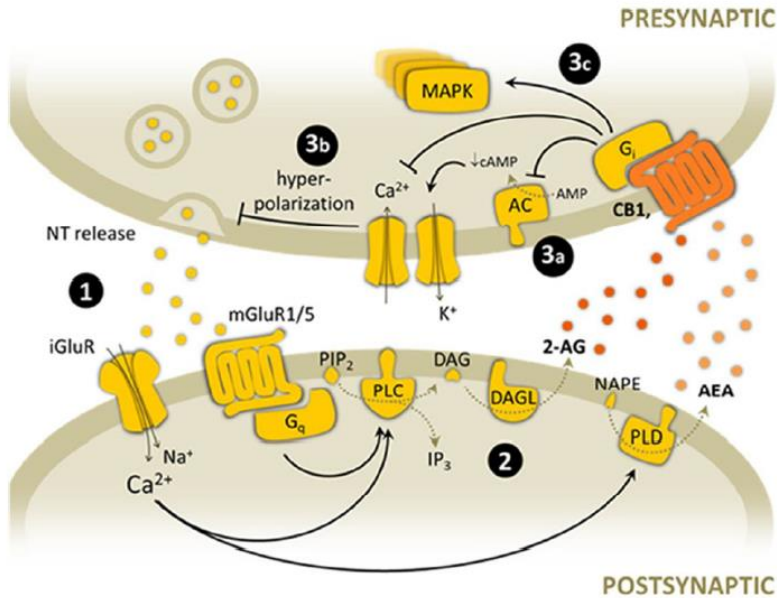


Figure 23. Endocannabinoid-mediated synaptic signaling. (1) Glutamate is released from presynaptic terminals and stimulates both ionotropic and metabotropic glutamate receptors, leading to postsynaptic depolarization through Ca^{2+} entrance and G_q -protein activation. (2) High Ca^{2+} concentration stimulates endocannabinoid synthesis through PLC and PLD. (3) Endocannabinoids are released to the synaptic cleft and consequently activate CB_1 presynaptic receptor. Some of the main downstream consequences of CB_1R activation and subsequent G_i -protein stimulation are (3a) inhibition of AC activity, (3b) membrane hyperpolarization after modulation of K^+ and Ca^{2+} channels, and subsequent inhibition of NT release, (3c) activation of protein kinase cascades such as MAPK pathway. NT, neurotransmitter; iGluR, ionotropic glutamate receptor; mGluR, metabotropic glutamate receptor; PIP_2 , phosphatidylinositol bisphosphate; DAG, diacylglycerol; 2-AG, 2-arachidonoylglycerol; NAPE, M-arachidonoyl-phosphatidylethanolamine; AEA, anandamide; PLC, phospholipase C; DAGL, diacylglycerol lipase; PLD, phospholipase D; AC, adenylyl cyclase; cAMP, cyclic AMP; MAPK, mitogen-activated protein kinase. Adapted from (Flores *et al.*, 2013).

3.3.3.4. Endocannabinoid modulation of brain reward system

CB_1R is expressed in the main structures of the mesocorticolimbic system, where it exhibits extensive modulatory influences on

excitatory and inhibitory signaling that lead to rewarding processing regulation and food intake (Parsons and Hurd, 2015). CB₁R expression is medium-high in the dorsal and ventral striatum, while CB₁R expression levels are relatively low in the VTA (Herkenham *et al.*, 1990; Tsou *et al.*, 1998; Martín-García *et al.*, 2016). At a cellular level, glutamatergic projecting neurons to the VTA and GABAergic interneurons expressing CB₁R in the presynaptic site are the main responsible in the regulation of DA projections from the VTA. CB₁R activation on axon terminals of GABAergic neurons in the VTA triggers the repression of GABA neurotransmission (DSI), and the reversion of this repressive input on DA neurons leads to augmented excitation of DA VTA neurons, that consequently promotes reward (D'Addario *et al.*, 2014). Furthermore, the activation of CB₁R also diminishes glutamatergic transmission (DSE) in the VTA and NAc, mainly controlling the activity of neurons projecting from the PFC (Melis *et al.*, 2004).

In the NAc, neurons activity is modulated by the moderate and abundant expression levels of CB₁R and DA receptors, respectively (Hernandez *et al.*, 2002; Salamone *et al.*, 2007). CB₁R are identified in the postsynaptic site of excitatory glutamatergic projections going from the PFC to NAc, and in the presynaptic sites of inhibitory GABAergic projections from the NAc, in MSNs, and in some interneurons (Figure 24). Thus, eCBs acting in the NAc may have an essential role in the substance-related rewarding effect modulation. Previous studies with rodents demonstrated that CB₁R antagonist microinjection in the NAc reduced GABA release of the projecting MSNs, leading to suppression in ethanol and saccharin

administration (Malinen and Hyytiä, 2008; Balla *et al.*, 2018). However, neurons of the NAc are additionally modulated by eCBs binding to CB₁R on glutamatergic terminals which induce a reduction in glutamate release and hyperphagia (Bellocchio *et al.*, 2010). Thus, the final effect of eCBs on rewarding processes depends on the functional balance between its actions on inhibitory GABAergic versus excitatory glutamatergic transmission.

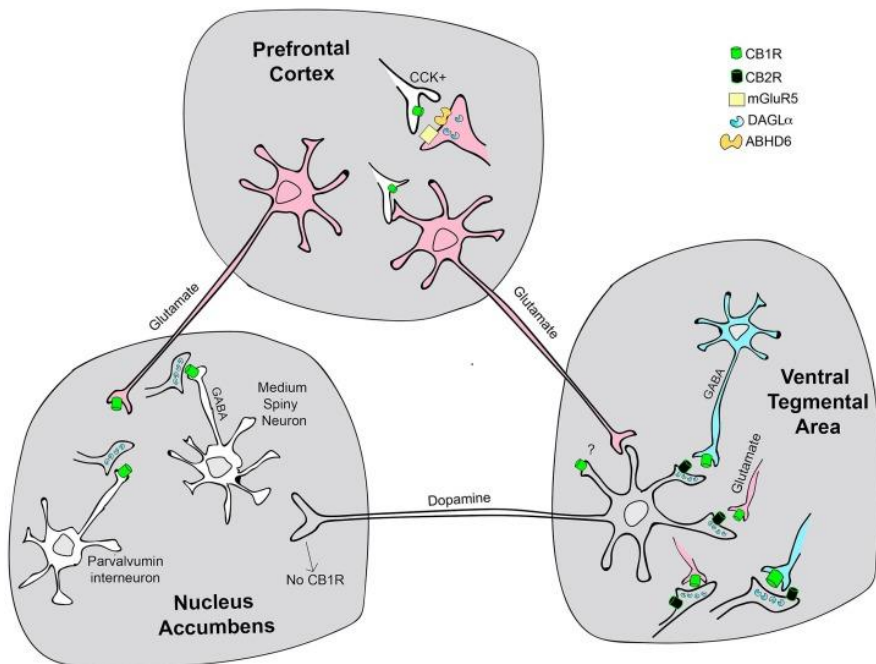


Figure 24. Functional localization of CB₁R and CB₂R in the main structures of the mesocorticolimbic circuit. CCK⁺: Cholecystinin-positive (Manzanares *et al.*, 2018).

Additionally, the eCB system may influence rewarding processes by modulation of sensory perception, such as palatability and olfaction. Local pharmacological and genetic manipulations demonstrated that cortical feedback projection to the main olfactory bulb crucially

regulates food intake via CB₁R (Soria-Gomez *et al.*, 2014). These findings reveal that eCBs of the mesocorticolimbic system have a prominent role in the reinforcing properties of drugs and food intake due to its neuronal activity regulation function. The eCB system is an emerging research target in food addiction and eating disorders.

3.3.3.5. The endocannabinoid system in food addiction and eating disorders

The widespread role of the eCB system as a modulator of homeostatic and hedonic aspects of food intake has prompted investigations into possible disruptions of this system in eating disorders. Previous studies in obese rodents and anorexia nervosa and binge eating disorder patients detected increased levels of AEA in comparison to control groups (Di Marzo *et al.*, 2001; Monteleone *et al.*, 2005). Consistent with these findings, PET studies detected increased CB₁R levels in cortical and subcortical areas in anorexia patients compared to healthy control (Gérard *et al.*, 2011). Furthermore, human genetic studies revealed a positive linkage between eating disorders and specific polymorphisms of genes encoding diverse components of the eCB system, such as CB₁R (Monteleone *et al.*, 2009). According to these findings, the eCB tone dysregulation of patients suffering from eating disorders may represent an adaptative response to maintain energy balance by potentiating internal orexigenic signals and easing the rewarding properties of food intake (Monteleone and Maj, 2013; D'Addario *et al.*, 2014).

Additionally, various preclinical and clinical studies have identified associations between obesity and hyperactivity of the eCB system

manifested as overproduction of eCBs or/and upregulation of cannabinoid receptors in central and peripheral tissues implicated in energy homeostasis (Di Marzo and Matias, 2005). These findings highlight the crucial role of the eCB system in the regulation of feeding hedonic aspects. However, although many preclinical and clinical studies focus on the implication of the eCB system in eating disorders and obesity, little is known about the involvement of this system in food addiction. Previous studies conducted in our laboratory using a validated food addiction mouse model revealed that long-term operant training to obtain highly palatable food-induced adaptative changes at epigenetic and protein levels in the eCB system (Mancino *et al.*, 2015). Specifically, a significant reduction in DNA methylation at CB₁R gene (*Cnr1*) promoter in the PFC was observed, which was associated with upregulation of gene expression and the subsequent augment of CB₁R protein in mice classified as food addicted. The participation of the CB₁R in the food addictive-like behavior was corroborated using pharmacological and genetic approaches. Administration of CB₁R antagonist rimonabant decreased the percentage of animals reaching the addiction scores. In accordance, the genetic deletion of CB₁R using CB₁KO mice decreased operant seeking behavior, and CB₁KO did not reach the criteria for addiction (Mancino *et al.*, 2015). Thus, CB₁R may modulate the primary glutamatergic neuronal output of PFC, ultimately affecting brain reward processes and consequently enhancing extracellular DA levels in the NAc. These results were further investigated in recent studies where Glu-CB₁-KO mice displayed a resilient phenotype to develop food addictive-like

behavior, which was associated with enhanced excitatory synaptic transmission of glutamatergic neurons in the PFC-NAc pathway (Domingo-Rodriguez *et al.*, 2020). According to this evidence, the eCB system plays a crucial role in regulating the overconsumption of high palatable food through the hedonic effect modulation triggered by food intake.

4. Dynamics in the transition to addiction: stages of the food addiction cycle

Food addiction can be conceptualized in three key, and not mutually exclusive elements describing food addictive-like behavior: (i) **habitual overeating**, (ii) **overeating to relieve a negative emotional state**, and (iii) **overeating despite adverse consequences**. These three stages depend principally on the basal ganglia, the extended amygdala, and the PFC (Moore *et al.*, 2017, 2018). These key elements interact, forming a recurring cycle that worsens over time, ending with the pathological state of compulsive intake. The transition of food addiction from controlled intake to loss of control involves neuroplastic changes in the brain that affect reward, stress, and executive functions (George F Koob and Volkow, 2010; Koob and Volkow, 2016) (Figure 25).

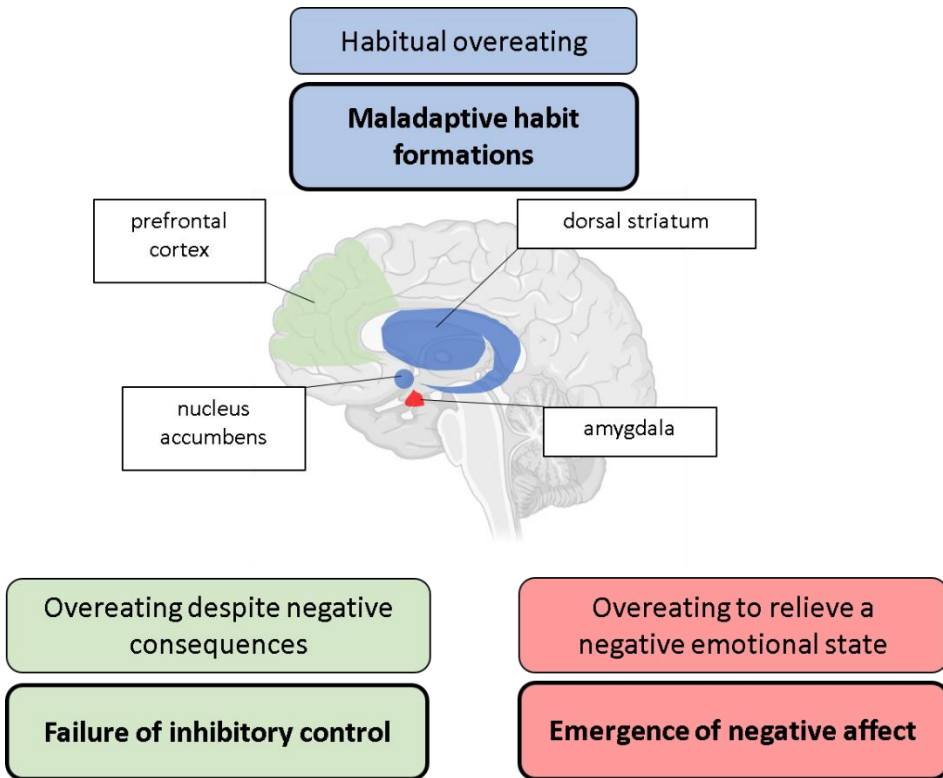


Figure 25. Model of the addiction cycle conceptualized in three stages with the corresponding brain areas involved, in which each dysfunction contributes to the compulsive overeating. The overall neurocircuitry correspond to three functional domains: habitual overeating (reward and incentive salience: basal ganglia (blue)), overeating to relieve a negative emotional state (negative emotional states and stress: extended amygdala (red)), and overeating despite negative consequences (craving, impulsivity, and executive function: PFC (green)). Adapted from (Koob and Volkow, 2016; Moore *et al.*, 2017).

4.1. Habitual overeating: maladaptive habit formation

Habitual overeating is the first element referring to the process by which a once goal-directed behavior becomes a maladaptive stimulus-driven habit. This process depends on the basal ganglia that include the NAc and dorsal components of the striatum, known for

their important roles in reward and reinforcement and habit formation, respectively (Moore *et al.*, 2018). Analogous to drugs of abuse, repeated stimulations of DA system in the NAc by palatable food and associated cues shifts signaling to dorso-striatal DA pathways leading to habit formation. Thus, compulsive eating reflects a maladaptive stimulus-driven habit which hijacks voluntary and goal-directed actions.

Maladaptive habit responses start with the union of environmental stimuli with food availability in the phenomenon named **conditioned reinforcement**. Repeated pairing of a cue with food induces the learned cue itself becomes salient in the phenomenon named **incentive salient** (Koob and Volkow, 2016). Both conditioned reinforcement and incentive salience may robustly augment eating desire and maintain food food-seeking even in the absence of food presentation or physiological needs, leading to habit formation (Velázquez-Sánchez *et al.*, 2015; Moore *et al.*, 2017). Thus, habit formation is the product of adaptive learning where voluntary actions become habitual through the reinforcement of these behaviors (Everitt and Robbins, 2005).

Stimuli associated with food delivery are enough to maintain compulsive-seeking behavior associated with food craving. Previous experiments in rodent models of operant conditioning maintained by palatable food paired with a cue light revealed that rats exhibited higher active lever responding even in a conditioned punishment compared to rats exposed to chow food (Velázquez-Sánchez *et al.*, 2015). Furthermore, compulsive food-seeking behavior was

observed in mice that continued responding on a palatable food-paired lever during a period signaled non-availability (Mancino *et al.*, 2015).

Several findings have hypothesized that the transition from controlled actions to habit-based responding behaviors comprises the shift from action-outcome ventrally dependent learning systems to dorsally dependent habit systems. As behavior is executed repetitively, there is a transition at the neural level from prefrontal cortical areas to striatal control where glutamatergic neurons from PFC and amygdala projecting to NAc lose their critical role (Everitt and Robbins, 2005). Recent evidence suggests that analogous to drugs of abuse, palatable foods may promote this shift in striatal circuits and consequently induce goal-directed actions in habitual systems (Ostlund *et al.*, 2010; Barker *et al.* Moreover, neuroimaging investigations in obese and healthy weight subjects exposed to palatable food detected activation of the caudate nucleus of the striatum, the area involved in goal-directed actions, and increased activity of the putamen, the area involved in habit responding. Obese subjects showed an impulsive eating behavior compared to healthy weight subjects (Babbs *et al.*, 2013; Moore *et al.*, 2018) (Table 3).

4.2. Overeating to relieve a negative emotional state: the emergence of a negative affect

Overeating to relieve a negative emotional state is the second element referred to performing a behavior, such as drug consumption or intake of palatable food, to alleviate a behavior, such as a drug

consumption or intake of palatable food, to alleviate a negative emotional state. This element may involve engagement in compulsive behaviors to suppress anxiety and distress before engagement or provide relief from anxiety and distress during and following engagement of the behavior (el-Guebaly *et al.*, 2012; Abramowitz and Jacoby, 2015). The neurobiological mechanisms underlying these processes are within-system inducing functional desensitization of DA transmission of the mesocorticolimbic system, and between-system neuroadaptations that comprise the recruitment of the stress system in the extended amygdala (Cottone *et al.*, 2009). Thus, a withdrawal-induced negative emotional state includes decreased reward, loss of motivation for ordinary rewards, and augmented anxiety (Moore *et al.*, 2017).

As controlled food intake progresses towards compulsive food intake, the hedonically rewarding properties of food may hold less importance in favor of food intake for preventing or improving negative states such as anxiety, depression or irritability, experienced symptoms occurring when preferred foods are not available (Parylak *et al.*, 2011).

Several studies in humans have reported that changing from a high-fat diet to a low-fat diet after one month of eating a high-fat diet induced mood effects that lead to increased anger and hostility (Wells *et al.*, 1998). Furthermore, negative emotional states such as irritability, nervousness, and anxiety appeared in human subjects that were restricted to food after overeating (Greeno and Wing, 1994). Thus, these findings suggest that repeated overconsumption of

palatable foods induces long-term neuroadaptations in the reward and stress pathways that promote anxious or depressive responses when desired foods are unavailable. Data collected from studies examining emotional factors in relation to binge eating supported that binge eaters present greater rates of psychiatric diagnoses, and increased prevalence of major depression, bipolar disorder and anxiety (Rosenbaum and White, 2015).

As previously mentioned, the withdrawal-induced adverse effects are within-system neuroadaptations and between-system neuroadaptations processes. **Within-system neuroadaptations** comprise changes in neurotransmitters that are implicated in reinforcing effect systems, inducing a decreased reward function signaling characterized by motivation loss towards rewards. Thus, high palatable foods may trigger disruptions in the DA system that lead to downregulation of D₂Rs in the striatum and reduction of DA basal levels in the NAc. In this context, previous investigations in obese and healthy weight individuals revealed that obese individuals showed a lower availability of D₂Rs associated with BMI (Wang *et al.*, 2001).

On the other hand, **between-system neuroadaptations** involve the engagement of the brain stress system situated in the extended amygdala. This system is not directly associated with the positive, rewarding effects, but it is retained and dysregulated by chronic stimulation of the rewarding system (Moore *et al.*, 2017). For example, previous studies in rodents demonstrated that rats withdrawn from intermittent access to palatable food displayed

increased anxiety and depressive-like behavior during withdrawal (Cottone *et al.*, 2009). Thus, these neuroadaptations aim to overcome the chronic presence of the problematic substance or food, limiting the reward and restoring normal function (Table 3).

4.3. Overeating despite aversive consequences: failure of inhibitory control

Overeating despite aversive consequences is the third element that describes the loss of executive control over food intake observed as a prolongation of maladaptive overeating in the face of the resulting physical and negative psychological consequences. The loss of control reflects alterations in inhibitory control mechanisms intended to suppress inappropriate actions (Deroche-Gamonet *et al.*, 2004b; Moore *et al.*, 2018). Dysfunctions in inhibitory control imply the disruption of frontostriatal circuitries. Concretely, the “Go circuit” and “Stop circuit” of the PFC to NAc pathway mediated by the orbitofrontal cortex and the PL (dlPFC in humans), respectively, play a crucial role in this stage. This frontostriatal communication between areas is modified throughout addiction leading to an increased orbitofrontal cortex to NAc (“Go circuit”) connectivity and a decreased PL to NAc (“Stop circuit”) communication (Hu *et al.*, 2019). Thus, as addiction progresses over time, the unbalance between these two circuits becomes more pronounced.

This last element has been mimicked in laboratory animals that show a compulsive behavior towards palatable food. Animals continue to consume palatable food even in the presence of an electric foot shock,

a conditioned stimulus that signals a punishment, or aversive conditions (Deroche-Gamonet *et al.*, 2004b; Mancino *et al.*, 2015; Velázquez-Sánchez *et al.*, 2015) (Table 3).

Table 3. A summary of the features of each element of compulsive eating behavior. Adapted from (Moore *et al.*, 2017, 2018).

Elements of compulsive eating behavior	Neurobiological mechanisms	Characteristic behavior	Primarily implicated brain area
<i>Habitual overeating</i>	Aberrant reward learning	Inability to reduce eating or seeking behavior following a decrease in food value or contingency	Basal ganglia
<i>Overeating to relieve a negative emotional state</i>	Affective habituation	Eating to cope with decreased sensitivity to reward	Basal ganglia
	Affective withdrawal	Eating to cope with negative affect	Extended amygdala
<i>Overeating despite negative consequences</i>	Decreased inhibitory control	Eating persists in conditions where it should normally be suppressed	Prefrontal cortex

5. Complex multifactorial nature of food addiction and eating disorders: gene and environment interaction

Recent progress has been made in behavioral genetics to highlight the importance of understanding genomics and epigenomics in food addiction and eating disorders. Findings from human behavioral genetic and molecular genetic studies have revealed that susceptibility to addiction development is heritable, highly polygenic and that the combination of environment and genetic factors

contributes to part of the observed phenotypic variation (Plomin and Daniels, 2011). The interaction between multiple gene networks and environmental factors strongly impacts brain function during development and throughout adulthood, influencing behavior, leading to different individuals' vulnerability or resilience to developing the disorder (Rafael Maldonado *et al.*, 2021). The vulnerability to addiction is associated with intrinsic factors such as gender, age, personality traits and comorbidity in psychopathological conditions, and extrinsic factors such as socioeconomic position, adverse life experiences, and addictive-substance availability (Dalle Molle *et al.*, 2017). The proportional importance of these factors fluctuates across the lifespan and the diverse stages of the disease (Ducci and Goldman, 2012).

The multifactorial nature of food addiction might explain why the vast majority of people that consume highly palatable food do not become addicted (Piazza and Deroche-Gamonet, 2013). Analogous to drugs of abuse, the repetitive exposure to the addictive substance induces long-lasting neuroadaptive changes in vulnerable individuals. Like drug addiction, food addiction may be the product of pathological response to highly palatable food in individuals with a vulnerable biological phenotype.

5.1. Genetic mechanisms of food addiction and eating disorders

The genetic mechanisms of multifactorial diseases indicate that the inheritance of the disorder has a polygenetic component, hindering

the determination of a person's risk of inheriting or passing these disorders (Volkow and Muenke, 2012). However, a multifactorial threshold model has been postulated (Reich *et al.*, 1975). In this model, a determined number of different genes and environmental variables are supposed to operate as risk and protective factors for the disease's development is considered a single entity admitted as "liability". The liability of individuals in a population creates a continuous variable that is regularly distributed throughout the population. Thus, if the combined impact of genetic and environmental variables pushes a person's liability over a certain threshold level, the individual will be affected and develop the disease (Figure 26).

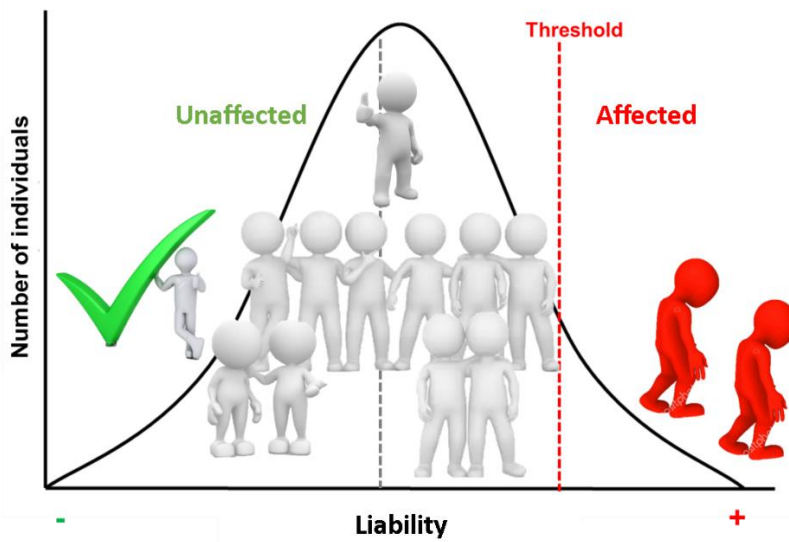


Figure 26. Multifactorial threshold model. The liability distribution for a multifactorial disease. An individual must exceed a threshold on this distribution to be affected with the diseases. Adapted from (Anthony *et al.*, 1994; Deroche-Gamonet *et al.*, 2004a).

Different genetic factors have been described as crucial determinants for a psychiatric disorder's risk or resilience. The genetic polymorphisms associated with addiction have been extensively studied, and evidence suggest that genes implicated in drug addiction may also participate in food addiction and obesity (Heber and Carpenter, 2011). Like substance use disorders, eating disorders are also found to aggregate within families (Bulik *et al.*, 1997) and individual differences in eating disorders may be explained by additive genetic factors (Munn *et al.*, 2010). In this context, shared environmental factors may significantly affect disordered eating in adoptive siblings, and the heritability of eating alterations is more pronounced in twins reared apart (Klump *et al.*, 2009). Thus, genetic and environmental factors play a crucial role in developing eating disorders.

Previous studies have employed different molecular and genetic approaches to study eating disorders, such as linkage, candidate-gene association, genome-wide association, and rare variants studies. Due to the importance of food and -related rewarding effects triggered by the increase of DA in the NAc, these studies have particularly focused on the genetic variations affecting the DA system (Volkow and Muenke, 2012). The A1 allele of the dopamine D₂R gene (*Taq1A*) is the most studied polymorphism. The *Taq1A* polymorphism is located more than 10 kilobase pairs downstream from the coding region of the *DRD2* gene or in the coding gene for the neighbored *ANKK1* gene (Neville *et al.*, 2004). Individuals containing the A1 allele of the *Taq1A* polymorphism (rs1800497) have been associated with the “reward deficiency syndrome”, a

syndrome consisting of a hypodopaminergic state induced by a faulty and decreased density of D₂R. Thus, the lack of D₂R gives rise to a higher risk of developing addictive, compulsive, and impulsive behaviors in the population. This affection may be explained by the possible compensatory performance for insufficient DA activity. Furthermore, *Taq1A* A1 allele has been directly associated with obesity and substance use disorders (Blum *et al.*, 1996, 2014, 2018), and further investigations revealed that D₂R and neighboring *ANKK1* single nucleotide polymorphisms are implicated in eating disorders (Davis *et al.*, 2008, 2009; Davis, 2013, 2017).

Moreover, addiction and obesity have been associated with other polymorphisms that participate in DA transmission. These polymorphisms are genes of DA receptors type 2, 3, and 4 (DRD2, DRD3, and DRD4, respectively) and genes for enzymes associated with DA degradation (Lindgren *et al.*, 2018). Differences in genotype for these particular genes may partially explain individual variation in eating behavior and susceptibility to weight gain (Stanfill *et al.*, 2015).

Research studies have begun to recognize the importance of considering **epistatic interactions** among polymorphic loci when addressing the simultaneous participation of numerous genes in the regulation pathways. Epistasis describes nearly any set of complex interactions among genetic loci (Phillips, 2008). Nikolova *et al.* were the first to apply a physiologically based “multilocus genetic profile score”, a composite genetic index that reflects the cumulative influence of numerous polymorphic loci with established functions

on a specific signaling pathway (Nikolova *et al.*, 2011). Thus, due to the simultaneous assessment of many functional loci, polymorphisms with non-significant independent effects might be included, which only collectively account for significant proportions of variability. Precisely, researchers designed a multilocus genetic profile representing the cumulative impact of functional polymorphisms on DA signaling, comprising DA receptor and DA degradation enzymes genes, which have been linked with variations in striatal DA signaling in an individual manner. This multilocus genetic profile might be employed to understand individual differences in reward-related ventral striatum variability. Finally, researchers demonstrated that the multilocus genetic profile score accounted for a greater proportion of variance in ventral striatum reactivity than each locus considered independently (Nikolova *et al.*, 2011).

Previous studies using this genetic methodology adapted to DA signaling revealed that food addiction YFAS-diagnosed patients showed an increased DA signaling compared to controls, suggesting a reward-based causal model progressing from an inherent biological susceptibility to an elevated risk of overeating (Davis, 2013). Furthermore, a recent study performed on slim individuals demonstrated that higher polygenic scores approximating DA signaling predicted increased food addiction symptoms and BMI. These findings suggest that emerging symptoms of food addiction and obesity risk may present identifiable biomarkers correlates in slim individuals (Romer *et al.*, 2019). Thus, risk-related neural and genetic fingerprints predicting subclinical symptoms of food

addiction may be helpful for the early identification and prevention of weight gain and obesity.

5.2. Epigenetic mechanisms of food addiction and eating disorders

Epigenetic mechanisms are promising candidates for the study of psychiatric disorders. The fact that not all individuals who consume drugs and high palatable food develop drug and food addiction, respectively, suggests the existence of individual resilient and vulnerable factors that contribute to the pathogenesis and persistence of addiction. As previously mentioned, experiences in life and environmental factors can shape epigenetic profiles that may modify individuals' vulnerability to addiction. Epigenetic mechanisms are a set of post-translational modifications that play an essential role in changing the brain for a lifetime, although they can also be reversible and transgenerationally transmitted (Nestler, 2014). Thus, epigenetic mechanisms can be seen as the vehicle through which the environment interacts with an individual's genome to determine all aspects of functions in health and disease. Epigenetic mechanisms include several types of post-translational adaptations such as **histone modifications, DNA methylation, and changes in miRNAs** (Nestler and Lüscher, 2019) (Figure 27).

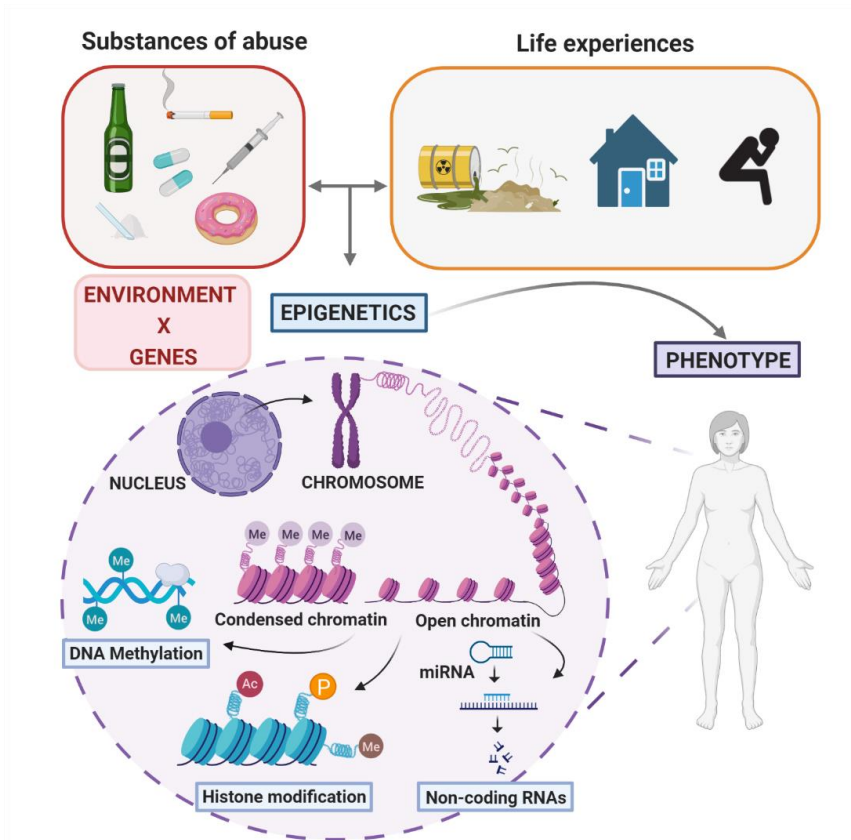


Figure 27. Epigenetic mechanisms alter individual's phenotype. Substances of abuse, diet, environmental factors, and experiences in life can modify epigenetic marks and reshape an individual's phenotype. Histone modification, DNA methylation, and non-coding RNAs are the most common epigenetic modifications. These modifications regulate gene expression without causing variations in the DNA sequence. The N-terminal tails of histones can undergo several post-transcriptional modifications, including acetylation, methylation, and phosphorylation, among others. Histone modification can lead to either activation or repression of gene expression, depending on the residues modified and the type of modification. DNA methylation is the covalent modification of cytosine residues in CpG dinucleotides within gene sequences. Contrary to histone modification, DNA methylation is associated with transcriptional silencing. However, DNA methylation in gene bodies is linked with active transcription. Non-coding RNAs include miRNAs that regulate gene expression through post-transcriptional silencing of genes (Rafael Maldonado *et al.*, 2021).

5.2.1. Histones modifications

Modification of histones is one of the most frequently studied epigenetic alterations in addiction. Histones are essential proteins that wrap DNA in the nucleus and condense it into chromatin. The basic building block of chromatin, also called a nucleosome, contains 147 DNA base pairs wrapped throughout an octamer comprised of two copies of H2A, H2B, H3, and H4 histones (Andrews and Luger, 2011). These proteins can undergo several post-translational modifications in which different functional groups are covalently added to amino acid residues of the N-terminal tails. Some of these modifications are acetylation, phosphorylation, and methylation, among others (Walker and Nestler, 2018).

Acetylation of histone occupancy on lysine residues diminishes electrostatic interaction between DNA and histone proteins, to make DNA more accessible to transcriptional regulators (Kouzarides, 2007). Histone lysine acetylation tends to be protective and leads to adaptive behaviors (Hitchcock and Matthew, 2014). This histone modification is continuously fluctuating throughout the brain after exposure to different drugs of abuse (Renthal *et al.*, 2008; Mashayekhi *et al.*, 2012; Rogge and Wood, 2013; Huang *et al.*, 2014).

On the other hand, histone **phosphorylation** is another post-translational modification occurring on serine, threonine, and tyrosine residues, and is generally associated with transcriptional activation. Drugs of abuse and natural reinforcements promote the nuclear accumulation of dopamine- and cAMP-regulated

phosphoprotein DARPP-32. The nuclear accumulation of DARPP-32 leads to an increase in H3 histone phosphorylation (Stipanovich *et al.*, 2009).

Histone lysine **methylation** is particularly complex and variable. Repeated exposure of drugs reduces global levels of histone methylation marks (H3K9me2, H3K9me3, and H3K27me2) in the NAc (Sun *et al.*, 2012; Aguilar-Valles *et al.*, 2014). On the other hand, drug exposure to methamphetamine may increase H3K4me2 and H3K4me3 levels in the NAc (Aguilar-Valles *et al.*, 2014). These studies are prototypical and suggest that regulation of histone methylation in response to drugs of abuse is complex and drug- and region-specific.

The identification of drug-induced transformations in histone acetylation, phosphorylation, and methylation in the NAc and other brain areas suggests that these modifications might be involved in the regulation of the addiction. More studies are needed to propose a molecular mechanism to explain these adaptations after exposure to the different drugs of abuse. However, evidence suggests that the combination of inherited predispositions, environmental stimuli, and exposure to addictive substances leading to histone modifications may have essential protective and/or risk factors in developing addiction.

Altogether, drug use may produce enduring alterations in gene expression via histone modifications to individuals carrying susceptibility genes exposed to adverse environmental factors. These post-translational transformations may influence susceptibility to

addictive disorders. Enhanced vulnerability to abuse drugs will then feedback into a higher risk of future drug consumption that will lead to further modifications to the epigenome and gene expression (Wong *et al.*, 2011) (Rafael Maldonado *et al.*, 2021).

5.2.2. DNA methylation

DNA methylation is a stable epigenetic mark that occurs with the covalent modification of DNA by DNA methyltransferases. In this modification, DNA methyltransferases trigger the addition of a methyl group to cytosine-phosphoguanine (CpG) at the C5 position (5-mC) (Bird, 2002). DNA methylation in gene promoters is associated with repression, whereas DNA methylation in gene bodies is associated with active transcription (Nestler and Lüscher, 2019). Repression of DNA by DNA methylation can be detrimental and lead to risks of developing addictive-like behaviors (Hitchcock and Matthew, 2014). However, little is known about the specific impact of DNA methylation on protective and risk factors in drug addiction, and most studies focus on the effect of drugs of abuse on the expression of DNA methyltransferases. Subchronic methamphetamine treatment induced different DNA methyltransferase 1 mRNA expression in the nucleus caudatus and NAc in rats, which increased DNA methylation (Numachi *et al.*, 2007). Other studies showed that repeated cocaine exposure increased the expression of methyl-CpG binding protein 2 and produced de novo DNA methylation (Bodetto *et al.*, 2013). Moreover, a recent study in alcohol use disorder subjects revealed that chronic alcohol drinking results in increased DNA methylation

of NR3C1 exon variant 1H, associated with reduced NR3C1 mRNA and protein expression levels in PFC other cortico-limbic regions (Gatta et al., 2019). However, a global mapping of DNA methylation changes in the brain at single-nucleotide resolution in response to drugs of abuse is still not available. The generation of DNA methylation genome-wide maps would allow a better understanding of the role of this epigenetic mark in drug addiction.

In the food addiction field, the formation of reward-related associative memories in rats upregulated essential plasticity genes in the VTA, which were correlated with memory strength and associated with gene-specific changes in DNA methylation (Day *et al.*, 2013). In addition, food addicted mice also showed a significant decrease in DNA methylation of the *CNR1* gene promoter in the PFC, associated with an upregulation of CB1 protein expression in the same brain area (S Mancino *et al.*, 2015).

Nowadays, recent epigenetic studies focus on determining the cell-type specificity of observed epigenetic alterations. For example, a study investigating the DNA-methylation cell-specificity in addiction demonstrated an elevated hypermethylated gene region in genes enriched preferentially in glutamatergic neurons but not in GABAergic neurons (Kozlenkov *et al.*, 2017).

Thus, epigenetic signatures have an essential role in vulnerability or resilience to addiction. The epigenetic mechanisms involve modifications in the stable-state expression levels of a set of genes, and also modifications in the stable-state expression levels of a set of genes and produce 'latent' changes in other genes' inducibility both

activation and inactivation (Nestler, 2014). Regulation of gene inducibility can be seen as “latent” in that it would not be evident by analysis of mRNA or protein levels. For instance, cocaine induces latent effects by changing the chromatin structure of many genes, which alter their inducibility in response to a subsequent stimulus. These latent changes can determine an individual’s vulnerability to addiction later in life upon drug exposure or affect relapse in long-term abstinent individuals after re-exposure to the drug. However, drugs or other environmental exposures can also induce transgenerational epigenetic inheritance of addiction vulnerability by epigenetic changes in germinal cells, which are then passed on to progeny and alter their vulnerability to addiction (Meaney and Szyf, 2005) (Rafael Maldonado *et al.*, 2021).

5.2.3. Non-coding RNA: microRNA

miRNAs are short RNA transcripts with around 22 nucleotides that are endogenously expressed by cells to regulate gene expression post-transcriptionally in a very dynamic way (Kenny, 2014). Identifying more than 2,000 miRNAs in the human genome suggests elevated conservation through evolution (Alles *et al.*, 2019), and each one may impact the post-transcription of thousands of protein-coding genes, eliciting a rising interest among the scientific community in addiction.

miRNAs are transcribed by RNA polymerase II in their native form and processed into so-called pri-miRNAs. Pri-miRNAs are processed by the Drosha enzyme into pre-miRNAs of around 70 nucleotides

and exported from the nucleus. Outside of the nucleus, they are further processed by the Dicer enzyme into a duplex RNA (dsRNA). Subsequently, the protein family Argonaute plays a crucial role in RNA silencing, being a component of the RNA-induced silencing complex (RISC). Together with Dicer and Argonaute, the dsRNA incorporates into RISC. RISC is responsible for the gene silencing phenomenon known as RNA interference (RNAi). Argonaute proteins bind different classes of small non-coding RNAs, including microRNAs (miRNAs). One RNA strand is removed from the dsRNA molecule, and the other RNA remains retained in the RISC as a mature molecule of miRNA (Figure 28). Ago 2 (one of the four members of the Argonaute family) has endonucleolytic activity, identifies the target mRNA-miRNA complementary sites, and degrades the target mRNA (Liu *et al.*, 2004). However, miRNAs can also block mRNA translation by preventing mRNA interaction with ribosomes and targeting mRNAs to processing bodies for degradation (Filipowicz *et al.*, 2008). In addition to these “canonical” miRNA roles in the cytoplasm, some findings have described miRNA targeting different cell compartments such as the nucleus and the cytoplasm and newer functions developed by miRNAs in these locations. These miRNAs can relocate to the nucleus, alter mRNA stability in the nucleolus, and affect alternative splicing (Catalanotto *et al.*, 2016). In neurons, miRNAs develop specific functions in dendrites and can be secreted to synapses in exosomes (Smith and PJ, 2018). When miRNAs bind to the 3’UTR of mRNAs, they affect mRNA translation and stability and mRNA distribution in dendrites and synapses (Most *et al.*, 2014).

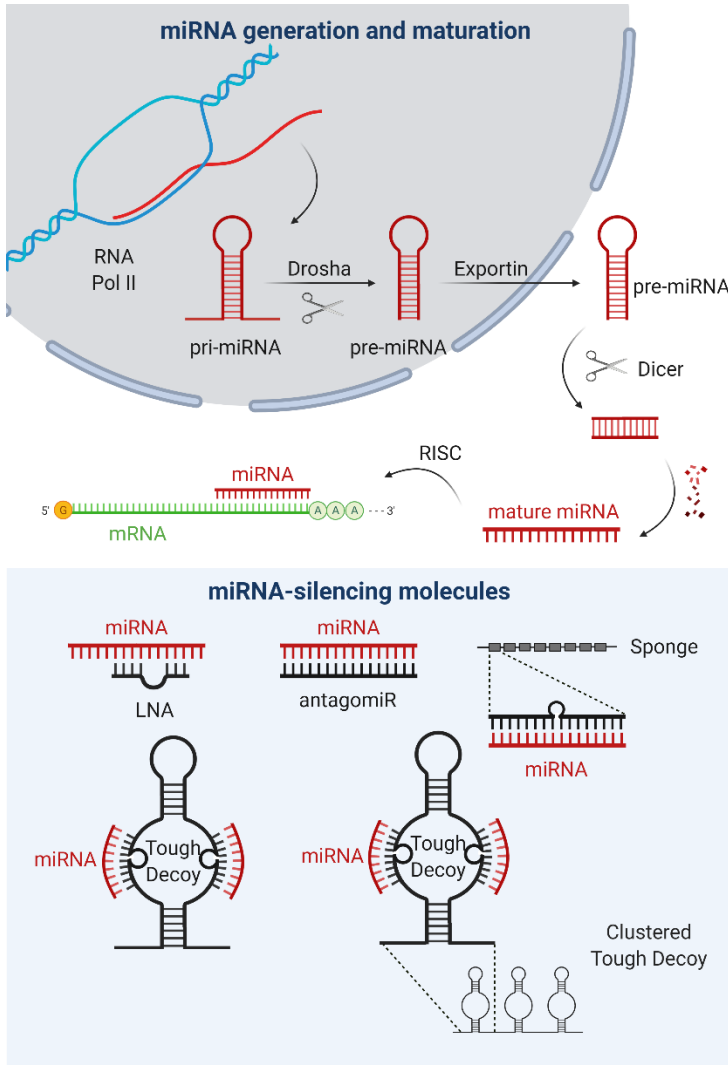


Figure 28. miRNA generation, maturation, and silencing mechanisms. miRNAs are transcribed by RNA polymerase II in their native form and processed into so-called pri-miRNAs. Pri-miRNAs are processed by the Drosha enzyme into pre-miRNAs and exported from the nucleus. At that point, they consist of around 70 nucleotides. The Dicer enzyme further processes them into a duplex (dsRNA) outside of the nucleus. Together with Dicer and Argonaute, the miRNA incorporates into an RNA-induced silencing complex (RISC). One RNA strand is removed, and the mature molecule of the miRNA is retained in the RISC. The miRNA silencing mechanisms comprise locked nucleic acid (LNA), antagomiR, sponges, and tough decoy (TuD). LNA use for miRNA knockdown is beneficial because these probes have a high affinity for their small RNA targets and exceptional mismatch-discrimination ability. AntagomiR consists of a single-stranded RNA molecule entirely complementary to the target miRNA. They

hybridize to prevent the union of the miRNA to an mRNA molecule. Sponges have up to eight regions antisense to target miRNAs located tandemly in the same transcript. Sponges, transcribed by RNA Pol II, can target different miRNAs from the same family. TuDs are 100 nucleotides long and form a hairpin structure that increases their stability and contains an unpaired region in the middle. Both strands from this unpaired region are complementary to the target miRNA. With the same TuD construct, there is the possibility of targeting two different miRNAs and forming TuD clusters to increase the number of miRNA-binding sites (Rafael Maldonado *et al.*, 2021).

According to the crucial role of miRNAs in synaptic plasticity and the emerging appreciation that maladaptive neuroplasticity mechanisms drive addiction, it is not surprising the relationship of several miRNAs with the addictive behavior. miR-132 and miR-212 are two examples of miRNAs with essential functions in synaptic plasticity and dendritic growth through the interaction with the brain-derived neurotrophic factor (BDNF). Inhibition of miR-132 reduces the number of mushroom-like spines while immature filopodia increases, whereas the deletion of miR-132 and miR-212 decreases dendritic length and complexity in the neurons of the hippocampus (Smith and PJ, 2018). miR-132 and miR-212 are upregulated in the striatum after cocaine administration and upon cocaine reinstatement (Quinn *et al.*, 2015; Sadakierska-Chudy *et al.*, 2017). Moreover, miR-132 and miR-212 are enriched in neurons in a CREB-dependent manner activated by cAMP during cocaine exposure (Hollander *et al.*, 2010). Thus, extended daily access to cocaine self-administration induced an augment of CREB phosphorylation in the dorsal striatum, and this effect was amplified by overexpression of miR-212, which decreased cocaine self-administration (Hollander *et al.*, 2010).

AntagomiR is an efficient tool for silencing miRNAs *in vivo*. This approach has been developed to study the effects of miRNAs directed regulation on gene expression (Krützfeldt *et al.*, 2005). It consists of a single-stranded RNA molecule entirely complementary to the target miRNA that hybridizes and prevents the association of the miRNA to an mRNA molecule (Scherr *et al.*, 2007). However, this useful technology is far from optimal as antagomiRs are unstable and quickly degraded.

Although the majority of miRNAs have been detected intracellularly, a significant number of miRNAs have been observed in the extracellular areas, including blood. This discovery attracted attention to the scientific community as circulating miRNAs could be employed as biomarkers for specific diseases. Nowadays, some research on miRNAs have obtained promising results when comparing circulating miRNAs between drug users and healthy controls (Smith and Kenny, 2018).

Despite these studies in the drug addiction framework, few specific investigations have been published studying the epigenetic changes during food addiction. Previous studies in our laboratory evaluated the epigenetic mark of CB₁R gene at a DNA methylation level, suggesting that the long-term operant training to obtain highly palatable food produced a significant reduction in promoter DNA methylation in the PFC of addicted mice. This reduction leads to an upregulation of CB₁R gene expression and the subsequent increase of CB₁R in the same brain area (Mancino *et al.*, 2015). Additionally, studies in the food addiction field are starting to employ potent

approaches for inhibition strategies such as “Sponges”, Tough Decoy inhibitors, or circular RNAs.

6. Animal models of food addiction and eating disorders

In recent years, accumulating evidence proposes the possibility of modeling food addiction in animals, and different conditions have been employed to this end. For example, many studies have used palatable food to originate overeating, obesity, binge eating, withdrawal symptoms, and food relapse in animal models. Although animal models may not reproduce the analogous internal and external factors involved in eating behaviors in humans, these animal models may mimic some relative roles of genetic and environmental variables, promoting a better control and understanding of the variables underlying behavioral, physiological, and molecular mechanisms. Specifically, inbred are among the most useful, extensively used to identify the genetic basis of addictive behaviors and strain-related differences in behavior (Di Segni *et al.*, 2014).

The validity of an animal model is evaluated by construct validity, face validity, and predictive validity. **Construct validity** refers to how precisely the mechanism used to induce the addictive phenotype in animals mimics the disease etiology in humans. **Face validity** indicates that the animal model reproduces anatomical, biochemical, neuropathological, or behavioral features of addiction in humans. Ultimately, **predictive validity** signifies that an animal phenotype

similarly responds to treatments as in humans (Nestler and Hyman, 2010).

6.1. Food addiction mouse model

Previous studies in our laboratory developed a food addiction mouse model with face and predictive validity for the first time. This mouse model mimicking food addiction is an operant conditioning model where mice are exposed to long-term operant training to obtain palatable food. Remarkably, two different extreme subpopulations of mice are identified at the end of the long-term operant training, referred to as the resilient or vulnerable phenotype to develop food addiction (Mancino *et al.*, 2015). The food addiction model was adapted from a previous mice model of cocaine addiction (Deroche-Gamonet *et al.*, 2004). Based on the DSM-IV clinical criteria, this model provides a unique tool to identify a percentage of drug-exposed rats that shift from controlled to compulsive self-administration, highlighting the interindividual differences between animals (Deroche-Gamonet *et al.*, 2004).

The **operant conditioning model** is based on the learning contingency in which a positive reinforcer, such as a drug or food, is delivered contingently to complete the schedule requirements (Sanchis-Segura and Spanagel, 2006). An operant chamber is used to conduct drug or food operant self-administration and is typically equipped with active and inactive operant switches, such as levers or nose poke. For instance, responding on the active lever will activate a pump or dispenser delivering drug or food. On the other hand,

responding on the inactive lever has no consequences. Stimuli such as light or tone is usually paired with active responses, facilitating the operant behavior (Figure 29).

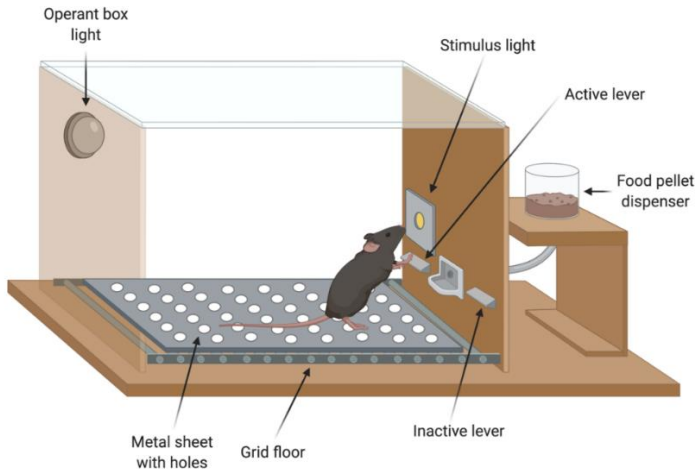


Figure 29. Scheme of an operant box to perform operant conditioning maintained by chocolate flavored-pellets. The chamber is provided with two retractable levers (active and inactive), a stimulus-light, and a food pellet dispenser. The floor of the chamber is a grid floor that delivers electric foot shocks. The grid floor is covered during operant self-administration sessions with a metal sheet with holes (Martín-García *et al.*, 2020).

The most common schedules of reinforcement used in drug or food self-administration are the fixed ratio (FR) and the progressive ratio (PR) schedules. A reinforcer is delivered under a FR schedule when the animal reaches a pre-established number of responses. For instance, an FR5 schedule corresponds to five active responses for single reward delivery. Usually, a time-out period of 15 s is initiated after each pellet delivery or drug infusion, where active responses are

not rewarded. Impulsive-like behavior is studied by evaluating active responses in the time-out period.

Moreover, the PR schedule is used to study the motivational effects of reward delivery. The required ratio to deliver the reward within the PR schedule augments following a pre-established progression. The maximum number of active responses that the animal performs to obtain one pellet is the last event completed, referred to as the “breaking point”. Thus, the breaking point is considered to be a measure of motivation. Finally, FR scheduled sessions can also be combined with a negative consequence (electric foot shock) associated with pellet delivery or drug infusion. Some animals will continue pressing the active lever for a reward delivery even in the presence of an electric foot shock. Thus, compulsive-like behavior is evaluated by scoring the number of shocks an animal will receive for reward obtainment (Mancino *et al.*, 2015; Domingo-Rodríguez *et al.*, 2020; Martín-García *et al.*, 2020).

The **food addiction model** consists on a long-term operant training maintained by chocolate-flavored pellets in daily sessions of 1h during 112 days. During the operant training schedule, three food addiction criteria are evaluated in two specific time periods: early and late periods. The three addictive-like criteria evaluated at both stages are (I) persistence to response when food is signaled as not available, (II) motivation towards food, and (III) compulsivity, which is referred to when mice continue pressing the lever and consuming the food despite negative consequences. An animal is considered positive for an addiction criterion when the score of the specific

behavioral test is above the 75th percentile of the global distribution. According to the number of addiction criteria reached in the early and late period, mice are categorized as resilient or vulnerable and non-addicted and addicted mice, respectively. At the end of the long-term operant training, mice considered food addicted (2-3 criteria) presented higher scores on each of the three addiction criteria than mice categorized as non-addicted (0-1 criteria). Moreover, addicted mice presented increased impulsivity and aversive learning (Mancino *et al.*, 2015; Domingo-Rodriguez *et al.*, 2020; Martín-García *et al.*, 2020).

As previously mentioned in section 2.2., the term food addiction has not still been included in the DSM-5 and is currently diagnosed by the validated tool YFAS 2.0 (Schulte and Gearhardt, 2017). This diagnostic tool is adapted from the substance use disorders criteria of the DSM-5. Remarkably, the food addiction model evaluates the three addiction criteria, which summarize the significant hallmarks of addiction specified in the DSM-5 and the food addiction diagnosis of the YFAS 2.0 (Table 4). Furthermore, the investigations performed using this model suggested a valid model with face and predictive validity as addicted mice represented ~20% of the population exposed to palatable food, a similar percentage value observed in humans (19.9%) (Kirrilly M Pursey *et al.*, 2014). Furthermore, the percentage of addicted animals was reduced by the administration of CB₁R antagonist rimonabant, correcting the food addiction-like behavior (Mancino *et al.*, 2015). These findings accentuate the importance of combining a vulnerable phenotype with chronic palatable food exposure in the development of compulsive

food self-administration. Altogether, the food addiction model is reliable for investigating the neurobiological mechanisms underpinning the transition from a controlled to compulsive food intake.

Table 4. Diagnostic items of drug use related disorders in DSM-4 and DSM-5, and of food addiction in YFAS 2.0, with their corresponding criteria measured in the mouse model of food addiction. Adapted from (Moore *et al.*, 2017; R. Maldonado *et al.*, 2021).

	DSM-IV	DSM-5	YFAS 2.0	Animal models
	Substance-related disorders	Substance-related and addictive disorders	Food addiction	Mice model of food addiction (2015)
	Substance abuse	Substance use disorders with severity	Self-report asking about "certain foods"*	3 main addictive domains
Diagnosis	At least 1 of these 4 criteria	At least of the 11 criteria (2-3 mild, 4-5 moderate, ≥6 severe)	Clinically significant or distress and 2 or more of the criteria (2-3 mild, 4-5 moderate, and ≥6 severe)	At least 2 of the 3 criteria
Criteria / Questions	1. Recurrent failure in major role obligations	1. Recurrent failure in role obligations	1. Recurrent failure in role obligation	
	2. Use in physically hazardous situations	2. Use in physically hazardous situations	2. Use in physically hazardous situations	
	3. Recurrent substance-related legal problems			
	4. Continued use despite social or interpersonal problems	3. Continued use despite social or interpersonal problems	3. Continued use despite social or interpersonal problems	
	Substance dependence			
	3 out of these 7 criteria			
Criteria / Questions	1. Tolerance	4. Tolerance	4. Tolerance	1. Persistence to response (difficulty to limit food use)
	2. Withdrawal	5. Withdrawal	5. Withdrawal	
	3. Consumed more (larger amount and for a longer period) than planned	6. Consumed more (larger amount and for a longer period) than planned	6. Consumed more (larger amount and for a longer period) than planned	
	4. Unable to cut down or stop	7. Unable to cut down or stop	7. Unable to cut down or stop	2. Motivation (strong motivation for the food)
		8. Craving	8. Craving	
	5. Great deal of time spent	9. Great deal of time spent	9. Great deal of time spent	
	6. Important social, work or recreational activities are given up because of use	10. Important social, work or recreational activities are given up because of use	10. Important social, work or recreational activities are given up because of use	
7. Use despite knowledge of physical/emotional consequences	11. Use despite knowledge of physical/emotional consequences	11. Use despite knowledge of physical/emotional consequences	3. Resistance to punishment (keep taking the food despite negative consequences)	

Additionally, diverse animal models of different eating disorders have been generated through different means such as selective breeding, genetic engineering, brain lesions, and environmental manipulations. For instance, some models of binge eating comprise voluntary binge eating in animals by limiting access to palatable food, incorporating cyclic periods of food deprivation, and using stressors (Avena *et al.*, 2012). Nevertheless, these models have several limitations. Deprivation of food induces and augments locomotor activity and corticosterone levels, leading to unstable binge-like eating patterns in short periods of time. Thus, developing a mouse model of binge-like eating behavior has proven to be more complex as minor stresses may significantly inhibit food intake (Teegarden and Bale, 2008).

6.2. Innovative technological approaches

Operant behavioral approaches are usually required to evaluate complex responses in animal models of drug or food addiction. Nowadays, novel techniques are available to be combined with operant approaches to dissect the interconnected brain networks that underpin addictive behavioral responses. These techniques include chemogenetics, calcium imaging, optogenetics, and electrophysiology. In addition, these innovative approaches have identified particular brain networks that could be targeted as potential therapies for future prevention and treatment of addiction (Rafael Maldonado *et al.*, 2021).

6.2.1. Chemogenetics

A chemogenetic technique that has been recently used to study the implication of specific cell populations in addiction is Designer Receptors Exclusively Activated by Designer Drugs (DREADDs). DREADD is based on GPCRs that allow the modification of a specific cell population to modulate the neuronal activity of a brain region or, even more precisely, the activity of a neuronal pathway. This modulation is performed through the depolarization or hyperpolarization of the neurons infected by a viral vector that contains the genetic information for excitatory (hM3Dq or hM3Ds) or inhibitory (hM4Di) GPCRs, respectively (Roth, 2016). The most common DREADD agonist used by the scientific community is clozapine-N-oxide (CNO). It has low brain penetrance and, via metabolic degradation, originates the antipsychotic drug clozapine in low concentrations, representing an additional active DREADD ligand (Gomez *et al.*, 2017). Despite the metabolic conversion, multiple research support the use of CNO. In addition, alternative DREADD agonists such as perlapine and compound 21 are also employed to substitute CNO (R. Maldonado *et al.*, 2021).

DREADDs have been extensively combined with behavioral studies to elucidate the reinforcing effects of drugs in the addictive processes (Urban and Roth, 2015). In this context, the activation of the excitatory DREADD, hM3Dq, by CNO chronically in the NAc reduced binge alcohol consumption (Purohit *et al.*, 2018; Pozhidayeva *et al.*, 2020). Furthermore, recent studies in the food addiction framework have used an updated DREADD technique more sophisticated called retro-DREADDS. This technique consists

of the inhibition or excitation of a neuronal population in a specific brain pathway, taking advantage of retrograde viral microinjection, which comprises an enzyme that recombines the DREADD. A study performed in our laboratory using the retro-DREADD technique from the mPFC to the NAc administrating CNO, evaluated the role of this pathway in an addictive-like behavior promoted by palatable food. The inhibition of mPFC projections to the NAc resulted in compulsive consumption of palatable food and enhancement of the addictive-like behavior (Domingo-Rodriguez *et al.*, 2020; R. Maldonado *et al.*, 2021) (Figure 30).

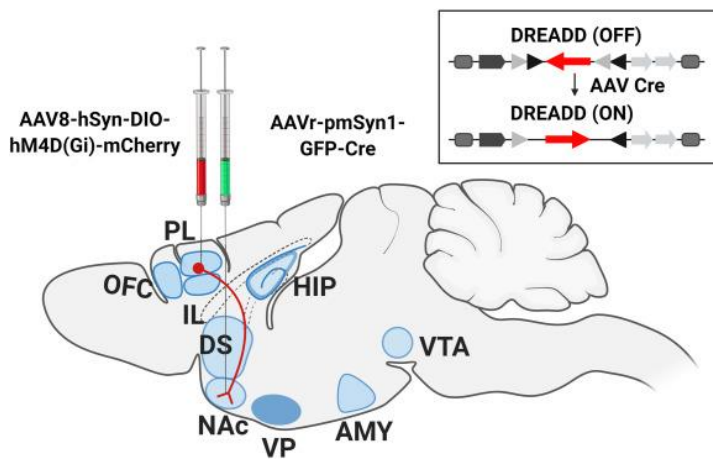


Figure 30. DREADDs approach for projection-specific modulation of neuronal activity. Representation of the mouse brain with the combinatorial viral strategy of the retro-DREADD approach. Selective chemogenetic inhibition of the mPFC to NAc neurons is produced by Cre-dependent hM4Di-mCherry injection in the mPFC and retrograde AAV with Cre recombinase in the NAc. Thus, hM4Di receptor expression only occurs in mPFC neurons that directly project to NAc. VTA, ventral tegmental area; NAc, nucleus accumbens; DS, dorsal striatum; AMY, amygdala; HIP, hippocampus; OFC, orbitofrontal cortex; PL, prelimbic; IL, infralimbic (R. Maldonado *et al.*, 2021).

6.2.2. Calcium imaging

Calcium imaging is based on the recordings of intracellular calcium influxes produced by the depolarization of neurons. Several optical techniques capture the intracellular calcium influxes based on genetically encoded calcium indicators (Yang and Yuste, 2017). Among these optical techniques, miniscopes allow for the first time the optical recordings of neuronal activity in awake, freely moving rodents that are employed in different behavioral models (Ghosh *et al.*, 2011) (Figure 31).

Few studies have used head-mounted miniscopes technology in behavioral studies to investigate the neuronal activity patterns during addiction. Increased neuronal activity patterns were recently reported with calcium recordings in neurons projecting from the mPFC to the NAc during cocaine-seeking, whereas the decreased activity of the same neurons was observed in a cocaine-free period (Cameron *et al.*, 2019). Specifically, selective recordings were performed from mPFC to NAc neurons during drug-seeking, and the activation of this network was associated with relapse prevention. Moreover, the activation of glutamatergic or GABAergic neurons in the ventral pallidum regulated differently cue-induced cocaine-seeking. Indeed, activation of glutamate neurons inhibited cocaine-seeking, while activating GABA or enkephalin neurons induced cocaine-seeking (Heinsbroek *et al.*, 2020). On the other hand, few studies using miniscopes have been published in the food addiction field. A previous study using freely behaving mice identified that individual GABAergic neurons of the lateral hippocampus preferentially encode aspects of either appetitive or consummatory behaviors, but

rarely both (Jennings *et al.*, 2015). Thus, miniscopes determine in a quantitative and qualitative strategy within cell resolution the particular neural activity in contrast to photometry that only captures the overall amount of fluorescence emitted in a quantitative strategy. Although miniscopes are currently the most contrasted *in vivo* calcium imaging system, new promising approaches are emerging, such as the optical fiberscope that allows high optical resolution in quantitative and qualitative strategies (R. Maldonado *et al.*, 2021).

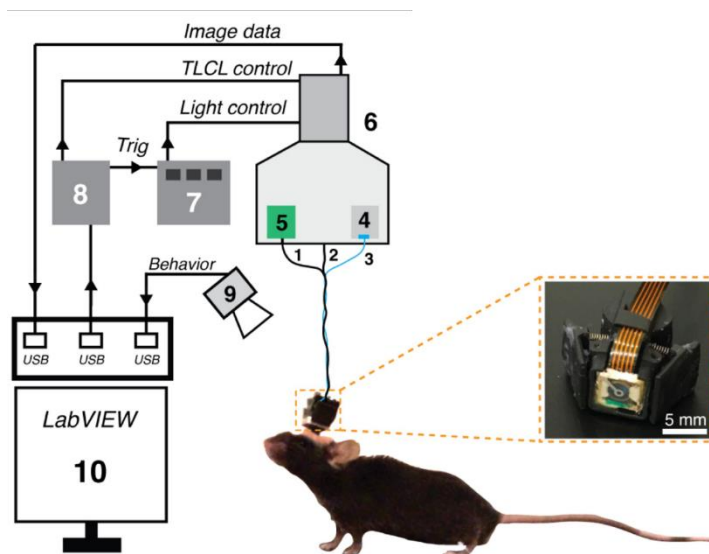


Figure 31. Schematic of the miniscopes and imaging system. 1. extension cable for the sensor; 2. wires allowing motionless electrical scanning; 3. optical fiber; 4. light source; 5. DAQ sensor; 6. rotary joint system; 7. light-emitting diodes driver; 8. DAQ Labview; 9. camera to record behavior; and 10, Labview user interface. Adapted from (Bagramyan *et al.*, 2021).

6.2.3. Optogenetics

Optogenetic manipulation of specific neural subpopulations has become a powerful strategy to understand behavioral paradigms.

This photo-dependent technique involves the introduction of genes encoding for photoactivatable ion channels, called opsins, in targeted neurons to enable depolarization or hyperpolarization. The most commonly used opsin to activate neural circuits is channelrhodopsin-2 (ChR2), a light-gated cation channel activated by blue light (450 – 490 nm wavelength). On the other hand, optogenetic inactivation of neural circuits is most commonly accomplished by employing the light-gated chloride pump halorhodopsin (NpHR), which is activated with yellow light (~590 nm wavelength). Indeed, other variants of these opsins have been developed, allowing the possibility of exciting two genetically distinct neuron populations within the same brain area (Rodriguez-Romaguera *et al.*, 2020) (Figure 32).

Opsins expression under the control of neuron -specific promoter is a method to manipulate diverse subtypes of neurons without using transgenic mouse lines. Using this method, previous studies manipulated glutamatergic projections from the basolateral amygdala to the NAc, suggesting that this pathway is crucial in reward-seeking (Stuber *et al.*, 2011). Moreover, further studies have used optogenetics to elucidate multiple circuit components involved in the motivational states of addiction (Britt and Bonci, 2013; Juarez *et al.*, 2019). Thus, the optogenetic technique combined with behavioral approaches has provided significant advances to understand the specific participation of relevant neuronal pathways in the development of addiction.

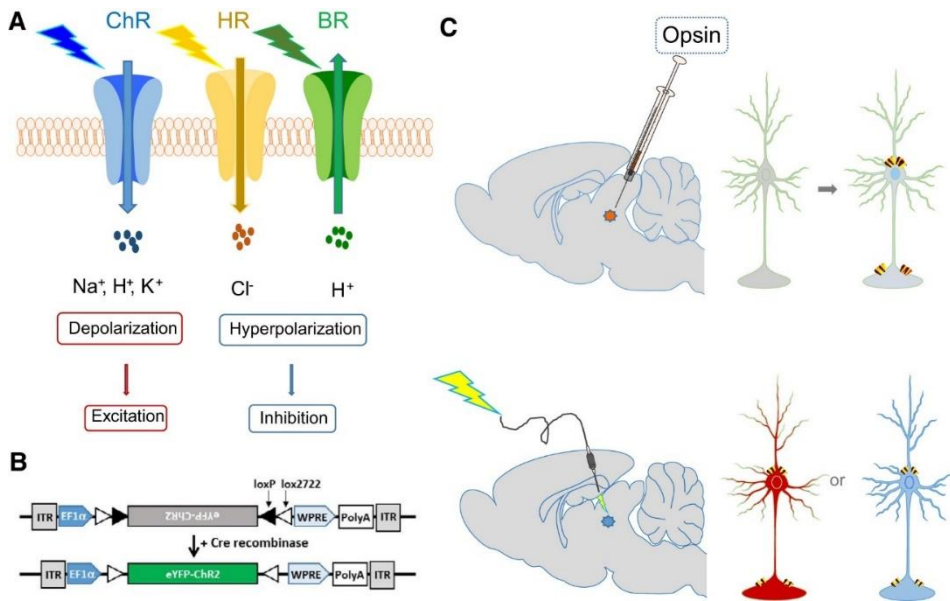


Figure 32. Optogenetics opsins. A. The most popular opsins include ChR, HR, and archaerhodopsin (BR). Light induction of ChR leads to neuronal depolarization, while illumination upon HR and BR leads to neuronal silencing. B. Normally, the double-floxed inverse open-reading frame (DIO) contains the inverted repeat (ITR), the elongation factor-1 α (EF1 α) promoter, an eYFP-ChR2 transgene surrounded by loxP sites and lox2722 sites oriented inward, a woodchuck hepatitis virus posttranscriptional regulatory element (WPRE), and a polyadenylation signal (polyA). Presence of Cre recombinase cleaves the loxP sites, leading in the expression of the eYFP-ChR2 transgene. C. Stereotaxic microinjection is needed to deliver a light-sensitive opsin packaged in a viral vector in the desired brain area. Once expressed, targeted neurons will contain opsins on the plasma membrane. An implanted fiber optic delivers light inducing depolarization or hyperpolarization of the targeted neurons (Jiang *et al.*, 2017).

7. Electrophysiological approaches

In vivo electrophysiological approaches explore the electrical activity of living neurons and investigate the molecular and cellular processes that govern their signaling. As previously commented, neurons communicate using electrical and chemical signals, and therefore

electrophysiology techniques listen in on these signals by recording electrical activity, allowing the decoding of intercellular and intracellular communications. In combination with behavioral approaches, this technique enables a real-time readout of neural functions and network capability in different brain states across a wide range of temporal and spatial scales. Different recording methods are comprised in electrophysiology research, such as electroencephalography (EEG) and *in vivo* extracellular recordings.

7.1. Electroencephalography recordings

EEG is a non-invasive technique that has been extensively used in the last four decades to record on the scalp of patients suffering from addiction. EEG data have been used to get an insight into the pharmacological modulation by drugs of abuse of ongoing neural oscillations, which are electric waves that travel across the brain.

The acute effect of different addictive drugs has been extensively studied. Acute administration of drugs of abuse, such as cocaine (Herning *et al.*, 1985), alcohol (Lukas *et al.*, 1986; Stenberg *et al.*, 1994; Little, 1999), THC (Lukas *et al.*, 1995), and benzodiazepines (Benowitz *et al.*, 1980; Manmaru and Matsuura, 1989) induced an increase in alpha and beta activity in healthy volunteers. By contrast, MDMA administration decreases alpha and theta power in MDMA naïve volunteers (Frei *et al.*, 2001). Theta activity also decreases after acute THC administration in healthy volunteers (Aaron B *et al.*, 2004; Zuurman *et al.*, 2008; Böcker *et al.*, 2010). Thus, it is well

known that acute administration of drugs of abuse tunes the rhythmic activity of neurons in the human brain (R. Maldonado *et al.*, 2021).

Other authors have focused on studying the acute effect of drugs on consumers. During resting states, cannabis users exhibited decreased delta and increased theta, beta, and gamma power compared to controls (Shikha Prashad and Detric, 2018). Alcohol users showed a decrease in delta and theta bands (Coutin-Churchman *et al.*, 2006). Cocaine-experienced users did not evidence persistent beta increase, commonly observed in inexperienced intranasal cocaine users (Heming *et al.*, 1994). Furthermore, predominantly in the beta band, were detected in heroin addicts compared to healthy controls (Motlagh *et al.*, 2018).

EEG studies have also focused on studying the neural correlates of food addiction in patients with three or more food addiction symptoms. For example, food addicted individuals presented an increase of delta and theta power in the right middle frontal gyrus, the right precentral gyrus, and the right insula and right inferior frontal gyrus, respectively. Moreover, food addicted patients presented elevated functional connectivity in frontoparietal areas in both alpha and theta brainwaves, associated with the number of food addiction symptoms (Imperator *et al.*, 2015).

EEG has also been used to study reward valuation processes and cognitive impairments using drug-related cues in patients with previous drug and food intake stories. These studies have focused on event-related potentials (ERPs), which are the means of time-locked EEG recordings to a stimulus or a response. P300 is the most

frequently employed index of neural resources assigned to reward studies among different ERPs types. A positive ERP appears 300 to 600 ms following stimulus presentation. P300s are implicated in memory, motivation, attention, and response inhibition using cognitive and emotional paradigms (Stewart and May, 2016).

Using oddball visual tasks, opioids (Lubman *et al.*, 2007, 2008, 2009), nicotine (Littel and Franken, 2011), alcohol (Bartholow *et al.*, 2010; Petit *et al.*, 2012), and cannabis (Henry *et al.*, 2014) users displayed greater P300s for substance-related cues than for non-substance-related cues. Furthermore, drug users exhibited generally higher P300s compared to controls. These studies indicate that consumers increased neural activity to process stimuli related to the selected drug of choice at the expense of other stimuli.

Several studies have also focused on studying EEG activity abnormalities when patients suffering from eating disorders are exposed to food cues. Authors of different studies observed that beta oscillations in resting states was augmented in frontocentral regions of individuals with a comorbid eating disorder and obesity, which positively correlated with eating disorder psychopathologies at rest and following exposure to food cues (Tammela *et al.*, 2010; Hume *et al.*, 2015; Bauer and Manning, 2016; Wolz *et al.*, 2017). ERP responses to food stimuli have also been investigated among individuals with eating and weight disorders. Studies revealed that patients suffering from eating disorders exhibited an increased attentional response to food cues compared to healthy controls. Moreover, P300s augmented during food-specific exposure but did

not differentiate overweight from control groups (Chami *et al.*, 2019).

The previous studies provide evidence of the potential usefulness of electrophysiological techniques to assess cerebral function in drug or food addiction patients. However, despite the advances in understanding the consequences of exposure to drugs of abuse and palatable food by recording neural activity on patients' scalp, EEG research in addiction and reward processes has significant limitations. Indeed, the electrical activity recorded by EEG electrodes is distant from the input source, coming from neurons in deep brain areas, which prevents the accurate study of brain regions altered during addiction. For that reason, direct extracellular electrophysiological recordings in better understand animals' specific brain areas and the neurocircuitry basis underlying addiction (R. Maldonado *et al.*, 2021).

7.2. In vivo extracellular recordings

In vivo extracellular recordings may detect neural activity in awake animals during different behavioral performances. Animals undergo stereotaxic surgery to implant electrodes to permit real-time monitoring of neural network activity. Neural activity is detected as local field potentials (LFP) and multi-unit (MUA) or single-unit activity (SUA) (Hong and Lieber, 2019). LFPs are voltage waves generated by synchronizing the activity of neuron populations interconnected in neural networks. MUA and SUA provide spike firing rate information of a group of neurons and single neurons.

Therefore, crucial information on brain circuitry and connectivity related to addictive-like behaviors can be obtained using *in vivo* extracellular recordings.

The effect of drugs of abuse on neurons firing rate has been extensively studied in anesthetized and awake animals. In anesthetized rats, cocaine (Koulchitsky *et al.*, 2012) and opioids (Khodayari *et al.*, 2019) produced a general decrease in the firing rate and bursting of VTA neurons after injection. Moreover, THC (Renard *et al.*, 2017; Norris *et al.*, 2019) and ethanol (Tu *et al.*, 2007) decreased medium spiny neurons activity in the anterior NAc and/ or PFC. By contrast, nicotine (Morel *et al.*, 2018) and amphetamines (Shi *et al.*, 2000) enhanced VTA DA cells' firing and bursting activity. Many studies have evaluated neuron synaptic plasticity in anesthetized animals with previous chronic drug intake (Moussawi *et al.*, 2009; Shen and Kalivas, 2013). Nevertheless, this thesis focuses on electrophysiological studies combined with operant behavioral approaches, and these studies in anesthetized animals are out of scope.

In vivo electrophysiological studies in addiction have also focused on neuronal firing responses related to brain reactivity to contingent drug-self administration. These studies record chronic activity in awake, freely moving animals trained for operant self-administration, and examine correlations between neural activity (LFPs and single-unit) and lever-pressing for intravenous administration of drugs or palatable pellets intake associated to drug or food-related cues (Figure 33).

Through an entire self-administration session, amphetamine (Haracz *et al.*, 1998) and cocaine (Peoples *et al.*, 1997, 2004; Kiyatkin *et al.*, 2000) infusions increased dopamine levels that tonically inhibited the majority of neurons in the striatum and the NAc. Nicotine self-administration sessions produced higher VTA DA neurons activity than saline self-administration sessions (Caillé *et al.*, 2009). Moreover, lever-pressing for drugs of abuse correlates with increases or decreases of glutamate-mediated firing in response to drug reward or drug-related cues. During cocaine and heroin self-administration sessions, distinct firing rates patterns were associated with the reinforced lever-presses (Carelli *et al.*, 1993; Chang *et al.*, 1994, 1997; Carelli and Deadwyler, 1996; Deadwyler *et al.*, 2004). In the NAc of rats trained to self-administer cocaine, a small percentage of neurons exhibited either increased or decreased firing rates seconds before lever-pressing (anticipatory responses). Half of the neuron population predominantly decreased firing rates minutes after lever-pressing (post-cocaine responses) (Chang *et al.*, 1994). In heroin self-administration sessions, NAc neurons displayed more post-heroin responses than PFC neurons, while the percentage of neurons firing before the lever-press was similar in the PFC and the NAc (Chang *et al.*, 1997). In ethanol self-administration, the recording from ensembles of single-units primarily located within the shell of the NAc during operant responding to oral ethanol in trained rats exhibits significant phasic changes, with alterations in firing rate related to operant response, tone stimulus, and ethanol delivery (Janak *et al.*, 1999). These results reveal the crucial role of the NAc in linking conditioned and unconditioned internal and external stimuli with

motor plans to allow for ethanol-seeking behavior to occur (R. Maldonado *et al.*, 2021).

Several studies have also focused on neuronal responses related to particular behavioral responses in the food addictive process. Evidence suggests that oscillatory activities of the mPFC and NAc correlate with impulsivity and pellet delivery outcomes. Power in gamma frequency LFP oscillations transiently increased in the PFC and the NAc during anticipation of reward-related cue signaling. Moreover, theta LFP power increased during the waiting period in these brain areas (Donnelly *et al.*, 2014). These neurophysiological findings further implicate the PFC and the NAc in reward outcome abnormalities (G F Koob and Volkow, 2010). In terms of firing rate, other studies have revealed that the firing activity of neurons in the mPFC and the NAc fluctuate between anticipatory responses (before lever-press) and post-reward responses (Chang *et al.*, 1997, 1994; Deadwyler *et al.*, 2004b). Moreover, recent studies in trained rats suggest that the firing dynamics of neurons in the mPFC, encode reward outcome and impulsivity (Sackett *et al.*, 2019). Thus, addictive-like behavior is associated with irregular delta, theta, and gamma oscillations and abnormal firing rates. However, connectivity measures between brain areas involved in drug and food addictive behaviors during reward processes remain mostly unknown. The elucidation of these interconnectivity may be crucial to clearly understanding the neurophysiological mechanisms responsible for addictive behaviors (R. Maldonado *et al.*, 2021).

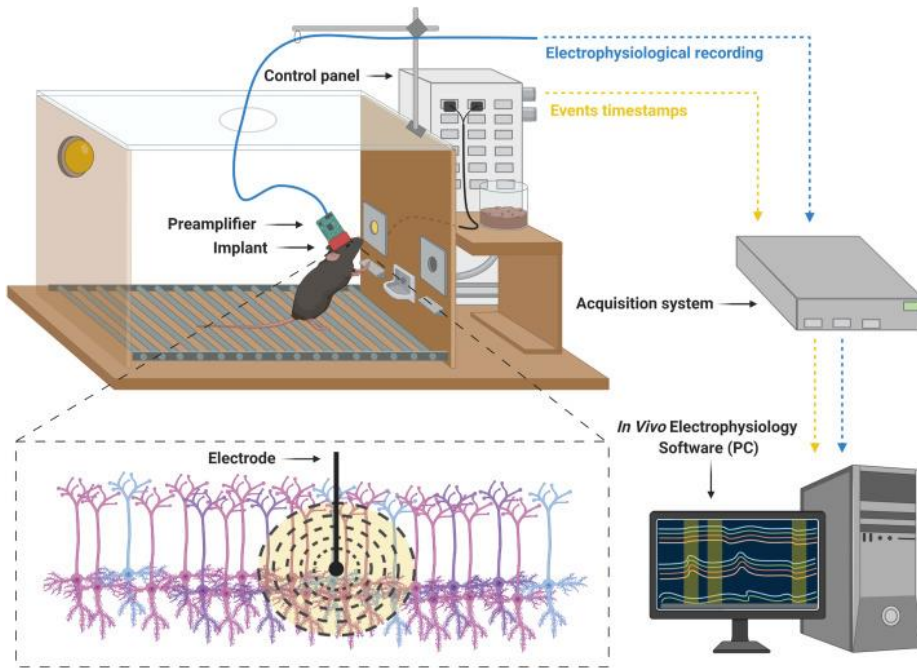


Figure 33. Electrophysiological recordings in awake, freely moving mice. Animals are trained to self-administer drugs of abuse or palatable food in operant boxes. A light stimulus (cue light) located above the active lever is paired contingently with reward delivery. Neural oscillatory activities are recorded during the entire session. The electrode implanted in the desired brain area records rhythmic changes in voltage generated by the synchronization of activity of neuron population interconnected in neural networks. Analogic signals recorded by the electrode are bandpass filtered and digitized by a preamplifier, later amplified by the acquisition system, and finally, visualized and stored in a computer via an *in vivo* electrophysiology system (blue arrow). The control panel processes timestamps events occurring along with the session and consequently signaled to the acquisition system to mark events duration in the electrophysiological recordings (yellow arrow) (R. Maldonado *et al.*, 2021).

8. Therapeutics for food addiction and eating disorders

The emerging inclusion of food addiction and eating disorders as a research framework has stimulated considerable research testing

innovative methods to treat eating disorders. As investigations better characterized the needs of individuals suffering from eating disorders, it was evident that these treatments had to be effective for compulsive eating pathologies, associated eating disorders psychopathologies, depressive psychopathologies, and often weight gain problems (Devlin, 2001). Notwithstanding, treatment investigations have extensively varied in their designs and methods, focusing primarily on binge eating and weight.

Review studies and analyses of the treatment literature have generally combined different specific specialized non-pharmacological and pharmacological treatments for reducing compulsive eating and associated psychopathologies. Among diverse therapies, non-pharmacological behavioral therapies have demonstrated that their benefit are quite durable with follow-up studies. However, weight loss does not generally occur (Grilo *et al.*, 2011). On the other hand, pharmacotherapy studies have revealed that certain medications have short-term efficacy relative to placebo for eating disorders (McElroy *et al.*, 2015; Reas and Grilo, 2015; Grilo *et al.*, 2016). Thus, eating disorders require a detailed treatment plan, including strategy combinations, tailored to meet individuals' needs and improve their eating behaviors.

8.1. Non-pharmacological treatments

8.1.1. Behavioral therapies

Behavioral therapies are effective alternatives that focus on correcting thinking and behavior, offering diverse, healthy attitudes

towards food. Specifically, these psychological interventions are centered on challenging and changing unhelpful distortions in cognition, such as thoughts, attitudes, beliefs, behaviors, and emotional regulation (McHugh *et al.*, 2010; Castelnuovo *et al.*, 2017; Linardon and Brennan, 2017). Cognitive behavior therapy and interpersonal psychotherapy are the two main strategies employed in behavioral therapies.

Cognitive behavior therapy and interpersonal psychotherapy are different specific therapies directly acting on the eating disorder. **Cognitive behavior therapy** plays an important role in helping the patient better confront eating disorder-related issues, such as negative emotions and depressed mood. This therapy may provide improved behavioral control over food consumption. On the other hand, **interpersonal psychotherapy** is centered on social relationships with other people, improving interpersonal skills. This therapy aims to reduce compulsive eating induced by problems in social relationships and communication skills. Although both therapies did not produce significant weight loss in comorbid patients, they have improved eating disorder psychopathology with short-term and long-term efficacy (Wilfley *et al.*, 2002; Wilson *et al.*, 2007). Notwithstanding, it is usually recommended a combination of behavioral and pharmacological therapies.

8.1.2. Brain stimulation therapeutics

The circuit-based therapeutics could be invasive, such as deep brain stimulation (DBS) or non-invasive, such as repetitive transcranial

magnetic stimulation (rTMS) and transcranial direct current stimulation (tDCS).

DBS is an invasive non-lesional neurosurgical procedure with surgical implantation of current circulating electrodes for the electrical stimulation of discrete brain areas. This stimulating therapy has been employed in diverse circuit-based neuropsychiatric conditions, such as compulsive disorder and depression (Alonso *et al.*, 2015; Cleary *et al.*, 2015). DBS therapy is a safe and efficacious treatment for Parkinson's disease (Honey *et al.*, 2017). Notwithstanding, DBS has limitations as the general stimulation provided in a determined brain area is not selective at cellular levels. To eliminate these limitations, many studies have designed a combinatorial approach with deep brain stimulation and pharmacological adjuvants that discard the opposing effects of the general stimulation. This approach was effective in preclinical models of cocaine addiction, where cocaine-induced modifications in synaptic plasticity and cocaine locomotor sensitization were reversed (Creed *et al.*, 2015). DBS has also been used in clinical studies with obese women. The stimulation of particular hypothalamic areas (homeostatic center) and NAc (reward system) induced a loss of body weight and, therefore, a reduced BMI (Harat *et al.*, 2016). These findings highlight the possibilities of deep brain stimulation for treating food addiction, eating disorders, and obesity. However, further research is needed to understand better the effectiveness and adverse effects originated by DMS in the food addiction framework.

rTMS and tDCS are non-invasive stimulation techniques that do not require surgical procedures. **rTMS** passes brief current pulses through a coil over the patient's scalp to originate an electromagnetic field that inhibits (low frequency, <5 Hz rTMS) or activates (high frequency, >5 Hz rTMS) target neurons. On the other hand, **tDCS** delivers a weak electrical current to brain regions through electrodes situated over the patient's scalp to either depolarize (anodal tDCS) or hyperpolarize (cathodal tDCS) resident neurons. Nowadays, most investigations have employed high-frequency rTMS and tDCS to ameliorate neuronal and cortical activity in the dlPFC, leading to an elevated control of executive functions.

A previous study in patients suffering from cocaine addiction suggested that cocaine consumption and craving were reduced after several trials using high-frequency rTMS of the dlPFC (Terraneo *et al.*, 2016). Moreover, analogous to these results, a decrease in food cravings and weight loss was detected in a cohort of obese individuals after several weeks of high-frequency dlPFC rTMS (Ferrulli *et al.*, 2019). Similarly, studies employing tDCS to stimulate the dlPFC of obese subjects observed a food craving reduction (Lee *et al.*, 2018).

The efficacy of dlPFC high-frequency rTMS in drug or food addiction-like behavior therapies might be elucidated by enhancing long-term neuroplastic variations that modulate cortical excitability. Due to the release of a wide variety of neurotransmitters, long-term plasticity originated at the dlPFC, being the primary area activated. This activation may enhance the stimulation of subcortical areas, which are secondly activated. Certainly, rTMS of the dlPFC at high

frequencies caused prolonged augmentation of DA levels in the ventral striatal complex (Diana *et al.*, 2017). These findings propose that rTMS and tDCS may play a crucial role in treating food addiction and obesity. Nevertheless, more investigations are required to better define stimulation parameters, frequency of the therapy, and the long-term sustainability of any positive effects.

8.1.3. Neurofeedback strategies

Other alternative non-pharmacological approaches used to treat addiction are neurofeedback strategies. In the last years these strategies have emerged as an imaging or recording modality employed to examine volitional control over targeted brain activity in the last years. Functional magnetic resonance imaging or EEG applied clinically to train patients to self-regulate areas of the brain, or circuitry, associated with addictive-like behaviors. The objective of this strategy is to promote normalized brain activity via associative learning and subsequently provide diverse strategies to patients to modify their psychological states (Hammond, 2011; Martz *et al.*, 2020). Few studies have focused in the treatment of substance use disorder and overeating using this strategy. A recent study suggested that after neurofeedback treatment, participants reduced binge eating episodes showing a decreased EEG high beta activity (Schmidt and Martin, 2020). Although these treatments are still in preliminary stages, evidence indicate that physiological changes serve as specific treatment mechanisms in neurofeedback against eating disorders. Decreasing cortical arousal may ameliorate eating behaviors,

therefore considering corresponding neurofeedback techniques in combination with pharmacological treatments for future treatments (Schmidt and Martin, 2020).

8.2. Pharmacotherapies

Pharmacological treatments aimed to treat food addiction, obesity, and eating disorders must address the dysfunctions at brain levels, and the use of pharmaceuticals including opioids, leptin, cannabinoids, and DA has been proposed to modulate these brain areas leading to a craving decrease and a correction in food intake. However, the current pharmacologic treatments for obesity have not succeeded in addressing the disease.

Silbutramine is a mixture of serotonin, norepinephrine, and DA reuptake inhibitors approved in 1977 to treat overweight. This drug did show promising effects on body weight but was discarded from the market in 2010 due to concerns of elevated risk of stroke and cardiovascular events (Padwal and Majumdar, 2007; Rucker *et al.*, 2007). **Orlistat** is nowadays the unique long-term pharmacologic treatment for obesity that is approved for up to a year duration. This drug reduces fat absorption in the gut by inhibiting gastrointestinal lipase, resulting in a modest weight loss. Orlistat is currently considered a good option due to its safety on cardiovascular effects. However, secondary effects such as diarrhea and excess gas have been presented in many individuals (Rössner *et al.*, 2000; Rucker *et al.*, 2007). Furthermore, **phentermine** and **diethylpropion** are

usually prescribed for obesity but have limited success (Wadden *et al.*, 2005).

Furthermore, preclinical studies induced an extensive range of promising pharmacological strategies that aim to target modulators of the brain reward system, such as opioids that play a major role in controlling appetite and food consumption. As such, opioid antagonists have been helpful in weight loss therapy, demonstrating a decrease in short-term food intake and in the pleasurable nature of palatable foods (Cota *et al.*, 2006). Investigations have revealed that opioid antagonists such as naltrexone, naloxone, and nalmefene may decrease caloric intake. Among these, **Naltrexone** preferentially acts on mu opioid receptor and is currently employed for treating alcohol and opioid addiction. Additionally, in the food addiction treatment, naltrexone use significantly decreases food intake and reward activation in normal-weight volunteers (Lee and Fujioka, 2009).

Other recent medications have been approved by the Food and Drug Administration (FDA) to treat obesity, having relevant implications for food addiction. These drugs are **contrave** (mixture of naltrexone and bupronion), **lorcaserin** and **topiramate**. In an obesity clinical trial, **contrave** reduced body weight in 48% of obese participants (Greenway *et al.*, 2010). Furthermore, **contrave** blunted hypothalamic activation to food cues and stimulated the activation of brain regions participating in inhibitory control, internal awareness and memory (G-J Wang *et al.*, 2014). **Lorcaserin** acts in serotonergic 5HT_{2C} receptors of the brain, enhancing satiety, whereas **topiramate** is an antiepileptic drug acting on GABAergic

and AMPA/kainite receptors that induces a decrease in appetite and weight. A clinical investigation using topiramate reported that prolonged administration of this drug resulted in a significant reduction of binge eating episodes with a corresponding weight loss (Milano *et al.*, 2013).

Finally, as previously commented, cannabinoid receptors may serve as another potential target for treating food addiction and obesity. A blockade of the eCB system has been proposed as a potential alternative. The most common, **rimonabant**, is an antagonist drug acting on CB₁R that was approved in Europe and more than 30 countries worldwide in 2006 for obesity treatment (Rinaldi-Carmona *et al.*, 1996). Although rimonabant was effective in enhancing weight loss, this medication was withdrawn from clinical use two years later due to adverse psychiatric effects, such as anxiety, depression, and suicidal ideas. Thereupon, new neutral CB₁R antagonists and/or peripherally restricted CB₁R antagonists unable to cross the blood-brain barrier have been developed and are under preclinical investigation (D'Addario *et al.*, 2014). On the other hand, pharmacological modulators of eCBs synthesis, instead of blockade of CB₁R, could provide a better physiological approach to treating obesity.

Objectives

General objective

The general objective of this thesis is to unravel the neurophysiological signatures involved in food addiction.

Objective 1: To study the prelimbic-nucleus accumbens core neurophysiological signatures in food addiction.

- 1.1. To characterize the prelimbic-nucleus accumbens core electrophysiological fingerprints of extreme phenotypes of food addicted and non-addicted mice.
- 1.2. To characterize the prelimbic-nucleus accumbens core electrophysiological marks of CB₁ receptor blockade in food addicted and non-addicted mice.

Chapter 1: Prelimbic to nucleus accumbens core neural dynamics in food addicted and non-addicted mice.

Objective 2: To study the prelimbic-nucleus accumbens core neurophysiological signatures in the transition from vulnerable to food addiction phenotype in mice.

Chapter 2: Evolution of prelimbic-nucleus accumbens core neural dynamics in mice vulnerable to develop food addiction.

Materials and Methods

Animals

Experiments were performed in C57BL/6J male mice (n=60). Mice (2 - 10 months old) were housed under conditions of controlled temperature ($23 \pm 1^\circ\text{C}$) and illumination (12 hours light/dark cycle), and all the tests were performed during the dark phase of a reverse light cycle. Mice were habituated to the experimental room and handled for one week before starting the experiments. All procedures had authorization from the Barcelona Biomedical Research Park Animal Research Ethics Committee (PRBB-CEEA) and complied with the guidelines of the European Union Council (EU Directive 2010/63/EU) and Spanish regulations (BOE 252/34367-91, 2005).

Operant behavior apparatus

Mouse operant chambers (Model ENV-307A-CT, Med Associates, Georgia, VT, USA) were used for operant responding maintained by chocolate flavored pellets. The operant chambers were equipped with two retractable levers, one randomly selected as the active lever and the other as the inactive. Pressing on the active lever resulted in a food pellet delivery paired with a stimulus-light (associated cue), located above the active lever, and while pressing on the inactive lever had no consequences. A food dispenser equidistant between the two levers permitted the delivery of food pellets when required. The floor of the chambers was a grid floor that served to deliver electric food shocks in the session of the shock-test and served as a contextual cue in the session of the shock-associated cue, the day after the shock session. A metal sheet with holes was placed above the grid floor during the rest of the self-administration sessions. Thus, mice could

discriminate between different contexts. The chambers were made of aluminum and acrylic and were located in sound- and light-attenuated boxes equipped with fans to provide ventilation and white noise.

Food pellets

During the operant conditioning sessions, after active responding by lever pressing, animals received a 20 mg chocolate-flavored pellet, a highly palatable isocaloric pellet (TestDiet, Richmond, IN, USA). These pellets had a similar caloric value (3.44 kcal/g: 20.6% protein, 12.7% fat, 66.7% carbohydrate) to the standard maintenance diet provided to mice in their home cage (3.52 kcal/g: 17.5% protein, 7.5% fat, 75% carbohydrate) with some slight differences in their composition: addition of chocolate flavor (2% pure unsweetened cocoa) and modification in the sucrose content. Indeed, although the carbohydrate content was similar in the standard diet (75%) and highly palatable isocaloric pellets (66.7%), the proportion of sucrose content in standard diet food was 8.3% and 50.1% in highly palatable isocaloric pellets.

Behavioral experiment

Daily self-administration sessions maintained by chocolate-flavored pellets were performed in operant boxes and lasted 1 hour. The beginning of each self-administration session was signaled by turning on a house light placed on the ceiling of the skinner box during the first 3 seconds. The self-administration sessions were composed of two pellet periods (active periods) of 25 minutes, separated by a pellet-free period of 10 minutes. Pellets were delivered contingently

after an active response paired with a stimulus light (cue light) during the pellet periods. A time-out period of 15 seconds was established after each pellet delivery, where the cue light was off, and no reinforcer was provided after responding on the active lever. Responses on the active lever and all the responses performed during the time-out period were recorded. During the pellet-free period, no pellet was delivered and this period was signaled by the illumination of the entire self-administration chamber. In the operant conditioning sessions, mice were under a fixed ratio 1 (FR1) schedule of reinforcement (one lever-press resulted in one pellet delivery) followed by an increased FR to 5 (FR5) (five lever-presses resulted in one pellet delivery) for the rest of the sessions. The criteria for the achievement of the operant responding were acquired when all of the following conditions were met: (1) mice maintained a stable responding with <20% deviation from the mean of the total number of reinforcers earned in three consecutive sessions (80% of stability); (2) at least 75% responding on the active lever; and (3) a minimum of 5 reinforcers per session. After each session mice were returned to their home cages.

Decision-making epochs were defined as the second prior to the first of the five lever presses in reward preceding trials (5 lever presses + cue light and reward delivery). Reward expectation epochs were defined as the second occurring immediately after the fifth lever press, when the cue light turns on and reward is delivered.

Three behavioral tests were used to evaluate the food addiction-like criteria as recently described and adapted from cocaine addiction-like in rats (Deroche-Gamonet *et al.*, 2004b; Deroche-Gamonet and Piazza, 2014). These three criteria summarized the significant hallmarks of addiction based on DSM-IV, specified in DSM-5 and now included in the food addiction diagnosis through the YFAS 2.03.

Persistence of response: Non-reinforced active responses during the pellet-free period (10 minutes), when the box was illuminated and signaling the unavailability of pellet delivery, were measured as persistence of food-seeking behavior. Mice were scored on this test for three consecutive days before the motivation test (see below).

Motivation: The progressive ratio schedule of reinforcement was used to evaluate the motivation for the chocolate-flavored pellets. The response required to earn one single pellet escalated according to the following series: 1, 5, 12, 21, 33, 51, 75, 90, 120, 155, 180, 225, 260, 300, 350, 410, 465, 540, 630, 730, 850, 1000, 1200, 1500, 1800, 2100, 2400, 2700, 3000, 3400, 3800, 4200, 4600, 5000, and 5500. The maximal number of responses that the animal performs to obtain one pellet was the last event completed, referred to as the breaking point. The maximum duration of the progressive ratio session was 5 h or until mice did not respond on any lever within 1 h.

Compulsivity: Total number of shocks in the session of shock test (50 min) performed after the motivation test, when each pellet

delivered was associated with punishment, were used to evaluate compulsivity-like behavior. Mice were placed in a self-administration chamber without the metal sheet with holes and consequently with the grid floor exposed (contextual cue). In this shock session, mice were under an FR5 schedule of reinforcement for 50 min with two scheduled changes: at the fourth active lever-response, mice received only an electric footshock (0.18 mA, 2 seconds) without pellet delivery, and at the fifth active lever-response, mice received another electric footshock with a chocolate-flavored pellet paired with the cue light. The schedule was reinitiated after 15 seconds of pellet delivery (time-out period) and after the fourth response if mice did not perform the fifth response within a minute.

Moreover, two additional phenotypic traits involved in the addictive-like behavior were evaluated.

Impulsivity: Non-reinforced active responses during the time-out periods (15 sec) after each pellet delivery were measured as impulsivity-like behavior, indicating the inability to stop a response once initiated (George F Koob and Volkow, 2010). The last three consecutive days of the self-administration period were considered.

Aversive learning: Measured with the shock-induced suppression test. In the shock-induced suppression test mice were placed in the self-administration chamber for 50 minutes with the same grid floor used during the shock test. However, during this FR5 self-

administration session, pressing the active lever had no consequences: no electric shock, no chocolate-flavored pellets, and no cue light. Non-reinforced active responses during this shock-induced suppression test are measured for the aversive associative learning (Figure 34).

After performing the behavioral tests to measure the food addiction-like behaviors, mice were categorized into two extreme subpopulations (addicted or extreme non-addicted animals) depending on the number of positive criteria that they had achieved. An animal was considered positive for an addiction-like criterion when the score of the specific behavioral test was above the 75th percentile of the normal distribution. Mice that achieved two or three addiction-like criteria were considered addicted animals, and mice that achieved none or one addiction-like criterion were considered extreme non-addicted animals.

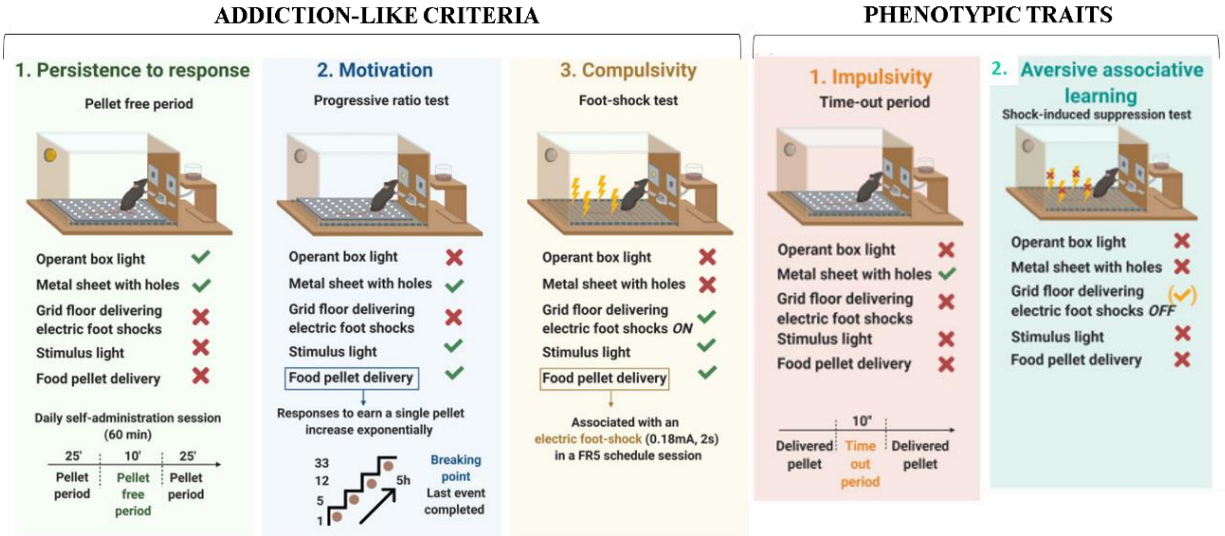


Figure 34. Addiction-like criteria and phenotypic traits of the behavioral experiment. Addiction-like criteria: (1) Persistence to response. Non-reinforced active responses during the pellet free period (10 min), when the box is illuminated and signaling the unavailability of pellet delivery, are used to evaluate the persistence of food-seeking. (2) Motivation. The progressive ratio test is used to evaluate the motivation for chocolate-flavored pellets. The responses to earn a single pellet increase exponentially. The maximal number of responses that the animal performs to obtain one pellet is the last event completed, referred to as the breaking point. (3) Compulsivity. The total number of shocks in the session of shock test, when each pellet delivered is associated with punishment, is used to evaluate compulsivity-like behavior. Phenotypic traits: (1) Impulsivity measured by the non-reinforced active responses not paired with a stimulus light during the time-out periods (15 s) after each pellet delivery. (2) Aversive associative learning measured by the shock-induced suppression test. Adapted from (Martín-García *et al.*, 2020).

Surgeries and electrode implantation

Mice were induced with a mixture of ketamine/xylazine and placed into a stereotaxic apparatus for intracranial electrode implantation. Anesthesia was maintained with isoflurane 0.25 - 2%. Four micro-screws were placed into the skull to stabilize the implant. An additional micro-screw was placed on the top of the cerebellum and used as a general ground. Two tungsten electrodes (25 μm wide; 100 to 400 k Ω ; Advent, UK) were unilaterally implanted in the PL mPFC (AP: 1.98 mm, ML: 0.3 mm, DV: -2.30 mm) and the NAc core (AP: 1.10 mm, ML: 1.0 mm, DV: -4.60 mm) (Figure 35). In addition, three reference electrodes were implanted in the *corpus callosum* and lateral ventricles (AP: 1.0 mm, 0.2 mm, -1.0 mm; ML: 1.0 mm, 0.8 mm, 1.70 mm; DV: -1.25 mm, -1.40 mm, -1.50 mm, respectively). The recorded hemisphere was chosen randomly. At the time of implantation, the electrodes had an impedance from 100 to 400 k Ω and were implanted with dental cement. Neural activity was recorded while the electrodes were being lowered down inside the brain to make sure they were implanted in tissue rich in neural activity. In addition, mice received after surgery a preventive treatment with an i.p. injection of the antibiotic gentamicin (Genta-Gobens; Laboratorios Normon, Spain; 1 mg/kg of body weight) and a subcutaneous (s.c.) injection of the anti-inflammatory agent meloxicam (Metacam; Boehringer Ingelheim, Rhein; 2 mg/kg of body weight) both diluted in sterile 0.9% physiological saline. After surgery, animals were allowed at least one week to recover, during which they familiarized themselves with the implant connected to the recording cable.

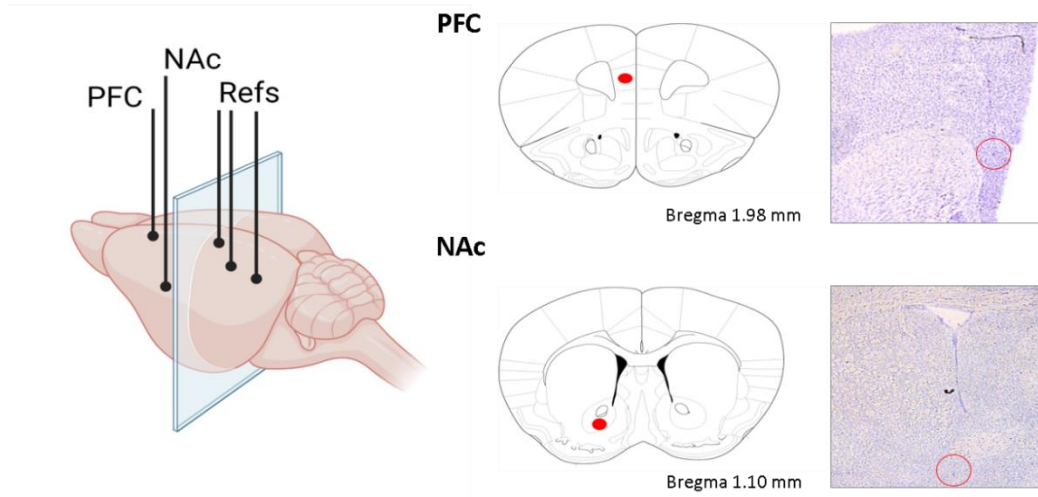


Figure 35. Representative and histological validation of electrode implantation in the mPFC and the NAc. Stereotrodes were unilaterally implanted in the prelimbic mPFC and the NAc core. Additionally, three reference electrodes were implanted in the corpus callosum and lateral ventricles. At the end of the experiment, electrode placements were confirmed by histological validation.

In vivo electrophysiological recordings

Electrophysiological recordings were conducted in the dark illumination cycle (from 8:00 a.m. to 7:30 p.m.). Animals were removed from their home cages, connected to the headstage and placed inside the skinner box to start the session. All the recordings (LFPs and MUA) were carried out with the multi-channel Open Ephys system at 0.1-6000 Hz and a sampling rate of 30 kHz with Intan RHD2132 amplifiers equipped with an accelerometer. Two animals were recorded simultaneously in two separate skinner boxes adapted for electrophysiological recordings. In brief, the boxes included an input-output board that collected relevant behavioral measures from the box (lever presses, pellet deliveries, houselight

activation, and cue light activation) and timestamped them in the electrophysiological files where the voltage signals were saved. We used two criteria to consider that operant responding was achieved during electrophysiological FR5 sessions. Operant responding during recordings was achieved when the total number of reinforcers earned in three consecutive sessions had more than a 60% of stability, and when reinforcement levels reached a minimum of 5 reinforcers per session. The electrophysiological recordings of Chapter 2 were performed with two different operant boxes per animal in order to record all the animals twice per week as a minimum. The additional operant box was a “fake operant box adapted to electrophysiology” that mimicked recordings conditions (wire connection, swivel, adapted feeder for implanted animals) but without producing electrophysiological data.

Pharmacology

The CB1 receptor blocker rimonabant was administered to mice at the end of the experimental protocol. Rimonabant (Sanofi-Aventis) was diluted in 5% ethanol, 5% Cremophor EL, and 90% saline. Rimonabant was injected by intraperitoneal (i.p.) in a dose of 3 mg/kg of body weight. Recordings of FR5 operant training sessions were performed 30 minutes after injection of the treatment.

Data and statistical analyses

All analyses were carried out with custom scripts programmed in Python. The files were first pre-processed to extract local field potentials (LFPs) and multi-unit activities (MUA). More

specifically, recorded signals from each electrode were detrended, notch-filtered to remove power line artifacts (50 Hz), and decimated to 1kHz offline to obtain LFPs. Noisy electrodes were discarded by visual inspection from individual channel spectrograms. The frequency bands considered for the band-specific analyses included: delta (2-5 Hz), theta (8-12 Hz), beta (18-25 Hz), low gamma (30-50 Hz), high gamma (50-100 Hz) and high-frequency oscillations (150-200 Hz).

Power spectral density results were calculated using the multi-taper method (time-frequency bandwidth; $TW = 5$ and $K = 9$ tapers; 1-200Hz range, non-overlapping sliding windows of 1 minute for spectrograms and power spectrum of the selected epoch, 1 second for decision-making, reward expectation, and phase changes of the FR5 sessions). Due to mathematical limitations of the multi-taper method, the stockwell method from the mne library (Gramfort *et al.*, 2013) was used for spectrograms of 1-second window during operant training sessions. Spectrograms were constructed using consecutive Fourier transforms.

Phase coherence between mPFC and NAc was estimated via weighted phase-lag index (wPLI, Butterworth filter of order 3), a measure of phase synchronization between areas aimed at removing the contribution of common source zero-lag effects that allowed us to estimate the synchronization between the mPFC and the NAc mitigating source signals affecting multiple regions simultaneously. First, we used Hilbert transformation to obtain instantaneous phases

from LFP. wPLI measures the asymmetry in the distribution of phase differences for each frequency band between the two-time series resulting in values ranging between 0 and 1, being a higher value a high asymmetric distribution as a consequence of a consistent phase-lag between signals in the two areas. wPLI reduces the probability of detecting false positive connectivity in the case of volume conducted noise sources with near zero phase lag and shows higher sensitivity in detecting real phase synchronization. These measures are not present in the result section of the thesis as no differences were reported between experimental groups.

Signal directionality between mPFC and NAc areas was calculated with the phase slope index (PSI) with a Python translation of MATLAB's `data2psi.m` (`epleng = 60s`, `segleng = 1s`) as in reference (Nolte *et al.*, 2008). PSI is a robust measure of directionality based on the conceptual, temporal argument supporting that the driver is earlier than the recipient. It quantifies the consistency of the direction within phase differences across frequencies. Given a specific bandwidth parameter, it computes the change in the phase difference between close frequency bins for each frequency bin, weighted with the coherence. Then, when phase difference changes consistently across frequencies and there is coherence, PSI deviates from zero (Bastos and Schoffelen, 2015). A positive slope reflects a PFC-to-NAc flow of information in a specific frequency range, while a negative slope reflects NAc-to-PFC signal directionality.

For the phase-amplitude coupling (PAC), we used two different functions depending on the size of the window to analyze. We used the modulation index (MI) developed by (Tort *et al.*, 2008) for over one minute windows. In addition, we used the Canolty method as implemented by (Onslow *et al.*, 2011) for the one-second windows reflecting decision-making and reward expectancy periods during the operant conditioning. First, low frequency (delta and theta) phases were divided into 18° bins (i.e., each cycle was divided into 20 bins), and gamma (low, high gamma) and hfo amplitudes were calculated for each phase bin. MI measured the divergence of the phase-amplitude distribution and was higher as the distribution deviated from the uniform distribution (i.e., no modulation). In order to choose specific frequency band pairs for the MI quantification, we represented overall MI in two-dimensional pseudocolor comodulation maps. A warmer color indicated coupling between the phase of the low-frequency bands (1-16 Hz; x-axis) and the amplitude of the high-frequency band (20-250 Hz; y-axis), while blue depicts the absence of coupling (Figure 36).

MUA was estimated by first subtracting the raw signals from each electrode with the signal from a nearby referencing electrode to remove artifacts generated by the animals' movement and present in all the channels. Then, continuous signals were filtered between 450-6000 Hz with Python and thresholded at -3 sigma standard deviations with Offline Sorter v4 (Plexon Inc.).

Statistical analyses were performed with Graphpad Prism 8.0 (Graphpad Software, Inc, San Diego, CA) and Statistical Package for

the Social Sciences 22.0 (SSPS Software, IBM Corp, Armonk, NY) softwares.

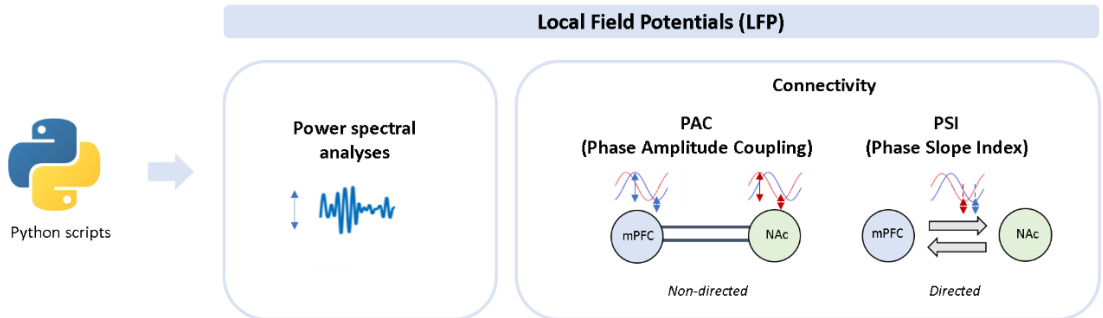


Figure 36. Classification of local field potential analyses. Power spectral analyses were performed to analyze the amplitude of the local field potentials in the PFC or the NAc locally. Phase amplitude coupling is performed locally or inter-regionally methods for short or long windows. First, we performed a band-pass filtering and extraction of phase and amplitude and then assessed correlations between amplitude and phase to quantify deviations of the uniform distribution from the amplitude vs phase histogram. The directed connectivity measure was the phase slope index, measuring the consistency of the direction of the change in the phase difference across frequencies. Spectrograms, comodulograms and quantifications will be used to present these analyses.

Histology

On the last day of electrophysiological recordings, small electrolytic lesions of the recording sites were carried out via electrical stimulation of the electrodes (100 Hz, 0.1 mA for 2 s) under anesthesia. Then, mice were sacrificed and their brains extracted and preserved in 2-methylbutane. Brains were sliced into 30 μm sections with a cryostat. Electrode placements were confirmed histologically by staining the brain slices using the Nissl method. Images were obtained and analyzed using light microscopy (Olympus BX61) with a 4x magnification. Electrodes with tips outside the targeted areas were discarded from data analyses.

*Experimental design***Chapter 1**

Thirty-one mice were trained in operant boxes for 112 days to develop food addictive-like behaviors (Mancino *et al.*, 2015; Domingo-Rodriguez *et al.*, 2020). The long-term operant conditioning started with a fixed ratio of one lever press to one pellet reward (FR1) schedule of reinforcement during five sessions and was followed by 105 sessions under FR5 (Figure 37a). One mouse that did not achieve the acquisition criteria after day 33 was excluded from the study. Persistence to response, motivation, and compulsivity were evaluated in the early (sessions 18-26) and late periods (sessions 104-112). After the behavioral evaluation during the late training period, mice were classified into two different phenotypes: addicted (covering two or three criteria) and non-addicted (covering none or one criterion) mice. An additional classification was performed to select extreme phenotypes according to the distribution of their values in P25, P50 and P75 percentiles values ($<P25 = 0$, $>P25 < P50 = 1$, $>P50 < P75 = 2$, $>P75 = 3$) in the different addiction-like criteria and phenotypic traits tests (5x compulsivity, 4.5x three days pellet-free period, 4x motivation, 3x ten days pellet-free period, 2.5x three days time-out, 2x ten days time-out, 1.5x three days reinforcement, 1x ten days reinforcement). These extreme subpopulations (extreme non-addicted and addicted mice) underwent stereotaxic surgery to implant electrodes in the prelimbic mPFC and the NAc core. Following recovery from surgery, recordings were performed in operant boxes adapted for electrophysiology for a short-term operant training (post-surgery FR5 sessions 1 to 10). Following these ten

sessions with electrophysiological recordings, mice were treated with rimonabant 3 mg/kg to investigate the effects on the neural substrates of the addictive phenotype. Recordings in standard cages and recordings during four FR5 sessions (post-surgery FR5 sessions 11 to 14) were performed to study the electrophysiological effects of rimonabant in the mPFC and the NAc core (Figure 37a).

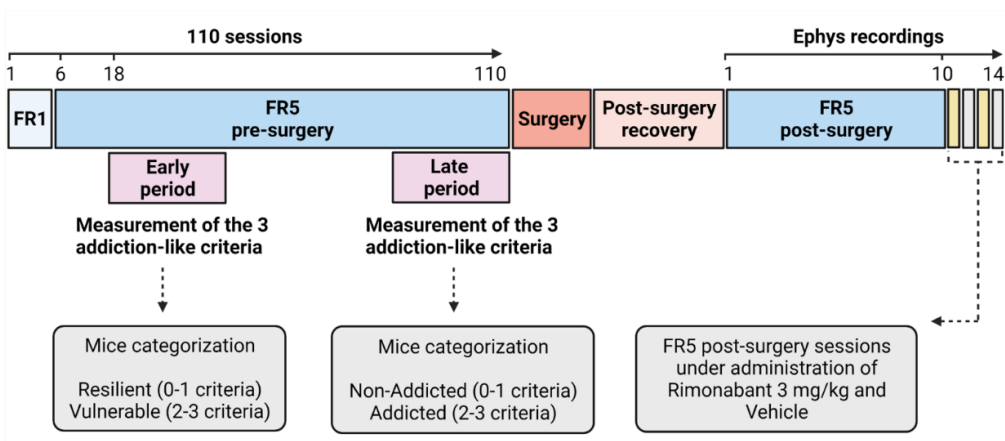


Figure 37a. Timeline of the experimental sequence. Mice were trained to acquire the operant conditioning maintained by chocolate-flavored pellets under FR1 (5 sessions) and FR5 (105 sessions) schedules of reinforcement. Mice categorization was performed according to the three addiction criteria and phenotypic traits in order to obtain extreme subpopulations: extreme non-addicted (0 criteria) and addicted (2-3 criteria) mice. These animals underwent stereotaxic surgery for electrode implantation the PL mPFC and the NAc core (n = 9 addicted mice and n = 9 extreme non-addicted mice). After recovery from surgery and habituation to the implant and the wire connection, electrophysiological recordings were performed in standard cages and operant boxes adapted for electrophysiology in the post-surgery FR5 sessions period (10 sessions). Subsequently, mice were treated with rimonabant 3 mg/kg and recordings were performed in standard cages and operant boxes during additional FR5 sessions (4 sessions).

Chapter 2

Twenty-eight mice started the experimental protocol with an FR1 schedule of reinforcement during two sessions and was followed by five sessions under FR5. These sessions were performed to lead the animals to learn the operant training and habituate themselves to the operant chambers. After these sessions were completed, animals underwent stereotaxic surgery to implant stereotrodes in the prelimbic mPFC and the NAc core. Following recovery from surgery, a habituation period to the wire was performed and the animals were re-trained in the task. Mice that accomplished more than 3 reinforcers per session, and obtained stability of 60% between sessions at the two different operant boxes (the standard one and the one adapted for electrophysiology), and performed more than 75% of responses in the active lever were ready to start the electrophysiological recordings of the medium-term operant training. These criteria were analyzed individually and mice that did not accomplish the acquisition criteria after day 33 after implantation (day 45 from the beginning of the experiment) were excluded from the study. The electrophysiological recordings were performed with two different operant boxes per animal in order to record all the animals twice per week as a minimum. The additional operant box was a “fake operant box adapted to electrophysiology” that mimicked recordings conditions (wire connection, swivel, adapted feeder for implanted animals) but without producing electrophysiological data. Electrophysiological recordings of the medium-term operant training started with 15 sessions of FR5 and subsequently, persistence to response, motivation and compulsivity were evaluated in the early

(session 18-26) and medium (session 52-60) periods (Figure 37b). Electrophysiological recordings lasted until the end of the medium period due to the signal quality and implant durability. After the behavioral evaluation during the medium training period, mice were classified into two different phenotypes: addicted (covering two or three criteria) and non-addicted (covering none or one criterion) mice, as in Chapter 1 (Figure 37b).

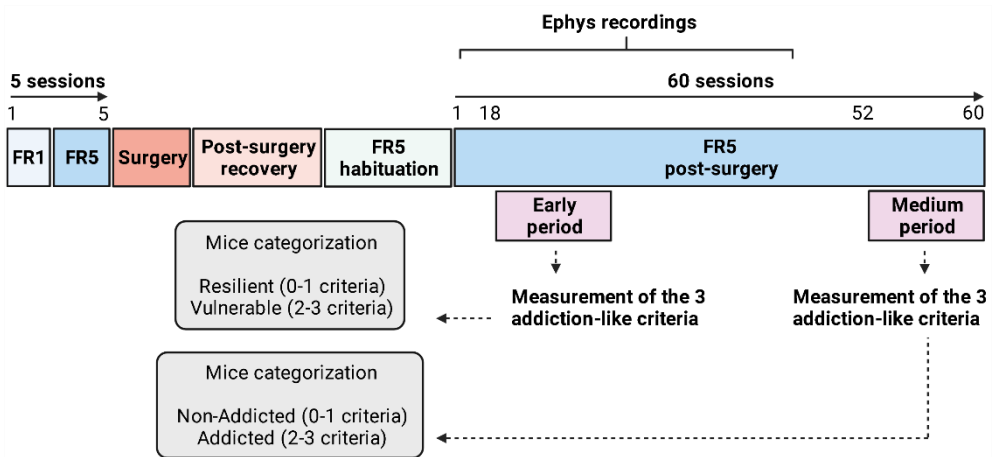


Figure 37b. Timeline of the experimental sequence. Mice were trained to acquire the operant conditioning maintained by chocolate-flavored pellets in five sessions (2 FR1 and 3 FR5 sessions). Electrode implantation in the PL mPFC and the NAc core was performed in all animals. After recovery and the habituation period, mice were recorded twice per week during the medium-term operant training (60 sessions). Addictive-like criteria were evaluated at the early and medium periods. Mice categorization was performed according to the three addiction criteria and phenotypic traits in order to obtain extreme subpopulations: non-addicted (0-1 criteria) and addicted (2-3 criteria) mice.

Results

Chapter 1

Prelimbic – nucleus accumbens core neural dynamics in food addicted mice

Pablo Calvé^{1,2}, Thomas Gener^{2,3,4}, Laura Ribalta¹, Sami Kummer¹,
Pau Nebot², Elena Martín-García^{*1,2}, M. Victoria Puig^{*2,3,4}, Rafael
Maldonado^{*1,2}

1 Laboratory of Neuropharmacology. Department of Medicine and Life Science,

Universitat Pompeu Fabra, Barcelona, Spain.

2 Hospital del Mar Medical Research Institute, Barcelona, Spain.

3 Catalan Institute of Nanoscience and Nanotechnology, CSIC and The Barcelona Institute of Science and Technology, Campus UAB, 08193 Bellaterra, Spain.

4 Institut de Neurociències, Universitat Autònoma de Barcelona, 08193 Bellaterra, Barcelona, Spain.

*These authors contributed equally to the study

IN PREPARATION

1.1. Electrophysiological characterization of extreme subpopulations of food addicted and non-addicted mice.

Categorization of extreme phenotypes of food addicted and non-addicted mice

To study the electrophysiological signatures of food addicted and non-addicted mice, we first categorized mice into addicted and non-addicted according to the food addiction animal model (Mancino *et al.*, 2015). Thus, we trained 31 C57Bl/6J adult male mice in the long operant protocol of food addiction for 112 days (Domingo-Rodriguez *et al.*, 2020) (Figure 37a; see Experimental design section of Chapter 1 in Methods). In fixed ratio 1 (FR1) sessions, mice started to acquire the operant behavior, and the number of reinforcers increased across sessions in all mice. When the effort to obtain one single pellet was augmented to FR5, the number of reinforcers declined during the first four FR5 sessions. However, previous reinforcement levels were quickly achieved at the fifth FR5 session and progressively increased across time (Figure 38). After surgical electrode implantation, mice significantly reduced the number of reinforcers from 51.16 to 41.18. At the end of the protocol, four days of pharmacological treatment were introduced using rimonabant and vehicle subsequently in a within-subject design. Results showed that rimonabant drastically reduced the number of reinforcers compared with the vehicle with the previous FR5 sessions (Figure 38).

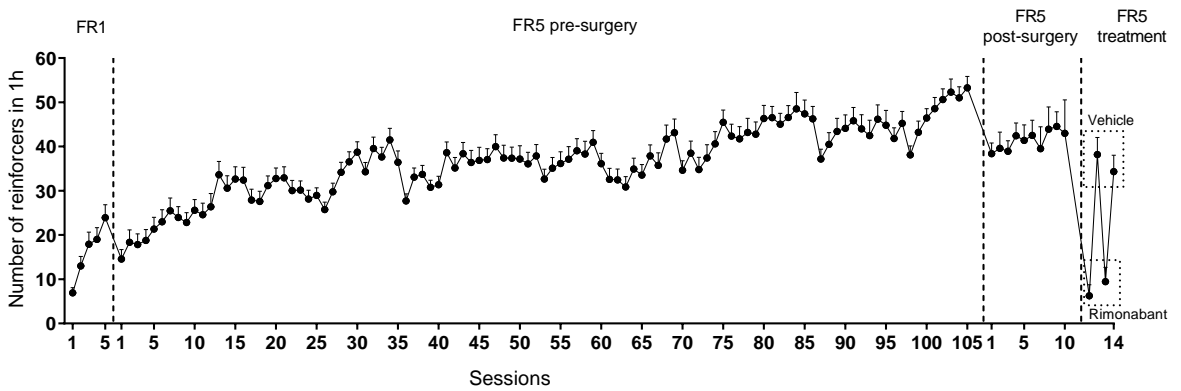


Figure 38. Acquisition of operant training maintained by chocolate-flavored pellets. Mean number of reinforcers during the acquisition training in FR1 and FR5 schedule of reinforcement ($n=31$, One-way ANOVA repeated measures, Supplementary Table 1), during electrophysiological recordings ($n=9-13$), and during rimonabant treatment ($n=9-11$). Differences are reported as mean \pm SEM.

Categorization of extreme phenotypes of food addicted and non-addicted mice was performed in the late period, between sessions (104-112), and 29.03% of the animals reached two or three addiction-like criteria and were considered as addicted ($n=9$). The rest of the animals (70.97%) reached none or one addiction-like criterion and were considered non-addicted ($n=22$) (Figure 39).

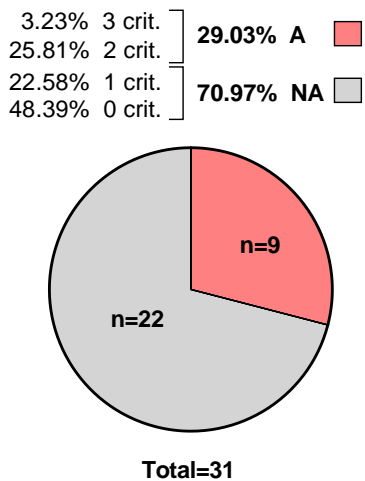


Figure 39. According to the late period, the distribution of animals with different scores for addiction-like behavior. Animals were assigned to a criteria subgroup based on the number of criteria met for which they scored equal to or above the 75th percentile.

Considering this phenotypic categorization of the late period, we evaluated if there were significant differences in the hallmarks of addiction between these groups of addicted and non-addicted mice in the early period (session 18-26). Results showed non-significant differences in the persistence of response, motivation, and compulsivity between addicted and non-addicted mice (Figure 40A-C). As expected, in the late period (session 104-112), addicted mice showed significantly higher persistence of response and increased motivation for reward obtention compared to non-addicted mice (U Mann–Whitney, $P < 0.01$, $P < 0.001$, Figure 40D-F). Moreover, addicted mice tended to show increased compulsivity values, although the difference between addicted and non-addicted animals was not significant (Figure 40F).

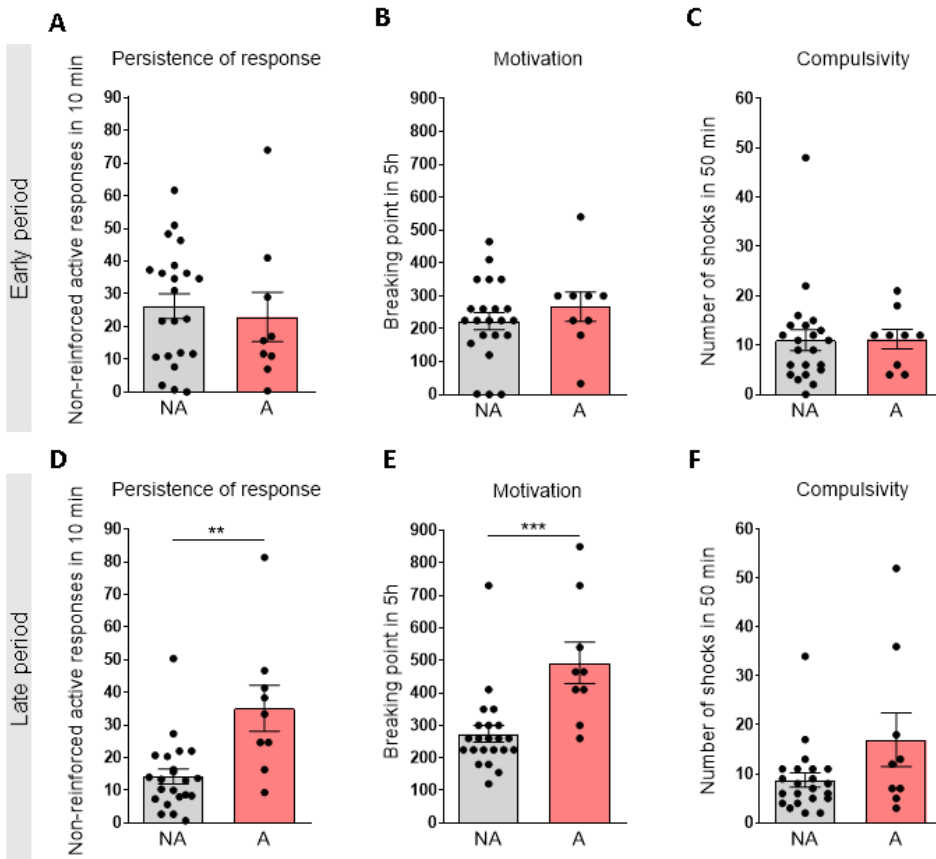


Figure 40. Behavioral tests of the three addiction criteria in both phenotypes at the early (A-C) and late (D-F) periods. (A,D) Persistence of response. Total number of non-reinforced active responses during three consecutive daily 10-min of pellet free period. (B,E) Motivation. Breaking point achieved in 5 h of PR schedule. The breaking point refers to the maximal effort that an animal is willing to do to earn one pellet. (C,F) Compulsivity. Number of shocks that mice received in 50 min in the shock test in which each pellet delivery was associated with a footshock (0.18 mA). Differences are reported as mean \pm SEM, U Mann-Whitney, ** $P < 0.01$, *** $P < 0.001$.

We further evaluated the reinforcing effects of chocolate-flavored pellets and importantly, in the FR5 late period, addicted mice showed a significantly increased number of reinforcers and lever-presses compared to their non-addicted peers (U Mann–Whitney, $P < 0.05$, P

< 0.01, Figure 41A-B). This effect was not observed in FR1 nor the FR5 early period. We also compared the levels of impulsivity in addicted and non-addicted mice, and only in the late period addicted mice showed significantly higher impulsivity which was measured by the inability to stop pressing the lever during the time-out period (15 s) after each pellet delivery (U Mann–Whitney, $P < 0.01$, Figure 41C). For the aversive associative cue reactivity test, in both early and late periods, addicted mice showed a slightly increased food-seeking compared to non-addicted mice, indicating decreased aversive cue reactivity, although the statistical difference was not significant (Figure 41D-E).

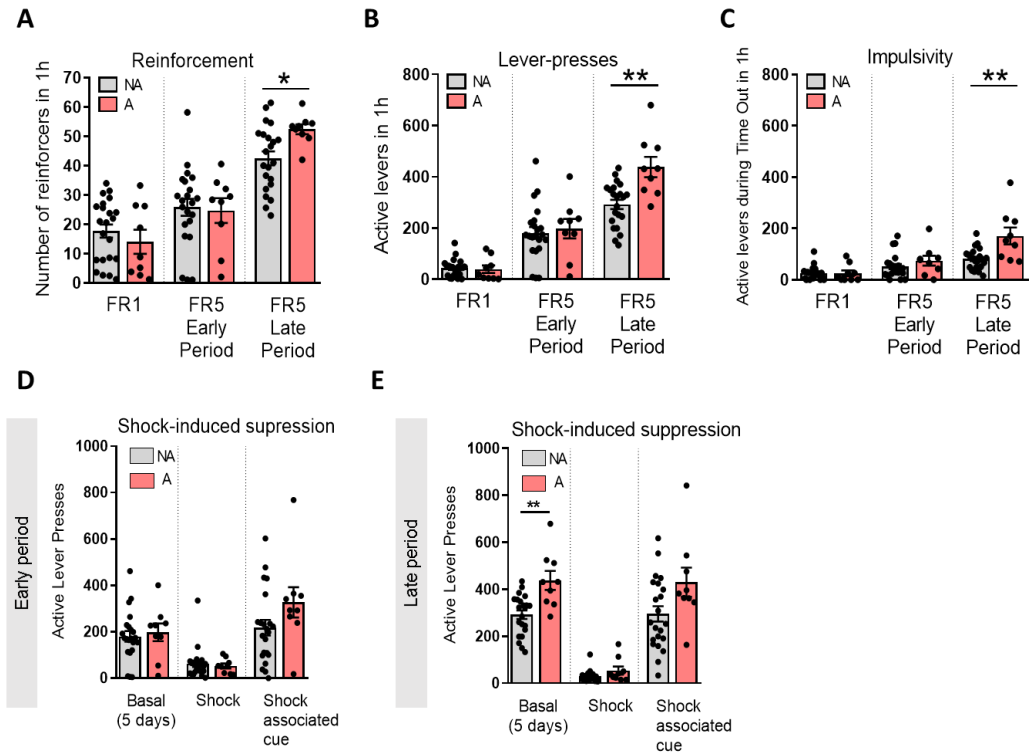


Figure 41. (A-C) Behavioral data of phenotypic traits in FR5 sessions represented by individual values with the mean and \pm SEM. FR1 corresponds to the five operant sessions of FR1, FR5 Early Period corresponds to the five FR5 sessions before the early period, FR5 Late Period corresponds to the five FR5 sessions before the late period. (A) Reinforcement levels were quantified by counting the number of reinforcers consumed in 1h operant session. (B) Number of total active lever-presses scored in 1h operant session. (C) Impulsivity. Number of non-reinforced active lever-presses during five consecutive daily time out (15 s) after each pellet delivery (U Mann-Whitney, * $P < 0.05$, ** $P < 0.01$). (D-E) Behavioral test of shock-induced suppression at the (D) early period and (E) late period represented by individual values with the mean of active levers and \pm SEM. Basal corresponds to the five FR5 sessions before compulsivity test (shock). Shock corresponds to the compulsivity test where each pellet delivery was associated with a punishment, an electric foot shock. Shock-associated cue corresponds to the number of non-reinforced active responses in 50 min in the following session after the shock test with the same discriminative stimulus (grid floor) as the shock test in which pressing the active lever had no consequences: no shock, no reward delivery and no cue light (U Mann-Whitney, ** $P < 0.01$).

We measured weekly bodyweight during the whole protocol to discard any potential predisposing effect on food addiction development and monitor its evolution. Results showed no basal differences between addicted and non-addicted mice. In addition, the evolution across time was similar and not affected by food addiction development (Figure 42), indicating that changes in the body weight did not explain the higher persistence of response, motivation, reinforcement, and impulsivity observed in addicted mice.

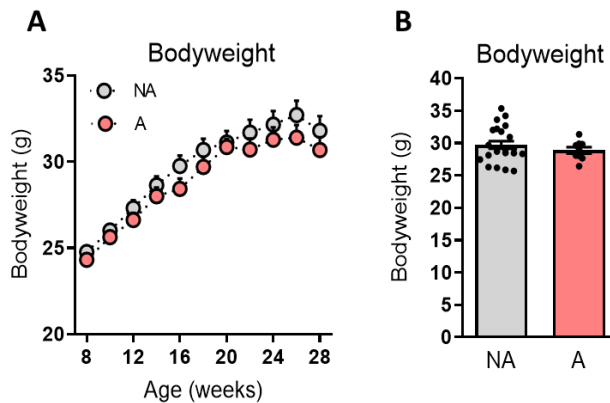


Figure 42. Bodyweight. (A) Measurements of body weight in grams across weeks in NA and A mice. (B) Averaged body weight data per phenotype.

To gain deeper insight into the main factors contributing to the development of addicted and non-addicted phenotypes, we performed a principal component analysis (PCA) of behavioral traits. The percentage of variance explained by the two principal components was 45.4% (PC1) and 22.1% (PC2). PCA allowed classifying the two extreme phenotypes in vulnerable (n=9) or resilient (n=22) to develop food addiction-like behaviors based on these criteria and phenotypic traits (Figure 43A). The main variables

contributing to PC1 were reinforcement, the addiction criterion of motivation, and the impulsivity trait, whereas the addiction criteria of compulsivity and persistence of response were the predominant in PC2 (Figure 43B-C).

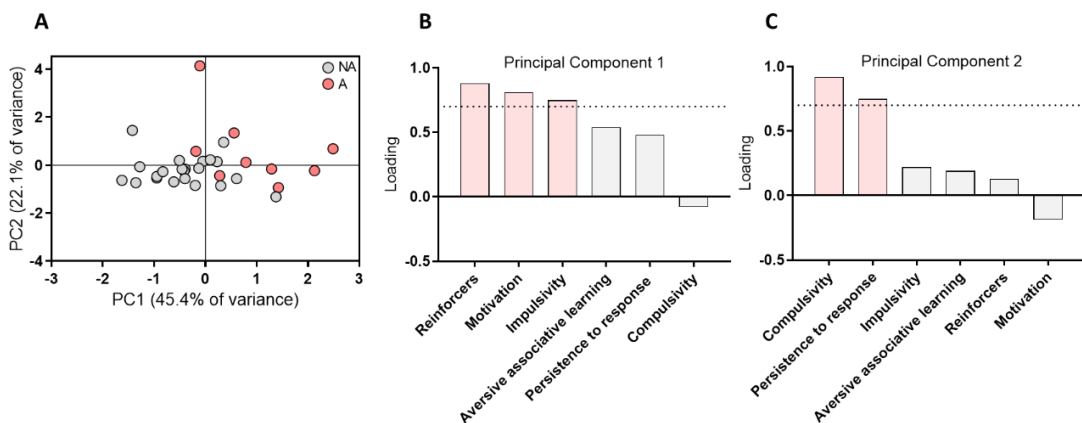


Figure 43. PCA analysis. (A) Mice subjects clustered by the presence of A or NA on the space yielded by two components of the PCA that account for the maximum data variance with factor loadings of principal component (PC) 1 (45.4%) and principal PC2 (22.1%). (B-C) The order of factor loading of the different variables in the (B) PC1 and (C) PC2 is represented. The dashed horizontal line marked loadings > 0.7 , mainly contributing to the component.

As reinforcement levels and motivation to pursue highly palatable pellets were the higher scores variables of the PC1 (0.88 and 0.81, respectively), and compulsivity and persistence of response had the higher load of the PC2 (0.92 and 0.75 respectively), we decided to focus the analysis on decision-making and reward expectation of FR5 sessions. Indeed, altered decision-making and outweighed reward expectation have been associated with motivation, rewarding processes of food consumption, compulsivity, and persistence of response (O’Doherty et al., 2017; Verharen et al., 2020).

Prelimbic - nucleus accumbens core gamma circuit communication signals are disrupted in addicted mice during decision-making and reward expectation.

To investigate the neurophysiological signatures underlying addictive-like behaviors, we selected mice at the tails of an inverted U-shape curve according to the quantitative individual scores obtained in the addiction-like criteria and phenotypic traits tests. Animals were classified according to the distribution of their scores in the specific behavioral tests. Scores below 25th percentile summed up 0 points, scores between 25th and 50th percentiles summed up 1 point, scores between 50th and 75th percentile summed up 2 points, and scores above 75th percentile summed up 3 points. Indeed, the number of points scored were multiplied by the importance of the behavioral test (5x compulsivity, 4.5x three days pellet-free period, 4x motivation, 3x ten days pellet-free period, 2.5x three days' time-out, 2x ten days time-out, 1.5x three days reinforcement, 1x ten days reinforcement). Extreme subpopulations of non-addicted (n=9) and addicted (n=9) mice (Figure 44) underwent stereotaxic surgery for electrode implantation in the PL mPFC and the NAc core.

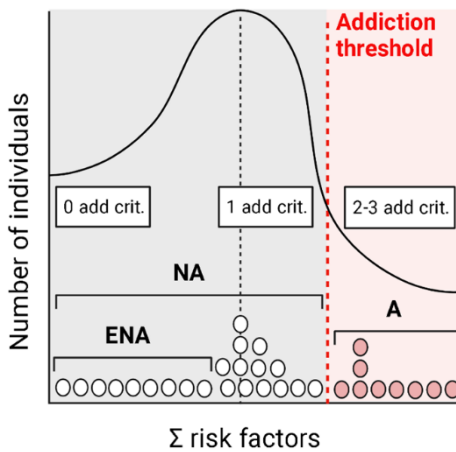


Figure 44. Representative scheme of the selection of animals situated at the extremes of the U-inverted shape curve, according to addictive-like criteria and phenotypic traits. Out of 31 animals, 22 were categorized as non-addicted (NA) (0 and 1 criterion accomplished) and 9 were categorized as addicted (A) (2 and 3 criteria accomplished). 9 extreme non-addicted (ENA) that accomplished 0 addiction-like criteria and obtained a low score in the addiction classification were selected in parallel with 9 A animals for electrode implantation.

After surgical recovery, electrophysiological recordings were performed in home cages immediately after the FR5 sessions. Locomotor activity was similar in both groups (Figure 45), and no significant differences in signal power were detected between addicted and extreme non-addicted mice neither in the PL mPFC nor in the NAc core. However, Igamma power was larger in the NAc core compared with the PL mPFC (Unpaired t-test, $P < 0.05$, Figure 46).

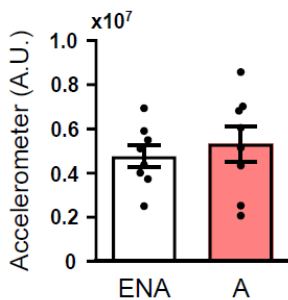


Figure 45. Locomotor activity in ENA and A mice during recordings in the standard cage after FR5 sessions. Accelerometer, variance of signals from the accelerometer integrated within the headstages. The corresponding quantification of the animal's mobility is presented as a ratio to the highest value in the baseline condition.

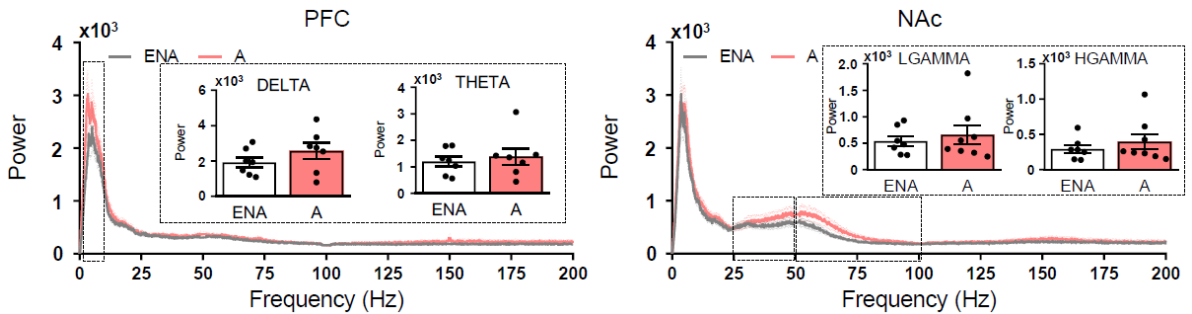


Figure 46. Power spectra of PL mPFC (left) and NAc core (right) signals during recordings of 20 min in the standard cage. Power values of delta and theta between ENA and A mice are shown in PL mPFC power spectra. Also, power values of lgamma and hgamma between ENA and A mice are shown in NAc core power spectra.

Furthermore, no significant differences were found in circuit communication (phase slope index, PSI) between addicted and extreme non-addicted mice. Notably, both groups exhibited a flow of information from the NAc core to the PL mPFC at theta and hgamma frequencies (NAc core to PL mPFC PSI, NAc core leads) and a PL mPFC to NAc core communication at lgamma frequencies (PL mPFC to NAc core PSI, PL mPFC leads) under basal conditions (Figure 47). Altogether, circuit communication measures suggested that neural signals of addicted and extreme non-addicted mice in the PL mPFC and the NAc core coordinated at theta, lgamma and hgamma frequencies after FR5 sessions. These connectivity fluctuations were frequency-specific and did not occur at other frequencies.

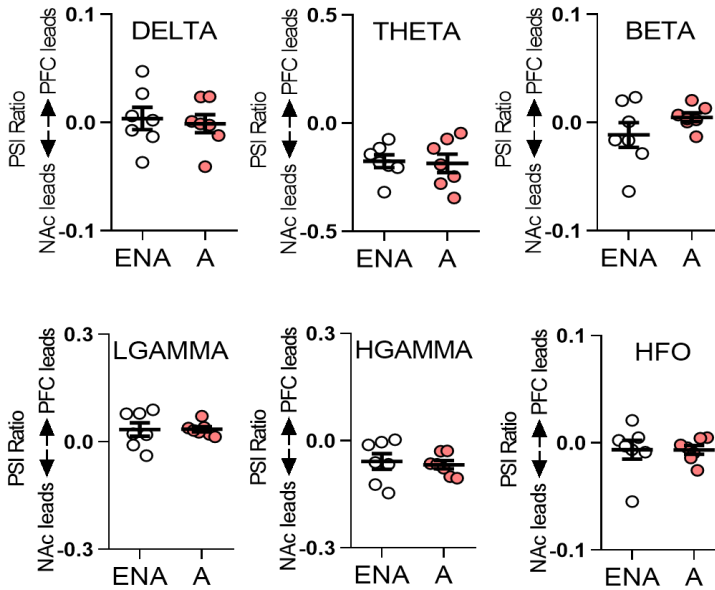


Figure 47. PL mPFC – NAc core circuit communication (PSI) at delta, theta, beta, lgamma, hgamma and hfo in ENA and A animals during recordings in the standard cage.

Addictive-like behavior was maintained after the surgery process during additional FR5 sessions (FR5 post-surgery). Addicted mice showed a higher number of reinforcers, an augmented number of lever-presses, and increased impulsivity compared to extreme non-addicted mice (Unpaired t-test, $P < 0.05$, $P < 0.01$, Figure 48).

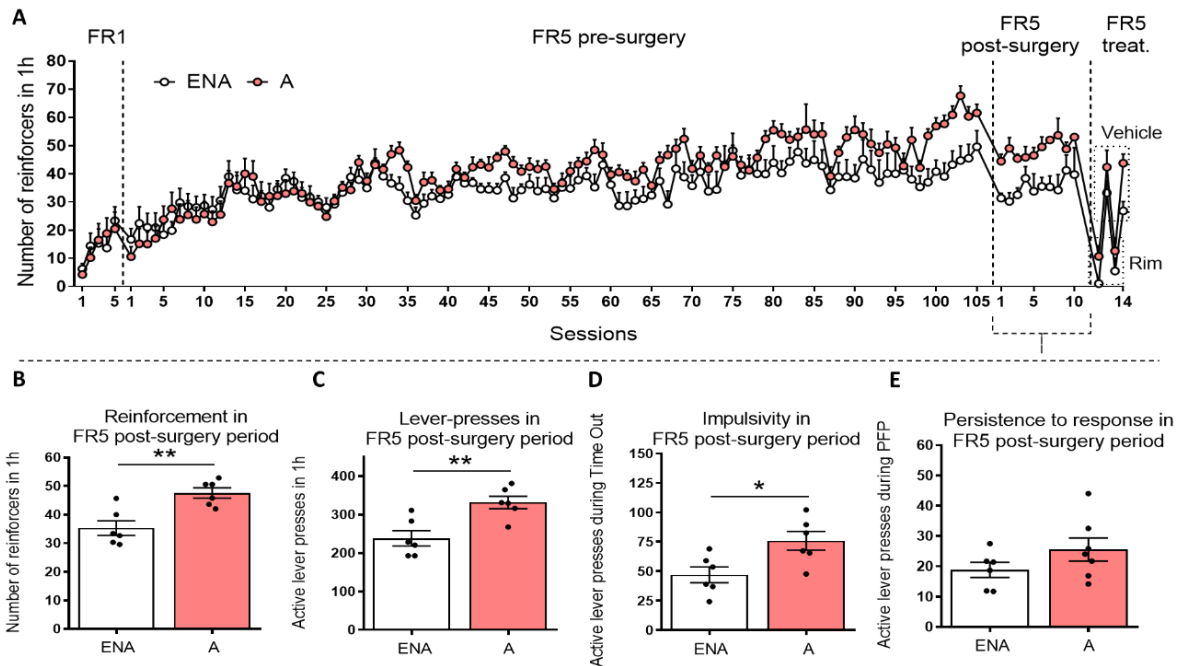


Figure 48. (A) Acquisition of operant training maintained by chocolate-flavored pellets in ENA ($n=9$) and A ($n=9$) mice. Mean number of reinforcers during the acquisition training in FR1 and FR5 schedule of reinforcement, during electrophysiological recordings, and rimonabant treatment. Differences are reported as mean \pm SEM. (B-E) During recordings of the FR5 post-surgery period, A mice maintained the addictive-like behavior during the operant sessions showing an increased (B) reinforcement, (C) number of lever-presses, and (D) impulsivity, in comparison with ENA mice. (E) Persistence of response was not significantly different between A and ENA mice. Differences are reported as mean \pm SEM, Unpaired t-test, * $P < 0.05$, ** $P < 0.01$.

In order to discard possible behavioral affections due to the surgery process, we compared reinforcement levels, number of active lever-presses and impulsivity at the different stages of the long-term operant training, remarking the maintenance of the addictive-like behavior at the end of the training schedule (Figure 49A-C). Significant differences in compulsivity and aversive cue reactivity were observed at the late period, being addicted mice more

compulsive and showing reduced aversive associative learning compared with extreme non-addicted mice (Figure 49D-E).

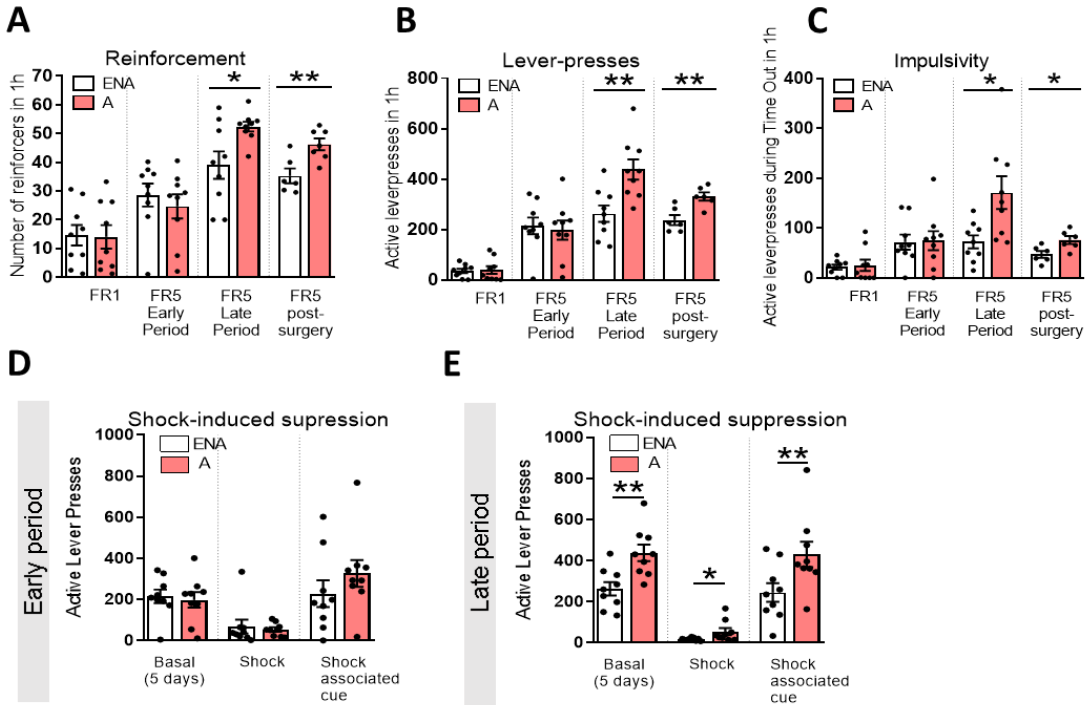


Figure 49. (A-C) A mice maintained the addictive-like behavior showing a higher number of reinforcers, an augmented number of lever-presses and increased impulsivity in comparison with ENA mice. Behavioral data of phenotypic traits in FR5 sessions are represented by individual values with the mean and \pm SEM. FR1 corresponds to the five operant sessions of FR1, FR5 Early Period corresponds to the five FR5 sessions before the early period, FR5 Late Period corresponds to the five FR5 sessions before the late period. FR5 post-surgery corresponds to the ten FR5 recording sessions after electrode implantation, recovery and habituation (A) Reinforcement levels quantified by counting the number of reinforcers consumed in 1h operant sessions. (B) Number of total active lever-presses scored in 1h operant session. (C) Impulsivity. Number of non-reinforced active lever-presses during five consecutive daily time out (15 s) after each pellet delivery (Unpaired t-test, * $P < 0.05$, ** $P < 0.01$). (D-E) Considering the phenotypic categorization used ($n=9$ addicted, $n=9$ extreme non-addicted), compulsivity and aversive associative learning were re-evaluated at the early (D) and late (E) periods. Significant differences in compulsivity and aversive associative learning were observed at the late period, being addicted mice more compulsive and showing an increased aversive associative learning compared with extreme non-addicted mice. Behavioral test of shock-induced suppression at the early period (D) and late period

(E) represented by individual values with the mean of active levers and \pm SEM. Basal corresponds to the five FR5 sessions before compulsivity test (shock). Shock corresponds to the compulsivity test where each pellet delivery was associated with a punishment, an electric foot shock. Shock-associated cue corresponds to the number of non-reinforced active responses in 50 min in the following session after the shock test with the same discriminative stimulus (grid floor) as shock test in which pressing the active lever had no consequences: no shock, no reward delivery and no cue light (Unpaired t-test, * $P < 0.05$, ** $P < 0.01$).

We next investigated the neurophysiological fingerprints of addicted and extreme non-addicted phenotypes during decision-making and reward expectation. In order to discard behavioral variability in the duration of rewarding trials for reward obtainment between addicted and extreme non-addicted mice, we selected reward preceding epochs (5 lever presses + cue light and reward delivery) during FR5 sessions that lasted one to three seconds, as these epochs length were the most abundant during rewarding preceding trials (Figure 50).

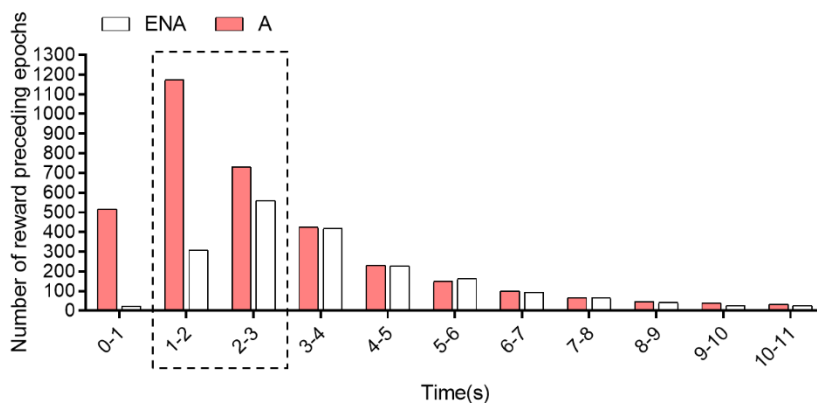


Figure 50. Sum of reward preceding epochs per duration of seconds in A and ENA mice. The dots dashed square indicates the duration of epochs selected for the analysis.

We considered decision-making epochs as 1s time windows occurring the second prior to the first of the five lever presses, just before the animal will press the lever (Figure 51).

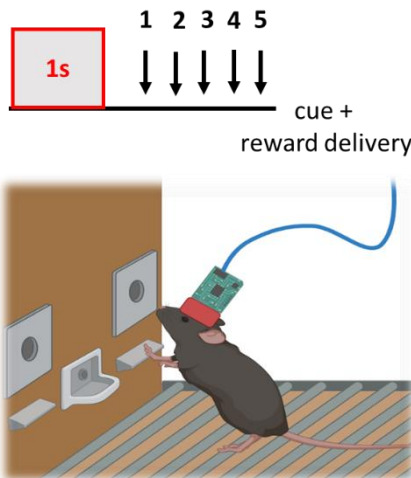


Figure 51. Schematic diagram illustrating decision-making epochs. Decision-making epochs were considered as 1s time windows occurring the second prior to the first of the five lever presses in reward preceding trials (5 lever presses + cue light and reward delivery).

During decision-making epochs, the power in the PL mPFC and in the NAc core was similar between extreme non-addicted and addicted mice and no significant differences were found at any frequency (Figure 52A). Differently, circuit communication measures revealed that hgamma and hfo were modified during decision-making in these subgroups of mice. Indeed, we found that extreme non-addicted mice displayed a NAc core to PL mPFC signaling at hgamma frequencies and a PL mPFC to NAc core communication at higher frequencies. However, addicted mice presented an opposite predominance of hgamma signaling (PL mPFC to NAc core PSI, PL mPFC leads) (Unpaired t-test, $P < 0.05$) and no clear directionality at higher frequencies was determined (Figure

52B). These results suggest that the directionality of these signals was disrupted in addicted mice. In contrast, addicted mice showed normal circuit communication at lower frequencies (Figure 52C).

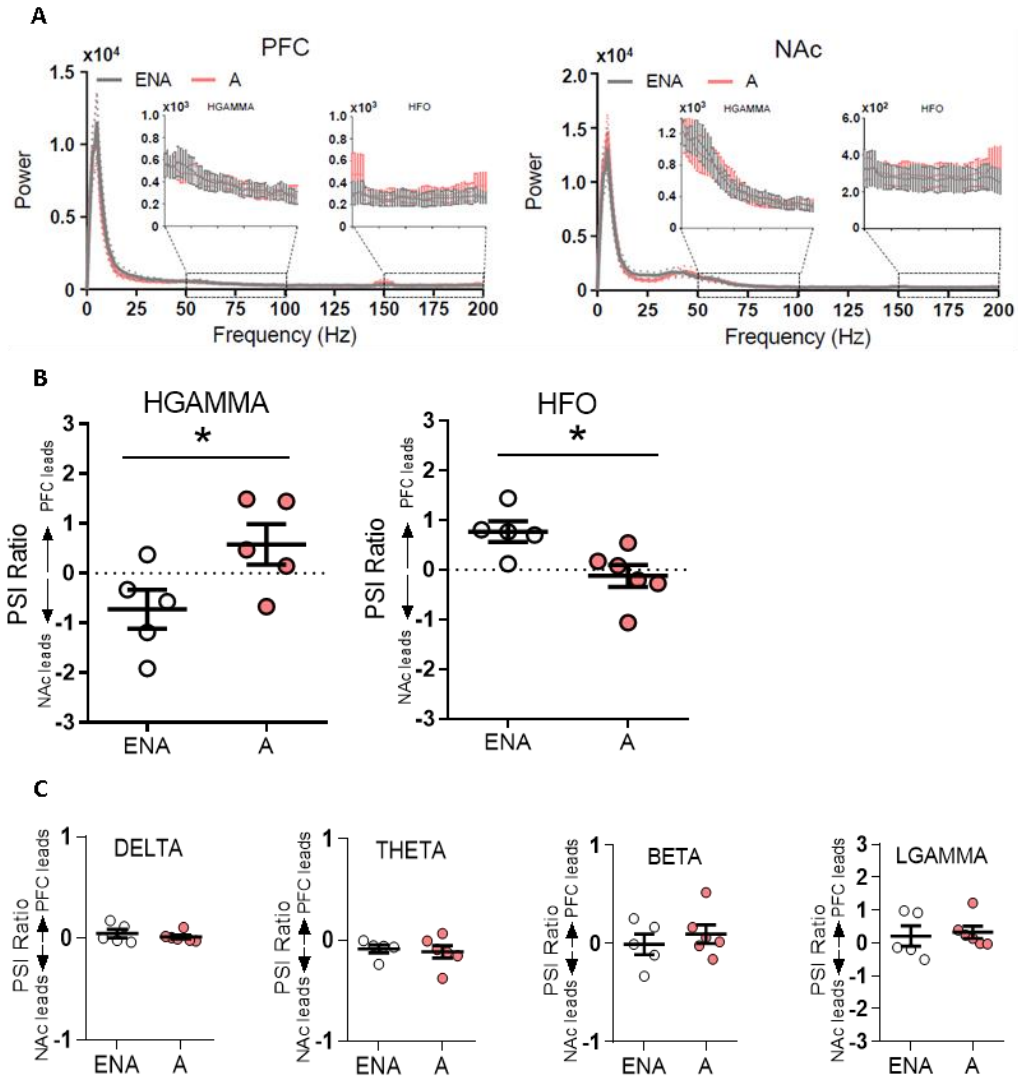


Figure 52. (A) Power spectra of neural signal in the PL mPFC (left) and the NAc core (right) in ENA and A mice during decision-making. Power values amplification of hgamma and hfo is also shown. (B) PL mPFC – NAc core circuit communication (PSI) at hgamma and hfo frequencies during decision-making. Data are represented as mean \pm SEM, Unpaired t-test, *P < 0.05. (C) PL mPFC – NAc core circuit communication (PSI) at delta, theta, beta and lgamma in ENA and A animals during decision-making.

Notably, a significant negative correlation was detected between the total number of reinforcers and the PL mPFC to NAc core hfo circuit communication (PSI) values when including both phenotypes (Pearson correlation, $P < 0.05$, Figure 53). Conversely, food intake and NAc core to PL mPFC hgamma communication (PSI) during decision-making did not correlate. These findings suggest that PL mPFC to NAc core connectivity is abnormal at hgamma and hfo ranges in addicted mice during decision-making and that hfo connectivity was associated with the number of reinforcers consumed.

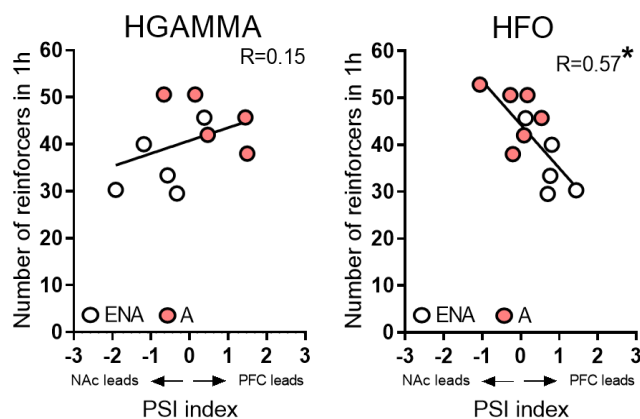


Figure 53. Pearson correlations between PL mPFC – NAc core circuit communication at hgamma (left) and hfo (right); and the number of reinforcers acquired in the FR5 operant sessions. PL mPFC to NAc core hfo PSI that emerged during decision making correlated negatively with reinforcement levels in ENA and A mice together. Differences are reported as mean \pm SEM, $*P < 0.05$.

With the aim of understanding neural synchrony in both phenotypes, we further investigated cross-frequency coupling between slow rhythms (1-16 Hz) and faster oscillations (50-250 Hz) both within the PL mPFC and the NAc core (local PAC or l-PAC: PL mPFC_{phase}-PL

mPFC_{amp} and NAc core_{phase}-NAc core_{amp}) and at the circuit level via coupling of NAc core phase with PL mPFC amplitude and vice versa (inter-regional PAC or ir-PAC: NAc core_{phase}-PL mPFC_{amp} and PL mPFC_{phase}-NAc core_{amp}). Coupling between the phase of slow oscillations with the amplitude of high-frequency oscillations was similar between phenotypes (Figure 54A-D).

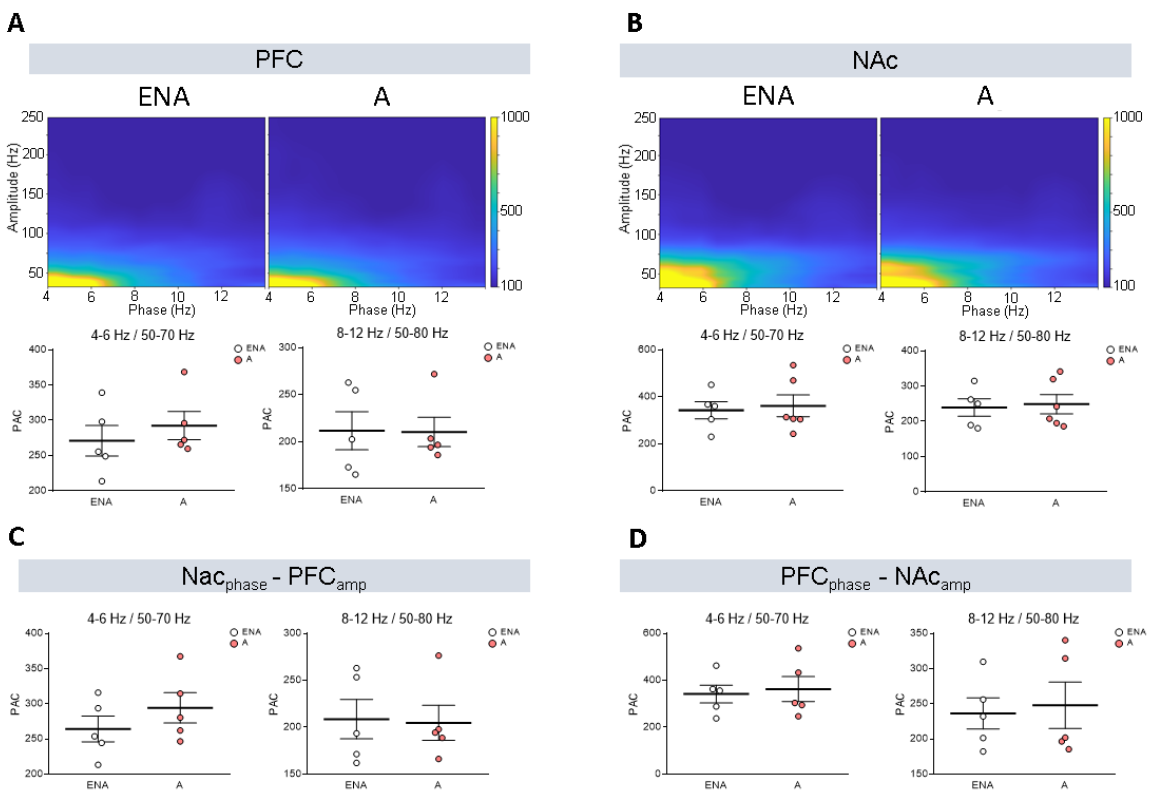


Figure 54. (A-D) Local and inter-regional cross-frequency coupling during decision-making (1s) in ENA and A mice. (A-B) Comodulation maps and quantification of delta-gamma and theta-gamma local coupling in the PL mPFC and the NAc core. The x-axis represents phase frequencies (4-14 Hz) and the y-axis represents amplitude frequencies (30-250 Hz). (C-D) Quantification of inter-regional modulation index between the NAc core phase (NAc core_p) and the PL mPFC amplitude (PL mPFC_a) and between the PL mPFC phase (PL mPFC_p) and the NAc core amplitude (NAc core_a).

We also investigated the differential neural substrates of reward expectation in addicted and extreme non-addicted mice. We considered reward expectation epochs as 1s time windows occurring the second immediately after the fifth lever press when the cue light turns on, and reward is delivered (Figure 55).

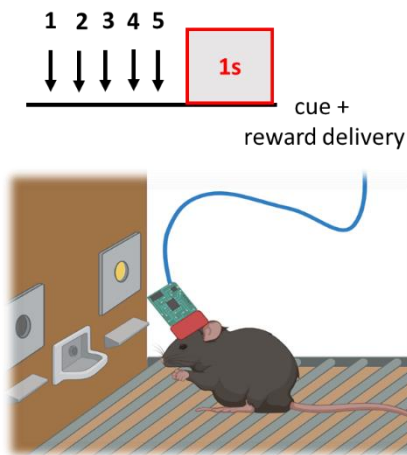


Figure 55. Schematic diagram illustrating reward expectation epochs. Reward expectation epochs were defined as the second occurring immediately after the fifth lever press, when the cue light turns on and reward is delivered.

During reward expectation epochs, no significant differences were observed in PL mPFC power between addicted and extreme non-addicted mice (Unpaired t-test, delta: $P = 0.22$; theta: $P = 0.52$, Figure 56A left, 56B left). However, addicted mice showed decreased power at lgamma frequencies in the NAc core (Unpaired t-test, $P < 0.01$, Figure 56B right, 56B right). Furthermore, we found that the power of NAc core lgamma oscillations during reward expectation correlated negatively with the number of reinforcers when including both genotypes (Pearson correlation, $P < 0.01$, Figure 56C). These results suggest that addicted mice present a disruption of NAc core

lgamma oscillations during expectation of reward, that may contribute to the elevated pellet intake behavior.

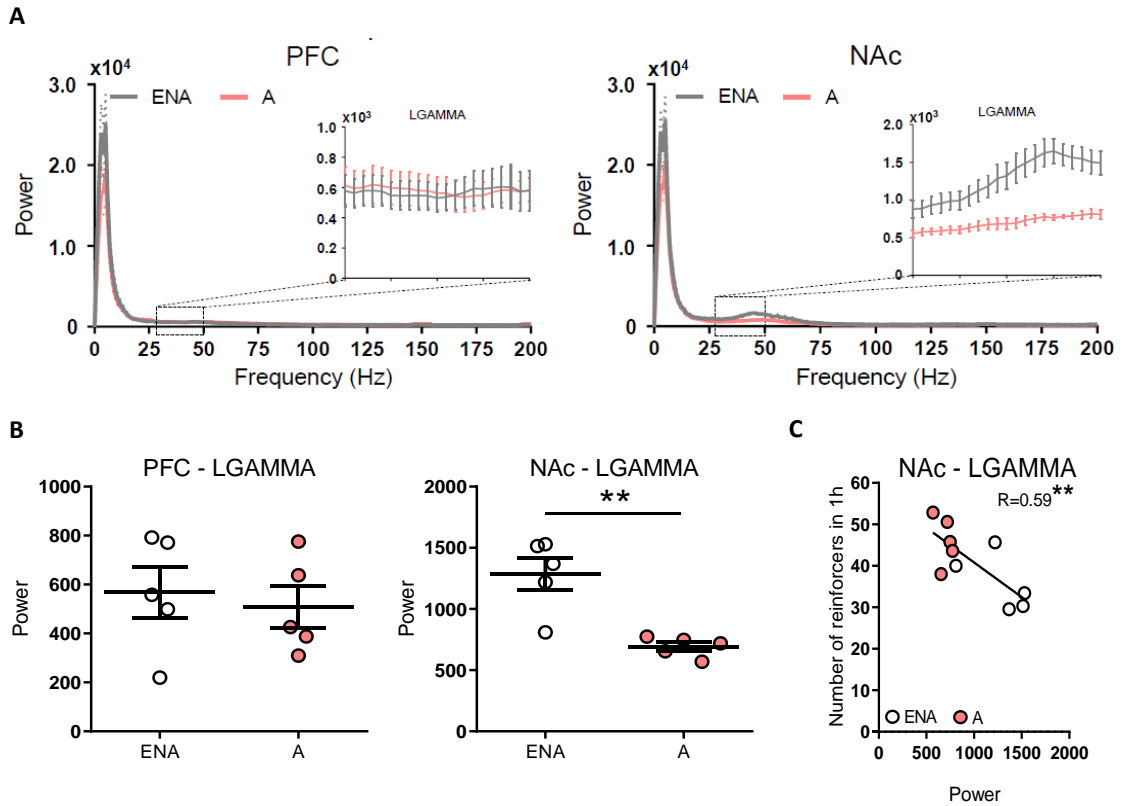


Figure 56. (A) Power spectra of neural signal in the PL mPFC (left) and the NAc core (right) in ENA and A mice during expectation of reward. Power values amplification of lgamma is also shown. (B) Corresponding quantification of lgamma power in the PL mPFC (left) and the NAc core (right) during expectation of reward. Data are represented as mean ± SEM, Unpaired t-test, **P < 0.01. (C) Pearson correlations between NAc core lgamma power and the number of reinforcers acquired in the FR5 operant sessions. Lgamma power negatively correlated with reinforcement levels in ENA and A mice together. Differences are reported as mean ± SEM, **P < 0.01.

In order to evaluate communication strength between the PL mPFC and NAc core during reward expectation, we quantified inter-

regional communication (PSI) in both phenotypes at this specific moment. Addicted animals showed normal PSI values with no significant differences being detected at any specific frequency range. In fact, a slight PL mPFC to NAc core signaling predominance was observed in both phenotypes at lgamma, hgamma and hfo (PL mPFC to NAc core PSI, PL mPFC leads) during the expectation of reward (Figure 57). These results indicate that the PL mPFC has a leading role in the communication between both areas during reward expectation, transferring neural signals to the NAc core at gamma and high frequencies.

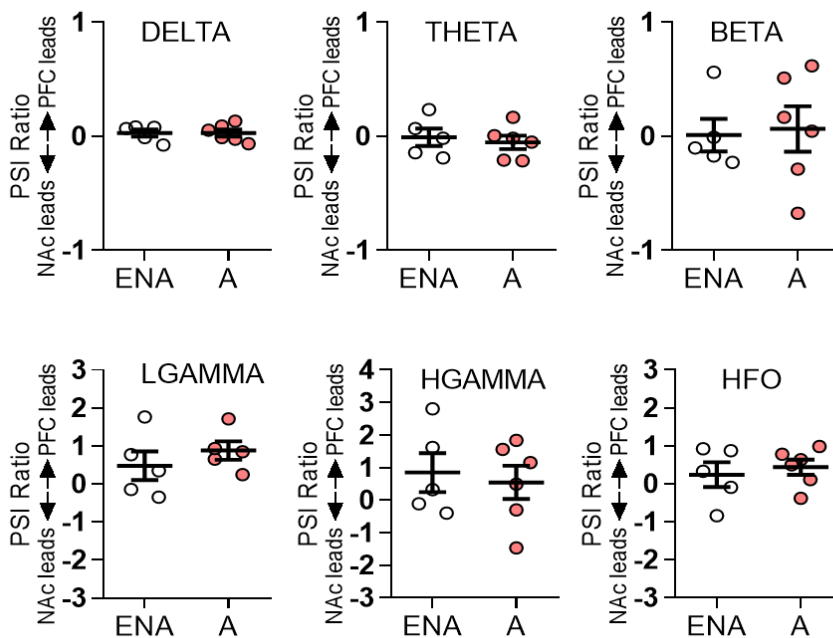


Figure 57. PL mPFC – NAc core circuit communication (PSI) at delta, theta, beta, lgamma, hgamma and hfo in ENA and A animals during expectation of reward.

We further investigated cross-frequency coupling during the expectation of reward. Correspondingly, theta-gamma coupling was reduced in the NAc core of addicted animals (Unpaired t-test, $P < 0.05$, Figure 58).

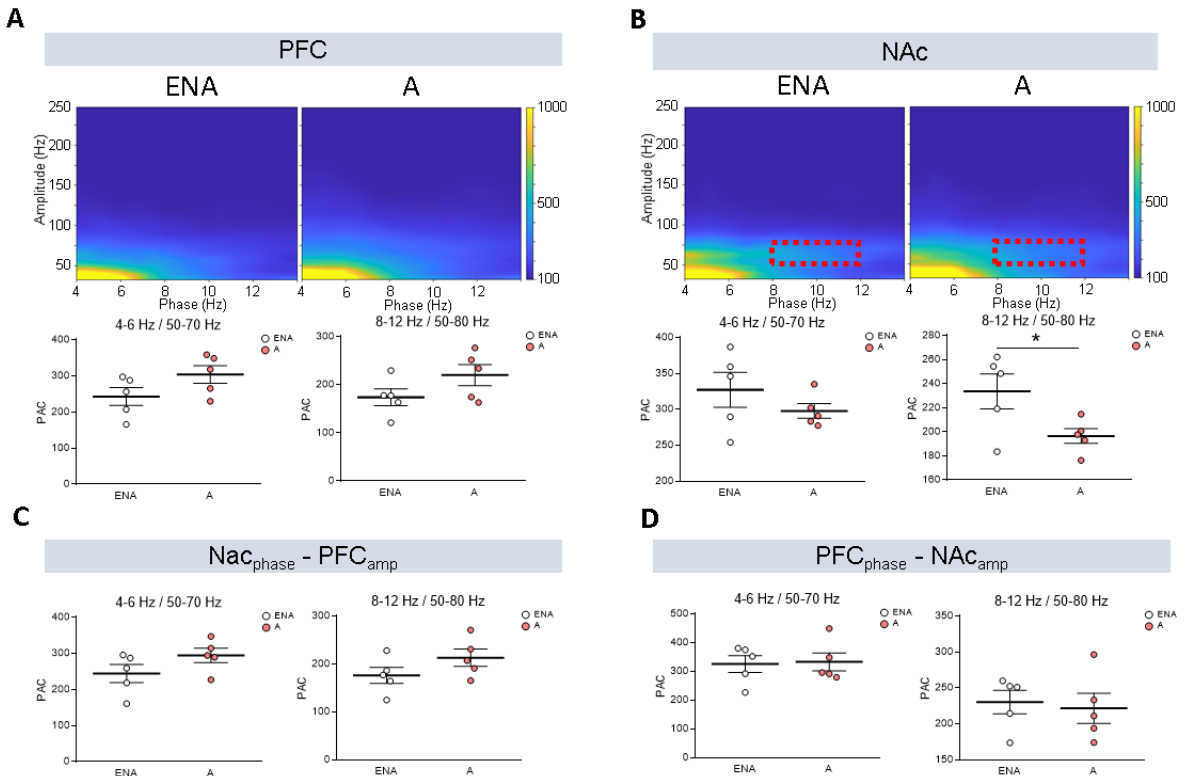


Figure 58. (A-D) Local and inter-regional cross-frequency coupling during reward expectation (1s) in ENA and A mice. (A-B) Comodulation maps and quantification of delta-gamma and theta-gamma local coupling in the PL mPFC and the NAc core (Unpaired t-test, $*P < 0.05$). The x-axis represents phase frequencies (4-14 Hz) and the y-axis represents amplitude frequencies (30-250 Hz). (C-D) Quantification of inter-regional modulation index between the NAc core phase (NAc core_p) and the PL mPFC amplitude (PL mPFC_a) and between the PL mPFC phase (PL mPFC_p) and the NAc core amplitude (NAc core_a).

Addicted mice exhibit abnormal prelimbic - nucleus accumbens core neural dynamics during rewarding periods.

Persistence of food-seeking behavior was measured by the responses for active lever presses during the 10 minutes of unavailability of pellet delivery, and this period (pellet-free period) was signaled by the illumination of the entire operant chamber. However, the pellet-free period was situated between two active periods (active period 1 and active period 2) of 25 minutes each one, where a cue light was turned on when the reward was delivered after the five active lever presses during rewarding periods. In order to gain insight on neural activity in the PL mPFC and the NAc core during the transition of these different periods of the operant FR5 session, we evaluated local power during the phase change from the first rewarding period (active period 1) to the beginning of the non-rewarding period (pellet-free period) and from the end of the pellet-free period to the beginning of the second rewarding period (active period 2). Changes between phases were analyzed in two seconds epochs (1s end reward to 1s start pellet-free period and 1s end pellet-free period to 1s start reward) (Figure 59).

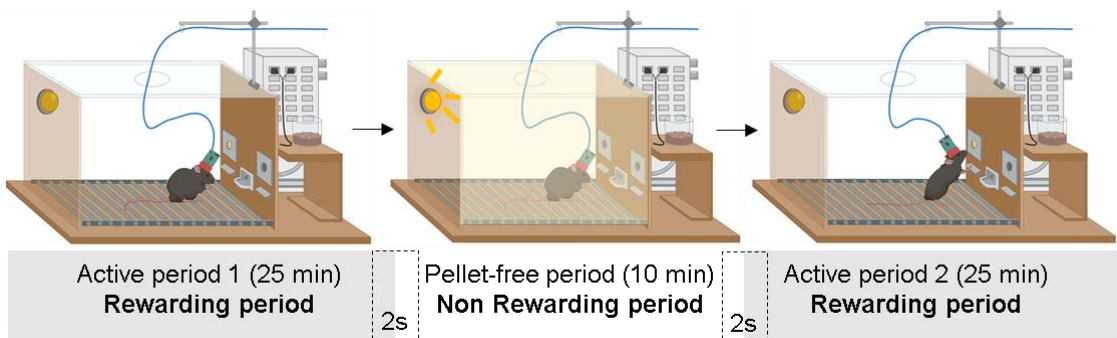


Figure 59. Schematic diagram illustrating the different periods of an FR5 operant session. The self-administration sessions are composed of two pellet periods (active periods) of 25 minutes separated by a pellet-free period of 10 minutes. During the pellet periods, pellets are delivered contingently after five active lever-presses paired with a cue light, whereas, during the pellet-free period, no pellet is delivered being this period signaled by the illumination of the entire self-administration chamber. Changes between phases were analyzed in two seconds epochs (1s end reward to 1s start pellet-free period and 1s end pellet-free period to 1s start reward).

Changes between periods were characterized by prominent hgamma and hfo in the PL mPFC and in the NAc core (Figure 60A-B). Local power at these frequency ranges was increased from the end of the reward to the start of the pellet-free period in the PL mPFC and in both areas, respectively (One-way ANOVA repeated measures, $P < 0.05$, $P < 0.01$, Figure 60C-D). Remarkably, during the pellet-free period (10 min), when no rewards were delivered, a decrease of PL mPFC and NAc core power was observed at delta, hgamma and hfo (One-way ANOVA repeated measures, $P < 0.05$, $P < 0.01$, $P < 0.001$, Figure 60C-D). Theta and beta oscillations were also reduced in the PL mPFC (One-way ANOVA repeated measures, $P < 0.05$, Figure 60C-D). Subsequently, at the beginning of the second active period (start reward), PL mPFC power at hgamma and hfo reached basal

levels (One-way ANOVA repeated measures, $P < 0.001$, $P < 0.05$, Figure 60 C-D). These power fluctuations across phases of the operant training session indicate that neural activity in both the PL mPFC and the NAc core may contribute to the encoding of relevant behaviors linked to persistence and reward. While changes in local PL mPFC and NAc core oscillations were identified during the different phase changes of the FR5 sessions, no significant differences were detected between addicted and extreme non-addicted mice (Figure 60C-D).

Results

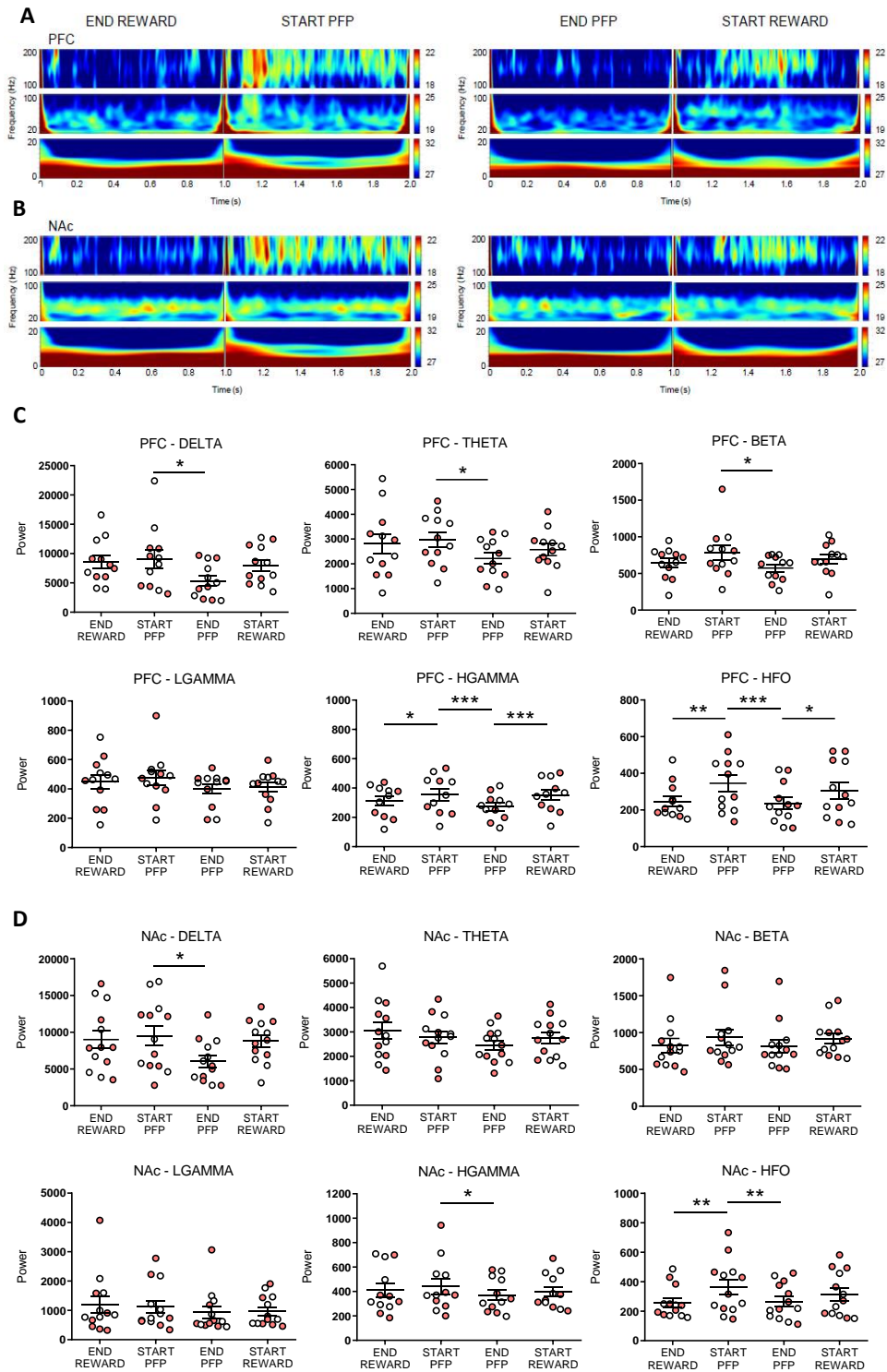


Figure 60. (A-B) Spectrograms of neural signals during the change between phases of the operant session (end reward to start PFP and end PFP to start reward) in the (A) PL mPFC and the (B) NAc core. The plots have been divided into 0-20, 20-100 and 100-200 Hz to facilitate the comparison. (C-D) Power quantification across phases of the operant session at delta, theta, beta, lgamma, hgamma and hfo in the (C) PL mPFC and the (D) NAc core. ENA mice correspond to white-colored dots, whereas A mice are represented with red-colored dots. Data are represented as mean \pm SEM, One-way ANOVA repeated measures, *P < 0.05, **P < 0.01, ***P < 0.001.

To find valuable neurophysiological biomarkers that differentiate addictive-like behaviors from resilient phenotypes during the different phases of the FR5 sessions, we assessed PL mPFC to NAc core circuit communication in each of the phases (end reward, start pellet-free period, end pellet-free period, start reward), as above. Remarkably, circuit communication analyses indicated a flow of information at lgamma and hgamma from the PL mPFC to the NAc core in extreme non-addicted mice (PL mPFC to NAc core PSI, PL mPFC leads) during rewarding periods (end reward). By contrast, addicted mice showed a predominance of lgamma and hgamma signaling that originated in the NAc core and traveled to the PL mPFC (NAc core to PL mPFC PSI, NAc core leads) during the same session periods (Unpaired t-test, $P < 0.05$, $P < 0.001$, Figure 61). These observations suggest that food sensitivity to reward might be encoded by lgamma and hgamma communication in PL mPFC to NAc core connectivity. Fluctuations of lgamma and hgamma signals in PL mPFC to NAc core circuits were frequency-specific at the end of rewarding periods and did not occur at other bands and periods (Figure 61).

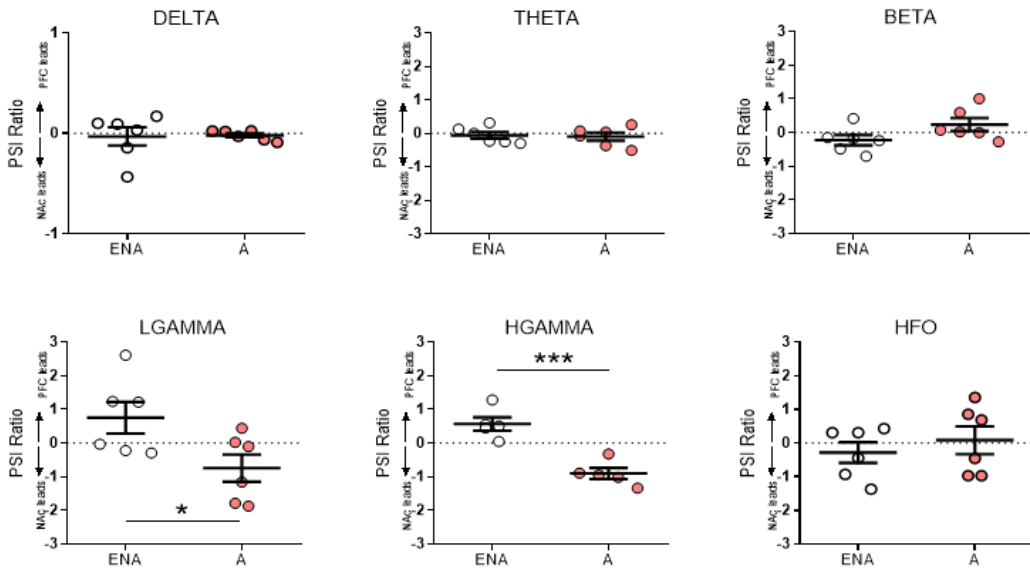


Figure 61. PL mPFC to NAc core circuit communication (PSI) at theta, lgamma, hgamma and hfo frequencies in ENA and A mice during the end of the rewarding period (end reward). Differences are reported as mean \pm SEM, Unpaired t-test, * $P < 0.05$, *** $P < 0.001$.

Correlations between circuit communication (PSI) and reward intake of the first rewarding period (active period 1) were examined to investigate this further. As expected, addicted mice showed more rewards and lever-presses than extreme non-addicted mice (Unpaired t-test, $P < 0.01$, $P < 0.01$, Figure 62).

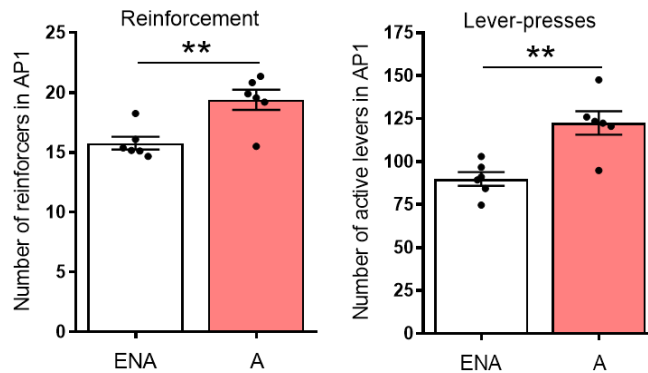


Figure 62. Behavioral data of reinforcement levels and the number of lever-presses in the first active period (AP1). Differences are reported as mean \pm SEM, Unpaired t-test, ** $P < 0.01$.

We found that PL mPFC - NAc core communication at hgamma, but not lgamma, correlated negatively with the number of reinforcers and active levers obtained in the first rewarding period, including both extreme genotypes (Pearson correlation, $P < 0.001$, Figure 63). Therefore, hgamma circuit connectivity seemed relevant for motivational values of rewards as it additionally significantly correlated with reinforcement and lever-presses in addicted mice (Pearson correlation, $P < 0.01$, $P < 0.05$, Figure 63).

Consistent with the literature (Goldstein and Volkow, 2011; Volkow and Morales, 2015; Scofield *et al.*, 2016), these evidence highlight the multifactorial concept of food addiction, suggesting that the NAc of addicted mice governs over the mPFC, whereas the mPFC of extreme non-addicted mice leads over the NAc. Furthermore, although electrophysiological signatures of the addictive-like

behavior were identified at the end of the first rewarding period, no more significant differences in circuit communication were found in the rest of the session periods analyzed (beginning pellet-free period, end pellet-free period, start reward) (Figure 64).

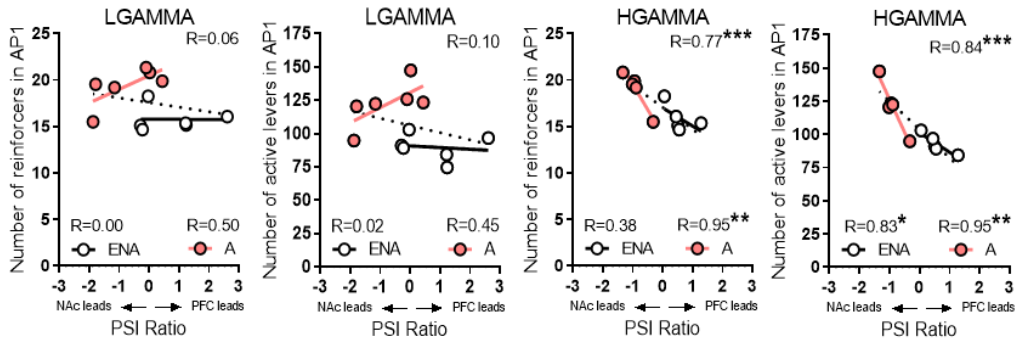


Figure 63. Pearson correlations between PL mPFC to NAc core circuit communication (PSI) at lgamma and hgamma bands; and behavioral data (number of reinforcers and lever-presses) acquired in the AP1 of the FR5 operant sessions. PL mPFC – NAc core communication at hgamma correlated with behavioral data in ENA and A mice together (marked with black dotted line) and separately (marked with a black line for ENA mice and with a red line for A mice). Differences are reported as mean \pm SEM, * $P < 0.05$, ** $P < 0.01$, *** $P < 0.001$.

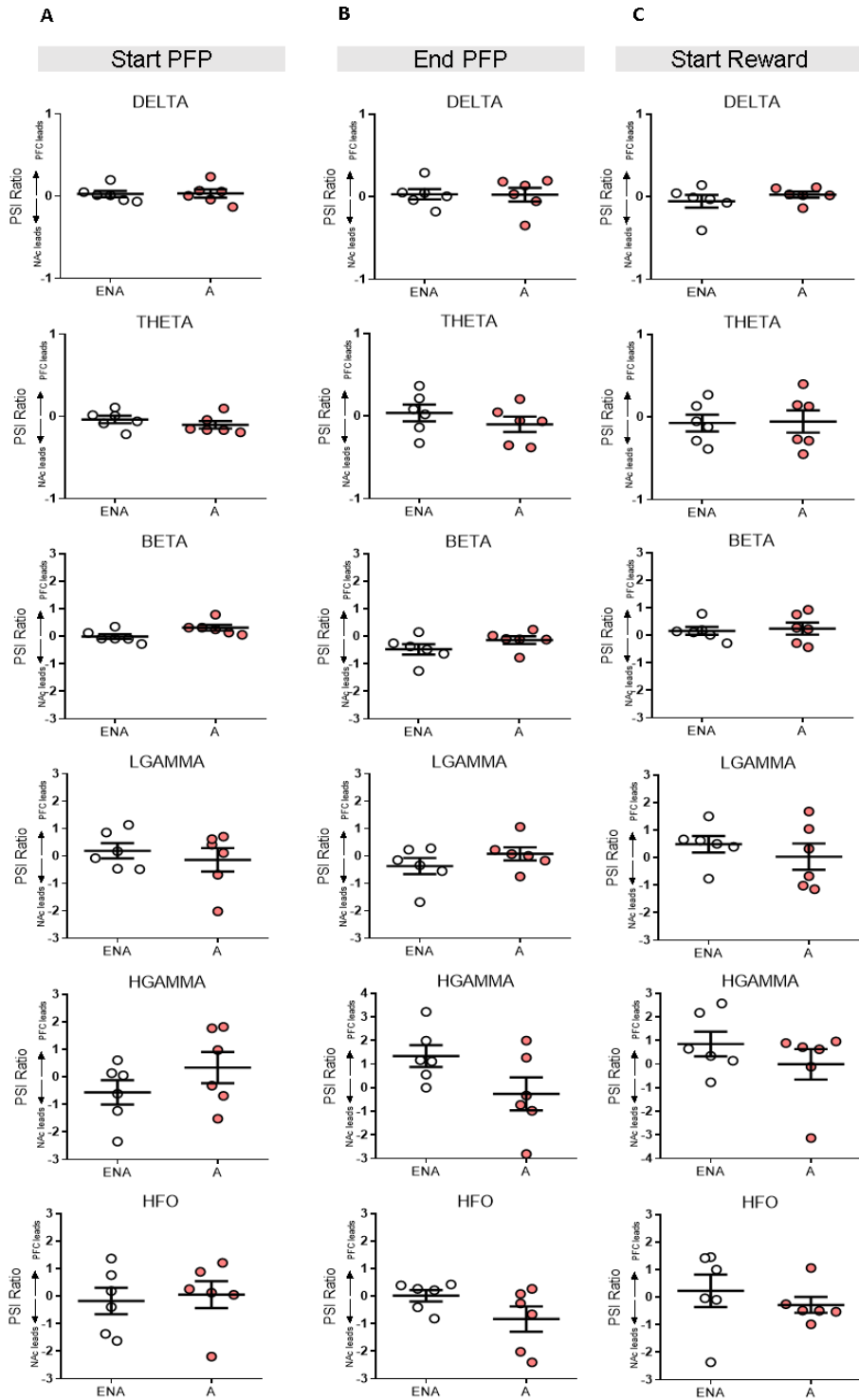


Figure 64. (A-C) PL mPFC to NAc core circuit communication (PSI) at delta, theta, beta, lgamma, hgamma and hfo frequencies in ENA and A mice during the (A) start of the pellet-free period, the (B) end of the pellet-free period, and the (C) beginning of the second active period (AP2) (start reward). Differences are reported as mean \pm SEM.

Supplementary Table 1.

Identification of extreme phenotypes of vulnerability and resilience to food addiction by long-term operant training.				
<i>Figure number</i>	<i>Statistical analysis</i>	<i>Factor name</i>	<i>Statistic value</i>	<i>P-value</i>
Figure 38	One-way ANOVA repeated measures	Operant training Time	F(115,3503)=15.49	P < 0.0001
Figure 40A	U Mann-Whitney	Early Period Persistence of response	U=83	n.s
Figure 40B	U Mann-Whitney	Early Period Motivation	U=77.50	n.s
Figure 40C	U Mann-Whitney	Early Period Compulsivity	U=86.50	n.s
Figure 40D	U Mann-Whitney	Late Period Persistence of response	U=28.50	P < 0.01
Figure 40E	U Mann-Whitney	Late Period Motivation	U=21.50	P < 0.001
Figure 40F	U Mann-Whitney	Late Period Compulsivity	U=65	n.s
Figure 41A	U Mann-Whitney	FR1 FR5 Early Period FR5 Late Period	U=84 U=97 U=42.50	n.s n.s P < 0.05
Figure 41B	U Mann-Whitney	FR1 FR5 Early Period FR5 Late Period	U=83.50 U=75 U=30.50	n.s n.s P < 0.01
Figure 41C	U Mann-Whitney	FR1 FR5 Early Period FR5 Late Period	U=80.50 U=67.50 U=38	n.s n.s P < 0.01
Figure 41D	U Mann-Whitney	Early Period Basal Shock Shock associated cue	U=75 U=97.50 U=56	n.s n.s n.s
Figure 41E	U Mann-Whitney	Late Period Basal Shock Shock associated cue	U=30.50 U=68 U=61	P < 0.01 n.s n.s
Figure 42A	2-WAY ANOVA	Bodyweight Phenotype Weeks Phenotype x Weeks	F(1, 319)=6.383 F(10, 319)=22.59 F(10,319)=0.1146	P < 0.05 P < 0.0001 n.s
Figure 42B	U Mann-Whitney	Bodyweight Phenotype	U=85	n.s

Supplementary Table 2.

Prelimbic-nucleus accumbens core gamma circuit communication signals are disrupted in addicted mice during decision-making and reward expectation.				
<i>Figure number</i>	<i>Statistical analysis</i>	<i>Factor name</i>	<i>Statistic value</i>	<i>P-value</i>
Figure 45	Unpaired t-test	Locomotion	t=0.5975	n.s
Figure 46	Unpaired t-test	PL mPFC power Delta Theta NAc core power Lgamma Hgamma PL mPFC vs NAc core (power) Lgamma Hgamma	t=1.191 t=0.5134 t=0.5443 t=0.7996 t=2.505 t=1.437	n.s n.s n.s n.s P < 0.05 n.s
Figure 47	Unpaired t-test	PSI Delta Theta Beta Lgamma Hgamma Hfo	t=0.3545 t=0.1721 t=1.352 t=0.01869 t=0.3517 t=0.02014	n.s n.s n.s n.s n.s n.s
Figure 48A	Unpaired t-test	Reinforcement	t=4.732	P < 0.0001
Figure 48B	Unpaired t-test	Reinforcement	t=3.927	P < 0.01
Figure 48C	Unpaired t-test	Lever-presses	t=3.658	P < 0.01
Figure 48D	Unpaired t-test	Impulsivity	t=2.772	P < 0.05
Figure 48E	Unpaired t-test	Persistence	t=1.427	n.s
Figure 49A	Unpaired t-test	FR1 FR5 Early Period FR5 Late Period FR5 Post-surgery	t=0.1063 t=0.6800 t=2.643 t=3.376	n.s n.s P < 0.05 P < 0.01
Figure 49B	Unpaired t-test	FR1 FR5 Early Period FR5 Late Period FR5 Post-surgery	t=0.1805 t=0.3339 t=3.386 t=3.658	n.s n.s P < 0.01 P < 0.01
Figure 49C	Unpaired t-test	FR1 FR5 Early Period FR5 Late Period FR5 Post-surgery	t=0.2975 t=0.1168 t=2.798 t=2.772	n.s n.s P < 0.05 P < 0.05
Figure 49D	Unpaired t-test	Early Period Basal Shock	t=0.3339 t=0.4105	n.s n.s

Results

		Shock associated cue	t=1.079	n.s
Figure 49E	Unpaired t-test	Early Period Basal Shock Shock associated cue	t=3.386 t=2.123 t=2.407	P < 0.01 P < 0.05 P < 0.01
Figure 52A	Unpaired t-test	PL mPFC Power Hgamma Hfo NAc core Power Hgamma Hfo	t=0.08792 t=0.4008 t=0.06407 t=0.1279	n.s n.s n.s n.s
Figure 52B	Unpaired t-test	PSI Hgamma Hfo	t=2.309 t=2.879	P < 0.05 P < 0.05
Figure 52C	Unpaired t-test	PSI Delta Theta Beta Lgamma	t=0.7386 t=0.3664 t=0.7337 t=0.3315	n.s n.s n.s n.s
Figure 53	Pearson correlation	PSI Hgamma Hfo	R=0.1413 R=0.5742	n.s P < 0.05
Figure 54A	Unpaired t-test	PAC PL mPFC Delta/Gamma Theta/Gamma	t=0.7250 t=0.0493	n.s n.s
Figure 54B	Unpaired t-test	PAC NAc core Delta/Gamma Theta/Gamma	t=0.3150 t=0.2474	n.s n.s
Figure 54C	Unpaired t-test	PAC NAc corep-PL mPFCa Delta/Gamma Theta/Gamma	t=1.064 t=0.139	n.s n.s
Figure 54D	Unpaired t-test	PAC PL mPFCp-NAc corea Delta/Gamma Theta/Gamma	t=0.3252 t=0.2882	n.s n.s
Figure 56A-B	Unpaired t-test	PL mPFC Power Lgamma NAc core power Lgamma	t=0.4479 t=4.336	n.s P < 0.01

Results

Figure 56C	Pearson correlation	NAC core Power Lgamma	R=0.5893	P < 0.01
Figure 57	Unpaired t-test	PSI Delta Theta Beta Lgamma Hgamma Hfo	t=0.02118 t=0.4621 t=0.2085 t=0.8999 t=0.3846 t=0.5305	n.s n.s n.s n.s n.s n.s
Figure 58A	Unpaired t-test	PAC PL mPFC Delta/Gamma Theta/Gamma	t=1.749 t=1.642	n.s n.s
Figure 58B	Unpaired t-test	PAC NAC core Delta/Gamma Theta/Gamma	t=1.123 t=2.356	n.s P < 0.05
Figure 58C	Unpaired t-test	PAC NAC corep-PL mPFCa Delta/Gamma Theta/Gamma	t=1.588 t=1.507	n.s n.s
Figure 58D	Unpaired t-test	PAC PL mPFCp-NAC corea Delta/Gamma Theta/Gamma	t=0.1786 t=0.3242	n.s n.s

Supplementary Table 3.

Addicted mice exhibit abnormal prelimbic-nucleus accumbens core neural dynamics during rewarding periods.				
<i>Figure number</i>	<i>Statistical analysis</i>	<i>Factor name</i>	<i>Statistic value</i>	<i>P-value</i>
Figure 60C	One-WAY ANOVA repeated measures	PL mPFC power		
		Delta		
		Phases	F(3,33)=3.714	P < 0.05
		Individuals	F(11,33)=4.196	P < 0.001
		End reward vs Start PFP		n.s
		End reward vs End PFP		n.s
		End reward vs Start reward		n.s
		Start PFP vs End PFP		P < 0.05
		Start PFP vs Start reward		n.s
		End PFP vs Start reward		n.s
		Theta		
		Phases	F(3,33)=2.828	n.s
		Individuals	F(11,33)=6.400	P < 0.0001
		End reward vs Start PFP		n.s
		End reward vs End PFP		n.s
		End reward vs Start reward		n.s
		Start PFP vs End PFP		P < 0.05
		Start PFP vs Start reward		n.s
		End PFP vs Start reward		n.s
		Beta		
		Phases	F(3,33)=2.269	n.s
Individuals	F(11,33)=6.071	P < 0.0001		
End reward vs Start PFP		n.s		
End reward vs End PFP		n.s		
End reward vs Start reward		n.s		
Start PFP vs End PFP		P < 0.05		
Start PFP vs Start reward		n.s		
End PFP vs Start reward		n.s		
Lgamma				
Phases	F(3,30)=1.662	n.s		
Individuals	F(10,30)=12.56	P < 0.0001		
End reward vs Start PFP		n.s		
End reward vs End PFP		n.s		
End reward vs Start reward		n.s		
Start PFP vs End PFP		n.s		

Results

		Start PFP vs Start reward End PFP vs Start reward Hgamma Phases Individuals End reward vs Start PFP End reward vs End PFP End reward vs Start reward Start PFP vs End PFP Start PFP vs Start reward End PFP vs Start reward Hfo Phases Individuals End reward vs Start PFP End reward vs End PFP End reward vs Start reward Start PFP vs End PFP Start PFP vs Start reward End PFP vs Start reward	 $F(3,33)=10.87$ $F(11,33)=21.54$ $F(3,33)=8.214$ $F(11,33)=14.32$	n.s n.s $P < 0.0001$ $P < 0.0001$ $P < 0.05$ n.s n.s $P < 0.001$ n.s $P < 0.001$ $P < 0.001$ $P < 0.0001$ $P < 0.01$ n.s n.s $P < 0.001$ n.s $P < 0.05$
Figure 60D	One-WAY ANOVA repeated measures	NAc core power Delta Phases Individuals End reward vs Start PFP End reward vs End PFP End reward vs Start reward Start PFP vs End PFP Start PFP vs Start reward End PFP vs Start reward Theta Phases Individuals End reward vs Start PFP End reward vs End PFP End reward vs Start reward Start PFP vs End PFP Start PFP vs Start reward End PFP vs Start reward Beta	 $F(3,36)=3.560$ $F(12,36)=3.434$ $F(3,36)=1.822$ $F(12,36)=5.105$	 $P < 0.05$ $P < 0.01$ n.s n.s n.s $P < 0.05$ n.s n.s n.s $P < 0.0001$ n.s n.s n.s n.s n.s n.s

Results

		Phases Individuals	F(3,36)=1.293 F(12,36)=8.057	n.s P < 0.0001
		End reward vs Start PFP End reward vs End PFP End reward vs Start reward Start PFP vs End PFP Start PFP vs Start reward End PFP vs Start reward		n.s n.s n.s n.s n.s n.s
		Lgamma Phases Individuals	F(3,36)=1.292 F(12,36)=14.24	n.s P < 0.0001
		End reward vs Start PFP End reward vs End PFP End reward vs Start reward Start PFP vs End PFP Start PFP vs Start reward End PFP vs Start reward		n.s n.s n.s n.s n.s n.s
		Hgamma Phases Individuals	F(3,33)=10.87 F(11,33)=21.54	n.s P < 0.0001
		End reward vs Start PFP End reward vs End PFP End reward vs Start reward Start PFP vs End PFP Start PFP vs Start reward End PFP vs Start reward		n.s n.s n.s P < 0.05 n.s n.s
		Hfo Phases Individuals	F(3,36)=6.620 F(12,36)=15.25	P < 0.05 P < 0.0001
		End reward vs Start PFP End reward vs End PFP End reward vs Start reward Start PFP vs End PFP Start PFP vs Start reward End PFP vs Start reward		P < 0.01 n.s n.s P < 0.01 n.s n.s
Figure 61	Unpaired t-test	PSI End reward Delta Theta Beta Lgamma Hgamma	t=0.1199 t=0.2547 t=1.8590 t=2.4150 t=5.6950	n.s n.s n.s P < 0.05 P < 0.001

Results

		Hfo	t=0.7126	n.s
Figure 62	Unpaired t-test	Reinforcement Lever-presses	t=3.6270 t=4.1123	P < 0.01 P < 0.01
Figure 63	Pearson correlation	Lgamma Reinforcement All ENA A Lever-presses All ENA A Hgamma Reinforcement All ENA A Lever-presses All ENA A	R=0.06487 R=0.0001 R=0.4999 R=0.1040 R=0.02109 R=0.4486 R=0.7666 R=0.3791 R=0.9475 R=0.8404 R=0.8263 R=0.9492	n.s n.s n.s n.s n.s n.s P < 0.001 n.s P < 0.01 P < 0.001 P < 0.05 P < 0.01
Figure 64	Unpaired t-test	PSI Start PFP Delta Theta Beta Lgamma Hgamma Hfo End PFP Delta Theta Beta Lgamma Hgamma Hfo Start Reward Delta Theta Beta Lgamma Hgamma Hfo	t=0.09459 t=1.013 t=1.340 t=0.6498 t=1.260 t=0.3404 t=0.05588 t=0.9906 t=1.426 t=1.165 t=1.909 t=1.690 t=0.9380 t=0.1073 t=0.3224 t=0.8069 t=1.037 t=0.7812	n.s n.s n.s n.s n.s n.s n.s n.s n.s n.s n.s n.s n.s n.s n.s n.s n.s n.s

1.2. Electrophysiological characterization of CB₁ antagonism in extreme non-addicted and addicted mice.

CB₁ receptors shape prefrontal – accumbens neural dynamics.

We aimed to investigate the acute effects of CB₁ antagonism on addictive-like behavior and prelimbic-nucleus accumbens core neural dynamics. A selective blocker of CB₁ receptors, rimonabant (3 mg/kg) was acutely administered to mice freely moving in a cage. Electrophysiological recordings were also performed to study the time-course of rimonabant's effect on PL mPFC - NAc core neurodynamics at 1, 16, and 19 minutes after rimonabant administration (n=4-6 addicted mice and n=5 extreme non-addicted mice). Rimonabant administration induced modest alterations in neural oscillations (Figure 65A-B) that did not affect locomotor activity (Figure 66).

In order to describe the electrophysiological effects of rimonabant in the PL mPFC and the NAc core independently of the addictive-like behavior, we quantified power in both areas, including addicted and extreme non-addicted mice together. Differences in power were observed between control and treated animals in the PL mPFC and the NAc core after 19 minutes of administration independent of addiction (Figure 67).

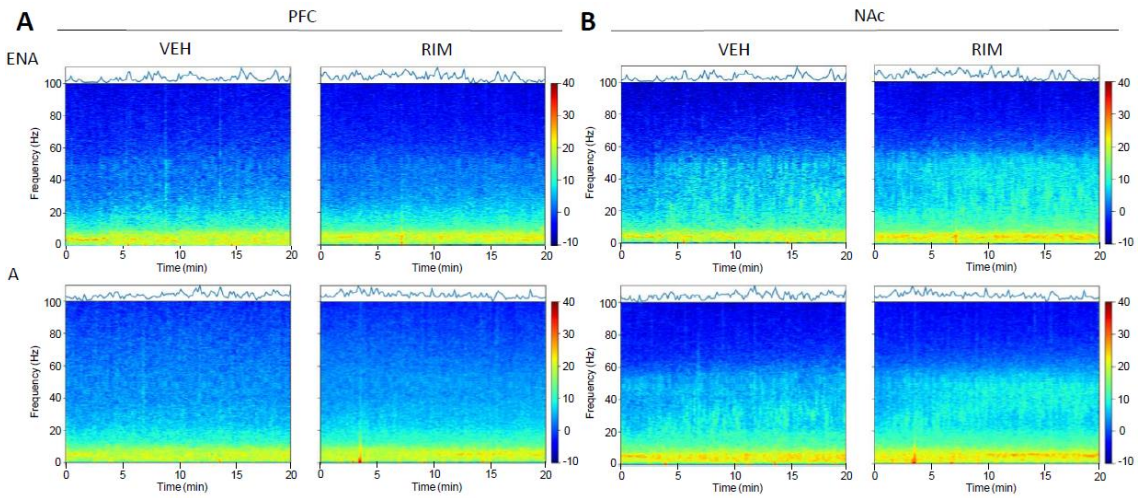
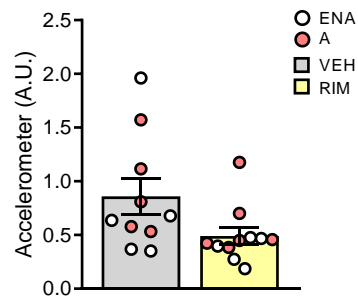


Figure 65. (A-B) Averaged spectrograms of signals of ENA and A mice under vehicle and rimonabant administration in the (A) PL mPFC and the (B) NAc core. Panels represent the raw data with the corresponding quantification of the animal's motility (accelerometer, variance of signals from the accelerometer integrated within headstages).

Figure 66. Locomotor activity in ENA (white dots) and A (red dots) mice during 20 min recordings in the standard cage after vehicle (grey) or rimonabant (yellow) administration. Accelerometer, variance of signals from the accelerometer integrated within the headstages. The corresponding quantification of the animal's mobility is presented as a ratio to the highest value in the baseline condition.



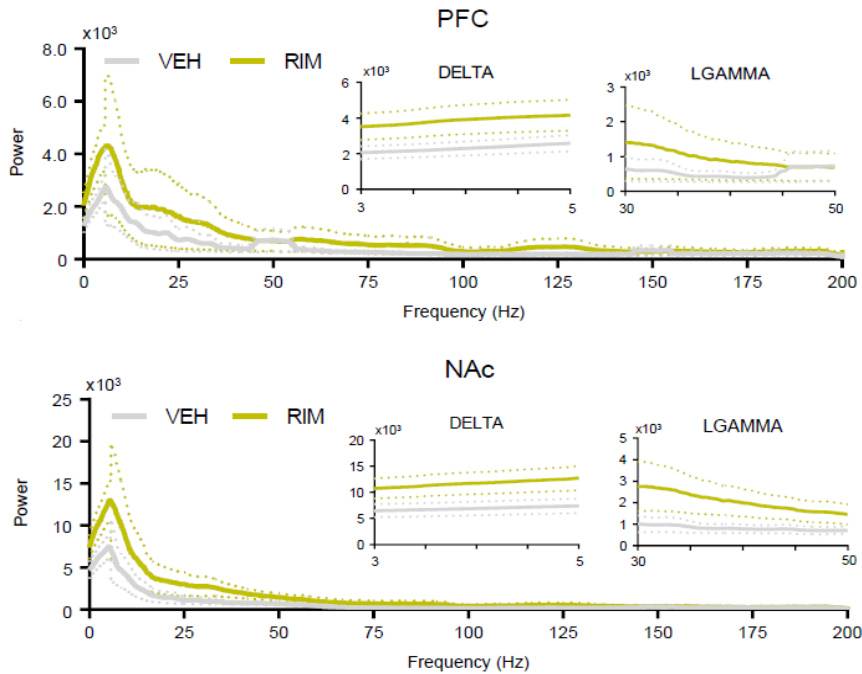


Figure 67. Power spectra of PL mPFC (top) and NAc core (down) signals at the 19th minute after administration of vehicle (grey) or rimonabant (yellow). Power values amplification of delta and lgamma are also shown.

Rimonabant progressively increased the delta band in the PL mPFC and the NAc core of both phenotypes compared to the vehicle (Two-way ANOVA multiple comparisons, $P < 0.05$, $P < 0.01$, Figure 67 and Figure 68). Additionally, rimonabant- treated animals showed a lgamma power amplification in the NAc core, but not in the PL mPFC (Two-way ANOVA, $P < 0.05$, $P < 0.01$, Figure 67 and Figure 68).

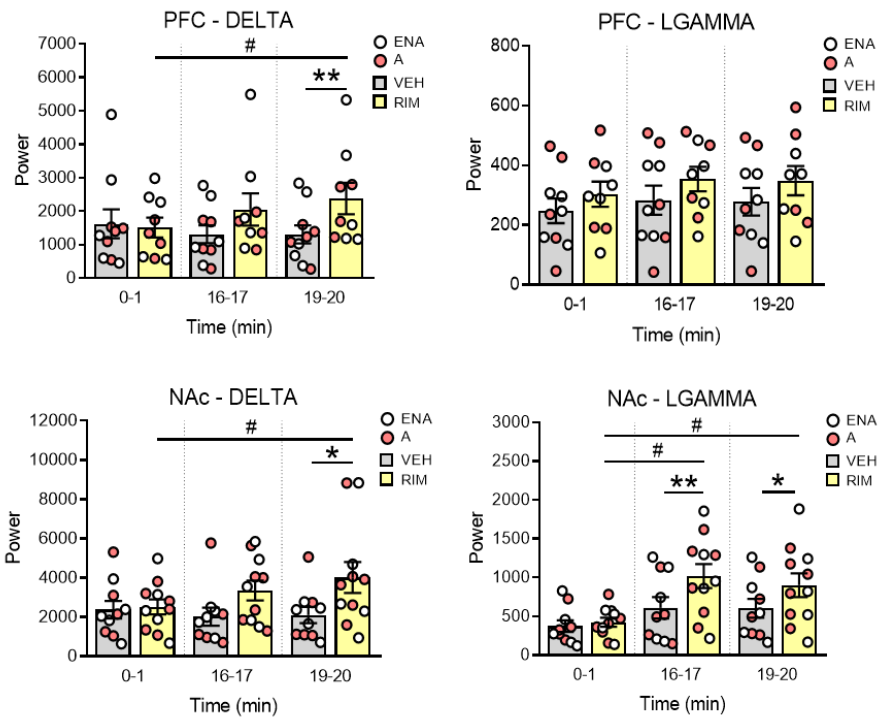


Figure 68. Corresponding power quantification of delta and lgamma frequencies across time (0-1, 16-17 and 19-20 min after administration of vehicle or rimonabant) in the PL mPFC (top) and the NAc core (down). ENA mice are represented with white colored dots whereas A mice are represented with red colored dots. Differences are reported as mean \pm SEM, Two-way ANOVA multiple comparisons, *P < 0.05, **P < 0.01, #P < 0.05.

The rest of the frequency bands followed a similar power pattern compared to the vehicle, both in the PL mPFC (Figure 69 left) and the NAc core (Figure 69 right).

Results

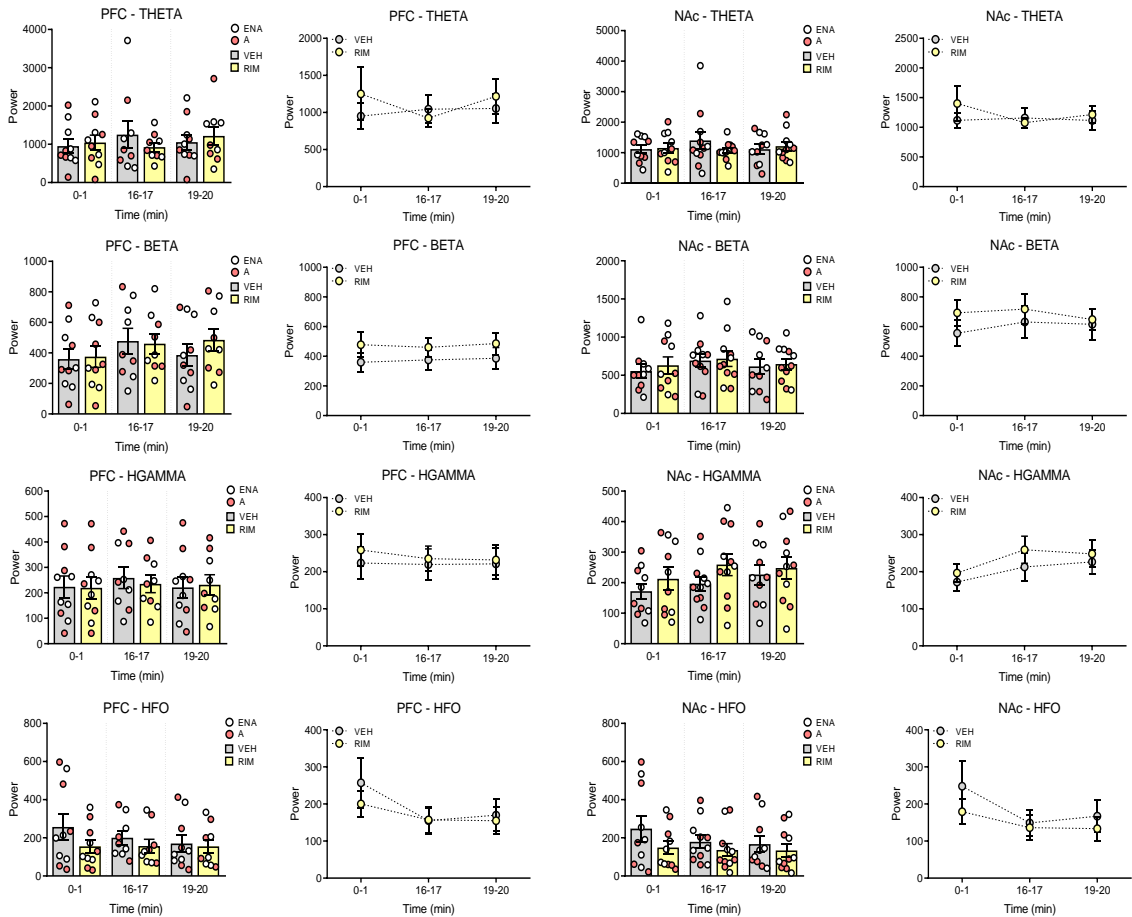


Figure 69. Power quantification of theta, beta, hgamma and hfo frequencies across time (0-1, 16-17 and 19-20 min after administration of vehicle or rimonabant) in the PL mPFC (left) and the NAc core (right). Within areas, in the left, power quantification by individual values (ENA and A mice) with the mean and \pm SEM. In the right, power quantification considering ENA and A mice as a unique experimental group. Differences are reported as mean \pm SEM.

To further assess circuit communication, we quantified circuit communication (PSI) and cross-frequency phase-amplitude coupling (PAC) under the administration of rimonabant. Remarkably, no significant differences were found in the circuit communication

measures (PSI) of the diverse frequency bands across time (Figure 70).

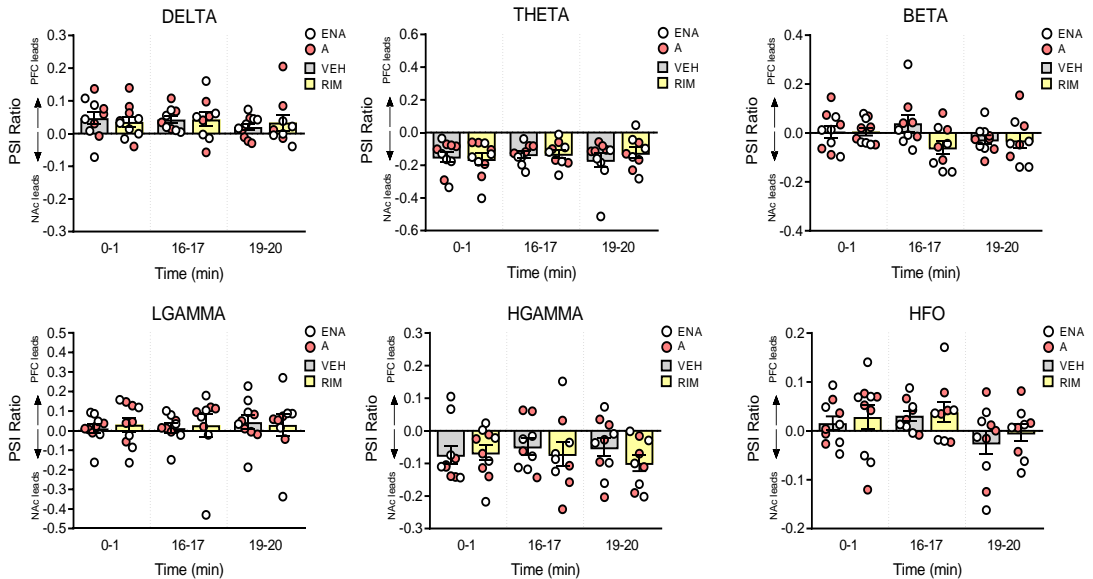


Figure 70. PL mPFC to NAc core circuit communication (PSI) at delta, theta, beta, lgamma, hgamma and hfo frequencies in ENA and A mice across time (0-1, 16-17 and 19-20 min after administration of vehicle or rimonabant). Data is reported as mean \pm SEM.

We further investigated cross-frequency coupling between slow rhythms (1-16 Hz) and faster oscillations (50-250 Hz) both within the PL mPFC and the NAc core (local PAC or l-PAC: PL mPFC_{phase}-PL mPFC_{amp} and NAc core_{phase}-NAc core_{amp}) and at the circuit level via coupling of NAc core phase with PL mPFC amplitude and vice versa (inter-regional PAC or ir-PAC: NAc core_{phase}-PL mPFC_{amp} and PL mPFC_{phase}-NAc core_{amp}). Locally in the PL mPFC, delta-hfo phase-amplitude coupling was detected, although no significant differences were observed between addicted and extreme non-addicted mice,

neither between rimonabant and vehicle treatments. By contrast, in the NAc core, addicted and extreme non-addicted mice exhibited robust delta-lgamma and delta-hfo coupling over time when treated with vehicle. After rimonabant, the delta-hfo (1-4 Hz with 150-250 Hz) coordination subsided after 19 minutes of drug administration (see panels marked with red dotted squares) (Paired t-test, $P < 0.05$, Figure 71 and Figure 72). At a circuit level, rimonabant effects were similar to those found in the NAc core. The phase of PL mPFC delta modulated the amplitude of NAc core hfo (PL mPFC_{phase}-NAc core_{amp}). As observed in the NAc core, rimonabant weakened this circuit coupling (Paired t-test, $P < 0.05$, Figure 71 and Figure 72). By contrast, no significant changes were detected for the reversed inter-regional coupling (that is, NAc core_{phase}-PL mPFC_{amp}) between the vehicle and rimonabant treated group. These findings demonstrate, yet again, a robust prefrontal-nucleus accumbens core communication that is sensitive to CB₁ pharmacological manipulation under basal conditions.

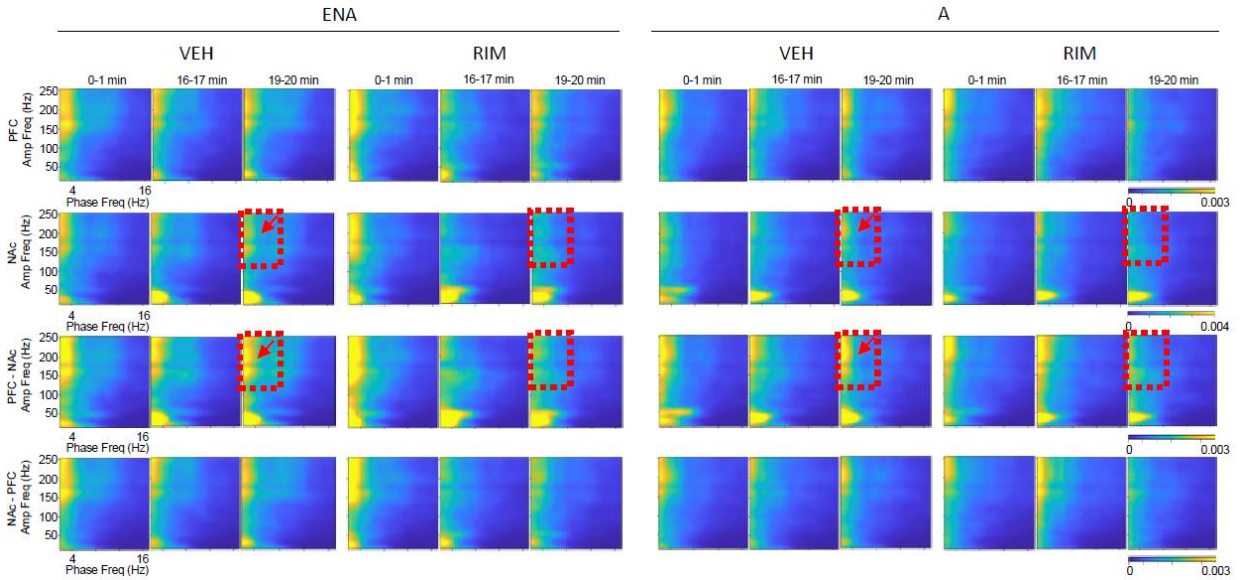


Figure 71. Comodulation maps quantifying local and inter-regional cross-frequency coupling in 1 minute periods (0-1, 16-17 and 19-20 min) in ENA and A mice. The x-axis represents phase frequencies (2-16 Hz) and the y-axis represents amplitude frequencies (10–250 Hz). Numbers on top indicate the minute after vehicle or rimonabant administration. In the top, local modulation index in the PL mPFC and the NAc core. In the bottom, inter-regional modulation index between the PL mPFC phase (PL mPFC_p) and the NAc core amplitude (NAc core_a) and between the NAc core phase (NAc core_p) and the PL mPFC amplitude (PL mPFC_a). The red dotted square indicates the coupling between delta and hfo present in normal conditions (vehicle), marked with a red arrow, that disappear after 19 minutes of rimonabant administration.

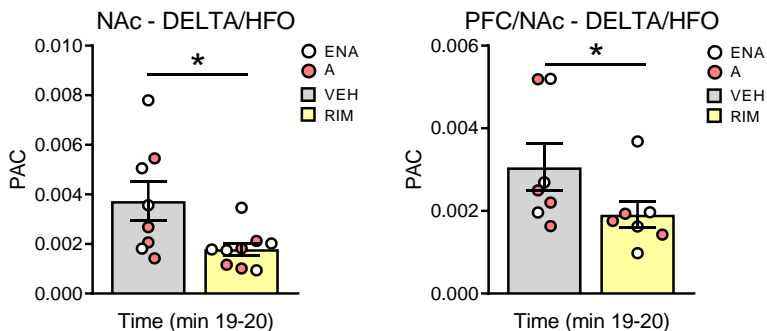


Figure 72. Corresponding quantification of local and inter-regional cross-frequency coupling in the 19-20 min period after administration in ENA and A mice. In the left, local NAc core delta-hfo coupling. In the right, inter-regional between PL mPFC phase (PL mPFC_p) and the NAc core amplitude (NAc core_a). Differences are reported as mean ±SEM, Paired t-test, *P < 0.05.

Next, we examined the firing rate of neuron populations (multi-unit activity, MUA) in addicted and extreme non-addicted mice and the differential effects of rimonabant treatment. Considering all animals, rimonabant decreased firing rates in population activity across time in the PL mPFC and the NAc core. NAc core firing rates also diminished in vehicle-treated animals (Two-way ANOVA multiple comparisons, $P < 0.05$, $P < 0.01$, Figure 73A left - B left). When dividing vehicle-treated animals by phenotype, addicted mice showed a similar PL mPFC firing rate pattern over time compared to extreme non-addicted mice (Figure 73A right). When treated with rimonabant, PL mPFC firing activity slightly decreased after 16 mins in extreme non-addicted mice and remained stable, close to the firing rate pattern of addicted mice (Two-way ANOVA multiple comparisons, $P < 0.05$, Figure 73A right). However, altered NAc core spiking activity was found in addicted animals. Remarkably, addicted mice showed a higher firing rate of population activity in comparison with extreme non-addicted mice when treated with vehicle (Two-way ANOVA repeated measures, $P < 0.05$, Figure 73B right). These results suggest that addicted mice, under basal conditions, have an altered increasing spiking activity of neuron population in the NAc core. However, when addicted mice were treated with rimonabant, the NAc core firing activity declined and reached the firing rate pattern of extreme non-addicted mice, correcting in this way the spiking activity alteration found in addicted mice (Figure 73B right).

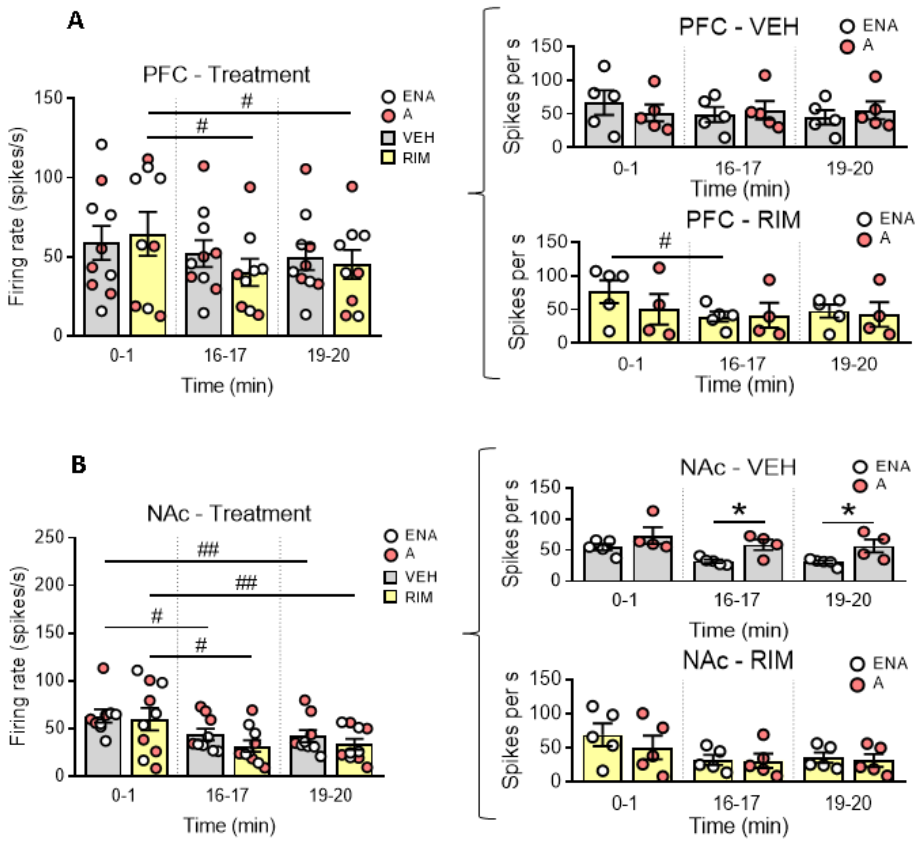


Figure 73. (A-B) Time-course of changes in the firing rate of neurons under vehicle and rimonabant treatment in the (A) PL mPFC and the (B) NAc core. Multi-unit activity was used in this analysis. Differences are reported as mean \pm SEM, Two-way ANOVA multiple comparisons, * $P < 0.05$, # $P < 0.05$, ## $P < 0.01$.

Altogether, the abnormal power, cross-frequency coupling and spiking activity unraveled a profound disruption of the NAc core microcircuitry oscillations and the prelimbic-nucleus accumbens core oscillation circuitry generated by rimonabant. By contrast, neural spiking activity alteration in addicted mice was corrected by blocking CB₁ receptors with rimonabant.

Rimonabant reduces reinforcement levels and restores abnormal prelimbic - nucleus accumbens core neural dynamics during decision-making and reward expectation.

We used rimonabant to investigate its putative therapeutical effects on addictive-like behavior and to rescue the potential of anomalous neural dynamics. Rimonabant was administered 30 minutes before the operant training session and neurophysiological recordings were performed during the entire FR5 session. Mice received a treatment alternated daily either with vehicle or rimonabant for four consecutive days (Figure 37a). As reported in previous studies (Maccioni *et al.*, 2008; Mancino *et al.*, 2015), the pharmacological effect of CB₁ antagonism had an impressive effect on addictive-like behavior. The number of reinforcers drastically decreased in addicted and extreme non-addicted mice compared to the vehicle group. (Mixed analysis ANOVA multiple comparisons, $P < 0.0001$, $P < 0.01$, Figure 74 left and Paired t-test, $P < 0.0001$, Figure 74 right).

We investigated if the effects of rimonabant were different in addicted and non-addicted mice. In addicted mice, reinforcement levels decreased to a percentage of 25.5% in comparison with basal levels. On the other hand, the number of reinforcers in treated non-addicted mice declined to levels close to 0 (Paired t-test, $P < 0.001$, Figure 75 left).

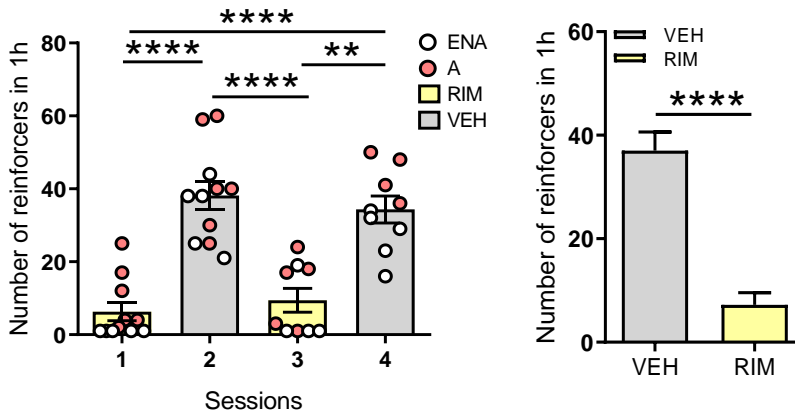


Figure 74. Reinforcement values of ENA and A mice under vehicle and rimonabant treatment. ENA mice are represented with white dots whereas A mice are shown with red dots. Grey bars indicate vehicle treatment and yellow bars indicate rimonabant treatment. In the left, number of reinforcers in 1h operant session during 4 consecutive days alternating vehicle and rimonabant administration. In the right, corresponding mean of reinforcement levels of the 2 sessions under vehicle and rimonabant administration assembling ENA and A mice together. Differences are reported as mean \pm SEM, Mixed analysis ANOVA multiple comparisons, ** $P < 0.01$, **** $P < 0.0001$ and Paired t-test, **** $P < 0.0001$.

Furthermore, in addicted mice, the decreased number of reinforcers consumed when treated with rimonabant correlated with the increase of NAc core γ power observed in the previous recordings performed in the cage (Pearson correlation, $P < 0.01$, Figure 75 right) and was not correlated in extreme non-addicted mice. This result suggests that NAc core γ oscillatory activity might play an important role in the regulation of high palatable food intake.

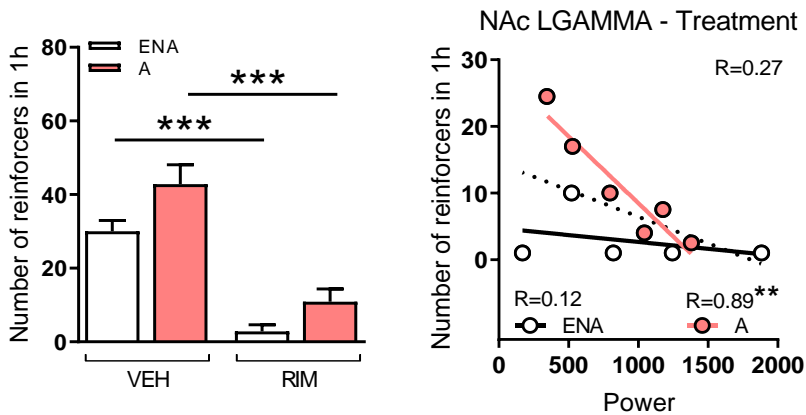


Figure 75. In the left, corresponding mean of reinforcement levels in ENA and A mice after vehicle and rimonabant administration. Data are represented as mean \pm SEM, Paired t-test, ***P < 0.001. In the right, Pearson correlation between the number of reinforcers in rimonabant treatment FR5 sessions and NAc core lgamma power increase observed after 19 minutes of rimonabant administration. Differences are reported as mean \pm SEM, **P < 0.01. The dotted line corresponds with linear regression of ENA and A mice together, whereas linear regressions in ENA and A mice separately are represented in black and red colored lines, respectively.

No correlation was detected between the decreased reinforcement levels and delta activity, neither in the PL mPFC nor in the NAc core (Figure 76).

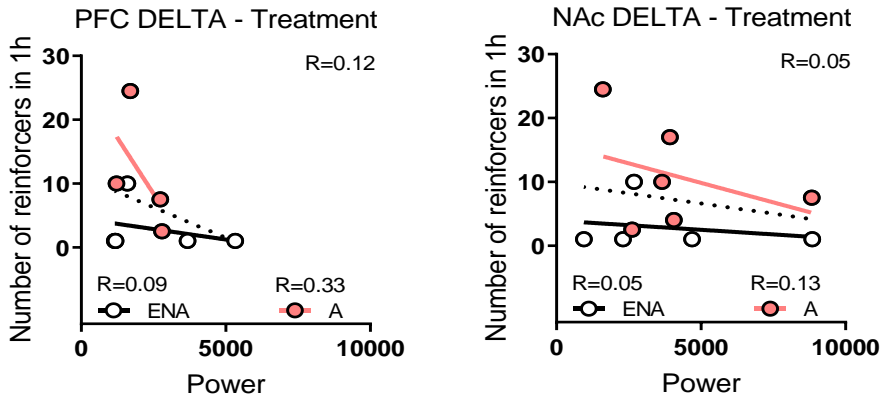


Figure 76. Pearson correlations between the number of reinforcers in rimonabant treatment FR5 sessions and delta power increase observed in the PL mPFC (left) and the NAc core (right) after 19 minutes of rimonabant administration. Differences are reported as mean \pm SEM. The dotted line corresponds with linear regression of ENA and A mice together, whereas linear regressions in ENA and A mice separately are represented in black and red colored lines, respectively.

Only one extreme non-addicted mouse had windows for electrophysiological analysis during rewarding preceding epochs (five lever-presses and reward delivery). Therefore, the lack of analysis windows in extreme non-addicted mice forced us to limit the study to the electrophysiological effects of rimonabant in only addicted mice.

We investigated the pharmacological effects of rimonabant on power activity and circuit communication during decision-making and reward expectation epochs. During decision-making periods, power in the PL mPFC of addicted mice did not vary when treated with rimonabant (Figure 77) while the power of hfo slightly decreased in the NAc core (Paired t-test, $P < 0.05$, Figure 77).

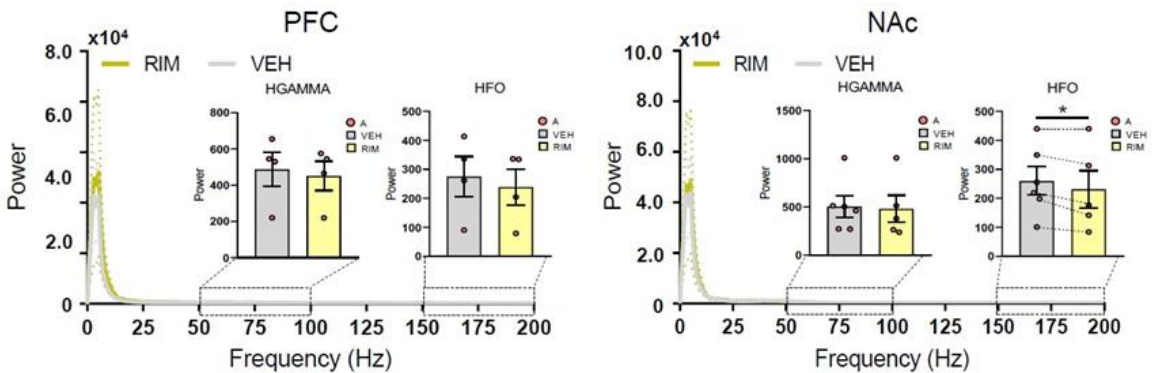


Figure 77. Power spectra of PL mPFC (left) and NAc core (right) signals during decision-making after administration of vehicle (grey) or rimonabant (yellow). The corresponding power quantification of hfo in the NAc core is also represented in the right. Red dots correspond to A animals. Data are represented as mean \pm SEM, Paired t-test, * $P < 0.05$.

In terms of neural information flow between the PL mPFC and the NAc core (PSI), we previously identified that NAc core-to-PL mPFC hgamma and PL mPFC-to-NAc core hfo signals were involved in decision-making in extreme non-addicted mice and were altered in addicted mice (Figure 52B and Figure 53). At high frequencies, the vehicle control group again displayed reversed directionality of signals compared with extreme non-addicted mice (NAc core to PL mPFC PSI, NAc core leads) (Unpaired t-test, $P < 0.05$, Figure 78). In rimonabant-treated addicted animals, the directionality of signals reversed, resembling those of extreme non-addicted animals (PL

mPFC to NAc core PSI, PL mPFC leads) (Paired t-test, $P < 0.05$, Figure 78).

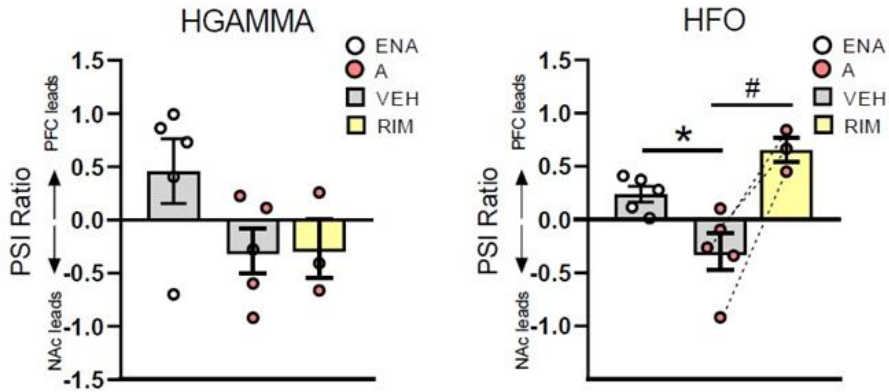


Figure 78. PL mPFC – NAc core circuit communication (PSI) at hgamma (left) and hfo (right) frequencies during decision-making under vehicle and rimonabant treatment. Data are represented as mean \pm SEM, Unpaired and Paired t-test, * $P < 0.05$, # $P < 0.05$.

Neural activities at other frequencies were unchanged (Figure 79).

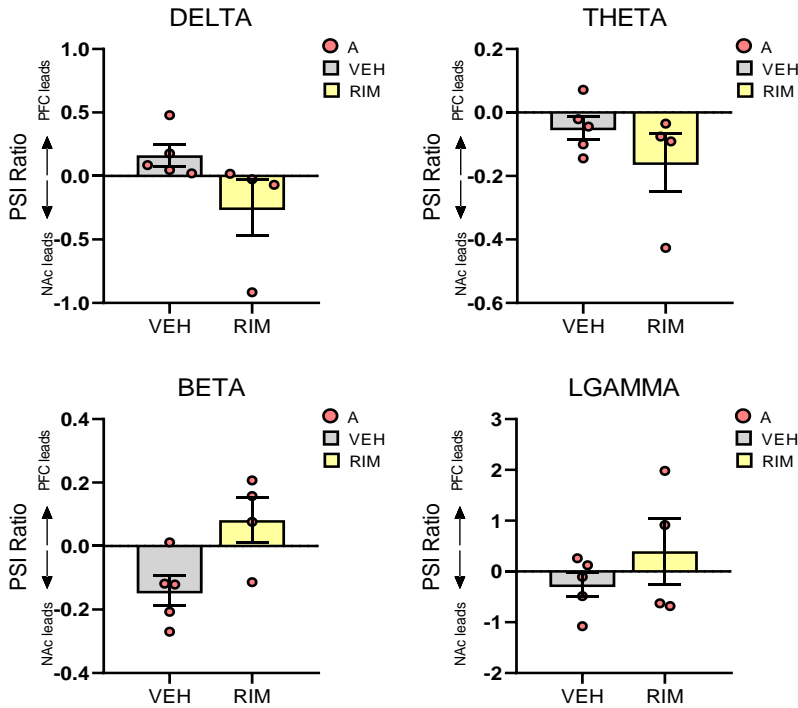


Figure 79. PL mPFC to NAc core circuit communication (PSI) at delta, theta, beta and lgamma frequencies in vehicle and rimonabant treated A mice during decision-making. Data is reported as mean \pm SEM.

Moreover, we studied phase-amplitude coupling during decision-making. Theta-gamma coupling in both areas was equivalent between phenotypes and not overtly affected by the treatment (Figure 80).

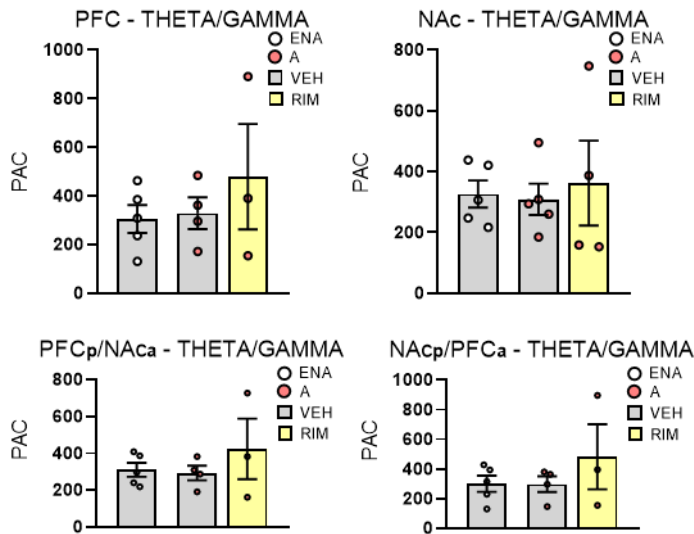


Figure 80. Quantification of local and inter-regional theta-gamma coupling in the PL mPFC and NAc core during decision-making (1s) in ENA and A mice treated with vehicle and rimonabant treated A mice.

These power and connectivity results evidenced that rimonabant corrected aberrant signals at high frequencies during decision-making in addicted animals.

We further studied the electrophysiological effects of CB₁ antagonism during reward expectation periods. No significant changes in PL mPFC power were detected in rimonabant-treated addicted mice compared to the vehicle group (Figure 81) independently of the addiction phenotype. In the NAc core, lgamma power was larger in rimonabant-treated mice (Paired t-test, $P < 0.01$, Figure 81). Furthermore, as previously described for decision-making epochs, we detected a power reduction at hfo in rimonabant-treated mice (Paired t-test, $P < 0.05$, Figure 81).

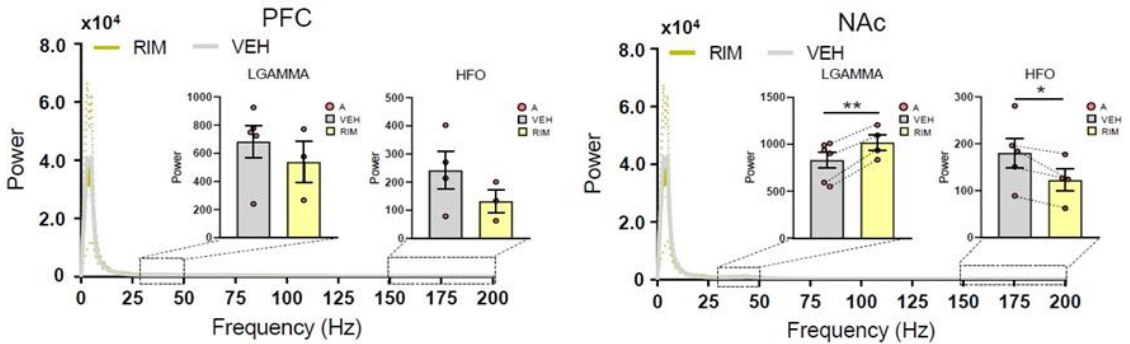


Figure 81. Power spectra of PL mPFC (left) and NAc core (right) signals during expectation of reward after administration of vehicle (grey) or rimonabant (yellow). Power values amplification of lgamma and hfo are also shown. Red dots correspond to A animals. Data are represented as mean \pm SEM, Paired t-test, * $P < 0.05$, ** $P < 0.01$.

Next, we studied the influence of rimonabant on circuit communication. ENA animals exhibited robust PL mPFC-to-NAc core lgamma signals and NAc core-to-PL mPFC hfo signals following vehicle injections. In addicted mice, this circuit coordination was disrupted. In fact, hfo traveled in the opposite direction, that is, from the PL mPFC to the NAc core, and these signals were rescued in the two animals that could be evaluated in this test (Unpaired and Paired t-test, $P < 0.05$ and $P < 0.05$, respectively, Figure 82).

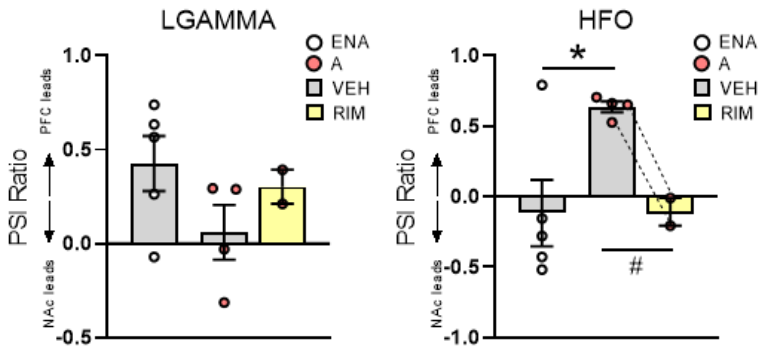


Figure 82. PL mPFC – NAc core circuit communication (PSI) at lgamma and hfo frequencies during reward expectation under vehicle and rimonabant treatment. Data are represented as mean \pm SEM. Unpaired and Paired t-test, *P < 0.05, #P < 0.05.

The rest of the frequency bands were unaltered by rimonabant during reward expectation periods (Figure 83).

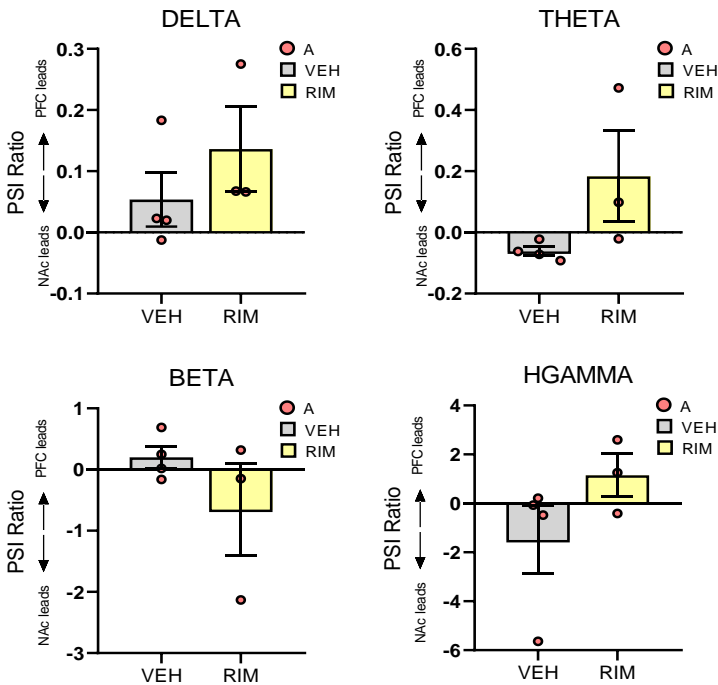


Figure 83. PL mPFC to NAc core circuit communication (PSI) at delta, theta, beta and hgamma frequencies in vehicle and rimonabant treated A mice during reward expectation. Data is reported as mean \pm SEM.

Additionally, theta-gamma coupling was again reduced in the NAc core of addicted animals during the expectation of reward (Unpaired t-test, $P < 0.05$, Figure 58B), however, it was not rescued by rimonabant (Figure 84).

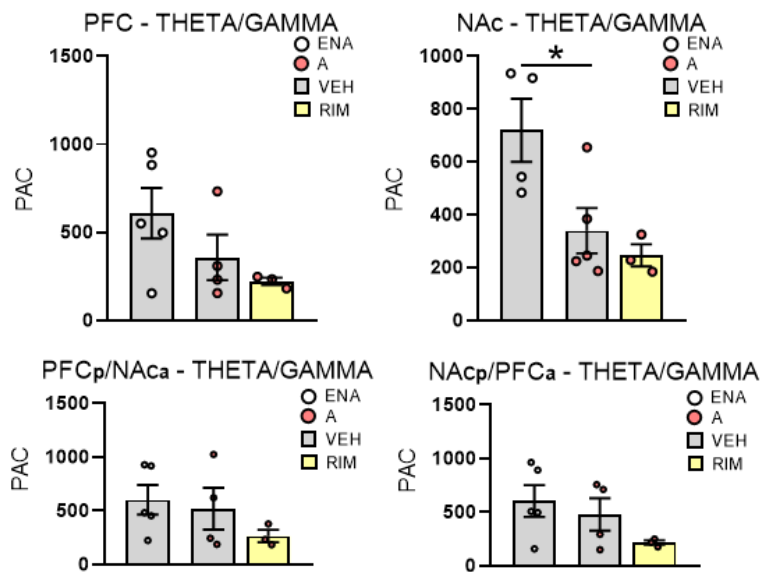


Figure 84. Quantification of local and inter-regional theta-gamma coupling in the PL mPFC and NAc core during expectation of reward (1s) in ENA and A mice treated with vehicle and rimonabant treated A mice. Differences are reported as mean \pm SEM, Unpaired t-test, * $P < 0.05$.

Finally, we aimed to study the effect of rimonabant during rewarding periods. Previously, we identified that circuit communication directionality of signals at lgamma and hgamma frequencies were disrupted in addicted mice during rewarding periods (end reward) (Figure 61-63). However, no correction effect was observed in

rimonabant-treated animals (extreme non-addicted and addicted) at any frequency range (Figure 85).

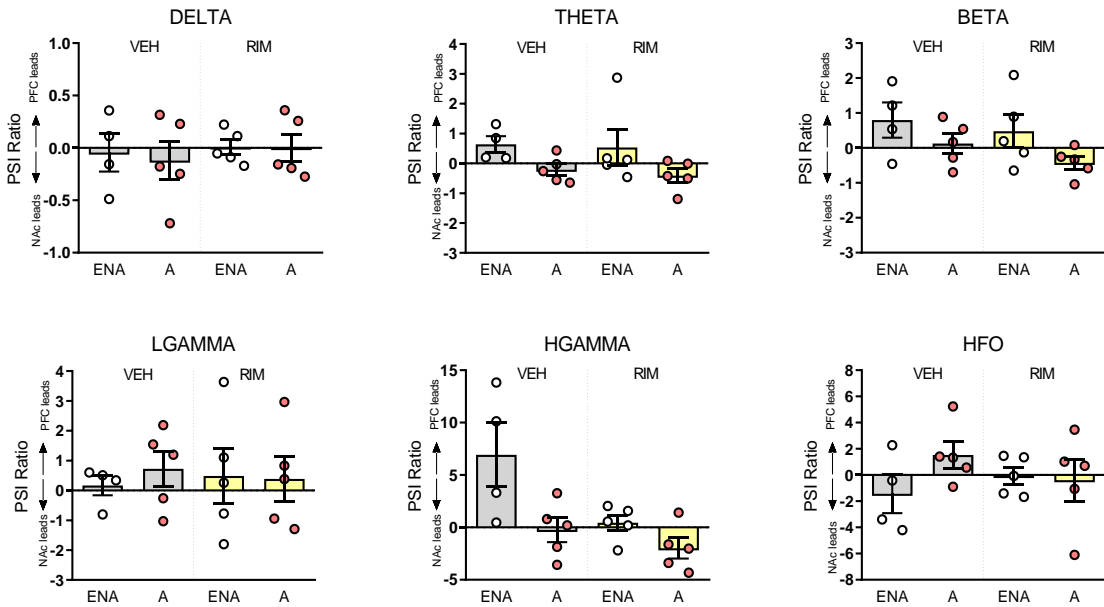


Figure 85. PL mPFC – NAc core circuit communication (PSI) at delta, theta, beta, lgamma, hgamma and hfo frequencies during the last second of the first rewarding period (end reward) under vehicle and rimonabant treatment. Data are represented as mean \pm SEM.

Results

		19-20	F(5, 45)=3.909	n.s
		Hfo		
		0-1		n.s
		16-17		n.s
		19-20		n.s
		Time		
		Rimonabant treatment		
		PL mPFC Power		
		Theta		
		0-1 vs 16-17		n.s
		0-1 vs 19-20		n.s
		16-17 vs 19-20		n.s
		Beta		
		0-1 vs 16-17		n.s
		0-1 vs 19-20		n.s
		16-17 vs 19-20		n.s
		Hgamma		
		0-1 vs 16-17		n.s
		0-1 vs 19-20	n.s	
		16-17 vs 19-20	n.s	
		Hfo		
		0-1 vs 16-17	P < 0.05	
		0-1 vs 19-20	n.s	
		16-17 vs 19-20	n.s	
		NAc core Power		
		Theta		
		0-1 vs 16-17	n.s	
		0-1 vs 19-20	n.s	
		16-17 vs 19-20	n.s	
		Beta		
		0-1 vs 16-17	n.s	
		0-1 vs 19-20	n.s	
		16-17 vs 19-20	n.s	
		Hgamma		
		0-1 vs 16-17	P < 0.01	
		0-1 vs 19-20	P < 0.01	
		16-17 vs 19-20	n.s	
		Hfo		
		0-1 vs 16-17	P < 0.05	
		0-1 vs 19-20	n.s	
		16-17 vs 19-20	n.s	
		Time		
		Vehicle treatment		
		PL mPFC Power		
		Theta		
		0-1 vs 16-17	n.s	
		0-1 vs 19-20	n.s	

Results

		16-17 vs 19-20 Beta 0-1 vs 16-17 0-1 vs 19-20 16-17 vs 19-20 Hgamma 0-1 vs 16-17 0-1 vs 19-20 16-17 vs 19-20 Hfo 0-1 vs 16-17 0-1 vs 19-20 16-17 vs 19-20 NAc core Power Theta 0-1 vs 16-17 0-1 vs 19-20 16-17 vs 19-20 Beta 0-1 vs 16-17 0-1 vs 19-20 16-17 vs 19-20 Hgamma 0-1 vs 16-17 0-1 vs 19-20 16-17 vs 19-20 Hfo 0-1 vs 16-17 0-1 vs 19-20 16-17 vs 19-20		n.s n.s n.s n.s n.s n.s n.s n.s P < 0.05 P < 0.05 n.s n.s n.s n.s n.s n.s P < 0.05 P < 0.05 n.s P < 0.05 P < 0.05 n.s
Figure 70	Two-way ANOVA multiple comparisons	Treatment PSI Delta 0-1 16-17 19-20 Theta 0-1 16-17 19-20 Beta 0-1 16-17 19-20 Lgamma 0-1 16-17 19-20	F(5, 40)=0.3995 F(5, 40)=1.089 F(5, 40)=2.239 F(5, 40)=0.3475	n.s n.s n.s n.s n.s n.s n.s n.s P < 0.05 n.s n.s n.s

Results

		Hgamma	F(5, 40)=0.3849	
		0-1		n.s
		16-17		n.s
		19-20		n.s
		Hfo	F(5, 40)=1.469	
		0-1		n.s
		16-17		n.s
		19-20		n.s
		Time		
		Rimonabant treatment		
		PSI		
		Delta		
		0-1 vs 16-17		n.s
		0-1 vs 19-20		n.s
		16-17 vs 19-20		n.s
		Theta		
		0-1 vs 16-17		n.s
		0-1 vs 19-20		n.s
		16-17 vs 19-20		n.s
		Beta		
		0-1 vs 16-17		n.s
		0-1 vs 19-20		n.s
		16-17 vs 19-20		n.s
		Lgamma		
		0-1 vs 16-17		n.s
		0-1 vs 19-20		n.s
		16-17 vs 19-20		n.s
		Hgamma		
		0-1 vs 16-17		n.s
		0-1 vs 19-20		n.s
		16-17 vs 19-20		n.s
		Hfo		
		0-1 vs 16-17		n.s
		0-1 vs 19-20		n.s
		16-17 vs 19-20		n.s
		Time		
		Vehicle treatment		
		PSI		
		Delta		
		0-1 vs 16-17		n.s
		0-1 vs 19-20		n.s
		16-17 vs 19-20		n.s
		Theta		
		0-1 vs 16-17		n.s
		0-1 vs 19-20		n.s
		16-17 vs 19-20		n.s
		Beta		

Results

Figure 73B	Two-way ANOVA multiple comparisons	NAc core firing rate	F(5, 40)=4.377	
		Treatment		
		0-1		n.s
		16-17		n.s
		19-20		n.s
		Time		
	One-way ANOVA Repeated measures	Rimonabant treatment		
		ENA	F(1.003,4.012)= 8.226	P < 0.05
			F(4,8)=5.782	P < 0.05
		A	F(1.442,5.767)= 4.549	n.s
			F(4,8)=15.88	P < 0.001
		Vehicle treatment		
ENA	F(1.205,4.820)= 11.02	P < 0.05		
	F(4,8)=0.3952	n.s		
A	F(1.835,5.506)= 1.686	n.s		
	F(3,6)=5.521	P < 0.05		

Supplementary Table 5.

Rimonabant reduces reinforcement levels and restores abnormal prelimbic - nucleus accumbens core neural dynamics during decision-making and reward expectation.					
<i>Figure number</i>	<i>Statistical analysis</i>	<i>Factor name</i>	<i>Statistic value</i>	<i>P-value</i>	
Figure 74 left	Mixed ANOVA repeated measures	Reinforcement	F(1.805,15.65)=70.06	n.s	
		Treatment			
	Mixed ANOVA multiple comparisons (Turkey's)	Sessions		q=17.73	P < 0.0001
		1 vs 2		q=1.593	n.s
		1 vs 3		q=17.07	P < 0.0001
		2 vs 3		q=15.60	P < 0.0001
		2 vs 4		q=1.612	n.s
3 vs 4	q=9.670	P < 0.01			
Figure 74 right	Paired t-test	Treatment	t=15.19	P < 0.0001	
Figure 75 left	Paired t-test	Treatment ENA A	t=13.70 t=10.39	P < 0.001 P < 0.001	
Figure 75 right	Pearson correlation	Reinforcement vs NAc core lgamma power All ENA A	R=0.27 R=0.12 R=0.89	n.s n.s P < 0.01	
Figure 76 left	Pearson correlation	Reinforcement vs PL mPFC delta power All ENA A	R=0.12 R=0.09 R=0.33	n.s n.s n.s	
Figure 76 right	Pearson correlation	Reinforcement vs NAc core delta power All ENA A	R=0.05 R=0.05 R=0.13	n.s n.s n.s	
Figure 77	Paired t-test	Treatment PL mPFC hfo power NAc core hfo power	t=1.964 t=3.064	n.s P < 0.05	

Results

Figure 78	Paired t-test	Treatment Hgamma PSI Hfo PSI	t=1.086 t=3.809	n.s n.s
Figure 79	Paired t-test	Treatment Delta PSI Theta PSI Beta PSI Lgamma PSI	t=1.324 t=1.740 t=2.912 t=0.8002	n.s n.s n.s n.s
Figure 80	Paired t-test	Treatment PL mPFC hfo power NAc core hfo power	t=1.358 t=3.532	n.s P < 0.05
Figure 81	Paired t-test	Treatment Lgamma PSI Hfo PSI	t=0.8070 t=2.106	n.s n.s
Figure 82	Paired t-test	Treatment Delta PSI Theta PSI Beta PSI Hgamma PSI	t=3.909 t=1.658 t=0.9231 t=1.107	n.s n.s n.s n.s
Figure 83	Paired t-test	Treatment Delta PSI ENA A Theta PSI ENA A Beta PSI ENA A Lgamma PSI ENA A Hgamma PSI ENA A Hfo PSI ENA A	t=0.2459 t=0.4884 t=0.2949 t=0.8934 t=0.4894 t=1.241 t=0.7251 t=0.2766 t=1.807 t=0.9506 t=1.094 t=0.7741	n.s n.s n.s n.s n.s n.s n.s n.s n.s n.s

Chapter 2

Evolution of prelimbic-nucleus accumbens core neural dynamics in mice vulnerable to develop food addiction.

Pablo Calvé^{1,2}, Laura Ribalta¹, Thomas Gener^{2,3,4}, Elena Martín-García^{*1,2}, M. Victoria Puig^{*2,3,4}, Rafael Maldonado^{*1,2}

1 Laboratory of Neuropharmacology. Department of Experimental and Health Sciences,

Universitat Pompeu Fabra, Barcelona, Spain.

2 Hospital del Mar Medical Research Institute, Barcelona, Spain.

3 Catalan Institute of Nanoscience and Nanotechnology, CSIC and The Barcelona Institute of Science and Technology, Campus UAB, 08193 Bellaterra, Spain.

4 Institut de Neurociències, Universitat Autònoma de Barcelona, 08193 Bellaterra, Barcelona, Spain.

*These authors contributed equally to the study.

IN PREPARATION

Categorization of extreme phenotypes of food addicted and non-addicted mice for posterior electrophysiological analyses at the medium period

Mice (n=28) started the experimental protocol with an FR1 schedule of reinforcement during two sessions and was followed by three sessions under FR5. After these five sessions were completed, animals underwent stereotaxic surgery to implant stereotrodes in the PL mPFC and the NAc core. Following recovery from surgery, a habituation period to the wire was performed, and animals that accomplished more than 3 reinforcers per session, obtained stability of 60% between sessions, and performed more than 75% of responses in the active lever accomplished the criteria to start the electrophysiological recordings of the medium-term operant training. Electrophysiological recordings of the medium-term operant training started with 15 sessions of FR5, and subsequently, the persistence of response, motivation and compulsivity were evaluated in the early (session 18-26) and medium (session 52-60) periods (Figure 37b; see Experimental design section of Chapter 2 in Methods, and Figure 86). Electrophysiological recordings lasted until the end of the medium period due to the signal quality and implant durability.

As previously reported in the animal batch of Chapter 1, when the effort to obtain one single pellet was increased to FR5, reinforcement values decreased. Subsequently, surgeries were performed and after recovery and habituation period that lasted between 2 and 3 weeks,

the number of reinforcers obtained in the valid sessions maintained stable until the medium period (Figure 86).

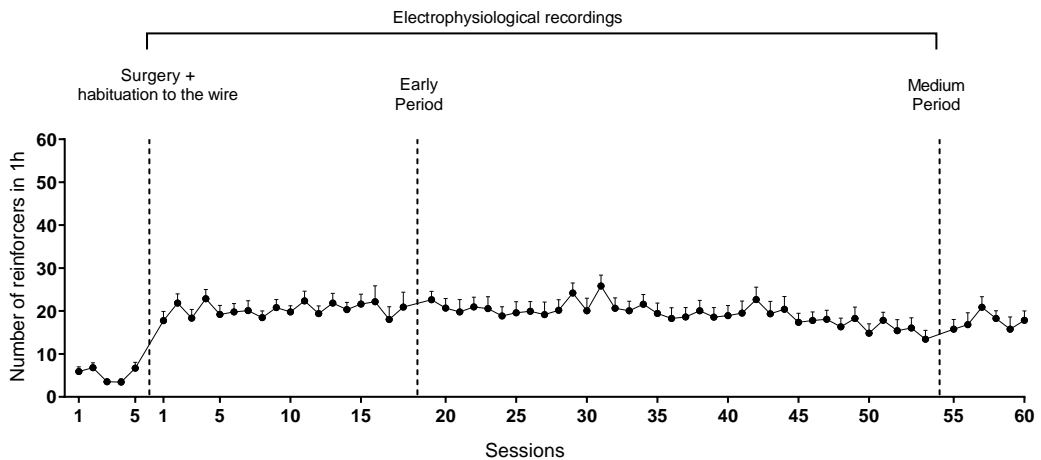


Figure 86. Acquisition of operant training maintained by chocolate-flavored pellets. Mean number of reinforcers during the acquisition training in FR5 schedule of reinforcement ($n=28$ at the beginning to $n=19$ at the end). Differences are reported as mean \pm SEM.

During the early period, $\frac{1}{4}$ of the animals reached two or three addiction-like criteria (25.00%) and were considered as vulnerable mice ($n=5$). At this early stage, the rest of animals that reached none or one addiction-like criterion (75.00%) were considered as resilient mice ($n=15$). The prevalence of resilience and vulnerability to food addiction was similar in the medium period. During the medium period, about $\frac{1}{4}$ of animals (26.32%) were considered as addicted mice ($n=5$) while the rest of animals (73.68%) were considered as non-addicted mice ($n=14$) (Figure 87). In addition, we observed that the prediction of the development of food addiction was of 25%, as

only one animal considered as vulnerable in the early period was categorized as addicted in the medium period.

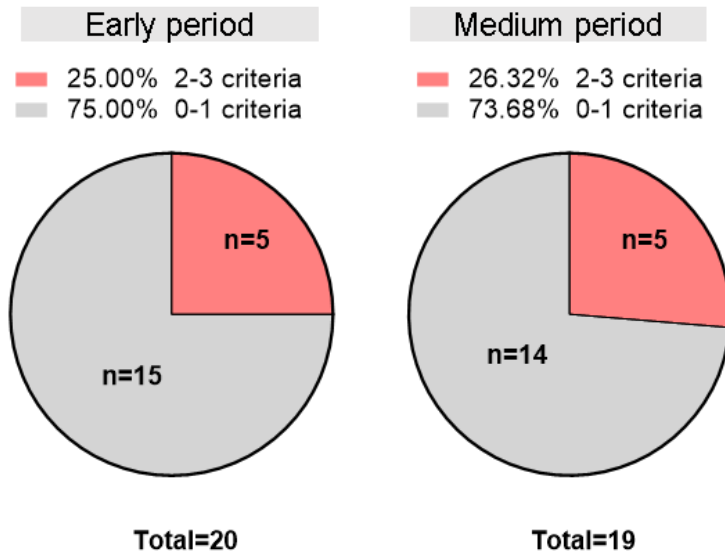


Figure 87. Distribution of animals with different scores for addiction-like behavior according to early and medium period. Animals were assigned to a criteria subgroup based on the number of criteria met for which they scored equal or above the 75th percentile.

Considering the different phenotypic categorization performed for the two time periods of the medium-term operant training, in the early period (session 18-26), significant differences were observed in the motivation and compulsivity tests between resilient and vulnerable mice. Moreover, vulnerable mice tended to show increased persistence values, although the difference between both subgroups was not significant (U Mann-Whitney, $P < 0.01$, $P < 0.001$, Figure 88A-C). By contrast, in the medium period (session 52-60), addicted

mice showed significantly higher persistence of response and increased motivation for reward obtention compared to non-addicted mice.

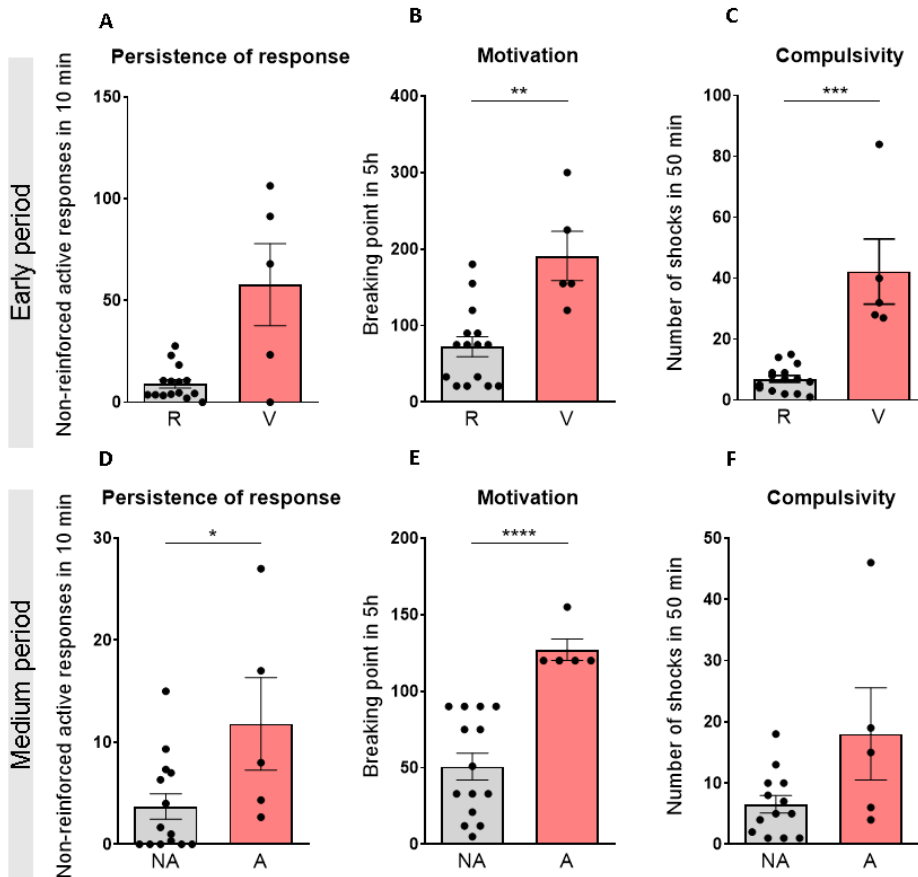


Figure 88. Behavioral tests of the three addiction criteria in resilient and vulnerable mice at the early (A-C), and in non-addicted and addicted mice at the medium period (D-F). (A, D) Persistence of response. Total number of non-reinforced active responses during three consecutive daily 10-min of pellet free period. (B, E) Motivation. Breaking point achieved in 5 h of PR schedule. The breaking point refers to the maximal effort that an animal is willing to do to earn one pellet. (C, F) Compulsivity. Number of shocks that mice received in 50 min in the shock test in which each pellet delivery was associated with a footshock (0.18 mA). Differences are reported as mean \pm SEM, U Mann-Whitney, * $P < 0.05$, ** $P < 0.01$, *** $P < 0.001$, **** $P < 0.0001$.

Additionally, addicted mice tended to show increased compulsivity values, although the difference between both phenotypes was not significant (U Mann-Whitney, $P < 0.05$, $P < 0.0001$, Figure 88D-F).

In terms of phenotypic traits, in the early stage of the operant training (FR5 early period) vulnerable mice showed a significantly augmented reinforcement level, impulsivity and aversive associative learning compared to the resilient group (U Mann-Whitney, $P < 0.05$, Figure 89A-C). Notwithstanding, these differences between phenotypes were not maintained until the medium (Figure 89D-F) period, although a tendency was present showing higher values in addicted mice.

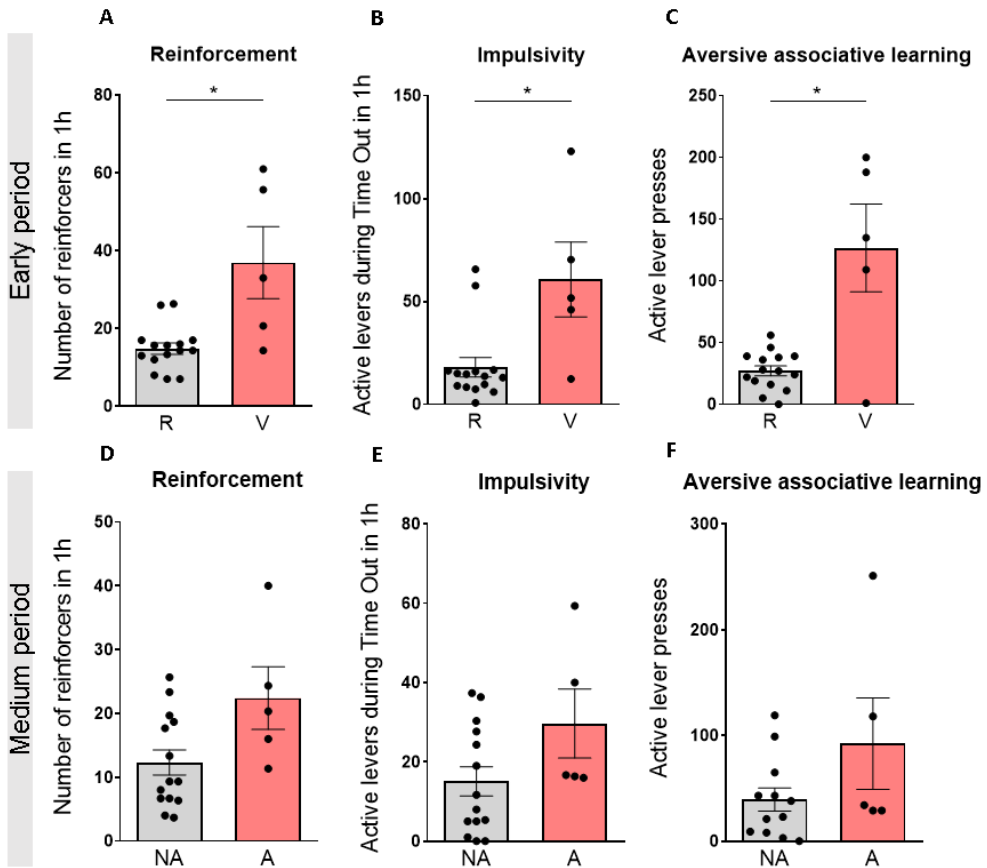


Figure 89. (A-F) Behavioral data of phenotypic traits in the FR5 sessions of early (A-C) and medium (D-F) periods represented by individual values with the mean and \pm SEM. (A, D) Reinforcement levels quantified by counting the number of reinforcers consumed in 1h operant sessions. (B, E) Impulsivity. Number of non-reinforced active lever-presses during five consecutive daily time out (15 s) after each pellet delivery. (C, F) Aversive associative learning that corresponds to the number of non-reinforced active responses in 50 min in the following session after the shock test with the same discriminative stimulus (grid floor) as shock test in which pressing the active lever had no consequences: no shock, no reward delivery and no cue light (U Mann-Whitney, * $P < 0.05$).

To investigate the evolution of neurophysiological signatures underlying addictive-like behaviors across operant training sessions,

we selected mice at the tails of an inverted U-shape curve according to the quantitative individual scores obtained in the addiction-like criteria and phenotypic traits tests of the medium period (session 52-60). The individual selection criteria are detailed in Chapter 1 and Methods. Extreme non-addicted (n=5) and addicted (n=5) mice were selected as candidates for the electrophysiological analysis of PL mPFC-NAc core circuitry. Considering the phenotypic categorization used, we compared addiction-like criteria and phenotypic traits at the medium period of the medium-term operant training, remarking the difference of the addictive-like behavior at the end of the training schedule (Figure 90 and Figure 91). Addicted mice showed a significantly increased persistence of response and motivation compared to their extreme non-addicted peers (Unpaired t-test, $P < 0.05$, $P < 0.0001$, Figure 90A-B). No differences were reported between both extreme phenotypes in the compulsivity test, although a remarked tendency was observed (Figure 90C). Moreover, addicted mice showed significantly higher reinforcement levels and impulsivity, which was measured by the inability to stop pressing the lever during the time-out period (15 s) after each pellet delivery (Unpaired t-test, $P < 0.05$, Figure 91A-B). By contrast, no differences were detected between extreme non-addicted and addicted mice in the aversive associative learning, although a tendency was present.

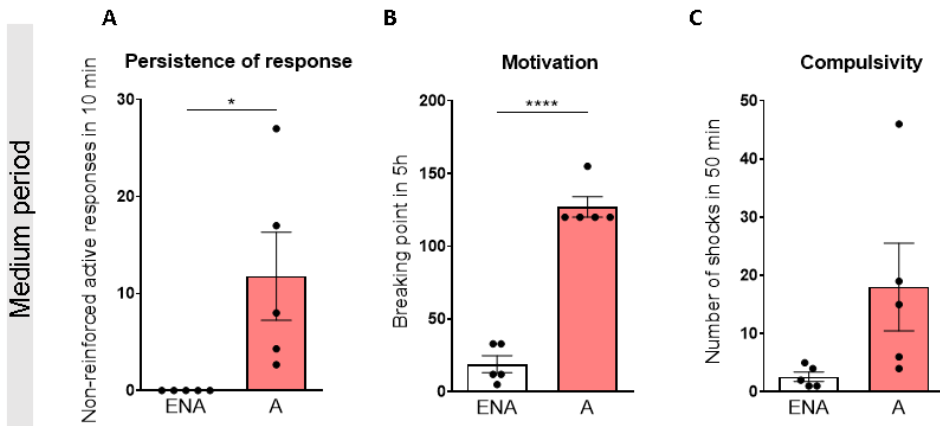


Figure 90. Behavioral tests of the three addiction criteria in addicted and extreme non-addicted at the medium period. (A) Persistence of response. Total number of non-reinforced active responses during three consecutive daily 10-min of pellet free period. (B) Motivation. Breaking point achieved in 5 h of PR schedule. The breaking point refers to the maximal effort that an animal is willing to do to earn one pellet. (C) Compulsivity. Number of shocks that mice received in 50 min in the shock test in which each pellet delivery was associated with a footshock (0.18 mA). Differences are reported as mean \pm SEM, Unpaired t-test, * $P < 0.05$, **** $P < 0.0001$.

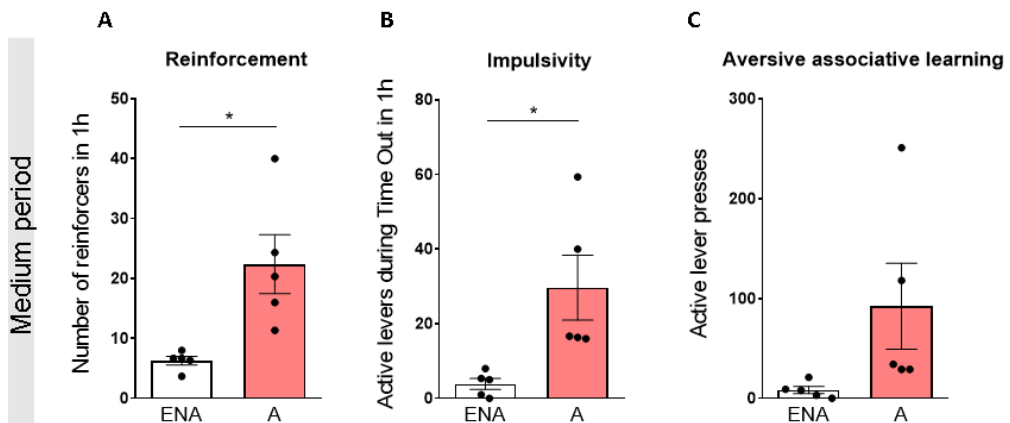


Figure 91. Behavioral data of phenotypic traits in the medium period represented by individual values with the mean and \pm SEM. (A) Reinforcement levels quantified by counting the number of reinforcers consumed in 1h operant sessions. (B) Impulsivity. Number of non-reinforced active lever-presses during five consecutive daily time out (15 s) after each pellet delivery. (C) Aversive associative learning that corresponds to the number of non-reinforced active responses in 50 min in the following session after the shock test with the same discriminative stimulus (grid floor) as shock test in which pressing the active lever had no consequences: no shock, no reward delivery and no cue light (Unpaired t-test, * $P < 0.05$).

Disruption of prelimbic - nucleus accumbens core gamma circuit communication signals during decision-making are still not present at the medium period stage.

In order to determine if neural circuitry disruptions were already present at the medium period, we next investigated the neurophysiological fingerprints of addicted and extreme non-addicted phenotypes during decision-making in the latest recording sessions (session 55-58) performed of the medium period. We selected reward preceding epochs (5 lever presses + cue light and reward delivery) during the three FR5 sessions of the medium period. As in the result section of Chapter 1, these reward preceding epochs were more abundant in short time periods that lasted one to three seconds (Figure 92). In order to obtain a higher number of epochs for electrophysiological analyses, we selected reward preceding epochs that lasted one to four seconds for the electrophysiological analysis.

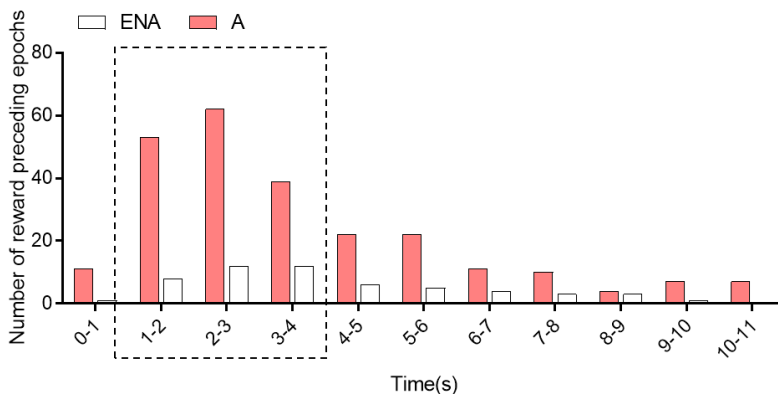


Figure 92. Sum of reward preceding epochs per duration of seconds in A and ENA mice during FR5 sessions of the medium period. The dots dashed square indicates the duration of epochs selected for the analysis.

During decision-making epochs, the power in the PL mPFC and in the NAc core was similar between extreme non-addicted and addicted mice and no significant differences were found at any frequency (Figure 93 and Figure 94). These findings were similar to the ones obtained in Chapter 1.

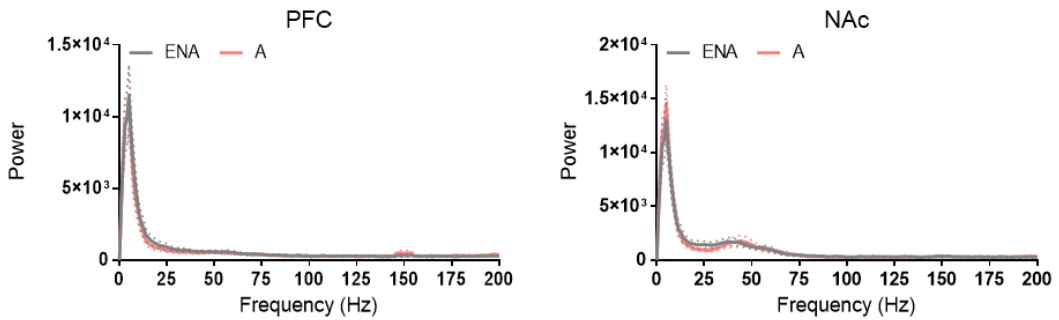


Figure 93. Power spectra of neural signals in the PL mPFC (left) and the NAc core (right) in extreme non-addicted and addicted mice during decision-making.

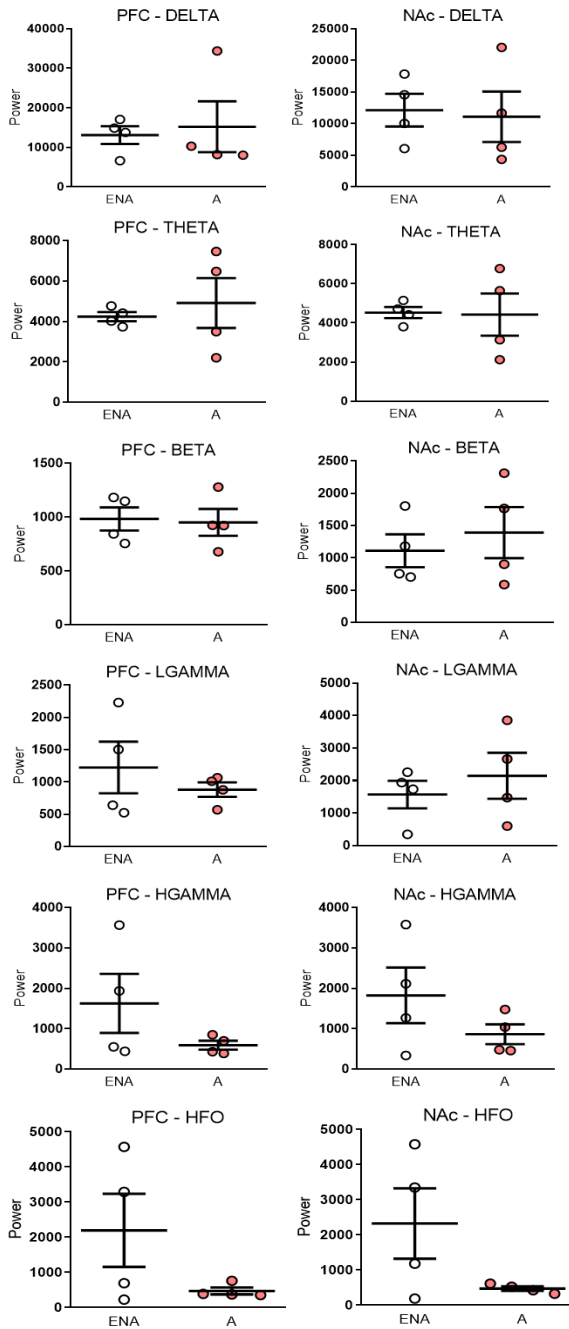


Figure 94. Power quantification of neural signaling in the PL mPFC (left) and the NAc core (right) in extreme non-addicted and addicted mice during decision-making.

Furthermore, as previously commented in Chapter 1, we observed that at the stage of the late period, extreme non-addicted mice displayed a NAc core to PL mPFC signaling at hgamma frequencies and a PL mPFC to NAc core communication at hfo. Indeed, the directionality of these signals was disrupted in addicted mice, showing a predominance of PL mPFC to NAc core hgamma signaling (PL mPFC to NAc core PSI, PL mPFC leads) and no clear directionality at higher frequencies (Figure 52 and 53). Notwithstanding, at the medium period stage, we did not observe differences in PL mPFC to NAc core circuit communication between extreme non-addicted and addicted mice (Figure 95). Thus, these results suggest that probably circuit communication during decision-making is disrupted at the late period stages of the long-term operant training.

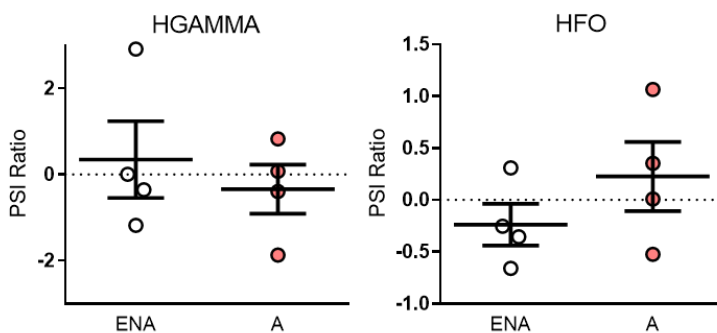


Figure 95. PL mPFC-NAc core circuit communication (PSI) at hgamma and hfo frequencies during decision-making.

Moreover, addicted mice showed normal circuit communication at lower frequencies in the medium period (Figure 96).

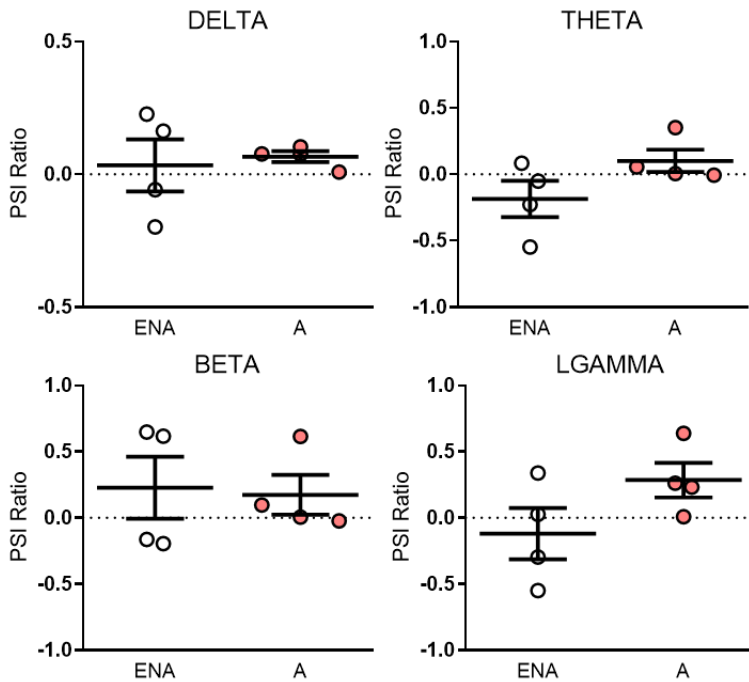


Figure 96. PL mPFC-NAc core circuit communication (PSI) at delta, theta, beta, and lgamma frequencies during decision-making.

Further analyses during decision-making, reward expectation and rewarding periods at different time periods of the medium-term operant training will confirm the initial altered neurophysiological fingerprints in vulnerable mice and how these abnormalities are developed and expressed in the addicted phenotype.

Supplementary Table 6.

Categorization of extreme phenotypes of food addicted and non-addicted mice for posterior electrophysiological analyses at the medium period				
<i>Figure number</i>	<i>Statistical analysis</i>	<i>Factor name</i>	<i>Statistic value</i>	<i>P-value</i>
Figure 88A	U Mann-Whitney	Early Period Persistence of response	U=15.50	n.s
Figure 88B	U Mann-Whitney	Early Period Motivation	U=5.500	P < 0.01
Figure 88C	U Mann-Whitney	Early Period Compulsivity	U=0	P < 0.001
Figure 88D	U Mann-Whitney	Medium Period Persistence of response	U=13	P < 0.05
Figure 88E	U Mann-Whitney	Medium Period Motivation	U=0	P < 0.0001
Figure 88F	U Mann-Whitney	Medium Period Compulsivity	U=15.50	n.s
Figure 89A	U Mann-Whitney	Early Period Reinforcement	U=10	P < 0.05
Figure 89B	U Mann-Whitney	Early Period Impulsivity	U=13	P < 0.05
Figure 89C	U Mann-Whitney	Early Period Aversive learning	U=14	P < 0.05
Figure 89D	U Mann-Whitney	Medium Period Reinforcement	U=14	n.s
Figure 89E	U Mann-Whitney	Medium Period Impulsivity	U=18	n.s
Figure 89F	U Mann-Whitney	Medium Period Aversive learning	U=19	n.s
Figure 90A	Unpaired t-test	Medium period ENA vs A Persistence of response	t=2.598	P < 0.05
Figure 90B	Unpaired t-test	Medium Period ENA vs A Motivation	t=11.83	P < 0.0001
Figure 90C	Unpaired t-test	Medium Period ENA vs A Compulsivity	t=2.033	n.s
Figure 91A	Unpaired t-test	Medium Period ENA vs A Reinforcement	t=2.033	P < 0.05
Figure 91B	Unpaired t-test	Medium Period ENA vs A Impulsivity	t=2.033	P < 0.05
Figure 91C	Unpaired t-test	Medium Period ENA vs A Aversive learning	t=2.033	n.s

Supplementary Table 7.

Disruption of prelimbic - nucleus accumbens core gamma circuit communication signals during decision-making are still not present at the medium period stage.				
<i>Figure number</i>	<i>Statistical analysis</i>	<i>Factor name</i>	<i>Statistic value</i>	<i>P-value</i>
Figure 94	Unpaired t-test	PL mPFC power		
		Delta	t=0.3134	n.s
		Theta	t=0.5384	n.s
		Beta	t=0.1937	n.s
		Lgamma	t=0.8260	n.s
		Hgamma	t=1.395	n.s
		Hfo	t=1.651	n.s
		NAc core power		
		Delta	t=0.2201	n.s
		Theta	t=0.09246	n.s
		Beta	t=0.5984	n.s
		Lgamma	t=0.7013	n.s
		Hgamma	t=1.317	n.s
		Hfo	t=1.847	n.s
Figure 95	Unpaired t-test	PSI		
		Hgamma	t=0.6495	n.s
		Hfo	t=1.193	n.s
Figure 96	Unpaired t-test	PSI		
		Delta	t=0.3294	n.s
		Theta	t=1.783	n.s
		Beta	t=0.1922	n.s
		Lgamma	t=1.736	n.s

Discussion

Nowadays, the easy access to hypercaloric and palatable foods with elevated addictive properties in Western societies is a crucial contributing factor to compulsive eating behavior and the consequent development of food addiction and obesity, which are closely associated (Kirrilly M Pursey *et al.*, 2014). In this thesis, we describe novel neurophysiological signatures underlying behaviors associated with food addiction within PL mPFC – NAc core circuits and the possible rescue by blocking the endocannabinoid system. Indeed, the neural network established between the PL mPFC and the NAc plays a key role in the inhibition of behavioral control (Koob, 2000; Volkow *et al.*, 2013; Moore *et al.*, 2017; Domingo-Rodriguez *et al.*, 2020), and this neural network is modulated by the endocannabinoid system (Mancino *et al.*, 2015; Covey *et al.*, 2017; Manzanares *et al.*, 2018). Therefore, the blockade of the endocannabinoid system by CB₁ receptors antagonism might be a protective strategy to rescue food addictive-like behaviors. In order to do so, we used a mouse operant behavioral model (Mancino *et al.*, 2015) combined with *in vivo* electrophysiological recordings. Understanding the neurophysiological fingerprints involved in addictive-like behaviors might be a significant advance in providing new information for personalized treatments for food addiction, obesity, and eating disorders.

We promoted food addiction in mice using a behavioral paradigm with high translational face validity to human addiction (Mancino *et al.*, 2015; Domingo-Rodriguez *et al.*, 2020). Thus, we mimicked the

development of addiction after repeated seeking of palatable food in an operant training during 112 sessions. This mouse model allowed to distinguish different subpopulations of mice vulnerable (29.03%) or resistant (70.97%) to develop food addiction. The percentage of mice that developed food addiction in this operant model was slightly higher than the prevalence reported in humans (19.9%) using the YFAS food addiction diagnosis (Kirrilly M Pursey *et al.*, 2014), and similar to animals addicted to cocaine (31.0%) (Deroche-Gamonet *et al.*, 2004b). These slight differences in the prevalence of addiction might be due to the different behavioral responses promoted by natural rewards and drugs of abuse, as well as by the different species (humans, rats, and mice) and experimental conditions required to accomplish these distinct experiments.

We found that addicted animals were characterized by increased food intake. Accordingly, previous investigations in our group observed differences in pellet intake between Glu-CB₁-KO and WT mice, suggesting that mutant mice consumed a decreased number of reinforcers that may contribute to the protective phenotype to develop food addiction (Domingo-Rodriguez *et al.*, 2020). Therefore, according to our previous results in the same genetic background (C57BL/6J), the increased number of reinforcers consumed by addicted mice might correspond to changes in the expression patterns of selective receptors, that may play crucial roles in the control of palatable food intake across the sessions of the long-term operant training. By contrast, recent studies using the same mouse strain and

experimental conditions did not observe significant differences in palatable pellet intake between non-addicted and addicted mice (García-Blanco *et al.*, 2022). Thus, this different result suggests that epigenetic and environmental factors might have influenced in the expression of certain addictive phenotypic traits during the development of this multifactorial disorder.

Food intake differences between non-addicted and addicted mice were not influenced by the body weight variable. Indeed, previous studies using the same animal model and chocolate-flavored pellets suggested that the body weight is not a predisposing factor in the development of the addictive-like behavior (Mancino *et al.*, 2015; Domingo-Rodriguez *et al.*, 2020; García-Blanco *et al.*, 2022). Moreover, the fact of using isocaloric chocolate-flavored pellets in our experiments allowed us to study more precisely the development of food addiction, leaving aside other possible contributing factors that may be present in foods containing high amounts of fat, which are related in the development of obesity. Notwithstanding, this thesis focuses on the behavioral traits expressed by the development of food addiction, not in the development of obesity.

Next, we studied the personality traits related to food addiction. Our findings revealed that addicted mice presented increased persistence, motivation, and impulsivity. These findings are supported by previous studies employing the same experimental approach with highly palatable pellets to develop food addiction in mice (Mancino

et al., 2015; Domingo-Rodriguez *et al.*, 2020). Indeed, persistence of response, motivation, compulsivity and impulsivity were the main hallmarks and phenotypic traits of addiction that were augmented in addicted mice in these previous investigations. In our results, the major hallmark compulsivity was not significantly difference between both phenotypes, although a tendency was present. One possible reason could be the small number of animals in the present study and the distinct mouse strain employed in both studies: a batch of 31 C57BL/6J mice was used in this study, whereas animal batches were of 56 C57BL/6J mice (Domingo-Rodriguez *et al.*, 2020) and 27 CD1 mice (Mancino *et al.*, 2015) in the previous studies. Therefore, the behavioral characterization performed in our cohort of animals has taken into account each specific endophenotype that may participate in this complex behavioral disease.

Additionally, PCA analysis of the mouse behavioral responses revealed a predominant load of two main traits, motivation and impulsivity, contributing to addiction-like behaviors, in a first component (PC1) defining these extreme phenotypes. A major weight in the second component (PC2) corresponded to compulsivity and persistence. Thus, these behavioral factors may depend on distinct brain areas participating in rewarding processes, that may influence in the development of food addiction. Accordingly, recent studies performed in our laboratory using the same operant protocol reported similar results in the PCA: motivation and impulsivity were the main traits found in PC1, while persistence of response and

compulsivity were the main hallmarks of food addiction in PC2 (García-Blanco *et al.*, 2022). All these behavioral factors were equally associated to the identical principal components in our analysis, except persistence of response that was associated to the PC1, instead of PC2. This different result in the association of persistence of response to the principal components may suggest that this addiction-like criterion might depend on multiple distinct mechanisms and the participation of diverse variables.

Previous studies performed over the last decade using modern circuit neuroscience tools offer abundant evidence supporting the notion that the NAc is a critical node of the circuitry that translates motivation into action. (Volkow *et al.*, 2017; Klawonn and Malenka, 2018; Volkow *et al.*, 2019). Indeed, recent investigations in rats using optogenetics revealed that the activation of MSNs expressing D2 receptors in the NAc increased motivation, whereas the inhibition of these neurons induced the opposite effect (Soares-Cunha *et al.*, 2018). Moreover, evidence has also demonstrated that the NAc is a key component of the neural components regulating impulsivity (Basar *et al.*, 2010). Previous studies in impulsive mice and humans suffering from impulsivity have revealed a prominent increase in NAc delta oscillations during anticipation of reward (Hemmings *et al.*, 2018). Thus, these findings support our results of the PCA, suggesting that the main traits of motivation and impulsivity might be associated with neural regulation of the NAc.

Previous studies have demonstrated that compulsivity and persistence may depend on dysfunctions in inhibitory control regulated by the mPFC (Goldstein and Volkow, 2011; Luigjes *et al.*, 2019). Indeed, human studies have suggested that deficits in prefrontal cortical function and subsequent loss of inhibitory control could be crucial in promoting compulsive drug use (Jentsch and Taylor, 1999; Naqvi and Bechara, 2010; Goldstein and Volkow, 2011). Moreover, a study using a rat model of compulsive drug-seeking in which cocaine-seeking persists in a subgroup of rats despite negative consequences has demonstrated that prolonged cocaine self-administration diminishes *ex vivo* intrinsic excitability of deep-layer neurons in the PFC, which was significantly more noticeable in compulsive drug-seeking animals (Chen *et al.*, 2013). Additionally, compensating for hypoactive PFC neurons with *in vivo* optogenetic PFC stimulation significantly prevented compulsive cocaine-seeking, whereas optogenetic PFC inhibition increased compulsive cocaine-seeking (Chen *et al.*, 2013). Thus, our findings on the PCA are strongly supported by the previous studies reported on the differential behavioral roles of the NAc and the mPFC in addiction, suggesting that abnormal function of both brain areas may have contributed to the observed behavioral traits.

Next, we aimed to study neurophysiological differences between addicted and extreme non-addicted mice in basal conditions, recording neural activity in their homecages immediately after FR5 sessions. We found that local power and PL mPFC-to-NAc core

circuit communication between addicted and extreme non-addicted mice was similar. Notwithstanding, both groups exhibited a flow of information from the NAc core to the PL mPFC at theta and hgamma frequencies (NAc core to PL mPFC PSI, NAc core leads) and a PL mPFC to NAc core communication at lgamma frequencies (PL mPFC to NAc core PSI, PL mPFC leads) under basal conditions. Thus, circuit communication measures suggested that neural signals of addicted and extreme non-addicted mice in the PL mPFC and the NAc core coordinated at theta, lgamma and hgamma frequencies after FR5 sessions. Previous studies have demonstrated that theta and gamma (lgamma and hgamma) oscillations are involved in cognition, executive functions and memory, especially in the mPFC. Indeed, several investigations using a genetic mouse model of cognitive dysfunction (*Zdhhc8^{+/-}*) revealed that theta-gamma coupling is increased when mice successfully performed a spatial working memory task, suggesting that the interaction between theta and gamma oscillations is associated with increased synchronization of neurons in the mPFC (Tamura *et al.*, 2017, 2018). Moreover, previous studies focusing in circuit communication signaling have demonstrated that theta and gamma oscillations fluctuate between different brain areas and are enhanced in the mPFC when performing working memory and executive function tasks (Lohani *et al.*, 2019; Alemany-González *et al.*, 2020; Lintas *et al.*, 2021). Thus, our findings demonstrating the communication between the PL mPFC and the NAc core after FR5 operant training sessions are supported by previous evidences on the specific role of theta, lgamma and

hgamma frequencies responsible for the communication between these two brain areas.

Theta and gamma oscillations also seem to participate in addictive-like behaviors. Previous studies focusing on impulsive behavior investigated LFPs in the mPFC and the NAc on a 5-choice serial reaction time task, and revealed that theta and gamma oscillatory activity increased during anticipation and waiting periods of reward (Donnelly *et al.*, 2014). Furthermore, recent studies investigating power and connectivity measures between the basolateral amygdala and the NAc in an appetitive conditioning associated with food demonstrated that theta and gamma oscillations in each region diverged in the presence of food-associated cues (Hsu *et al.*, 2020). These studies confirm that oscillatory activity at theta and gamma frequencies may fluctuate between brain areas that participate in rewarding mechanisms and addictive-like behaviors. Indeed, these oscillatory activity changes at theta and gamma frequencies may depend on the modulation of heterogeneous neural ensembles cooperating locally and between different brain areas. In that sense, the activation and/or inhibition of these neural ensembles might be triggered by reward-induced changes in glutamatergic, GABAergic and DA signaling.

According to our results, the predominance of the NAc core signaling over the PL mPFC observed under basal conditions at theta and hgamma frequencies after FR5 sessions might represent the

prolonged activation of the NAc by the DA system triggered by the consumption of palatable reinforcers during operant food-seeking sessions. On the other hand, the generation of lgamma oscillations migrating from the PL mPFC to the NAc core might correspond to the enhancement of the mPFC activity produced by the proper performance of the acquired task. These results on lgamma oscillations are supported by previous studies demonstrating the participation of this specific frequency band during rewarding trials in a PR schedule of reinforcement (Hernández-González *et al.*, 2017).

We next evaluated the different behavioral traits that characterize the maintenance of the addictive-like behavior at the end of the training schedule. As expected, addicted mice showed increased number of active leverpresses and reinforcements. As previously mentioned, reinforcement and motivation to pursue highly palatable pellets were the main scores variables of the PC1. In that context, in order to study the reinforcing value of the reward, we have focused in two main features that participate in reward-related behaviors: decision-making and reward expectation. Indeed, altered decision-making and outweighed reward expectation have been linked with reinforcing processes of food consumption (O'Doherty *et al.*, 2017; Verharen *et al.*, 2020). For that purpose, we considered decision-making epochs as 1s time windows occurring the second prior to the first leverpress in reward preceding trials (5 lever presses + cue light and reward delivery). Moreover, reward expectation epochs were defined as the

second occurring immediately after the fifth leverpress, when the cue light turns on and reward is delivered.

Our findings suggested that PL mPFC – NAc core circuit communication at high frequencies (hgamma and hfo) was disrupted in addicted mice during decision-making. We observed that addicted mice presented an altered PL mPFC to NAc core hfo signaling, compared to extreme non-addicted mice. Furthermore, the directionality of hgamma signaling in addicted mice (PL mPFC to NAc core) was opposite to hgamma signaling in extreme non-addicted mice (NAc core to PL mPFC). Notably, the directionality of signals at hfo correlated with the number of reinforcers implying that neural dysfunctions at this specific frequency between the mPFC and the NAc favored addictive-like behaviors. Gamma and hfo are believed to reflect neuronal network coordination involved in attention, being these frequency bands recognized as potential biomarkers in cognitive disorders (Kucewicz *et al.*, 2014; Mably and Colgin, 2018). Previous evidence have demonstrated that gamma and hfo in the PFC are altered in several cognitive disorders, including Alzheimer, Down syndrome and schizophrenia diseases, among others (Guggisberg *et al.*, 2007; Amemiya and Redish, 2018; Tamura *et al.*, 2018). Indeed, studies in animal models of intellectual disability (Ts65Dn and *Ophn1*^{-y}) revealed that mPFC and hippocampal gamma oscillations were reduced in these models, suggesting the presence of a network malfunction (Powell *et al.*, 2014; Alemany-González *et al.*, 2020). Additionally, it is well known

that cognitive impairment lead by alterations in the PFC and the hippocampus are closely associated with poor decision-making (Domenech and Koehlin, 2015; Ho *et al.*, 2021; Tavares and Tort, 2022), which is also a characteristic of addiction (Koffarnus and Kaplan, 2018; Verdejo-Garcia and Chong, 2021). Thus, these previous results support our findings suggesting that alterations of gamma and hfo during decision-making may participate in the expression of behavioral anomalies linked to food addiction.

Our findings revealing disrupted circuit communication between the PL mPFC and the NAc core at hfo during decision-making are strengthened by previous evidence, suggesting that coordination at hfo may be characteristic of nucleus accumbens microcircuits (Olszewski *et al.*, 2013). These oscillations are present during different healthy brain states and increase within schizophrenia and other mental disorders when they likely spread from the NAc to several brain regions, including the mPFC (Hunt *et al.*, 2009; Goda *et al.*, 2015; Delgado-Sallent *et al.*, 2021). Thus, our results highlight the importance of these oscillations in the mesocorticolimbic pathway, suggesting that hfo of addicted mice might be generated and consequently hijacked by the NAc during decision-making, leading to a predominance of neural signals controlled by the NAc that migrate to the mPFC. This disruption in the circuit communication of addicted mice triggered by an extensive heterogeneity of neural ensembles might represent the increased food intake shown by addicted mice.

Next, we investigated the differential neural substrates of reward expectation in addicted and extreme non-addicted mice. Addicted mice showed local desynchronization of gamma rhythms in the NAc core during the expectation of rewards, with a reduction of lgamma oscillations that correlated with reinforcement levels. Moreover, addicted mice presented a decreased theta-gamma coupling in the NAc core. The NAc plays a crucial role in reward prediction during reward-seeking behavior (Day *et al.*, 2011), and changes in theta and gamma oscillations have been reported in the ventral striatum and PFC areas (Van Der Meer and Redish, 2009; Kalenscher *et al.*, 2010; Gruber *et al.*, 2013). Previous studies have revealed that these fluctuations in theta and gamma oscillatory activity are triggered by the local and interregional modulation of dopaminergic, glutamatergic and GABAergic signaling, among others (Furth *et al.*, 2013; Chen *et al.*, 2014; Lally *et al.*, 2014; Fuhrmann *et al.*, 2015; Wang *et al.*, 2020). Specifically, DA is the crucial neurotransmitter released in the NAc during the obtainment and consumption of rewards (drugs or food) (Volkow and Morales, 2015). Additionally, glutamate and GABA are also co-released from distinct sets of excitatory and inhibitory neurons in the PFC and VTA (Bouarab *et al.*, 2019). Thus, our findings showing an altered gamma power and a disrupted theta-gamma coordination in the NAc of addicted mice during the expectancy of reward might be influenced by the activation of DA release in the NAc triggered by the rewarding process.

Previous studies in humans have demonstrated that addiction is associated with a decrease in DA release in response to drugs of abuse, suggesting that the altered release of DA might reflect disrupted neurophysiology of DA neurons within the reward system (Volkow *et al.*, 2010). These DA neurons are also involved in the expectation of reward, and previous studies have demonstrated that DA neurons signals apparently are involved in the prediction of reward (Schultz *et al.*, 1993, 1997; Schultz, 1998). This hypothesis about the involvement of DA neurons in reward prediction suggests that in situations requiring a repeated learning task, DA neurons are activated by primarily rewards during each learning phase. However, DA neurons cease in the responding to reward when the reward becomes fully predictable (Schultz *et al.*, 1993). Therefore, the information related to rewards is a complex learning mechanism within the participation of DA neurons in the NAc and interconnected areas. Deficiencies in these circuits where the same DA neurons are involved may affect diverse behavioral aspects of the rewarding process, such as anticipatory responses, expectation, and reward intake.

An interesting hypothesis to explain addiction is based on a chronic basal deficiency in brain reward (Volkow *et al.*, 1999, 2002b; Comings and Blum, 2000; Morgan *et al.*, 2002; Dalley *et al.*, 2007), suggesting that the “reward deficiency syndrome” is a type of self-medication, ultimately affecting DA signaling in the brain reward

circuitry of addicted individuals. The reduced DA transmission in the NAc of addicted users during rewarding periods causes the need of consuming a higher amount of rewards that imply a constant release of DA, and consequently will lead to a higher risk of presenting multiple addictive-like behaviors (Blum *et al.*, 2018). All these hypotheses arguing a DA hypoactivation in the NAc of addicted subjects during rewarding periods are in agreement with our findings in the NAc core of addicted mice during expectation of reward. We suggest that the lgamma hypoactivation and theta-gamma coupling disruption observed in addicted mice may be supported by the “reward deficiency syndrome”, and the consequent alterations induced in the encoding of reward prediction. These deficient behaviors for reward satiation may partially be reflected in addicted mice that present a reduced gamma oscillatory activity in the NAc core during expectation of reward, and consequently need to press the lever multiple times to obtain a higher number of rewards and reach basal levels of dopamine in the NAc.

We next investigated oscillatory activity in the PL mPFC and the NAc core during the different phase changes of the operant FR5 sessions. For this purpose, neural activities were studied in both phenotypes together during the transition from the first rewarding period (active period 1) to the beginning of the non-rewarding period (pellet-free period), and in the transition from the end of the pellet-free period to the beginning of the second rewarding period (active period 2). A cue light was turned on during rewarding periods when

the reward was delivered after five active lever presses. By contrast, during non-rewarding periods (pellet-free periods), no pellets were delivered, and this period was signaled by the illumination of the entire operant chamber.

We found that during the different phase changes of the operant sessions, neural signaling in the PL mPFC-NAc core circuitry of both phenotypes was characterized by fluctuations in the power of hgamma and hfo in both, the PL mPFC and the NAc core. This finding suggests that oscillatory activities > 50 Hz (hgamma and hfo) in both areas contributed to the encoding of relevant behaviors closely associated with persistence, as oscillatory activity at these frequencies decreased during the pellet-free period, that is the period where active leverpresses are not reinforced and animals persist to obtain the reward. Furthermore, these oscillatory activities also contributed to the encoding of reward, as these brain rhythms increased at the beginning of the second active period, when mice detect the initiation of the rewarding period. Previous studies in rodents have also demonstrated that gamma fluctuations and changes in firing rates play a significant role during waiting periods where reward is not delivered (Roesch *et al.*, 2012; McCracken and Grace, 2013; Donnelly *et al.*, 2014). Thus, the decrease of hgamma and hfo in both the PL mPFC and NAc core during the pellet-free period may correspond with the increased persistence to obtain a palatable pellet over time, as animals must wait a 10 minutes period to obtain a reinforcer. Once the second active period started, prominent

increases of hfo were detected, particularly in the PL mPFC. Indeed, several studies revealed that gamma and hfo of the striatum augmented in periods of reward delivery, suggesting that these oscillatory frequencies are involved in rewarding behaviors (Van Der Meer and Redish, 2009). Thus, these evidences support our findings that demonstrate the increase of hfo in the detection of entering again into the rewarding period, highlighting the importance of oscillatory activities > 50 Hz within mPFC – NAc circuits.

To find valuable neurophysiological biomarkers that differentiate addictive-like behaviors from resilient phenotypes during the different phases of the FR5 sessions, we assessed PL mPFC to NAc core circuit communication in each of the phases previously evaluated. At the end of the first rewarding period, addicted mice also exhibited abnormal directionality of signals within this circuit. Indeed, we identified a predominance of lgamma and hgamma signaling that traveled from the NAc core to the PL mPFC, opposite to the PL mPFC to NAc core signaling observed in extreme non-addicted mice. Remarkably, these reversed NAc to mPFC hgamma signals correlated strongly with increased food intake and lever presses in addicted mice. These findings are supported by previous literature suggesting that drugs of abuse or palatable foods hijack the mesocorticolimbic circuitry in addicted subjects (Moore *et al.*, 2017, 2018; Volkow *et al.*, 2019). Indeed, extensive exposure of drugs or foods increase DA in the reward circuit, underlying their rewarding effects. In parallel, previous studies have revealed that the activation

of DA triggered by drugs of abuse also reduces top-down processes modulated by the mPFC (Goldstein and Volkow, 2011), suggesting that the inability to stop consuming drugs suffered by addicted patients may be due to a failure of behavioral inhibitory control (Goldstein and Volkow, 2002; Ceceli *et al.*, 2022). Accordingly, our results demonstrated a predominance of NAc core signaling over the PL mPFC of addicted mice that was associated with the increased reinforcement levels at the end of the first rewarding period. We hypothesize that these altered communication signalings governed by the NAc in addicted mice during the persistent seeking to obtain rewards might be explained by a possible disruption of the mPFC, which is incapable of controlling the inhibition of palatable pellets intake.

Craving behaviors are measured by the persistence of reward seeking and depend on the modulation of multiple neurotransmitters acting at synaptic levels. Several studies have demonstrated that diverse neurotransmitters are modulated in the mesolimbic pathway by the endocannabinoid system (Covey *et al.*, 2017; Manzanares *et al.*, 2018), which plays a crucial role in reinforcing and motivational properties of highly palatable foods (Maccioni *et al.*, 2008; Mancino *et al.*, 2015). CB₁ receptors are the prominent subtype receptor in the CNS that have attracted much recent interest due to its potential therapeutically avenue in eating disorders and obesity (Mackie, 2006). Indeed, eCBs are critical modulators of reinforcing behaviors partially by their influence on dopaminergic projections to the NAc.

However, it has been suggested that DA neurons do not express CB₁ receptors. Thus, the actions of eCBs and exogenous cannabinoids at the level of the dopaminergic cell bodies in the VTA are indirect and likely inhibit the release of glutamate, GABA and other neurotransmitters (Cheer *et al.*, 2000; Wilson and Nicoll, 2002; Julian *et al.*, 2003; Mateo *et al.*, 2017). These receptors are preferentially at the presynaptic level in different brain areas of the rewarding pathway, acting as a regulatory feedback mechanism to modulate synaptic transmission (D'Addario *et al.*, 2014). In the mesocorticolimbic pathway, CB₁ receptors are highly expressed in the striatum, whereas low expression levels of CB₁ receptors are found in the VTA (Tsou *et al.*, 1998; Koob, 2000; Wise, 2004). At the behavioral level, the reinforcement modulation processing by the CB₁ receptors and eCBs has been extensively studied using diverse behavioral paradigms (Soria *et al.*, 2005; Shoaib, 2008; Oleson *et al.*, 2021). However, the electrophysiological characterization of CB₁ antagonism in the PL mPFC and NAc core pathway on addictive behavior is still unknown. For that reason, we aimed to investigate the acute effects of CB₁ antagonism on behavior and correlate these responses with the PL mPFC – NAc core neural dynamics of addicted and extreme non-addicted mice.

To elicit a selective blockade of CB₁ receptors, rimonabant (3 mg/kg) was acutely administered to mice freely moving in a homecage. In basal conditions, rimonabant progressively augmented delta oscillations in the PL mPFC and the NAc core and lgamma

oscillations in the NAc core, while not affecting general mobility in both groups of animals. Additionally, the enhanced delta power in the PL mPFC and the NAc core weakened delta-hfo coordination locally in the NAc core and at a circuit level, disrupting the coupling between the amplitude of NAc core hfo and the phase of PL mPFC delta. However, the blockade of CB₁ receptors did not affect the circuit's directionality of signals. All these neural alterations observed by rimonabant administration affected extreme non-addicted and addicted mice together, and no differences were reported between both extreme subpopulations. These findings evidence the main effect of CB₁ receptors on local neural activities during basal conditions with limited actions of the circuit's communication.

Several studies have previously focused on the electrophysiological fingerprints of CB₁ modulation in the NAc, demonstrating changes in delta and gamma oscillations (Hernandez and Cheer, 2012; Ramlakhan *et al.*, 2020; Jenkins *et al.*, 2021). Gamma oscillations are believed to provide temporal structures that induce the alignment of spike trains within and between different brain areas, facilitating the encoding of diverse afferent projections into NAc spiking patterns (Kalenscher *et al.*, 2010). Thus, the changes in neural coordination and activation patterns shown in this study might reveal the heterogeneity of neural ensembles participating locally in the mPFC and the NAc, and interregionally in the mPFC-to-NAc pathway, suggesting that antagonism of CB₁ receptors might have influenced

neural encoding via alterations of glutamatergic and/or GABAergic signaling (Robbe *et al.*, 2002). In that sense, the inhibition of CB₁ receptors might have arrested eCB-mediated reduction of glutamatergic release in the NAc core, revealing an enhanced excitatory synaptic transmission at gamma frequencies in the targeted MSNs in the NAc core. On the other hand, previous studies have identified that the increase of delta oscillations seems to be the consequence of the hyperpolarization of neurons due to the activation of CB₁ receptors (Dasilva *et al.*, 2014). Interestingly, our findings are supported by this evidence as we observe the opposite effects when blocking CB₁ receptors. The increase of delta oscillations in the PL mPFC and NAc core revealed in mice treated with rimonabant might reflect the depolarization of glutamatergic neurons in the mPFC and afferent MSNs of the NAc led by the blockade of CB₁ receptors. Notwithstanding, further experiments using other techniques, such as optogenetics or chemical approaches, would be necessary to identify neural specificity within and between areas.

Furthermore, we studied the effects of rimonabant in the spiking activity of addicted and extreme non-addicted mice. Interestingly, addicted animals treated with vehicle exhibited increased spiking activity in the NAc core compared to their extreme non-addicted peers. Remarkably, we observed that rimonabant decreased spiking activity both in the PL mPFC and the NAc core, and the spiking activity increase previously detected in addicted mice was not observed when treated with rimonabant. These findings suggest that

the NAc core of addicted mice is highly activated during basal conditions. The blockade of CB₁ receptors induced the correction of this altered firing activity, decreasing spiking activity levels in addicted mice to the normal firing activity levels of extreme non-addicted mice. In the presence of rimonabant, glutamatergic projections from the mPFC to the NAc might have disarranged glutamatergic transmission at the synapse in the NAc. Moreover, several studies have identified specific subtypes of spiking interneurons in the NAc that play crucial roles in firing properties (Tepper *et al.*, 2010). One of the fundamental electrophysiological features of specific types of fast-spiking interneurons is their maintained high action potential firing frequencies in the NAc. It has been discovered that some of these fast-spiking interneurons uniquely express CB₁ receptor (Winters *et al.*, 2012). This particular neuron type of fast-spiking interneurons expressing CB₁ receptors extensively overlaps with fast-spiking interneurons expressing parvalbumin and may thus represent a different neural population in the NAc (Wright *et al.*, 2017). Indeed, our results are sustained by these evidences as the inhibitory effect of CB₁ receptor in this specific subtype of neurons may lead to a decrease in the spiking activity of the NAc. Yet again, these findings point to a main effect of rimonabant on NAc microcircuits during basal conditions.

We then examined rimonabant's rescuing effects of neural activities associated with food addiction. As reported in previous studies (Maccioni *et al.*, 2008; Mancino *et al.*, 2015), the pharmacological

blockade of CB₁ receptors had an impressive effect on the reversion of addictive-like behavior. Accordingly, our results revealed that rimonabant reduced the number of reinforcers obtained by addicted and extreme non-addicted animals in the operant paradigm. Together with the previous studies, these results suggest that CB₁ receptor is a crucial component of the neural substrates mediating reinforcing properties of high palatable food. Moreover, we found that the decreased number of reinforcers consumed when treated with rimonabant correlated with the increase of NAc core γ power observed in the previous recordings performed in the homecage, suggesting that NAc core γ oscillations might play a crucial role in controlling high palatable food intake. In that context, our previous analysis of the operant training recordings revealed that γ oscillations in the PL mPFC to NAc core circuit were associated with reinforcement levels, suggesting an important role in food seeking behavior. Thus, the increase of γ oscillations in the NAc core observed in mice treated with rimonabant might reflect the depolarization of afferent MSNs of the NAc core led by the antagonism of CB₁ receptors. Indeed, the modulatory activity in NAc afferent MSNs at γ frequencies induced by rimonabant may influence glutamatergic and GABAergic neurotransmission within the PL mPFC to NAc core pathway, affecting behavioral inhibitory control. Therefore, once again the association of this brain wave band with reinforcement levels when blocking CB₁ receptors highlights the participation of the endocannabinoid system in food seeking behavior.

To gain a deeper insight into the pharmacological effect of rimonabant during decision-making and expectation of reward, we investigated power activity and circuit communication in these epochs, analyzing the same behavioral intervals than in the previous section. In terms of neural communication between the PL mPFC and the NAc core (PSI), our previous analysis identified that NAc core to PL mPFC hgamma and PL mPFC to NAc core hfo signals were involved in decision-making in extreme non-addicted mice and were altered in addicted mice. Interestingly, the blockade of CB₁ receptors by rimonabant restored mPFC control of the circuit in addicted mice during decision-making. Moreover, the directionality of signals was reversed in rimonabant-treated addicted animals resembling those of extreme non-addicted animals.

Several studies have focused on understanding the relationship between decision-making, gamma oscillations, and CB₁ receptor modulation in prefrontal-hippocampal circuits (Kucewicz *et al.*, 2011), concluding that systemic CB₁ receptor activation contributes to the dynamic coordination of limbic-cortical interactions that are related to network dysfunctions. In our findings, we observe a similar neural dynamics disfunction at hfo in the PL mPFC to NAc core pathway of addicted mice that is corrected by the blockade of CB₁ receptors with rimonabant. Hfo are generated in the NAc and migrate to different brain areas (Hunt *et al.*, 2008, 2009). Thus, dysfunctions in the NAc core of addicted mice might influence the communication at these specific frequencies during decision-making.

We previously hypothesized that hfo of addicted mice might be hijacked by the NAc during altered decision-making. Under the presence of rimonabant, the blockade of CB₁ receptors may induce the activation of presumably glutamatergic projections from the PL mPFC and the NAc core, restoring the functionality of the mPFC in addicted mice and consequently leading to the reversion of hfo communication in this circuit. Altogether, our findings highlight the correction of the addictive-like behavior with CB₁ antagonism, suggesting that a part from gamma oscillations, hfo also play a crucial role in reinforcing behaviors towards palatable food, especially during decision-making. However, further experiments are needed to confirm the specific identification of these neural alterations and their correction by pharmacological treatment.

We also studied the electrophysiological effect of CB₁ antagonism during reward expectation periods. No significant changes of PL mPFC power were detected between addicted mice treated with vehicle and with rimonabant. However, we found that lgamma power in the NAc core was larger in addicted mice treated with rimonabant than in vehicle-treated mice during reward expectation epochs. We previously revealed that addicted mice presented a reduced NAc power at lgamma frequencies compared to extreme non-addicted mice during expectation of reward. Therefore, the increased lgamma NAc power induced by rimonabant in addicted mice showed a correcting effect that restored lgamma NAc power to normal power

levels. Indeed, these results are consistent with the previous augment of Igamma power observed in the NAc core of rimonabant treated animals during basal recordings.

We previously suggested that the decreased Igamma NAc power observed in addicted mice during expectancy of reward may reflect disruptions of NAc DA neurons involved in rewarding processes. Thus, blockade of CB₁ receptors and its consequent modification on presumably glutamatergic transmission within the mPFC to NAc projections may have participated in the indirect modulation of NAc DA release. Indeed, previous studies have studied the influence of CB₁ receptors on NAc DA release by the regulation of VTA to NAc pathway (Lupica and Riegel, 2005), and by the involvement of other CB₁- expressing projections innervating the NAc from different brain areas (Cheer *et al.*, 2004). Additionally, other studies demonstrated that rimonabant reduced the increase of extracellular DA in the NAc triggered by high palatable food, confirming that the mesocorticolimbic dopaminergic system is involved, at least in part, in the effect of CB₁ receptor antagonists on food intake (Melis *et al.*, 2007). Therefore, we suggest that the significant increase of Igamma power in the NAc core of addicted animals after rimonabant administration during the expectation of reward could underlie a possible modulation of DA in the NAc, triggered by the indirect participation of afferent projections expressing CB₁ receptors. The fact that CB₁ receptors are not expressed in DA MSNs and the crucial participation they have in the regulation of other neurotransmitters

hinders the obtainment of clear hypothesis. Further experiments studying the activation and/or inhibition of diverse projections innervating the NAc will be needed to clarify these findings.

Additionally, theta-gamma coupling was again reduced in the NAc core of addicted animals during expectation of reward as previously described, however this response was not rescued by rimonabant. These findings suggest that coordination between theta and gamma frequencies during expectation of reward may depend on alternative neural pathways that are not influenced by the blockade of CB₁ receptors. In agreement, previous studies in humans evaluating the role of frontal theta rhythms during expectation of reward suggested that DA may be the main neurotransmitter mediating frontal theta oscillatory activity (Gruber *et al.*, 2013). In that context, a possible modulation of DA MSNs innervating the NAc may reverse the decreased NAc theta-gamma coupling observed in addicted mice during reward expectation.

The aim of our second objective was to identify the evolution of abnormal mPFC to NAc neural dynamics in the transition from vulnerable to addicted phenotype. For this purpose, mice performed a medium-term operant training to develop food addictive-like behavior during 60 sessions. These animals underwent stereotaxic surgery at the beginning of the training with the purpose of recording neural activity during all the sessions since the beginning to the medium period training. Animals were categorized in addicted and

non-addicted mice at the medium period stage in order to avoid implant falls and signal quality losses during our recordings. This technical limitation makes not possible the evolution of the neural dynamics at a late period of operant training.

We identified that 26.32% of the animals accomplished 2 or 3 criteria in the medium training period and were therefore vulnerable to develop food addiction. The remaining animals (73.68%) accomplished 1 or none criterion and were considered as resilient mice. These percentages in the categorization of the animals were analogous to the percentage of vulnerable and resilient mice in Chapter 1 (29.03% and 70.97%, respectively), suggesting that the distribution of animals in the Gaussian curve was similar in both cohorts of animals.

Furthermore, we observed that addicted mice that were categorized in the medium period presented a significantly higher persistence of response and motivation. Interestingly, addicted animals that were categorized in the late period in Chapter 1 also showed increased values in these two hallmarks of addiction. By contrast, compulsivity trait was not significantly higher in addicted mice, neither in the medium period categorization of Chapter 2, nor on late period categorization of Chapter 1. Considering the close similitudes in the expression of addictive-like behaviors in both groups of addicted mice, we suggest that persistence of response and motivation towards highly palatable pellets may be expressed in the medium stages of the

food addiction cycle. Previous studies have reported that persistence may be developed by an habitual palatable food seeking (Mancino *et al.*, 2015; Moore *et al.*, 2017). In accordance, mice are exposed everyday to palatable pellets in daily sessions of 1h where they must seek the reward by pressing a lever. Thus, after 60 sessions of operant training, it is expected to observe individual differences in behavior during the pellet-free period when no pellets are available but addicted mice persist pressing the lever. Additionally, motivation is another behavioral hallmark of food addiction that has been expressed in addicted mice at the late period stages of the long-term operant training (Mancino *et al.*, 2015; Domingo-Rodriguez *et al.*, 2020; García-Blanco *et al.*, 2022). In agreement, our results highlight the expression of motivation in addicted mice at the medium period, suggesting that this major hallmark might be expressed at the same time periods than persistence. Recent findings in our group using similar operant training protocols in male CD1 mice have revealed that the prediction of developing food addiction during the late period considering the data obtained in the medium period was of 50%, suggesting that half of addicted mice categorized at the medium period will continue being addicted at the late period. Furthermore, this prediction was even higher in female CD1 mice that showed 80% of prediction in developing food addiction comparing early and late periods.

In terms of phenotypic traits, we found that addicted mice that were classified in the medium period did not show significant differences

in reinforcement levels and impulsivity compared to their non-addicted peers, although a tendency was present. In contrast, differences in the number of reinforcers and impulsivity were observed between addicted and non-addicted mice categorized at the late period of Chapter 1. This difference between the phenotypic traits of addicted mice of Chapter 1 and addicted mice of Chapter 2 might also depend on the number of animals employed in each experiment, as only 19 mice reached the medium period in Chapter 2.

To study the electrophysiological fingerprints at the medium period, we selected mice at the curve ends according to the individual scores obtained in the addiction-like criteria and phenotypic traits evaluated in the medium period. Addicted mice presented a significantly increased persistence of response, motivation, and impulsivity compared to extreme non-addicted mice. Reinforcement levels were also higher in addicted mice compared with extreme non-addicted mice. Thus, when selecting extreme animals, behavioral results of Chapter 2 were similar to those obtained in Chapter 1.

We next studied the neurophysiological fingerprints of addicted and extreme non-addicted phenotypes during decision-making in the medium period. We observed that no differences in local power and circuit communication signaling were revealed between addicted and extreme non-addicted mice during decision-making. Moreover, no clear directionability of signals at hgamma and hfo was detected in

both phenotypes during decision-making. Thus, these findings suggest that circuit communication during decision-making is not still altered at the medium period stage. By contrast, our previous findings of Chapter 1 revealed that addicted mice presented a disrupted circuit communication at hgamma and hfo during decision-making in late period stages. Indeed, further analysis will confirm if the alterations in PL mPFC to NAc core communication detected in Chapter 1 are present at the medium period stages in reward expectation and rewarding periods.

The transition of the neuroplastic changes occurring in the development of food addiction still remain elusive, although some studies have focused in understanding the transition from vulnerable to addiction using drugs of abuse. Several authors have studied the neuroadaptive changes related with the transition to addiction in self-administration models of drug reinforcement and addictive-like behavior (Kalivas, 2005; Kasanetz *et al.*, 2010), suggesting that long term depressions in prelimbic mPFC and NAc mediated by specific receptors was impaired in drug addicted rats (Kasanetz *et al.*, 2010) at the late period stages of the addiction cycle. These synaptic alterations were not observed at the early stages of drug self-administration, when addictive-like behaviors were not present (Kasanetz *et al.*, 2013). Moreover, long term depression modifications occurred earlier in the NAc than in the PFC (Kasanetz *et al.*, 2013), suggesting that synaptic plasticity changes may be sequential and progress over time in a NAc to PFC direction.

Altogether, our results in food addicted mice during decision-making and the previous reports about drug addiction and long-term depressions support the idea that anomalous synaptic plasticity and communication between the mPFC and NAc at hgamma and hfo frequencies may participate in the transition from vulnerable to food addiction phenotype. Indeed, further analysis of electrophysiological recordings during the operant sessions performed between the early and medium period will reveal the evolution of possible disruptions in neural communication between areas.

In conclusion, the present doctoral thesis has identified new electrophysiological signatures of food addictive-like behaviors in two extreme subpopulations of mice. Accordingly, PL mPFC to NAc core signaling was disrupted at high frequencies during decision-making in addicted animals. Moreover, addicted mice exhibited reduced low gamma oscillations and theta-gamma coupling in the NAc core during reward expectancy. Altered PL mPFC to NAc core connectivity and gamma synchrony in the NAc core was also associated with increased reinforcement levels, underlying the functional relevance of these abnormalities. These findings could open new therapeutic research possibilities for food addiction and other neurological disorders with alterations in food intake, such as obesity or eating disorders (Moore *et al.*, 2018; Pursey *et al.*, 2021). Thus, the induction of brain oscillations by neuronal stimulation at specific frequency ranges may restore neural circuits disrupted in

food addictive-like behaviors, leading to the improvement of these behaviors. Indeed, recent studies in Alzheimer's disease have focused in improving cognitive traits by the enhancement of oscillatory stimulation (Chan *et al.*, 2021).

Moreover, our results highlight CB₁ receptors as significant modulators of the top-down cortico-striatal pathways mediating control over food intake and its associated neurophysiological fingerprints. We found that neural disruptions presented in addicted mice during basal conditions, decision-making and reward expectation were reversed by blocking CB₁ receptors with rimonabant. Specifically, increased spiking activity of addicted mice was reduced to extreme non-addicted firing rate levels during basal conditions. In FR5 session recordings, hfo circuit communication between the PL mPFC and the NAc core was corrected to normal levels during decision-making and reward expectation. Moreover, alterations in NAc gamma oscillatory activity of addicted mice were reversed during reward expectancy. In that sense, the generation of new pharmacological tools with high affinity to CB₁ receptors in selective neurons could be another possible approach to battle addictive-like behaviors. Further research would be needed to design novel selective and safe candidate drugs acting at these levels.

Finally, we have demonstrated that the expression of addiction traits during the transition from vulnerable to food addiction phenotypes is similar between the categorization of addicted mice at the medium

period and late period, suggesting that neural alterations in addictive-like behavior may be present at the medium training period. However, we did not observe disruptions in neural communication within the PL mPFC to NAc pathway during decision-making at these period stage. Indeed, further analysis of decision-making, reward expectation, and rewarding periods are needed at different stages of the medium-term operant training to better understand neural alterations related to addictive-like behaviors. For this purpose, we will perform a complete characterization of the PL mPFC and NAc core neural signatures of extreme non-addicted and addicted mice at this medium period to evaluate if similar neural disruptions to those previously revealed in Chapter 1 could also be identified at this medium period. Next, we will characterize the same electrophysiological fingerprints of the selected animals at the early training period. Finally, we will study in these groups of animals the evolution of the neural alterations obtained at the medium period since the early period. These studies will allow to elucidate how neural activity in vulnerable mice is modified across FR5 sessions until the expression of the addiction phenotype at the medium training period. Additionally, these studies should be repeated in female mice considering possible gender differences.

To conclude, this thesis provides new neurophysiological evidences which could help to identify novel strategies to address this pathology.

Conclusions

The present thesis allows to draw the following conclusions:

1. PL mPFC and NAc core neural signals of addicted and extreme non-addicted mice coordinated at theta, lgamma and hgamma frequencies after FR5 sessions.
2. PL mPFC – NAc core circuit communication at high frequencies (hgamma and hfo) is disrupted in addicted mice during decision-making characterized by dysfunctional prefrontal output that may favor addictive-like behaviors.
3. Local gamma rhythms in the NAc core of addicted mice are desynchronized during the expectation of rewards suggesting a key role in reward seeking behavior.
4. Oscillatory activities >50 Hz in the PL mPFC and NAc core contributed to the encoding of relevant behaviors closely associated with persistence and reward.
5. Addicted mice enhanced gamma NAc core to PL mPFC connectivity during rewarding periods highlighting their pathological nature.
6. Blockade of CB₁ receptors with rimonabant evidenced a main effect on local neural activities at delta, lgamma and hfo bands during basal conditions.

7. Addicted mice exhibited increased spiking activity in the NAc core compared to extreme non-addicted mice during basal conditions.
8. The altered spiking activity in the NAc core of addicted mice during basal conditions was reversed after rimonabant administration.
9. The blockade of CB₁ receptors by rimonabant restored PL mPFC control of the hfo circuit in addicted mice during decision-making.
10. The blockade of CB₁ receptors by rimonabant corrected NAc core control of the circuit during reward expectation in addicted mice normalizing gamma synchrony in the NAc.
11. PL mPFC – NAc core circuit communication at high frequencies during decision-making is not still disrupted in addicted mice at the medium period stage.
12. Further analysis during decision-making, reward expectation, and rewarding periods at different stages of the medium-term operant training will be performed to study the evolution of neural abnormalities in addicted mice.

13. Our findings provide neurophysiological evidence supporting the acceptance of the food addiction construct, which could open new diagnostic and/or therapeutic possibilities for this pathology and for other psychiatric disorders with alterations in food intake behavior.

Bibliography

Aaron B, I., Michael E, S. and Gevins, A. (2004) Effects of marijuana on neurophysiological signals of working and episodic memory, *Psychopharmacology*, 17(6), pp. 214–222.

Abdalla, M. M. I. (2017) Central and peripheral control of food intake., *Endocrine regulations*. Germany, 51(1), pp. 52–70.

Abramowitz, J. S. and Jacoby, R. J. (2015) Obsessive-compulsive and related disorders: a critical review of the new diagnostic class., *Annual review of clinical psychology*. United States, 11, pp. 165–186.

Aguilar-Valles, A. *et al.* (2014) Methamphetamine-Associated Memory is Regulated by a Writer and an Eraser of Permissive Histone Methylation, *Biol Psychiatry*, 76(1), pp. 57–65.

Aleman-González, M. *et al.* (2020) Prefrontal-hippocampal functional connectivity encodes recognition memory and is impaired in intellectual disability, *Proceedings of the National Academy of Sciences of the United States of America*, 117(21).

Alger, B. E. and Kim, J. (2011) Supply and demand for endocannabinoids., *Trends in neurosciences*, 34(6), pp. 304–315.

Alles, J. *et al.* (2019) An estimate of the total number of true human miRNAs, *Nucleic Acids Research*, 47(7), pp. 3353–3364.

Alonso-Alonso, M. *et al.* (2015) Food reward system: current perspectives and future research needs, *Nutrition reviews*. 2015/04/09. Oxford University Press, 73(5), pp. 296–307.

Alonso, P. *et al.* (2015) Deep Brain Stimulation for Obsessive-Compulsive Disorder: A Meta-Analysis of Treatment Outcome and

- Predictors of Response., *PloS one*, 10(7), p. e0133591.
- Amemiya, S. and Redish, A. D. (2018) Hippocampal Theta-Gamma Coupling Reflects State-Dependent Information Processing in Decision Making., *Cell reports*, 22(12), pp. 3328–3338.
- American Psychiatric Association (2013) *Diagnostic and Statistical Manual of Mental Disorders, 5th Edition (DSM-5)*. Washington, DC. USA.
- Andrews, A. J. and Luger, K. (2011) Nucleosome Structure(s) and Stability: Variations on a Theme, *Annual Review of Biophysics*, 40(1), pp. 99–117.
- Anthony, J. C., Warner, L. a. and Kessler, R. C. (1994) Comparative epidemiology of dependence on tobacco, alcohol, controlled substances, and inhalants: Basic findings from the National Comorbidity Survey., *Experimental and Clinical Psychopharmacology*, 2(3), pp. 244–268.
- de Araujo, I. E., Schatzker, M. and Small, D. M. (2020) Rethinking Food Reward, *Annual Review of Psychology*. Annual Reviews, 71(1), pp. 139–164.
- Asadi, A. *et al.* (2022) Obesity and gut-microbiota-brain axis: A narrative review., *Journal of clinical laboratory analysis*. United States, p. e24420.
- Atwood, B. K. and Mackie, K. (2010) CB2: a cannabinoid receptor with an identity crisis., *British journal of pharmacology*, 160(3), pp. 467–479.

Avena, N. M., Bocarsly, M. E. and Hoebel, B. G. (2012) Animal models of sugar and fat bingeing: relationship to food addiction and increased body weight., *Methods in molecular biology (Clifton, N.J.)*. United States, 829, pp. 351–365.

Babbs, R. K. *et al.* (2013) Decreased caudate response to milkshake is associated with higher body mass index and greater impulsivity., *Physiology & behavior*, 121, pp. 103–111.

Bagramyan, A. *et al.* (2021) Focus-tunable microscope for imaging small neuronal processes in freely moving animals, *Photon. Res. OSA*, 9(7), pp. 1300–1309.

Baik, J.-H. (2013) Dopamine signaling in reward-related behaviors., *Frontiers in neural circuits*, 7, p. 152.

Ball, K. T., Combs, T. A. and Beyer, D. N. (2011) Opposing roles for dopamine D1- and D2-like receptors in discrete cue-induced reinstatement of food seeking., *Behavioural brain research*. Netherlands, 222(2), pp. 390–393.

Balla, A. *et al.* (2018) Cannabinoid-1 receptor neutral antagonist reduces binge-like alcohol consumption and alcohol-induced accumbal dopaminergic signaling., *Neuropharmacology*, 131, pp. 200–208.

Bartholow, B. D., Lust, S. A. and Tragesser, S. L. (2010) Specificity of P3 Event-related potential reactivity to alcohol cues in individuals low in alcohol sensitivity, *Psychology of Addictive Behaviors*, 24(2), pp. 220–228.

Basar, K. *et al.* (2010) Nucleus accumbens and impulsivity.,

Progress in neurobiology. England, 92(4), pp. 533–557.

Bastos, A. M. and Schoffelen, J.-M. (2015) A Tutorial Review of Functional Connectivity Analysis Methods and Their Interpretational Pitfalls., *Frontiers in systems neuroscience*, 9, p. 175.

Bauer, L. O. and Manning, K. J. (2016) Challenges in the Detection of Working Memory and Attention Decrements among Overweight Adolescent Girls., *Neuropsychobiology*, 73(1), pp. 43–51.

Beaulieu, J.-M. and Gainetdinov, R. R. (2011) The physiology, signaling, and pharmacology of dopamine receptors., *Pharmacological reviews*. United States, 63(1), pp. 182–217.

Bello, N. T. and Hajnal, A. (2010) Dopamine and binge eating behaviors., *Pharmacology, biochemistry, and behavior*, 97(1), pp. 25–33.

Bellocchio, L. *et al.* (2010) Bimodal control of stimulated food intake by the endocannabinoid system., *Nature neuroscience*. United States, 13(3), pp. 281–283.

Bénard, G. *et al.* (2012) Mitochondrial CB₁ receptors regulate neuronal energy metabolism., *Nature neuroscience*. United States, 15(4), pp. 558–564.

Benowitz, N. L. *et al.* (1980) Metabolic and psychophysiologic studies of cannabidiol-hexobarbital interaction, *Clinical Pharmacology & Therapeutics*, 28(1), pp. 115–120.

Berridge, K. C. (1996) Food reward: brain substrates of wanting and liking., *Neuroscience and biobehavioral reviews*. United States,

20(1), pp. 1–25.

Berrios, J. *et al.* (2016) Loss of UBE3A from TH-expressing neurons suppresses GABA co-release and enhances VTA-NAc optical self-stimulation., *Nature communications*, 7, p. 10702.

Bird, A. (2002) DNA methylation patterns and epigenetic memory, *Genes and Development*, 16, pp. 16–21.

Blanco-Gandia, M. C., Montagud-Romero, S. and Rodríguez-Arias, M. (2021) Binge eating and psychostimulant addiction., *World journal of psychiatry*, 11(9), pp. 517–529.

Blevins, J. E. *et al.* (2000) Effects of threonine injections in the lateral hypothalamus on intake of amino acid imbalanced diets in rats., *Brain research*. Netherlands, 879(1–2), pp. 65–72.

Blevins, J. E. and Baskin, D. G. (2010) Hypothalamic-brainstem circuits controlling eating, *Forum of nutrition*. 2009/11/27, 63, pp. 133–140.

Blum, K. *et al.* (1996) Increased prevalence of the Taq I A1 allele of the dopamine receptor gene (DRD2) in obesity with comorbid substance use disorder: a preliminary report, *Pharmacogenetics and Genomics*, 6(4).

Blum, K., Thanos, P. K. and Gold, M. S. (2014) Dopamine and glucose, obesity, and reward deficiency syndrome., *Frontiers in Psychology*. Blum, Kenneth: 101 Colorado Street, Suite 1702, Austin, TX, US, 78701, drd2gene@gmail.com: Frontiers Media S.A.

Blum, K. *et al.* (2018) Introducing Precision Addiction Management

of Reward Deficiency Syndrome, the Construct That Underpins All Addictive Behaviors , *Frontiers in Psychiatry* . Available at: <https://www.frontiersin.org/article/10.3389/fpsyt.2018.00548>.

Bock, R. *et al.* (2013) Strengthening the accumbal indirect pathway promotes resilience to compulsive cocaine use., *Nature neuroscience*, 16(5), pp. 632–638.

Böcker, K. B. E. *et al.* (2010) Cannabinoid modulations of resting state EEG theta power and working memory are correlated in humans, *Journal of Cognitive Neuroscience*, 22(9), pp. 1906–1916.

Bodetto, S. P. *et al.* (2013) Cocaine represses protein phosphatase-1C β through DNA methylation and Methyl-CpG Binding Protein-2 recruitment in adult rat brain, *Neuropharmacology*. Elsevier Ltd, 73, pp. 31–40.

Bosier, B., Muccioli, G. G., Hermans, E. and Lambert, D. M. (2010) Functionally selective cannabinoid receptor signalling: therapeutic implications and opportunities., *Biochemical pharmacology*. England, 80(1), pp. 1–12.

Bouarab, C., Thompson, B. and Polter, A. M. (2019) VTA GABA Neurons at the Interface of Stress and Reward, *Frontiers in Neural Circuits*, 13.

Bozarth, M. A. and Wise, R. A. (1983) Neural substrates of opiate reinforcement, *Progress in Neuro-Psychopharmacology and Biological Psychiatry*, 7(4), pp. 569–575.

Bray, G. A. (2004) Medical consequences of obesity., *The Journal of clinical endocrinology and metabolism*. United States, 89(6), pp.

2583–2589.

Brimblecombe, K. R. and Cragg, S. J. (2017) The Striosome and Matrix Compartments of the Striatum: A Path through the Labyrinth from Neurochemistry toward Function., *ACS chemical neuroscience*. United States, 8(2), pp. 235–242.

Britt, J. P. and Bonci, A. (2013) Optogenetic interrogations of the neural circuits underlying addiction., *Current opinion in neurobiology*, 23(4), pp. 539–545.

Bromberg-Martin, E. S., Matsumoto, M. and Hikosaka, O. (2010) Dopamine in motivational control: rewarding, aversive, and alerting., *Neuron*, 68(5), pp. 815–834.

Bruinsma, K. and Taren, D. L. (1999) Chocolate: food or drug?, *Journal of the American Dietetic Association*. United States, 99(10), pp. 1249–1256.

Brusco, A., Tagliaferro, P., Saez, T. and Onaivi, E. S. (2008) Postsynaptic localization of CB2 cannabinoid receptors in the rat hippocampus., *Synapse (New York, N.Y.)*. United States, 62(12), pp. 944–949.

Bulik, C. M., Sullivan, P. F., Fear, J. L. and Joyce, P. R. (1997) Eating disorders and antecedent anxiety disorders: a controlled study., *Acta psychiatrica Scandinavica*. United States, 96(2), pp. 101–107.

Burdyga, G. *et al.* (2006) Ghrelin receptors in rat and human nodose ganglia: putative role in regulating CB-1 and MCH receptor abundance., *American journal of physiology. Gastrointestinal and liver physiology*. United States, 290(6), pp. G1289-97.

Burghardt, P. R. *et al.* (2015) Endogenous Opioid Mechanisms Are Implicated in Obesity and Weight Loss in Humans., *The Journal of clinical endocrinology and metabolism*, 100(8), pp. 3193–3201.

Burgos-Robles, A., Vidal-Gonzalez, I. and Quirk, G. J. (2009) Sustained conditioned responses in prelimbic prefrontal neurons are correlated with fear expression and extinction failure., *The Journal of neuroscience : the official journal of the Society for Neuroscience*, 29(26), pp. 8474–8482.

Burrows, T., Skinner, J., McKenna, R. and Rollo, M. (2017) Food Addiction, Binge Eating Disorder, and Obesity: Is There a Relationship?, *Behavioral sciences (Basel, Switzerland)*, 7(3).

Burrows, T. *et al.* (2018) Food addiction and associations with mental health symptoms: a systematic review with meta-analysis., *Journal of human nutrition and dietetics : the official journal of the British Dietetic Association*. England, 31(4), pp. 544–572.

Caillé, S. *et al.* (2009) Voluntary nicotine consumption triggers in vivo potentiation of cortical excitatory drives to midbrain dopaminergic neurons, *Journal of Neuroscience*, 29(33), pp. 10410–10415.

Calabresi, P. *et al.* (2014) Direct and indirect pathways of basal ganglia: a critical reappraisal., *Nature neuroscience*. United States, 17(8), pp. 1022–1030.

Calu, D. J. *et al.* (2013) Optogenetic inhibition of dorsal medial prefrontal cortex attenuates stress-induced reinstatement of palatable food seeking in female rats., *The Journal of neuroscience : the*

- official journal of the Society for Neuroscience*, 33(1), pp. 214–226.
- Cameron, C. M. *et al.* (2019) Increased Cocaine Motivation Is Associated with Degraded Spatial and Temporal Representations in IL-NAc Neurons, *Neuron*. Elsevier Inc., 103(1), pp. 80-91.e7.
- Carelli, R. M., King, V. C., Hampson, R. E. and Deadwyler, S. A. (1993) Firing patterns of nucleus accumbens neurons during cocaine self-administration in rats, *Brain Research*, 626(1–2), pp. 14–22.
- Carelli, R. M. and Deadwyler, S. A. (1996) Dual factors controlling activity of nucleus accumbens cell-firing during cocaine self-administration, *Synapse*. Synapse, 24(3), pp. 308–311.
- Caron, A. and Richard, D. (2017) Neuronal systems and circuits involved in the control of food intake and adaptive thermogenesis., *Annals of the New York Academy of Sciences*. United States, 1391(1), pp. 35–53.
- Carr, D. B. and Sesack, S. R. (2000) Projections from the rat prefrontal cortex to the ventral tegmental area: target specificity in the synaptic associations with mesoaccumbens and mesocortical neurons., *The Journal of neuroscience : the official journal of the Society for Neuroscience*, 20(10), pp. 3864–3873.
- Cassin, S. E. *et al.* (2019) Ethical, Stigma, and Policy Implications of Food Addiction: A Scoping Review., *Nutrients*, 11(4).
- Castelnuovo, G. *et al.* (2017) Cognitive behavioral therapy to aid weight loss in obese patients: Current perspectives., *Psychology Research and Behavior Management*. Castelnuovo, Gianluca: Clinical Psychology Lab, Istituto Auxologico Italiano IRCCS, San

Giuseppe Hospital, Strada Cadorna 90 – Piancavallo di Oggebbio, Verbania, Italy, 28824, gianluca.castelnuovo@auxologico.it: Dove Medical Press Ltd.

Castillo, P. E., Younts, T. J., Chávez, A. E. and Hashimoto, Y. (2012) Endocannabinoid signaling and synaptic function., *Neuron*, 76(1), pp. 70–81.

Castro, D. C. and Bruchas, M. R. (2019) A Motivational and Neuropeptidergic Hub: Anatomical and Functional Diversity within the Nucleus Accumbens Shell., *Neuron*, 102(3), pp. 529–552.

Catalanotto, C., Cogoni, C. and Zardo, G. (2016) MicroRNA in control of gene expression: An overview of nuclear functions, *International Journal of Molecular Sciences*, 17(10).

Ceceli, A. O., Bradberry, C. W. and Goldstein, R. Z. (2022) The neurobiology of drug addiction: cross-species insights into the dysfunction and recovery of the prefrontal cortex., *Neuropsychopharmacology: official publication of the American College of Neuropsychopharmacology*, 47(1), pp. 276–291.

Chami, R. *et al.* (2019) Neural responses to food stimuli among individuals with eating and weight disorders: a systematic review of event-related potentials., *International review of psychiatry (Abingdon, England)*. England, 31(4), pp. 318–331.

Chan, D. *et al.* (2021) Induction of specific brain oscillations may restore neural circuits and be used for the treatment of Alzheimer's disease., *Journal of internal medicine*. England, 290(5), pp. 993–1009.

Chang, J. Y., Sawyer, S. F., Lee, R. S. and Woodward, D. J. (1994) Electrophysiological and pharmacological evidence for the role of the nucleus accumbens in cocaine self-administration in freely moving rats, *Journal of Neuroscience*, 14(3 I), pp. 1224–1244.

Chang, J. Y., Zhang, L. L., Janak, P. H. and Woodward, D. J. (1997) Neuronal responses in prefrontal cortex and nucleus accumbens during heroin self-administration in freely moving rats, *Brain Research*, 754(1–2), pp. 12–20.

Cheer, J. F., Marsden, C. A., Kendall, D. A. and Mason, R. (2000) Lack of response suppression follows repeated ventral tegmental cannabinoid administration: an in vitro electrophysiological study, *Neuroscience*, 99(4), pp. 661–667.

Cheer, J. F. *et al.* (2004) Cannabinoids enhance subsecond dopamine release in the nucleus accumbens of awake rats., *The Journal of neuroscience : the official journal of the Society for Neuroscience*, 24(18), pp. 4393–4400.

Chen, B. T. *et al.* (2013) Rescuing cocaine-induced prefrontal cortex hypoactivity prevents compulsive cocaine seeking, *Nature*. Nature Publishing Group, 496(7445), pp. 359–362.

Chen, C.-M. A. *et al.* (2014) GABA level, gamma oscillation, and working memory performance in schizophrenia, *NeuroImage: Clinical*, 4, pp. 531–539.

Di Chiara, G. and Imperato, A. (1988) Drugs abused by humans preferentially increase synaptic dopamine concentrations in the mesolimbic system of freely moving rats, *Proceedings of the*

National Academy of Sciences, 85(14), pp. 5274 LP – 5278.

Di Chiara, G. (2002) Nucleus accumbens shell and core dopamine: differential role in behavior and addiction., *Behavioural brain research*. Netherlands, 137(1–2), pp. 75–114.

Childers, S. R. and Deadwyler, S. A. (1996) Role of cyclic AMP in the actions of cannabinoid receptors., *Biochemical pharmacology*. England, 52(6), pp. 819–827.

Cifuentes, L. and Acosta, A. (2021) Homeostatic regulation of food intake., *Clinics and research in hepatology and gastroenterology*. France, 46(2), p. 101794.

Cleary, D. R., Ozpinar, A., Raslan, A. M. and Ko, A. L. (2015) Deep brain stimulation for psychiatric disorders: where we are now., *Neurosurgical focus*. United States, 38(6), p. E2.

Comings, D. E. and Blum, K. (2000) Reward deficiency syndrome: genetic aspects of behavioral disorders., *Progress in brain research*. Netherlands, 126, pp. 325–341.

Conceição, E. M. *et al.* (2014) What is ‘grazing’? Reviewing its definition, frequency, clinical characteristics, and impact on bariatric surgery outcomes, and proposing a standardized definition., *Surgery for obesity and related diseases : official journal of the American Society for Bariatric Surgery*. United States, 10(5), pp. 973–982.

Cooper, S., Robison, A. J. and Mazei-Robison, M. S. (2017) Reward Circuitry in Addiction, *Neurotherapeutics : the journal of the American Society for Experimental NeuroTherapeutics*. Springer US, 14(3), pp. 687–697.

Cossrow, N. *et al.* (2016) Estimating the Prevalence of Binge Eating Disorder in a Community Sample From the United States: Comparing DSM-IV-TR and DSM-5 Criteria., *The Journal of clinical psychiatry*. United States, 77(8), pp. e968-74.

Cota, D., Tschöp, M. H., Horvath, T. L. and Levine, A. S. (2006) Cannabinoids, opioids and eating behavior: the molecular face of hedonism?, *Brain research reviews*. Netherlands, 51(1), pp. 85–107.

Cottone, P. *et al.* (2009) CRF system recruitment mediates dark side of compulsive eating., *Proceedings of the National Academy of Sciences of the United States of America*, 106(47), pp. 20016–20020.

Coutin-Churchman, P., Moreno, R., Añez, Y. and Vergara, F. (2006) Clinical correlates of quantitative EEG alterations in alcoholic patients, *Clinical Neurophysiology*, 117(4), pp. 740–751.

Covelo, I. R. *et al.* (2014) Manipulation of GABA in the ventral pallidum, but not the nucleus accumbens, induces intense, preferential, fat consumption in rats., *Behavioural brain research*, 270, pp. 316–325.

Covey, D. P. *et al.* (2017) Endocannabinoid modulation of dopamine neurotransmission, *Neuropharmacology*. 2017/04/25, 124, pp. 52–61.

Creed, M., Pascoli, V. J. and Lüscher, C. (2015) Addiction therapy. Refining deep brain stimulation to emulate optogenetic treatment of synaptic pathology., *Science (New York, N.Y.)*. United States, 347(6222), pp. 659–664.

Creed, M. *et al.* (2016) Convergence of Reinforcing and Anhedonic

Cocaine Effects in the Ventral Pallidum., *Neuron*, 92(1), pp. 214–226.

Crunelle, C. L. *et al.* (2012) Substrates of neuropsychological functioning in stimulant dependence: a review of functional neuroimaging research, *Brain and Behavior*. John Wiley & Sons, Ltd, 2(4), pp. 499–523.

Cummings, D. E. *et al.* (2001) A preprandial rise in plasma ghrelin levels suggests a role in meal initiation in humans., *Diabetes*. United States, 50(8), pp. 1714–1719.

Cummings, D. E. (2006) Ghrelin and the short- and long-term regulation of appetite and body weight., *Physiology & behavior*. United States, 89(1), pp. 71–84.

D’Addario, C. *et al.* (2014) Endocannabinoid signaling and food addiction, *Neuroscience & Biobehavioral Reviews*, 47, pp. 203–224.

Dalle Molle, R. *et al.* (2017) Gene and environment interaction: Is the differential susceptibility hypothesis relevant for obesity?, *Neuroscience and biobehavioral reviews*, 73, pp. 326–339.

Dalley, J. W. *et al.* (2007) Nucleus accumbens D2/3 receptors predict trait impulsivity and cocaine reinforcement., *Science (New York, N.Y.)*, 315(5816), pp. 1267–1270.

Dasilva, M., Grieve, K. L., Cudeiro, J. and Rivadulla, C. (2014) Anandamide activation of CB1 receptors increases spontaneous bursting and oscillatory activity in the thalamus, *Neuroscience*, 265, pp. 72–82.

Davis, C. *et al.* (2008) Reward sensitivity and the D2 dopamine receptor gene: A case-control study of binge eating disorder., *Progress in neuro-psychopharmacology & biological psychiatry*. England, 32(3), pp. 620–628.

Davis, C. *et al.* (2011) Evidence that ‘food addiction’ is a valid phenotype of obesity., *Appetite*. England, 57(3), pp. 711–717.

Davis, C. (2013) A narrative review of binge eating and addictive behaviors: shared associations with seasonality and personality factors., *Frontiers in psychiatry*, 4, p. 183.

Davis, C. (2017) A commentary on the associations among ‘food addiction’, binge eating disorder, and obesity: Overlapping conditions with idiosyncratic clinical features., *Appetite*. England, 115, pp. 3–8.

Davis, C. A. *et al.* (2009) Dopamine for ‘wanting’ and opioids for ‘liking’: a comparison of obese adults with and without binge eating., *Obesity (Silver Spring, Md.)*. United States, 17(6), pp. 1220–1225.

Day, J. J., Jones, J. L. and Carelli, R. M. (2011) Nucleus accumbens neurons encode predicted and ongoing reward costs in rats, *The European journal of neuroscience*. 2010/12/29, 33(2), pp. 308–321.

Day, J. J. *et al.* (2013) DNA methylation regulates associative reward learning Jeremy, *Nature Neuroscience*, 16(10), pp. 1445–1452.

Deadwyler, S. A., Hayashizaki, S., Cheer, J. and Hampson, R. E. (2004) Reward, memory and substance abuse: Functional neuronal circuits in the nucleus accumbens, in *Neuroscience and Biobehavioral Reviews*. Elsevier Ltd, pp. 703–711.

Delgado-Sallent, C. *et al.* (2021) Atypical, but Not Typical, Antipsychotic Drugs Reduce Hypersynchronized Prefrontal-Hippocampal Circuits during Psychosis-Like States in Mice: Contribution of 5-HT_{2A} and 5-HT_{1A} Receptors., *Cerebral cortex* (New York, N.Y. : 1991). United States.

Deroche-Gamonet, V., Belin, D. and Piazza, P. V. (2004b) Evidence for addiction-like behavior in the rat, *Science*, 305(5686), pp. 1014–1017.

Deroche-Gamonet, V. and Piazza, P. V. (2014) Psychobiology of cocaine addiction: Contribution of a multi-symptomatic animal model of loss of control, *Neuropharmacology*. Elsevier, 76(PART B), pp. 437–449.

Devlin, M. J. (2001) Binge-eating disorder and obesity. A combined treatment approach., *The Psychiatric clinics of North America*. United States, 24(2), pp. 325–335.

Diana, M. *et al.* (2017) Rehabilitating the addicted brain with transcranial magnetic stimulation., *Nature reviews. Neuroscience*. England, 18(11), pp. 685–693.

DiFeliceantonio, A. G. and Small, D. M. (2019) Dopamine and diet-induced obesity, *Nature Neuroscience*, 22(1), pp. 1–2.

Domenech, P. and Koechlin, E. (2015) Executive control and decision-making in the prefrontal cortex, *Current Opinion in Behavioral Sciences*, 1, pp. 101–106.

Domingo-Rodriguez, L. *et al.* (2020) A specific prelimbic-nucleus accumbens pathway controls resilience versus vulnerability to food

- addiction, *Nature Communications*. Springer US, 11(1), pp. 1–16.
- Donnelly, N. A. *et al.* (2014) Oscillatory activity in the medial prefrontal cortex and nucleus accumbens correlates with impulsivity and reward outcome, *PLoS ONE*, 9(10), pp. 14–17.
- Douglas, R. J. and Martin, K. A. C. (2004) Neuronal circuits of the neocortex., *Annual review of neuroscience*. United States, 27, pp. 419–451.
- Dreyer, J. K., Herrik, K. F., Berg, R. W. and Hounsgaard, J. D. (2010) Influence of phasic and tonic dopamine release on receptor activation., *The Journal of neuroscience : the official journal of the Society for Neuroscience*, 30(42), pp. 14273–14283.
- Ducci, F. and Goldman, D. (2012) The genetic basis of addictive disorders., *The Psychiatric clinics of North America*, 35(2), pp. 495–519.
- el-Guebaly, N. *et al.* (2012) Compulsive features in behavioural addictions: the case of pathological gambling., *Addiction (Abingdon, England)*, 107(10), pp. 1726–1734.
- Everitt, B. J. and Robbins, T. W. (2005) Neural systems of reinforcement for drug addiction: from actions to habits to compulsion., *Nature neuroscience*. United States, 8(11), pp. 1481–1489.
- Fazzino, T. L., Rohde, K. and Sullivan, D. K. (2019) Hyper-Palatable Foods: Development of a Quantitative Definition and Application to the US Food System Database, *Obesity*. John Wiley & Sons, Ltd, 27(11), pp. 1761–1768.

Feldman, J. and Eysenck, S. B. (1986) Addictive personality traits in bulimic patients., *Personality and Individual Differences*. Netherlands: Elsevier Science, 7(6), pp. 923–926.

Fernandez-Aranda, F., Karwautz, A. and Treasure, J. (2018) Food addiction: A transdiagnostic construct of increasing interest, *European Eating Disorders Review*, 26(6), pp. 536–540.

Ferrulli, A. *et al.* (2019) Weight loss induced by deep transcranial magnetic stimulation in obesity: A randomized, double-blind, sham-controlled study, *Diabetes, Obesity and Metabolism*, 21(8), pp. 1849–1860.

Ferssiwi, A., Cardo, B. and Velley, L. (1987) Gustatory preference-aversion thresholds are increased by ibotenic acid lesion of the lateral hypothalamus in the rat., *Brain research*. Netherlands, 437(1), pp. 142–150.

Filipowicz, W., Bhattacharyya, S. N. and Sonenberg, N. (2008) Mechanisms of post-transcriptional regulation by microRNAs: Are the answers in sight?, *Nature Reviews Genetics*. Nat Rev Genet, pp. 102–114.

Finlayson, G. (2017) Food addiction and obesity: unnecessary medicalization of hedonic overeating., *Nature reviews. Endocrinology*. England, 13(8), pp. 493–498.

Fletcher, P. C. and Kenny, P. J. (2018) Food addiction: a valid concept?, *Neuropsychopharmacology: official publication of the American College of Neuropsychopharmacology*, 43(13), pp. 2506–2513.

Flint, A. J. *et al.* (2014) Food-addiction scale measurement in 2 cohorts of middle-aged and older women, *The American journal of clinical nutrition*. 2014/01/22. American Society for Nutrition, 99(3), pp. 578–586.

Flores, A., Maldonado, R. and Berrendero, F. (2013) Cannabinoid-hypocretin cross-talk in the central nervous system: what we know so far, *Frontiers in neuroscience*. Frontiers Media S.A., 7, p. 256.

Ford, C. P. (2014) The role of D2-autoreceptors in regulating dopamine neuron activity and transmission, *Neuroscience*. 2014/01/23, 282, pp. 13–22.

Fox, M. K. *et al.* (2006) Relationship between portion size and energy intake among infants and toddlers: evidence of self-regulation., *Journal of the American Dietetic Association*. United States, 106(1 Suppl 1), pp. S77-83.

Frei, E. *et al.* (2001) Localization of MDMA-induced brain activity in healthy volunteers using low resolution brain electromagnetic tomography (LORETA), *Human Brain Mapping*, 14(3), pp. 152–165.

Friedman, J. M. (2004) Modern science versus the stigma of obesity., *Nature medicine*. United States, 10(6), pp. 563–569.

Fuhrmann, F. *et al.* (2015) Locomotion, Theta Oscillations, and the Speed-Related Firing of Hippocampal Neurons Are Controlled by a Medial Septal Glutamatergic Circuit., *Neuron*. United States, 86(5), pp. 1253–1264.

Furth, K. E. *et al.* (2013) Dopamine, cognitive function, and gamma

oscillations: role of D4 receptors, *Frontiers in cellular neuroscience*. Frontiers Media S.A., 7, p. 102.

Galaj, E., Bi, G.-H., Yang, H.-J. and Xi, Z.-X. (2020) Cannabidiol attenuates the rewarding effects of cocaine in rats by CB2, 5-HT(1A) and TRPV1 receptor mechanisms., *Neuropharmacology*, 167, p. 107740.

García-Blanco, A. *et al.* (2022) MicroRNAs signatures associated with vulnerability to food addiction in mice and humans, *The Journal of Clinical Investigation*. The American Society for Clinical Investigation.

Gearhardt, A. N., Corbin, W. R. and Brownell, K. D. (2009) Preliminary validation of the Yale Food Addiction Scale, *Appetite*, 52(2), pp. 430–436.

Gearhardt, A. N. *et al.* (2012) An examination of the food addiction construct in obese patients with binge eating disorder., *The International journal of eating disorders*, 45(5), pp. 657–663.

Gearhardt, A. N., Boswell, R. G. and White, M. A. (2014) The association of ‘food addiction’ with disordered eating and body mass index., *Eating behaviors*, 15(3), pp. 427–433.

Gearhardt, A. N., Corbin, W. R. and Brownell, K. D. (2016) Development of the Yale Food Addiction Scale Version 2.0., *Psychology of Addictive Behaviors*, 30(1), pp. 113–121.

Gearhardt, A. N. and Hebebrand, J. (2021) The concept of ‘food addiction’ helps inform the understanding of overeating and obesity: YES., *The American journal of clinical nutrition*. United States,

113(2), pp. 263–267.

Gérard, N. *et al.* (2011) Brain type 1 cannabinoid receptor availability in patients with anorexia and bulimia nervosa., *Biological psychiatry*. United States, 70(8), pp. 777–784.

Gerfen, C. R., Baimbridge, K. G. and Thibault, J. (1987) The neostriatal mosaic: III. Biochemical and developmental dissociation of patch-matrix mesostriatal systems., *The Journal of neuroscience : the official journal of the Society for Neuroscience*, 7(12), pp. 3935–3944.

Gerfen, C. R. and Surmeier, D. J. (2011) Modulation of striatal projection systems by dopamine., *Annual review of neuroscience*, 34, pp. 441–466.

Ghosh, K. K. *et al.* (2011) Miniaturized integration of a fluorescence microscope, *Nature Methods*, 8(10), pp. 871–878.

Giuliano, C. *et al.* (2012) Inhibition of opioid transmission at the μ -opioid receptor prevents both food seeking and binge-like eating., *Neuropsychopharmacology : official publication of the American College of Neuropsychopharmacology*, 37(12), pp. 2643–2652.

Glass, M. J., Billington, C. J. and Levine, A. S. (1999) Role of lipid type on morphine-stimulated diet selection in rats, *American Journal of Physiology-Regulatory, Integrative and Comparative Physiology*. American Physiological Society, 277(5), pp. R1345–R1350.

Goda, S. A. *et al.* (2015) Aberrant high frequency oscillations recorded in the rat nucleus accumbens in the methylazoxymethanol acetate neurodevelopmental model of schizophrenia., *Progress in*

neuro-psychopharmacology & biological psychiatry. England, 61, pp. 44–51.

Goldstein, R. Z. and Volkow, N. D. (2002) Drug addiction and its underlying neurobiological basis: neuroimaging evidence for the involvement of the frontal cortex, *The American journal of psychiatry*, 159(10), pp. 1642–1652.

Goldstein, R. Z. and Volkow, N. D. (2011) Dysfunction of the prefrontal cortex in addiction: neuroimaging findings and clinical implications, *Nat Rev Neurosci.*, 23(1), pp. 1–7.

Gomez, J. L. *et al.* (2017) Chemogenetics Revealed: DREADD Occupancy and Activation Via Converted Clozapine, *Science*, 507(August), pp. 503–507.

Gong, J.-P. *et al.* (2006) Cannabinoid CB2 receptors: immunohistochemical localization in rat brain., *Brain research*. Netherlands, 1071(1), pp. 10–23.

González-Muniesa, P. *et al.* (2017) Obesity, *Nature Reviews Disease Primers*, 3(1), p. 17034.

Gordon, E. L., Ariel-Donges, A. H., Bauman, V. and Merlo, L. J. (2018) What is the evidence for ‘food addiction?’ A systematic review, *Nutrients*, 10(4), pp. 1–30.

Gramfort, A. *et al.* (2013) MEG and EEG data analysis with MNE-Python., *Frontiers in neuroscience*, 7, p. 267.

Greenberg, J. L. Overlapping addictions and self-esteem among college men and women., *Addictive behaviors*, pp. 565–571.

Greeno, C. G. and Wing, R. R. (1994) Stress-induced eating., *Psychological bulletin*. United States, 115(3), pp. 444–464.

Greenway, F. L. *et al.* (2010) Effect of naltrexone plus bupropion on weight loss in overweight and obese adults (COR-I): a multicentre, randomised, double-blind, placebo-controlled, phase 3 trial., *Lancet (London, England)*. England, 376(9741), pp. 595–605.

Grilo, C. M. *et al.* (2011) Cognitive-behavioral therapy, behavioral weight loss, and sequential treatment for obese patients with binge-eating disorder: a randomized controlled trial., *Journal of consulting and clinical psychology*, 79(5), pp. 675–685.

Grilo, C. M., Reas, D. L. and Mitchell, J. E. (2016) Combining Pharmacological and Psychological Treatments for Binge Eating Disorder: Current Status, Limitations, and Future Directions., *Current psychiatry reports*. United States, 18(6), p. 55.

Gruber, M. J. *et al.* (2013) Expected reward modulates encoding-related theta activity before an event, *NeuroImage*, 64, pp. 68–74.

Guggisberg, A. G., Dalal, S. S., Findlay, A. M. and Nagarajan, S. S. (2007) High-frequency oscillations in distributed neural networks reveal the dynamics of human decision making., *Frontiers in human neuroscience*, 1, p. 14.

Gutiérrez-Rodríguez, A. *et al.* (2018) Localization of the cannabinoid type-1 receptor in subcellular astrocyte compartments of mutant mouse hippocampus., *Glia*. United States, 66(7), pp. 1417–1431.

Haliloglu, B. and Bereket, A. (2015) Hypothalamic obesity in children: pathophysiology to clinical management., *Journal of*

pediatric endocrinology & metabolism : JPEM. Germany, 28(5–6), pp. 503–513.

Hammond, D. C. (2011) What is Neurofeedback: An Update, *Journal of Neurotherapy*. Routledge, 15(4), pp. 305–336.

Haracz, J. L. *et al.* (1998) Amphetamine effects on striatal neurons: implications for models of dopamine function., *Neuroscience and biobehavioral reviews*. United States, 22(5), pp. 613–622.

Harat, M. *et al.* (2016) Nucleus accumbens stimulation in pathological obesity., *Neurologia i neurochirurgia polska*. Poland, 50(3), pp. 207–210.

Hebebrand, J. *et al.* (2014) ‘Eating addiction’, rather than ‘food addiction’, better captures addictive-like eating behavior., *Neuroscience and biobehavioral reviews*. United States, 47, pp. 295–306.

Hebebrand, J. and Gearhardt, A. N. (2021) The concept of ‘food addiction’ helps inform the understanding of overeating and obesity: NO., *The American journal of clinical nutrition*. United States, 113(2), pp. 268–273.

Heber, D. and Carpenter, C. L. (2011) Addictive genes and the relationship to obesity and inflammation., *Molecular neurobiology*. Springer, 44(2), pp. 160–5.

Heidbreder, C. A. and Groenewegen, H. J. (2003) The medial prefrontal cortex in the rat: Evidence for a dorso-ventral distinction based upon functional and anatomical characteristics, *Neuroscience and Biobehavioral Reviews*, 27(6), pp. 555–579.

Heinsbroek, J. A. *et al.* (2020) Opposing Regulation of Cocaine Seeking by Glutamate and GABA Neurons in the Ventral Pallidum., *Cell reports*. Elsevier B.V., 30(6), pp. 2018-2027.e3.

Heming, R. *et al.* (1994) Cocaine-Induced Increases in EEG Alpha and Beta Activity : Evidence for Reduced Cortical Processing, 11(1).

Hemmings, W. *et al.* (2018) Closing the loop on impulsivity via nucleus accumbens delta-band activity in mice and man, *Proceedings of the National Academy of Sciences*. Proceedings of the National Academy of Sciences, 115(1), pp. 192–197.

Henry, E. A. *et al.* (2014) Cannabis cue reactivity and craving among never, infrequent and heavy cannabis users, *Neuropsychopharmacology*. Nature Publishing Group, 39(5), pp. 1214–1221.

Herkenham, M. *et al.* (1990) Cannabinoid receptor localization in brain., *Proceedings of the National Academy of Sciences of the United States of America*, 87(5), pp. 1932–1936.

Hernández-González, S. *et al.* (2017) A Cognition-Related Neural Oscillation Pattern, Generated in the Prelimbic Cortex, Can Control Operant Learning in Rats., *The Journal of neuroscience : the official journal of the Society for Neuroscience*, 37(24), pp. 5923–5935.

Hernandez, G. and Cheer, J. F. (2012) Effect of CB1 receptor blockade on food-reinforced responding and associated nucleus accumbens neuronal activity in rats, *The Journal of neuroscience : the official journal of the Society for Neuroscience*. Society for Neuroscience, 32(33), pp. 11467–11477.

Hernandez, P. J., Sadeghian, K. and Kelley, A. E. (2002) Early consolidation of instrumental learning requires protein synthesis in the nucleus accumbens., *Nature neuroscience*. United States, 5(12), pp. 1327–1331.

Herning, R. I. *et al.* (1985) Cocaine increases EEG beta: A replication and extension of Hans Berger's historic experiments, *Electroencephalography and Clinical Neurophysiology*, 60(6), pp. 470–477.

Hetherington, M. M. and MacDiarmid, J. I. (1993) 'Chocolate addiction': a preliminary study of its description and its relationship to problem eating., *Appetite*. England, 21(3), pp. 233–246.

Hilker, I. *et al.* (2016) Food Addiction in Bulimia Nervosa: Clinical Correlates and Association with Response to a Brief Psychoeducational Intervention., *European eating disorders review : the journal of the Eating Disorders Association*. England, 24(6), pp. 482–488.

Hitchcock, L. N. and Matthew, L. K. (2014) Histone-mediated epigenetics in addiction, *Prog Mol Biol Transl Sci*, 128(1), pp. 51–87.

Ho, M.-H. *et al.* (2021) Decision-Making in People With Dementia or Mild Cognitive Impairment: A Narrative Review of Decision-Making Tools, *Journal of the American Medical Directors Association*, 22(10), pp. 2056-2062.e4.

van Hoeken, D. and Hoek, H. W. (2020) Review of the burden of eating disorders: mortality, disability, costs, quality of life, and

- family burden., *Current opinion in psychiatry*, 33(6), pp. 521–527.
- Hollander, J. A. *et al.* (2010) Striatal microRNA controls cocaine intake through CREB signalling., *Nature*, 466(7303), pp. 197–202.
- Honey, C. R. *et al.* (2017) Deep Brain Stimulation Target Selection for Parkinson’s Disease., *The Canadian journal of neurological sciences. Le journal canadien des sciences neurologiques*. England, 44(1), pp. 3–8.
- Hopkins, M. *et al.* (2000) The Regulation of Food Intake in Humans., in Feingold, K. R. *et al.* (eds). South Dartmouth (MA).
- Hopkins, M. and Blundell, J. E. (2016) Energy balance, body composition, sedentariness and appetite regulation: pathways to obesity., *Clinical science (London, England: 1979)*. England, 130(18), pp. 1615–1628.
- Horsager, C., Færk, E., Lauritsen, M. B. and Østergaard, S. D. (2021) Food addiction comorbid to mental disorders: A nationwide survey and register-based study, *International Journal of Eating Disorders*, 54(4), pp. 545–560.
- Hsu, C.-C. *et al.* (2020) Reward-related dynamical coupling between basolateral amygdala and nucleus accumbens., *Brain structure & function*, 225(6), pp. 1873–1888.
- Hu, S. S.-J. and Mackie, K. (2015) Distribution of the Endocannabinoid System in the Central Nervous System., *Handbook of experimental pharmacology*. Germany, 231, pp. 59–93.
- Hu, Y. *et al.* (2019) Compulsive drug use is associated with

imbalance of orbitofrontal- and prelimbic-striatal circuits in punishment-resistant individuals, *Proceedings of the National Academy of Sciences*, 116(18), pp. 9066 LP – 9071.

Huang, Y. Y. *et al.* (2014) D1/D5 receptors and histone deacetylation mediate the gateway effect of LTP in hippocampal dentate gyrus, *Learning and Memory*, 21(3), pp. 153–160.

Hübel, C., Marzi, S. J., Breen, G. and Bulik, C. M. (2019) Epigenetics in eating disorders: a systematic review., *Molecular psychiatry*, 24(6), pp. 901–915.

Hume, D. J. *et al.* (2015) Electrophysiological indices of visual food cue-reactivity. Differences in obese, overweight and normal weight women., *Appetite*. England, 85, pp. 126–137.

Hunt, M. J., Garcia, R., Large, C. H. and Kasicki, S. (2008) Modulation of high-frequency oscillations associated with NMDA receptor hypofunction in the rodent nucleus accumbens by lamotrigine., *Progress in neuro-psychopharmacology & biological psychiatry*. England, 32(5), pp. 1312–1319.

Hunt, M. J., Matulewicz, P., Gottesmann, C. and Kasicki, S. (2009) State-dependent changes in high-frequency oscillations recorded in the rat nucleus accumbens., *Neuroscience*. United States, 164(2), pp. 380–386.

Hyman, S. E., Malenka, R. C. and Nestler, E. J. (2006) NEURAL MECHANISMS OF ADDICTION: The Role of Reward-Related Learning and Memory, *Annual Review of Neuroscience*, 29(1), pp. 565–598.

Ifland, J. *et al.* (2015) Clearing the confusion around processed food addiction., *Journal of the American College of Nutrition*. United States, 34(3), pp. 240–243.

Imperator, C. *et al.* (2015) Modification of EEG functional connectivity and EEG power spectra in overweight and obese patients with food addiction: An eLORETA study., *Brain imaging and behavior*. United States, 9(4), pp. 703–716.

Ivezaj, V., White, M. A. and Grilo, C. M. (2016) Examining binge-eating disorder and food addiction in adults with overweight and obesity., *Obesity (Silver Spring, Md.)*, 24(10), pp. 2064–2069.

Jaber, M., Robinson, S. W., Missale, C. and Caron, M. G. (1996) Dopamine receptors and brain function., *Neuropharmacology*. England, 35(11), pp. 1503–1519.

Jager, G. and Witkamp, R. F. (2014) The endocannabinoid system and appetite: relevance for food reward., *Nutrition research reviews*. England, 27(1), pp. 172–185.

Janak, P. H., Chang, J. Y. and Woodward, D. J. (1999) Neuronal spike activity in the nucleus accumbens of behaving rats during ethanol self-administration, *Brain Research*, 817(1–2), pp. 172–184.

Jasinska, A. J., Chen, B. T., Bonci, A. and Stein, E. A. (2015) Dorsal medial prefrontal cortex (MPFC) circuitry in rodent models of cocaine use: implications for drug addiction therapies., *Addiction biology*, 20(2), pp. 215–226.

Jenkins, B. W., Buckhalter, S., Perreault, M. L. and Khokhar, J. Y. (2021) Cannabis Vapor Exposure Alters Neural Circuit Oscillatory

Activity in a Neurodevelopmental Model of Schizophrenia: Exploring the Differential Impact of Cannabis Constituents, *Schizophrenia Bulletin Open*, 3(1).

Jennings, J. H. *et al.* (2015) Visualizing hypothalamic network dynamics for appetitive and consummatory behaviors., *Cell*, 160(3), pp. 516–527.

Jentsch, J. D. and Taylor, J. R. (1999) Impulsivity resulting from frontostriatal dysfunction in drug abuse: implications for the control of behavior by reward-related stimuli., *Psychopharmacology*. Germany, 146(4), pp. 373–390.

Jiang, J., Cui, H. and Rahmouni, K. (2017) Optogenetics and pharmacogenetics: principles and applications, *American Journal of Physiology-Regulatory, Integrative and Comparative Physiology*. American Physiological Society, 313(6), pp. R633–R645.

Johnson, P. M. and Kenny, P. J. (2010) Dopamine D2 receptors in addiction-like reward dysfunction and compulsive eating in obese rats., *Nature neuroscience*, 13(5), pp. 635–641.

Juarez, B., Liu, Y., Zhang, L. and Han, M.-H. (2019) Optogenetic investigation of neural mechanisms for alcohol-use disorder., *Alcohol (Fayetteville, N.Y.)*, 74, pp. 29–38.

Julian, M. D. *et al.* (2003) Neuroanatomical relationship between type 1 cannabinoid receptors and dopaminergic systems in the rat basal ganglia, *Neuroscience*, 119(1), pp. 309–318.

Kabanova, A. *et al.* (2015) Function and developmental origin of a mesocortical inhibitory circuit., *Nature neuroscience*. United States,

18(6), pp. 872–882.

Kalenscher, T., Lansink, C. S., Lankelma, J. V. and Pennartz, C. M. A. (2010) Reward-associated gamma oscillations in ventral striatum are regionally differentiated and modulate local firing activity, *Journal of Neurophysiology*, 103(3), pp. 1658–1672.

Kalivas, P. W. (2005) How do we determine which drug-induced neuroplastic changes are important?, *Nature neuroscience*. United States, 8(11), pp. 1440–1441.

Kano, M. *et al.* (2009) Endocannabinoid-mediated control of synaptic transmission., *Physiological reviews*. United States, 89(1), pp. 309–380.

Kasanetz, F. *et al.* (2010) Transition to addiction is associated with a persistent impairment in synaptic plasticity, *Science*, 328(5986), pp. 1709–1712.

Kasanetz, F. *et al.* (2013) Prefrontal synaptic markers of cocaine addiction-like behavior in rats, *Molecular Psychiatry*, 18(6), pp. 729–737.

Katona, I. and Freund, T. F. (2012) Multiple functions of endocannabinoid signaling in the brain., *Annual review of neuroscience*, 35, pp. 529–558.

Kawamura, Y. *et al.* (2006) The CB1 cannabinoid receptor is the major cannabinoid receptor at excitatory presynaptic sites in the hippocampus and cerebellum., *The Journal of neuroscience : the official journal of the Society for Neuroscience*, 26(11), pp. 2991–3001.

- Kenny, P. J. (2014) Epigenetics, microRNA, and addiction, *Dialogues in Clinical Neuroscience*, 16(3), pp. 335–344.
- Kessler, R. C. *et al.* (2013) The prevalence and correlates of binge eating disorder in the World Health Organization World Mental Health Surveys., *Biological psychiatry*, 73(9), pp. 904–914.
- Khan, Z. U. *et al.* (1998) Differential regional and cellular distribution of dopamine D2-like receptors: an immunocytochemical study of subtype-specific antibodies in rat and human brain., *The Journal of comparative neurology*. United States, 402(3), pp. 353–371.
- Khodayari, S., Pakdel, F. G., Shahabi, P. and Naderi, S. (2019) Acute tramadol-induced cellular tolerance and dependence of ventral tegmental area dopaminergic neurons: An in vivo electrophysiological study, *Basic and Clinical Neuroscience*, 10(3), pp. 209–224.
- Kiyatkin, E. A., Kiyatkin, D. E. and Rebec, G. V (2000) Phasic inhibition of dopamine uptake in nucleus accumbens induced by intravenous cocaine in freely behaving rats., *Neuroscience*. United States, 98(4), pp. 729–741.
- Klawonn, A. M. and Malenka, R. C. (2018) Nucleus Accumbens Modulation in Reward and Aversion, *Cold Spring Harbor symposia on quantitative biology*. 2019/01/23, 83, pp. 119–129.
- Klump, K. L. *et al.* (2009) Genetic and environmental influences on disordered eating: An adoption study., *Journal of abnormal psychology*, 118(4), pp. 797–805.

- Koch, M. *et al.* (2015) Hypothalamic POMC neurons promote cannabinoid-induced feeding., *Nature*, 519(7541), pp. 45–50.
- Koffarnus, M. N. and Kaplan, B. A. (2018) Clinical models of decision making in addiction., *Pharmacology, biochemistry, and behavior*, 164, pp. 71–83.
- Kolaczynski, J. W. *et al.* (1996) Acute and chronic effects of insulin on leptin production in humans: Studies in vivo and in vitro., *Diabetes*. United States, 45(5), pp. 699–701.
- Koob, G. F. (2000) Neurobiology of addiction. Toward the development of new therapies., *Annals of the New York Academy of Sciences*. United States, 909, pp. 170–185.
- Koob, G. F. and Le Moal, M. (2008) Addiction and the brain antireward system., *Annual review of psychology*. United States, 59, pp. 29–53.
- Koob, G F and Volkow, N. D. (2010) Neurocircuitry of addiction, *Neuropsychopharmacology: official publication of the American College of Neuropsychopharmacology*. Nature Publishing Group, 35(1), pp. 217–238.
- Koob, G. F. and Volkow, N. D. (2016) Neurobiology of addiction: a neurocircuitry analysis, *The Lancet Psychiatry*, 3(8), pp. 760–773.
- Koob, G. F. (2017) Antireward, compulsivity, and addiction: seminal contributions of Dr. Athina Markou to motivational dysregulation in addiction., *Psychopharmacology*. Germany, 234(9–10), pp. 1315–1332.

Koulchitsky, S. *et al.* (2012) Differential effects of cocaine on dopamine neuron firing in awake and anesthetized rats, *Neuropsychopharmacology*. Nature Publishing Group, 37(7), pp. 1559–1571.

Kouzarides, T. (2007) Chromatin Modifications and Their Function, *Cell*, 128(4), pp. 693–705.

Kozlenkov, A. *et al.* (2017) DNA Methylation Profiling of Human Prefrontal Cortex Neurons in Heroin Users Shows Significant Difference between Genomic Contexts of Hyper- and Hypomethylation and a Younger Epigenetic Age., *Genes*, 8(6).

Kreitzer, A. C. and Malenka, R. C. (2008) Striatal plasticity and basal ganglia circuit function., *Neuron*, 60(4), pp. 543–554.

Krützfeldt, J. *et al.* (2005) Silencing of microRNAs in vivo with ‘antagomirs’., *Nature*. England, 438(7068), pp. 685–689.

Kucewicz, M. T., Tricklebank, M. D., Bogacz, R. and Jones, M. W. (2011) Dysfunctional Prefrontal Cortical Network Activity and Interactions following Cannabinoid Receptor Activation, *Journal of Neuroscience*. Society for Neuroscience, 31(43), pp. 15560–15568.

Kucewicz, M. T. *et al.* (2014) High frequency oscillations are associated with cognitive processing in human recognition memory, *Brain : a journal of neurology*. 2014/06/11. Oxford University Press, 137(Pt 8), pp. 2231–2244.

Kupchik, Y. M. *et al.* (2015) Coding the direct/indirect pathways by D1 and D2 receptors is not valid for accumbens projections., *Nature neuroscience*, 18(9), pp. 1230–1232.

Kupchik, Y. M. and Kalivas, P. W. (2017) The Direct and Indirect Pathways of the Nucleus Accumbens are not What You Think., *Neuropsychopharmacology: official publication of the American College of Neuropsychopharmacology*, 42(1), pp. 369–370.

Kure Liu, C. *et al.* (2019) Brain Imaging of Taste Perception in Obesity: a Review., *Current nutrition reports*, 8(2), pp. 108–119.

Lally, N. *et al.* (2014) Glutamatergic correlates of gamma-band oscillatory activity during cognition: a concurrent ER-MRS and EEG study., *NeuroImage*. United States, 85 Pt 2, pp. 823–833.

Lammel, S. *et al.* (2012) Input-specific control of reward and aversion in the ventral tegmental area, *Nature*, 491(7423), pp. 212–217.

Lanciego, J. L. *et al.* (2011) Expression of the mRNA coding the cannabinoid receptor 2 in the pallidal complex of *Macaca fascicularis*., *Journal of psychopharmacology (Oxford, England)*. United States, 25(1), pp. 97–104.

Laporte, S. A., Miller, W. E., Kim, K.-M. and Caron, M. G. (2002) beta-Arrestin/AP-2 interaction in G protein-coupled receptor internalization: identification of a beta-arrestin binding site in beta 2-adaptin., *The Journal of biological chemistry*. United States, 277(11), pp. 9247–9254.

Lau, B. K., Cota, D., Cristino, L. and Borgland, S. L. (2017) Endocannabinoid modulation of homeostatic and non-homeostatic feeding circuits., *Neuropharmacology*. England, 124, pp. 38–51.

Lee, D. J., Elias, G. J. B. and Lozano, A. M. (2018) Neuromodulation

for the treatment of eating disorders and obesity, *Therapeutic advances in psychopharmacology*. 2017/12/08. SAGE Publications, 8(2), pp. 73–92.

Lee, M. W. and Fujioka, K. (2009) Naltrexone for the treatment of obesity: review and update., *Expert opinion on pharmacotherapy*. England, 10(11), pp. 1841–1845.

Lennerz, B. and Lennerz, J. K. (2018) Food Addiction, High-Glycemic-Index Carbohydrates, and Obesity., *Clinical chemistry*, 64(1), pp. 64–71.

Lerma-Cabrera, J. M., Carvajal, F. and Lopez-Legarrea, P. (2016) Food addiction as a new piece of the obesity framework., *Nutrition journal*, 15, p. 5.

Limpens, J. H. W. *et al.* (2015) Pharmacological inactivation of the prelimbic cortex emulates compulsive reward seeking in rats., *Brain research*. Netherlands, 1628(Pt A), pp. 210–218.

Linardon, J. and Brennan, L. (2017) The effects of cognitive-behavioral therapy for eating disorders on quality of life: A meta-analysis., *The International journal of eating disorders*. United States, 50(7), pp. 715–730.

Lindgren, E. *et al.* (2018) Food addiction: A common neurobiological mechanism with drug abuse, *Frontiers in Bioscience - Landmark*, 23(5), pp. 811–836.

Lintas, A. *et al.* (2021) Operant conditioning deficits and modified local field potential activities in parvalbumin-deficient mice, *Scientific Reports*, 11(1), p. 2970.

Littel, M. and Franken, I. H. (2011) Implicit and explicit selective attention to smoking cues in smokers indexed by brain potentials, *Journal of Psychopharmacology*, 25(4), pp. 503–513.

Little, H. J. (1999) The contribution of electrophysiology to knowledge of the acute and chronic effects of ethanol, *Pharmacology and Therapeutics*, 84(3), pp. 333–353.

Liu, J. *et al.* (2004) Argonaute2 is the catalytic engine of mammalian RNAi, *Science*. Science, 305(5689), pp. 1437–1441.

Lohani, S. *et al.* (2019) Dopamine Modulation of Prefrontal Cortex Activity Is Manifold and Operates at Multiple Temporal and Spatial Scales, *Cell Reports*. ElsevierCompany., 27(1), pp. 99-114.e6.

Lubman, D. I., Allen, N. B., Peters, L. A. and Deakin, J. F. W. (2007) Electrophysiological evidence of the motivational salience of drug cues in opiate addiction, *Psychological Medicine*, 37(8), pp. 1203–1209.

Lubman, D. I., Allen, N. B., Peters, L. A. and Deakin, J. F. W. (2008) Electrophysiological evidence that drug cues have greater salience than other affective stimuli in opiate addiction, *Journal of Psychopharmacology*, 22(8), pp. 836–842.

Lubman, D. I. *et al.* (2009) Responsiveness to drug cues and natural rewards in opiate addiction: Associations with later heroin use, *Archives of General Psychiatry*, 66(2), pp. 205–213.

Luigjes, J. *et al.* (2019) Defining Compulsive Behavior, *Neuropsychology review*. 2019/04/23. Springer US, 29(1), pp. 4–13.

Lukas, S. E., Mendelson, J. H., Benedikt, R. A. and Jones, B. (1986) EEG alpha activity increases during transient episodes of ethanol-induced euphoria, *Pharmacology, Biochemistry and Behavior*, 25(4), pp. 889–895.

Lukas, S. E., Mendelson, J. H. and Benedikt, R. (1995) Electroencephalographic correlates of marijuana-induced euphoria, *Drug and Alcohol Dependence*, 37(2), pp. 131–140.

Lupica, C. R. and Riegel, A. C. (2005) Endocannabinoid release from midbrain dopamine neurons: a potential substrate for cannabinoid receptor antagonist treatment of addiction., *Neuropharmacology*. England, 48(8), pp. 1105–1116.

Lüscher, C. and Slesinger, P. A. (2010) Emerging roles for G protein-gated inwardly rectifying potassium (GIRK) channels in health and disease., *Nature reviews. Neuroscience*, 11(5), pp. 301–315.

Lustig, R. H., Schmidt, L. A. and Brindis, C. D. (2012) The toxic truth about sugar, *Nature*, 482(7383), pp. 27–29.

Lutz, B., Marsicano, G., Maldonado, R. and Hillard, C. J. (2015) The endocannabinoid system in guarding against fear, anxiety and stress., *Nature reviews. Neuroscience*, pp. 705–718.

Lutz, T. A. *et al.* (2001) The anorectic effect of a chronic peripheral infusion of amylin is abolished in area postrema/nucleus of the solitary tract (AP/NTS) lesioned rats., *International journal of obesity and related metabolic disorders : journal of the International Association for the Study of Obesity*. England, 25(7), pp. 1005–1011.

Mably, A. J. and Colgin, L. L. (2018) Gamma oscillations in

cognitive disorders, *Current Opinion in Neurobiology*, 52, pp. 182–187.

Maccioni, P. *et al.* (2008) Suppression by the cannabinoid CB1 receptor antagonist, rimonabant, of the reinforcing and motivational properties of a chocolate-flavoured beverage in rats, *Behavioural Pharmacology*, 19(3), pp. 197–209.

MacDonald, A. J. *et al.* (2020) Regulation of food intake by astrocytes in the brainstem dorsal vagal complex., *Glia*, 68(6), pp. 1241–1254.

Mackie, K. (2006) Mechanisms of CB1 receptor signaling: endocannabinoid modulation of synaptic strength., *International journal of obesity (2005)*. England, 30 Suppl 1, pp. S19-23.

Maldonado, Rafael *et al.* (2021) Genomics and epigenomics of addiction, *American Journal of Medical Genetics, Part B: Neuropsychiatric Genetics*, 186(3), pp. 128–139.

Maldonado, R. *et al.* (2021) Vulnerability to addiction, *Neuropharmacology*, 186.

Malinen, H. and Hyytiä, P. (2008) Ethanol self-administration is regulated by CB1 receptors in the nucleus accumbens and ventral tegmental area in alcohol-preferring AA rats., *Alcoholism, clinical and experimental research*. England, 32(11), pp. 1976–1983.

Mancino, S *et al.* (2015) Epigenetic and Proteomic Expression Changes Promoted by Eating Addictive-Like Behavior, *Neuropsychopharmacology*., p. 10.

Manmaru, S. and Matsuura, M. (1989) Quantification of benzodiazepine-induced topographic EEG changes by a computerized wave form recognition method: application of a principal component analysis, *Electroencephalography and Clinical Neurophysiology*, 72(2), pp. 126–132.

Mannella, F., Gurney, K. and Baldassarre, G. (2013) The nucleus accumbens as a nexus between values and goals in goal-directed behavior: a review and a new hypothesis, *Frontiers in behavioral neuroscience*. Frontiers Media S.A., 7, p. 135.

Manzanas, J. *et al.* (2018) Role of the endocannabinoid system in drug addiction., *Biochemical pharmacology*. England, 157, pp. 108–121.

Margolis, E. B. *et al.* (2012) Identification of Rat Ventral Tegmental Area GABAergic Neurons, *PLOS ONE*. Public Library of Science, 7(7), p. e42365. Available at: <https://doi.org/10.1371/journal.pone.0042365>.

Marhe, R., van de Wetering, B. J. M. and Franken, I. H. A. (2013) Error-related brain activity predicts cocaine use after treatment at 3-month follow-up., *Biological psychiatry*. United States, 73(8), pp. 782–788.

Markus, C. R., Rogers, P. J., Brouns, F. and Schepers, R. (2017) Eating dependence and weight gain; no human evidence for a ‘sugar-addiction’ model of overweight., *Appetite*. England, 114, pp. 64–72.

Martín-García, E. *et al.* (2010) Central and peripheral consequences of the chronic blockade of CB1 cannabinoid receptor with

rimonabant or taranabant., *Journal of neurochemistry*. England, 112(5), pp. 1338–13351.

Martín-García, E. *et al.* (2016) Differential Control of Cocaine Self-Administration by GABAergic and Glutamatergic CB1 Cannabinoid Receptors., *Neuropsychopharmacology : official publication of the American College of Neuropsychopharmacology*, 41(9), pp. 2192–2205.

Martín-García, E., Domingo-Rodríguez, L. and Maldonado, R. (2020) An Operant Conditioning Model Combined with a Chemogenetic Approach to Study the Neurobiology of Food Addiction in Mice., *Bio-protocol*, 10(19), p. e3777.

Martz, M. E., Hart, T., Heitzeg, M. M. and Peltier, S. J. (2020) Neuromodulation of brain activation associated with addiction: A review of real-time fMRI neurofeedback studies, *NeuroImage: Clinical*, 27, p. 102350.

Di Marzo, V. *et al.* (2001) Leptin-regulated endocannabinoids are involved in maintaining food intake., *Nature*. England, 410(6830), pp. 822–825.

Di Marzo, V., Bifulco, M. and De Petrocellis, L. (2004) The endocannabinoid system and its therapeutic exploitation., *Nature reviews. Drug discovery*. England, 3(9), pp. 771–784.

Di Marzo, V. and Matias, I. (2005) Endocannabinoid control of food intake and energy balance., *Nature neuroscience*. United States, 8(5), pp. 585–589.

Mashayekhi, F. J. *et al.* (2012) Expression levels of the BDNF gene

and histone modifications around its promoters in the ventral tegmental area and locus ceruleus of rats during forced abstinence from morphine, *Neurochemical Research*, 37(7), pp. 1517–1523.

Mateo, Y. *et al.* (2017) Endocannabinoid Actions on Cortical Terminals Orchestrate Local Modulation of Dopamine Release in the Nucleus Accumbens, *Neuron*, 96(5), pp. 1112-1126.e5.

Max, B. (1989) This and that: chocolate addiction, the dual pharmacogenetics of asparagus eaters, and the arithmetic of freedom., *Trends in pharmacological sciences*. England, 10(10), pp. 390–393.

McAllister, S. D. and Glass, M. (2002) CB(1) and CB(2) receptor-mediated signalling: a focus on endocannabinoids., *Prostaglandins, leukotrienes, and essential fatty acids*. Scotland, 66(2–3), pp. 161–171.

McCracken, C. B. and Grace, A. A. (2013) Persistent cocaine-induced reversal learning deficits are associated with altered limbic cortico-striatal local field potential synchronization, *Journal of Neuroscience*, 33(44), pp. 17469–17482.

McElroy, S. L., Guerdjikova, A. I., Mori, N. and Keck, P. E. J. (2015) Psychopharmacologic treatment of eating disorders: emerging findings., *Current psychiatry reports*. United States, 17(5), p. 35.

McFarland, K. and Kalivas, P. W. (2001) The circuitry mediating cocaine-induced reinstatement of drug-seeking behavior., *The Journal of neuroscience: the official journal of the Society for Neuroscience*, 21(21), pp. 8655–8663.

McHugh, R. K., Hearon, B. A. and Otto, M. W. (2010) Cognitive behavioral therapy for substance use disorders., *The Psychiatric clinics of North America*, 33(3), pp. 511–525.

Meaney, M. J. and Szyf, M. (2005) Environmental programming of stress responses through DNA methylation: Life at the interface between a dynamic environment and a fixed genome, *Dialogues in Clinical Neuroscience*, 7(2), pp. 103–123.

Van Der Meer, M. and Redish, A. D. (2009) Low and high gamma oscillations in rat ventral striatum have distinct relationships to behavior, reward, and spiking activity on a learned spatial decision task , *Frontiers in Integrative Neuroscience* . Available at: <https://www.frontiersin.org/article/10.3389/neuro.07.009.2009>.

Melis, M. *et al.* (2004) Endocannabinoids Mediate Presynaptic Inhibition of Glutamatergic Transmission in Rat Ventral Tegmental Area Dopamine Neurons through Activation of CB1 Receptors, *Journal of Neuroscience*, 24(1), pp. 53–62.

Melis, T. *et al.* (2007) The cannabinoid antagonist SR 141716A (Rimonabant) reduces the increase of extra-cellular dopamine release in the rat nucleus accumbens induced by a novel high palatable food., *Neuroscience letters*. Ireland, 419(3), pp. 231–235.

Meule, A. and Gearhardt, A. N. (2014) Food addiction in the light of DSM-5, *Nutrients*, 6(9), pp. 3653–3671.

Meule, A. (2015) Back by popular demand: A narrative review on the history of food addiction research, *Yale Journal of Biology and Medicine*, 88(3), pp. 295–302.

Meule, A. (2019) A Critical Examination of the Practical Implications Derived from the Food Addiction Concept, *Current obesity reports*. Springer US, 8(1), pp. 11–17.

Milano, W. *et al.* (2013) The pharmacological options in the treatment of eating disorders., *ISRN pharmacology*, 2013, p. 352865.

Miller, E. K. and Cohen, J. D. (2001) An integrative theory of prefrontal cortex function, *Annual Review of Neuroscience*, 24, pp. 167–202.

Mishra, A., Anand, M. and Umesh, S. (2017) Neurobiology of eating disorders - an overview, *Asian Journal of Psychiatry*. Elsevier B.V., 25, pp. 91–100.

Missale, C. *et al.* (1998) Dopamine receptors: from structure to function., *Physiological reviews*. United States, 78(1), pp. 189–225.

Mogenson, G. J., Jones, D. L. and Yim, C. Y. (1980) From motivation to action: functional interface between the limbic system and the motor system., *Progress in neurobiology*. England, 14(2–3), pp. 69–97.

Monory, K. *et al.* (2006) The endocannabinoid system controls key epileptogenic circuits in the hippocampus., *Neuron*, 51(4), pp. 455–466.

Monteleone, P. *et al.* (2005) Blood levels of the endocannabinoid anandamide are increased in anorexia nervosa and in binge-eating disorder, but not in bulimia nervosa., *Neuropsychopharmacology : official publication of the American College of Neuropsychopharmacology*. England, 30(6), pp. 1216–1221.

Monteleone, P. *et al.* (2009) Association of CNR1 and FAAH endocannabinoid gene polymorphisms with anorexia nervosa and bulimia nervosa: evidence for synergistic effects., *Genes, brain, and behavior*. England, 8(7), pp. 728–732.

Monteleone, P. and Maj, M. (2013) Dysfunctions of leptin, ghrelin, BDNF and endocannabinoids in eating disorders: beyond the homeostatic control of food intake., *Psychoneuroendocrinology*. England, 38(3), pp. 312–330.

Moore, C. F., Sabino, V., Koob, G. F. and Cottone, P. (2017) Pathological Overeating: Emerging Evidence for a Compulsivity Construct, *Neuropsychopharmacology*. Nature Publishing Group, 42(7), pp. 1375–1389.

Moore, C. F., Panciera, J. I., Sabino, V. and Cottone, P. (2018) Neuropharmacology of compulsive eating, *Philosophical transactions of the Royal Society of London. Series B, Biological sciences*. The Royal Society, 373(1742), p. 20170024.

Moorman, D. E., James, M. H., McGlinchey, E. M. and Aston-Jones, G. (2015) Differential roles of medial prefrontal subregions in the regulation of drug seeking., *Brain research*, 1628(Pt A), pp. 130–146.

Morales, M. and Margolis, E. B. (2017) Ventral tegmental area: cellular heterogeneity, connectivity and behaviour., *Nature reviews. Neuroscience*. England, 18(2), pp. 73–85.

Morales, P., Reggio, P. H. and Jagerovic, N. (2017) An Overview on Medicinal Chemistry of Synthetic and Natural Derivatives of

- Cannabidiol., *Frontiers in pharmacology*, 8, p. 422.
- Morel, C. *et al.* (2018) Nicotinic receptors mediate stress-nicotine detrimental interplay via dopamine cells' activity, *Molecular Psychiatry*, 23(7), pp. 1597–1605.
- Morgan, D. *et al.* (2002) Social dominance in monkeys: dopamine D2 receptors and cocaine self-administration., *Nature neuroscience*. United States, 5(2), pp. 169–174.
- Morris, M. J., Na, E. S. and Johnson, A. K. (2008) Salt craving: the psychobiology of pathogenic sodium intake., *Physiology & behavior*, 94(5), pp. 709–721.
- Most, D., Workman, E. and Adron Harris, R. (2014) Synaptic adaptations by alcohol and drugs of abuse: Changes in microRNA expression and mRNA regulation, *Frontiers in Molecular Neuroscience*, 7(DEC), pp. 1–10.
- Motlagh, F. *et al.* (2018) Acute effects of methadone on EEG power spectrum and event-related potentials among heroin dependents. *Psychopharmacology*, pp. 3273–3288.
- Moussawi, K. *et al.* (2009) N-Acetylcysteine Reverses Cocaine Induced Metaplasticity, *Nature Neuroscience*, 12(2), pp. 182–189.
- Munn, M. A. *et al.* (2010) Bivariate analysis of disordered eating characteristics in adolescence and young adulthood., *The International journal of eating disorders*, 43(8), pp. 751–761.
- Naqvi, N. H. and Bechara, A. (2010) The insula and drug addiction: an interoceptive view of pleasure, urges, and decision-making.,

Brain structure & function, 214(5–6), pp. 435–450.

Nathan, P. J. *et al.* (2012) Opioid receptor modulation of hedonic taste preference and food intake: a single-dose safety, pharmacokinetic, and pharmacodynamic investigation with GSK1521498, a novel μ -opioid receptor inverse agonist., *Journal of clinical pharmacology*. England, 52(4), pp. 464–474.

Navarrete, F. *et al.* (2013) Role of CB2 cannabinoid receptors in the rewarding, reinforcing, and physical effects of nicotine., *Neuropsychopharmacology: official publication of the American College of Neuropsychopharmacology*, 38(12), pp. 2515–2524.

Nestler, E. J. and Hyman, S. E. (2010) Animal models of neuropsychiatric disorders., *Nature neuroscience*, 13(10), pp. 1161–1169.

Nestler, E. J. (2014) Epigenetic Mechanisms of Drug Addiction, *Neuropharmacology*, 76, pp. 1–7.

Nestler, E. J. and Lüscher, C. (2019) The Molecular Basis of Drug Addiction: Linking Epigenetic to Synaptic and Circuit Mechanisms, *Neuron*, 102(1), pp. 48–59.

Neville, M. J., Johnstone, E. C. and Walton, R. T. (2004) Identification and characterization of ANKK1: A novel kinase gene closely linked to DRD2 on chromosome band 11q23.1, *Human Mutation*, 23(6), pp. 540–545.

Nikolova, Y. S., Ferrell, R. E., Manuck, S. B. and Hariri, A. R. (2011) Multilocus Genetic Profile for Dopamine Signaling Predicts Ventral Striatum Reactivity, *Neuropsychopharmacology*, 36(9), pp. 1940–

1947.

Nolte, G. *et al.* (2008) Robustly estimating the flow direction of information in complex physical systems, *Physical Review Letters*, 100(23), pp. 1–4.

Norgren, R., Hajnal, A. and Mungarndee, S. S. (2006) Gustatory reward and the nucleus accumbens., *Physiology & behavior*, 89(4), pp. 531–535.

Norris, C. *et al.* (2019) The Bivalent Rewarding and Aversive properties of Δ 9-tetrahydrocannabinol are Mediated Through Dissociable Opioid Receptor Substrates and Neuronal Modulation Mechanisms in Distinct Striatal Sub-Regions, *Scientific Reports*, 9(1), pp. 1–14.

Numachi, Y. *et al.* (2007) Methamphetamine alters expression of DNA methyltransferase 1 mRNA in rat brain, *Neuroscience Letters*, 414(3), pp. 213–217.

O’Doherty, J. P., Cockburn, J. and Pauli, W. M. (2017) Learning, Reward, and Decision Making., *Annual review of psychology*, 68, pp. 73–100.

Oleson, E. B. and Cheer, J. F. (2012) A brain on cannabinoids: the role of dopamine release in reward seeking., *Cold Spring Harbor perspectives in medicine*, 2(8).

Oleson, E. B., Hamilton, L. R. and Gomez, D. M. (2021) Cannabinoid Modulation of Dopamine Release During Motivation, Periodic Reinforcement, Exploratory Behavior, Habit Formation, and Attention, *Frontiers in Synaptic Neuroscience*, 13.

Olszewski, M. *et al.* (2013) NMDA receptor antagonist-enhanced high frequency oscillations: are they generated broadly or regionally specific?, *European neuropsychopharmacology : the journal of the European College of Neuropsychopharmacology*. Netherlands, 23(12), pp. 1795–1805.

Onaivi, E. S. (2006) Neuropsychobiological evidence for the functional presence and expression of cannabinoid CB2 receptors in the brain., *Neuropsychobiology*. Switzerland, 54(4), pp. 231–246.

Onaolapo, A. Y. and Onaolapo, O. J. (2018) Food additives, food and the concept of ‘food addiction’: Is stimulation of the brain reward circuit by food sufficient to trigger addiction?, *Pathophysiology : the official journal of the International Society for Pathophysiology*. Switzerland, 25(4), pp. 263–276.

Onslow, A. C. E., Bogacz, R. and Jones, M. W. (2011) Quantifying phase-amplitude coupling in neuronal network oscillations., *Progress in biophysics and molecular biology*. England, 105(1–2), pp. 49–57.

Opland, D. M., Leininger, G. M. and Myers, M. G. J. (2010) Modulation of the mesolimbic dopamine system by leptin., *Brain research*, 1350, pp. 65–70.

Padwal, R. S. and Majumdar, S. R. (2007) Drug treatments for obesity: orlistat, sibutramine, and rimonabant., *Lancet (London, England)*. England, 369(9555), pp. 71–77.

Parmar, R. M. and Can, A. S. (2022) Physiology, Appetite And Weight Regulation., in. Treasure Island (FL).

Parsons, L. H. and Hurd, Y. L. (2015) Endocannabinoid signalling in reward and addiction., *Nature reviews. Neuroscience*, 16(10), pp. 579–594.

Parylak, S. L., Koob, G. F. and Zorrilla, E. P. (2011) The dark side of food addiction, *Physiology & Behavior*. Elsevier, 104(1), pp. 149–156.

Pascoli, V. *et al.* (2018) Stochastic synaptic plasticity underlying compulsion in a model of addiction., *Nature*. England, 564(7736), pp. 366–371.

Peciña, S. and Berridge, K. C. (2005) Hedonic hot spot in nucleus accumbens shell: where do mu-opioids cause increased hedonic impact of sweetness?, *The Journal of neuroscience: the official journal of the Society for Neuroscience*, 25(50), pp. 11777–11786.

Pelchat, M. L. *et al.* (2004) Images of desire: food-craving activation during fMRI., *NeuroImage*. United States, 23(4), pp. 1486–1493.

Peoples, L. L., Uzwiak, A. J., Gee, F. and West, M. O. (1997) Operant behavior during sessions of intravenous cocaine infusion is necessary and sufficient for phasic firing of single nucleus accumbens neurons, *Brain Research*, 757(2), pp. 280–284.

Peoples, L. L., Lynch, K. G., Lesnock, J. and Gangadhar, N. (2004) Accumbal Neural Responses during the Initiation and Maintenance of Intravenous Cocaine Self-Administration, *Journal of Neurophysiology*, 91(1), pp. 314–323.

Perry, C. J., Sergio, L. E., Crawford, J. D. and Fallah, M. (2015) Hand placement near the visual stimulus improves orientation selectivity in

- V2 neurons., *Journal of neurophysiology*, 113(7), pp. 2859–2870.
- Pertwee, R. G. *et al.* (2010) International Union of Basic and Clinical Pharmacology. LXXIX. Cannabinoid receptors and their ligands: beyond CB₁ and CB₂., *Pharmacological reviews*, 62(4), pp. 588–631.
- Peters, J., LaLumiere, R. T. and Kalivas, P. W. (2008a) Infralimbic prefrontal cortex is responsible for inhibiting cocaine seeking in extinguished rats, *The Journal of neuroscience : the official journal of the Society for Neuroscience*. Society for Neuroscience, 28(23), pp. 6046–6053.
- Peters, J., Vallone, J., Laurendi, K. and Kalivas, P. W. (2008b) Opposing roles for the ventral prefrontal cortex and the basolateral amygdala on the spontaneous recovery of cocaine-seeking in rats., *Psychopharmacology*. Germany, 197(2), pp. 319–326.
- Petit, G. *et al.* (2012) Alcohol-related context modulates performance of social drinkers in a visual go/no-go task: A preliminary assessment of event-related potentials, *PLoS ONE*, 7(5), pp. 1–11.
- Phillips, P. C. (2008) Epistasis--the essential role of gene interactions in the structure and evolution of genetic systems., *Nature reviews. Genetics*, 9(11), pp. 855–867.
- Piazza, P. V. and Deroche-Gamonet, V. (2013) A multistep general theory of transition to addiction., *Psychopharmacology*, 229(3), pp. 387–413.
- Piazza, P. V., Cota, D. and Marsicano, G. (2017) The CB1 Receptor as the Cornerstone of Exostasis., *Neuron*. United States, 93(6), pp. 1252–1274.

Picciotto, M. R. and Kenny, P. J. (2013) Molecular mechanisms underlying behaviors related to nicotine addiction, *Cold Spring Harbor perspectives in medicine*. Cold Spring Harbor Laboratory Press, 3(1), pp. a012112–a012112.

Pierce, K. L., Premont, R. T. and Lefkowitz, R. J. (2002) Seven-transmembrane receptors., *Nature reviews. Molecular cell biology*. England, 3(9), pp. 639–650.

Piomelli, D. (2003) The molecular logic of endocannabinoid signalling., *Nature reviews. Neuroscience*. England, 4(11), pp. 873–884.

Pistillo, F., Clementi, F., Zoli, M. and Gotti, C. (2015) Nicotinic, glutamatergic and dopaminergic synaptic transmission and plasticity in the mesocorticolimbic system: focus on nicotine effects., *Progress in neurobiology*. England, 124, pp. 1–27.

Plomin, R. and Daniels, D. (2011) Why are children in the same family so different from one another?, *International Journal of Epidemiology*, 40(3), pp. 563–582.

Powell, A. D. *et al.* (2014) Reduced Gamma Oscillations in a Mouse Model of Intellectual Disability: A Role for Impaired Repetitive Neurotransmission?, *PLOS ONE*. Public Library of Science, 9(5), p. e95871. Available at: <https://doi.org/10.1371/journal.pone.0095871>.

Pozhidayeva, D. Y. *et al.* (2020) Chronic Chemogenetic Stimulation of the Nucleus Accumbens Produces Lasting Reductions in Binge Drinking and Ameliorates Alcohol-Related Morphological and Transcriptional Changes., *Brain sciences*, 10(2).

Puente, N. *et al.* (2011) Polymodal activation of the endocannabinoid system in the extended amygdala., *Nature neuroscience*. United States, 14(12), pp. 1542–1547.

Purohit, K. *et al.* (2018) Pharmacogenetic Manipulation of the Nucleus Accumbens Alters Binge-Like Alcohol Drinking in Mice, *Alcoholism: Clinical and Experimental Research*, 42(5), pp. 879–888.

Pursey, Kirrilly M. *et al.* (2014) The prevalence of food addiction as assessed by the yale food addiction scale: A systematic review, *Nutrients*, 6(10), pp. 4552–4590.

Pursey, K. M., Davis, C. and Burrows, T. L. (2017) Nutritional Aspects of Food Addiction, *Current Addiction Reports*, 4(2), pp. 142–150.

Pursey, K. M., Collins, R., Skinner, J. and Burrows, T. L. (2021) Characteristics of individuals seeking addictive eating treatment., *Eating and weight disorders : EWD*. Germany, 26(8), pp. 2779–2786.

Qi, J. *et al.* (2016) VTA glutamatergic inputs to nucleus accumbens drive aversion by acting on GABAergic interneurons., *Nature neuroscience*, 19(5), pp. 725–733.

Quinn, R. K. *et al.* (2015) Distinct miRNA expression in dorsal striatal subregions is associated with risk for addiction in rats, *Translational Psychiatry*. Nature Publishing Group, 5(2).

Ramlakhan, J. U. *et al.* (2020) The Role of Gamma Oscillations in the Pathophysiology of Substance Use Disorders., *Journal of*

personalized medicine, 11(1).

RANDOLPH, T. G. (1956) The descriptive features of food addiction; addictive eating and drinking., *Quarterly journal of studies on alcohol*. United States, 17(2), pp. 198–224.

Raybould, H. E. *et al.* (2006) Detection of macronutrients in the intestinal wall., *Autonomic neuroscience: basic & clinical*. Netherlands, 125(1–2), pp. 28–33.

Reas, D. L. and Grilo, C. M. (2015) Pharmacological treatment of binge eating disorder: update review and synthesis., *Expert opinion on pharmacotherapy*, 16(10), pp. 1463–1478.

Reich, T., Cloninger, C. R. and Guze, S. B. (1975) The multifactorial model of disease transmission: I. Description of the model and its use in psychiatry., *The British Journal of Psychiatry*. United Kingdom: Royal College of Psychiatrists, pp. 1–10.

Renard, J. *et al.* (2017) Adolescent THC Exposure Causes Enduring Prefrontal Cortical Disruption of GABAergic Inhibition and Dysregulation of Sub-Cortical Dopamine Function /631/378/2571 /631/378/1689/1799 /9 /9/30 /82 /82/1 article, *Scientific Reports*. Springer US, 7(1), pp. 1–14.

Renthal, W. *et al.* (2008) Δ FosB mediates epigenetic desensitization of the c-fos gene after chronic amphetamine exposure, *Journal of Neuroscience*, 28(29), pp. 7344–7349.

Reynolds, S. M. and Berridge, K. C. (2001) Fear and feeding in the nucleus accumbens shell: rostrocaudal segregation of GABA-elicited defensive behavior versus eating behavior., *The Journal of*

neuroscience : the official journal of the Society for Neuroscience, 21(9), pp. 3261–3270.

Ribeiro, G. and Oliveira-Maia, A. J. (2021) Sweet taste and obesity, *European journal of internal medicine*. 2021/02/13. Elsevier Science, 92, pp. 3–10.

Rinaldi-Carmona, M. *et al.* (1996) Characterization of two cloned human CB1 cannabinoid receptor isoforms., *The Journal of pharmacology and experimental therapeutics*. United States, 278(2), pp. 871–878.

Robbe, D. *et al.* (2002) Endogenous cannabinoids mediate long-term synaptic depression in the nucleus accumbens., *Proceedings of the National Academy of Sciences of the United States of America*, 99(12), pp. 8384–8388.

Robinson, T. E. and Berridge, K. C. (2003) Addiction., *Annual Review of Psychology*. US: Annual Reviews, pp. 25–53.

Rodriguez-Romaguera, J. *et al.* (2020) Developments from Bulk Optogenetics to Single-Cell Strategies to Dissect the Neural Circuits that Underlie Aberrant Motivational States, *Cold Spring Harbor perspectives in medicine*, p. a039792.

Roesch, M. R. *et al.* (2012) Willingness to wait and altered encoding of time-discounted reward in the orbitofrontal cortex with normal aging., *The Journal of neuroscience : the official journal of the Society for Neuroscience*, 32(16), pp. 5525–5533.

Rogers, P. J. (2017) Food and drug addictions: Similarities and differences., *Pharmacology, biochemistry, and behavior*. United

States, 153, pp. 182–190.

Rogge, G. A. and Wood, M. A. (2013) The role of histone acetylation in cocaine-induced neural plasticity and behavior, *Neuropsychopharmacology*. Nature Publishing Group, 38(1), pp. 94–110.

Romer, A. L. *et al.* (2019) Dopamine genetic risk is related to food addiction and body mass through reduced reward-related ventral striatum activity., *Appetite*, 133, pp. 24–31.

Rosenbaum, D. L. and White, K. S. (2015) The relation of anxiety, depression, and stress to binge eating behavior., *Journal of health psychology*. England, 20(6), pp. 887–898.

Rossi, M. A. and Stuber, G. D. (2018) Overlapping Brain Circuits for Homeostatic and Hedonic Feeding., *Cell metabolism*, 27(1), pp. 42–56.

Rossi, M. A. *et al.* (2019) Obesity remodels activity and transcriptional state of a lateral hypothalamic brake on feeding., *Science (New York, N.Y.)*, 364(6447), pp. 1271–1274.

Rössner, S. *et al.* (2000) Weight loss, weight maintenance, and improved cardiovascular risk factors after 2 years treatment with orlistat for obesity. European Orlistat Obesity Study Group., *Obesity research*. United States, 8(1), pp. 49–61.

Roth, B. L. (2016) DREADDs for Neuroscientists, *Neuron*. Elsevier Ltd, 89(4), pp. 683–694.

Rozin, P. and Stoess, C. (1993) Is there a general tendency to become

- addicted?, *Addictive behaviors*. England, 18(1), pp. 81–87.
- Rucker, D. *et al.* (2007) Long term pharmacotherapy for obesity and overweight: updated meta-analysis., *BMJ (Clinical research ed.)*, 335(7631), pp. 1194–1199.
- Ruehle, S. *et al.* (2013) Cannabinoid CB1 receptor in dorsal telencephalic glutamatergic neurons: distinctive sufficiency for hippocampus-dependent and amygdala-dependent synaptic and behavioral functions., *The Journal of neuroscience: the official journal of the Society for Neuroscience*, 33(25), pp. 10264–10277.
- Russell-Mayhew, S., von Ranson, K. M. and Masson, P. C. (2010) How does overeaters anonymous help its members? A qualitative analysis., *European eating disorders review: the journal of the Eating Disorders Association*. England, 18(1), pp. 33–42.
- Russo, S. J. and Nestler, E. J. (2013) The brain reward circuitry in mood disorders., *Nature reviews. Neuroscience*, 14(9), pp. 609–625.
- Sadakierska-Chudy, A. *et al.* (2017) Prolonged Induction of miR-212/132 and REST Expression in Rat Striatum Following Cocaine Self-Administration, *Molecular Neurobiology*. Humana Press Inc., 54(3), pp. 2241–2254.
- Salamone, J. D., Correa, M., Farrar, A. and Mingote, S. M. (2007) Effort-related functions of nucleus accumbens dopamine and associated forebrain circuits., *Psychopharmacology*. Germany, 191(3), pp. 461–482.
- Salgado, S. and Kaplitt, M. G. (2015) The nucleus accumbens: A comprehensive review, *Stereotactic and Functional Neurosurgery*,

93(2), pp. 75–93.

Sanchis-Segura, C. and Spanagel, R. (2006) REVIEW: Behavioural assessment of drug reinforcement and addictive features in rodents: an overview, *Addiction Biology*. John Wiley & Sons, Ltd, 11(1), pp. 2–38.

Sandoval, D. (2008) CNS GLP-1 regulation of peripheral glucose homeostasis, *Physiology & behavior*. 2008/05/27, 94(5), pp. 670–674.

Sandoval, D., Cota, D. and Seeley, R. J. (2008) The Integrative Role of CNS Fuel-Sensing Mechanisms in Energy Balance and Glucose Regulation, *Annual Review of Physiology*. Annual Reviews, 70(1), pp. 513–535.

Sangha, S. *et al.* (2014) Alterations in reward, fear and safety cue discrimination after inactivation of the rat prelimbic and infralimbic cortices., *Neuropsychopharmacology: official publication of the American College of Neuropsychopharmacology*, 39(10), pp. 2405–2413.

Schaumberg, K. *et al.* (2017) The Science Behind the Academy for Eating Disorders' Nine Truths About Eating Disorders., *European eating disorders review: the journal of the Eating Disorders Association*, 25(6), pp. 432–450.

Scherr, M. *et al.* (2007) Lentivirus-mediated antagomir expression for specific inhibition of miRNA function, *Nucleic Acids Research*, 35(22).

Schienze, A., Schäfer, A., Hermann, A. and Vaitl, D. (2009) Binge-

eating disorder: reward sensitivity and brain activation to images of food., *Biological psychiatry*. United States, 65(8), pp. 654–661.

Schlicker, E. and Kathmann, M. (2001) Modulation of transmitter release via presynaptic cannabinoid receptors., *Trends in pharmacological sciences*. England, 22(11), pp. 565–572.

Schmidt, J. and Martin, A. (2020) The Influence of Physiological and Psychological Learning Mechanisms in Neurofeedback vs. Mental Imagery Against Binge Eating, *Applied Psychophysiology and Biofeedback*, 45(4), pp. 293–305.

Schneeberger, M., Gomis, R. and Claret, M. (2014) Hypothalamic and brainstem neuronal circuits controlling homeostatic energy balance, *Journal of Endocrinology*. Bristol, UK: Bioscientifica Ltd, 220(2), pp. T25–T46.

Schulte, Erica M., Avena, N. M. and Gearhardt, A. N. (2015) Which foods may be addictive? The roles of processing, fat content, and glycemic load, *PLoS ONE*, 10(2), pp. 1–18.

Schulte, E. M., Yokum, S., Potenza, M. N. and Gearhardt, A. N. (2016) Neural systems implicated in obesity as an addictive disorder: from biological to behavioral mechanisms., *Progress in brain research*. Netherlands, 223, pp. 329–346.

Schulte, E. M. and Gearhardt, A. N. (2017) Development of the Modified Yale Food Addiction Scale Version 2.0., *European eating disorders review : the journal of the Eating Disorders Association*. England, 25(4), pp. 302–308.

Schulte, E. M. and Gearhardt, A. N. (2018) Associations of Food

Addiction in a Sample Recruited to Be Nationally Representative of the United States., *European eating disorders review : the journal of the Eating Disorders Association*. England, 26(2), pp. 112–119.

Schulte, E. M., Wadden, T. A. and Allison, K. C. (2020) An evaluation of food addiction as a distinct psychiatric disorder, *International Journal of Eating Disorders*, 53(10), pp. 1610–1622.

Schultz, W., Apicella, P. and Ljungberg, T. (1993) Responses of monkey dopamine neurons to reward and conditioned stimuli during successive steps of learning a delayed response task., *The Journal of neuroscience : the official journal of the Society for Neuroscience*, 13(3), pp. 900–913.

Schultz, W., Dayan, P. and Montague, P. R. (1997) A neural substrate of prediction and reward., *Science (New York, N.Y.)*. United States, 275(5306), pp. 1593–1599.

Schultz, W. (1998) Predictive reward signal of dopamine neurons., *Journal of neurophysiology*. United States, 80(1), pp. 1–27.

Scofield, M. D. *et al.* (2016) The nucleus accumbens: Mechanisms of addiction across drug classes reflect the importance of glutamate homeostasis, *Pharmacological Reviews*, 68(3), pp. 816–871.

Di Segni, M. *et al.* (2014) Animal models of compulsive eating behavior, *Nutrients*. MDPI, 6(10), pp. 4591–4609.

Sellayah, D., Cagampang, F. R. and Cox, R. D. (2014) On the evolutionary origins of obesity: a new hypothesis., *Endocrinology*. United States, 155(5), pp. 1573–1588.

Seroogy, K. *et al.* (1988) A subpopulation of dopaminergic neurons in rat ventral mesencephalon contains both neurotensin and cholecystokinin., *Brain research*. Netherlands, 455(1), pp. 88–98.

Seroogy, K. B. *et al.* (1994) Dopaminergic neurons in rat ventral midbrain express brain-derived neurotrophic factor and neurotrophin-3 mRNAs., *The Journal of comparative neurology*. United States, 342(3), pp. 321–334.

Sesack, S. R. and Grace, A. A. (2010) Cortico-Basal Ganglia reward network: microcircuitry., *Neuropsychopharmacology: official publication of the American College of Neuropsychopharmacology*, 35(1), pp. 27–47.

Shen, H. and Kalivas, P. W. (2013) Reduced LTP and LTD in prefrontal cortex synapses in the nucleus accumbens after heroin self-administration, *International Journal of Neuropsychopharmacology*, 16(5), pp. 1165–1167.

Shi, W. X. *et al.* (2000) Dual effects of D-amphetamine on dopamine neurons mediated by dopamine and nondopamine receptors, *Journal of Neuroscience*, 20(9), pp. 3504–3511.

Shikha Prashad, E. S. and Dedrick, F. M. F. (2018) Cannabis users exhibit increased cortical activation during resting state compared to non-users, *Neuroimage*, 179, pp. 176–186.

Shimura, T., Imaoka, H. and Yamamoto, T. (2006) Neurochemical modulation of ingestive behavior in the ventral pallidum, *European Journal of Neuroscience*. John Wiley & Sons, Ltd, 23(6), pp. 1596–1604.

Shoaib, M. (2008) The cannabinoid antagonist AM251 attenuates nicotine self-administration and nicotine-seeking behaviour in rats., *Neuropharmacology*. England, 54(2), pp. 438–444.

Van Sickle, M. D. *et al.* (2005) Identification and functional characterization of brainstem cannabinoid CB2 receptors., *Science (New York, N.Y.)*. United States, 310(5746), pp. 329–332.

de Silva, P. and Eysenck, S. (1987) Personality and addictiveness in anorexic and bulimic patients., *Personality and Individual Differences*. Netherlands: Elsevier Science, 8(5), pp. 749–751.

Small, D. M. and DiFeliceantonio, A. G. (2019) Processed foods and food reward., *Science (New York, N.Y.)*. United States, 363(6425), pp. 346–347.

Smink, F. R. E., van Hoeken, D. and Hoek, H. W. (2012) Epidemiology of eating disorders: incidence, prevalence and mortality rates., *Current psychiatry reports*, 14(4), pp. 406–414.

Smith, A. C. . and Kenny, P. . (2018) MicroRNAs regulate synaptic plasticity underlying drug addiction A., *Genes, Brain and Behavior*, 17.

Smith, D. G. and Robbins, T. W. (2013) The neurobiological underpinnings of obesity and binge eating: a rationale for adopting the food addiction model., *Biological psychiatry*. United States, 73(9), pp. 804–810.

Soares-Cunha, C. *et al.* (2018) Nucleus Accumbens Microcircuit Underlying D2-MSN-Driven Increase in Motivation, *eNeuro*. Society for Neuroscience, 5(2).

Soria-Gomez, E., Bellocchio, L. and Marsicano, G. (2014) New insights on food intake control by olfactory processes: the emerging role of the endocannabinoid system., *Molecular and cellular endocrinology*, 397(1–2), pp. 59–66.

Soria, G. *et al.* (2005) Lack of CB1 cannabinoid receptor impairs cocaine self-administration., *Neuropsychopharmacology: official publication of the American College of Neuropsychopharmacology*. England, 30(9), pp. 1670–1680.

Stamatakis, A. M. *et al.* (2013) A unique population of ventral tegmental area neurons inhibits the lateral habenula to promote reward., *Neuron*, 80(4), pp. 1039–1053.

Stanfill, A. G. *et al.* (2015) Neurogenetic and Neuroimaging Evidence for a Conceptual Model of Dopaminergic Contributions to Obesity, *Biological research for nursing*. 2015/01/09, 17(4), pp. 413–421.

Stefanik, M. T. *et al.* (2013) Optogenetic inhibition of cocaine seeking in rats, *Addiction Biology*. John Wiley & Sons, Ltd, 18(1), pp. 50–53.

Steindel, F. *et al.* (2013) Neuron-type specific cannabinoid-mediated G protein signalling in mouse hippocampus., *Journal of neurochemistry*. England, 124(6), pp. 795–807.

Stenberg, G., Sano, M., Rosen, I. and Ingvar, D. H. (1994) EEG topography of acute ethanol effects in resting and activated normals, *Journal of Studies on Alcohol*, 55(6), pp. 645–656.

Steward, T. *et al.* (2018) Food addiction and impaired executive

functions in women with obesity, *European Eating Disorders Review*. John Wiley & Sons, Ltd, 26(6), pp. 574–584.

Stewart, J. L. and May, A. C. (2016) *Electrophysiology for addiction medicine: From methodology to conceptualization of reward deficits*. 1st edn, *Progress in Brain Research*. 1st edn. Elsevier B.V.

Stipanovich, A. *et al.* (2009) A phosphatase cascade by which natural rewards and drugs of abuse regulate nucleosomal response in the mouse, *Nature*, 453(7197), pp. 879–884.

Stoltz, S. G. (1984) Recovering from foodaholism., *Journal for Specialists in Group Work*. United Kingdom: Taylor & Francis, 9(1), pp. 51–61.

Stuber, G. D. *et al.* (2011) Excitatory transmission from the amygdala to nucleus accumbens facilitates reward seeking., *Nature*, 475(7356), pp. 377–380.

Sugiura, T., Kishimoto, S., Oka, S. and Gokoh, M. (2006) Biochemistry, pharmacology and physiology of 2-arachidonoylglycerol, an endogenous cannabinoid receptor ligand., *Progress in lipid research*. England, 45(5), pp. 405–446.

Sun, H. S. *et al.* (2012) Morphine epigenomically regulates behavior through alterations in histone H3 lysine 9 dimethylation in the nucleus accumbens, *Journal of Neuroscience*, 32(48), pp. 17454–17464.

Taha, S. A. *et al.* (2009) Convergent, not serial, striatal and pallidal circuits regulate opioid-induced food intake., *Neuroscience*, 161(3), pp. 718–733.

Tammela, L. I. *et al.* (2010) Brain electrical activity during food presentation in obese binge-eating women., *Clinical physiology and functional imaging*. England, 30(2), pp. 135–140.

Tamura, H., Shiosaka, S. and Morikawa, S. (2018) Trophic modulation of gamma oscillations: The key role of processing protease for Neuregulin-1 and BDNF precursors., *Neurochemistry international*. England, 119, pp. 2–10.

Tamura, M. *et al.* (2017) Hippocampal-prefrontal theta-gamma coupling during performance of a spatial working memory task., *Nature communications*, 8(1), p. 2182.

Tavares, L. C. S. and Tort, A. B. L. (2022) Hippocampal-prefrontal interactions during spatial decision-making., *Hippocampus*. United States, 32(1), pp. 38–54.

Teegarden, S. L. and Bale, T. L. (2008) Effects of stress on dietary preference and intake are dependent on access and stress sensitivity., *Physiology & behavior*, 93(4–5), pp. 713–723.

Tepper, J. M., Tecuapetla, F., Koós, T. and Ibáñez-Sandoval, O. (2010) Heterogeneity and diversity of striatal GABAergic interneurons., *Frontiers in neuroanatomy*, 4, p. 150.

Terraneo, A. *et al.* (2016) Transcranial magnetic stimulation of dorsolateral prefrontal cortex reduces cocaine use: A pilot study, *European Neuropsychopharmacology*. Elsevier, 26(1), pp. 37–44.

Timper, K. and Brüning, J. C. (2017) Hypothalamic circuits regulating appetite and energy homeostasis: pathways to obesity, *Disease models & mechanisms*. The Company of Biologists Ltd,

10(6), pp. 679–689.

Tokita, K., Armstrong, W. E., St John, S. J. and Boughter, J. D. J. (2014) Activation of lateral hypothalamus-projecting parabrachial neurons by intraorally delivered gustatory stimuli., *Frontiers in neural circuits*, 8, p. 86.

Tort, A. B. L. *et al.* (2008) Dynamic cross-frequency couplings of local field potential oscillations in rat striatum and hippocampus during performance of a T-maze task., *Proceedings of the National Academy of Sciences of the United States of America*, 105(51), pp. 20517–20522.

Touzani, K. and Sclafani, A. (2002) Area postrema lesions impair flavor-toxin aversion learning but not flavor-nutrient preference learning., *Behavioral Neuroscience*. Sclafani, Anthony: Dept of Psychology, Brooklyn Coll of the City U New York, Brooklyn, NY, US, 11210, asclafani@gc.cuny.edu: American Psychological Association, pp. 256–266.

Tritsch, N. X. and Sabatini, B. L. (2012) Dopaminergic modulation of synaptic transmission in cortex and striatum., *Neuron*, 76(1), pp. 33–50.

Tsou, K. *et al.* (1998) Immunohistochemical distribution of cannabinoid CB1 receptors in the rat central nervous system., *Neuroscience*. United States, 83(2), pp. 393–411.

Tu, Y. *et al.* (2007) Ethanol inhibits persistent activity in prefrontal cortical neurons, *Journal of Neuroscience*, 27(17), pp. 4765–4775.

Tuulari, J. J. *et al.* (2017) Feeding Releases Endogenous Opioids in

Humans., *The Journal of neuroscience : the official journal of the Society for Neuroscience*, 37(34), pp. 8284–8291.

Urban, D. J. and Roth, B. L. (2015) DREADDs (Designer Receptors Exclusively Activated by Designer Drugs): Chemogenetic Tools with Therapeutic Utility, *Annual Review of Pharmacology and Toxicology*, 55(1), pp. 399–417.

Usiello, A. *et al.* (2000) Distinct functions of the two isoforms of dopamine D2 receptors., *Nature*. England, 408(6809), pp. 199–203.

Velázquez-Sánchez, C. *et al.* (2015) Seeking behavior, place conditioning, and resistance to conditioned suppression of feeding in rats intermittently exposed to palatable food., *Behavioral neuroscience*, 129(2), pp. 219–224.

Verdejo-Garcia, A. and Chong, T. T.-J. (2021) Targeting goal-based decision-making for addiction recovery., *Pharmacology, biochemistry, and behavior*. United States, 210, p. 173275.

Verharen, J. P. H., Adan, R. A. H. and Vanderschuren, L. J. M. J. (2020) How Reward and Aversion Shape Motivation and Decision Making: A Computational Account., *The Neuroscientist : a review journal bringing neurobiology, neurology and psychiatry*. United States, 26(1), pp. 87–99.

Volkow, N. D. *et al.* (1999) Prediction of reinforcing responses to psychostimulants in humans by brain dopamine D2 receptor levels., *The American journal of psychiatry*. United States, 156(9), pp. 1440–1443.

Volkow, N. D. *et al.* (2002a) ‘Nonhedonic’ food motivation in

humans involves dopamine in the dorsal striatum and methylphenidate amplifies this effect., *Synapse (New York, N.Y.)*. United States, 44(3), pp. 175–180.

Volkow, N. D. *et al.* (2002b) Role of dopamine in the therapeutic and reinforcing effects of methylphenidate in humans: results from imaging studies., *European neuropsychopharmacology : the journal of the European College of Neuropsychopharmacology*. Netherlands, 12(6), pp. 557–566.

Volkow, N. D. and O'Brien, C. P. (2007) Issues for DSM-V: Should Obesity Be Included as a Brain Disorder?, *American Journal of Psychiatry*. American Psychiatric Publishing, 164(5), pp. 708–710.

Volkow, Nora D. *et al.* (2008) Low dopamine striatal D2 receptors are associated with prefrontal metabolism in obese subjects: Possible contributing factors, *NeuroImage*. Academic Press, 42(4), pp. 1537–1543.

Volkow, Nora D, Wang, G.-J., Fowler, J. S. and Telang, F. (2008) Overlapping neuronal circuits in addiction and obesity: evidence of systems pathology., *Philosophical transactions of the Royal Society of London. Series B, Biological sciences*, 363(1507), pp. 3191–3200.

Volkow, N. D. *et al.* (2010) Addiction: decreased reward sensitivity and increased expectation sensitivity conspire to overwhelm the brain's control circuit., *BioEssays : news and reviews in molecular, cellular and developmental biology*, 32(9), pp. 748–755.

Volkow, N. D. *et al.* (2011a) Addiction: Beyond dopamine reward circuitry, *Proceedings of the National Academy of Sciences*, 108(37),

pp. 15037 LP – 15042.

Volkow, N. D., Wang, G.-J. and Baler, R. D. (2011b) Reward, dopamine and the control of food intake: implications for obesity., *Trends in cognitive sciences*, 15(1), pp. 37–46.

Volkow, N. D. and Muenke, M. (2012) The genetics of addiction., *Human genetics*, pp. 773–777.

Volkow, N. D., Wang, G.-J., Tomasi, D. and Baler, R. D. (2013) Obesity and addiction: neurobiological overlaps., *Obesity reviews : an official journal of the International Association for the Study of Obesity*, 14(1), pp. 2–18.

Volkow, N. D. and Baler, R. D. (2015) NOW vs LATER brain circuits: implications for obesity and addiction., *Trends in neurosciences*. England, 38(6), pp. 345–352.

Volkow, N. D. and Morales, M. (2015) The Brain on Drugs: From Reward to Addiction, *Cell*. Elsevier Inc., 162(4), pp. 712–725.

Volkow, N. D., Koob, G. F. and McLellan, A. T. (2016) Neurobiologic Advances from the Brain Disease Model of Addiction, *New England Journal of Medicine*, 374(4), pp. 363–371.

Volkow, Nora D., Wise, R. A. and Baler, R. (2017) The dopamine motive system: Implications for drug and food addiction, *Nature Reviews Neuroscience*, 18(12), pp. 741–752.

Volkow, N. D., Michaelides, M. and Baler, R. (2019) The Neuroscience of Drug Reward and Addiction., *Physiological reviews*, 99(4), pp. 2115–2140.

de Vries, S.-K. and Meule, A. (2016) Food Addiction and Bulimia Nervosa: New Data Based on the Yale Food Addiction Scale 2.0., *European eating disorders review: the journal of the Eating Disorders Association*. England, 24(6), pp. 518–522.

Wadden, T. A. *et al.* (2005) Randomized trial of lifestyle modification and pharmacotherapy for obesity., *The New England journal of medicine*. United States, 353(20), pp. 2111–2120.

Walker, D. M. and Nestler, E. J. (2018) Neuroepigenetics and addiction, *Handb Clin Neurol*, 148, pp. 747–765.

Wang, Gene-Jack *et al.* (2014) BMI Modulates Calorie-Dependent Dopamine Changes in Accumbens from Glucose Intake, *PLOS ONE*. Public Library of Science, 9(7), p. e101585. Available at: <https://doi.org/10.1371/journal.pone.0101585>.

Wang, G-J *et al.* (2014) Effect of combined naltrexone and bupropion therapy on the brain's reactivity to food cues., *International journal of obesity (2005)*, 38(5), pp. 682–688.

Wang, G. J. *et al.* (2001) Brain dopamine and obesity., *Lancet (London, England)*. Elsevier, 357(9253), pp. 354–7.

Wang, L. *et al.* (2020) Modulation of Hippocampal Gamma Oscillations by Dopamine in Heterozygous Reeler Mice in vitro, *Frontiers in Cellular Neuroscience*, 13.

Weiner, B. and White, W. (2007) The Journal of Inebriety (1876-1914): history, topical analysis, and photographic images., *Addiction (Abingdon, England)*. England, 102(1), pp. 15–23.

Wells, A. S., Read, N. W., Laugharne, J. D. and Ahluwalia, N. S. (1998) Alterations in mood after changing to a low-fat diet., *The British journal of nutrition*. England, 79(1), pp. 23–30.

Westlake, T. M. *et al.* (1994) Cannabinoid receptor binding and messenger RNA expression in human brain: an in vitro receptor autoradiography and in situ hybridization histochemistry study of normal aged and Alzheimer's brains., *Neuroscience*. United States, 63(3), pp. 637–652.

Westwater, M. L., Fletcher, P. C. and Ziauddeen, H. (2016) Sugar addiction: the state of the science., *European journal of nutrition*, 55(Suppl 2), pp. 55–69.

Wexler, B. E. *et al.* (2001) Functional Magnetic Resonance Imaging of Cocaine Craving, *American Journal of Psychiatry*, 158(1), pp. 86–95.

WHO (2017) No Title.

Wiepkema, P. R. (1971) Behavioural factors in the regulation of food intake., *The Proceedings of the Nutrition Society*. England, 30(2), pp. 142–149.

Wildes, J. E. *et al.* (2012) Emotion and eating disorder symptoms in patients with anorexia nervosa: an experimental study., *The International journal of eating disorders*, 45(7), pp. 876–882.

Wilfley, D. E. *et al.* (2002) A randomized comparison of group cognitive-behavioral therapy and group interpersonal psychotherapy for the treatment of overweight individuals with binge-eating disorder., *Archives of general psychiatry*. United States, 59(8), pp.

713–721.

Williams, G. (2012) Aromatase up-regulation, insulin and raised intracellular oestrogens in men, induce adiposity, metabolic syndrome and prostate disease, via aberrant ER- α and GPER signalling., *Molecular and cellular endocrinology*. Ireland, 351(2), pp. 269–278.

Wilson, G. T., Grilo, C. M. and Vitousek, K. M. (2007) Psychological treatment of eating disorders., *The American psychologist*. United States, 62(3), pp. 199–216.

Wilson, R. I. and Nicoll, R. A. (2002) Endocannabinoid signaling in the brain., *Science (New York, N.Y.)*. United States, 296(5568), pp. 678–682.

Winters, B. D. *et al.* (2012) Cannabinoid receptor 1-expressing neurons in the nucleus accumbens., *Proceedings of the National Academy of Sciences of the United States of America*, 109(40), pp. E2717-25.

Wise, R. A. (2004) Dopamine, learning and motivation., *Nature reviews. Neuroscience*. England, 5(6), pp. 483–494.

Wise, R. A. (2005) Forebrain substrates of reward and motivation, *The Journal of comparative neurology*, 493(1), pp. 115–121.

Wiss, D. A., Avena, N. and Rada, P. (2018) Sugar Addiction: From Evolution to Revolution, *Frontiers in psychiatry*. Frontiers Media S.A., 9, p. 545.

Wolz, I. *et al.* (2017) Subjective craving and event-related brain

response to olfactory and visual chocolate cues in binge-eating and healthy individuals., *Scientific reports*, 7, p. 41736.

Wonderlich, S. A. *et al.* (2009) The validity and clinical utility of binge eating disorder., *The International journal of eating disorders*. United States, 42(8), pp. 687–705.

Wong, C. C. Y., Mill, J. and Fernandes, C. (2011) Drugs and addiction: An introduction to epigenetics, *Addiction*, 106(3), pp. 480–489.

Wright, W. J., Schlüter, O. M. and Dong, Y. (2017) A Feedforward Inhibitory Circuit Mediated by CB1-Expressing Fast-Spiking Interneurons in the Nucleus Accumbens., *Neuropsychopharmacology: official publication of the American College of Neuropsychopharmacology*, 42(5), pp. 1146–1156.

Yang, H. *et al.* (2018) Nucleus Accumbens Subnuclei Regulate Motivated Behavior via Direct Inhibition and Disinhibition of VTA Dopamine Subpopulations, *Neuron*. Elsevier Inc., 97(2), pp. 434-449.e4.

Yang, W. and Yuste, R. (2017) In vivo imaging of neural activity, *Nature Methods*. Nature Publishing Group, pp. 349–359.

Yeomans, M. R. and Gray, R. W. (2002) Opioid peptides and the control of human ingestive behaviour., *Neuroscience and biobehavioral reviews*. United States, 26(6), pp. 713–728.

Yilmaz, Z., Hardaway, J. A. and Bulik, C. M. (2015) Genetics and Epigenetics of Eating Disorders., *Advances in genomics and genetics*, 5, pp. 131–150.

Zhang, H.-Y. *et al.* (2021) Repeated cocaine administration upregulates CB(2) receptor expression in striatal medium-spiny neurons that express dopamine D(1) receptors in mice., *Acta pharmacologica Sinica*. United States.

Zigman, J. M., Bouret, S. G. and Andrews, Z. B. (2016) Correction to ‘Obesity Impairs the Action of the Neuroendocrine Ghrelin System’: [Trends in Endocrinology and Metabolism, 27 (2016) 54-63]., *Trends in endocrinology and metabolism: TEM*. United States, 27(5), p. 348.

Zipfel, S., Schmidt, U. and Giel, K. E. (2022) The hidden burden of eating disorders during the COVID-19 pandemic, *The Lancet Psychiatry*. Elsevier Ltd, 9(1), pp. 9–11.

Zou, S. and Kumar, U. (2018) Cannabinoid Receptors and the Endocannabinoid System: Signaling and Function in the Central Nervous System., *International journal of molecular sciences*, 19(3).

Zuurman, L. *et al.* (2008) Effect of intrapulmonary tetrahydrocannabinol administration in humans, *Journal of Psychopharmacology*, 22(7), pp. 707–716.

Annex

Annex I: R Maldonado, P Calvé, A García-Blanco, L Domingo-Rodriguez, E Senabre, E Martín-García. (2021) Vulnerability to addiction., *Neuropharmacology*.

Annex II: R Maldonado, P Calvé, A García-Blanco, L Domingo-Rodriguez, E Senabre, E Martín-García. (2021) Genomics and epigenomics of addiction., *American Journal of Medical Genetics, Part B: Neuropsychiatric Genetics*.

Annex III: Carlo Matera, Pablo Calvé*, Verònica Casadó-Anguera*, Rosalba Sortino*, Alexandre M. J. Gomila, Estefanía Moreno, Thomas Gener, Cristina Delgado, Pau Nebot, Davide Costazza, Sara Conde-Berriozabal, Mercè Masana, Jordi Hernando, Vicent Casadó, M. Victoria Puig, Pau Gorostiza. (2022) Reversible photocontrol of dopaminergic transmission in wild-type animals., *ChemRxiv*.

Annex IV: Natalia Soldevila-Domenech[#], Laura Tío[#], Jone Llorente-Onaindia, Elena Martín-García, Pau Nebot, Rafael de la Torre, Alba Gurt, Rafael Maldonado* and Jordi Monfort* and the Covidmar Study Group. (2020) COVID-19 incidence in patients with immunomediated inflammatory diseases: Influence of Immunosuppressant Treatments., *Frontiers in Pharmacology*.

Annex V: Josep Blanch-Rubió*, Natalia Soldevila-Domenech*, Laura Tío, Jone Llorente-Onaindia, Manuel Ciria-Recasens, Luciano Polino, Alba Gurt, Rafael de la Torre, Rafael Maldonado, Jordi Monfort, and the Covidmar Study Group. (2020) Influence of anti-osteoporosis treatments on the incidence of COVID-19 in patients with non-inflammatory rheumatic conditions., *Aging*.



Invited review

Vulnerability to addiction



R. Maldonado^{a,b,*}, P. Calvé^a, A. García-Blanco^a, L. Domingo-Rodríguez^a, E. Senabre^a,
E. Martín-García^a

^a Laboratory of Neuropharmacology-Neurophar, Department of Experimental and Health Sciences, Universitat Pompeu Fabra (UPF), Barcelona, Spain
^b Hospital Del Mar Medical Research Institute (IMIM), Barcelona, Spain

ARTICLE INFO

Keywords:

Addiction
DSM-5
Inhibitory control
DREADD
Electrophysiology
Calcium imaging
Therapeutic approach

ABSTRACT

Addiction is a chronic brain disease that has dramatic health and socioeconomic consequences worldwide. Multiple approaches have been used for decades to clarify the neurobiological basis of this disease and to identify novel potential treatments. This review summarizes the main brain networks involved in the vulnerability to addiction and specific innovative technological approaches to investigate these neural circuits. First, the evolution of the definition of addiction across the Diagnostic and Statistical Manual of Mental Disorders (DSM) is revised. We next discuss several innovative experimental techniques that, combined with behavioral approaches, have allowed recent critical advances in understanding the neural circuits involved in addiction, including DREADDs, calcium imaging, and electrophysiology. All these techniques have been used to investigate specific neural circuits involved in vulnerability to addiction and have been extremely useful to clarify the neurobiological basis of each specific component of the addictive process. These novel tools targeting specific brain regions are of great interest to further understand the different aspects of this complex disease. This article is part of the special issue on 'Vulnerabilities to Substance Abuse'.

1. Introduction

Addiction is a chronic relapsing disorder characterized by the loss of inhibitory control over drug-seeking and taking, and maintenance of drug use despite negative consequences (Koob and Volkow, 2016). This brain disease has a multifactorial origin with several environmental factors and gene networks interacting among them, leading to a vulnerable phenotype to develop the addictive process (Hamer, 2002). The Diagnostic and Statistical Manual of Mental Disorders (DSM), the tool for diagnosing mental illness used by the American Psychiatric Association, has highly evolved from the eighties to the nineties in the criteria used to diagnose addiction (Fig. 1). In 1980, the third edition of the DSM (DSM-III) defined addiction mainly based on the two significant physical effects produced by the long-term exposure to drugs of abuse, tolerance to the drug, and withdrawal symptoms when stopping drug use (American Psychiatric Association, 1980). In 1994, this drug-centered definition changed with the DSM-IV, and these two criteria were no longer necessary for the diagnosis of addiction. The diagnosis was given in the DSM-IV only when the patient met a minimum of three out of seven criteria, and five of the seven diagnosis criteria were focused on behavioral markers (American Psychiatric

Association, 1994).

The current DSM fifth edition (American Psychiatric Association, 2013) combines the DSM-IV categories of substance abuse and substance dependence into a single substance use disorder, measured with eleven criteria on a continuum from mild to severe. Thus, the categorical approach of DSM-IV has evolved into a dimensional approach in the DSM-5 that consists of condensing abuse and dependence as dimensions into a single manifestation of a disorder with varying levels of severity (Kopak et al., 2012). Each specific substance is a new separate use disorder, but nearly all substances are diagnosed based on the same overarching criteria (American Psychiatric Association, 2013). A diagnosis of substance dependence previously required three criteria in the DSM-IV, but now mild substance-use disorder in the DSM-5 requires only two symptoms, while severe requires a minimum of six. In the DSM-5, the term addiction is now synonymous with the concept of severe substance-use disorder (Volkow et al., 2016). Problems with law enforcement are not present anymore because cultural considerations make the criteria challenging to apply internationally. Hence, the concept of addiction in the DSM-IV and DSM-5 remains behavioral-centered, and the alterations of loss of inhibitory control emerge as relevant for the transition to addiction. In agreement, the

* Corresponding author. Laboratory of Neuropharmacology, Universitat Pompeu Fabra, Dr. Aiguader, 88, Barcelona, 08003, Spain.
E-mail addresses: rafael.maldonado@upf.edu (R. Maldonado), elena.martin@upf.edu (E. Martín-García).

<https://doi.org/10.1016/j.neuropharm.2021.108466>

Received 1 October 2020; Received in revised form 3 December 2020; Accepted 14 January 2021

Available online 20 January 2021

0028-3908/© 2021 The Authors. Published by Elsevier Ltd. This is an open access article under the CC BY-NC-ND license

<http://creativecommons.org/licenses/by-nc-nd/4.0/>.

Tenth Revision of the International Classification of Diseases and Health Problems (ICD-10) defines the dependence syndrome as being a cluster of behavioral, physiological, and cognitive phenomena in which the habit of substance use occurs on a much higher urgency for an individual than other activities that once had more salient value. However, the crucial feature of dependence in the ICD-10 is the desire to take the drug and the high probability of relapse after a period of abstinence (WHO, 2020). The DSM-5 also includes gambling disorder as the only diagnosable condition in a new category of behavioral addictions. The controversial concept of food addiction is not included in the DSM-5, although this concept is evolving, and the Yale Food Addiction Scale (YFAS) is the current tool used for the diagnosis of food addiction (Gearhardt et al., 2009) in its updated version YFAS v2.0 (Gearhardt et al., 2016).

The individual vulnerability to addiction is a crucial component in the development of the pathology. Thus, drug-taking initiation does not necessarily lead to addiction, and not all drug users become addicted. Out of 100 people initiating drug use, around 15 to 17 develop an addiction (Anthony et al., 1994), and the range of variation depends on

the pharmacological drug properties, the environment, and the genetic susceptibility (Nestler et al., 2016). After the initiation of drug use, resilient individuals can stop and control consumption. In contrast, occasional use in vulnerable individuals is followed by regular use, and finally, addiction develops with a high risk of relapse even after prolonged periods of abstinence. Currently, relapse is a cause of maximum preoccupation at the clinical level with difficult therapeutic approaches.

The diagnostic criteria used in the manuals of psychiatry must be considered when animal models are used to study addiction's neurobiology (Piazza and Deroche-Gamonet, 2013). An animal model of drug addiction has been generated based on five behavioral criteria of DSM-IV/5 clustered in three particular behavioral hallmarks of addiction with the following correspondence (Fig. 1): 1) persistence to response (criteria 3 and 4 of DSM-IV, and 6 and 7 of DSM-5), 2) motivation for the drug (criteria 5 and 6 of DSM-IV, and 9 and 10 of DSM-5), 3) compulsivity defined as an alteration of inhibitory control despite negative consequences (criterion 7 of DSM-IV, and 11 of DSM-5) (Deroche-Gamonet et al., 2004). As the DSM-IV addiction criteria were maintained in the DSM-5, the three hallmarks that englobe them have

<p>DSM-III (1980) Criteria for Substance Abuse</p> <p>All of these three criteria should be accomplished</p> <ol style="list-style-type: none"> 1. Disturbance of social or occupational functioning. 2. Pattern of pathological use. <p>3. Impairment in social or occupational functioning due to substance use.</p>	<p>DSM-IV (1994) Criteria for Substance Abuse</p> <p>At least one of these four criteria should be accomplished</p> <ol style="list-style-type: none"> 1. Recurrent failure to fulfill major role obligations. 2. Recurrent substance use in physically hazardous situations. 3. Recurrent substance-related legal problems. 4. Continued substance use despite persistent or recurrent social or interpersonal problems. 	<p>DSM-5 (2013) Criteria for Substance Use</p> <p>At least one of the eleven criteria: (0-1 unaffected; 2-3 mild; 4-5 moderate; 6 or more severe)</p> <ol style="list-style-type: none"> 1. Recurrent failure to fulfill major role obligations. 2. Recurrent substance use in physically hazardous situations. 3. Continued substance use despite persistent or recurrent social or interpersonal problems. 	<p>Hallmarks of addiction rat/mouse model</p> <p>(Deroche-Gamonet et al. 2004, Kasanetz et al. 2010, Mancini et al. 2015, Domingo-Rodriguez et al. 2020)</p> <ol style="list-style-type: none"> 1. Persistence to response (criteria 3-4 in DSM-IV and 6-7 in DSM-5).
<p>DSM-III (1980) Criteria for Substance Dependence</p> <p>One out of these two criteria should be accomplished</p> <ol style="list-style-type: none"> 1. Tolerance. 2. Withdrawal. 	<p>DSM-IV (1994) Criteria for Substance Dependence</p> <p>Three out of these seven criteria should be accomplished</p> <ol style="list-style-type: none"> 1. Tolerance. 2. Withdrawal. 3. The substance is often taken in larger amounts or even a longer period than intended. 4. Persistent desire or unsuccessful efforts to cut down. 5. Considerable time spent in obtaining the substance or using, or recovering from its effects. 6. Important social, work, or recreational activities given up because use. 7. Continued use despite knowledge of problems caused by or aggravated by use. 	<ol style="list-style-type: none"> 4. Tolerance. 5. Withdrawal. 6. The substance is often taken in larger amounts or even a longer period than intended. 7. Persistent desire or unsuccessful efforts to cut down. 8. Craving. 9. Considerable time spent in obtaining the substance or using, or recovering from its effects. 10. Important social, work, or recreational activities given up because use. 11. Continued use despite knowledge of problems caused by or aggravated by use. 	<ol style="list-style-type: none"> 2. Motivation (criteria 5-6 in DSM-IV and 9-10 in DSM-5). 3. Compulsivity (criteria 7 in DSM-IV and 11 in DSM-5).

Fig. 1. Evolution of the diagnosis criteria of drug addiction in DSM-III, DSM-IV, and DSM-5, and comparison with their corresponding criteria measured in the rodent models of addiction.

been continuously used as a reference to develop animal models of drug and food addiction and to elucidate the neurobiological mechanisms underlying these processes (Augier et al., 2018; Deroche-Gamonet et al., 2004; Domingo-Rodriguez et al., 2020; Kasanetz et al., 2010; Mancino et al., 2015).

Here we review the correspondence between the diagnostic criteria in the DSM and the behavioral hallmarks used in translational research with animal models to link these behavioral responses with recent advances in the neurobiology of addiction. Operant behavioral approaches are usually required to evaluate in animals these complex responses, and novel techniques are now available to be combined with these operant approaches in order to dissect the brain interconnected networks that underlie these responses. These techniques include optogenetics, DREADDs, calcium imaging, electrophysiology, and whole-brain 3-D imaging. Whole-brain 3-D imaging approaches comprise optical clearing methods that allow a three-dimensional reconstruction of brain tissue structures. Among different clearing methods, PACT (passive CLARITY technique) and uDISCO (ultimate DISCO) possess excellent clearing capability on mouse brain samples. PACT removes cell membranes and protein by sodium dodecyl sulfate to decrease the sample's

scattering while preserving native epitope with acrylamide hydrogel. uDISCO employs essential organic compounds that render tissue transparent by protein denaturation and lipid removal. Among others, these clearing methods have provided essential tools for mapping brain wiring diagrams and promoted advances in circuit-based approaches (Kimbrough et al., 2020; Para-Damas and Saura, 2020; Ueda et al., 2020; Vigouroux et al., 2017). Moreover, optogenetic manipulation of specific neural subpopulations has become a powerful strategy to understand behavioral paradigms, already discussed in excellent recent review articles (Chen et al., 2018; Deubner et al., 2019; Rodriguez-Romaguera et al., 2020). The recent advances obtained by combining DREADDs, calcium imaging, and electrophysiology with operant behavioral approaches will be discussed in this review. All together, these techniques have identified particular brain networks that could be targeted as potential therapies for future prevention and treatment of addiction.

2. Neurocircuitry of addiction

The neurocircuitry underlying addiction lies initially in the brain reward system. Within this system, several interconnected networks

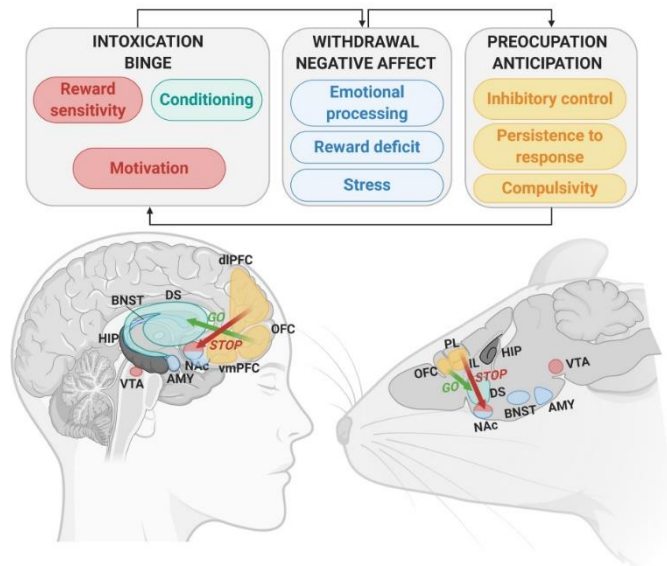


Fig. 2. Schematic representation of human and mouse brain areas involved in reward sensitivity, conditioning, emotional processing, and inhibitory control circuits. These interconnected circuits are underlying the three addiction stages, i.e., binge/intoxication, withdrawal/negative affect, and preoccupation/anticipation, that interact with each other forming a recurring cycle that worsens over time, leading to compulsive seeking despite adverse consequences. This final loss of control seems to be the result of an imbalance between the Stop and Go top-down cortical circuits with a hypofunction of the PL-ventral striatum network and hyperactivity of the OFC-dorsal striatum networks. VTA, ventral tegmental area; NAc, nucleus accumbens; DS, dorsal striatum; AMY, amygdala; BNST, bed nucleus of the stria terminalis; HIP, hippocampus; dIPFC, dorsolateral prefrontal cortex; vmPFC, ventromedial prefrontal cortex; OFC, orbitofrontal cortex; PL, prelimbic; IL, infralimbic.

involved in reward sensitivity, conditioning, emotional processing, and inhibitory control are first recruited by drug exposure and later modified by long-lasting neuroadaptations (Volkow et al., 2019). These networks can be clustered in three major neurobiological circuits: the basal ganglia, the extended amygdala, and the prefrontal cortex (Koob and Volkow, 2016). These three major neurobiological circuits have its correspondence to three stages of the transition to addiction, i.e., binge/intoxication, the withdrawal/negative affect, and the pre-occupation/anticipation stage, that interact with each other forming a recurring cycle in which addiction can be conceptualized (Koob and Volkow, 2010). The three behavioral hallmarks used in the addiction animal model, motivation, persistence to response, and compulsivity, can be integrated into these three stages of the addictive process. Thus, the motivation for the drug has its correspondence with the intoxication stage; whereas, the persistence to response and the compulsivity-like behavior have their phenotypic similarity in the pre-occupation/anticipation stage (Fig. 2). Motivation is connected to reward processing and is related to the mesolimbic dopamine neurons projecting from the ventral tegmental area (VTA) to the nucleus accumbens (NAc) (Lindgren et al., 2017). Persistence to response reveals the difficulty of animals to stop reward-seeking. This behavioral hallmark is related to a persistent desire and an ineffective effort to cut down the response due to habit formation or disruption of extinction learning and mainly involves the participation of the prefrontal cortex (PFC), the dorsal striatum, and the hippocampus (Schmitzer-Torbert et al., 2015). The compulsivity-like behavior is related to the connectivity strength of the medial PFC (mPFC) glutamatergic projections to the NAc (Domingo-Rodriguez et al., 2020). This establishment of addiction behavioral hallmarks in animal research based on human diagnostic criteria has helped to study the neurobiological substrates underlying addiction, taking into account each specific endophenotype that integrates this complex behavioral disease.

During the intoxication stage, the rewarding effects of drugs of abuse are related to a massive burst of dopamine in the NAc (Di Chiara and Imperato, 1998; Koob and Bloom, 1998). The dopaminergic neurons that project from the VTA to the NAc involved in these rewarding effects integrate the mesolimbic pathway critically involved in goal-directed behavior (Lammel et al., 2012; Yang et al., 2018). This reward pathway drives the motivation for natural reinforcers, such as food, indicating that drugs are hijacking the circuits underlying natural rewards (Kelley and Berridge, 2002). The physiological role of this circuit provides a neurobiological explanation for the capability of foods, mostly those rich with sugars, to trigger addictive behaviors similar to drugs of abuse (Volkow et al., 2013; Wise, 2002).

Phasic dopamine firing in the NAc produced by addictive substance intake promotes a strong association between environmental neutral stimuli and the reward through the process of conditioning (Koob and Volkow, 2010). With the repeated pairing stimulus-reward over time, the learned cue becomes salient and acquires the ability to increase dopamine in the NAc by itself in anticipation of the reward (Pecina and Berridge, 2013). Thus, the motivational drive towards the reinforcer now may occur with the addictive substance-predictive cue's exposure, in the absence of drug or food presentation and the absence of physiological needs, facilitating the transition to habit-like compulsive seeking (Everitt and Robbins, 2005). This transition from controlled actions to more habit-based behaviors involves a shift from the ventral striatum in favor of progressive recruitment of the dorsal striatum (Balleine and O'Doherty, 2010; Everitt and Robbins, 2013). Within the dorsal striatum, the dorsolateral portion of this area (DLS) has been proposed to play a particular role in the formation and expression of stimulus-response habits in contrast to the dorsomedial portion (DMS), involved in the acquisition of drug-seeking and goal-directed behavior (Everitt and Robbins, 2016; Lipton et al., 2019). Thus, dopamine receptor blockade in the DLS decreased cocaine-seeking after prolonged training in mice but was ineffective during the acquisition phase. In contrast, dopamine receptor blockade in the DMS modified

cocaine-seeking acquisition but did not affect prolonged training when habit formation was established (Murray et al., 2012). In agreement, electrophysiological studies revealed a DMS neuronal activation during the acquisition of a specific learning task, which was progressively decreased over training corresponding to the time frame when DLS activity emerged to drive habitual performance (Grenel and Costa, 2013; Smith and Graybiel, 2013; Thorn et al., 2010). Therefore, the repetitive consummatory behavior leads to a reduction of the glutamate inputs from the PFC to the NAc and the DMS governing the goal-directed behavior in favor of glutamate projections from sensory-motor cortical areas and dopaminergic projections from the substantia nigra to the lateral portion of the dorsal striatum leading to the habitual drug-seeking (Everitt and Robbins, 2013, 2016). However, recent data have raised questions about the relevance of 'habit-formation' in addiction development since drug-taking behaviors were reported to only require dopamine inputs from the ventral striatum but not from the dorsal striatum (Singer et al., 2019).

As addiction progresses, abstinence of the addictive substance results in a strong negative emotional state (anhedonia, anxiety, depression, among other symptoms) that leads to an increased urge to consume the addictive substance to ameliorate these negative symptoms rather than for its primary reinforcing value (Pavlyk et al., 2011). The neurobiological substrate underlying this stage is the recruitment of the brain's stress systems in the extended amygdala and the activation of the hypothalamic-pituitary-adrenal axis triggered by stress mediators, such as the corticotropin-releasing factor (Koob and Volkow, 2016). In parallel, the chronic activation of the reward system leads to neuroadaptations producing a decreased reward function characterized by loss of motivation for natural rewards and the lack of interest in activities not associated with the reinforcer. Indeed, neuroimaging studies revealed a lower availability of dopamine type 2 receptors (D2Rs) and decreased dopamine release in the striatum in drug-addicted individuals, similar to the downregulation of these receptors reported in obese individuals (Volkow and Wise, 2005; Wang et al., 2001). Striatal D2Rs availability correlates with lower metabolic activity in PFC regions in these subjects (Goldstein and Volkow, 2011; Volkow et al., 2008). These neuroadaptations contribute to the emergence of the negative state associated with the withdrawal, driving to a craving that increases the vulnerability to relapse.

During the preoccupation stage, the exposure to conditioned cues leads to an augmentation of the craving associated with a hypofunction of frontal areas involved in the top-down inhibitory control (Goldstein and Volkow, 2011). This loss of inhibitory control over drug or food-seeking leads to continue use despite negative consequences. Only a small percentage of people who consume addictive substances reach this stage, pointing out the individual differences between vulnerable and resilient phenotypes (Deroche-Gammonet et al., 2004; Piazza and Deroche-Gammonet, 2013). One frontal area involved in behavioral control that has received considerable attention is the PFC (Miller and Cohen, 2001). The PFC is a collection of several brain areas involved in cognitive processes that are closely implicated in addiction (Moorman et al., 2015). The PFC receives dopamine inputs from the VTA and sends glutamatergic projections to the dorsal and ventral striatum, modulating the striatal-pallidal-thalamocortical system to the VTA, exercising feedback control over the dopaminergic system (Koob and Volkow, 2016). Drug-induced PFC alterations contribute to the dysregulation of reward circuits and higher-order executive functions. The PFC is crucial in the transition to addiction, as the disorder emerges from an imbalance between execution and inhibition of behavior, with excessive motivation uncontrolled by impaired self-regulation, through altered PFC performances. The PFC includes the orbitofrontal cortex (OFC) and the medial PFC (mPFC) (Koob and Volkow, 2010). The mPFC contains several sub-regions that seem to play distinct functional roles: the medial precentral, anterior cingulate, prelimbic (PL), and infralimbic (IL) cortex (Heidbreder and Goensewegen, 2003). These three last sub-regions of the mPFC have been widely related to drug addictive

processes. The PL cortex has been reported to promote cocaine-seeking, whereas the IL cortex has been proposed to suppress cocaine-seeking after extinction (Mooman et al., 2015). However, both PL and IL cortices drive and inhibit drug-seeking depending on the behavioral context, the type of drug, and the previous history of drug consumption, suggesting that multiple subcircuits within each of these mPFC areas may play unique behavioral functions (Mooman et al., 2015; Rign et al., 2014). The anterior cingulate cortex has been mainly involved in attentional selectivity and discrimination learning participating in the generation of impulsive actions (Perry et al., 2011) and cues-induced cocaine reinstatement (Kalivas and Volkow, 2005). Another area recently related to cue-induced cocaine reinstatement is the lateral habenula, which regulates dopaminergic signaling from the limbic forebrain to the brainstem nuclei. The main role attributed to the lateral habenula is the processing of aversive information and behavioral flexibility (Nau et al., 2020).

The orbitofrontal cortex is involved in appropriate flexible behavior and goal-directed decision making (Wilkenheiser and Schoenbaum, 2016). Early studies support a crucial role of this area in the inhibitory control of inappropriate responses in a current context (Perry et al., 2011). In contrast, more recent studies argued against response inhibition as the primary role of the orbitofrontal cortex, suggesting a more relevant role in associative learning and decision-making (Strubiner et al., 2015). The orbitofrontal cortex in rodents is part of the olfactory system, and the possible differential role of the sub-regions of this cortical area has not yet been well defined (den Hartog et al., 2016; Lucantonio et al., 2012; Wilkenheiser and Schoenbaum, 2016).

Within the PFC, the anterior insular cortex that corresponds to the agranular insula in rodents (Naqvi and Bechara, 2009) appears to have an interoceptive function integrating autonomic and visceral information with emotion and motivation and has been shown to be involved in the maintenance of drug addiction (Naqvi and Bechara, 2009), and food anticipatory activity (Gavrilu et al., 2017). The role of the insula in drug addiction seems related to maladaptive interoceptive control over behavior (Naqvi and Bechara, 2009; Stewart et al., 2014; Verdejo-Garcia et al., 2012; Verdejo-Garcia and Bechara, 2009). Accordingly, this brain structure is activated during craving (Bonson et al., 2002; Brody et al., 2002; Naqvi et al., 2007), and tobacco smokers with insula damage stopped smoking easily without experiencing craving or relapse (Naqvi et al., 2007). Furthermore, anterior insular cortex lesions modulate the loss of control over cocaine intake in rats (Rotge et al., 2017). Other frontal cortical areas, such as the granular insula (Forget et al., 2010), have also been involved in drug addiction. Interestingly, the granular insula's integrity is necessary for exhibiting motivation to take nicotine and relapse to nicotine seeking, but not similar behavioral responses mediated by food (Forget et al., 2010).

The frontal areas send glutamatergic projections in a top-down manner to different brain areas such as VTA, NAc, dorsal striatum, hippocampus, and amygdala, controlling the basal ganglia and the extended amygdala microcircuits (Parsons and Hurd, 2015). Specific 'Go circuits' and 'Stop circuits' have been identified depending on if their recruitment promotes or difficult the transition to addiction-like behaviors (Bock et al., 2013; Picciotto, 2013). The Go circuit produces an activation of the OFC neurons that directly connect to the medial striatum cluster, which includes the NAc core and the medial wall of the dorsal striatum (Hu et al., 2019; Pascoli et al., 2018; Wall et al., 2019). In turn, the 'Stop circuit' activates the excitatory synaptic transmission in PL mPFC neurons projecting to the NAc core inhibiting compulsive-like behavior (Fig. 2) (Domingo-Rodríguez et al., 2020; Hu et al., 2019). An imbalance between both circuits is crucial in the transition to addiction. Identifying the individual strength of both networks may help for restoring the physiological balance between them.

The dorsolateral PFC (dlPFC) in humans is equivalent to the PL area in rodents, and the ventromedial PFC (vmPFC) in humans corresponds to the IL area in rodents (Heidbreder and Groenewegen, 2003). Human neuroimaging studies showed that dlPFC activity increased in response

to cocaine-related cues, and this activation was associated with craving and a high risk of relapse (Wexler et al., 2001). Similarly, rodent studies using drug self-administration reinstatement paradigms reported decreased cocaine- and food-reinstatement behavior after pharmacological PL inactivation (McFarland and Kalivas, 2001). However, compelling evidence suggests that dlPFC and PL circuits also have an essential inhibitory role in regulating reward-seeking behavior. Thus, brain imaging studies revealed a reduced dlPFC activation in cocaine abusers performing response inhibition tasks (Crunelle et al., 2012). In parallel, the PL area's pharmacological inactivation reduced a footshock-associated stimulus's ability to decrease cocaine responding and increased punishment resistance in animals responding for sucrose (Limpens et al., 2015). A reduction of PL neurons excitability was revealed after prolonged cocaine self-administration exposure, with the most substantial effect shown in shock-resistant rats (Chen et al., 2013). In some studies, the dlPFC appears to stimulate cocaine-seeking in the reinstatement model while, in others, it suppresses cocaine-seeking when a shock is associated. This contradiction may be explained considering the associative learning process where the activity in the dlPFC promotes the performance of the most potent behavioral response at the expense of a minus well-learned response (Jasinakla et al., 2015; Smith and Laikis, 2018). Therefore, the dorsal dlPFC, equivalent to the PL area, is recruited in appetitive associative learning promoting drug-seeking responses in reinstatement and also in aversive learning producing avoidance in the presence of harmful consequences of compulsive taking. It is important to underline that the specific circuits driving or suppressing behavior may depend on multiple factors, including the animal model, the behavioral context, and the nature of the drug investigated (Mooman et al., 2015). Indeed, the role of mPFC neurons in reward processing is more complicated than a simple PL vs. IL dichotomy, and both subregions have overlapping functions depending on these factors. The heterogeneous functions within the mPFC may reflect the importance of multiple interconnected subcircuits within each of these areas of mPFC necessary to support unique functions (Mooman et al., 2015). Therefore the mPFC must be considered a structurally subdivided region with multiple specific neural networks that connect different sets of neurons to achieve its complex function in the rational control of the behavioral responses.

3. DREADD approaches on behavioral studies

Innovative techniques have been combined in the last years with behavioral approaches to study the neurobiological substrate of addiction. A chemogenetic technique that has been recently used to study the implication of specific cell populations in addiction is Designer Receptors Exclusively Activated by Designer Drugs (DREADDs). DREADD is based on G protein-coupled receptors (GPCRs) that allow the modification of a specific cell population to modulate the neuronal activity of a brain region or, even more precisely, the activity of a neuronal pathway. This modulation is done through the depolarization or hyperpolarization of the neurons infected by a viral vector that contains the genetic information for excitatory (hM3Dq or hM3Ds) or inhibitory (hM4Di) GPCRs, respectively (Roth, 2016). The first and prototypical DREADD agonist, clozapine-N-oxide (CNO), has low brain penetration and, via metabolic degradation, produces the antipsychotic drug clozapine in low concentrations that represents an additional active DREADD ligand (Gomez et al., 2017). In spite of this metabolic conversion, multiple studies support the use of CNO, taken into account several mandatory requirements. Indeed, CNO use requires appropriate controls by the administration of CNO to non-DREADD-expressing animals in order to exclude potential off-target effects of CNO and/or clozapine (Mahler and Aston-Jones, 2018).

Alternative DREADD agonists have been used instead of CNO, such as perlapine and compound 21, although substantial systemic doses are required to activate DREADDs *in vivo*, and the use of appropriate controls are also necessary for potential off-target actions (Chen et al., 2015;

Thompson et al., 2018). Recently, a potent and selective agonist for muscarinic-based DREADDs named deschloroclozapine has been reported to show 100-fold better affinity and potency for hM3Dq and hM4Di than CNO or compound 21 (Nagai et al., 2020). Deschloroclozapine quickly penetrated the brain and activated hM3Dq and hM4Di in less than 10 min post-injection in rodents and decreased off-target binding compared to CNO *in vitro* (Nagai et al., 2020).

Although cholinergic DREADDs are the most widely chemogenetic tool used in the neuroscience field, other non-cholinergic DREADDs have also been developed. Based on the κ -opioid receptor, KORD (κ -opioid DREADD) has been developed to be activated by the selective inert ligand salvinorin B (SALB). KORD can be expressed in mice together with CNO-responsive DREADDs, a promising bidirectional chemogenetic manipulation of neural circuits (Vardy et al., 2015). Ion channel approaches have also been developed to obtain DREADDs. Thus, modified glutamate-gated chloride channels have been developed to inhibit neuronal transmission using the drug ivermectin as a selective ligand (Frazier et al., 2013). In addition, a promising set of modular ion channels and ultrapotent ligands have been developed, such as novel chemogenetic agonists derived from the clinically approved drug varicaine and novel sub-nanomolar potency agonists with high selectivity for the chemogenetic receptors (Magnus et al., 2019).

In the last years, DREADDs have been widely combined with behavioral studies to elucidate the neurobiological correlates of addiction to different drugs in rodents (Urban and Roth, 2015). Here, we briefly summarized only the main studies that have used DREADDs to dissect the role of specific neuronal pathways in the binge intoxication, withdrawal/negative affect, and preoccupation/anticipation stages of addiction. The use of DREADDs in other responses related to addictive processes has been revised in recent articles (Dobrzanski and Kosut, 2017; Runegard et al., 2019; Yager et al., 2015).

Most DREADD studies focus on the reinforcing effects of drugs of abuse responsible for the binge intoxication stage of the addictive process. The reinforcing effects are regulated by the release of dopamine from the VTA to the NAc, and VTA neurons are regulated at the same time by the GABAergic medial spiny neurons of the NAc (Koob and Volkow, 2016). In agreement, the activation of the excitatory DREADD, hM3Dq, by CNO chronically in the NAc reduces binge alcohol consumption (Pozhidayeva et al., 2020; Purohit et al., 2018). Cell-type-specific *in vivo* chemogenetic manipulation in a model of repeated cycles of alcohol consumption and withdrawal in mice demonstrated that chemogenetic excitation of D1-medium spiny neurons in the NAc mimicked glutamatergic strengthening, promoting alcohol consumption. Inhibition of D2-medium spiny neurons produced the same effect by mimicking strengthening of GABAergic inputs (Cheng et al., 2017). In cocaine self-administration, DREADD inhibition of D2-medium spiny neurons using a chemogenetic approach, enhanced the motivation to obtain cocaine (Bock et al., 2013). In contrast, DREADD activation of the mesolimbic dopaminergic pathway using Cre-recombinase expressing CAV2 vector increased cocaine motivation in rats (Boender et al., 2014). The enhancement of VTA dopamine activity via excitatory DREADDs increased both the affinity of cocaine for DAT and the development of cocaine conditioned place preference in mice with a clear sexual dimorphism (Calipari et al., 2017).

DREADDs have also been used to investigate the role of limbic regions in the negative affect rise during drug abstinence and relapse. Interestingly, inhibition of the insula with DREADDs reduces the hyperactivity of the BNST in abstinence from alcohol, and the excitation of the BNST with DREADDs enhances the negative affect that leads to relapse (Centanni et al., 2019). Inhibition of the lateral habenula also reduces cocaine self-administration and diminishes cue-induced cocaine reinstatement (Nair et al., 2020). In contrast, DREADD BNST inhibition enhances cue-induced reinstatement (Perez et al., 2020). In the NAc, DREADD-mediated glutamate release by glial cells inhibited cue-induced reinstatement of cocaine-seeking by stimulating release-regulating mGluR2/3 autoreceptors (Scofield et al., 2015).

Methamphetamine reinstatement was also modulated by chemogenetic manipulations of glial glutamate release within the NAc core, and astrocyte-specific Gq-coupled expression DREADDs inhibited methamphetamine seeking promoted by cues (Siensen et al., 2019).

In the phase of preoccupation and anticipation of the addiction cycle, the neurobiology of compulsivity has been studied using DREADDs. Cocaine-induced perseverative behaviors in mice were associated with altered synaptic plasticity in accumbal D2-medium spiny neurons integrated into the 'Stop circuit'. A potentiation of glutamatergic input to this 'Stop circuit' produced resilience toward compulsive cocaine-seeking (Bock et al., 2013). These data provide a possible input-output link of a protective mechanism against compulsive behavior due to the enhanced activity induced by cocaine of glutamatergic circuits synapsing onto D2-medium spiny neurons within the NAc. Strengthening the accumbal D2-medium spiny neurons promoted resilience to compulsive cocaine use (Bock et al., 2013). The loss of inhibitory control over palatable food has been studied using the retro-DREADD technique. The retro-DREADD technique consists of the inhibition or excitation of a neuronal population in a specific pathway within a brain region, taking advantage of retrograde viral microinjection, which contains an enzyme that recombinates the DREADD. A study using the retro-DREADD technique from the mPFC to the NAc administering CNO chronically in a constant release for four weeks through minipumps evaluated the role of this pathway in an addictive-like behavior promoted by palatable food. The inhibition of these mPFC projections to the NAc core resulted in compulsive consumption of palatable food and enhancement of the addictive-like behavior (Fig. 3) (Domingo-Rodriguez et al., 2020).

4. Calcium approaches in combination with behavioral studies

Another pioneering technique easy to combine with behavioral approaches to determine neuronal activity *in vivo* in animals is calcium imaging. Calcium imaging is based on the recordings of intracellular calcium influxes caused by depolarization of the neuronal cells. Several optical techniques capture the intracellular calcium influxes based on genetically encoded calcium indicators (Yang and Yuste, 2017). In this review, we focus on the head-mounted miniscopes technology as the most promising technique to combine with behavioral studies that may provide crucial advances in the neuroscience field in the following years. Indeed, miniscopes allow for the first time the optical recordings of neuronal activity in awake, freely moving rodents that can be used in different behavioral models (Ghosh et al., 2011).

Few studies have used head-mounted miniscopes technology in behavioral studies to investigate the neuronal activity patterns during addiction. A recent study has combined calcium imaging and DREADDs to modulate neuronal activity and observe the resulting neuronal activity pattern during cocaine-seeking behavior through calcium imaging (Heinsbroek et al., 2020). Activation of glutamate or GABA neurons in the ventral pallidum regulated differently cue-induced cocaine-seeking. Indeed, activation of glutamate neurons inhibited cocaine-seeking, while activating GABA or enkephalin neurons induced cocaine-seeking (Heinsbroek et al., 2020). Differential neuronal activity patterns were also recently reported combining electrophysiological and calcium recordings. Thus, increased activity of neurons projecting from the IL cortex to the NAc was revealed during cocaine-seeking, whereas the decreased activity of the same neurons was observed in a cocaine-free period (Cameron et al., 2019). Specifically, selective recordings were performed from IL-NAc neurons during drug-seeking, and the activation of this network was associated with relapse prevention. This decreased activity with susceptibility to relapse suggests that strengthening the activity of IL to NAc neurons could be a promising strategy for relapse prevention. Therefore, the calcium imaging technique is a promising optical tool that may provide a considerable contribution in the near future to understand better the neuronal activity patterns of brain regions of the brain currently involved in addiction.

Miniscopes can determine in a quantitative and qualitative strategy

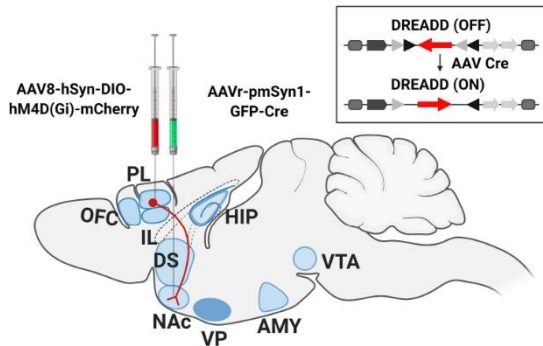


Fig. 3. A potential approach for projection-specific modulation of neuronal activity using DREADDs. The mouse brain, with the combinatorial viral strategy of the retro-DREADD approach, is represented. Selective chemo-genetic inhibition of prelimbic (PL) medial prefrontal cortex to nucleus accumbens (Nac) core neurons is produced by Cre-dependent hM4Di-mCherry injection in the PL and retrograde AAV with Cre recombinase in the NAc. Thus, hM4Di receptor expression only occurs in PL neurons that directly project to NAc. VTA, ventral tegmental area; NAc, nucleus accumbens; DS, dorsal striatum; AMY, amygdala; HIP, hippocampus; OFC, orbitofrontal cortex; PL, prelimbic; IL, infralimbic.

within cell resolution the particular neural activity in contrast to photometry that only captures the overall amount of fluorescence emitted in a quantitative strategy. Although miniscopes are currently the most contrasted *in vivo* calcium imaging system, new promising approaches are emerging, such as the optical fiber scope that also allows high optical resolution in quantitative and qualitative strategies (Dussaux et al., 2015). It should also be mentioned that calcium ions are the most used target due to their critical role in neuronal depolarization. However, other ion indicators, including potassium or sodium, and other potential markers like pH and membrane, are also emerging (Bischof et al., 2019).

5. Electrophysiological approaches combined with behavioral studies

In vivo electrophysiology is employed to record the electrical activity of neurons in combination with behavioral approaches. This technique enables a real-time readout of neural functions and network capability in different brain states across a wide range of temporal and spatial scales. Electroencephalography (EEG) is a non-invasive technique that has been widely used in the last four decades to record on the scalp of patients suffering from addiction. EEG data have been used to get an insight into the pharmacological modulation by drugs of abuse of ongoing neural oscillations, which are electric waves that travel across the brain. The acute effect of different addictive drugs has been extensively studied. Acute administration of drugs of abuse, such as cocaine (Heming et al., 1985), alcohol (Little, 1999; Lukas et al., 1986; Steinberg et al., 1994), THC (Lukas et al., 1995), and benzodiazepines (Benowitz et al., 1980; Mammari and Matsura, 1989) induced an increase in alpha and beta activity in healthy volunteers. By contrast, MDMA administration reveals a decrease in alpha and theta power in MDMA naive volunteers (Fivel et al., 2001). Theta activity is also decreased after acute THC administration in healthy volunteers (Anton B et al., 2004; Bocker et al., 2010; Zuurman et al., 2000). Thus, it is well known that acute administration of drugs of abuse tunes the rhythmic activity of neurons in the human brain. Other authors have focused on studying the acute effect of drugs on consumers. During resting states, cannabis users exhibited decreased delta and increased theta, beta, and gamma power compared to controls (Shikha Prasad and Dedrick, 2018). Alcohol users showed a decrease in delta and theta bands (Coutin-Churchman et al., 2006). Cocaine experienced users did not evidence persistent beta

increase, which is commonly observed in inexperienced intranasal cocaine users (Heming et al., 1994). Furthermore, abnormal brain activities, predominantly in the beta band, were detected in heroin addicts compared to healthy controls (Motlagh et al., 2013).

EEG has also been used to study reward valuation processes and cognitive impairments using drug-related cues in patients with previous drug intake stories. These studies have focused on event-related potentials (ERPs), which are the means of EEG recordings that are time-locked to a stimulus or a response. Among different ERPs types, P300 is the most frequently employed index of neural resources assigned to reward studies. It is a positive ERP that appears 300–600 ms following stimulus presentation. P300s are implicated in memory, motivation, attention, and response inhibition using cognitive and emotional paradigms (Stewart and May 2016). Using oddball visual tasks, opioid (Labman et al., 2007, 2008, 2009), nicotine (Littel and Franken, 2011), alcohol (Bartholow et al., 2010; Petit et al., 2012), and cannabis (Henry et al., 2014) users displayed greater P300s for substance-related cues than for non-substance-related cues. Furthermore, drug users exhibited generally higher P300s compared to controls. These studies indicate that consumers increased neural activity to process stimuli related to the selected drug of choice at the expense of other stimuli.

Despite the advances in understanding the consequences of exposure to drugs of abuse by recording neural activity on patients' scalp, EEG research in addiction and reward processes has significant limitations. Indeed, the electrical activity recorded by EEG electrodes is distant from the input source, coming from neurons in deep brain areas, which prevents the accurate study of brain regions altered during addiction. For that reason, direct extracellular electrophysiological recordings in specific brain areas of animals have emerged to acquire a better understanding of the neurocircuitry basis underlying addiction.

In vivo extracellular recordings may detect neural activity in awake animals during different behavioral performances. Animals undergo stereotaxic surgery to implant electrodes to permit real-time monitoring of neural network activity. Neural activity is detected as local field potentials (LFP) and multi-unit (MUA) or single-unit activity (SUA) (Hong and Lieber, 2019). LFPs are voltage waves generated by the synchronization of the activity of neuron populations interconnected in neural networks. MUA and SUA provide spike firing rate information of a group of neurons and single neurons, respectively. Therefore, crucial information on brain circuitry and connectivity related to addictive-like behaviors can be obtained using *in vivo* extracellular recordings.

The effect of drugs of abuse in neurons' firing rate has been extensively studied in anesthetized and awake animals. In anesthetized rats, cocaine (Koulchitsky et al., 2012) and opioids (Khodayari et al., 2019) produced a general decrease in the firing rate and bursting of VTA neurons after injection. Moreover, THC (Norris et al., 2019; Renard et al., 2017) and ethanol (Tu et al., 2007) decreased medium spiny neurons activity in the anterior NAc and/or PFC. By contrast, nicotine (Morel et al., 2018) and amphetamines (Shi et al., 2000) enhanced VTA DA cells' firing and bursting activity. Many studies have evaluated neuron synaptic plasticity in anesthetized animals with previous chronic drug-intake (Moussawi et al., 2009; Shen and Kalivas, 2013). Nevertheless, our review focuses on electrophysiological studies combined with operant behavioral approaches, and these studies in anesthetized animals are out of scope.

Many electrophysiological studies in addiction have focused on neuronal firing responses related to brain reactivity to contingent drug-self administration. These studies record chronic activity in awake, freely moving animals trained for operant self-administration and examine correlations between neural activity (LFPs and single-unit) and lever-pressing for intravenous administration of drugs or drug-related cues (Fig. 4). Through an entire self-administration session, amphetamine (Haez et al., 1998) and cocaine (Kiyatkin, 2002; Peoples et al., 1997, 2004) infusions increased dopamine levels that tonically inhibited the majority of neurons in the striatum and the NAc. Nicotine self-administration sessions produced higher activity in VTA DA neurons compared to saline self-administration sessions (Caillé et al., 2009).

Moreover, lever-pressing for drugs of abuse correlates with increases or decreases of glutamate-mediated firing in response to drug reward or drug-related cues. During cocaine and heroin self-administration sessions, distinct firing rates patterns were associated to the reinforced lever-presses (Carelli et al., 1993; Carelli and Deadwyler, 1996; Chang et al., 1994, 1997; Deadwyler et al., 2004). In the NAc of rats trained to self-administer cocaine, a small percentage of neurons exhibited either increased or decreased firing rates seconds before lever-pressing (anticipatory responses). Half of the neuron population predominantly decreased firing rates minutes after lever-pressing (post-cocaine responses) (Chang et al., 1994). In heroin self-administration sessions, NAc neurons displayed more post-heroin responses than PFC neurons, while the percentage of neurons firing before the lever-press was similar in the PFC and the NAc (Chang et al., 1997). In ethanol self-administration, the recording from ensembles of single-units primarily located within the shell of the NAc during operant responding for oral ethanol in trained rats exhibits significant phasic changes, with alterations in firing rate related to operant response, tone stimulus, and ethanol delivery (Janak et al., 1999). These results reveal the crucial role of the NAc in linking together conditioned and unconditioned internal and external stimuli with motor plans to allow for ethanol-seeking behavior to occur.

Several studies have also focused on neuronal responses related to particular behavioral responses involved in the addictive process. Evidence suggests that oscillatory activities of the mPFC and NAc correlate with impulsivity and reward outcomes. According to neuron firing rates,

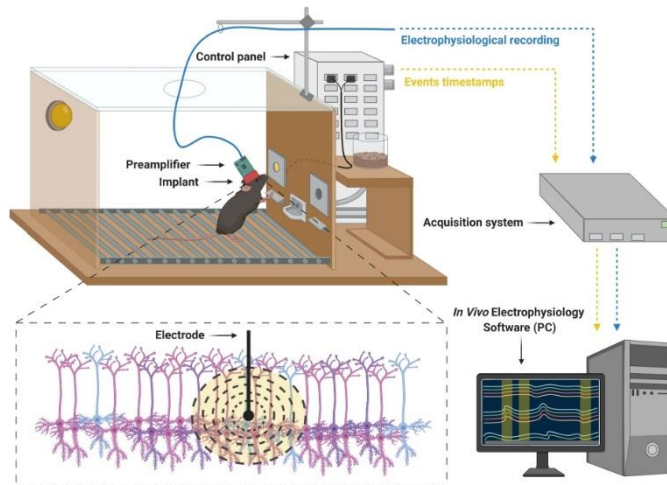


Fig. 4. Electrophysiological recordings in awake, freely moving mice. Experimental set up: Animals are trained to self-administer a drug of abuse or palatable food in operant boxes. A light stimulus (cue light) located above the active lever is paired contingently with reward delivery. Neural oscillatory activities (LFPs) are recorded during the entire session. The electrode implanted in the desired brain area records rhythmic changes in voltage generated by the synchronization of activity of neuron population interconnected in neural networks. Analogic signals recorded by the electrode are bandpass filtered and digitized by a preamplifier, later amplified by the acquisition system, and finally, visualized and stored in a computer via an *in vivo* electrophysiology software (blue arrow). The control panel processes timestamps events occurring along with the session and consequently signaled to the acquisition system to mark events duration in the electrophysiological recordings (yellow arrow).

more impulsive rats showed a more significant shift in the proportion of small/immediate PL neurons than less impulsive rats (Sackett et al., 2019). Power in gamma frequency LFP oscillations transiently increased in the PPC and the NAc during signaling cue anticipation (Donnelly et al., 2014). Moreover, theta LFP power increased during the waiting period in these brain areas (Donnelly et al., 2014). These neurophysiological findings further implicate the PPC and the NAc in reward outcome abnormalities (Koob and Volkow, 2010). However, connectivity measures between brain areas involved in addictive behaviors during reward processes remain mostly unknown. The elucidation of these interconnectivities may be crucial to clearly understand the neurophysiological mechanisms responsible for addictive behaviors.

6. Possible novel therapeutic approaches for addiction

Despite the amount of work devoted to addiction research, few treatments are currently available for substance use disorders. In most cases, these treatments combine psychosocial approaches with pharmacotherapy. Up to date, the most effective pharmacological treatments approved by the U.S. Food and Drug Administration (FDA) are agonist treatments, also called 'substitution therapies' (Sanjesi et al., 2020). They have proven to be the most robust approach to treat opioid and nicotine use disorders. They consist of a molecule that mimics the drug's molecular mechanism by binding to the same receptor. Their efficacy relies on their specific pharmacological properties, which make them less abusable than the original drug. Thus, methadone is an opioid agonist used to treat opioid use disorder due to its slower onset of action on the μ -opioid receptor (Schuckit, 2016), the receptor responsible for the addictive properties of all the prototypical opioid drugs (Lofwall et al., 2018). Buprenorphine presents a partial agonist activity on μ -opioid receptor to treat opioid use disorder (Schuckit, 2016). Varenicline is a partial agonist that activates $\alpha 4 \beta 2$ nAChR, only to 50% of the maximal nicotine effect, and is used to treat nicotine use disorder (Prochaska and Benowitz, 2019). Another partial $\alpha 4 \beta 2$ nAChR agonist of interest for nicotine abuse treatment termed cytisine has not yet been approved by the FDA (Prochaska and Benowitz, 2019).

On the other hand, opioid antagonists, such as naloxone and naltrexone, reverse and prevent opioid effects by blocking the opioid receptors. Naloxone is a μ -opioid antagonist used to reverse an opioid overdose, and take-home naloxone programs aim to prevent fatal overdose (Bell and Strang, 2020). Naltrexone mainly antagonizes μ -opioid receptors and has been approved by the FDA to treat alcohol (Kranzler and Soyka, 2018) and opioid (Strang et al., 2020) use disorder. Nalmefene, a μ and δ opioid receptor antagonist and κ opioid receptor partial agonist, appeared to act similarly as naltrexone and effectively reduced alcohol consumption in heavy drinkers when combined with psychological support (Wang et al., 2020). A recent approach to improve adherence and safety in opioid use disorder is based on a new depot and implant formulations of buprenorphine and naltrexone (Bell and Strang, 2020). Depot buprenorphine compared with sublingual buprenorphine plus naltrexone has revealed not inferior effect (Lofwall et al., 2018), whereas another depot buprenorphine preparation revealed a superior effect to a placebo (Haight et al., 2019).

In addition to agonist and antagonist treatments, of particular importance are other approaches such as topiramate, bupropion, and disulfiram. The FDA first approved topiramate, a GABA/glutamatergic modulator, for the treatment of seizures, epilepsy, and migraines. Topiramate eventually decreases the activity of the mesocorticolimbic dopaminergic system and is currently used with limited efficacy in the treatment of alcohol (Kranzler and Soyka, 2018), cocaine (Kampman, 2019), and methamphetamine/amphetamine (Siefried et al., 2020) use disorder. Bupropion, a non-tricyclic antidepressant that inhibits mainly dopamine reuptake, reduces cocaine craving (Frisman, 2007). Bupropion has also been approved to treat nicotine use disorder (Prochaska and Benowitz, 2019). Interestingly, naltrexone in combination with bupropion is rising as a possible treatment for

methamphetamine/amphetamine use disorder (Siefried et al., 2020) and binge eating disorder (Valbrun and Zvonarev, 2020). In 2014, the FDA approved this combination of naltrexone and bupropion for obesity management. The fact that a drug used to treat drug addiction provides such an outcome when administered to patients suffering from binge eating disorder and abnormal eating patterns underlines the similarities in neuronal circuits shared with drug use disorders (Lindgren et al., 2017). The Disulfiram was the first medication approved for the treatment of alcohol use disorder. Disulfiram mechanism of action consists of inhibiting aldehyde dehydrogenase and increasing toxic metabolites of alcohol if ingested. Instead of having a direct pharmacological effect, its effectiveness lies in the patient's will to avoid the subsequent unpleasant effects (Kranzler and Soyka, 2018). However, disulfiram also inhibits dopamine β -hydroxylase, which converts dopamine to norepinephrine (Kampangaew et al., 2019) and has also been used for the treatment of cocaine use disorder (Kosten et al., 2013). Notably, a genetic variation in the SLC6A3 gene, encoding DAT, has been associated with disulfiram effectiveness for cocaine addiction, with patients with higher DAT levels having better treatment outcomes than those with lower DAT levels (Kampangaew et al., 2019). As pharmacologic treatments have proven to be insufficient in fighting addiction, new techniques are rising as promising options to treat substance use disorders. One of these techniques is transcranial magnetic stimulation (TMS), which consists of the induction of an electromagnetic field to depolarize neurons and eventually modulate brain excitability (Terraneo et al., 2016; Volkow et al., 2019). Applying repetitive TMS in the mPFC of patients suffering from cocaine use disorder showed promising results (Terraneo et al., 2016). The possible efficacy of this treatment relies on the role of top-down inhibition exerted by the mPFC on the reward system, a function diminished in cocaine use disorder (Volkow et al., 2019). A variation of TMS is termed deep TMS (dTMS). The H-coil use in this technique allows a more in-depth, bilateral brain structure stimulation compared to the traditional repeated TMS 8-coil, without increasing the stimulation intensity in the cortical regions and possible consequent side effects (Addolorato et al., 2017). Promising results with dTMS were obtained when applied to the PFC of patients suffering from nicotine (Dinu-Klein et al., 2014) and alcohol (Addolorato et al., 2017) use disorders. This technique has also been reported to reduce food cravings in obese individuals (Ferrulli et al., 2019). Deep brain stimulation is another promising technique for treating addiction in humans that has been revert compulsivity by targeting the NAC (Xu et al., 2020). It is based on a surgical intervention that consists of placing bipolar electrodes over specific brain regions and stimulating them with an implanted pulse generator (Salling and Martínez, 2016). Finally, the current development of innovative neuroimaging techniques, such as task-based functional magnetic resonance imaging, positron emission tomography, and diffusion tensor imaging, among others, is opening the possibility to study individual predisposition to addiction to tailor treatments and predict outcomes (Voon et al., 2020).

7. Concluding remarks

The knowledge of the neurobiological substrate underlying addictive processes has been improved largely in recent years due, in part, to important technical innovations in neurosciences and the availability of novel behavioral models. The previous behavioral models in animals to evaluate addiction were focused on particular effects of drugs of abuse or specific behavioral responses related to drug exposure. In contrast, we have now ground-breaking behavioral models validated in rodents that incorporate the main hallmarks that characterized this disease in human patients. These models are based on complex operant behavioral techniques that mimic the development of the addictive processes and allow to identify individuals vulnerable and resilient to develop the disease imitating the human conditions, where only a minority of individuals that consumed the drug of abuse become addicted. The current use of these novel behavioral models with high translational value is offering

valuable information more easier to translate to the human clinical conditions than that obtained with the early behavioral models.

New techniques have also been recently developed to be combined with these sophisticated behavioral approaches in order to identify the specific neuronal pathways involved in these complex behaviors. Early optogenetic studies combined with behavioral approaches have first provided significant advances to understand the specific involvement in the addiction of relevant neuronal pathways. The current availability of novel chemogenetic techniques that can also be combined with these behavioral approaches has allowed to advance an additional step to dissect the precise role of these specific brain networks. The possibility to maintain the modifications in the activity of these neuronal networks during long-term periods represents an additional advantage of these chemogenetic techniques.

The use of head-mounted miniscopes and *in vivo* electrophysiological techniques in awake, freely moving rodents in combination with the behavioral approaches are other pioneering techniques that have recently allowed to better understand the neuronal activity patterns during addiction. These technologies now allow a real-time readout of neural functions and network capability in specific brain areas and pathways and have recently provided important results to clarify the substrate of addiction. At the present moment, few studies have combined these innovative technological and behavioral approaches together in the field of addiction. The results obtained have already been of great interest, but they represent only the first step for future studies that will certainly provide definitive advances in understanding the neurobiological bases of this complex disease. The identification of the precise involvement of the crucial neuronal pathways underlying each stage of the addiction process will allow to identify potential targets to develop more efficient therapeutic approaches. The possibility to apply in a near-future novel technologies to selectively modulate the excitability of these specific neuronal pathways may open new avenues for the treatment of addictive processes, which have enormous health and socio-economic burden worldwide at the present moment.

Acknowledgments

This work was supported by the Spanish Ministerio de Economía y Competitividad-MINECO (#SAF2017-84060-R-AEI/FEDER-UE), the Spanish Instituto de Salud Carlos III, RETICS-RTA (#RD12/0028/0023), the Generalitat de Catalunya, AGAUR (#2017-SGR-669), ICREA-Acadèmia (#2015) and the Spanish Ministerio de Sanidad, Servicios Sociales e Igualdad, Plan Nacional Sobre Drogas of the Spanish Ministry of Health (#PNSD-20170166) to R.M., Fundació La Marató-TV3 (#2016/20-30) and Plan Nacional Sobre Drogas of the Spanish Ministry of Health (#PNSD-2019006) to E.M.-G. Figures are created with BioRender.com.

References

Aaron, B. I., Michael, E. S., Gewins, A., 2004. Effects of marijuana on neurophysiological signals of working and episodic memory. *Psychopharmacology (Berl)* 17, 214–222.

Addolorato, G., Antonelli, M., Cocciolillo, F., Vassallo, G.A., Tardi, C., Sestito, L., Mirijello, A., Ferrulli, A., Pizzuto, D.A., Camardese, G., Miceli, A., Diana, M., Giordano, A., Gubazzini, A., Di Giuda, D., 2017. Deep transcranial magnetic stimulation of the dorsolateral prefrontal cortex in alcohol use disorder patients: effects on dopamine transporter availability and alcohol intake. *Eur. Neuropsychopharmacol* 27, 450–461.

American Psychiatric Association, 2013. *Diagnostic and Statistical Manual of Mental Disorders*, fifth ed. DSM-5, Washington, DC, USA.

American Psychiatric Association, 1994. *Diagnostic and Statistical Manual of Mental Disorders*, fourth ed. DSM-IV, Washington.

American Psychiatric Association, 1980. *Diagnostic and Statistical Manual of Mental Disorders*, third ed. DSM-III, Washington.

Anthony, J.C., Warner, L.A., Kessler, R.C., 1994. Comparative epidemiology of dependence on tobacco, alcohol, controlled substances, and inhalants: basic findings from the National Comorbidity Survey. *Exp. Clin. Psychopharmacol* 2, 244–268.

Augier, E., Buhse, E., Dalmann, R.S., Lüscher, V., Augier, G., Doss, E., Bachleier, R., Farris, S., Nätt, D., Doyne Mayfield, R., Ademski, L., Hellig, M., 2018. A molecular mechanism for choosing alcohol over an alternative reward. *Science* 360, 1321–1326.

Balleine, B.W., O'Doherty, J.P., 2010. Human and rodent homologues in action control: contextual determinants of goal-directed and habitual action. *Neuropsychopharmacology* 35 (1), 45–69.

Bartholow, B.D., Lust, S.A., Trageser, S.L., 2010. Specificity of P3 Event-related potential reactivity to alcohol cues in individuals low in alcohol sensitivity. *Psychol. Addict. Behav.* 24, 220–228.

Bell, J., Strang, J., 2020. Medication treatment of opioid use disorder. *Biol. Psychiatr.* 67, 82–88.

Benowitz, N.L., Nguyen, T.-L., Jones, R.T., Henning, R.L., Bachman, J., 1980. Metabolic and psychophysiological studies of cannabis/helloresorbital interaction. *Clin. Pharmacol. Ther.* 28, 115–120.

Bischof, H., Burgstaller, S., Waldeck-Weiermair, M., Rauter, T., Schiagl, M., Ramadani-Muja, J., Graier, W.F., Mall, R., 2019. Live-cell imaging of physiologically relevant neural ions using genetically encoded FRET-based probes. *Cells* 8, 492.

Bock, R., Shin, J.H., Kaplan, A.R., Dohi, A., Markley, F., Krasser, P.F., Gemel, C.M., Christensen, C.H., Adreier, M.F., Alvarez, V.A., 2013. Strengthening the accumbal indirect pathway promotes resilience to compulsive cocaine use. *Nat. Neurosci.* 16, 432–438.

Boeker, K.B.E., Hunault, C.C., Gerlitsen, J., Kruidenier, M., Mendoga, T.T., Kenemans, J. L., 2010. Cannabinoid modulations of resting state EEG theta power and working memory are correlated in humans. *J. Cognit. Neurosci.* 22, 1906–1916.

Bonafas, A.J., De Jong, J.W., Beekhoudt, L., Luitjens, M.C.M., Van Der Plasse, G., Adas, R.A.H., 2014. Combined use of the canine adenosine-2 and DREADD technology to activate specific neural pathways in vivo. *PLoS One* 9, 1–6.

Bonson, K.R., Grant, S.J., Costoreggi, C.S., Links, J.M., Mettelife, J., Weyl, H.L., Koutnik, V., Ernst, M., London, E.D., 2002. Neural systems and cue-induced cocaine craving. *Neuropsychopharmacol. Off. Publ. Am. Coll. Neuropsychopharmacol.* 26, 376–386.

Brodly, A.L., Mandelblat, M.A., London, E.D., Childress, A.R., Lee, G.S., Bota, R.G., Ho, M.J., Saxena, S., Baxter, L.R., Madson, D., Jarvis, M.E., 2002. Brain metabolic changes during cigarette craving. *Arch. Gen. Psychiatr.* 59, 1162–1172.

Caillé, S., Guillem, K., Cadot, M., Manzoni, O., Georges, F., 2009. Voluntary nicotine consumption triggers in vivo potentiation of cortical excitatory drives to midbrain dopaminergic neurons. *J. Neurosci.* 29, 10410–10415.

Calipari, E.S., Juárez, B., Morel, C., Walker, D.M., Cahill, M.E., Ribeiro, E., Roman-Ortiz, C., Ramakrishnan, C., Deisseroth, K., Han, M.H., Nader, E.J., 2017. Dopaminergic dynamics underlying sex-specific cocaine reward. *Nat. Commun.* 8.

Cameron, C.M., Margenau, M., Choi, J.Y., Egeci, E.A., Witten, I.E., 2019. Increased cocaine motivation is associated with degraded spatial and temporal representations in IL-Nac neurons. *Neuron* 103 (80–91.e7).

Carelli, R.M., Deadwyler, S.A., 1996. Dual factors controlling activity of nucleus accumbens core firing during cocaine self-administration. *Synapse* 24, 300–311.

Carelli, R.M., King, V.C., Hampson, R.E., Deadwyler, S.A., 1993. Firing patterns of nucleus accumbens neurons during cocaine self-administration in rats. *Brain Res.* 626, 14–22.

Centanni, S.W., Morris, B.D., Luchinger, J.R., Bedus, G., Fettyer, T.L., Patel, S., Winder, D.G., 2019. Endocannabinoid control of the insular bed nucleus of the stria terminalis circuit regulates negative affective behavior associated with alcohol abstinence. *Neuropsychopharmacology* 44, 526–537.

Chang, J.Y., Scovier, S.F., Lee, R.S., Woodward, D.J., 1994. Electrophysiological and pharmacological evidence for the role of the nucleus accumbens in cocaine self-administration in freely moving rats. *J. Neurosci.* 14, 1224–1244.

Chang, J.Y., Zhang, L.L., Janak, P.H., Woodward, D.J., 1997. Neuroanatomical responses in prefrontal cortex and nucleus accumbens during heroin self-administration in freely moving rats. *Brain Res.* 754, 12–20.

Chen, B.T., Yau, H.-J., Hatch, C., Kusumoto-Yoshida, H., Cho, S.L., Hopf, F.W., Bonci, A., 2013. Rescuing cocaine-induced prefrontal cortex hypoactivity prevents compulsive cocaine seeking. *Nature* 496, 359–362.

Chen, I.W., Papagaitanous, E., Emiliani, V., 2018. Towards circuit optimization. *Curr. Opin. Neurobiol.* 50, 179–189.

Chen, X., Choo, H., Huang, X.P., Yang, X., Steier, O., Roth, B.L., Jin, J., 2015. The first structure-function relationship studies for designer receptors exclusively activated by designer drugs. *ACS Chem. Neurosci.* 6, 476–484.

Cheung, Y., Huang, C.C.Y., Ma, T., Wei, X., Wang, X., Lu, J., Wang, J., 2017. Distinct synaptic strengthening of the ventral direct and indirect pathways drive alcohol consumption. *Biol. Psychiatr.* 61, 918–929.

Coutin-Churchman, P., Moreno, R., Añez, V., Vergara, F., 2006. Clinical correlates of quantitative EEG alterations in alcoholic patients. *Clin. Neurophysiol.* 117, 740–751.

Crunelle, C.L., Veltman, D.J., Booij, J., Emswiler-van Oortmerssen, K., van den Brink, W., 2012. Substrates of neuropsychological functioning in stimulant dependence: a review of functional neuroimaging research. *Brain Behav* 2, 499–523.

Deadwyler, S.A., Hayashizaki, S., Cheer, J., Hampson, R.E., 2004. Reward, memory and substance abuse: functional neuronal circuits in the nucleus accumbens. *Neurosci. Biobehav. Rev.* 27, 703–711.

den Hartog, C., Zamudio-Bulcock, P., Nairnval, S., Gilstrap, M., Eaton, B., Fedorovich, H., Motts, A., Woodward, J.J., 2016. Inactivation of the lateral subthalamic nucleus increases drinking in ethanol-dependent but not non-dependent mice. *Neuropharmacology* 107, 451–459.

Deroche-Gamonet, V., Belin, D., Piazza, P.V., 2004. Evidence for addiction-like behavior in the rat. *Science* 305, 1014–1017.

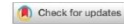
Dehaene, J., Coulin, P., Diester, I., 2019. Optogenetic approaches to study the mammalian brain. *Curr. Opin. Struct. Biol.* 57, 157–163.

Di Ciano, P., Imperato, A., 1988. Drugs abused by humans preferentially increase synaptic dopamine concentrations in the mesolimbic system of freely moving rats. *Proc. Natl. Acad. Sci. U.S.A.* 85, 5274–5278.

- Dinnar-Klein, L., Dannon, P., Hadar, A., Rosenberg, O., Roth, Y., Kotler, M., Zangen, A., 2014. Smoking cessation induced by deep repetitive transcranial magnetic stimulation of the prefrontal and insular cortices: a prospective, randomized controlled trial. *Biol. Psychiatry* 76, 742–749.
- Dobrzanski, G., Rosent, M., 2017. Application of the DREADD technique in biomedical brain research. *Pharmacol. Rep.* 69, 213–221.
- Domingo-Rodriguez, J., Ruiz de Azua, I., Dominguez, E., Senabre, E., Serra, L., Kummer, S., Navandar, M., Boddéhausen, S., Hofmann, C., Andero, R., Gerber, S., Navarrete, M., Dierssen, M., Lutz, B., Martín-García, E., Maldonado, R., 2020. A specific prefrontal-nucleus accumbens pathway controls resilience versus vulnerability to food addiction. *Nat. Commun.* 11, 1–16.
- Donnelly, N.A., Holtzman, T., Rich, P.D., Nevado-Holgado, A.J., Fernando, A.B.P., Van Dijk, G., Holzhammer, T., Paul, O., Rubner, P., Paulsen, O., Robbins, T.W., Dalley, J.W., 2014. Oscillatory activity in the medial prefrontal cortex and nucleus accumbens correlates with impulsivity and reward outcome. *PLoS One* 9.
- Dusaux, C., Szabo, V., Chastagner, Y., Fodor, J., Léger, J.F., Bourdieu, L., Perroy, J., Ventalon, C., 2018. Fast confocal fluorescence imaging in freely behaving mice. *Sci. Rep.* 8.
- Everitt, B.J., Robbins, T.W., 2016. Drug addiction: updating actions to habits to compulsions ten years on. *Annu. Rev. Psychol.* 67, 23–50.
- Everitt, B.J., Robbins, T.W., 2013. From the ventral to the dorsal striatum: evolving views of their roles in drug addiction. *Neurosci. Biobehav. Rev.* 37 (9), 1946–1954.
- Everitt, B.J., Robbins, T.W., 2005. Neural systems of reinforcement for drug addiction: from actions to habits to compulsion. *Nat. Neurosci.* 8, 1481–1489.
- Ferrulli, A., Macci, C., Terruzzi, I., Manarini, S., Ambrogi, F., Adamo, M., Milani, V., Luzzi, L., 2019. Weight loss induced by deep transcranial magnetic stimulation in obesity: a randomized, double-blind, sham-controlled study. *Diabetes Obes. Metabol.* 21, 1849–1860.
- Fogge, B., Pushparaj, A., Le Fell, B., 2010. Granular insular cortex inactivation as a novel therapeutic strategy for nicotine addiction. *Biol. Psychiatry* 68, 265–271.
- Frazier, S.J., Cohen, B.N., Lester, H.A., 2013. An engineered glutamate-gated chloride (GLGC) channel for sensitive, consistent neuronal silencing by ivectinectin. *J. Biol. Chem.* 288, 21029–21042.
- Fret, E., Camuna, A., Parvul-Marqui, R., Lehmann, D., Hell, D., Vollenweider, F.X., 2001. Localization of MDMA-induced brain activity in healthy volunteers using low resolution brain electromagnetic tomography (LORETA). *Hum. Brain Mapp.* 14, 152–165.
- Fridman, W.H., 2007. Smoking Cessation Pharmacotherapy — Nicotine and Nicotinic Preparations 10–22.
- Gavril, A.M., Hood, S., Robinson, B., Anil, S., 2017. Effects of bilateral anterior cingulate insula lesions on food anticipatory activity in rats. *PLoS One* 12, e0179970.
- Gearhardt, A.N., Corbin, W.R., Brownell, K.D., 2016. Development of the Yale food addiction scale version 2.0. *Psychol. Addict. Behav.* 30, 113–121.
- Gearhardt, A.N., Corbin, W.R., Brownell, K.D., 2009. Preliminary validation of the Yale food addiction scale. *Appetite* 52, 430–436.
- Ghosh, K.K., Burns, L.D., Cocker, E.D., Nimmejhan, A., Ziv, Y., Gamal, A.E., Schmitzer, M.J., 2011. Miniaturized integration of a fluorescence microscope. *Nat. Methods* 8, 871–878.
- Goldstein, R.Z., Volkow, N.D., 2011. Dysfunction of the prefrontal cortex in addiction: neuroimaging findings and clinical implications. *Nat. Rev. Neurosci.* 12, 652–669.
- Gomez, J.L., Bonaventura, J., Lesiak, W., Mathews, R.B., Syta-Shah, P., Rodriguez, L. A., Ellis, R.J., Richie, C.T., Harvey, B.K., Danals, R.F., Pomper, M.G., Bonci, A., Michaelides, M., 2017. Chemogenetics revealed: DREADD occupancy and activation via converted diacylglycerol. *Science* 357, 503–507.
- Gremel, C.M., Coats, R.M., 2013. Orbitofrontal and striatal circuits dynamically encode the shift between goal-directed and habitual actions. *Nat. Commun.* 4.
- Haight, B.R., Lemmel, S.M., Luffino, C.M., Fofala, P.J., Zhao, Y., Garofalo, A.S., Greenwald, M.R., Nadigelli, V.R., Ling, W., Heilbroner, C., 2019. Efficacy and safety of a monthly buprenorphine depot injection for opioid use disorder: a multicenter, randomized, double-blind, placebo-controlled, phase 3 trial. *Lancet (London, England)* 393, 778–790.
- Hamer, D., 2002. *Genetics. Rethinking behavior genetics.* *Science* 298, 71–72.
- Haracz, J.L., Tschanz, J.T., Wang, Z., Griffith, K.E., Rebec, G.V., 1998. Amphetamine effects on striatal nucleus: implications for models of dopamine function. *Neurosci. Biobehav. Rev.* 22, 613–622.
- Heidbreder, C.A., Groenewegen, H.J., 2003. The medial prefrontal cortex in the rat: evidence for a dorso-ventral distinction based upon functional and anatomical characteristics. *Neurosci. Biobehav. Rev.* 27, 555–579.
- Heinrichs, J.A., Bobolitis, A.C., Derscheidovitz, E., Assal, A., Chalhoub, R.M., Cowan, C.W., Kalivas, P.W., 2020. Opposing regulation of cocaine seeking by glutamate and GABA neurons in the ventral pallidum. *Cell Rep.* 30, 2018–2027 e3.
- Hemig, R., Ph, D., Glover, B.J., Koopel, B., Phillips, R.L., Ph, D., London, E.D., Ph, D., 1994. Cocaine induced increases in EEG Alpha and Beta Activity: Evidence for Reduced Cortical Processing 11.
- Henry, E.A., Kape, J.T., Bryan, A.D., Hutchison, K.E., Ito, T.A., 2014. Cannabis cue reactivity and craving among never, infrequent and heavy cannabis users. *Neuropsychopharmacol. Off. Publ. Am. Coll. Neuropsychopharmacol.* 39, 1214–1221.
- Hemig, R.J., Jones, R.T., Hooker, W.D., Mendelson, J., Blackwell, L., 1985. Cocaine increases EEG beta: a replication and extension of Hans Berger's historic experiments. *Electroencephalogr. Clin. Neurophysiol.* 60, 470–477.
- Hong, G., Lieber, C.M., 2019. Novel electrode technologies for neural recordings. *Nat. Rev. Neurosci.* 20, 330–345.
- Hu, Y., Salmeron, B.J., Kramova, I.N., Gu, H., Lu, H., Bonci, A., Cadet, J.L., Stein, E.A., Yang, Y., 2019. Compulsive drug use is associated with imbalance of orbitofrontal and prefrontal circuits in punishment-resistant individuals. *Proc. Natl. Acad. Sci. U.S.A.* 116 (15), 9868–9871. doi:10.1073/pnas.1810097116.
- Janak, P.H., Chang, J.W., Woodward, D.J., 1999. Neuronal spike activity in the nucleus accumbens of behaving rats during ethanol self-administration. *Brain Res.* 817, 172–184.
- Jankauskas, A.J., Chen, B.T., Bonci, A., Stein, E.A., 2015. Dorsal medial prefrontal cortex (MPFC) circuitry in rodent models of cocaine use: implications for drug addiction therapies. *Addiction Biol.* 20, 215–226.
- Kalivas, P.W., Volkow, N.D., 2005. The neural basis of addiction: a pathology of motivation and choice. *Am. J. Psychiatry* 162, 1403–1413.
- Kamponang, J.P., Spillio, C.J., Nielsen, E.M., Harding, M.J., Ye, A., Hanson, S.C., Kosten, T.R., Nielsen, D.A., 2019. Pharmacogenetic role of dopamine transporter (SLC6A3) variation on response to disulfiram treatment for cocaine addiction. *Am. J. Addict.* 28, 311–317.
- Kampanan, K.M., 2019. The Treatment of Cocaine Use Disorder 1–8.
- Kanarek, F., Deroche-Gamonet, V., Beson, N., Balado, E., Lafourcade, M., Manzoni, O., Piazza, P.V., 2010. Transition to addiction is associated with a persistent impairment in synaptic plasticity. *Science* 328, 1709–1712.
- Kelley, A.E., Berridge, K.C., 2002. The neuroscience of natural rewards: relevance to addictive drugs. *J. Neurosci.* 22, 3306–3311.
- Khodayari, S., Paldel, F.G., Shahabi, P., Naderi, S., 2019. Acute tramadol-induced cellular tolerance and dependence of ventral tegmental area dopaminergic neurons in vivo electrophysiological study. *Basic Clin. Neurosci.* 10, 209–224.
- Kimbrough, A., Lurie, D.J., Collazo, A., Krefeldt, M., Sidhu, H., MacEde, G.C., D'Esposito, M., Conner, C., George, O., 2020. Brain-wide functional architecture remodeling by alcohol dependence and abstinence. *Proc. Natl. Acad. Sci. U.S.A.* 117, 2149–2159.
- Kiyatkin, E.A., 2002. Dopamine in the nucleus accumbens: cellular actions, drug- and behavior-associated fluctuations, and a possible role in an organism's adaptive signaling. *Behav. Brain Res.* 137, 27–46.
- Koob, G.F., Bloom, F.E., 1988. Cellular and molecular mechanisms of drug dependence. *Science* 242, 715–723.
- Koob, G.F., Volkow, N.D., 2016. Neurobiology of addiction: a neurocircuitry analysis. *The Lancet Psychiatry* 3, 760–773.
- Koob, G.F., Volkow, N.D., 2010. Neurocircuitry of addiction. *Neuropsychopharmacology* 35, 217–238.
- Kopak, A.M., Proctor, S.L., Hoffmann, N.G., 2012. An assessment of the compatibility of DSM-5 and proposed DSM-5 criteria in the diagnosis of cannabis use disorder. *Subst. Use Misuse* 47, 1328–1338.
- Kosten, T.R., Wu, G., Huang, W., Harding, M.J., Hanson, S.C., Lappalainen, J., Nielsen, D. A., 2013. Pharmacogenetic randomized trial for cocaine abuse: disulfiram and dopamine D₂-hydroxylase. *Biol. Psychiatry* 73, 219–224.
- Koukhtchik, S., De Backer, B., Quereumont, E., Charlier, C., Sautin, V., 2012. Differential effects of cocaine on dopamine neuron firing in awake and anesthetized rat. *Neuropsychopharmacology* 37, 1559–1571.
- Kranke, H.R., Soyka, M., 2018. Diagnosis and pharmacotherapy of alcohol use disorder a review. *JAMA, J. Am. Med. Assoc.* 320, 815–824.
- Lammel, S., Lim, B.K., Ran, C., Huang, K.W., Besten, J., Tye, K.M., Deisseroth, K., Malenka, R.C., 2012. Input-specific control of reward and aversion in the ventral tegmental area. *Nature* 491, 212–217.
- Limpens, J.H.W., Damsteegt, R., Broekhoven, H.M., Voom, P., Vanderschueren, L.J.M.J., 2015. Pharmacological inactivation of the prefrontal cortex enables compulsive reward seeking in rats. *Brain Res.* 1620, 210–218.
- Lindgren, E., Gray, R., Miller, G., Tyler, R., Wiers, C.E., Volkow, N.D., Wang, G.-J., 2017. Food addiction: a common neurobiological mechanism with drug abuse. *Front. Biosci. Landmark Ed.* 23, 811–836.
- Lipton, D.M., Gonzalez, B.J., Citri, A., 2019. Dorsal striatal circuits for habits, compulsions and addictions. *Front. Syst. Neurosci.* 13, 28.
- Littel, M., Franken, L.H., 2011. Implicit and explicit selective attention to smoking cues in smokers indexed by brain potentials. *J. Psychopharmacol.* 25, 503–513.
- Little, H.J., 1999. The contribution of electrophysiology to knowledge of the acute and chronic effects of ethanol. *Pharmacol. Ther.* 64, 333–353.
- Lofwall, M.R., Walsh, S.L., Nunes, E.V., Bailey, G.L., Sigmon, S.C., Kampman, K.M., Frost, M., Tiberg, F., Linden, M., Siskind, B., Oomsen, S., Peterson, S., Chen, M., Kim, S., 2018. Weekly and monthly subcutaneous buprenorphine depot formulations vs daily sublingual buprenorphine with naloxone for treatment of opioid use disorder: a randomized clinical trial. *JAMA Intern. Med.* 178, 764–773.
- Lubman, D.I., Allen, N.B., Peters, L.A., Deskin, J.F.W., 2008. Electrophysiological evidence that drug cues have greater salience than other affective stimuli in opiate addiction. *J. Psychopharmacol.* 22, 836–842.
- Lubman, D.I., Allen, N.B., Peters, L.A., Deskin, J.F.W., 2007. Electrophysiological evidence of the motivational salience of drug cues in opiate addiction. *Psychol. Med.* 37, 1203–1209.
- Lubman, D.I., Yucel, M., Kettle, J.W.L., Scuffield, A., Mackenzie, T., Simmons, J.G., Allen, N.B., 2009. Responsiveness to drug cues and natural rewards in opiate addiction: associations with later heroin use. *Arch. Gen. Psychiatry* 66, 205–213.
- Lucanato, F., Galzano, T.A., Shahan, Y., Niv, Y., Schoenbaum, G., 2012. The impact of orbitofrontal dysfunction on cocaine addiction. *Nat. Neurosci.* 15, 358–366.
- Lukas, S.E., Mendelson, J.H., Benediti, R., 1995. Electroencephalographic correlates of marijuana-induced euphoria. *Drug Alcohol Depend.* 37, 131–140.
- Lukas, S.E., Mendelson, J.H., Benediti, R.A., Jones, R., 1986. EEG alpha activity increases during transient episodes of ethanol-induced euphoria. *Pharmacol. Biochem. Behav.* 25, 889–895.
- Magmas, C.J., Lee, P.H., Bonaventura, J., Zemla, R., Gomez, J.L., Ramirez, M.H., Hu, X., Gulvan, A., Bassi, J., Michaelides, M., Stimson, S.M., 2019. Unpleasant

- chemogenetics for research and potential clinical applications. *Science* 344, 139–140.
- Mahler, S.V., Aston-Jones, G., 2010. CNO EvDf: Considerations for the Use of DREADDs in Behavioral Neuroscience. *NeuroPsychopharmacology*.
- Mancino, S., Burokas, A., Gutiérrez-Cuesta, J., Gutiérrez-Martos, M., Martín-García, E., Pucci, M., Palomni, A., D'Aldofrio, C., Maccarone, M., Maldonado, R., 2015. Epigenetic and proteomic expression changes promoted by eating addictive-like behavior. *NeuroPsychopharmacology* 40, 2788–2800.
- Mammano, S., Matsuyama, M., 1989. Quantification of benzodiazepine-induced topographic EEG changes by a computerized wave form recognition method: application of a principal component analysis. *Electroencephalogr. Clin. Neurophysiol.* 72, 126–132.
- McFarland, K., Kalivas, P.W., 2001. The nucleus mediating cocaine-induced reinstatement of drug-seeking behavior. *J. Neurosci.* 21, 6655–6663.
- Miller, E.K., Cohen, J.D., 2001. An integrate theory of PFC function. *Annu. Rev. Neurosci.* 24, 167–202.
- Moorman, D.E., James, M.H., McGillicuddy, E.M., Aston-Jones, G., 2015. Differential roles of medial prefrontal subregions in the regulation of drug seeking. *Brain Res.* 1628, 130–146.
- Morel, C., Fernandez, S.P., Pantouli, F., Meys, F.J., Marti, F., Tolu, S., Parnaudou, S., Marie, H., Tronche, F., Makon, U., Moretti, M., Gotti, C., Han, M.H., Bailey, A., Munné, M., Bunk, J., Fauré, P., 2019. Nicotinic receptors mediate stress-nicotinic detrimental interplay via dopamine cell activity. *Mol. Psychiatry* 23, 1597–1605.
- Motilish, F., Ibrahim, F., Rashid, R., Shafiqabady, N., Seghatoleslam, T., Habibi, H., 2018. Acute Effects of Methadone on EBO Power Spectrum and Event-Related Potentials Among Heroin Dependents. *2273–2280*.
- Mousavi, K., Paschioni, A., Moran, M., Olive, M.F., Gas, J.T., Lavin, A., Kalivas, P.W., 2009. N-acetylcysteine reverses cocaine induced metaplasticity. *Nat. Neurosci.* 12, 182–189.
- Murray, J.E., Bello, D., Ewitt, B.J., 2012. Double dissociation of the dorsomedial and dorsolateral striatal control over the acquisition and performance of cocaine seeking. *NeuroPsychopharmacology* 37, 2456–2466.
- Nagai, Y., Miyakawa, N., Takawa, H., Hori, Y., Oiyama, K., Ji, B., Takahashi, M., Huang, X., Slovacek, S.T., DiBerto, J.F., Xiong, Y., Uryushikina, T., Hirabayashi, T., Fujimoto, A., Mimura, K., English, J.G., Liu, J., Inoue, K., Kumata, K., Seki, C., Ono, M., Shimizu, M., Zhang, M., Tomita, Y., Nakahara, J., Sahara, T., Takada, M., Higuchi, M., Jin, J., Roth, B.L., Mizumoto, T., 2020. Deschloroamphetamine, a potent and selective chemogenetic activator enables rapid neuronal and behavioral modulations in mice and monkeys. *Nat. Neurosci.* 23 (9), 1157–1167.
- Nair, S.G., Srinivas, D.S., Estabrook, M.M., Chisholm, A.D., Silva, P.R., Neumaier, J.F., 2020. Effect of chemogenetic inhibition of lateral habenula neuronal activity on cocaine- and food-seeking behaviors in the rat. *Addiction Biol.* 1–14.
- Naqvi, N.H., Bechara, A., 2009. The hidden island of addiction: the insula. *Trends Neurosci.* 32, 56–67.
- Naqvi, N.H., Rubinst, D., Damasio, H., Bechara, A., 2007. Damage to the insula disrupts addiction to cigarette smoking. *Science* 315, 531–534.
- Nestler, E.J., Peña, C.J., Kundakovic, M., Mitchell, A., Alkarkas, S., 2016. Epigenetic basis of mental illness. *Neuroscientist* 22, 447–463.
- Norris, C., Szabadkó, H.J., Perrini, B., Roshchik, V., Laviolette, S.R., 2019. The bivalent rewarding and aversive properties of Δ^9 -tetrahydrocannabinol are mediated through dissociable opioid receptor substrates and neuronal modulation mechanisms in distinct striatal subregions. *Sci. Rep.* 9, 1–14.
- Parra-Damian, A., Saura, C.A., 2020. Tissue clearing and expansion methods for imaging brain pathology in neurodegeneration: from circuits to synapses and beyond. *Front. Neurosci.* 14.
- Parsons, L.H., Hurd, Y.L., 2015. Endocannabinoid Signaling in Reward and Addiction. *Psychol. Sci.* 26, 149–156.
- Parsons, L.H., Koob, G.F., Zorilla, E.P., 2011. The dark side of food addiction. *Physiol. Behav.* 104, 149–156.
- Pascoli, V., Hiver, A., Van Zessen, R., Loureiro, M., Achagui, R., Harada, M., Flakowski, J., Lüscher, C., 2018. Stochastic synaptic plasticity underlying compulsion in a model of addiction. *Nature* 564, 366–371.
- Pecina, S., Berridge, K.C., 2013. Dopamine or opioid stimulation of nucleus accumbens shell amplifies cue-triggered "wanting" for reward: entire core and medial shell mapped as substrates for PIT enhancement. *Eur. J. Neurosci.* 37, 1529–1540.
- Peoples, L.L., Lynch, K.G., Lemcoe, J., Gengodhar, N., 2004. Accumbal neural responses during the initiation and maintenance of intravenous cocaine self-administration. *J. Neurophysiol.* 91, 314–323.
- Peoples, L.L., Uzviski, A.J., Gee, F., West, M.O., 1997. Operant behavior during sessions of intravenous cocaine infusion is necessary and sufficient for phasic firing of single nucleus accumbens neurons. *Brain Res.* 757, 280–284.
- Peres, R.E., Bazu, A., Nabit, B.P., Harris, N.A., Folkes, O.M., Patel, S., Gilibach, R., Hein, L., Winder, D.G., 2020. $\alpha 2A$ -adrenergic heteroreceptors are required for stress-induced reinstatement of cocaine conditioned place preference. *NeuroPsychopharmacology* 1–9.
- Perry, J.L., Joseph, J.E., Jiang, Y., Zimmerman, R.S., Kelly, T.H., Dama, M., Huetti, P., Dwek, L.P., Bardo, M.T., 2011. Prefrontal cortex and drug abuse vulnerability: stimulation to prevention and treatment interventions. *Brain Res. Rev.* 65, 124–149.
- Petit, G., Konradi, C., Noel, X., Verbanck, P., Campanella, S., 2012. Alcohol-related context modulates performance of social drinkers in a visual go/no-go task: a preliminary assessment of event-related potentials. *PLoS One* 7, 1–11.
- Piazza, P.V., Deroche-Gamonet, V., 2013. A multiple general theory of transition to addiction. *Psychopharmacology (Berl)* 229, 387–413.
- Picciotto, M.R., 2013. An indirect resilience to addiction. *Nat. Publ. Gr.* 16, 521–523.
- Pozhildayeva, D.V., Farris, S.P., Goeke, C.M., Firsick, E.J., Towrnley, K.G., Guizetti, M., Ozburn, A.R., 2020. Chronic chemogenetic stimulation of the nucleus accumbens produces lasting reductions in binge drinking and ameliorates alcohol-related morphological and transcriptional changes. *Brain Sci.* 10.
- Prochaska, J.J., Besowitz, N.L., 2019. Current Advances in Research in Treatment and Recovery | Nicotine Addiction.
- Purohit, K., Purohit, P.K., Kern, J., Logan, R.W., Liu, Z., Huang, Y., McClung, C.A., Crabbe, J.C., Ozburn, A.R., 2018. Pharmacogenetic manipulation of the nucleus accumbens alters binge-like alcohol drinking in mice. *Alcohol Clin. Exp. Res.* 42, 879–888.
- Randeni, M., Rotroen, J., Nunes, E.V., Lee, J.D., Novo, P., Levan, O., Ott, J., Pavlicova, M., Scodes, J., Erek, M.J., 2020. Variants of opioid genes and response to treatment of opioid use disorder with buprenorphine-naloxone versus extended-release naltrexone in Caucasians. *Am. J. Drug Alcohol Abuse* 1–8.
- Renard, J., Szabadkó, H.J., Kramar, C.P., Johnson, C.E.L., Mouni, R., Roshchik, W.J., Laviolette, S.R., 2017. Adolescent THC exposure causes enduring prefrontal cortical disruption of GABAergic inhibition and dysregulation of sub-cortical dopamine function. *Sci. Rep.* 7, 1–14. /631/378/2571/631/378/1699/1799/9/9/20/62/82/1 article.
- Riga, D., Matsos, M.R., Glatz, A., Smit, A.B., Spiljor, S., Van den Oever, M.C., 2014. Optogenetic dissection of medial prefrontal cortex circuitry. *Front. Syst. Neurosci.* 8, 230.
- Rodríguez-Romaguera, J., Nambudini, V.M.K., Baziri, M.L., Stamatialis, A.M., Stuber, G., 2020. Developments from bulk optogenetics to single-cell strategies to dissect the neural circuits that underlie aberrant motivational states. *Cold Spring Harbor Perspect. Med.* 8, a039792.
- Rotge, J.-Y., Cozack, P.J., Daniel, M.-L., Bellu-Rausant, A., Everitt, B.J., Belin, D., 2017. Bidirectional regulation over the development and expression of loss of control over cocaine intake by the anterior insula. *Psychopharmacology (Berlin)* 234, 1623–1631.
- Roth, B.L., 2016. DREADDs for neuroscientists. *Neuron* 89, 663–694.
- Rungegard, A.H., Fitzpatrick, C.M., Woldbye, D.P.D., Andreassen, J.T., Sørensen, A.T., Giedd, U., 2019. Modulating dopamine signaling and behavior with chemogenetics: concepts, progress, and challenges. *Pharmacol. Rev.* 71, 123–156.
- Sackett, D.A., Moschak, T.M., Carelli, R.M., 2019. Prelimbic cortical neurons track preferred reward value and reflect impulsive choice during delay discounting. *Neurosci. J. Neurosci.* 39, 3109–3115.
- Salling, M.C., Martínez, D., 2016. Brain stimulation in addiction. *NeuroPsychopharmacology* 41, 2798–2809.
- Schmitzer-Torbert, N., Apertolidou, S., Amos, R., O'Rear, C., Kaster, M., Stowers, J., Ritz, R., 2015. Post-training cocaine administration facilitates habit learning and requires the infralimbic cortex and dorsolateral striatum. *Neurobiol. Learn. Mem.* 118, 105–112.
- Schultz, M.A., 2016. Treatment of opioid-use disorders. *N. Engl. J. Med.* 375, 357–368.
- Schofield, M.D., Roge, H.A., Seng, R.J., Lu, H., Hayden, G.G., Kalivas, P.W., 2015. Gq-DREADD selectively initiates glutamate release and inhibits cue-induced cocaine seeking. *Biol. Psychiatry* 70, 441–451.
- Shen, H., Kalivas, P.W., 2013. Reduced LTP and LTD in prefrontal cortex synapses in the nucleus accumbens after heroin self-administration. *Int. J. NeuroPsychopharmacol.* 16, 1165–1167.
- Shi, W.X., Pun, C.L., Zhang, X.X., Jones, M.D., Bunney, B.S., Shi, W.X., 2000. Dual effects of D-amphetamine on dopamine neurons mediated by dopamine and non-dopamine receptors. *J. Neurosci.* 20, 3504–3511.
- Shikha Prashad, E.S., Dedrick, F.M.F., 2018. Cannabis users exhibit increased cortical activation during resting state compared to non-users. *Neuroimage* 179, 176–186.
- Siefried, K.J., Acherson, L.S., Litzstein, N., Ezzard, N., 2020. Pharmacological treatment of methamphetamine/amphetamine dependence - a systematic review. *CNS Drugs* 34, 337–365.
- Siemsen, B.M., Siemsen, B.M., Reichel, C.M., Leong, K.C., Garcia-Keller, C., Gipson, C.D., Spence, S., McFadden, J.A., Hooper, K.N., Kalivas, P.W., Scofield, M.D., 2019. Effects of methamphetamine self-administration and extinction on astrocyte structure and function in the nucleus accumbens core. *Neuroscience* 406, 528–541.
- Singer, B.F., Fadanel, M., Kawa, A.B., Robinson, T.E., 2018. Are cocaine-seeking "habits" necessary for the development of addiction-like behavior in rats? *J. Neurosci.* 38, 60–73.
- Smith, K.S., Graybiel, A.M., 2013. A dual operator view of habitual behavior reflecting cortical and striatal dynamics. *Neuron* 79, 361–374.
- Smith, R.J., Ludewig, L.S., 2018. Behavioral and neural mechanisms underlying habitual and compulsive drug seeking. *Prog. Neuro Psychopharmacol. Biol. Psychiatry* 87, 11–21.
- Steinaker, T.A., Coech, N.K., Schoenbaum, G., 2015. What the orbitofrontal cortex does not do. *Nat. Neurosci.* 18, 620–627.
- Stenberg, G., Sazo, M., Rosen, I., Ingvar, D.H., 1974. EEG topography of acute ethanol effects in resting and activated normals. *J. Stud. Alcohol* 55, 645–656.
- Stewart, J.L., Connolly, C.G., May, A.C., Tapert, S.F., Witmann, M., Paulus, M.P., 2014. Striatal and insula dysfunction during reinforcement learning differentiates abstinent and relapsed methamphetamine-dependent individuals. *Addiction* 109, 460–471.
- Stewart, J.L., May, A.C., 2016. *ElectroPhysiology for Addiction Medicine: from Methodology to Case-Optimization of Reward Deficits*, 1st Ed. Progress in Brain Research. Elsevier B.V.
- Strang, J., Volkow, N.D., Degenhardt, L., Hickman, M., Johnson, K., Koob, G.F., Marshall, B.D.L., Tyndall, M., Walsh, S.L., 2020. Opioid use disorder. *Nat. Rev. Dis. Prim.* 6.
- Terrence, A., Leggio, L., Salardini, M., Ermani, M., Bonci, A., Gallimberti, L., 2016. Transcranial magnetic stimulation of dorsolateral prefrontal cortex reduces cocaine use: a pilot study. *Eur. NeuroPsychopharmacol.* 26, 37–44.
- Thompson, L.J., Khajeholli, E., Bradley, S.J., Novotny, J.S., Huang, X.P., Slocum, S., Jin, J., Liu, J., Xiong, Y., Olson, R.H.J., DiBerto, J.F., Boyt, K.M., Pan, M.M., Par, D.,

- Molloy, C., Burdgaard, C., Sexton, P.M., Kash, T.L., Krasner, M.J., Christopoulos, A., Roth, B.L., Tobin, A.E., 2018. DREADD Agonist 21 is an effective agonist for muscarinic-based DREADDs in vitro and in vivo. *ACS Pharmacol. Transl. Sci.* 1, 61–72.
- Thorn, C.A., Atallah, H., Howe, M., Graybiel, A.M., 2010. Differential dynamics of activity changes in denolateral and dorsomedial striatal loops during learning. *Neuron* 66, 781–795.
- Tu, Y., Kroemer, S., Abarbany, K., Lapish, C., Seamans, J., Chandler, L.J., Woodward, J.J., 2007. Ethanol inhibits persistent activity in prefrontal cortical neurons. *J. Neurosci.* 27, 4765–4775.
- Ueda, H.R., Erniik, A., Chung, K., Gradinaru, V., Chédatol, A., Tomancak, P., Keller, P.J., 2020. Tissue clearing and its applications in neuroscience. *Nat. Rev. Neurosci.* 21, 61–79.
- Urban, D.J., Roth, B.L., 2015. DREADDs (designer receptors exclusively activated by designer drugs): chemogenetic tools with therapeutic utility. *Annu. Rev. Pharmacol. Toxicol.* 55, 399–417.
- Valtun, L.P., Zvonarev, V., 2020. The opioid system and food intake: use of opiate antagonists in treatment of binge eating disorder and abnormal eating behavior. *J. Clin. Med. Res.* 12, 41–63.
- Vardy, E., Robinson, J.E., Li, C., Olsen, R.H.J., DiBerio, J.F., Giguere, P.M., Sassano, P.M., Huang, X.-P., Zhu, H., Urban, D.J., White, K.L., Rittiner, J.E., Crowley, N.A., Pleil, K.E., Manzoni, C.M., Mosier, P.D., Song, J., Kuhl, T.L., Malanga, C.J., Krasner, M.J., Roth, B.L., 2015. A new DREADD facilitates the multiplexed chemogenetic interrogation of behavior. *Neuron* 86, 936–946.
- Verdejo-García, A., Bechara, A., 2009. A somatic marker theory of addiction. *Neuropharmacology* 56 (Suppl. 1), 45–62.
- Verdejo-García, A., Clark, L., Dunn, B.D., 2012. The role of interoception in addiction: a critical review. *Neurosci. Biobehav. Rev.* 36, 1857–1869.
- Vigouros, R.J., Belle, M., Chédatol, A., 2017. Neuroscience in the third dimension: shedding new light on the brain with tissue clearing. *Mol. Brain* 10, 1–10.
- Volkow, N.D., Koob, G.F., McLellan, A.T., 2016. Neurobiological advances from the brain disease model of addiction. *N. Engl. J. Med.* 374, 363–371.
- Volkow, N.D., Michelberger, M., Baler, R.D., 2019. The neuroscience of drug reward and addiction. *Physiol. Rev.* 99, 2115–2140.
- Volkow, N.D., Wang, G.-J., Telang, F., Fowler, J.S., Thanos, P.K., Logan, J., Alexoff, D., Ding, Y.-S., Wong, C., Ma, Y., Pradhan, K., 2008. Low dopamine striatal D2 receptors are associated with prefrontal metabolism in obese subjects: possible contributing factors. *Neuroimage* 42, 1537–1543.
- Volkow, N.D., Wang, G.-J., Tomasi, D., Baler, R.D., 2013. Obesity and addiction: neurobiological overlaps. *Obes. Rev.* 14, 2–13.
- Volkow, N.D., Wise, R.A., 2005. How can drug addiction help us understand obesity? *Nat. Neurosci.* 8, 555–560.
- Voon, V., Grodin, E., Mandali, A., Morris, L., Bonnamy, N., Weidacher, K., Kwako, L., Goldman, D., Koob, G.F., Momenan, R., 2020. Addictive Neuroimaging Assessment (ANIA): towards an integrative framework for alcohol use disorder. *Neurosci. Biobehav. Rev.* 113, 492–506.
- Wall, N.R., Neumann, P.A., Beier, K.T., Mohkari, A.K., Luo, L., Malenka, R.C., 2019. Complementary genetic targeting and monozygotic input mapping reveal recruitment and refinement of distributed corticostriatal ensembles by cocaine. *Neuron* 104, 916–930 e5.
- Wang, G.-J., Volkow, N.D., Logan, J., Pappas, N.R., Wong, C.T., Zhu, W., Netusil, N., Fowler, J.S., 2001. Brain dopamine and obesity. *Lancet (London, England)* 357, 354–357.
- Wang, S.C., Chen, Y.C., Chen, S.J., Lee, C.H., Cheng, C.M., 2020. Alcohol addiction, gut microbiota, and alcoholism treatment: a review. *Int. J. Mol. Sci.* 21, 1–11.
- Wexler, B.E., Gottschalk, C.H., Fulbright, R.K., Prohovnik, I., Lacadro, C.M., Rounsaville, B.J., Gore, J.C., 2001. Functional magnetic resonance imaging of cocaine craving. *Am. J. Psychiatr.* 158, 86–95.
- WHO, 2020. Management of substance abuse. Retrieved from:** https://www.who.int/substance_abuse/terminology/definitions/en/.
- Wilentz, A.M., Schoenbaum, G., 2016. Over the river, through the woods: cognitive maps in the hippocampus and orbitofrontal cortex. *Nat. Rev. Neurosci.* 17, 513–523.
- Wise, R.A., 2002. Brain reward circuitry: insights from untested incentives. *Neuron* 36 (2), 229–240.
- Xu, L., Nan, J., Liu, Y., 2020. The nucleus accumbens: a common target in the comorbidity of depression and addiction. *Front. Neural Circ.* 14.
- Yager, L.M., Garcia, A.F., Wunsch, A.M., Ferguson, S.M., 2015. The ins and outs of the striatum: role in drug addiction. *Neuroscience* 301, 529–541.
- Yang, H., de Jong, J.W., Tak, Y., Peck, J., Bsteup, H.S., Lammel, S., 2018. Nucleus accumbens subnuclei regulate motivated behavior via direct inhibition and disinhibition of VTA dopamine subpopulations. *Neuron* 97, 434–449 e4.
- Yang, W., Yuste, R., 2017. In vivo imaging of neural activity. *Nat. Methods* 14 (4), 349–359.
- Zuurman, L., Roy, C., Schoemaker, R.C., Hozekamp, A., Den Hartigh, J., Besder, J.C.M.E., Verpoorte, R., Pinquier, J.L., Cohen, A.F., Van Gerven, J.M.A., 2008. Effect of intrapulmonary tetrahydrocannabinol administration in humans. *J. Psychopharmacol.* 22, 707–716.



Received: 18 September 2020 | Revised: 4 March 2021 | Accepted: 24 March 2021
 DOI: 10.1002/ajmg.b.32843

REVIEW ARTICLE



Genomics and epigenomics of addiction

Rafael Maldonado^{1,2} | Pablo Calvé¹ | Alejandra García-Blanco¹ |
 Laura Domingo-Rodríguez¹ | Eric Senabre¹ | Elena Martín-García¹

¹Laboratory of Neuropharmacology: Neurophar, Department of Experimental and Health Sciences, Universitat Pompeu Fabra (UPF), Barcelona, Spain

²Hospital del Mar Medical Research Institute (IMIM), Barcelona, Spain

Correspondence

Elena Martín-García and Rafael Maldonado, Laboratory of Neuropharmacology, Universitat Pompeu Fabra, Dr. Aiguader, 88, Barcelona 08003, Spain.

Email: elena.martin@upf.edu (E.M.-G.) and rafael.maldonado@upf.edu (R.M.)

Funding information

Agència de Gestió d'Ajuts Universitaris i de Recerca (AGAUR), Grant/Award Number: 2017-SGR-449; Fundació la Marató de TV3, Grant/Award Number: 2016/20-30; ICREA-Academia, Grant/Award Number: 2015; Spanish Instituto de Salud Carlos III, RETICS-RTA, Grant/Award Number: RD12/0028/0023; Spanish Ministerio de Economía y Competitividad-MINECO, Grant/Award Number: SAF-2017-84060-R-AEI/FEDER-UE; Plan Nacional Sobre Drogas of the Spanish Ministry of Health, Grant/Award Numbers: 2017I068, 2019I006

Abstract

Recent progress in the genomics and epigenomics of addiction has contributed to improving our understanding of this complex mental disorder's etiology, filling the gap between genes, environment, and behavior. We review the behavioral genetic studies reporting gene and environment interactions that explain the polygenic contribution to the resilience and vulnerability to develop addiction. We discuss the evidence of polymorphic candidate genes that confer susceptibility to develop addiction as well as the studies of specific epigenetic marks that contribute to vulnerability and resilience to addictive-like behavior. A particular emphasis has been devoted to the miRNA changes that are considered potential biomarkers. The increasing knowledge about the technology required to alter miRNA expression may provide promising novel therapeutic tools. Finally, we give future directions for the field's progress in disentangling the connection between genes, environment, and behavior.

KEYWORDS

DNA methylation, endophenotype, epigenetic, genes-environment interaction, multifactorial, polygenic

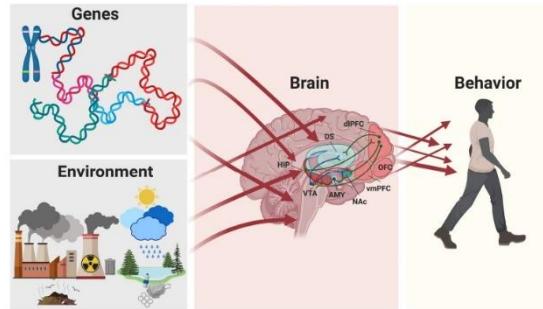
1 | INTRODUCTION

Significant findings from the behavioral genetics field have contributed to our understanding of individual differences in behavior. Research in humans in this area applies studies of monozygotic identical twins, family investigations, and adoption studies. These studies have pointed out that psychiatric disorders, personality traits, and cognition have a significant polygenic influence. However, the environment and the interaction between both factors are essential. Molecular genetic studies in humans and animals have shown that the susceptibility for psychiatric disorders such as addiction is heritable, highly polygenic, and that the combination of environmental and genetic factors contributes to the observed phenotypic variation (Plomin & Daniels, 2011). Thus, addiction has a complex multifactorial pattern of inheritance. This multifactorial genetic model aims to explain how the interaction between multiple gene networks and environmental factors strongly impacts

brain function early during development and later throughout the adulthood period influencing behavior (Figure 1). Hence, genes are not single direct triggers of mental disorders but contribute to confer risk for pathological behavior development, accounting for a significant fraction of total variation (Hamer, 2002). In this context, the present article aims to discuss why some individuals are vulnerable to develop addiction, while others are resilient to certain environmental risk factors, even if access to the drug is present. Several genetic and neurobiological factors of vulnerability and resilience have been identified in human and animal studies. For example, to manipulate a vulnerable phenotype to develop food addiction was generated by manipulating the activity of "top-down" cortical circuits using chemogenetic approaches, whereas a cell-type gene deletion has promoted resilience to food addiction (Domingo-Rodríguez et al., 2020).

The interaction between genes and environment is now better understood with the recent advances in the epigenetics field. Epigenetics

FIGURE 1 Addiction has a multifactorial inheritance pattern with an interaction between different gene networks and multiple environmental factors that strongly impact brain function both during development and throughout adulthood, influencing behavior



refers to changes that regulate gene expression without causing variation in the DNA sequence. The main epigenetic mechanisms comprise DNA methylation, histone modifications, and non-coding microRNAs (miRNAs). These changes are reversible, but early life epigenetic modifications of genes in the brain may lead to behavioral patterns of response that can last for life. Indeed, an individual's experience can modify the chromatin topography within the brain in a region-specific and cell-type-specific manner. The environment can produce different gene expression changes, even in genetically identical individuals, such as the monozygotic twins (Nestler, 2014). A significant contribution to the field was the knowledge that these epigenetic signatures may have a trans-generational behavioral transmission pattern, such as in the case of exploratory, nurturing, and anxiety-related behaviors (Meaney & Szyf, 2005). Consequently, epigenetics concedes an explanation for the gap of the pathway from genotype to phenotype. Addiction is a multifactorial complex disorder in which genes and environment interact with each other. Nowadays, we can study genes in sufficient detail to move beyond the nature-nurture dichotomy. Hereditary influences ("nature") comprise variations, polymorphisms in DNA sequences, transmitted from generation to generation over an evolutionary time scale. The environment ("nurture") influences gene expression during an individual's lifetime, which also has a major consequence on the phenotype (Robinson, 2004). Thus, nurture is the personal experience in each individual's life established for the interactions with the environment as childhood, economics, or social relationships, that modifies the genetic factors defined by nature. In the postgenomic era, there has been a shift within the scientific community from mere acceptance of nature and nurture mutual effects to a more complex understanding of gene-environment interaction. It is well-known that DNA is both inherited and environmentally reactive through different mechanisms, including epigenetics. For behavior, gene expression in the brain is the primary readout of the interaction between genetic and environmental factors. This modulation involves complex probabilistic interactions between genes and the environment, rather than merely additive effects. Understanding that phenotypes are the developmental result of interactions between genes

and the environment is essential to avoid oversimplification by focusing on monogenic traits (Haskel-Ittah, Duncan, & Yarden, 2020). Thus, the environment is more salient in influencing the phenotype than predicted and may affect phenotype acting at different levels, including gene regulation via epigenetics and mutations by changing the DNA sequence. This modulation is termed phenotypic plasticity. Classical genetic approaches, such as adoption and twin research-based methods, have identified the influence of the environment controlling genes and the environment separately (Plomin & Daniels, 2011). The influence of a nonshared environment was significant in genetic studies because it made individuals differ although being genetically similar. Indeed, genetic influence never explains all percentages of variance for complex phenotypes such as addiction, and the remaining variance is related to environmental influences. In animal models, the environment's influence has been translationally modeled using childhood separation procedures after birth or stress induction (Meaney & Szyf, 2005). Moreover, the manipulation of genetic factors in animals contributed to an evolving field with a promising future to decipher the neurobiological substrate of complex multifactorial disorders, such as addiction.

Human genetic findings are crucial to discover underlying loci for complex human diseases such as addiction, but these findings are frequently limited to the population under study. Thus, genome-wide association study (GWAS) studies in humans cannot reliably capture complex multifactorial disease neurobiology without further mechanistic studies. These studies must complement animal research to straightforwardly discover molecular networks linked with altered phenotypes with temporal, cell-type-specific, and brain-area resolution. Mice are the leading source for genetic complex disease-related research. Recent progress in DNA-sequencing, DNA-cloning, bioinformatics, viral delivery approaches, and gene editing have advanced the resources of mouse genetics. The link of animal studies with human genetics has been improved in recent years mainly due to the new tools available for molecular discovery and the efforts in translational research. Thus, animal studies are now able to genetic variants discovered in humans to a relevant biological process and often to a

pharmacological target. Human and animal genetic studies' connections offer an efficient approach to biological discovery and clinical translation (Sau, Philip, Reinholdt, & Chesler, 2019). The link of animal studies with human genetics has also significantly improved, resulting in new tools for discovering molecular underpinnings and translational research. Thus, animal studies may link a human genetic variant discovered to a relevant biological process and often to a pharmacological target. Human and animal genetic studies' connection offers an efficient and economical approach to biological discovery and clinical translation (Saul et al., 2019).

The current review aims to examine how behavioral genetic research has contributed to advancing our understanding of the links between genes, environment, and behavior and the substrate of resilience and vulnerability to addiction. It is a state-of-the-art review that offers new perspectives on addiction genetics and epigenetics with a comprehensive search of current literature to underline areas for further research. This review helps to understand the existing state of knowledge and priorities for future research. First, we review the genetics of vulnerability and resilience underlying candidate genes linked to these two distinct dimensions' etiology and developmental profiles. Second, we examine the epigenetics of vulnerability and resilience. At each step, we discuss the strengths and limitations of applying the different methodological approaches, such as GWAS or epigenetics, to investigate individual differences in vulnerability and resilience. Third, we focus on miRNAs as potential biomarkers due to their capacity to be secreted extracellularly and systemic circulation. Finally, we review novel approaches to alter miRNAs expression that, together with the increasing knowledge about miRNAs, may open new promising therapeutic tools.

2 | GENETICS OF VULNERABILITY AND RESILIENCE IN ADDICTION

The genetic factor plays an essential role in the individual susceptibility to develop addiction. The quantitative genetic theory began in the early part of the 19th century to answer the dichotomy between qualitative Mendelian genetics and quantitative normal distributions (Plomin & Daniels, 2011). In the 20th century, this theory progressed, and the liability threshold model emerged, highlighting a normal risk distribution for bimodal effects (affected or unaffected). Later, this model was applied in human genetics and established today's fundamental concepts (Martin, Daly, Robinson, Hyman, & Neale, 2019). This theory leads to the multifactorial model, where individuals' phenotypes follow a normal distribution, with the majority located in the center of the inverted U-shaped curve and the minorities representing the extremes subpopulations of a resilient or vulnerable continuous phenotypic variation where some individuals may pass a certain threshold and become affected (Figure 2). This model suggested that several minor genetic and environmental factors, combined interactively, could provide phenotypic variation along a continuum for binary human diseases and traits, introducing the statistical theory of the modern liability threshold model (Martin et al., 2019). Such models

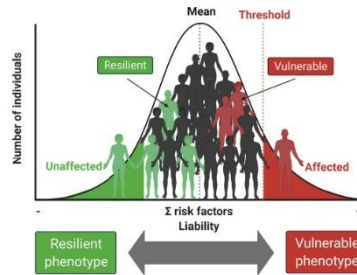


FIGURE 2 In the multifactorial addiction model, the genetic factor plays an essential role in the vulnerable or resilient individual susceptibility to developing this brain disease. In this model, the individuals' phenotypes follow a normal distribution. The majority are located in the center of the inverted U-shaped curve. The minorities represent the extremes subpopulations of a resilient or vulnerable quantitative continuum of a phenotype where some individuals can pass a certain threshold and become affected

are relevant to mostly all common psychiatric disorders, which are not monogenic disorders.

In substance use disorder, classical twin, adoption, and family human studies estimate that 40–60% of the population variability in becoming addicted is attributable to genetic factors (Agrawal et al., 2012). The heritability of cocaine addiction is among the highest among psychiatric disorders, estimated at around 65% for women (Kendler, Karkowski, Neale, & Prescott, 2000) and 79% for men (Kendler & Prescott, 1998). Concerning other abuse drugs, the heritability calculated was 48–66% for alcohol abuse, 60% for nicotine dependence, and 54% for opioid use disorder (Agrawal et al., 2012; Kendler & Prescott, 1998; Tsuang et al., 1998). The inheritance of addiction does not follow a Mendelian transmission pattern, which means that the heritability is polygenic, involving multiple gene variants, complex networks of gene–gene, epistasis (complex interactions among genetic loci), and gene–environment interactions, among others (Phillips, 2008; Volkow & Muenke, 2012). The advances in the knowledge of the neurobiological substrates underlying substance use disorders have allowed performing hypothesis-driven candidate gene studies to evaluate suspected connections between specific genes and addiction endophenotypes (Caspi & Moffitt, 2006). Endophenotypes are the quantifiable mechanisms alongside the pathway between a complex psychiatric disease and the distal genotype. They can be biochemical, neurophysiological, neuroanatomical, endocrinological, cognitive, or neuropsychological (Gottesman, 2005). Endophenotypes have supposed an advance since they are heritable neurobiological substrates at an intermediate position in the pathway between the disease and the genotype. They represent more clear

traces of genetic mechanisms than the disease syndrome itself, supporting the notion that psychiatric diagnoses can be deconstructed, resulting in a more precise and successful analysis (Gottesman, 2005). Multiple addiction endophenotypes have been studied, but we have focused our review on the reward processing linked to the dopaminergic system, as the most directly related to the initiation of the addictive process taken into account its involvement in the primary rewarding effects of all drugs of abuse and natural rewards. Although all abuse drugs lead to a release of dopamine in the brain reward region, the nucleus accumbens (NAc) is essential to differentiate opioid and psychostimulant use disorders from a behavioral and neurobiological point of view (Badani, Belin, Epstein, Calu, & Shaham, 2011). One candidate gene widely studied is the *DRD2* gene that encodes for the dopamine-type 2 receptor (D2R), with a specific polymorphism conferring a high risk of "reward deficiency syndrome," consisting of a hypodopaminergic state due to reduced levels of D2R density (Blum et al., 2000; Febo et al., 2017). The reduction of D2R levels can produce a decrease of feeling pleasure for usual incentives and a need to compensate for this deficiency, promoting a high risk for multiple addictive, impulsive, and compulsive behaviors overall drugs of abuse (Tsou et al., 2019). Hence, other polymorphisms in the dopamine system, such as the dopamine receptors genes for dopamine receptors type 2, 3, and 4 (*DRD2*, *DRD3*, and *DRD4*), the dopamine transporter (*DAT1*) gene, and enzymes involved in dopamine degradation (catechol-*o*-methyl-transferase, [*COMT*]) have also a link with addiction and obesity and have been discussed in other review articles (Lindgren et al., 2017; Sanna et al., 2020; S. C. Wang, Chen, Lee, & Cheng, 2019).

Despite these early addiction genetics findings, it was not until the GWAS method's emergence that geneticists could identify novel associations and provide new genes of interest as potential addiction treatment targets. This method performs statistical analyses on many polymorphisms throughout the whole genome, solving the inherent bias problem of analyzing only the hypothesis-driven candidate-genes with known or suspected connections to the addiction endophenotype of interest (Crist, Reiner, & Berrettini, 2019). Based on factor analysis of the Diagnostic and Statistical Manual of Mental Disorders (DSM) symptoms, GWAS for substance use disorders produced statistically robust and clinically interesting results. Detailed meta-analyses for candidate gene studies and GWAS for alcohol, tobacco, cannabis, cocaine, and opioids are discussed in another review that includes 150 meta-analyses for SUD (Lopez-Leon, González-Giraldo, Wegman-Ostrosky, & Forero, 2021). For example, the earliest and most relevant findings with clinical relevance derived from GWAS studies related to nicotine and alcohol addiction (Hancock, Markunas, Bierut, & Johnson, 2018). Thus, GWAS results of nicotine dependence revealed genetic variations in nicotinic acetylcholine receptor subunit genes such as *CHRNA3*, *CHRNA6*, and enzymes involved in nicotine metabolism *CYP2A6* and *CYP2B6* (Furberg et al., 2010; Hancock et al., 2015; Thorgeirsson et al., 2010). GWAS meta-analyses identified targets in chromosome 15q and 20q, in which the cholinergic receptor nicotinic alpha genes (*CHRNA*) are located. The SNPs identified in several GWAS were located in the *CHRNA3*, *CHRNA4*,

CHRNA3, *DBH* (dopamine beta-hydroxylase), and *PEX2* genes. Besides, candidate gene studies revealed the strongest associations with the dopamine receptor 2 gene (*DRD2*), the galanin receptor 1 gene (*GALR1*), and with tetrapeptide repeat domain 12 (*TTTC12*) (Lopez-Leon et al., 2021). Interestingly, the cholinergic receptor nicotinic subunit *CHRNA2* has been implicated with cannabis use disorder (Demontis et al., 2019). A recent GWAS of nicotine metabolism and cigarette consumption, measured in current smokers of European descent, showed a fine-mapping of chromosome 19 revealing putatively causal variants mapping to *CYP2A6*, *MAP3K10*, *ADCK4*, and *CYP2B6*, in addition to a novel chromosome 4 region mapping to *TMPPRS11E* and several *UGT2* genes (Buchwald et al., 2020). The authors identified SNPs associated with nicotine clearance estimated and metabolism and identified novel loci influencing the nicotine metabolism and tobacco exposure phenotypes. Studies on alcohol use disorder showed genes associated with alcohol pharmacokinetics, such as alcohol dehydrogenase (*ADH1B-ADH1C*) and aldehyde dehydrogenase (*ALDH2*) as well some other genes linked with regulatory protein functions, such as the *SERPINC1*, *GCKR*, *SGOL1*, *KLB*, *AUTS2*, and *TF* (Clarke et al., 2017; Takeuchi et al., 2011; Way et al., 2015). Other GWAS studies showed more neuropsychiatric candidate genes identified, such as the GABA transporter 1 (*SLC6A1*) and Adrenoceptor Alpha 2A (*ADRA2A*) gene (Adkins et al., 2015). In addition, candidate gene studies showed associations that were protective against alcohol use disorder, including the alcohol dehydrogenase genes (*ADH1B*, *ADH1C*) and the aldehyde dehydrogenase 2 (*ALDH2*). Other genes significantly associated with alcohol dependence and alcohol use disorder were three dopamine-related genes (*DRD2*, *DRD4*, and *SLC6A3*), serotonin-related genes (*SLC6A4*, *HTR2A*), GABA receptor genes (*GABRA2* and *GABRB2*), an opioid receptor gene (*OPRM1*), and the tumor necrosis factor (*TNF*) (Lopez-Leon et al., 2021). Significant variants from GWAS of opioid use disorder were associated with genes encoding potassium voltage-gated ion channels, such as the *KCNQ2* and *KCNK1* (Crist et al., 2019). A recent meta-analysis of GWAS revealed that the *HIST1H2BD* gene was associated with cocaine dependence, a gene located in a region on chromosome 6, which has been previously associated with schizophrenia (Cabana-Dominguez et al., 2019). Regarding food addiction, only one GWAS study provided results of genetic variations to our knowledge. An enrichment for gene members of the MAPK signaling pathway was revealed, but no candidate SNP coincident for substance use disorder was significantly associated with food addiction due to a possible limited study power (Cornelis et al., 2016). Therefore, some studies have the limitation of insufficiently powered GWAS sample sizes for complex traits tested, and the GWAS-identified SNPs only explain a small proportion of the phenotypic variance to develop the addictive behavior emphasizing the polygenic multifactorial component of addiction (Martin et al., 2019; Vink, 2016). Indeed, GWAS studies revealed that most SNPs are produced in non-coding sequence, changing RNA expression and DNA methylation, ultimately altering gene activity. This evidence highlights the importance of understanding the cross-talk between genetics and epigenetics in the individual susceptibility to addiction since this complex disease is

mediated by the interplay between genetic and epigenetic factors in many cells (Maurano et al., 2012).

Recent studies have recognized the importance of gene interaction complexity and integrate DNA, RNA, and protein sequence data with GWAS findings (Hancock et al., 2018). Similarly, other investigations considered the simultaneous involvement of multiple genes in the regulation of pathways underpinning addiction. Remarkably, a study used the powerful multilocus genetic profile method, a combined genetic index reflecting the effect of numerous polymorphic loci functionality relevant to a specific neurobiological mechanism (Nikolova, Ferrell, Manuck, & Hariri, 2011). The polygenic risk score method uses entire GWAS datasets, with several million loci, and has been proposed as a complementary method to investigate complex traits' polygenic architecture by considering a large set of SNPs simultaneously (Lewis & Vassos, 2020). In this method, a GWAS is conducted on an initial discovery sample, and the *p*-values of SNPs are obtained. Subsequently, an independent target sample is analyzed by constructing a polygenic risk score consisting of each subject's associated alleles' weighted sum. This polygenic risk score has been used to predict individual genetic liability for drug addiction (Barr et al., 2020; Chen et al., 2018; Frank et al., 2012; Vink et al., 2014). Few studies have been developed using this method in addiction. This method allows the inclusion of several polymorphisms with minor independent effects but with jointly significant effects. A multilocus genetic profile represents the cumulative impact of functional polymorphisms on dopamine signaling, comprising *COMPT*, *DAT*, *DRD2*, and *DRD4* genes, which individually produce variation in striatal dopamine signaling, that can explain individual differences in reward-related ventral striatum variability (Nikolova et al., 2011). A study employing this genetic methodology to food addiction found a significantly increased dopamine signaling in the food addiction group compared with controls supporting a reward-based causal model progressing from an inherent biological susceptibility to increased risk for overeating, and ultimately to develop addiction to hyperpalatable food (Davis et al., 2013). Another study described variations in a multilocus genetic score related to dopamine signaling associated with sugar consumption differences in children with intrauterine growth restriction, suggesting that dopamine function is involved in these children's behavioral features (Silveira et al., 2018).

3 | EPIGENETICS OF VULNERABILITY AND RESILIENCE

The fact that not all individuals who consume drugs develop addiction suggests the existence of individual resilient and vulnerable factors that contribute to addiction's pathogenesis and persistence. Experiences in life and environmental factors can shape epigenetic profiles that may modify individuals' vulnerability to addiction. Epigenetic mechanisms are a set of posttranslational modifications that play an essential role in changing the brain for a lifetime, although they can also be reversible and transgenerationally transmitted. The diversity of epigenetic modifications described in addiction due to exposure to

drugs of abuse include histone posttranslational modifications, DNA methylation, and changes in miRNAs (Figure 3).

Modification of histones is one of the most frequently studied epigenetic alterations in addiction. Histones are essential proteins that wrap DNA in the nucleus and condense it into chromatin. The basic building block of chromatin, also called a nucleosome, contains 147 DNA base pairs wrapped throughout an octamer comprising two copies of H2A, H2B, H3, and H4 histones (Andrews & Luger, 2011). These proteins can undergo several posttranslational modifications in which different functional groups are covalently added to amino acid residues of the N-terminal tails. Some of these modifications are acetylation, phosphorylation, and methylation, among others (Walker & Nestler, 2018). Acetylation of histone occupancy on lysine residues decreases electrostatic interaction between DNA and histone proteins to make DNA more accessible to transcriptional regulators (Kouzarides, 2007). Histone

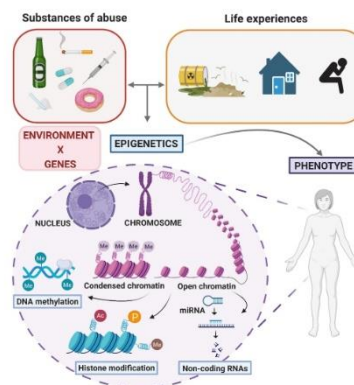


FIGURE 3 Epigenetic mechanisms alter individuals phenotype. Substances of abuse, environmental factors, and life experiences can modify epigenetic marks and reshape an individual's phenotype. Histone modification, DNA methylation, and non-coding RNAs are the most common epigenetic modifications. These modifications regulate gene expression without causing variations in the DNA sequence. The N-terminal tails of histones can undergo several posttranslational modifications, including acetylation, methylation, and phosphorylation, among others. Histone modification can lead to either activation or repression of gene expression, depending on the residues modified and the type of modification. DNA methylation is the covalent modification of cytosine residues in CpG dinucleotides within gene sequences. Contrary to histone modification, DNA methylation is associated with transcriptional silencing. However, DNA methylation in gene bodies is linked with active transcription. Non-coding RNAs include miRNAs that regulate gene expression through posttranscriptional silencing of genes

phosphorylation can occur on serine, threonine, and tyrosine residues and is generally associated with transcriptional activation (Rossetto, Avvakumov, & Côté, 2012). On the other hand, histone methylation occurs on lysine, and it is associated with either repression or activation of gene expression, depending on the number of methyl residues added (Kouzarides, 2002). Histone lysine acetylation tends to be protective and leads to adaptive behaviors (Hitchcock & Matthew, 2014). Histone lysine acetylation is continuously fluctuating throughout the brain after exposure to different drugs of abuse, including cocaine (Rogge, Singh, Dang, & Wood, 2013), nicotine (Huang et al., 2014), morphine (Mashayekhi et al., 2012), heroin (Egervari et al., 2017), and amphetamine (Renthal et al., 2008), among others. Specifically, histone deacetylases 3 negatively regulates cocaine-induced conditioned place preference acquisition (Rogge et al., 2013). Concerning nicotine, it has been shown that the application of a histone deacetylase inhibitor can mimic the priming effects of nicotine (Huang et al., 2014). With morphine, there are tissue and promoter-specific histone modifications around the BDNF gene's individual promoters in response to chronic morphine and withdrawal (Mashayekhi et al., 2012). Heroin use leads to hyperacetylation of histone H3 in the dorsal striatum that produces glutamate transcription changes (Egervari et al., 2017). Studies performed with chronic amphetamine administration showed increased histone H3 methylation on the *c-fos* promoter and increased expression levels of the H3 histone methyltransferase, KMT1A (lysine methyltransferase 1A, formerly SUV39H1) (Renthal et al., 2008). In the last years, histones' acetylation and phosphorylation have been widely studied using candidate gene approaches in response to cocaine (Rogge et al., 2013; Sadri-Vakili, 2015). These studies confirm that acute or repeated exposure to some abusive drugs can increase H3 and H4 acetylation in several brain areas involved in the reward circuitry. Nevertheless, more studies are needed to precise their specific roles in addiction physiology.

Histone phosphorylation is another posttranslational modification usually observed in substance use disorder. Drugs of abuse and natural reinforcements promote the nuclear accumulation of dopamine-regulated and cAMP-regulated phosphoprotein DARPP-32. The nuclear accumulation of DARPP-32 leads to an increase in H3 histone phosphorylation (Stipanovich et al., 2009). Another common histone modification is lysine methylation. Histone lysine methylation is particularly complex and variable. Repeated exposure of drugs, such as cocaine and morphine, reduces global levels of histone methylation marks (H3K9me2 and H3K9me3) in the NAC (Sun et al., 2012). On the other hand, methamphetamine exposure decreases H3K27me2 levels but increases H3K4me2 and H3K4me3 levels in the NAC (Aguilar-Valles et al., 2014). These studies are prototypical and suggest that histone methylation regulation in response to drugs of abuse is complex and drug-specific and region-specific. Correlations of altered transcript levels with activating and repressive marks of methylation have also been investigated after cocaine exposure. Exonic enrichment of H3K4me1, H3K4me3, and H3K36me3 were positively correlated with transcriptional levels, whereas H3K9me2, H3K9me3, and H3K27me3 were negatively correlated (Feng et al., 2014), suggesting novel regulation modes on the epigenome in the NAC by which cocaine alters the brain. Identifying drug-induced transformations in

histone acetylation, phosphorylation, and methylation in the NAC and other brain areas suggests that these modifications might involve drug addiction regulation. More studies are needed to propose a molecular mechanism to explain these adaptations after exposure to the different drugs of abuse. However, evidence suggests that the combination of inherited predispositions, environmental stimuli, and exposure to addictive substances leading to histone modifications may represent protective and risk factors in developing addiction.

It has been recently shown that dopamine is associated with chromatin to form a previously unknown epigenetic regulation called "dopaminylation." Rats undergoing withdrawal from cocaine showed an accumulation of histone H3 glutamine 5 dopaminylation (H3Q5dop) in the VTA. Consequently, intra-VTA viral manipulations were produced to induce decreasing levels of H3Q5dop. This manipulation prevented cocaine-mediated gene expression changes and cocaine-seeking behavior in rats during withdrawal (Lepack et al., 2020). This previously uncharacterized chromatin modification opens a new research window in the underlying substance use disorder's epigenetic regulation mechanisms.

In summary, drug use may produce enduring alterations in gene expression via histone modifications to individuals carrying susceptibility genes exposed to adverse environmental factors. These post-translational transformations may influence susceptibility to addictive disorders. Enhanced vulnerability to abuse drugs can give feedback at an increased risk of future drug consumption, leading to further modifications on the epigenome and gene expression (Wong, Mill, & Fernandes, 2011).

DNA methylation is a stable epigenetic mark that occurs with the covalent modification of DNA by DNA methyltransferases. In this modification, DNA methyltransferases trigger the addition of a methyl group to cytosine-phosphoguanine (CpG) at the C5 position (5-mC) (Bird, 2002). DNA methylation in gene promoters is associated with repression, whereas DNA methylation in gene bodies is associated with active transcription (Nestler & Luscher, 2019). Repression of DNA by DNA methylation can be detrimental and enhance the risk to develop addiction and depressive-like behaviors (Hitchcock & Matthew, 2014). However, little is known about the specific impact of DNA methylation in protective and risk factors in substance use disorder, and most studies focus on the specific effect of drugs of abuse in the expression of DNA methyltransferases. Methamphetamine self-administration paired with electrical footshocks resulted in differential DNA hydroxymethylation and increased expression of potassium channel mRNAs in the NAC of those rats that showed a resilient phenotype against the adverse consequences associated with methamphetamine (Cadet, Patel, & Jayanthi, 2019). Subchronic methamphetamine treatment-induced different patterns of DNA methyltransferase 1 mRNA expression in the nucleus caudatus and NAC in rats, which increased DNA methylation (Numachi et al., 2007). Other studies showed that repeated cocaine exposure increased the expression of methyl-CpG binding protein 2 and produced de novo DNA methylation (Bodetto et al., 2013). By contrast, nicotine microinjections in the mouse cortex and hippocampus decreased mRNA and DNA methyltransferase 1 expression levels but increased glutamic acid decarboxylase 67 (GAD₆₇) expression levels in the frontal cortex (Satta et al., 2008).

Moreover, a recent study in alcohol use disorder subjects revealed that chronic alcohol drinking results in increased DNA methylation of NR3C1 exon variant 1H, associated with reduced NR3C1 mRNA and protein expression levels in PFC and other cortico-limbic regions (Gatta et al., 2021). Oxycodone also produced demethylation of genes implicated in synaptic plasticity (synaptophysin and postsynaptic density protein 95) in the VTA of rats, which can be prevented with oxytocin pretreatment (Fan, Shi, & Zhao, 2019). However, a global mapping of DNA methylation changes in the brain at single-nucleotide resolution in response to abuse drugs is still not available. The generation of DNA methylation genome-wide maps would allow a better understanding of the role of this epigenetic mark in substance use disorder.

The study of epigenetic marks is currently moving one step forward due to the latest technological advances. The combination of next-generation sequencing (NGS) and chromatin immunoprecipitation (ChIP) has now provided novel descriptive information about the presence of epigenetic marks involved in addiction and other neurological diseases. Even though this information is of great importance, the real revolution relies on the technology that enables the induction of discrete epigenetic marks in brain cells. This technology is termed "neuroepigenetic editing." Before its existence, experiments in animal models were based on the overexpression or underexpression of related epigenetic enzymes (as histone or chromatin modification enzymes), which target hundreds of genes and, therefore, have undesirable off-target effects and unpredictable compensatory consequences. In contrast, neuroepigenetic editing techniques, produce single and locus-specific epigenetic modifications, thus allowing to establish a causal relationship between the epigenetic mark and its consequence. There are three main strategies to produce discrete neuroepigenetic editions: zinc-finger proteins (Heller et al., 2014), transcription activator-like effectors (Heller et al., 2014), and clustered regularly interspaced short palindromic repeats CRISPR/Cas9. Among them, CRISPR/Cas9 stands out due to the simplicity of its design, the low price of the synthesis, the scalability, versatility, and most importantly, the cell specificity and temporal precision. For instance, CRISPR/Cas9 has been used to target methyl-CpG-binding proteins (Swiech et al., 2015), and Cas9 has also been used after its fusion with DNA methylating enzymes to edit the methylation profile of specific enhancers and promoters (Liu et al., 2016). CRISPR/Cas9 applications in the mammalian nervous system exceed this manuscript's aim and have been deeply reviewed before (Day, 2019; Savell et al., 2019). Therefore, neuroepigenetic editing, although recent, is proving to be a very promising field in basic and translational research.

In the food addiction field, the formation of reward-related associative memories in rats upregulated essential plasticity genes in the VTA correlated with memory strength and associated with gene-specific changes in DNA methylation (Day et al., 2013). Food addicted mice also showed a significant decrease in DNA methylation of the *CNR1* gene promoter in the PFC, which was associated with an upregulation of CB1 protein expression in the same brain area (Mancino et al., 2015).

Thus, epigenetic signatures have an essential role in vulnerability or resilience to addiction. The epigenetic mechanisms involve modifications

in the stable-state expression levels of a set of genes and produce "latent" changes in other genes' inducibility, activation, and inactivation (Nestler, 2014). Regulation of gene inducibility can be seen as "latent" in that it would not be evident by analysis of mRNA or protein levels. For instance, cocaine induces latent effects by changing the chromatin structure at many genes, which alter their inducibility in response to a subsequent stimulus. These latent changes can determine an individual's vulnerability to addiction later in life upon drug exposure or affect relapse in long-term abstinent individuals after re-exposure to the drug. However, drugs or other environmental exposures can also induce trans-generational epigenetic inheritance of addiction vulnerability by epigenetic changes in germinal cells, which are then passed on to progeny and alter their vulnerability to addiction (Meaney & Szyf, 2005).

4 | miRNAs OF VULNERABILITY AND RESILIENCE: ALTERATION OF miRNA EXPRESSION AS A NOVEL THERAPEUTICAL TOOL

Non-coding RNAs that do not translate into proteins play an essential role in cell function. Among these, miRNAs are of particular relevance for cell biology and are related to many processes, including addiction.

miRNAs are short RNA transcripts with around 22 nucleotides that are endogenously expressed by cells to regulate gene expression post-transcriptionally in a very dynamic way (Kenny, 2014). The identification of more than 2,000 miRNAs in the human genome suggests high conservation through evolution (Alles et al., 2019). Each one can impact the posttranscription of thousands of protein-coding genes, eliciting a rising interest among the scientific community in most diverse fields, including addiction.

miRNAs are transcribed by RNA polymerase II in their native form and processed into so-called pri-miRNAs. Pri-miRNAs are processed by the Drosha enzyme into pre-miRNAs of around 70 nucleotides and exported from the nucleus. Outside of the nucleus, they are further processed by the Dicer enzyme into a duplex RNA (dsRNA). The protein family Argonaute plays a crucial role in RNA silencing, being a component of the RNA-induced silencing complex (RISC). Together with Dicer and Argonaute, the dsRNA incorporates into RISC. RISC is responsible for the gene silencing phenomenon known as RNA interference (RNAi). Argonaute proteins bind different classes of small non-coding RNAs, including microRNAs (miRNAs). One RNA strand is removed from the dsRNA molecule, and the other RNA remains retained in the RISC as a mature molecule of miRNA (Figure 4). Ago 2 (one of the four members of the Argonaute family) has endonucleolytic activity, identifies the target mRNA-miRNA complementary sites, and degrades the target mRNA (Liu et al., 2004). However, miRNAs can also block mRNA translation by preventing mRNA interaction with ribosomes and targeting mRNAs to processing bodies for degradation (Filipowicz, Bhattacharyya, & Sonenberg, 2008). In addition to these "canonical" miRNA roles in the cytoplasm, some findings have described miRNA targeting different cell compartments such as the nucleus and the cytoplasm and newer functions developed by

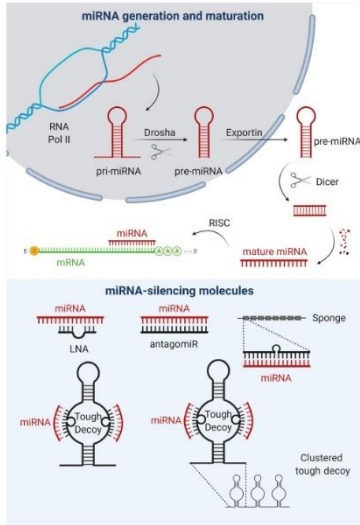


FIGURE 4 miRNA generation, maturation, and silencing mechanisms. miRNAs are transcribed by RNA polymerase II in their native form and processed into so-called pri-miRNAs. Pri-miRNAs are processed by the Drosha enzyme into pre-miRNAs and exported from the nucleus. At that point, they consist of around 70 nucleotides. The Dicer enzyme further processes them into a duplex (dsRNA) outside of the nucleus. Together with Dicer and Argonaute, the miRNA incorporates into an RNA-induced silencing complex (RISC). One RNA strand is removed, and the mature molecule of the miRNA is retained in the RISC. The miRNA silencing mechanisms comprise locked nucleic acid (LNA), antagomiR, sponges, and tough decoy (TuD). LNA use for miRNA knockdown is beneficial because these probes have a high affinity for their small RNA targets and exceptional mismatch-discrimination ability. AntagomiR consists of a single-stranded RNA molecule entirely complementary to the target miRNA. They hybridize to prevent the union of the miRNA to a mRNA molecule. Sponges have up to eight regions antisense to target miRNAs located tandemly in the same transcript. Sponges, transcribed by RNA Pol II, can target different miRNAs from the same family. TuDs are 100 nucleotides long and form a hairpin structure that increases their stability and contains an unpaired region in the middle. Both strands from this unpaired region are complementary to the target miRNA. With the same TuD construct, there is the possibility of targeting two different miRNAs and forming TuD clusters to increase the number of miRNA-binding sites

miRNAs in these locations. These miRNAs can relocate to the nucleus, alter mRNA stability in the nucleolus, and affect alternative splicing (Catalanotto, Cogoni, & Zardo, 2016). In neurons, miRNAs develop specific functions in dendrites and can be secreted to synapses in exosomes (Smith & Kenny, 2018). When miRNAs bind to the 3'UTR of mRNAs, they affect mRNA translation and stability and mRNA distribution in dendrites and synapses (Most, Workman, & Adron Harris, 2014).

miRNAs play a role in synaptic plasticity events closely related to addition development (Smith & Kenny, 2018). Synaptic plasticity processes, such as enlargement of dendritic spines, changes in AMPA/NMDA receptor ratio, and activation of metalloproteases, are related to opiates, nicotine, and cocaine relapse (Smith & Kenny, 2018). miR-132 and miR-212 are two examples of miRNAs with essential functions in synaptic plasticity and dendritic growth through the interaction with the brain-derived neurotrophic factor (BDNF). Inhibition of miR-132 reduces the number of mushroom-like spines while immature filopodia increases, whereas the deletion of miR-132 and miR-212 decreases dendritic length and complexity in the neurons of the hippocampus (Smith & Kenny, 2018). miR-132 and miR-212 are upregulated in the striatum after cocaine administration (Sadakierska-Chudy et al., 2017) and upon cocaine reinstatement (Quinn et al., 2015).

Alongside the increasing knowledge about miRNAs, the technology required to alter miRNA expression moves forward. Inhibition and overexpression of miRNAs are now possible by specific experimental approaches, therefore becoming promising therapeutic tools. As miRNAs eventually achieve their target miRNA's degradation, their suppression would correlate with their target mRNAs' overexpression or an increased translation. The opposite would happen when overexpressed with downregulation of their target mRNAs or a decreased gene expression. Most strategies to date that aimed to inhibit miRNAs consist of delivering a DNA vector encoding for the RNA-based inhibitory molecule, thus providing a long-lasting expression. In vitro studies have demonstrated that locked nucleic acids (LNA) are also very potent tools. They consist of a short synthetic RNA oligonucleotide containing a modified nucleotide, which sharply increases its stability (Papargyri, Pontoppidan, Andersen, Koch, & Hagedorn, 2020; Rasmussen & Roberts, 2007). The use of LNA for the knockdown of miRNA is beneficial because these probes have a high affinity for their small RNA targets and excellent mismatch-discrimination capability (Rasmussen & Roberts, 2007). The structurally most straightforward approach for miRNA inhibition in vivo is antagomiR. It consists of a single-stranded RNA molecule entirely complementary to the target miRNA that hybridizes and prevents the miRNA's union to an mRNA molecule (Scherr et al., 2007). This useful technology is far from being optimal, as antagomiRs are unstable and degraded quickly. To overcome this limitation, "Sponges" have been generated with up to eight regions antisense to target miRNAs located tandemly in the same transcript (Ebert, Neilson, & Sharp, 2007). Sponges transcribed by RNA Pol II can target different miRNAs from the same family,

However, one of the most potent approaches for miRNA inhibition strategies is the Tough Decoy inhibitor (TuD) (Bak, Hollensen, Primo, & Sørensen, 2013; Hollensen et al., 2018). TuDs are 100 nucleotides long and form a hairpin structure that increases their stability and contains an unpaired region in the middle. Both strands from this unpaired region are complementary to the target miRNA. TuD technology was first described by expressing them through RNA Pol III (Haraguchi, Ozaki, & Iba, 2009). However, TuDs can also be transcribed by RNA Pol II, which confers higher tissue specificity (Bak et al., 2013). The latest advances show the possibility of targeting two different miRNAs with the same TuD construct and forming TuD clusters to increase the number of miRNA-binding sites (Hollensen, Bak, Haslund, & Mikkelsen, 2013). These novel inhibitors (Sponges and TuDs) may be further improved by the insertion of a short region (four nucleotides) of self-complementary nucleotides that form a “bulge.” “Bulge” makes inhibitors less likely to be degraded by the Argonaute complex after miRNA pairing (Ebert et al., 2007; Yoo, Hajjar, & Jeong, 2017).

Interestingly, circular RNAs (circRNAs) were discovered to be naturally expressed by cells from most tissues. One well-known circRNA is ciRS-7 that contains 70 times the complementary sequence for a miRNA termed miR-7. ciRS-7 acts as a “sponge” by binding miR-7, and its circular structure makes it more resistant to exonucleases (Hansen et al., 2013). Recently, other endogenously expressed circRNAs have been described to different sponge miRNAs, opening the door for more miRNA inhibition possibilities for therapeutic purposes (Li et al., 2020). Methods for in vitro and in vivo generation of circRNAs have successfully been developed (Ebermann, Schnarr, & Müller, 2020).

The novel technology required to alter miRNAs expression has potential therapeutic utility. The capacity to be secreted extracellularly and to the systemic circulation has led miRNAs to be considered potential biomarkers for diagnosing and preventing addiction. They can constitute relevant indicators of a resilient or vulnerable phenotype to addiction. The technology required to alter miRNA expression is dynamically progressing, becoming promising therapeutic tools in the field of addiction.

5 | FUTURE DIRECTIONS

Recent research advances have allowed a better understanding of the genetic and epigenetic bases underlying addiction development. The interaction between multiple environmental factors and polygenic influences is responsible for the development of this disease. Multiple gene variants have been reported to participate in the individual vulnerability to develop addiction. Several of these variants were initially identified by using gene candidate approaches. However, GWAS's more recent use has provided a rapid advance in these genetic mechanisms' knowledge. The recent technological improvements in these GWAS approaches would provide definitive progress for better understand the complex interactions among the multiple genes involved in the pathogenesis of addiction. Innovative genomic

approaches now combine animal and human studies for cross-talks and validation of the data, which mainly improves the identification of the functional relevance of the candidate genes identified.

The recent advances in the knowledge of the complex mechanisms involved in the epigenetic control of gene expression and the novel technological tools to manipulate these mechanisms will allow us to definitively understand the capability of environmental factors to modify gene expression and their influence on the development of the addictive processes. Identifying these epigenetic factors opens new possibilities to define more precise biomarkers of vulnerability and resilience to addiction and may open innovative therapeutic perspectives that are still unexploited.

All these genetic and epigenetic tools are now available. The use of these novel tools in creative and well-designed experimental approaches would undoubtedly allow in a near-future definitive advance to clarify the involvement of these mechanisms in addiction development. This knowledge will be crucial to develop new therapeutic strategies for better management of addict patients.

ACKNOWLEDGMENTS

This work was supported by the Spanish Ministerio de Economía y Competitividad-MINECO (#SAF2017-84060-R-AEI/FEDER-UE), the Spanish Instituto de Salud Carlos III, RETICS-RTA (#RD12/0028/0023), the Generalitat de Catalunya, AGAUR (#2017-SGR-669), ICREA-Acadèmia (#2015) and the Spanish Ministerio de Sanidad, Servicios Sociales e Igualdad, Plan Nacional Sobre Drogas of the Spanish Ministry of Health (#PNSD-2017068) to R.M., Fundació La Marató-TV3 (#2016/20-30) and Plan Nacional Sobre Drogas of the Spanish Ministry of Health (#PNSD-2019006) to E.M.-G. Figures created with BioRender.com.

DATA AVAILABILITY STATEMENT

Data sharing not applicable – no new data generated, or the article describes entirely theoretical research.

ORCID

Alejandra García-Blanco  <https://orcid.org/0000-0002-9155-4660>

Elena Martín-García  <https://orcid.org/0000-0002-4487-3028>

REFERENCES

- Adkins, D. E., Clark, S. L., Copeland, W. E., Kennedy, M., Conway, K., Angold, A., ... Costello, E. J. (2015). Genome-wide meta-analysis of longitudinal alcohol consumption across youth and early adulthood. *Twin Research and Human Genetics*, 18, 335–347.
- Agrawal, A., Verweij, K. J. H., Gillespie, N. A., Heath, A. C., Lessov-Schlaggar, C. N., Martin, N. G., ... Lynskey, M. T. (2012). The genetics of addiction: a translational perspective. *Translational Psychiatry*, 2(7), e140.
- Aguilar-Valles, A., Vaissière, T., Griggs, E. M., Mikaelsson, M. A., Takács, I. F., Young, E. J., ... Miller, C. A. (2014). Methamphetamine-associated memory is regulated by a writer and an eraser of permissive histone methylation. *Biological Psychiatry*, 76, 57–65.
- Alles, J., Fehlmann, T., Fischer, U., Backes, C., Galata, V., Minet, M., ... Meese, E. (2019). An estimate of the total number of true human miRNAs. *Nucleic Acids Research*, 47, 3353–3364.
- Andrews, A. J., & Luger, K. (2011). Nucleosome structure(s) and stability: Variations on a theme. *Annual Review of Biophysics*, 40, 99–117.

- Badani, A., Belin, D., Epstein, D., Calu, D. J., & Shaham, Y. (2011). Opiate versus psychostimulant addiction: The differences do matter. *Nature Reviews Neuroscience*, 12, 685–700.
- Bak, R. O., Hollensen, A. K., Primo, M. N., & Sørensen, C. D. (2013). Potent microRNA suppression by RNA pol II-transcribed 'tough Decoy' inhibitors. *RNA*, 19, 280–293.
- Barr, P. B., Kishan, A., Su, J., Johnson, E. C., Meyers, J. L., Wetherill, L., ... Dick, D. M. (2020). Using polygenic scores for identifying individuals at increased risk of substance use disorders in clinical and population samples. *Translational Psychiatry*, 10(1). <http://dx.doi.org/10.1038/s41398-020-00865-8>.
- Blum, K., Braverman, E. R., Holder, J. M., Lubar, J. F., Monasta, V. J., Miller, D., ... Comings, D. E. (2000). Reward deficiency syndrome: A biogenetic model for the diagnosis and treatment of impulsive, addictive, and compulsive behaviors. *Journal of Psychoactive Drugs*, 32, 1–112.
- Bird, A. (2002). DNA methylation patterns and epigenetic memory. *Genes & Development*, 16(1), 6–21. <http://dx.doi.org/10.1101/gad.947102>.
- Bodetto, S. P., Carouge, D., Fonteneau, M., Dietrich, J. B., Zwiller, J., & Anglard, P. (2013). Cocaine represses protein phosphatase-1C β through DNA methylation and methyl-CpG binding protein-2 recruitment in adult rat brain. *Neuropharmacology*, 73, 31–40.
- Buchwald, J., Chenoweth, M. J., Palvialainen, T., Zhu, G., Benner, C., Gordon, S., ... Tyndale, R. F. (2020). Genome-wide association meta-analysis of nicotine metabolism and cigarette consumption measures in smokers of European descent. *Molecular Psychiatry*. <https://doi.org/10.1038/s41380-020-0702-z>.
- Cabana-Domínguez, J., Shivalkar, A., Fernández-Castillo, N., & Comand, B. (2019). Genome-wide association meta-analysis of cocaine dependence: Shared genetics with comorbid conditions. *Progress in Neuro-Psychopharmacology & Biological Psychiatry*, 94, 109667.
- Caded, J. L., Patel, R., & Jayanthi, S. (2019). Compulsive methamphetamine taking and abstinence in the presence of adverse consequences: Epigenetic and transcriptional consequences in the rat brain. *Pharmacology, Biochemistry, and Behavior*, 179, 98–108.
- Caspi, A., & Moffitt, T. E. (2006). Gene-environment interactions in psychiatry: Joining forces with neuroscience. *Nature Reviews Neuroscience*, 7, 583–590.
- Catalanotto, C., Cogoni, C., & Zardo, G. (2016). MicroRNA in control of gene expression: An overview of nuclear functions. *International Journal of Molecular Sciences*, 17, 1712.
- Chen, L.-S., Hartz, S. M., Baker, T. B., Ma, Y., La Saccone, N., & Bierut, L. J. (2018). Use of polygenic risk scores of nicotine metabolism in predicting smoking behaviors. *Pharmacogenomics*, 19(18), 1383–1394. <http://dx.doi.org/10.2217/pgs-2018-0081>.
- Clarke, T. K., Adams, M. J., Davies, G., Howard, D. M., Hall, L. S., Padmanabhan, S., ... McIntosh, A. M. (2017). Genome-wide association study of alcohol consumption and genetic overlap with other health-related traits in UKbiobank (N=112117). *Molecular Psychiatry*, 22, 1376–1384.
- Comelis, M. C., Flint, A., Field, A. E., Kraft, P., Han, J., Rimm, E. B., & Van Dam, R. M. (2016). A genome-wide investigation of food addiction. *Obesity*, 24, 1336–1341.
- Crist, R. C., Reiner, B. C., & Berrettini, W. H. (2019). A review of opioid addiction genetics. *Current Opinion in Psychology*, 27, 31–35.
- Davis, C., Loxton, N. J., Levitan, R. D., Kaplan, A. S., Carter, J. C., & Kennedy, J. L. (2013). 'Food addiction' and its association with a dopaminergic multilocus genetic profile. *Physiology & Behavior*, 118, 63–69.
- Day, J. J. (2019). Genetic and epigenetic editing in nervous system. *Dialogues in Clinical Neuroscience*, 21, 359–368.
- Day, J. J., Childs, D., Guzman-Karlsson, M. C., Kibe, M., Moulden, J., Song, E., ... Sweatt, J. D. (2013). DNA methylation regulates associative reward learning. *Nature Neuroscience*, 16, 1445–1452.
- Demontis, D., Rajagopal, V. M., Thorgeirsson, T. E., Als, T. D., Grove, J., Leppä, K., ... Bergum, A. D. (2019). Genome-wide association study implicates CHRNA2 in cannabis use disorder. *Nature Neuroscience*, 22, 1066–1074.
- Domingo-Rodríguez, L., Ruiz de Azua, I., Domínguez, E., Senabre, E., Serra, I., Kummer, S., ... Maldonado, R. (2020). A specific prefrontal nucleus accumbens pathway controls resilience versus vulnerability to food addiction. *Nature Communications*, 11, 782.
- Ebermann, C., Schnarr, T., & Müller, S. (2020). Recent advances in understanding circular RNAs. *F1000Research*. <https://doi.org/10.12688/f1000research.25060>.
- Ebert, M. S., Nelson, J. R., & Sharp, P. A. (2007). MicroRNA sponges: Competitive inhibitors of small RNAs in mammalian cells. *Nature Methods*, 4, 721–726.
- Egervari, G., Landry, J., Callens, J., Fullard, J. F., Roussos, P., Keller, E., & Hurd, Y. L. (2017). Striatal H3K27 acetylation linked to glutamatergic gene dysregulation in human heroin abusers holds promise as therapeutic target. 81, 585–594.
- Fan, X. Y., Shi, G., & Zhao, P. (2019). Methylation in Syn and Pcd95 genes underlie the inhibitory effect of oxytocin on oxytocin-induced conditioned place preference. *European Neuropsychopharmacology*, 29, 1464–1475.
- Febbo, M., Blum, K., Badgalyan, R. D., Baron, D., Thanos, P. K., Colon-Perez, L. M., ... Gold, M. S. (2017). Dopamine homeostasis: Brain functional connectivity in reward deficiency syndrome. *Frontiers in Bioscience (Landmark Ed)*, 22, 669–669.
- Feng, J., Wilkinson, M., Liu, X., Purushothaman, I., Ferguson, D., Valou, V., ... Shen, L. (2014). Chronic cocaine-regulated epigenomic changes in mouse nucleus accumbens. *Genome Biology*, 15, R65.
- Filipowicz, W., Bhattacharya, S. N., & Sonenberg, N. (2008). Mechanisms of post-transcriptional regulation by microRNAs: Are the answers in sight? *Nature Reviews Genetics*, 9, 102–114.
- Frank, J., Cichon, S., Treutlein, J., Riedinger, M., Mattheisen, M., Hoffmann, P., & Rietschel, M. (2012). Genome-wide significant association between alcohol dependence and a variant in the ADH gene cluster. *Addiction Biology*, 17(1), 171–180. <http://dx.doi.org/10.1111/j.1369-1600.2011.00395.x>.
- Furberg, H., Kim, Y., Dackor, J., Boerwinkle, E., Franceschini, N., Ardisino, D., ... Sullivan, P. F. (2010). Genome-wide meta-analyses identify multiple loci associated with smoking behavior. *Nature Genetics*, 42, 441–447.
- Gatta, E., Grayson, D. R., Auta, J., Saudagar, V., Dong, E., Chen, Y., ... Guidotti, A. (2021). Genome-wide methylation in alcohol use disorder subjects: Implications for an epigenetic regulation of the cortico-limbic glucocorticoid receptors (NR3C1). *Molecular Psychiatry*, 26(3), 1029–1041.
- Gottesman, I. (2005). The Endophenotype concept in psychiatry: Etymology and strategic intentions. *International Journal of Dermatology*, 44, 1031–1034.
- Hamer, D. (2002). Genetics. Rethinking behavior genetics. *Science*, 298, 71–72.
- Hancock, D. B., Markunas, C. A., Bierut, L. J., & Johnson, E. O. (2018). Human genetics of addiction: New insights and future directions. *Current Psychiatry Reports*, 20, 8.
- Hancock, D. B., Reginsson, G. W., Gaddis, N. C., Chen, X., Saccone, N. L., Lutz, S. M., ... Stefansson, K. (2015). Genome-wide meta-analysis reveals common splice site acceptor variant in CHRNA4 associated with nicotine dependence. *Translational Psychiatry*, 5, 651.
- Hansen, T. B., Jensen, T. I., Clausen, B. H., Bramsen, J. B., Finsen, B., Damgaard, C. K., & Kjems, J. (2013). Natural RNA circles function as efficient microRNA sponges. *Nature*, 495, 384–388.
- Haraguchi, T., Ozaki, Y., & Iba, H. (2009). Vectors expressing efficient RNA decoys achieve the long-term suppression of specific microRNA activity in mammalian cells. *Nucleic Acids Research*, 37, e43.
- Haskei-Httah, M., Duncan, R. G., & Yarden, A. (2020). Students' understanding of the dynamic nature of genetics: Characterizing undergraduates' explanations for interaction between genetics and environment. *CBE Life Sciences Education*, 19, 1–13.

- Heller, E. A., Cates, H. M., Peña, C. J., Sun, H., Shao, N., Feng, J., ... Nestler, E. J. (2014). Locus-specific epigenetic remodeling controls addiction- and depression-related behaviors. *Nature Neuroscience*, *17*, 1720–1727.
- Hitchcock, L. N., & Matthew, L. K. (2014). Histone-mediated epigenetics in addiction. *Progress in Molecular Biology and Translational Science*, *128*, 51–87.
- Hollensen, A. K., Andersen, S., Hjerth, K., Bak, R. O., Hansen, T. B., Kjems, J., ... Mikkelsen, J. G. (2018). Enhanced tailored MicroRNA sponge activity of RNA pol II-transcribed TuD hairpins relative to ectopically expressed ciRS7-derived circRNAs. *Molecular Therapy—Nucleic Acids*, *13*, 365–375.
- Hollensen, A. K., Bak, R. O., Haskind, D., & Mikkelsen, J. G. (2013). Suppression of microRNAs by dual-targeting and clustered tough decoy inhibitors. *RNA Biology*, *10*, 406–414.
- Huang, Y. Y., Levine, A., Kandel, D. B., Yin, D., Colnaghi, L., Drisaldi, B., & Kandel, E. R. (2014). D1/D5 receptors and histone deacetylation mediate the gateway effect of LTP in hippocampal dentate gyrus. *Learning & Memory*, *21*, 153–160.
- Kendler, K. S., Karkovskiy, L. M., Neale, M. C., & Prescott, C. A. (2000). Illicit psychoactive substance use, heavy use, abuse, and dependence in a US population-based sample of male twins. *Archives of General Psychiatry*, *57*, 261–269.
- Kendler, K. S., & Prescott, C. A. (1998). Cocaine use, abuse and dependence in a population-based sample of female twins. *The British Journal of Psychiatry*, *173*, 345–350.
- Kenny, P. J. (2014). Epigenetics, microRNA, and addiction. *Dialogues in Clinical Neuroscience*, *16*, 335–344.
- Kouzarides, T. (2007). Chromatin modifications and their function. *Cell*, *128*, 693–705.
- Kouzarides, T. (2002). Histone methylation in transcriptional control. *Current Opinion in Genetics & Development*, *12*, 198–209.
- Lepack, A. E., Werner, C. T., Stewart, A. F., Fulton, S. L., Zhong, P., Farrelly, L. A., ... Maze, I. (2020). Dopaminergic histone H3 in ventral tegmental area regulates cocaine seeking. *Science*, *368*, 197–201.
- Lewis, C. M., & Vassos, E. (2020). Polygenic risk scores: From research tools to clinical instruments. *Genome Medicine*, *12*, 44.
- Li, J., Huang, C., Zou, Y., Ye, J., Yu, J., & Gui, Y. (2020). CircTLK1 promotes the proliferation and metastasis of renal cell carcinoma by sponging miR-136-5p. *Molecular Cancer*, *19*, 1–17.
- Lindgren, E., Gray, K., Miller, G., Tyler, R., Viers, C. E., Volkow, N. D., & Wang, G.-J. (2017). Food addiction: A common neurobiological mechanism with drug abuse. *Frontiers in Bioscience (Landmark Ed)*, *23*, 811–836.
- Liu, J., Camell, M. A., Rivas, F. V., Marsden, C. G., Thomson, J. M., Song, J. J., ... Hannon, G. J. (2004). Argonaute2 is the catalytic engine of mammalian RNAi. *Science*, *305*, 1437–1441.
- Liu, X. S., Wu, H., Ji, X., Stelzer, Y., Wu, X., Czuderna, S., ... Jaenisch, R. (2016). Editing DNA methylation in the mammalian genome. *Cell*, *167*, 233–247.
- Lopez-Leon, S., Gonzalez-Giraldo, Y., Wegman-Ostrosky, T., & Forero, D. A. (2021). Molecular genetics of substance use disorders: An umbrella review. *Neuroscience & Biobehavioral Reviews*, *124*, 358–369.
- Mancino, S., Burokas, A., Gutierrez-Cuesta, J., Gutierrez-Martos, M., Martin-Garcia, E., Pucci, M., ... Maldonado, R. (2015). Epigenetic and proteomic expression changes promoted by eating addictive-like behavior. *Neuropsychopharmacology*, *40*, 2788–2800.
- Martin, A. R., Daly, M. J., Robinson, E. B., Hyman, S. E., & Neale, B. M. (2019). Predicting polygenic risk of psychiatric disorders. *Biological Psychiatry*, *86*, 97–109.
- Mashayekhi, F. J., Rasti, M., Rahvar, M., Mokarram, P., Namavar, M. R., & Owji, A. A. (2012). Expression levels of the BDNF gene and histone modifications around its promoters in the ventral tegmental area and locus coeruleus of rats during forced abstinence from morphine. *Neurochemical Research*, *37*, 1517–1523.
- Maurano, M. T., Humbert, R., Rynes, E., Thurman, R. E., Haugen, E., Wang, H., ... Stamatoyanopoulos, J. A. (2012). Systematic localization of common disease-associated variation in regulatory DNA. *Science*, *337*, 1190–1195.
- Meaney, M. J., & Szyf, M. (2005). Environmental programming of stress responses through DNA methylation: Life at the interface between a dynamic environment and a fixed genome. *Dialogues in Clinical Neuroscience*, *7*, 103–123.
- Most, D., Workman, E., & Adron-Harris, R. (2014). Synaptic adaptations by alcohol and drugs of abuse: Changes in microRNA expression and mRNA regulation. *Frontiers in Molecular Neuroscience*, *7*, 1–10.
- Nestler, E. J. (2014). Epigenetic mechanisms of drug addiction. *Neuropharmacology*, *76*, 1–7.
- Nestler, E. J., & Luscher, C. (2019). The molecular basis of drug addiction: Linking epigenetic to synaptic and circuit mechanisms. *Neuron*, *102*, 48–59.
- Nikolova, Y. S., Ferrell, R. E., Manuck, S. B., & Hariri, A. R. (2011). Multilocus genetic profile for dopamine signaling predicts ventral striatum reactivity. *Neuropsychopharmacology*, *36*, 1940–1947.
- Numachi, Y., Shen, H., Yoshida, S., Fujiyama, K., Toda, S., Matsuoka, H., ... Sato, M. (2007). Methamphetamine alters expression of DNA methyltransferase 1 mRNA in rat brain. *Neuroscience Letters*, *414*, 213–217.
- Papargyri, N., Pontopidan, M., Andersen, M. R., Koch, T., & Hagedorn, P. H. (2020). Chemical diversity of locked nucleic acid-modified antisense oligonucleotides allows optimization of pharmaceutical properties. *Molecular Therapy—Nucleic Acids*, *19*, 706–717.
- Phillips, P. C. (2008). Epistasis—the essential role of gene interactions in the structure and evolution of genetic systems. *Nature Reviews Genetics*, *9*, 855–867.
- Plomin, R., & Daniels, D. (2011). Why are children in the same family so different from one another? *International Journal of Epidemiology*, *40*, 563–582.
- Quinn, R. K., Brown, A. L., Goldie, B. J., Levi, E. M., Dickson, P. W., Smith, D. W., ... Dayas, C. V. (2015). Distinct miRNA expression in dorsal striatal subregions is associated with risk for addiction in rats. *Translational Psychiatry*, *5*, e503.
- Rasmussen, S., & Roberts, P. (2007). Functional studies of microRNA based on knockdown using locked nucleic acid probes. *Nature Methods*, *4*(4), iii–iv.
- Renthal, W., Carle, T. L., Maze, I., Covington, H. E., Truong, H. T., Alibhai, I., ... Nestler, E. J. (2008). ΔFosB mediates epigenetic desensitization of the c-fos gene after chronic amphetamine exposure. *The Journal of Neuroscience*, *28*, 7344–7349.
- Robinson, G. E. (2004). Beyond nature and nurture. *Science*, *304*, 397–399.
- Rogge, G. A., Singh, H., Dang, R., & Wood, M. A. (2013). HDAC3 is a negative regulator of cocaine-context-associated memory formation. *The Journal of Neuroscience*, *33*, 6623–6632.
- Rossetto, D., Avvakumov, N., & Côté, J. (2012). Histone phosphorylation. *Epigenetics*, *7*, 1098–1108.
- Sadkierska-Chudy, A., Frankowska, M., Mszkiel, J., Wydra, K., Jastrzębska, J., & Filip, M. (2017). Prolonged induction of miR-212/132 and REST expression in rat striatum following cocaine self-administration. *Molecular Neurobiology*, *54*, 2241–2254.
- Sadri-Vakili, G. (2015). Cocaine triggers epigenetic alterations in the corticostriatal circuit. *Brain Research*, *1628*, 50–59.
- Sanna, M., Li, X., Visconti, A., Freidin, M. B., Sacco, C., Ribero, S., ... Han Jiali, F. M. (2020). Looking for sunshine: Genetic predisposition to sun-seeking in 265,000 individuals of European ancestry. *The Journal of Investigative Dermatology*, *141*, 779–786.
- Satta, R., Maloku, E., Zhubi, A., Pibiri, F., Hajos, M., Costa, E., & Guidotti, A. (2008). Nicotine decreases DNA methyltransferase 1 expression and glutamic acid decarboxylase 67 promoter methylation in GABAergic interneurons. *Proceedings of the National Academy of Sciences of the United States of America*, *105*, 16356–16361.

- Saul, M. C., Philip, V. M., Reinholdt, L. G., & Chesler, E. J. (2019). High-diversity mouse populations for complex traits. *Trends in Genetics*, 35, 501–514.
- Savell, K. E., Zipperly, M. E., Tuscher, J. J., Duke, C. G., Phillips, R. A., Bauman, A. J., ... Day, J. J. (2019). A dopamine-induced gene expression signature regulates neuronal function and cocaine response. *BioRxiv*, 2019. 781872.
- Scherr, M., Venturini, L., Battmer, K., Schaller-schoenitz, M., Schaefer, D., Dallmann, I., ... Eder, M. (2007). Lentivirus-mediated antagomir expression for specific inhibition of miRNA function. *Nucleic Acids Research*, 35, e149.
- Silveira, P. P., Pokhvisneva, I., Gaudreau, H., Atkinson, L., Fleming, A. S., Sokolowski, M. B., ... Meaney, M. J. (2018). Fetal growth interacts with multilocus genetic score reflecting dopamine signaling capacity to predict spontaneous sugar intake in children. *Appetite*, 120, 596–601.
- Smith, A. C., & Kenny, P. (2018). MicroRNAs regulate synaptic plasticity underlying drug addiction. *Genes, Brain and Behaviour*, 17, e12424.
- Stipanovich, A., Valjent, E., Matamales, M., Ahn, J., Maroteaux, M., Bertran-Gonzalez, J., ... Girault, J. (2009). A phosphatase cascade by which natural rewards and drugs of abuse regulate nucleosomal response in the mouse. *Nature*, 453, 879–884.
- Sun, H. S., Maze, I., Dietz, D. M., Scobie, K. N., Kennedy, P. J., Damez-Werno, D., ... Nestler, E. J. (2012). Morphine epigenomically regulates behavior through alterations in histone H3 lysine 9 dimethylation in the nucleus accumbens. *The Journal of Neuroscience*, 32, 17454–17464.
- Swiech, L., Heidenreich, M., Banerjee, A., Habib, N., Li, Y., Trombetta, J., ... Zhang, F. (2015). In vivo interrogation of gene function in the mammalian brain using CRISPR-Cas9. *Nature Biotechnology*, 33, 102–106.
- Takeuchi, F., Isono, M., Nabika, T., Katsuya, T., Sugiyama, T., Yamaguchi, S., ... Kato, N. (2011). Confirmation of ALDH2 as a major locus of drinking behavior and of its variants regulating multiple metabolic phenotypes in a Japanese population. *Circulation Journal*, 75, 911–918.
- Thorgeirsson, T. E., Gudbjartsson, D. F., Surakka, I., Vink, J. M., Amin, N., Geller, F., ... Stefansson, K. (2010). Sequence variants at CHRN3-CHRNA6 and CYP2A6 affect smoking behavior. *Nature Genetics*, 42, 448–453.
- Tsou, C. C., Chou, H. W., Ho, P. S., Kuo, S. C., Chen, C. Y., Huang, C. C., ... Huang, S. Y. (2019). DRD2 and ANKK1 genes associate with late-onset heroin dependence in men. *The World Journal of Biological Psychiatry*, 20, 605–615.
- Tsuang, M. T., Lyons, M. J., Meyer, J. M., Doyle, T., Eisen, S. A., Goldberg, J., ... Eaves, L. (1998). Co-occurrence of abuse of different drugs in men: The role of drug-specific and shared vulnerabilities. *Archives of General Psychiatry*, 55, 967–972.
- Vink, J. M. (2016). Genetics of addiction: Future focus on gene x environment interaction? *Journal of Studies on Alcohol and Drugs*, 77, 684–687.
- Vink, J. M., Hottenga, J. J., de Geus, E. J. C., Willemsen, G., Neale, M. C., Furberg, H., & Boomsma, D. I. (2014). Polygenic risk scores for smoking: predictors for alcohol and cannabis use?. *Addiction*, 109(7), 1141–1151. <http://dx.doi.org/10.1111/add.12491>
- Volkow, N. D., & Muenke, M. (2012). The genetics of addiction. *Human Genetics*, 131, 773–777.
- Walker, D. M., & Nestler, E. J. (2018). Neuroepigenetics and addiction. *Handbook of Clinical Neurology*, 148, 747–765.
- Wang, S. C., Chen, Y. C., Lee, C. H., & Cheng, C. M. (2019). Opioid addiction, genetic susceptibility, and medical treatments: A review. *International Journal of Molecular Sciences*, 20, 4294.
- Way, M., McQuillin, A., Saini, J., Ruparel, K., Lydall, G. J., Guernini, L., ... Gurling, H. M. D. (2015). Genetic variants in or near *adh1b* and *adh1c* affect susceptibility to alcohol dependence in a british and irish population. *Addiction Biology*, 20, 594–604.
- Wong, C. C. Y., Mill, J., & Fernandes, C. (2011). Drugs and addiction: An introduction to epigenetics. *Addiction*, 106, 480–489.
- Yoo, J., Hajjar, R. J., & Jeong, D. (2017). Generation of efficient miRNA inhibitors using tough decoy constructs. *Methods in Molecular Biology*, 1521, 41–53.

How to cite this article: Maldonado R, Calvé P, García-Blanco A, Domingo-Rodríguez L, Senabre E, Martín-García E. Genomics and epigenomics of addiction. *Am J Med Genet Part B*. 2021;186B: 128–139. <https://doi.org/10.1002/ajmg.b.32843>

Recently submitted to ChemRxiv

Reversible photocontrol of dopaminergic transmission in wild-type animals

Carlo Matera^{1,2,3}, Pablo Calvé^{4,#}, Verónica Casadó-Anguera^{5,#}, Rosalba Sortino^{1,2,#}, Alexandre M. J. Gomila^{1,2}, Estefanía Moreno⁵, Thomas Gener⁴, Cristina Delgado⁴, Pau Nebot⁴, Davide Costazza¹, Sara Conde-Berriozabal⁶, Mercè Masana⁶, Jordi Hernando⁷, Vicent Casadó⁵, M. Victoria Puig⁴, Pau Gorostiza^{1,2,8,*}

1. Institute for Bioengineering of Catalonia (IBEC), The Barcelona Institute for Science and Technology, Barcelona 08028, Spain
2. Biomedical Research Networking Center in Bioengineering, Biomaterials and Nanomedicine (CIBER-BBN), Madrid 28029, Spain
3. Department of Pharmaceutical Sciences, University of Milan, 20133 Milan, Italy
4. Hospital del Mar Medical Research Institute (IMIM), Barcelona Biomedical Research Park, Barcelona 08003, Spain
5. Department of Biochemistry and Molecular Biomedicine, Faculty of Biology, Institute of Biomedicine of the University of Barcelona, University of Barcelona, Barcelona, Spain
6. Department of Biomedical Sciences, Faculty of Medicine and Health Sciences, Institute of Neuroscience, University of Barcelona, IDIBAPS, CIBERNED, Barcelona, Spain
7. Department of Chemistry, Autonomous University of Barcelona (UAB), Cerdanyola del Vallès 08193, Spain
8. Catalan Institution for Research and Advanced Studies (ICREA), 08010 Barcelona, Spain

Equal contribution

ABSTRACT

Understanding the dopaminergic system is a priority in neurobiology and neuropharmacology. Dopamine receptors are involved in the modulation of fundamental physiological functions and dysregulation of dopaminergic transmission is associated with major neurological disorders. However, the available tools to dissect the endogenous dopaminergic circuits have limited specificity, reversibility, resolution, or require genetic manipulation. Here we introduce azodopa, a novel photoswitchable ligand that enables reversible spatiotemporal control of dopaminergic transmission. We demonstrate that azodopa activates D₁-like receptors *in vitro* in a light-dependent manner. Moreover, it enables reversibly photocontrolling zebrafish motility on a time scale of seconds and allows separating the retinal component of dopaminergic neurotransmission. Azodopa increases the overall neural activity in the cortex of anesthetized mice and displays illumination-dependent activity in individual cells. Azodopa is the first photoswitchable dopamine agonist with demonstrated efficacy in wildtype animals and opens the way to remotely controlling dopaminergic neurotransmission for fundamental and therapeutic purposes.

Keywords: photochromism, photoswitch, azobenzene, light, agonist, apomorphine, dopamine, G protein-coupled receptor, GPCR, behavior, biased signaling, neural oscillation, brainwave, *in vivo* electrophysiology, photopharmacology, optopharmacology, azologization, caged compound, optogenetics

INTRODUCTION

Dopamine receptors (DARs) are members of the class A G protein-coupled receptor (GPCR) family and are prominent in the vertebrate central nervous system (CNS). Their primary endogenous ligand is the catecholaminergic neurotransmitter dopamine, a metabolite of the amino acid tyrosine. Among the many neuromodulators used by the mammalian brain to regulate circuit function and plasticity, dopamine (Figure 1a) stands out as one of the most behaviorally powerful.^{1,2} Dopaminergic neurons are critically involved in diverse vital CNS functions, including voluntary movement, feeding, reward, motivation, sleep, attention, memory, and cognition. The extracellular concentration of dopamine oscillates following day/night cycles and plays important physiological roles in the regulation of olfaction, retinal function,³ and circadian rhythms.⁴ Disentangling these diverse components of DAR signaling and dopaminergic transmission is an unmet need both of basic research and medicine, because their abnormal function leads to complex medical conditions such as Parkinson's and Huntington's diseases, schizophrenia, attention deficit hyperactivity disorder, Tourette's syndrome, drug abuse, and addiction.¹ To date, five subtypes of DARs have been cloned:

D₁, D₂, D₃, D₄, and D₅. Based on their coupling to either G_{αs,off} proteins or G_{αi/o} proteins, which respectively stimulate or inhibit the production of the second messenger cAMP, DARs are classified as D₁-like receptors (D₁, D₅) or D₂-like receptors (D₂, D₃, D₄). However, both classes are known to signal through multiple pathways. Targeting these receptors using specific agonists and antagonists allows to modulate dopaminergic transmission and dopamine-dependent functions. Indeed, hundreds of compounds interfering with the dopaminergic system have been developed, and many of them are clinically used to treat various disorders. They also constitute pharmacological tools to study the role of dopamine in synaptic and neural circuits^{5,6} as well as the mechanisms underlying dopamine-related debilitating conditions.⁷ However, conventional ligands cannot differentiate among specific neuronal sub-populations in heterogeneous brain regions where multiple neuronal subtypes exist, thus potentially activating DARs that mediate distinct or even opposing physiological functions.² For this reason, the lack of circuit selectivity is a confounding element in basic research and likely cause of the poor safety as well as efficacy of many dopaminergic drugs. Hence, methods to activate DARs noninvasively with high spatiotemporal resolution are required both for research and therapeutic purposes.

Pursuing a traditional pharmacological approach would hardly pay off in such a physiological scenario, because a drug generally affects its target in multiple CNS regions at once and its effect is slowly reversible. Light is an unparalleled input signal to noninvasively manipulate biological systems in precisely designated patterns, and photopharmacology,⁸⁻¹⁰ which relies on molecular photoswitches to regulate bioactive compounds, has already been successful in GPCRs,¹¹⁻¹⁶ ion channels,^{17,18} and enzymes.^{19,20} The possibility of using light as an external stimulus to manipulate specific populations of dopaminergic neurons has generated enormous interest in neurobiology since the invention of optogenetics,^{21,22} in particular to elucidate the basis of complex behavioural and cognitive processes.^{23,24} However, the achievements of optogenetics rely on the overexpression of exogenous proteins that lack critical aspects of endogenous GPCR signaling, including their native ligand binding sites, downstream molecular interactions, and other elements that can affect receptor dynamics. Thus, current optogenetic tools may provide partial or sometimes inaccurate insights of biological processes. In addition, the application of genetic manipulation techniques to human subjects is still importantly hampered by safety (possible immune responses against the gene transfer), regulatory, and economic issues. Complementary approaches to address some of these limitations have been proposed. Trauner, Isacoff and collaborators developed light-gated DARs through a combined chemical-genetic method in which a weakly photoswitchable ligand was tethered via a maleimide-thiol conjugation to a genetically engineered cysteine residue at the target receptor in order to improve photocontrol.²⁵ They have also used a genetically targeted membrane anchor to tether a dopaminergic ligand via SNAP-tag labeling.¹⁵ Unlike the exogenous optogenetics tools described above, light-gated receptors bear a single-point mutation and provide a nearly physiological study system, but they still require gene delivery and overexpression. Genetics-free methods have also been described. For instance, Etchenique, Yuste and collaborators developed a caged dopamine compound based on ruthenium-bipyridine chemistry and used it to activate dendritic spines with two-photon excitation.²⁶ More recently, Gmeiner *et al.* described two caged DAR antagonists that can serve as valuable tools for light-controlled blocking of D₂/D₃ receptors.²⁷ However, notwithstanding its virtues, uncaging is an irreversible chemical process, while a photopharmacological modulation based on reversible, byproduct-free molecular photoswitches has important advantages *in vivo*. It is noteworthy in this regard the work published by König and collaborators, who developed a set of photochromic small molecules by incorporation of dithienylethenes and fulgides into known dopamine receptor ligands.²⁸ Two of those compounds, named 29 and 52, showed an interesting isomer-dependent (open vs closed form) efficacy at activating D₂ receptors, although neither *in situ* photoswitching nor *in vivo* validation of their effects were reported. We present here the design, synthesis and photopharmacological characterization

of the first chemical tool that enables the reversible photocontrol of native dopamine receptors in wildtype animals. Notably, it can be used to separate the retinal component of dopaminergic neurotransmission in zebrafish and manipulate brain waves in mice.

RESULTS

Design Strategy & Synthesis. Aryl azo compounds, especially azobenzenes, have emerged as the photoswitches of choice in photopharmacology because of their physical and chemical properties, which make them especially suitable for biological applications.^{29,30} An elegant strategy for the incorporation of an azobenzene into a bioactive ligand¹¹ relies on the isosteric replacement of the two-atom linker between the two aromatic rings with a diazene unit ($-N=N-$),^{11,20,31-33} which entails minimal perturbation of pharmacophore and drug-like properties, thus accounting for the success of this so-called azologization approach.³¹ However, to the best of our knowledge, this strategy is not applicable to any of the dopamine agonists known, since the scaffold of an isomerizable aryl azo compound is not directly present in their structure.

In the quest for a freely diffusible drug-like dopaminergic photoswitch, we noticed that most agonists (especially to D_1 receptors, see Figure 1a) are rigid or semi-rigid, conformationally restrained structures in which essential pharmacophoric features are held in their mutual position.³⁴ Indeed, two main routes can be identified in the early development of dopamine agonists, namely the rigidification of the dopamine molecule and the dissection of apomorphine, one of the first potent dopamine agonists to be found.³⁵ Dopamine rigidification led to the discovery of potent agonists, whereas the apomorphine de-rigidification generally reduced its efficacy.^{36,37} It stands then to reason that governing the geometry of such structures would enable the control of their biological effects. This could be achieved by “building” upon a semi-rigid and photoisomerizable molecular frame the structural elements required for DAR activation, and using light as external control signal. Common features in the dopamine agonist pharmacophore model are: (I) a cationic site point (an amino group) that forms a salt bridge with an aspartic acid residue in the receptor’s third transmembrane helix (TM3); (II) one or two hydrogen bond acceptor/donor sites (e.g., hydroxy groups), that interact with serine residues in TM5; and (III) an aromatic ring system that takes part in $\pi-\pi$ interactions with hydrophobic residues in TM6.^{38,39} On these grounds, we devised a photoswitchable dopamine agonist by decorating an azobenzene molecule with two hydroxyl substituents (II) on one phenyl ring, and an amino group (I) connected through a short linker to the other phenyl ring (III) (Figure 1b). This molecule, that we named azodopa, carries the main DAR binding determinants and enables to change their relative position upon photoisomerization, as predicted from the binding poses of the *trans* and *cis* isomers into a homology model of the D_1 receptor⁴⁰ (Figure 1b). Azodopa was synthesized in two steps via an azo-coupling reaction between commercially available 2-(2-(dimethylamino)ethyl)aniline and 1,2-dihydroxybenzene (see Scheme S1 and SI for detailed synthetic procedures and physicochemical characterization).

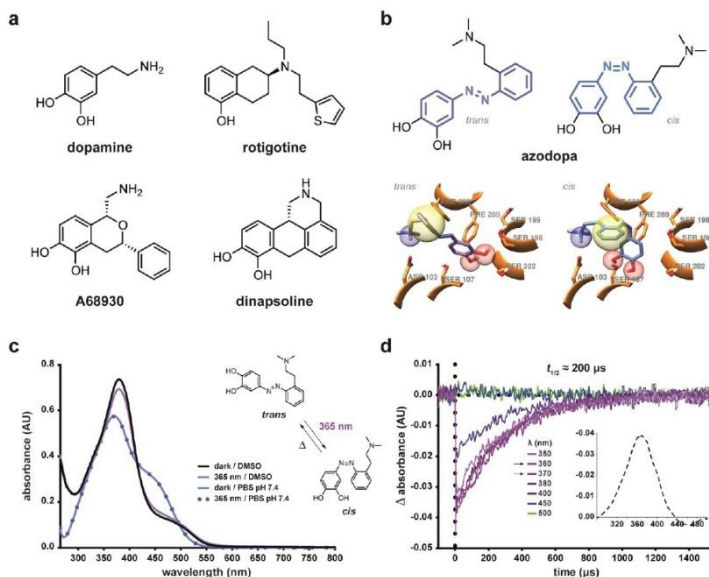


Figure 1. Design, structure, and photochromism of azodopa. (a) Chemical structure of dopamine and representative (semi)rigidified derivatives: rotigotine (nonselective agonist), A68930 (D_2 agonist), and dinapsoline (D_2 agonist). (b) Chemical structure of the photochromic dopamine ligand azodopa (*trans* and *cis* isomers) and corresponding predicted binding poses into a homology model of the D_2 receptor.⁴⁰ Key interacting residues in the binding pocket are shown in orange. Essential pharmacophoric features for D_2 receptor binding are highlighted: blue spheres represent cationic site points and H-bond donors, i.e. the protonated amino function that can form a salt bridge and a hydrogen bond with Asp103 and Ser107, respectively; red spheres represent H-bond acceptors, i.e. the hydroxyl groups of the catechol ring that can interact with Ser198, Ser199, and Ser202; yellow spheres represent hydrophobic elements, i.e. the aromatic ring that can form π - π interactions with Phe288 and Phe289. The mutual position and orientation of such pharmacophoric features in the receptor-bound conformation should affect binding affinity and efficacy of the ligands. Molecular docking was performed with AutoDock Vina (PyRx 0.8 interface) applying a protocol described in detail elsewhere.²⁰ The docking poses shown here are only intended for illustrative purposes. (c) Photochromic behavior of azodopa (50 μM) studied with steady-state spectroscopy in aqueous (PBS, pH 7.4) and organic (DMSO) solutions. As lifetimes of *cis*-hydroxazobenzenes are very short in polar protic solvents, no changes in the absorption spectrum of aqueous solutions of azodopa could be observed after illumination with 365 nm light (3 min). (d) Photochromic behavior of azodopa (30 μM) investigated by transient absorption spectroscopy in water (only representative traces are shown for the sake of clarity; see Figure S7 for the full experiment). Transient absorption time traces were measured at different wavelengths upon excitation of *trans*-azodopa with a 5-ns pulsed laser at $\lambda = 355 \text{ nm}$ (3 mJ/pulse energy) and 25 °C. Thermal relaxation half-life of the *cis*-isomer (200 μs) was estimated applying an exponential one-phase decay model (GraphPad Prism 6). Inset: Transient absorption spectrum of *trans*-azodopa upon pulsed irradiation at $\lambda = 355 \text{ nm}$ recorded at $t = 0 \mu\text{s}$. X-values represent wavelength (nm), Y-values represent ΔA (arbitrary units, AU).

Photochemical Characterization. An essential condition for azodopa to function as a photoswitchable dopamine ligand is that it photoisomerizes between two different configurations (*trans* and *cis*). We first characterized it by steady-state UV-Vis absorption spectroscopy (Figure 1c), which revealed an absorption maximum at 370 nm in aqueous solution (PBS, pH 7.4) and at 380 nm in DMSO. It is known that the thermal *cis*-to-*trans* isomerization of 4-hydroxazobenzenes follows a very fast kinetics in polar protic solvents via solvent-assisted proton transfer tautomerization,

whereas it proceeds more slowly in aprotic and nonpolar solvents.⁴¹ In agreement, no changes in the absorption spectrum of azodopa could be detected with a conventional UV-Vis spectrophotometer upon illumination at 365 nm in aqueous buffer because of the short lifetime of its *cis* isomer in this medium, and only a small change could be recorded in a polar but aprotic solvent such as DMSO (Figure 1c). No measurements were performed in nonpolar solvents (e.g., toluene) because of the very poor solubility of our compound in this kind of media. We next determined the optimal isomerization wavelength and lifetime of *cis*-azodopa by means of transient-absorption spectroscopy with ns-time resolution. Upon pulsed excitation of azodopa in aqueous media with UV and violet light, an instantaneous and remarkable decrease of the absorption signal was detected, which can be ascribed to the depletion of the *trans* ground electronic state due to the photoinduced formation of the corresponding *cis* isomer (Figure 1d).^{41,42} The initial absorption value was quickly recovered because of the fast thermal *cis*-to-*trans* back-isomerization which restores the initial concentration of the *trans* isomer with an estimated half-life of about 200 μ s (Figure 1d). Thus, since conversion to the *trans* form occurs almost immediately after turning the light off, we performed all biological experiments under continuous illumination. Overall, our absorption spectroscopy studies showed that azodopa undergoes *trans*-to-*cis* photoisomerization upon illumination with UV and violet light and it spontaneously reverts to its full *trans* isomer in a fraction of a millisecond once the light is switched off. Other mechanisms like excited-state intramolecular proton transfer could also play a role. In any case, azodopa should allow fast regulation of DAR activity using a single illumination source to induce *trans*-to-*cis* isomerization.

In Vitro Pharmacology. We next tested the effects of azodopa on D₂-like receptors, for which freely diffusible photoswitchable agonists have not been reported. First, we evaluated the binding affinity of azodopa in mammalian D₁-like and D₂-like receptors using competitive radioligand binding experiments performed either in the dark or under illumination at 365 nm (see SI for details).^{43,44} Azodopa displayed a good capacity to bind to D₁-like and D₂-like receptors, with higher affinity in the *trans* configuration in both cases. In particular for D₁-like receptors, we calculated an almost 4-fold decrease in affinity at 365 nm ($K_d^{\text{dark}} = 600$ nM, $K_d^{365\text{nm}} = 2200$ nM) (Figure S8 and Table S1). Since the activation of D₁-like receptors promotes cyclic adenosine monophosphate (cAMP) formation and phosphorylation by ERK1/2, we also investigated the ability of azodopa to behave as a D₁-like agonist by studying cAMP accumulation (Figure 2a) and ERK1/2 phosphorylation (Figure 2b) in cells overexpressing human D₁ receptors, both in the dark and under continuous illumination at 365 nm (to compare the 'full *trans*' vs the '*cis*-enriched' form, respectively). Intracellular cAMP accumulation was measured in HEK-293T cells transiently transfected with D₁ receptors in a time-resolved fluorescence resonance energy transfer (TR-FRET) assay. We found that azodopa induced cAMP accumulation in a dose- and light-dependent manner (Figure 2a). In particular, we observed substantial differences between the two forms at 5 μ M and 10 μ M, with the *trans* form being significantly more effective at inducing cAMP production than the *cis*-enriched form at the same concentrations. When cells were co-treated with the D₁-like antagonist SKF83566 (300 nM), the effect of azodopa was largely reduced or even disappeared, indicating that azodopa activates D₁ receptors. In cAMP assays performed in non-transfected HEK-293T cells used as negative control, azodopa (10 μ M), dopamine (1 μ M) and SKF38393 (300 nM) did not produce any effect (Figure S9). ERK1/2 phosphorylation was measured in HEK-293T cells transiently transfected with D₁ by western blot analysis using phospho-ERK1/2 antibody. The application of azodopa (10 μ M) promoted ERK1/2 phosphorylation to an extent that was significantly different between the two conditions (dark vs light). The full *trans* form displayed an efficacy 3.6-fold greater than the *cis*-enriched form (Figure 2b), in agreement with the observations in cAMP accumulation assays. Again, co-treatment of the cells with SKF83566 abolished azodopa responses, showing that the effects observed were mediated by D₁. Although we have not thoroughly characterized the pharmacological activity

profile, azodopa displayed D_1 -mediated photoactivity (blocked by SKF83566) also in zebrafish (see later).

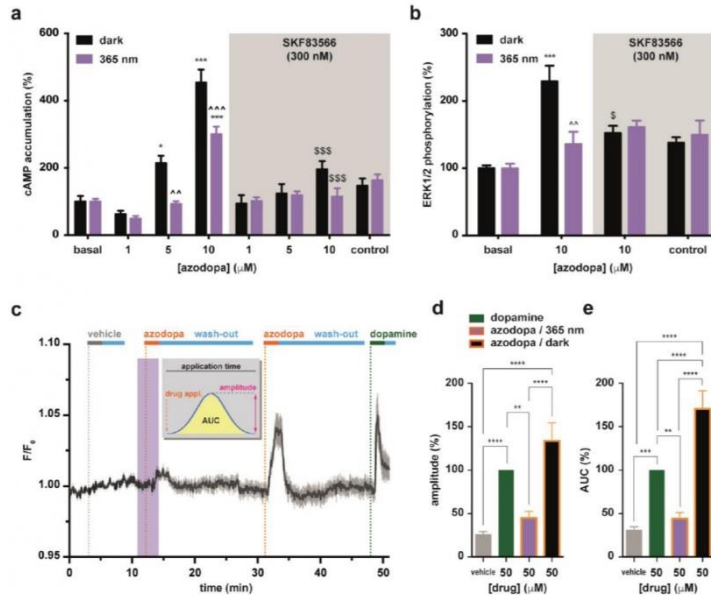


Figure 2. *In vitro* pharmacological characterization of azodopa. (a) Effect on D_1 -mediated adenylyl cyclase activation. cAMP accumulation experiments in HEK-293T cells transiently transfected with D_1 and treated with different concentrations of azodopa, in the dark (black bars) or under illumination (purple bars), in the presence (gray area) or not (white area) of a D_1 -like receptor antagonist (SKF83566). Values are represented in percentage vs basal levels of cAMP. Data are mean \pm S.E.M. (6 experiments performed in quadruplicate). Statistical differences were analyzed by two-way ANOVA followed by Tukey's post-hoc test (* $p < 0.05$ vs basal; ** $p < 0.01$ vs dark; *** $p < 0.001$ vs controls non-pretreated with the antagonist). (b) Effect on D_1 -mediated ERK1/2 activation. ERK1/2 phosphorylation was determined in HEK-293T cells transiently transfected with D_1 and treated with different concentrations of azodopa, in the dark (black bars) or under illumination (purple bars), in the presence (gray area) or not (white area) of a D_1 -like antagonist (SKF83566). Values are represented in percentage vs basal levels of ERK1/2 phosphorylation. Data are mean \pm S.E.M. (3 or 4 experiments performed in triplicate or quadruplicate). Statistical differences were analyzed by two-way ANOVA followed by Tukey's post-hoc test (*** $p < 0.001$ vs basal; ** $p < 0.01$ vs dark; \$ $p < 0.05$ vs controls non-pretreated with the antagonist). (c–e) Effect on D_1 -mediated intracellular calcium release compared to dopamine. (c) Real-time calcium imaging response (averaged traces, black line, $n = 24$ cells) in HEK-293T cells co-expressing D_1 receptors and R-GECO1 as calcium indicator. Traces were recorded upon direct application of azodopa (50 μ M, orange bars) in the dark (white area) and under illumination (purple area). Shadow represents \pm S.E.M.'. Gray and green bars indicate the application of vehicle (control) and dopamine (reference agonist), respectively. Light blue bars indicate wash-out periods. See example frames and raw data traces of individual cells in Supplementary Figure S10, and Supplementary Video S1 for the entire movie. Two values of the calcium responses generated by azodopa were calculated (Origin 8 software) and compared: the peak amplitude $\Delta F/F_0$ (d), calculated as the difference between the maximal and the minimal intensity of each response (**** $p < 0.0001$ for vehicle vs dopamine; **** $p < 0.0001$ for vehicle vs azodopa/dark; **** $p < 0.0001$ for azodopa/365nm vs azodopa/dark; ** $p = 0.035$ for dopamine vs azodopa/365nm), and the area under the curve (AUC) (e), calculated as the integral over the entire application time of vehicle or drugs (**** $p < 0.0001$ vehicle vs dopamine; **** $p < 0.0001$ for vehicle vs azodopa/dark; **** $p < 0.0001$ for dopamine vs azodopa/dark; **** $p < 0.0001$ for azodopa/365nm vs azodopa/dark; **** $p < 0.0001$ for vehicle vs dopamine; ** $p = 0.0025$ for dopamine vs azodopa/365nm). Data are mean \pm S.E.M. ($n = 40$ cells from 3 independent experiments). Data were normalized over the maximum response obtained with the saturating concentration of dopamine (50 μ M)

and were analyzed by one-way ANOVA followed by Tukey's post-hoc test for statistical significance. All statistical analyses (panels a, b, d, e) were performed with GraphPad Prism 6.

It is known that D₁ receptors are also linked to other second messenger systems. These include receptor-mediated activation of phospholipase C (G_q coupling) to generate inositol 1,4,5-trisphosphate (IP₃) which participates in phosphoinositide turnover and calcium-regulated signaling pathways in the brain.⁴⁵ IP₃ receptors are mainly located in the endoplasmic reticular membrane where IP₃ can mobilize Ca²⁺ from intracellular stores.⁴⁵ Thus, as a complementary method to characterize azodopa *in vitro*, we performed Ca²⁺-imaging experiments in HEK-293T cells co-expressing D₁ receptors and R-GECO1 as calcium indicator, and used dopamine as a control (Figure 2cde, Supplementary Figures S10 and S11, Supplementary Video 1). Azodopa (50 μM) was applied to the cells both in the dark and under illumination with UV light. Dopamine (50 μM) was tested as reference agonist. Robust increases of intracellular calcium were observed by the application of azodopa in the dark (pure *trans* isomer), whereas only weak increases were recorded when azodopa was applied under illumination (Figure 2c and Figure S10). Calcium responses were quantified and compared by peak amplitude and area under the curve (AUC). The analysis of these parameters showed that, *trans*-azodopa stimulates the release of intracellular calcium (like dopamine) and this effect is abolished under illumination. In this experiment, *trans*-azodopa displayed significantly higher efficacy than dopamine (Figure 2de). No responses were observed in control experiments in HEK cells (n = 25) not expressing D₁, thus confirming that the calcium oscillations were elicited by a specific interaction at this receptor (Figure S11). Moreover, we verified that *trans*-azodopa fully recovers its efficacy after long (60 min) exposure to 365 nm light, demonstrating that its effects are reversibly photodependent and are not due to an irreversible photodegradation of the molecule (Figure S20 and Figure S21). Our results in calcium imaging experiments suggest that *trans*-azodopa activates the G_q/phospholipase C pathway, in addition to the canonical G_s/adenylyl cyclase pathway already investigated. Such intriguing behavior has been described also for other dopamine agonists.⁴⁵

Taken as a whole, the results from our *in vitro* experiments illustrated in Figure 2 show that *trans*-azodopa is a full agonist at D₁-like receptors and that its effects can be partially or completely switched off with light. The reduction of azodopa efficacy under illumination can be attributed to the photoisomerization process which decreases the partial concentration of the *trans* isomer at the target receptor and/or disrupts the ligand interaction(s) at the binding pocket.

Behavioral effects in zebrafish larvae. The promising photopharmacological profile of azodopa prompted to use it *in vivo* to study dopaminergic neurotransmission. For that purpose, we designed a behavioral assay to record and quantify the locomotor activity of living animals as a function of drug concentration and illumination. It is known that dopamine plays a pivotal role in motor control in humans, as it activates striatal direct pathway neurons that directly project to the output nuclei of the basal ganglia through D₁ receptors, whereas it inhibits striatal indirect pathway neurons that project to the external pallidum through D₂ receptors.⁴⁶ We chose zebrafish larvae (*Danio rerio*) as animal model for our experiments because of their transparency, that facilitates the delivery of light, and their morphological, genetic, and behavioral similarity to higher vertebrates.^{10,47-52} Indeed, a functional nervous system is established after only 4–5 days of embryonic development in zebrafish, enabling them to perform complex behaviors, such as swimming and exploratory activity. In particular, the major dopaminergic pathways in mammals are also represented in the zebrafish brain, and homologous receptors for most of the mammalian subtypes have been identified in these animals. Humans and zebrafish share 100% of the amino acids in the binding site for D₁ and D₃ receptors, and 85–95% for D₂ and D₄ receptors, and generally similar effects are observed for

dopaminergic ligands in zebrafish and in mammals.⁵¹ As a rule of thumb, dopamine receptor agonists increase the locomotor activity, whereas antagonists decrease it.⁵³ However, disentangling the action of drugs on the multiple components of dopaminergic transmission (including different brain regions,² the regulation of retinal function³ and of circadian rhythms⁴) constitutes an unmet need of pharmacology and medicine. Therefore, we set to test azodopa *in vivo* and to take advantage of photocontrolling dopaminergic responses.

Zebrafish larval movements were tracked using a ZebraBox device for automated behavioral recording. Zebrafish larvae at 6 days post-fertilization (6 dpf) were randomly divided into control (vehicle) and treatment groups (with azodopa added to water). Each individual was placed in a separate well of a 96-well plate. Our setup allowed exposing the animal to controlled cycles of dark and 365 nm UV illumination, using the following protocol: dark (20 min, for adaptation), UV light (30 s), dark (20 min), and then four cycles of UV light (30 s) and dark (5 min) (see SI for details and Supplementary Video S2). In order to identify alterations in behavior, we measured multiple properties of locomotor activity to determine the activity level.⁵⁴ In particular, we focused on fast movements and measured swimming distances and duration of fast swimming, defined as speed $\geq 6 \text{ mm}\cdot\text{s}^{-1}$.

We first studied a wide concentration range (spanning from 1 nM to 1 mM azodopa) to determine if behavioral effects could be observed without signs of acute toxicity. No significant differences in locomotor activity were observed between the control group and the treatment groups up to a concentration of 10 μM neither in the dark nor upon illumination (Figure S12). A strong increase in swimming activity was recorded at 1 mM, but the effect ceased after 30 min, possibly because the fish were exhausted. We observed the most interesting alterations of the behavioral profile at 100 μM (Figure 3abcd and Figure S12). The changes in the swimming activity over time for this group and the control group are plotted in Figure 3a (full experiment represented in Figure S12; see also Video S2). We detected a progressive increase in activity for 30–40 min and relatively small photoresponses (e.g. at 20 min in Figure 3a) which is often due to the slow uptake of the drug in the fish.¹⁴ After this period, animals treated with 100 μM azodopa displayed a high swimming activity in the dark that was sustained for the whole duration of the experiment, and that was abolished during each period of UV illumination (30 s bouts between minute 40 and 60 in Figure 3a). These results agree with the intracellular signaling photoresponses observed *in vitro* and confirm a *trans-on/cis-off* dopamine agonist profile. An averaged time course (between 40–41.5 min, integrated every 5 s) of the swimming activity is magnified in Figure 3b. Representative trajectories of individual fish in wells containing the vehicle or 100 μM azodopa in the dark (40–40.5 min) and under illumination (40.5–41 min) are shown in Figure 3c, where green and red lines indicate slow ($< 6 \text{ mm}\cdot\text{s}^{-1}$) and fast ($\geq 6 \text{ mm}\cdot\text{s}^{-1}$) swimming periods, respectively (see Figure S13 for the entire plate and SI for experimental details and analysis). Figure 3d shows the quantification and statistical analysis of the total distances swum by the control group and the treatment group (100 μM azodopa) during the last four cycles, namely once the maximum effect of the drug was reached and maintained (30 s pre-illumination, 30 s illumination, and 30 s post-illumination periods). Fish treated with azodopa covered a distance three times longer than the control group during the same dark periods, and this effect was blocked under illumination. Interestingly, we also noticed a reduction in swimming activity during the first 30 s of dark after each illumination pulse in the treatment group, likely because the fish needed some time to recover the maximum level of activity. The differences between the total distances swum by the treatment group during the 30 s periods of dark (pre- or post-illumination) and the 30 s periods of illumination were also statistically significant (Figure 3d).

Next, we sought to verify whether the effect of azodopa on zebrafish locomotor activity is dose-dependent by testing a range of concentrations around 100 μM . For our analysis, we averaged the distance swum by each group during the last four consecutive dark-light cycles (30 s integration).

We observed that azodopa increased the swimming activity in the dark in a dose-dependent manner, while the effect under 365 nm illumination was smaller at all concentrations and yielded a weak dose dependence (Figure 3e; see also Figure S14 for a representation of the activity profile at all concentrations). Moreover, we observed that co-application of the D₁-like antagonist (SKF83566 at 50 μ M) abolished the behavioral effects produced by azodopa at 100 μ M in the dark, and restored zebrafish activity to control levels (Figure 3e and Figure S15). These experiments allow to exclude the participation of adrenergic receptors in the photoresponses *in vivo*,¹⁴ and support the hypothesis that that they are mediated by D₁-like rather than D₂-like receptors (SKF83566 is thousand-fold more potent in the formers). However, they cannot rule out the involvement of 5-HT₂ receptors, as the antagonist binds them with only 20-fold weaker potency.

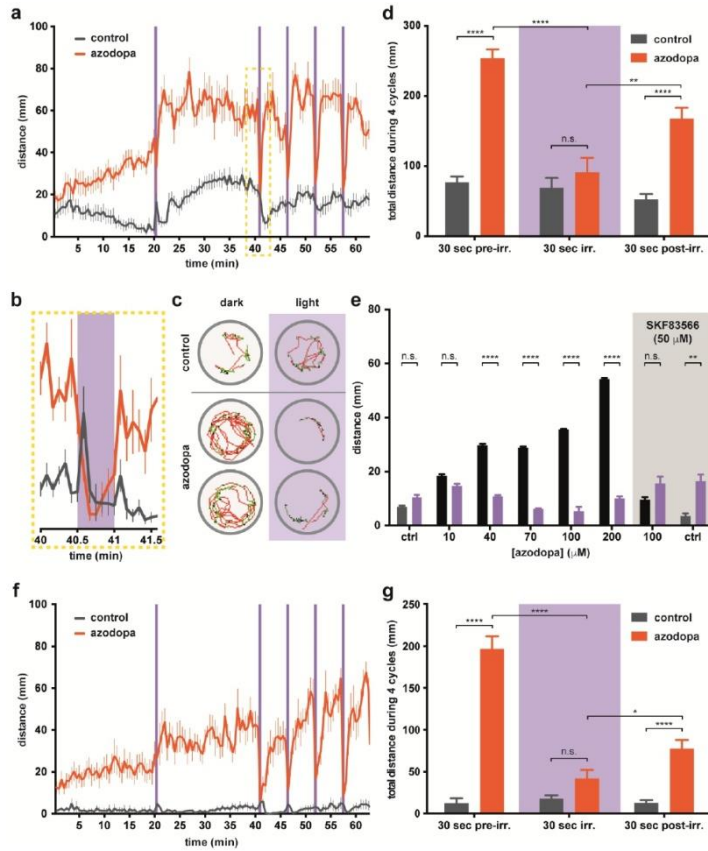


Figure 3. Behavioral effects of azodopa in zebrafish. (a–e) Experiments with normal zebrafish. (a) Swimming activity (distance/time) in larvae exposed to vehicle (control, gray line) or 100 μ M azodopa (treatment, orange line) in the dark (white areas) or under illumination with 365 nm light (purple bars). Data are mean \pm S.E.M. ($n = 11$ –12 individuals/group). (b) Representative time frame (40–41.5 min) of the swimming activity integrated every 5 s, showing how the effect of azodopa can be completely shut down upon illumination. The spike of activity observed for the control group upon illumination represent the startle response to the light stimulus. (c) Exemplary trajectories of individual larvae in one well containing the vehicle and two wells containing 100 μ M azodopa in the dark (40–40.5 min) and under illumination (40.5–41 min). Green lines and red lines indicate slow and fast swimming periods, respectively. The remarkable and light-dependent difference in behavior between untreated and azodopa-treated fish can be appreciated by observing these trajectories and the supplementary Video S2. (d) Quantification of the total distances swum by the control group (vehicle) and the treatment group (100 μ M azodopa) during 4 consecutive cycles of illumination (30 s) and dark (30 s before and after illumination). Data are mean \pm S.E.M. ($n = 11$ –12 individuals/group) and were analyzed by two-way ANOVA followed by Tukey's post-hoc test (**** $p < 0.0001$; ** $p = 0.0037$). (e) Dose-response study of azodopa (white area) and effect of a co-administered D_2 -like antagonist (gray box). Different groups of larvae were exposed to increasing concentrations of azodopa. For

quantification, the average distance swum by each group during the last 4 consecutive dark-light cycles (30 s integration) was considered. The graph shows that *trans*-azodopa (black bars) increases the fish locomotor activity in a dose-dependent manner, but its effects are abolished by the co-administration of a potent and selective D₁-like antagonist (SKF83566, 50 μ M). Data are mean \pm S.E.M. (n = 12 individuals/group) and were analyzed by two-way ANOVA followed by Sidak's post-hoc test (**** p < 0.0001; ** p = 0.0063). (f,g) Experiments with blinded zebrafish. (f) Swimming activity (distance/time) in larvae exposed to vehicle (control, gray line) or 100 μ M azodopa (treatment, orange line) in the dark (white areas) or under illumination with 365 nm light (purple bars). Data are mean \pm S.E.M. (n = 12 individuals/group). (g) Quantification of the total distances swum by the control group (vehicle) and the treatment group (100 μ M azodopa) during 4 consecutive cycles of illumination (30 s) and dark (30 s before and after illumination). Data are mean \pm S.E.M. (n = 12 individuals/group) and were analyzed by two-way ANOVA followed by Tukey's post-hoc test (**** p < 0.0001; * p = 0.0232). All statistical analyses (panels d, e, g) were performed with GraphPad Prism 6.

To tell apart the contribution of visual responses to (1) the changes in fish locomotion and (2) the dopaminergic modulation with azodopa, we repeated the experiments with blinded zebrafish larvae. The zebrafish retina contains four different cone photoreceptor subtypes (UV, S, M, L), each one defined by the expression of specific opsins that confer a particular wavelength-sensitivity. UV cones express SWS1, an opsin with peak sensitivity in the UV range ($\lambda_{max} = 354$ nm),⁵⁵ therefore the removal of functional UV cones can be used to suppress UV-dependent behaviors.⁵⁶ Blinded zebrafish larvae were obtained via a noninvasive blinding technique that induces photoreceptor apoptosis while preserving the rest of the retina (see SI for details).⁵⁷ They were remarkably inactive and unresponsive to illumination (Figure 3fg). The activity profile of azodopa-treated blinded zebrafish was qualitatively like the one observed with azodopa-treated normal zebrafish (Figures 3f and 3a, respectively). Azodopa (100 μ M) produced a remarkable increase of the swimming activity of blind larvae for the entire experiment during the dark periods, and this effect was abolished upon illumination. Quantification of the total distances swum by the control group and the treatment group (100 μ M azodopa) during the last four dark/light cycles confirmed our observations: the locomotion of blinded animals could be significantly photoswitched with azodopa. The overall decrease in swimming activity of blinded zebrafish (Figure 3fg) compared to normal zebrafish (Figure 3abcde) is due to the induced blindness, which reduces their exploratory tendencies. This phenomenon is more pronounced in the control-blinded group, which is almost immobile, and make the effect of azodopa on locomotion appear even stronger: azodopa-treated blinded larvae cover a total distance 16 times longer (during pre-illumination periods) and 6 times longer (during post-illumination periods) than the one swum by control animals (Figure 3g).

The fact that azodopa can elicit behavioral photoresponses in blinded zebrafish and that they have similar magnitude than those in normal fish show that retinal photoreceptors are not directly involved in the observed change in locomotion upon illumination. Instead, photoresponses must be attributed to other dopaminergic circuits in the CNS (present both in blinded and normal larvae) that are effectively put under the control of light with azodopa. Interestingly, the time course of photoresponses does display differences between blinded and normal larvae, and these must be ascribed to the presence of visual inputs in normal animals. The most outstanding one is the recovery of locomotion after turning off UV light in the presence of azodopa, which is significantly faster in normal zebrafish larvae than in blinded ones (see 4 cycles in Figures 3a, 3f, and quantification in Supplementary Figure S16). Thus, azodopa enables time-resolved behavioral experiments that contain unique information about the dopaminergic modulation of retinal function,³ and that will be further investigated with spatially-resolved neuronal activity maps.

Overall, behavioral responses in zebrafish larvae agree with our previous findings *in vitro* and confirm that azodopa is a reversible photoswitchable dopaminergic agonist displaying dose-dependent locomotor effects. In addition, we demonstrated that zebrafish larvae, previously exposed to azodopa and dark-light cycles, recovered normal swimming behavior after washout (see Figure S22 and SI), and were still alive about 48 hours after the experiment. The robust photocontrol

of behavior and the apparent absence of acute toxicity encouraged us to test the potential of azodopa in a mammalian model.

Electrophysiological recordings in anesthetized mice. We studied whether azodopa modulates neural activity in the cortex of mice. For such experiments, we developed a custom set-up that combined *in vivo* electrophysiological recordings and the possibility to illuminate with 365 nm LEDs. The Open Ephys data acquisition system was used to record neural activity via an octrode (4 two-wire stereotrode array) inserted in the superficial layers of the secondary motor cortex (M2) with a large craniotomy that allowed exposure of cortical tissue (Figure 4a).

We first investigated the effects of azodopa in the absence of light in two mice anesthetized with isoflurane (Mouse 1 and Mouse 2, Figure 4b-e). In each animal, we recorded spiking activity of individual neurons (single unit activity, SUA) and local field potentials (LFPs) in M2 before and after the administration of *trans*-azodopa. We quantified mean firing rates (spikes per second) and LFP power from 1 to 10 Hz. Transient oscillatory signals observed in LFPs reflect the summed synchronized activity of neural networks and are also called neural oscillations. Neural oscillations between 1 and 10 Hz have been associated with cognitive processing during alertness and slow waves during slow wave sleep and anesthesia (i.e., UP and DOWN states). The experiments started after cortical activity was stable for at least 10 minutes. Then, we recorded baseline neural activity for 10 more minutes. During this period, slow fluctuations of neural activity were observed both at the single-neuron and LFP levels that were associated with UP and DOWN states typically observed during anesthesia (Figure 4b). Later, 10 μ l of *trans*-azodopa at 3 μ M concentration were administered manually on the surface of the cortex with a standard pipette. Azodopa increased neural activity few seconds after its administration. The effects were transient in many neurons and the general activity remained elevated for at least 5 minutes (Figure 4c). There was a boost in the firing rate of individual neurons that no longer followed the UP and DOWN cycles. In addition, more neurons could be identified after *trans*-azodopa administration (21 neurons during baseline and 33 neurons after azodopa in mouse 1; see also Supplementary Figure S17). In fact, in mouse 2, we isolated 23 neurons during baseline and only 10 neurons after *trans*-azodopa because spiking activity was so elevated that spikes from different neurons co-occurred altering the shape of the waveforms and thus preventing their classification. Corresponding with the increased spiking activity of neurons, the power of oscillatory activities augmented, although moderately compared to changes in firing rate (Figure 4c, bottom panel). Statistical analyses confirmed significant increases of firing rate and 1–10 Hz power when combining the two animals (Figure 4de).

We next investigated the effects of azodopa under 365 nm illumination in two more mice anesthetized with isoflurane (Mouse 3 and Mouse 4, Supplementary Figures S17-S19). In each mouse, we first injected 0.5 ml of saline and later 0.5 ml 3 μ M azodopa in consecutive experiments. Solutions were administered with an infusion pump over the course of one minute to avoid environmental noise and to allow electrophysiological recordings during the administration. Moreover, drug administration was conducted under illumination so that azodopa penetrated cortical tissue in an inactive form. Then, we illuminated the motor cortex with five consecutive cycles of one-minute of darkness (OFF) and one-minute of light (ON) (Supplementary Figure S17). Here, we focused on differential spiking activity during light and dark cycles because azodopa displayed a stronger effect than on the power of neural oscillations in the previous experiments (Figure 4).

After the injection of saline, the mean firing rate of neurons remained like baseline levels and neural activity slightly increased during the light cycles compared to the dark cycles (Supplementary Figure S17). In the presence of azodopa, neural activity increased as in direct application experiments

(Figure 4) and some neurons showed rapid and reversible changes in their firing patterns during the ON and OFF light cycles. Interestingly, some of these neurons decreased their spiking activity during the light periods (DARK-ON) and others increased it (LIGHT-ON; Supplementary Figures S18 and S19). Although these heterogeneous effects of light cancelled each other out in the global average (Supplementary Figure S17c), manual pooling of single unit recordings yielded significant differences in neural activity between dark and light conditions (Supplementary Figure S19). Since dopamine receptors are expressed both in excitatory and inhibitory neurons of the frontal cortex, we hypothesize that DARK-ON neurons may correspond to those expressing D₂-like receptors, which decrease their firing rates when azodopa is deactivated by light, and LIGHT-ON neurons may be cells affected indirectly by network effects driven by DARK-ON neurons.

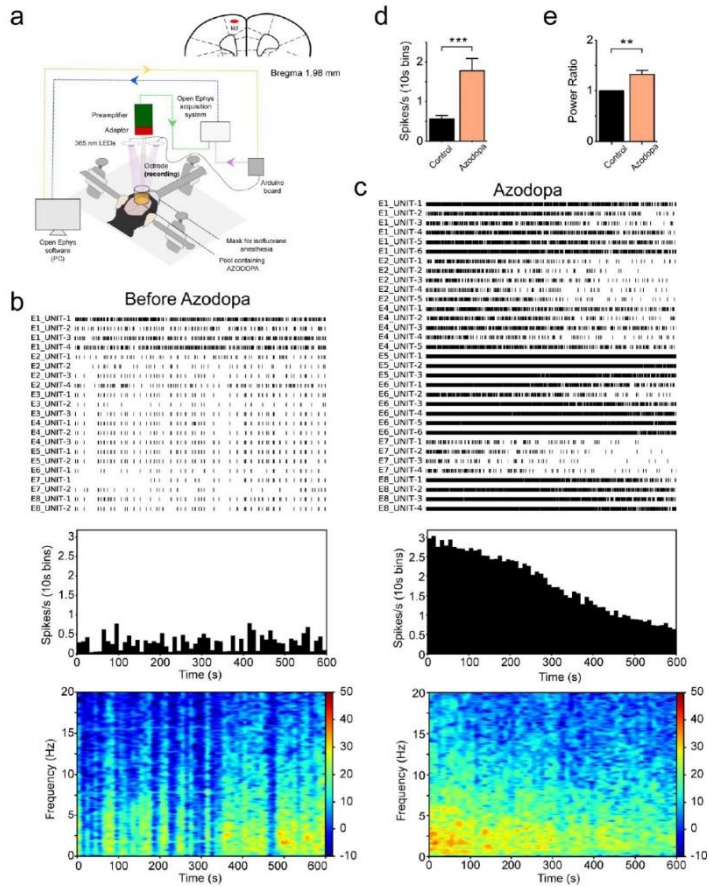


Figure 4. Effect of cortical administration of *trans*-azodopa on electrophysiological recordings in anesthetized mice. (a) Animals were anesthetized with isoflurane and placed in a stereotaxic apparatus. A craniotomy was drilled above the secondary motor cortex (M2) and an octrode was inserted in the superficial layers. Analog signals were bandpass filtered and digitized by a preamplifier, amplified by an Open Ephys data acquisition system (green arrow), and finally visualized and recorded in a PC (blue arrow). Neural activity was recorded during baseline conditions and after administration of *trans*-azodopa on the cortical surface (3 μ M concentration in 10 μ l volume). See the Supplementary Information for further details of the setup and Supplementary Figures S17-S19 for the effect of illumination on azodopa. (b) Neural activity during baseline conditions in Mouse 1. Raster plot of spiking activity in the cortex of one mouse for 10 minutes. Each row depicts the spiking activity of a single neuron (unit), each tick representing an action potential. We used arrays of 8 electrodes (octrodes) in each animal from which several units could be recorded. Neurons are labeled by their electrode number (E1 to E8). Firing rates were stable and followed the UP and DOWN slow fluctuations typical of

anesthesia. The quantification of firing rates and average time-frequency spectrogram of the power of neural oscillations ($n = 8$ electrodes) are shown below. (c) Neural activity after the administration of $3 \mu\text{M}$ *trans*-azodopa in Mouse 1 (zero indicates the time of administration). Azodopa boosted the firing rate of neurons and increased the power of neural oscillations. (d) Azodopa increased spiking activity of cortical neurons. Mean firing rate of neurons before and after the administration of *trans*-azodopa. Data are mean \pm S.E.M. ($n = 44$ neurons during baseline vs 43 neurons after azodopa in two mice) and were analyzed with an unpaired T-test ($*** p = 0.0002$). (e) Azodopa increased the power (1–10 Hz) of neural oscillations in the two animals. Due to the large differences in the baseline power of the two mice, we normalized the power to its baseline for visualization purposes only. Data are mean \pm S.E.M. ($n = 16$ channels per condition from two mice) and were analyzed with a paired T-test ($** p = 0.0011$).

Overall, our first *in vivo* studies in anesthetized mice indicate that *trans*-azodopa exerts excitatory actions on brain cortical microcircuits, as reflected by the increased spiking and oscillatory activities. The effects of azodopa were transient; the firing rate of many neurons was increased for few minutes while in others the elevated firing lasted more than 10 minutes. This could be due to the diffusion (and therefore dilution) of azodopa within cortical tissue over time, and possibly to its metabolic washout and reuptake by synaptic terminals.⁵⁸ The increase of cortical activity by *trans*-azodopa is consistent with our results from functional studies in cell cultures and suggests that *trans*-azodopa may act as a dopamine agonist also in the mouse brain.⁵⁹ The general excitatory action of azodopa was modulated by UV light in individual neurons, some of which revealed a decrease in spiking activity while others increased it. These heterogeneous responses to D₂-like receptor activation in wildtype animals bear physiological relevance and are currently being studied.

DISCUSSION

Understanding the dopaminergic system dynamics is a central question in neurobiology and neuropharmacology. In fact, DARs are involved in the modulation of fundamental physiological functions such as voluntary movement, motivation, cognition, emotion, reward, and neuroendocrine secretion, among others, and a dysregulation of the dopaminergic transmission is unavoidably associated with major psychiatric and neurological disorders. However, the available techniques to dissect neuronal circuits and their role in pathological conditions have several shortcomings. Electrical stimulation lacks cellular specificity and conventional pharmacological manipulation lacks temporal and spatial resolution.⁶⁰ Optogenetic tools allow the modulation of specific neural circuit elements with millisecond precision, but are limited by non-uniform expression of the optogenetic actuators and generation of non-physiological patterns of activity throughout the targeted population of neurons. Here we introduce a novel photopharmacological agonist that enables reversible spatiotemporal control of intact dopaminergic pathways *in vivo*. We show that azodopa triggers DAR-mediated cAMP accumulation and ERK1/2 phosphorylation as well as phospholipase C activation in its *trans* configuration, and its efficacy can be reduced or switched off under illumination. Accordingly, azodopa allows the reversible photocontrol of zebrafish motility on a time scale of seconds, increasing the swimming activity exclusively in the *trans* active state. Azodopa can be bath-applied, does not require microinjection or genetic manipulation and is compatible with high throughput behavioral screening in wildtype or transgenic fish, and with other treatments including pharmacological ones. For example, the inactivity of blinded larvae under control conditions can be risen to levels comparable to normal (untreated) animals by adding *trans*-azodopa in the water without illumination. In addition, locomotion is reduced to control levels upon photoisomerization to the *cis* form, which suggests that azodopa might be used to interfere with extracellular dopamine/melatonin cycles in the retina involved in circadian rhythms.³ Furthermore, the intriguing observation that DAR activation by azodopa *cis-trans* isomerization (dark relaxation) produces faster behavioral responses in normal fish than in blinded ones offers new opportunities to interrogate the dopaminergic modulation of retinal circuits with spatiotemporal, pharmacological, and cell-type specificity.⁶¹ Our results thus complement recently reported genetic-

photopharmacological agonists,¹⁵ photopharmacological antagonists,²⁵ and caged dopaminergic ligands,⁶⁸ and open the way to dissect dopaminergic neurotransmission in intact animals. Characterizing in detail the pharmacological profile and safety of azodopa was not the aim of this work but experiments with zebrafish in the presence of a selective antagonist suggested that D₁-like receptors are the main mediators of the photocontrolled behavior.

trans-Azodopa also exerts excitatory actions on brain cortical microcircuits at firing rates and frequency bands relevant for behavior in mice.⁶² In agreement with our *in vitro* studies, azodopa induced a general increase in neural excitability, although the time course and light dependence of the responses was heterogeneous in individual neurons. We identified cortical neurons with light-ON and dark-ON patterns, which is expected when administering in the intact brain an agonist of dopamine receptors that are expressed both in excitatory and inhibitory neurons. These responses must be characterized further, but it must be noted that isoflurane anesthesia produces profound inhibitory effects on brain activity. The activity of neural networks may be more difficult to modulate under anesthesia than during alertness, which prompts to evaluate the effects of azodopa under light/dark regimes in awake mice.

From a photochromic point of view, azodopa displays a short half-life of thermal relaxation, which is useful in neurobiology since a single wavelength of light allows to rapidly toggle the photoswitch between its two isomers. However, azodopa requires UV light for deactivation, which is normally undesired in photopharmacology because of poor tissue penetration and potential phototoxicity. Moreover, azodopa is active in the most thermodynamically stable configuration (*trans*). Although there are clinical conditions that might take advantage of a dark-active drug that can be deactivated on demand (e.g. to reduce levodopa-induced dyskinesia in Parkinson's disease),⁶³ light-activatable compounds are generally preferred for research and clinical purposes. Hence, new dopaminergic photoswitches must be developed that are active in the less thermodynamically stable configuration⁶⁴ and photoisomerize with visible⁶⁵ or infrared light^{66,67} in order to unleash their full potential as photopharmacological tools.

In summary, azodopa is a photochromic activator of endogenous dopamine receptors that does not require genetic manipulation, as well as the first photoswitchable dopaminergic agonist with demonstrated efficacy *in vivo* in intact wild-type animals, including mammals. This ligand allows analyzing the different components of the dopaminergic circuitry and is a breakthrough to develop new photoswitchable drugs potentially useful to manage neurological conditions, including movement disorders and addiction.

AUTHOR INFORMATION

(*) Corresponding Author: pau@icrea.cat

(#) P.C., V.C.-A., and R.S. contributed equally.

Author Contributions: C.M. designed and synthesized azodopa. C.M. and J.H. conducted spectroscopic studies. V.C.-A., E.M., V.C. and R.S. performed *in vitro* studies. C.M., A.M.J.G., D.C., S.C.-B. and M.M. performed behavioral studies. P.C., T.G., C.D., and P.N. performed electrophysiological recordings in mice. P.C., P.N. and M.V.P. analyzed electrophysiological data in mice. P.G., M.V.P. and V.C. supervised the project. P.G., M.V.P. and V.C. acquired funding and administered the project. P.G. conceived and designed the research. C.M. and P.G. wrote the manuscript with contribution from all authors. All authors have given approval to the final version of the manuscript.

Notes: The authors declare no competing financial interest.

DATA AVAILABILITY

The datasets generated during and/or analysed during the current study are available from the corresponding author on reasonable request.

ACKNOWLEDGMENTS

The authors wish to thank Ewa Blasiak (Jagiellonian University, Kraków) for donating the plasmid encoding the human D₁ receptor, Marcin Kolaczowski and Adam Bucki (Jagiellonian University, Kraków) for providing the homology model of the D₁ dopamine receptor, Fabio Riefolo (IBEC Barcelona) for his help with HPLC analyses, and Jordi Ortiz (Autonomous University of Barcelona) for useful discussions. Molecular graphics and analyses were performed with the UCSF Chimera package. Chimera is developed by the Resource for Biocomputing, Visualization, and Informatics at the University of California, San Francisco (supported by NIGMS P41-GM103311). Mass spectrometry was performed at the IRB Barcelona Mass Spectrometry Core Facility, which actively participates in the BMBS European COST Action BM 1403 and is a member of Proteored, PRB2-ISCIII, supported by grant PRB2 (IPT13/0001 – ISCIII/GEFI/ FEDER). This project has received funding from the EU Horizon 2020 Framework Programme for Research and Innovation (Human Brain Project WaveScaleS, Specific Grant Agreement 2 No. 785907; NEUROPA project, Grant Agreement No. 863214), AGAUR/Generalitat de Catalunya (CERCA Programme), Ministerio de Economía y Competitividad and European Regional Development Funds (Grant no. SAF2017-87629-R to V.C., SAF2016-80726-R to M.V.P., and SAF2017-88076-R to M.M.), Generalitat de Catalunya (Grant no. 2017-SGR-1497 to V.C., 2017-SGR-210 to M.V.P., and 2017-SGR-00465 to J.H.). CECH project. The CECH project is co-financed by the European Union Regional Development Fund within the framework of the ERDF Operational Program of Catalonia 2014-2020 with a grant of 50% of total eligible cost. All experiments on animals were conducted according to the European Directive 2010/63/EU and Spanish regulations RD 53/2013 for the care and use of laboratory animals. Experiments on mice were authorized by the PRBB Animal Research Ethics Committee and the local government.

REFERENCES

1. Beaulieu, J.-M. & Gainetdinov, R. R. The physiology, signaling, and pharmacology of dopamine receptors. *Pharmacol. Rev.* **63**, 182–217 (2011).
2. Tritsch, N. X. & Sabatini, B. L. Dopaminergic modulation of synaptic transmission in cortex and striatum. *Neuron* **76**, 33–50 (2012).
3. Firsov, M. L. & Astakhova, L. A. The Role of Dopamine in Controlling Retinal Photoreceptor Function in Vertebrates. *Neurosci Behav Physiol* **46**, 138–145 (2015).
4. Korshunov, K. S., Blakemore, L. J. & Trombley, P. Q. Dopamine: A Modulator of Circadian Rhythms in the Central Nervous System. *Front Cell Neurosci* **11**, 91 (2017).
5. Puig, M. V. & Miller, E. K. The role of prefrontal dopamine D1 receptors in the neural mechanisms of associative learning. *Neuron* **74**, 874–886 (2012).
6. Puig, M. V. & Miller, E. K. Neural Substrates of Dopamine D2 Receptor Modulated Executive Functions in the Monkey Prefrontal Cortex. *Cereb. Cortex* **25**, 2980–2987 (2015).
7. Beaulieu, J.-M., Espinoza, S. & Gainetdinov, R. R. Dopamine receptors - IUPHAR Review 13. *Br. J. Pharmacol.* **172**, 1–23 (2015).
8. Lerch, M. M., Hansen, M. J., van Dam, G. M., Szymanski, W. & Feringa, B. L. Emerging Targets in Photopharmacology. *Angew. Chem. Int. Ed. Engl.* **55**, 10978–10999 (2016).
9. Hübl, K., Morstein, J. & Trauner, D. In Vivo Photopharmacology. *Chem. Rev.* **118**, 10710–10747 (2018).
10. PIANOWSKI, Z. L. *Molecular Photoswitches: Synthesis, Properties, and Applications*. (VCH, 2021).
11. Pittolo, S. *et al.* An allosteric modulator to control endogenous G protein-coupled receptors with light. *Nat. Chem. Biol.* **10**, 813–815 (2014).
12. Agnetta, L. *et al.* Fluorination of Photoswitchable Muscarinic Agonists Tunes Receptor Pharmacology and Photochromic Properties. *J. Med. Chem.* **62**, 3009–3020 (2019).
13. Riefolo, F. *et al.* Optical Control of Cardiac Function with a Photoswitchable Muscarinic Agonist. *J. Am. Chem. Soc.* **141**, 7628–7636 (2019).
14. Prischich, D. *et al.* Adrenergic Modulation With Photochromic Ligands. *Angew. Chem. Int. Ed. Engl.* **60**, 3625–3631 (2021).
15. Donthamsetti, P. *et al.* Cell specific photoswitchable agonist for reversible control of endogenous dopamine receptors. *Nature Communications* **12**, 4775–13 (2021).
16. Berizzi, A. E. & Goudet, C. Strategies and considerations of G-protein-coupled receptor photopharmacology. *Adv Pharmacol* **88**, 143–172 (2020).
17. Bregestovski, P., Maleeva, G. & Gorostiza, P. Light-induced regulation of ligand-gated channel activity. *Br. J. Pharmacol.* **172**, 5870 (2017).

18. Izquierdo-Serra, M. *et al.* Optical control of endogenous receptors and cellular excitability using targeted covalent photoswitches. *Nature Communications* **7**, 12221 (2016).
19. Szymanski, W., Ourailidou, M. E., Velema, W. A., Dekker, F. J. & Feringa, B. L. Light-Controlled Histone Deacetylase (HDAC) Inhibitors: Towards Photopharmacological Chemotherapy. *Chemistry - A European Journal* **21**, 16517–16524 (2015).
20. Matera, C. *et al.* Photoswitchable Antimetabolite for Targeted Photoactivated Chemotherapy. *J. Am. Chem. Soc.* **140**, 15764–15773 (2018).
21. Steinberg, E. E. & Janak, P. H. Establishing causality for dopamine in neural function and behavior with optogenetics. *Brain Res.* **1511**, 46–64 (2013).
22. Stauffer, W. R. *et al.* Dopamine Neuron-Specific Optogenetic Stimulation in Rhesus Macaques. *Cell* **166**, 1564–1571.e6 (2016).
23. Chang, C. Y. *et al.* Brief optogenetic inhibition of dopamine neurons mimics endogenous negative reward prediction errors. *Nat. Neurosci.* **19**, 111–116 (2016).
24. Hare, B. D. *et al.* Optogenetic stimulation of medial prefrontal cortex Drd1 neurons produces rapid and long-lasting antidepressant effects. *Nature Communications* **10**, 223–12 (2019).
25. Donthamsetti, P. C. *et al.* Optical Control of Dopamine Receptors Using a Photoswitchable Tethered Inverse Agonist. *J. Am. Chem. Soc.* **139**, 18522–18535 (2017).
26. Araya, R., Andino-Pavlovsky, V., Yuste, R. & Etchenique, R. Two-photon optical interrogation of individual dendritic spines with caged dopamine. *ACS Chem Neurosci* **4**, 1163–1167 (2013).
27. Gienger, M., Hübner, H., Löber, S., König, B. & Grmeiner, P. Structure-based development of caged dopamine D2/D3 receptor antagonists. *Sci Rep* **10**, 829 (2020).
28. Lachmann, D. *et al.* Photochromic Dopamine Receptor Ligands Based on Dithienylethenes and Fulgides. *Chemistry - A European Journal* **23**, 13423–13434 (2017).
29. Szymanski, W., Beierle, J. M., Kistemaker, H. A. V., Velema, W. A. & Feringa, B. L. Reversible photocontrol of biological systems by the incorporation of molecular photoswitches. *Chem. Rev.* **113**, 6114–6178 (2013).
30. Broichhagen, J., Frank, J. A. & Trauner, D. A Roadmap to Success in Photopharmacology. *Acc. Chem. Res.* **48**, 1947–1960 (2015).
31. Schoenberger, M., Damijonaitis, A., Zhang, Z., Nagel, D. & Trauner, D. Development of a new photochromic ion channel blocker via azologization of fomocaine. *ACS Chem Neurosci* **5**, 514–518 (2014).
32. Borowiak, M. *et al.* Photoswitchable Inhibitors of Microtubule Dynamics Optically Control Mitosis and Cell Death. *Cell* **162**, 403–411 (2015).
33. Morstein, J., Awale, M., Reymond, J.-L. & Trauner, D. Mapping the Azolog Space Enables the Optical Control of New Biological Targets. *ACS Cent Sci* **5**, 607–618 (2019).
34. Casagrande, C. & Bertolini, G. in *Perspectives in Receptor Research* **24**, 67–84 (Elsevier, 1996).
35. Rodenhuis, N. New, centrally acting dopaminergic agents with an improved oral bioavailability: synthesis and pharmacological evaluation. (s.n., 2000).
36. Pettersson, I. & Liljefors, T. Structure-activity relationships for apomorphine congeners. Conformational energies vs. biological activities. *Journal of Computer-Aided Molecular Design* **1**, 143–152 (1987).
37. Cannon, J. G., Borgman, R. J., Aleem, M. A. & Long, J. P. Centrally acting emetics. 7. Hofmann and Emde degradation products of apomorphine. *J. Med. Chem.* **16**, 219–224 (1973).
38. Malo, M., Brive, L., Luthman, K. & Svensson, P. Investigation of D₃ receptor-agonist interactions using a combination of pharmacophore and receptor homology modeling. *ChemMedChem* **7**, 471–82–338 (2012).
39. Malo, M., Brive, L., Luthman, K. & Svensson, P. Investigation of D₁ receptor-agonist interactions and D₄/D₂ agonist selectivity using a combination of pharmacophore and receptor homology modeling. *ChemMedChem* **7**, 483–94–338 (2012).
40. Kolaczkowski, M., Bucki, A., Feder, M. & Pawlowski, M. Ligand-optimized homology models of D₁ and D₂ dopamine receptors: application for virtual screening. *Journal of Chemical Information and Modeling* **53**, 638–648 (2013).
41. Garcia-Amorós, J., Sánchez-Ferrer, A., Massad, W. A., Nonell, S. & Velasco, D. Kinetic study of the fast thermal cis-to-trans isomerisation of para-, ortho- and polyhydroxyazobenzenes. *Phys Chem Chem Phys* **12**, 13238–13242 (2010).
42. Izquierdo-Serra, M. *et al.* Two-photon neuronal and astrocytic stimulation with azobenzene-based photoswitches. *J. Am. Chem. Soc.* **136**, 8693–8701 (2014).
43. Ferré, S. *et al.* G protein-coupled receptor oligomerization revisited: functional and pharmacological perspectives. *Pharmacol. Rev.* **66**, 413–434 (2014).
44. Casadó, V. *et al.* Useful pharmacological parameters for G-protein-coupled receptor homodimers obtained from competition experiments. Agonist-antagonist binding modulation. *Biochem. Pharmacol.* **78**, 1456–1463 (2009).
45. Jin, L.-Q., Wang, H.-Y. & Friedman, E. Stimulated D1 dopamine receptors couple to multiple G α proteins in different brain regions. *J. Neurochem.* **78**, 981–990 (2001).
46. Chiken, S. *et al.* Dopamine D1 Receptor-Mediated Transmission Maintains Information Flow Through the Cortico-Striato-Entopeduncular Direct Pathway to Release Movements. *Cereb. Cortex* **25**, 4885–4897 (2015).
47. Basnet, R. M., Zizioli, D., Taweedet, S., Finazzi, D. & Memo, M. Zebrafish Larvae as a Behavioral Model in Neuropharmacology. *Biomedicines* **7**, 23 (2019).
48. Howe, K. *et al.* The zebrafish reference genome sequence and its relationship to the human genome. *Nature* **496**, 498–503 (2013).
49. Kalueff, A. V., Stewart, A. M. & Gerlai, R. Zebrafish as an emerging model for studying complex brain disorders. *Trends Pharmacol. Sci.* **35**, 63–75 (2014).
50. Lange, M. *et al.* The ADHD-susceptibility gene *lphn3.1* modulates dopaminergic neuron formation and locomotor activity during zebrafish development. *Mol. Psychiatry* **17**, 946–954 (2012).

51. Ek, F. *et al.* Behavioral Analysis of Dopaminergic Activation in Zebrafish and Rats Reveals Similar Phenotypes. *ACS Chem Neurosci* **7**, 633–646 (2016).
52. Levitas-Djerbi, T. & Appelbaum, L. Modeling sleep and neuropsychiatric disorders in zebrafish. *Curr. Opin. Neurobiol.* **44**, 89–93 (2017).
53. Irons, T. D., Kelly, P. E., Hunter, D. L., Macphail, R. C. & Padilla, S. Acute administration of dopaminergic drugs has differential effects on locomotion in larval zebrafish. *Pharmacol. Biochem. Behav.* **103**, 792–813 (2013).
54. Ingebretson, J. J. & Masino, M. A. Quantification of locomotor activity in larval zebrafish: considerations for the design of high-throughput behavioral studies. *Front Neural Circuits* **7**, 109 (2013).
55. Raymond, P. A., Barthel, L. K. & Curran, G. A. Developmental patterning of rod and cone photoreceptors in embryonic zebrafish. *J. Comp. Neurol.* **359**, 537–550 (1995).
56. Guggiana-Nilo, D. A. & Engert, F. Properties of the Visible Light Phototaxis and UV Avoidance Behaviors in the Larval Zebrafish. *Front Behav Neurosci* **10**, 160 (2016).
57. Taylor, S., Chen, J., Luo, J. & Hitchcock, P. Light-induced photoreceptor degeneration in the retina of the zebrafish. *Methods Mol. Biol.* **884**, 247–254 (2012).
58. Kaufman, D. M. & Milstein, M. J. in *Kaufman's Clinical Neurology for Psychiatrists* 501–525 (Elsevier, 2013). doi:10.1016/B978-0-7234-3748-2.00021-9
59. Roffman, J. L. *et al.* Dopamine D1 signaling organizes network dynamics underlying working memory. *Sci Adv* **2**, e1501672 (2016).
60. Nieh, E. H., Kim, S.-Y., Namburi, P. & Tye, K. M. Optogenetic dissection of neural circuits underlying emotional valence and motivated behaviors. *Brain Res.* **1511**, 73–92 (2013).
61. Roy, S. & Field, G. D. Dopaminergic modulation of retinal processing from starlight to sunlight. *J Pharmacol Sci* **140**, 86–93 (2019).
62. Alemany-González, M. *et al.* Prefrontal-hippocampal functional connectivity encodes recognition memory and is impaired in intellectual disability. *Proc. Natl. Acad. Sci. U.S.A.* **117**, 11788–11798 (2020).
63. Aubert, I. *et al.* Increased D1 dopamine receptor signaling in levodopa-induced dyskinesia. *Ann. Neurol.* **57**, 17–26 (2005).
64. Cabré, G. *et al.* Synthetic Photoswitchable Neurotransmitters Based on Bridged Azobenzenes. *Org. Lett.* **21**, 3780–3784 (2019).
65. Garrido-Charles, A. *et al.* Fast photoswitchable molecular prosthetics control neuronal activity in the cochlea. *bioRxiv* 2021.05.25.445123 (2021). doi:10.1101/2021.05.25.445123
66. Pittolo, S. *et al.* Reversible silencing of endogenous receptors in intact brain tissue using 2-photon pharmacology. *Proc. Natl. Acad. Sci. U.S.A.* **116**, 13680–13689 (2019).
67. Cabré, G. *et al.* Rationally designed azobenzene photoswitches for efficient two-photon neuronal excitation. *Nature Communications* **10**, 907–12 (2019).
68. Sitkowska K. *et al.* Red-light-sensitive BODIPY photoprotecting groups for amines and their biological application in controlling heart rhythm. *Chem. Commun. (Camb)* **56**:5480–5483 (2020).

SUPPLEMENTARY INFORMATION

Reversible photocontrol of dopaminergic transmission in wild-type animals

Carlo Matera^{1,2,3}, Pablo Calvé^{4,5}, Verónica Casadó-Anguera^{5,6}, Rosalba Sortino^{1,2,8}, Alexandre M. J. Gomila^{1,2}, Estefania Moreno⁵, Thomas Gener⁸, Cristina Delgado⁴, Pau Nebot⁴, Davide Costazza¹, Sara Conde-Berriozabal⁶, Mercè Masana⁵, Jordi Hernando⁷, Vicent Casadó⁵, M. Victoria Puig⁴, Pau Gorostiza^{1,2,8,*}

1. Institute for Bioengineering of Catalonia (IBEC), The Barcelona Institute for Science and Technology, Barcelona 08028, Spain
2. Biomedical Research Networking Center in Bioengineering, Biomaterials and Nanomedicine (CIBER-BBN), Madrid 28029, Spain
3. Department of Pharmaceutical Sciences, University of Milan, 20133 Milan, Italy
4. Hospital del Mar Medical Research Institute (IMIM), Barcelona Biomedical Research Park, Barcelona 08003, Spain
5. Department of Biochemistry and Molecular Biomedicine, Faculty of Biology, Institute of Biomedicine of the University of Barcelona, University of Barcelona, Barcelona, Spain
6. Department of Biomedical Sciences, Faculty of Medicine and Health Sciences, Institute of Neuroscience, University of Barcelona, IDIBAPS, CIBERNED, Barcelona, Spain
7. Department of Chemistry, Autonomous University of Barcelona (UAB), Cerdanyola del Vallès 08193, Spain
8. Catalan Institution for Research and Advanced Studies (ICREA), 08010 Barcelona, Spain

Equal contribution

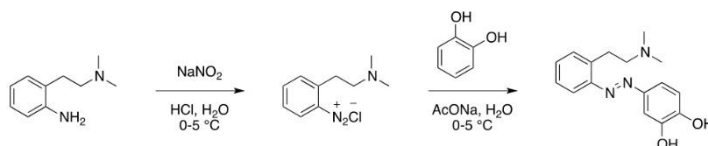
TABLE OF CONTENTS

1. Chemical Synthesis & Characterization
2. Photochemical Characterization
3. Radioligand Binding Assays
4. cAMP Accumulation Assays
5. ERK Phosphorylation Assays
6. Ca²⁺ Imaging Assays
7. Behavioral Assays in Zebrafish
8. Electrophysiological Recordings in Mice
9. Azodopa Resistance to Photodegradation
10. Recovery of Normal Swimming Behavior of Zebrafish Larvae after Washout
11. Additional References

1. Chemical Synthesis & Characterization

All chemicals and solvents are from commercial suppliers and used without purification. Reactions were monitored by thin layer chromatography (TLC: EMD/Millipore, silica gel 60 on aluminium support, layer thickness: 200 μm , particle size: 10-12 μm) by visualisation under 254 and/or 365 nm lamp. Nuclear magnetic resonance spectrometry (NMR): Varian-Mercury 400 MHz. Chemical shifts (δ) are reported in parts per million (ppm) against the reference compound tetramethylsilane using the signal of the residual non-deuterated solvent [Methanol- d_4 $\delta = 3.31$ ppm (^1H), $\delta = 49.00$ ppm (^{13}C)]. High-performance Liquid Chromatography (HPLC) apparatus: Waters Alliance 2695 separation module coupled to Waters 2996 photodiode detector (PDA) with MassLynx 4.1 software for data acquisition; XSelect CSH C18 OBD Preparative Column (130 \AA , 5 μm , 10 mm X 150 mm); mobile phase: water w/0.1% formic acid (solvent A) and acetonitrile w/0.1% formic acid (solvent B); elution method: flow 3 mL/min, gradient 0.0-1.0 min, 0% B; 1.0-7.0 min, 0-100% B; 7.0-8.0min, 100% B; 8.0-9.0 min, 100-0% B; 9.0-10.0 min, 0% B; runtime 10 min. Mass spectroscopy (MS) apparatus: Waters ACQUITY QDa detector (single quad mass detector) equipped with an electrospray ionization (ESI) interface. Spectra have been scanned between 100 and 1000 Da with values every 0.1 seconds and peaks are given as mass/charge (m/z) ratio. High resolution mass spectrometry analyses were performed with a LTQ-FT Ultra Mass Spectrometer (Thermo Scientific) with NanoESI positive ionization. A sample of the final compound was reconstituted in 100 μL of MeOH and diluted 1/100 with $\text{CH}_3\text{CN}/\text{H}_2\text{O}$ /formic acid (50:50:1) for MS analysis. The sample was introduced by direct infusion (Automated Nanoelectrospray). The NanoMate (Advion BioSciences, Ithaca, NY, USA) aspirated the samples from a 384-well plate (protein Lobind) with disposable, conductive pipette tips, and infused the samples through the nanoESI Chip (which consists of 400 nozzles in a 20x20 array) towards the mass spectrometer. Spray voltage was 1.70 kV, delivery pressure 0.50 psi and m/z range 50-2000 Da. Data were acquired with Xcalibur software, vs.2.0SR2 (ThermoScientific). Elemental composition from experimental exact mass monoisotopic value was obtained with a dedicated algorithm integrated in Xcalibur software. Data are reported as mass-to-charge ratio (m/z) of the corresponding positively charged molecular ion.

Synthetic Procedure. Azodopa was prepared in fair yield (about 63%) via an azo coupling reaction between freshly diazotized 2-(2-(dimethylamino)ethyl)aniline and 1,2-dihydroxybenzene (**Scheme S1**).



Scheme S1. Chemical synthesis of azodopa.

4-((2-(2-(dimethylamino)ethyl)phenyl)diazenyl)benzene-1,2-diol [azodopa]. In a round-bottom flask, to a mixture of 2-(2-(dimethylamino)ethyl)aniline (165 mg, 1.00 mmol) in water (3 mL) was added concentrated HCl (0.4 mL), and the obtained solution was cooled to 0-5 °C. A precooled solution (0-5 °C) of NaNO₂ (76 mg, 1.10 mmol) in water (0.5 mL) was added dropwise to the first solution under vigorous stirring and the resulting mixture was stirred for 30 min at 0-5 °C. The so-obtained yellowish aqueous solution of 2-(2-(dimethylamino)ethyl)benzenediazonium chloride was then added dropwise into a second round-bottom flask containing a mixture of 1,2-dihydroxybenzene (332 mg, 3.00 mmol) and sodium acetate (907 mg, 11.00 mmol) in water (3 mL) at 0-5 °C under vigorous stirring. This final mixture was then allowed to slowly warm up to room temperature and stirred for 12 h (reaction color turned from yellow to dark orange/red). The reaction crude was filtered and then directly purified by reverse-phase HPLC (see the general section above for details) to provide azodopa as a dark orange formate salt (63% yield; purity ≥ 98% as determined by HPLC-PDA analysis).

NMR data are given for the *trans* isomer.

¹H NMR (400 MHz, Methanol-*d*₄) δ 8.54 (s, 1H), 7.65 (dd, *J* = 7.9, 1.3 Hz, 1H), 7.48 – 7.38 (m, 4H), 7.35 (ddd, *J* = 7.9, 6.7, 2.1 Hz, 1H), 6.93 (d, *J* = 8.4 Hz, 1H), 3.51 – 3.40 (m, 2H), 3.15 – 3.05 (m, 2H), 2.71 (s, 6H).

¹³C NMR (101 MHz, Methanol-*d*₄) δ 169.95, 151.61, 151.08, 148.20, 147.30, 136.53, 131.92, 131.84, 129.31, 121.15, 116.78, 116.01, 107.52, 60.08, 43.61, 27.83.

*R*_t (HPLC-PDA) = 6.53 min (*trans*).

HRMS (*m/z*) calculated for C₁₆H₂₀N₂O₂⁺ [M+H]⁺: 286.1550, found: 286.1546 (Δ_{ppm} = -1.41).

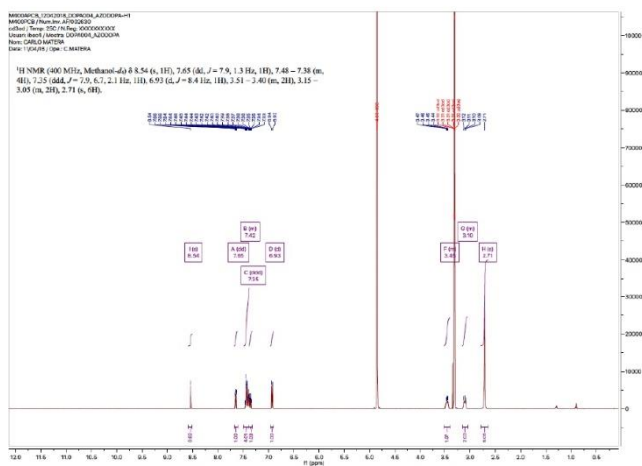
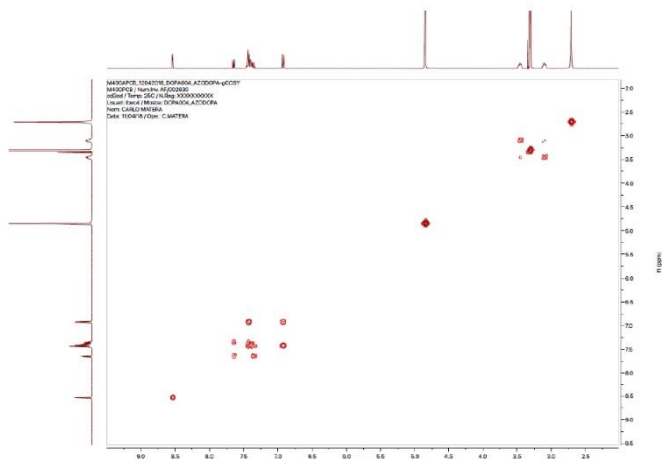
Figure S1. ¹H-NMR spectrum of azodopa.

Figure S2. gCOSY spectrum of azodopa.

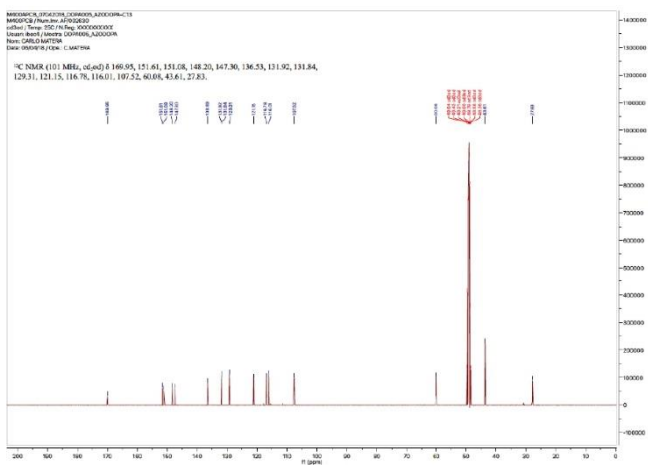
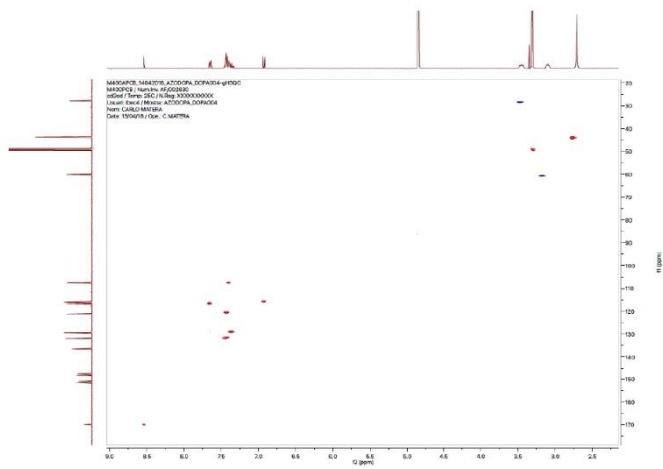
Figure S3. ¹³C-NMR spectrum of azodopa.

Figure S4. gHSQC NMR spectrum of azodopa.

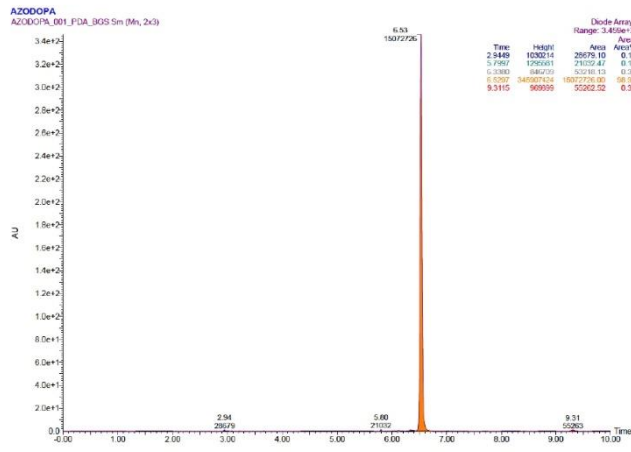


Figure S5. HPLC-PDA chromatogram of azodopa.

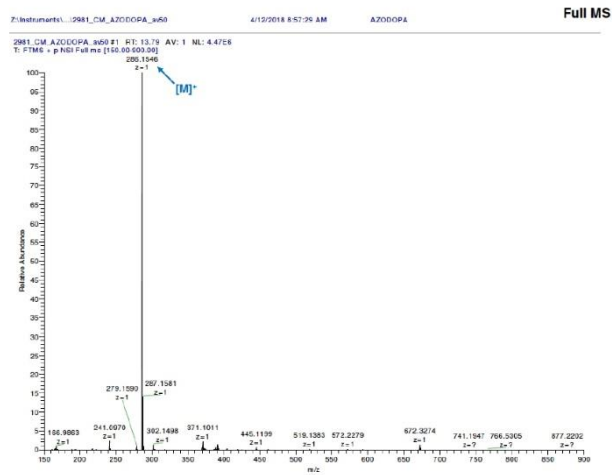


Figure S6. High-resolution mass spectrum of azodopa.

2. Photochemical Characterization

Steady-state UV-Vis spectra were recorded with a Shimadzu UV-1800 UV-VIS Spectrophotometer using standard quartz cuvettes (10 mm optical path). Photoisomerization was accomplished by irradiating azodopa with a Viber Lourmat UV Lamp (365 nm, 6 W) for 1–3 min. Transient absorption measurements were recorded with a nanosecond laser flash photolysis system (LKII, Applied Photophysics) equipped with a Nd:YAG laser (Brilliant, Quantel) as pump source ($\lambda_{exc} = 355$ nm), a Xe lamp as probe source, and a photomultiplier tube (PMT, R928, Hamamatsu) coupled to a spectrograph as detector. Thermal relaxation half-life was estimated applying an exponential one-phase decay model (GraphPad Prism 6).

The thermal relaxation half-life of the *cis* isomer is about 200 μ s and thus conversion to the *trans* form occurs almost immediately after turning the light off. For this reason, all biological experiments were performed under continuous illumination.

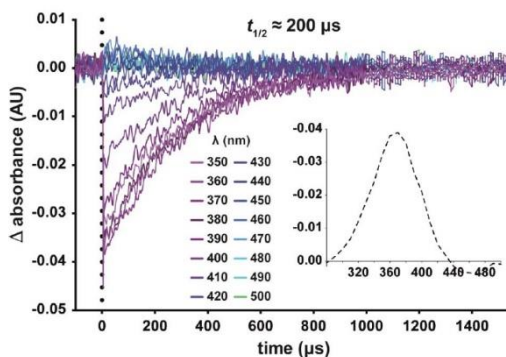


Figure S7. Photochromic behavior of azodopa investigated by transient absorption spectroscopy in water. Transient absorption time traces were measured at different wavelengths upon excitation of *trans*-azodopa (30 μ M) with a 5 ns pulsed laser at $\lambda = 355$ nm (3 mJ/pulse energy) and 25 °C. Thermal relaxation half-life of the *cis*-isomer (200 μ s) was estimated applying an exponential one-phase decay model (GraphPad Prism 6). Inset: Transient absorption spectrum of *trans*-azodopa upon pulsed irradiation at $\lambda = 355$ nm recorded at $t = 0$ μ s. X-values represent wavelength (nm), Y-values represent ΔA (arbitrary units, AU).

3. Radioligand Binding Assays

Brains of male and female sheep of 4-6 months old were freshly obtained from the local slaughterhouse. Brain striatum was disrupted with a Polytron homogenizer (PTA 20 TS rotor, setting 3; Kinematica, Basel, Switzerland) for two 5 s periods in 10 volumes of 50 mM Tris-HCl buffer, pH 7.4, containing a proteinase inhibitor cocktail (Sigma, St. Louis, MO, USA). Membranes were obtained by centrifugation twice at 105 000 g for 45 min at 4 °C. The pellet was stored at -80 °C, washed once more as described above and resuspended in 50 mM Tris-HCl buffer for immediate use. Membrane protein was quantified by the bicinchoninic acid method (Pierce Chemical Co., Rockford, IL, USA) using bovine serum albumin dilutions as standard. Binding experiments were performed with membrane suspensions at room temperature in 50 mM Tris-HCl buffer, pH 7.4, containing 10 mM MgCl₂.

For D₁-like receptor competition-binding assays, membrane suspensions (0.2 mg of protein/ml) were incubated for 90 min with a constant free concentration of 1 nM (non-irradiated curve) or 3 nM (irradiated curve) of the D₁-like receptor antagonist [³H]SCH23390 (PerkinElmer, Wellesley, MA, USA) and increasing concentrations of azodopa (from 1 nM to 100 μM). For saturation-binding assays, membrane suspensions (0.2 mg of protein/ml) were incubated for 2 h at room temperature in 50 mM Tris-HCl buffer, pH 7.4, containing 10 mM MgCl₂ with increasing concentrations of the D₁-like receptor antagonist [³H]SCH23390 (from 0.08 to 7.5 nM of free radioligand concentration for the irradiated curve and from 0.02 to 2.3 nM of free radioligand concentration for the non-irradiated curve) (K_{DA1}(dark): 0.3 ± 0.1* nM, K_{DA1}(UV): 1.6 ± 0.6 nM, (*) p < 0.05 vs UV, unpaired t-test, n=5). Non-specific binding was determined in the presence of 20 μM of non-labeled SCH23390. Even though both competition curves appear similar, due to the lower affinity of the radioligand upon illumination (Figure S8a), we calculated an almost 4-fold decrease in affinity at 365 nm (see Table S1).

For D₂-like receptor competition-binding assays, membrane suspensions (0.2 mg of protein/ml) were incubated for 2 h with a constant free concentration of 0.8 nM of the D₂ antagonist [³H]YM-09151-2 (K_{DA1} = 0.30 nM) and increasing concentrations of azodopa. Nonspecific binding was determined in the presence of 30 μM of dopamine because at this concentration dopamine does not displace the radioligand from sigma receptors.

During the incubation period, incubates were irradiated or not with UV light. Experiments under illumination were performed by continuously irradiating with a Vilber Lourmat transilluminator (model ECX-F20.L, 365 nm, 6 x 8 W). In both binding assays, free and membrane-bound ligands were separated by rapid filtration of 500 μl aliquots in a cell harvester (Brandel, Gaithersburg, MD, USA) through Whatman GF/C filters embedded in 0.3% polyethylenimine that were subsequently washed for 5 s with 5 ml of ice-cold 50 mM Tris-HCl buffer. The filters were incubated with 10 mL of Ultima Gold MV scintillation cocktail (PerkinElmer) overnight at room temperature and radioactivity counts were determined using a Tri-Carb 2800 TR scintillation counter (PerkinElmer) with an efficiency of 62%.

Data were analyzed according to the “dimer model” developed by Casadó and collaborators.¹ The model assumes GPCR dimers as a main functional unit and provides a more robust analysis of parameters obtained from saturation and competition experiments with orthosteric ligands, as compared with the commonly used “two-independent-site model”.^{1,2} The equation describing the saturation experiment in non-cooperative conditions is:

$$A_{\text{bound}} = \frac{2 A R_T}{2K_{DA1} + A}$$

where A represents the radioligand concentration, R_T the total number of dimers (being B_{max} = 2R_T), and K_{DA} the affinity of the radioligand.

To calculate the macroscopic equilibrium dissociation constants from competition experiments, when A and the competitor B are both non-cooperative and there is non-allosteric modulation between A and B, the following equation was applied:

$$A_{\text{bound}} = \frac{\left(4 K_{DA1} A + 2 A^2 + \frac{2 K_{DA1} A B}{K_{DB1}}\right) R_T}{4 K_{DA1}^2 + 4 K_{DA1} A + A^2 + \frac{2 K_{DA1} A B}{K_{DB1}} + \frac{4 K_{DA1}^2 B}{K_{DB1}} + \frac{K_{DA1}^2 B^2}{K_{DB1}^2}}$$

where B represents the assayed competing compound concentration and K_{DB} the affinity of the competing ligand.

Radioligand competition and saturation curves were analyzed by nonlinear regression using the commercial Grafit curve-fitting software (Erithacus Software, Surrey, UK), by fitting the binding data to the mechanistic dimer receptor model, as described in detail elsewhere.³

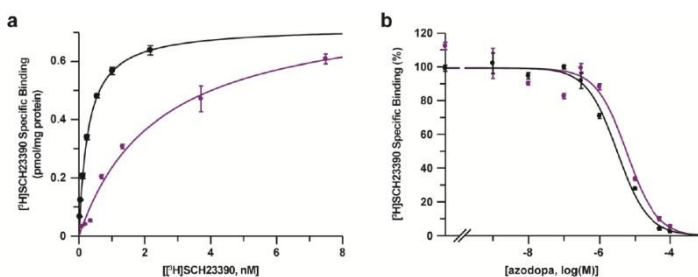


Figure S8. (a) Radioligand saturation binding experiments. Saturation experiments for D_1 in sheep brain striatum membranes. Saturation assays (0.2 mg protein/ml) were performed, and data were fitted as indicated above. These experiments were performed with increasing concentrations of the D_1 antagonist [³H]SCH23390 in the presence (purple) or absence (black) of UV irradiation during the incubation period of 1 h. Data are mean \pm S.E.M. values from a representative experiment performed in triplicate. Affinity values of [³H]SCH23390 appear in Table S1. **(b) Radioligand competition binding experiments.** Competition experiments for D_1 in sheep brain striatum membranes. Competition assays (0.2 mg protein/ml) were performed, and data were fitted as indicated above. The D_1 antagonist [³H]SCH23390 at 1 nM was displaced with increasing concentrations of azodopa in the presence (purple) or absence (black) of UV irradiation during the incubation period. Data are mean \pm S.E.M. values from a representative experiment performed in triplicate. 100% of [³H]SCH23390 specific binding = 1.1 ± 0.1 pmol/mg protein ($n = 9$ experiments performed in triplicate). Affinity values of azodopa (K_{DB}) appear in Table S1.

	D_1 (*)	D_2 (*)
dark	K_{DB} : 600 ± 100 nM	K_{DB} : 210 ± 30 nM
UV	K_{DB} : 2200 ± 600 nM	K_{DB} : 900 ± 300 nM

Table S1. Binding affinity of azodopa for D_1 and D_2 in the dark and under illumination. Affinity values obtained by fitting data from competition experiments of [³H]SCH23390 and [³H]YM-09151-2 vs azodopa to the dimer receptor model. Data are mean \pm S.E.M. from 3–5 experiments performed with different striatal homogenates of 3–4 animals. Statistical differences between the values obtained were calculated by an unpaired t-test. (*) $p < 0.05$ for affinity under UV vs in dark.

In conclusion, we found that azodopa has 3-fold greater affinity for D_2 -like than D_1 -like receptors, and in both cases the affinity is higher in the dark (*trans* isomer).

4. cAMP Accumulation Assays

Cell culture and transfection. For cAMP determinations, the human receptor construct of D_1 receptor fused to full-length yellow variant of green fluorescent protein (EYFP) was used.⁴ 2 μ g of plasmid cDNA was transfected into HEK-293T cells using polyethylenimine (Sigma-Aldrich) in 25-cm² cell culture flasks. Cells were maintained in culture with Dulbecco's modified Eagle's medium (Sigma-Aldrich) supplemented with 2

mM L-glutamine, MEM nonessential amino acid solution (1/100), 100U/ml penicillin/streptomycin, and 5% (vol/vol) of heat-inactivated fetal bovine serum and kept in an incubator at 37 °C and 5% CO₂. All experiments were performed approximately 48 hours after transfection.

Experimental protocol. Homogeneous time-resolved fluorescence energy transfer (HTRF) assays were performed using the Lance Ultra cAMP kit (PerkinElmer), based on competitive displacement of a europium chelate-labelled cAMP tracer bound to a specific antibody conjugated to acceptor beads. We first established the optimal cell density which provides a response that covers most of the dynamic range of the cAMP standard curve. Thus, 1200 cells in growing in medium containing 30 µM zardaverine were put into each well of a white ProxiPlate 384-well microplate (PerkinElmer). Cells were pretreated or not with the D₁-like receptor antagonists SKF83566 (Tocris) for 5 min before the activation with azodopa for 15 min. During these 15 minutes, cells were irradiated or not with UV light to induce the *trans/cis* isomerization of the compound. Experiments under illumination were performed by continuously irradiating with a Vilber Lourmat transilluminator (model ECX-F20.L, 365 nm, 6 x 8 W). Fluorescence at 665 nm was analyzed on a PHERAstar Flagship microplate reader equipped with an HTRF optical module (BMGLab technologies, Offenburg, Germany). cAMP assays were also performed in non-transfected HEK-293T cells. In these cells, the effect of azodopa at 10 µM, dopamine at 1 µM and the D₁-like receptor agonist SKF38393 at 300 nM was tested to ensure that all the effects observed were D₁-dependent. Statistical differences were analyzed by two-way ANOVA followed by Tukey's post-hoc test (GraphPad Prism 6).

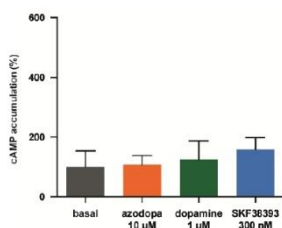


Figure S9. Effect of D₁ agonists on the adenylyl cyclase activity in non-transfected HEK-293T cells. As a negative control experiment, cAMP accumulation was determined in non-transfected HEK-293T cells activated with the D₁ dopamine agonists azodopa (10 µM, orange), dopamine (1 µM, green) or SKF38393 (300 nM, blue) for 15 minutes. Values are represented in % vs basal levels (gray) of cAMP. Data are mean ± S.E.M. of 3 experiments performed in quadruplicate.

5. ERK Phosphorylation Assays

Cell culture and transfection. For ERK1/2 phosphorylation determinations, the human receptor construct of D₁ receptor fused to full-length yellow variant of green fluorescent protein (EYFP) was used.⁴ 2 µg of plasmid cDNA was transfected into HEK-293T cells using polyethylenimine (Sigma-Aldrich) in 25 cm² cell culture flasks. Cells were maintained in culture with Dulbecco's modified Eagle's medium (Sigma-Aldrich) supplemented with 2 mM L-glutamine, MEM nonessential amino acid solution (1/100), 100U/ml penicillin/streptomycin, and 5% (vol/vol) of heat-inactivated fetal bovine serum and kept in an incubator at 37 °C and 5% CO₂. All experiments were performed approximately 48 hours after transfection.

Experimental protocol. The day of the experiment, cells were starved by treating them with serum free media for 3-4 h at 37 °C. After that, cells were incubated with the indicated antagonist for 5 min and then, with azodopa for 7 min at 37 °C. As for cAMP assays, cells were irradiated or not with UV light during the azodopa incubation. Experiments under illumination were performed by continuously irradiating with a Vilber Lourmat transilluminator (model ECX-F20.L, 365 nm, 6 x 8 W). Then, cells were rinsed with ice-cold

phosphate-buffered saline and lysed by adding 200 μ l ice-cold lysis buffer (50 mM Tris-HCl [pH 7.4], 50 mM NaF, 150 mM NaCl, 45 mM β -glycerophosphate, 1% Triton X-100, 20 mM phenyl-arsine oxide, 0.4 mM NaVO₄, and protease inhibitor cocktail). The cellular debris was removed by centrifugation at 13 000 g for 5 min at 4 °C, and the protein was quantified. To determine the level of ERK1/2 phosphorylation, equivalent amounts of protein were separated by electrophoresis on a denaturing 10% SDS polyacrylamide gel and transferred onto polyvinylidene difluoride membranes. Odyssey blocking buffer (LI-COR Biosciences, Lincoln, NE) was then added, and the membrane was rocked for 90 minutes. The membranes were then probed with a mixture of a mouse anti-phospho-ERK1/2 antibody (1:2500; Sigma-Aldrich) and rabbit anti-ERK1/2 antibody that recognizes both phosphorylated and nonphosphorylated ERK1/2 (1:40000; Sigma-Aldrich) overnight at 4 °C. The 42- and 44-kDa bands corresponding to ERK1 and ERK2 were visualized by the addition of a mixture of IRDye 800 (anti-mouse) antibody (1:10000; Sigma-Aldrich) and IRDye 680 (anti-rabbit) antibody (1:10000; Sigma-Aldrich) for 2 hours and scanned by the Odyssey infrared scanner (LICOR Biosciences). Band densities were quantified using the scanner software and exported to Excel (Microsoft, Redmond, WA). The level of phosphorylated ERK1/2 isoforms was normalized for differences in loading using the total ERK1/2 protein band intensities. Statistical differences were analyzed by two-way ANOVA followed by Tukey's post-hoc test (GraphPad Prism 6).

6. Ca²⁺ Imaging Assays

Cell culture and transfection. HEK-293T cells were purchased from the European Collection of Authenticated Cell Culture. Cells were maintained at 37 °C in a humidified atmosphere with 5% CO₂ and grown in Dulbecco's Modified Eagle's Medium (DMEM) and Ham's F-12 Nutrient Mixture (DMEM/F12 1:1, Life Technologies), supplemented with 10% fetal bovine serum (FBS, Life Technologies) and antibiotics (1% penicillin/streptomycin, Sigma-Aldrich). Plasmid pcDNA 3.1 (+) encoding human D₁ receptor was obtained as a kind gift from Ewa Błasiak (Department of Physical Biochemistry, Jagiellonian University, Kraków, Poland). Transient expression of the human D₁ dopamine receptor and the genetically encoded calcium indicator R-GECO-1 (Addgene) (ratio1:1) was induced by using the X-tremeGENE 9 DNA Transfection Reagent (Roche Applied Science) following the manufacturer's instructions. The day after, cells were harvested with Accutase® (Sigma-Aldrich) and seeded onto 16 mm glass coverslips (Fisher Scientific) pretreated with poly-L-Lysine (Sigma-Aldrich) to favor cell adhesion. Preconfluent cultures were used for experiments at 48–72 hours after transfection.

Experimental protocol. The bath solution used for single cell intracellular calcium recordings contained: 140 mM NaCl, 5.4 mM KCl, 1 mM MgCl₂, 10 mM HEPES, 10 mM glucose and 2 mM CaCl₂, and was adjusted to pH 7.40 with aqueous NaOH. Before each experiment, cells were mounted on the recording chamber (Open Diamond Bath Imaging Chamber for Round Coverslips from Warner Instruments). Cells were rinsed with fresh solution, and the recording chamber was filled with 1 ml recording solution and placed on an IX71 inverted microscope (Olympus) with a XLUMPLFLN 20XW x20/1 water immersion objective (Olympus). R-GECO1 was excited during 50 ms at 562 nm by using a Polychrome V light source (Till Photonics) equipped with a Xenon Short Arc lamp (Ushio) and a 585 nm dichroic beam splitter (Chroma Technology). Emission at 600 nm was filtered by ET630/75nm emission filter (Chroma Technology) and finally collected by a C9100-13 EM-CCD camera (HAMAMATSU). Images were acquired at room temperature with an imaging interval of 4 s with the SmartLux software (HEKA). Imaging analysis was performed with FIJI (ImageJ). Dopamine (50 μ M, Sigma-Aldrich) was used as agonist to stimulate D₁ receptors expressed in HEK-293T cells. Addition of dopamine, azodopa or vehicle (0.1% DMSO) was carried out by carefully pipetting a small volume during image acquisition into the accessory pool of the recording chamber to assure a good mixing of the solution. Photoisomerization of azodopa was achieved by continuously irradiating with a Vilber Lourmat UV Lamp (365 nm, 6 W) for 3 minutes before application. R-GECO1 is a red-shifted Ca²⁺ fluorescent indicator and it was chosen because imaging at longer wavelength minimizes the effect of the unwanted fluorescence generated by continuously illuminating the specimen with 365 nm light. Data were normalized over the maximum response obtained with dopamine at 50 μ M. The Origin 8 software was used to calculate the values of the

peak amplitude and the values of the area under the curve (AUC). AUC values correspond to the integral of the curves over each drug application interval. Statistical differences were analyzed by one-way ANOVA followed by Tukey's post-hoc test (GraphPad Prism 6).

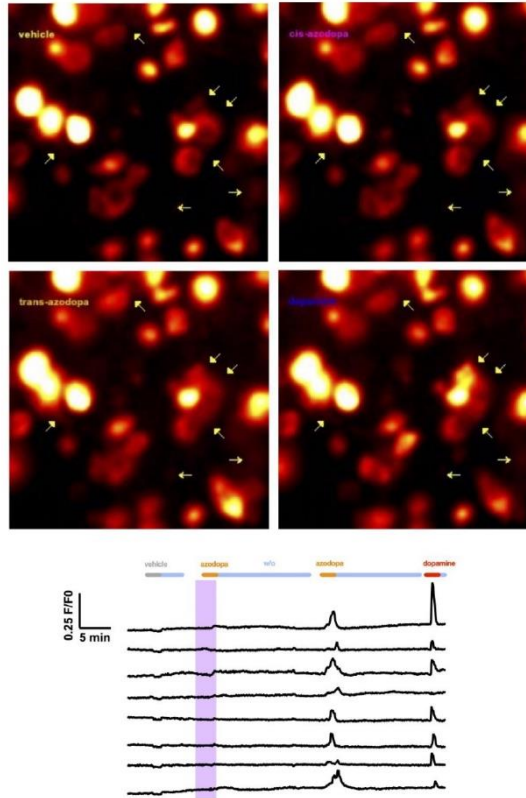


Figure S10. Effect of azodopa on D_1 -mediated intracellular calcium release. Example frames from Supplementary Movie 2 (top images; arrows indicating cells responding to *trans*-azodopa and dopamine over the time course of the experiment) and real-time calcium imaging response traces (bottom panel) in HEK-293T cells co-expressing D_1 receptors and R-GECO1 as calcium indicator. Single-cell calcium traces for 8 representative cells are shown. Traces were recorded upon direct application of azodopa ($50 \mu\text{M}$, orange bars) in the dark (white area) and under illumination (purple area). Shadow represents \pm S.E.M.'. Gray and green bars indicate the application of vehicle (control) and dopamine (reference agonist), respectively. Light blue bars indicate wash-out periods.

S12

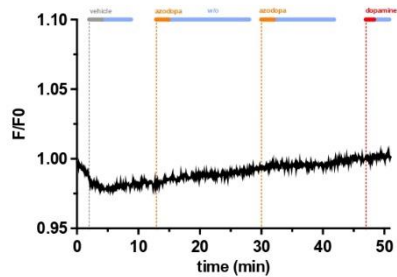


Figure S11. Calcium imaging experiments in control cells. Real-time calcium imaging in HEK-293T cells ($n = 25$) expressing R-GECO1 but not D_2 . No calcium oscillations were recorded upon the application of vehicle (gray), azodopa (orange) under illumination and in the dark, or dopamine (green). Data are mean \pm S.E.M.

7. Behavioral Assays in Zebrafish

Animal housing. Wild-type zebrafish embryos (Tupfel long-fin strain) were purchased from the animal facility of the Barcelona Biomedical Research Park (PRBB) and raised in darkness for 6 days at 28.5 °C in UV filtered tap water in Petri dishes (daily cleaned and refilled). Animal development was checked every 24 hours. Unhealthy or abnormal embryos and larvae were removed and euthanized in tricaine methanesulfonate 0.02%. All experiments and procedures were conducted according to the European Directive 2010/63/EU.

Blindness induction. For the experiments with blinded zebrafish, larvae underwent a non-invasive and highly specific blinding technique that induces photoreceptor apoptosis in the dorsal and central retina.⁵ The light-lesioning procedure was performed in a thermostatic and well-ventilated room equipped with small fans for air circulation and heat dissipation. Larvae at 5 days post-fertilization (dpf) were placed inside a 25 mm Petri dish containing 20 ml of UV filtered tap water, inserted in a closed mirrored chamber, and then exposed to 135 000 lux light emitted by a mercury lamp (model Olympus U-LH100HG) for 30 min. Temperature was monitored throughout the whole procedure.

Assay protocol. Behavioral studies were conducted on wild-type zebrafish larvae at 6 dpf. Vehicle and compounds were added with a multichannel pipette to exclude differences related to a delay in the application of each solution. Movements were recorded and analyzed using the ZebraBox tracking system and the ZebraLab software (ViewPoint Life Science, France). On the morning of the test, 6 dpf larvae were moved into a new batch of fresh water and checked for motility capabilities and possible physical mutations. Larvae were then randomly divided into control and treatment groups. Each individual was placed in a separate well of a 96 well plate, each containing 200 μ l of fresh UV filtered water and left undisturbed in the dark for 30 min to get acquainted with the new setting (habituation time). Afterwards, 100 μ l of water were removed from each well and replaced with 100 μ l of a double concentrated vehicle or treatment solution. At this point, the plate was inserted into the ZebraBox and the recording period started. Activity was recorded for a total of 62.5 min. Animals were exposed to controlled cycles of dark and 365 nm UV light, using the following protocol of illumination: dark (20 min, for adaptation), UV light (30 sec), dark (20 min), and then four cycles of UV light (30 sec) and dark (5 min). Illumination at 365 nm was performed with a built-in array of 12 LEDs placed 12 cm away from the multiwell plate. Light intensity, measured with a Newport 1916-C optical power meter coupled to a Newport 918D-SL-OD3R detector, was 5.9 mW·cm⁻². All experiments were conducted at 12.00 pm (UTC+01:00).

Tracking and analysis of swimming activity. Alterations of locomotor activity were determined by monitoring and measuring fast movements, swimming distances and duration of high-speed swimming. In particular, the dependent variables measured included: total distance travelled, distance travelled at ≤ 2 $\text{mm}\cdot\text{s}^{-1}$, distance travelled at $2\text{--}6$ $\text{mm}\cdot\text{s}^{-1}$, distance travelled at ≥ 6 $\text{mm}\cdot\text{s}^{-1}$, time spent moving, time spent freezing, and number of bursts. The arbitrary cut-off for motility (6 $\text{mm}\cdot\text{s}^{-1}$) was chosen because no variance was found among the groups at lower speeds. Total movements were not considered to limit the error of the video recording on minimal movements. Data were analyzed by two-way ANOVA with Tukey's post-hoc test or uncorrected Fisher's least significant difference test for statistical significance (GraphPad Prism 6).

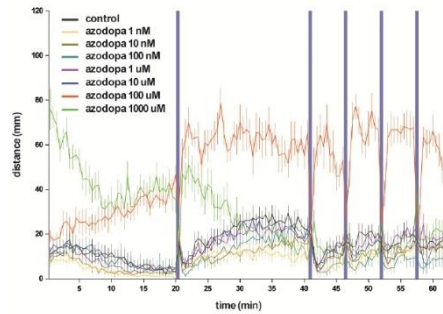


Figure S12. Effects of azodopa on the locomotor activity of zebrafish larvae. Swimming activity (distance moved over time) in larvae exposed to vehicle (control group) or azodopa in a wide range of concentrations (from 1 nM to 1 mM) in the dark (white areas) or under illumination with 365 nm light (purple bars). Up to a concentration of 10 μM azodopa, no significant differences in the locomotor activity were detected in comparison with the control group. A great increase of the swimming activity was recorded at 1 mM (green line), but the effect eventually disappeared in about 30 min, when fish were possibly exhausted. The most interesting and representative alterations of the behavioral profile were observed at 100 μM . Only fast movements (speed ≥ 6 $\text{mm}\cdot\text{s}^{-1}$) were considered and integrated every 30 s. Data are mean \pm S.E.M. ($n = 11\text{--}12$ individuals/condition).

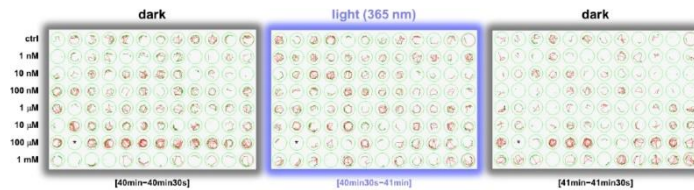


Figure S13. Tracking of zebrafish larvae movement in a 96-well plate. Trajectories of individual larvae treated with the vehicle (control group) or azodopa (from 1 nM to 1 mM) in different lighting conditions. Green lines and red lines indicate slow and fast swimming periods, respectively. Larvae treated with 100 μM azodopa show higher activity in the dark in comparison with the controls, while they returned to control levels of activity under illumination. Trajectories were extrapolated from the same experiment represented in Figure 3 (panels a–d) and Figure S12. (*) Dead larvae excluded from the analysis.

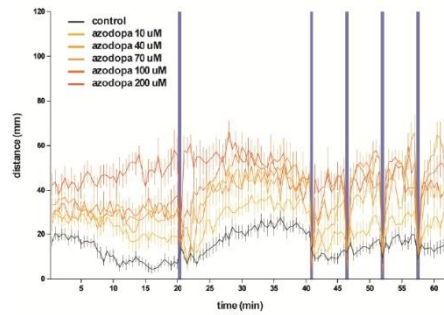


Figure S14. Effects of azodopa on the locomotor activity of zebrafish larvae. Swimming activity (distance moved over time) in larvae exposed to vehicle (control group) or azodopa in a small range of concentrations (from 10 μM to 200 μM) in the dark (white areas) or under illumination with 365 nm light (purple bars). Azodopa induced a dose-dependent increase of the swimming activity in the dark. Only fast movements (speed $\geq 6 \text{ mm}\cdot\text{s}^{-1}$) were considered and integrated every 30 s. Data are mean \pm S.E.M. ($n = 12$ individuals/condition).

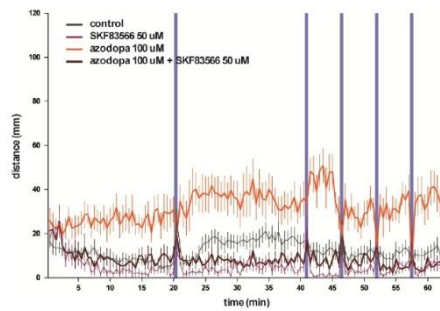


Figure S15. The effects of azodopa on zebrafish locomotor activity are counteracted by a D_2 antagonist. (a) Swimming activity (distance moved over time) in larvae exposed to vehicle (control group), azodopa (100 μM), SKF83566 (50 μM , D_2 -selective antagonist), or azodopa + SKF83566 (100 μM and 50 μM , respectively), in the dark (white areas) or under illumination with 365 nm light (purple bars). The co-application of a D_2 antagonist abolished the behavioral effects produced by azodopa, restoring a more basal level of activity (brown line), and suggesting that azodopa locomotor effects are D_2 -mediated. Only fast movements (speed $\geq 6 \text{ mm}\cdot\text{s}^{-1}$) were considered and integrated every 30 s. Data are mean \pm S.E.M. ($n = 12$ individuals/condition).

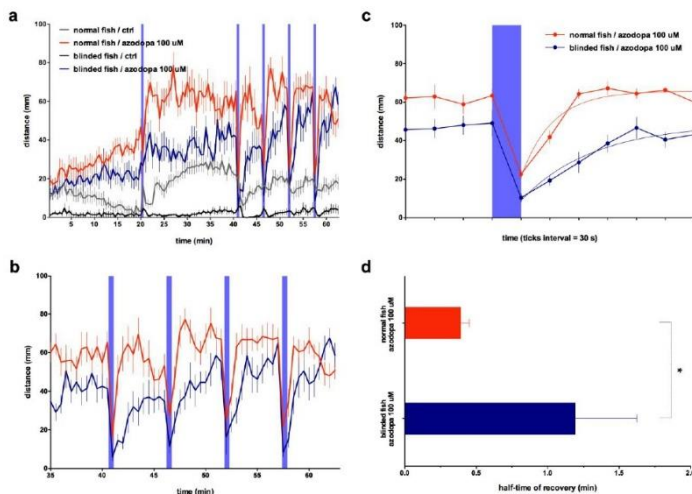


Figure S16. Azodopa produces faster behavioral responses in normal fish than in blinded fish upon *cis-to-trans* isomerization. (a) Swimming activity (distance moved over time) in normal and blinded zebrafish larvae exposed to vehicle (control group) or azodopa (100 μ M) in the dark (white areas) or under illumination with 365 nm light (purple bars). (b) Zoomed view of the last 4 dark-light cycles from panel 'a' to compare the kinetics of photoresponse in normal fish versus blinded fish. (c) Average of swimming activity (distance moved over time) in normal and blinded zebrafish larvae exposed to azodopa ($n = 11-12$ individuals/condition, 4 last consecutive dark-light-dark periods). Blinded zebrafish needed more time to recover the maximum level of activity when the light was switched off, likely because of the absence of visual response. The recovery of activity in normal and blinded fish fitted a pseudo-first-order model (non-linear regression based on one-phase association kinetics; $R^2_{\text{normal}} = 0.8553$, $R^2_{\text{blinded}} = 0.7168$; solid curves in orange and blue), with statistically different rate constants ($K_{\text{normal}} = 1.83 \pm 0.39$, $K_{\text{blinded}} = 0.80 \pm 0.35$; F test, $p < 0.05$). (d) In order to statistically compare the half-times of recovery, data points from each dark-light-dark period were analyzed independently by nonlinear regression and refitted to a one-phase association curve. The four half-times from either the normal group or the blinded group curves were then averaged and analyzed by an unpaired two-tailed t-test (* $p < 0.05$). All analyses were performed with GraphPad Prism 6.

8. Electrophysiological Recordings in Mice

Animals. Young adult male mice (C57BL/6, $n = 4$) were obtained from the local colony at the Barcelona Biomedical Research Park Animal Facility. Mice were 3 months old and weighed 20-25 g at the time of the experiments. All procedures were conducted in compliance with EU directive 2010/63/EU and Spanish guidelines (Laws 32/2007, 6/2013 and Real Decreto 53/2013) and were authorized by the local Animal Research Ethics Committee and the local government (Generalitat de Catalunya).

Surgeries. Mice were anesthetized with isoflurane at 0.5-2% and placed in a stereotaxic apparatus. A heating pad was placed between the animal and the stereotaxic frame to maintain body temperature. The level of anesthesia was regularly tested by tail-pinching, retraction of the hind paws and changes in body temperature. A craniotomy was unilaterally drilled above the secondary motor cortex (M2: AP +2.0 mm, L

0.8 mm from bregma). Dental cement was used to build a small pool around the craniotomy that contained the saline or azodopa solutions. One custom-made octrode with 8 independent electrodes (4 two-wire stereotrodes) was inserted approximately 200 μm deep into the superficial layers of the M2. The stereotrodes were made by twisting a strand of tungsten wire of 25 μm of diameter (Advent, UK) and had impedances that ranged from 100 to 400 $\text{k}\Omega$.

Electrophysiological recordings and pharmacology. Neural signals were recorded with the multi-channel Open Ephys system at a sampling rate of 30 kHz. The electrode wires were pinned to an adaptor to facilitate their connection to an Intan RHD2132 preamplifier that bandpass filtered (0.1-6 kHz) and digitized the analogic signals. These were later amplified and processed by the Open Ephys data acquisition system and finally visualized and stored in a PC via the Open Ephys GUI software. During the recordings, the exposed electrophysiological parts (octrode, adaptor, amplifier, LEDs) were shielded with aluminum foil to prevent environmental and electrical noise to interfere with the recordings. Experiments started when the anesthesia level and the electrophysiological signals were stable for 10 minutes. We recorded neural signals for 10 minutes under baseline conditions. Then, azodopa was administered with a standard 20 μl pipette at a 3 μM concentration in 10 μl volume. After the administration, the recordings started again and continued for 10 more minutes. After the experiments ended, the mice were euthanized.

Photoswitching experiments. Azodopa was photoswitched with 365 nm light from two LEDs controlled by the computer via an Arduino board (yellow arrow, Figure 4a in the main article). This allowed a precise control of the illumination periods (one-minute ON cycles) that were timestamped to the Open Ephys recording file (purple arrow, Figure 4a in the main article; results of illumination in Supplementary Figures S17-S19). In two mice, the two LEDs were placed on top of their heads so that light was directed towards the craniotomy for illumination with 365 nm light. The Arduino UNO board turned on and off the two LEDs and sent analogical triggers to the Open Ephys data acquisition system that included them as timestamps in the electrophysiological recordings. The illumination patterns consisted in one-minute ON one-minute OFF cycles. In these experiments, we first performed controls with saline, where 0.5 ml of saline were administered into the pool via an infusion pump at 0.5 ml per minute. Subsequently, the experiment was repeated with 0.5 ml 3 μM azodopa. We conducted continuous recordings that included a 5 minute baseline and 12 minute epochs after saline or azodopa administration with ON/OFF illumination cycles of UV light. The first illumination cycle started simultaneously to the drug administration (1 minute period). The goal was to inactivate azodopa while it accumulated in the pool. After the experiments ended, the mice were euthanized.

Data analysis. Recorded signals from each electrode were filtered offline to extract spiking activity and local field potentials (LFPs). Spiking activity was estimated by first subtracting the raw signal from each electrode with the mean signal of the 8 electrodes, which removed artifacts present in all the electrodes. Then, continuous signals were filtered between 450-6000 Hz with Python (Butterworth bandpass filter, order 2) and saved as NEX files. Spike sorting was performed with the Offline Sorter v4 software (Plexon Inc.). We first thresholded the signal and removed noise artifacts manually. Then, the K-means algorithm was used for automatic sorting of spikes to minimize any bias in the analyses. To obtain LFPs, signals were detrended and decimated to 1 kHz with custom-written scripts in Python. Spectrograms were constructed using the spectrogram function of the SciPy package (10 s windows, no overlap) and power was quantified with the multitaper power method of the spectral_connectivity package in Python. The taper parameters chosen for the analyses were: time-half-bandwidth product = 5, 9 tapers.

Statistical analysis. The firing rate of individual neurons was compared between baseline and azodopa and between saline and azodopa with an unpaired *t*-test (baseline vs azodopa, $n = 44$ vs 43 neurons; saline vs azodopa, $n = 57$ vs 67 neurons). For each electrode, the mean firing rate of all neurons and LFP power (1 to 10 Hz) were compared between conditions with a paired *t*-test ($n = 2$ mice, 8 electrodes per mouse). In the photoswitching experiments, the firing rates of individual neurons and LFP power were compared between the light and dark cycles with a paired *t*-test. We omitted the first light cycle (when saline or azodopa were injected) and compared the following 5 light cycles with the prior 5 dark cycles. We identified neurons that

fired more in the dark than during light cycles (dark-ON neurons) and neurons with the opposite pattern (8 light-ON neurons) in Mouse 3. Statistical analyses were conducted with the GraphPad Prism 6 statistical package.

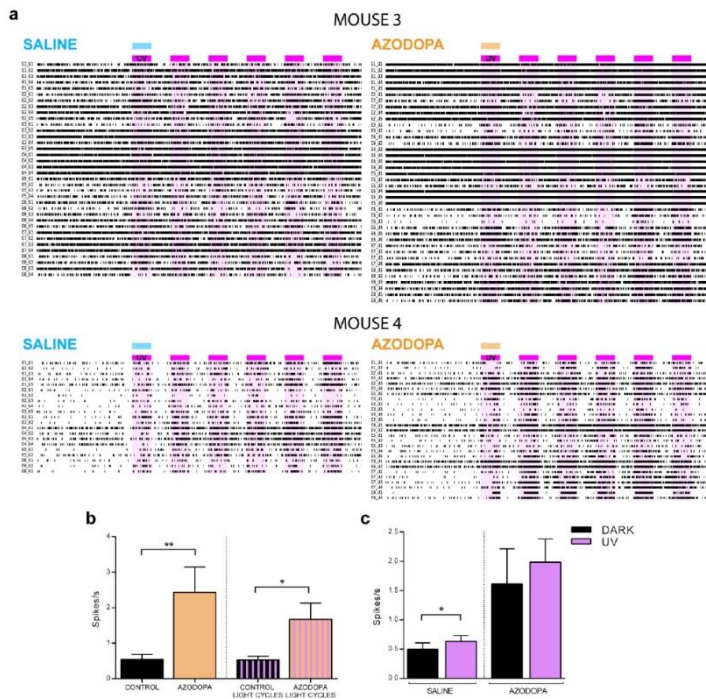


Figure S17. Effect of azodopa and illumination on spiking activity *in vivo*. (a) Raster plots of spiking activity in two mice anesthetized with isoflurane. Each row depicts the spiking activity of a single neuron (unit), each tick representing an action potential. We used arrays of 8 electrodes (octrodes) in each animal from which several units could be recorded. Neurons are labeled by their electrode number (E1 to E8). Six one-minute cycles of UV light are also shown (purple lines). Saline (0.5 ml) and azodopa (3 μ M in 0.5 ml) were administered with an infusion pump during the first light cycle (blue and orange lines). Individual neurons in the secondary motor cortex recorded after the injection of saline and azodopa were isolated offline with the Offline Sorter software. Notice that different neurons, particularly in Mouse 3, respond to illumination with opposite firing patterns, some increasing their spiking activity (light-ON pattern) while others decreasing it (dark-ON pattern; see also Figure S18 below). (b) As in Mouse 1 and Mouse 2 in the dark (solid bars on the left, data from Figure 4 in the main text), azodopa increased the firing rate of neurons with illumination in Mouse 3 and Mouse 4 (striped bars on the right, $n = 57$ neurons after saline vs 67 neurons after azodopa in two mice; mean firing rate per electrode, $n = 15$ channels, paired t -test, $^*p = 0.0246$). This increase was not significantly affected by the application of light cycles. (c) After saline, the averaged spiking rate was higher during the light than the dark cycles. After azodopa application this tendency in the averaged firing rate was maintained but not significant differences were obtained due to the cancellation of the opposing responses to light and darkness of individual neurons (see selected traces in Figure S18).

S18

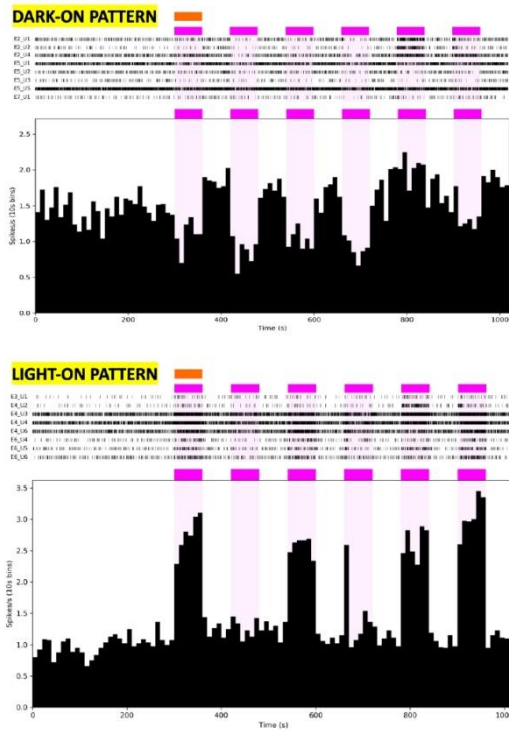


Figure S18. Individual neurons in the same mouse display opposite photoswitching patterns of spiking activity with azodopa. In Mouse 3, upon application of azodopa neurons can respond to light with opposite firing patterns, some decreasing their spiking activity during the light cycles (DARK-ON pattern, 8 pooled recordings) and others increasing it during the same cycles (LIGHT-ON pattern, 8 pooled recordings).

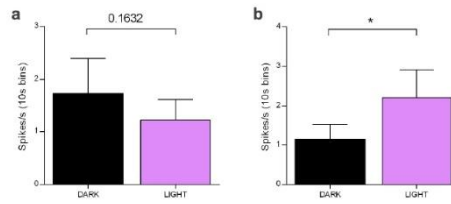


Figure S19. Photoswitching of spiking activity *in vivo* with azodopa. Quantification of the firing rate of (a) 8 neurons that decrease their spiking activity during the light cycles (dark-ON pattern) and (b) 8 neurons that increase their spiking activity during the light cycles (light-ON pattern). All neurons were recorded in Mouse 3. We compared the average spiking activity during the first 5 cycles of illumination (omitting the first cycle when azodopa was injected) with their previous 5 dark cycles (paired *t*-test; * *p* = 0.013).

9. Azodopa Resistance to Photodegradation

We verified in two ways that azodopa does not undergo significant irreversible photodegradation under the assay conditions, i.e. that the efficacy of the *trans* isomer can be maintained unaltered even after prolonged exposure to 365 nm light: (a) we analyzed a sample of azodopa by HPLC-PDA-MS before and after illumination (3 min and 60 min) (Figure S20), and (b) we compared in calcium imaging experiments the efficacy in the dark of a sample of azodopa that was pre-illuminated with 365 nm light for 60 min (named azodopa-60 for simplicity) with another sample of azodopa from the same batch but never exposed to light (Figure S21).

We did not detect any significant variation in the composition of the sample by HPLC-PDA-MS. Moreover, the efficacy in the dark of azodopa-60 was statistically not different from the efficacy of the non-illuminated sample.

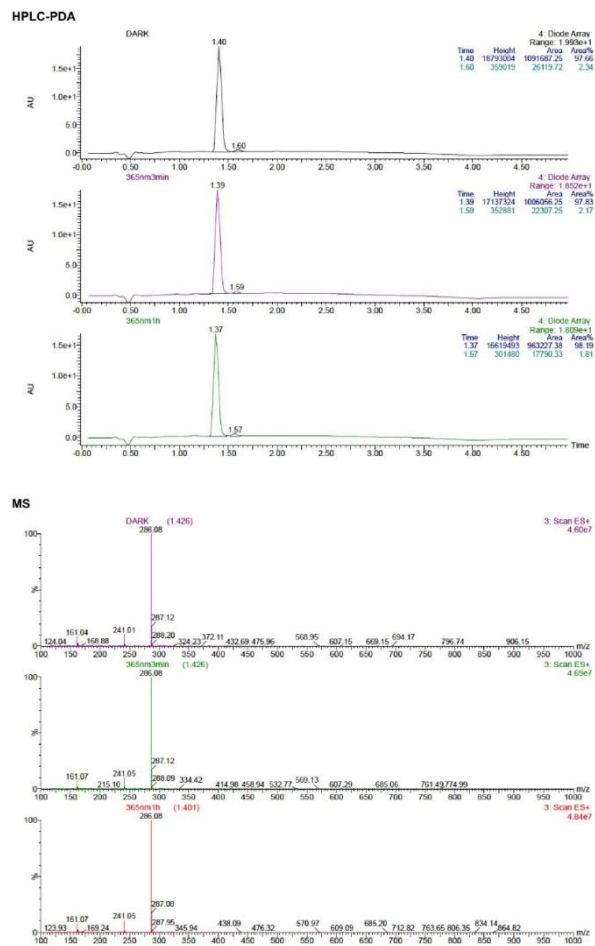


Figure S20. HPLC-PDA chromatograms and corresponding mass spectra of azodopa (50 μ M) before and after illumination with a Vilber Lourmat UV Lamp (365 nm, 6 W) for 3 min and 60 min (top: dark; middle: 365 nm, 3 min; bottom: 365 nm, 60 min). No significant variations in the composition of the sample were detected.

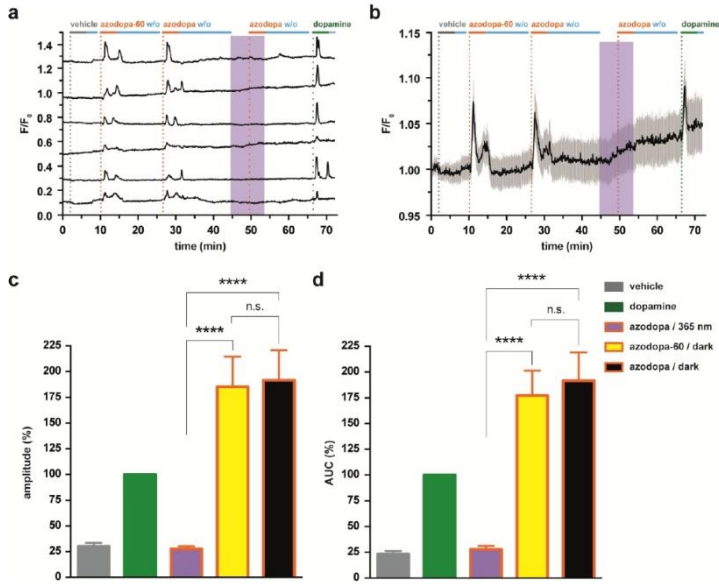


Figure S21. *trans*-Azodopa maintains its efficacy in calcium imaging experiments also after prolonged pre-exposure to ultraviolet light. Real-time calcium imaging response in HEK-293T cells co-expressing D_1 receptors and R-GECO1 as calcium indicator. (a) Single traces from 6 representative cells. (b) Averaged traces from 21 cells. Shadow represents \pm S.E.M.'. Traces were recorded upon direct application of azodopa (200 μ M, orange bars) in the dark (white areas) and under illumination (purple area). Azodopa-60 stands for "pre-irradiated azodopa" (Vilber Lourmat UV Lamp, 365 nm, 6 W, 60 min). Gray and green bars indicate the application of vehicle (control) and dopamine (reference agonist, 50 μ M), respectively. Light blue bars indicate wash-out periods. Two values of the calcium responses generated by azodopa were calculated (Origin 8 software) and compared: the peak *amplitude* $\Delta F/F_0$ (c), calculated as the difference between the maximal and the minimal intensity of each response (**** $p < 0.0001$ for azodopa/365 nm vs azodopa-60/dark; **** $p < 0.0001$ for azodopa/365 nm vs azodopa/dark), and the area under the curve (AUC) (d), calculated as the integral over the entire application time of vehicle or drugs (**** $p < 0.0001$ azodopa/365 nm vs azodopa-60/dark; **** $p < 0.0001$ for azodopa/365 nm vs azodopa/dark). Data are mean \pm S.E.M. ($n = 34$ cells from 3 independent experiments). Data were normalized over the maximum response obtained with the saturating concentration of dopamine (50 μ M) and were analyzed by one-way ANOVA followed by Tukey's post-hoc test for statistical significance. All statistical analyses were performed with GraphPad Prism 6. As shown, no statistical difference was observed between azodopa and azodopa-60 neither in amplitude nor in AUC of the calcium responses generated.

10. Recovery of Normal Swimming Behavior of Zebrafish Larvae after Washout

We demonstrated that zebrafish larvae, previously treated with azodopa 100 μ M and exposed to dark-light cycles, recover normal swimming behavior after washout (Figure S22, see caption for details). After the first experiment (panel a), the fish were transferred and maintained in fresh water for more than 1 hour, and the motility experiment was repeated using the same protocol of illumination (panel b). As shown in the figure, the two groups of fish displayed comparable swimming activity and reactivity to illumination after washout (panel b), independently if they had been previously exposed to azodopa or control solution. Moreover, all the larvae, kept in fresh water, were still alive after about 48 hours.

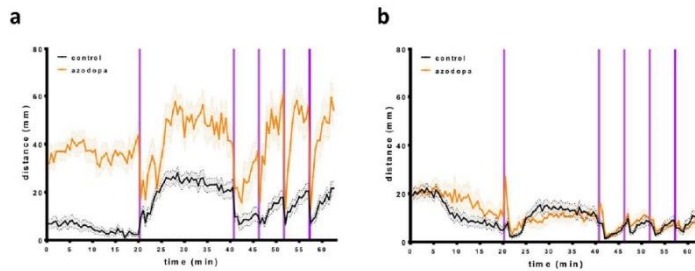


Figure S22. Recovery of normal swimming behavior of zebrafish larvae after washout. (a) Swimming activity (distance/time) in larvae exposed to vehicle (control, gray line) or 100 μ M azodopa (treatment, orange line) in the dark (white areas) or under illumination with 365 nm light (purple bars), following the same experimental procedure and illumination protocol shown in Figure 3. (b) Swimming activity (distance/time) in larvae previously exposed to vehicle (control, gray line) or 100 μ M azodopa (treatment, orange line) after washout. Washout procedure: fish were washed in fresh water (5 ml \times 5 times, in a period of >1 hour) and then added to a new 96-well plate; each individual was placed into the same well position as in the first experiment; before starting the second experiment, all larvae were disturbed by adding 100 μ l of water to each well in order to reproduce the same distress as in the first experiment (vehicle or treatment solution addition). Data are mean \pm S.E.M. (n = 24 individuals/group).

11. Additional References

- Casadó, V. *et al.* Old and new ways to calculate the affinity of agonists and antagonists interacting with G-protein-coupled monomeric and dimeric receptors: the receptor-dimer cooperativity index. *Pharmacol. Ther.* **116**, 343–354 (2007).
- Ferré, S. *et al.* G protein-coupled receptor oligomerization revisited: functional and pharmacological perspectives. *Pharmacol. Rev.* **66**, 413–434 (2014).
- Casadó, V. *et al.* Useful pharmacological parameters for G-protein-coupled receptor homodimers obtained from competition experiments. Agonist-antagonist binding modulation. *Biochem. Pharmacol.* **78**, 1456–1463 (2009).
- Ferrada, C. *et al.* Marked changes in signal transduction upon heteromerization of dopamine D1 and histamine H3 receptors. *Br. J. Pharmacol.* **157**, 64–75 (2009).
- Taylor, S., Chen, J., Luo, J. & Hitchcock, P. Light-induced photoreceptor degeneration in the retina of the zebrafish. *Methods Mol. Biol.* **884**, 247–254 (2012).



COVID-19 Incidence in Patients With Immunomediated Inflammatory Diseases: Influence of Immunosuppressant Treatments

OPEN ACCESS

Edited by:
Salvatore Salomone,
University of Catania, Italy

Reviewed by:
Philip C. Robinson,
The University of
Queensland, Australia
Jessias J. Manson,
University College London Hospitals
NHS Foundation Trust,
United Kingdom

***Correspondence:**
Rafael Maldonado
rafmaldonado@up.edu

¹These authors have contributed
equally to this work and share first
authorship

²These authors have contributed
equally to this work and share senior
authorship

³ORCID:
Rafael Maldonado
0000-0002-4359-8773

Specialty section:
This article was submitted to
Experimental Pharmacology
and Drug Discovery,
a section of the journal
Frontiers in Pharmacology

Received: 14 July 2020
Accepted: 16 October 2020
Published: 21 December 2020

Citation:
Soldevila-Domenech N, Tio L,
Llorente-Onaindia J, Martín-García E,
Nebot P, Torre Pladà, Gurt A,
Maldonado R and Monfort J (2020)
COVID-19 Incidence in Patients With
Immunomediated Inflammatory
Diseases: Influence of
Immunosuppressant Treatments.
Front. Pharmacol. 11:583260.
doi: 10.3389/fphar.2020.583260

Natalia Soldevila-Domenech^{1,2†}, Laura Tio^{3†}, Jone Llorente-Onaindia^{3†},
Elena Martín-García^{3,4}, Pau Nebot^{1,3}, Rafael de la Torre^{1,2,5}, Alba Gurt⁶,
Rafael Maldonado^{3,4,4†} and Jordi Monfort^{3,7*} and the Covidmar Study Group

¹Integrative Pharmacology and Systems Neuroscience Research Group, Neurosciences Research Program, Hospital del Mar Medical Research Institute (IMIM), Barcelona, Spain, ²Department of Experimental and Health Sciences, Universitat Pompeu Fabra (CEXS-UPF), Barcelona, Spain, ³IMIM Hospital Del Mar Medical Research Institute, PRBB, Barcelona, Spain, ⁴Laboratory of Neuropharmacology, Department of Experimental and Health Sciences, Universitat Pompeu Fabra, PRBB, Barcelona, Spain, ⁵Spanish Biomedical Research Centre in Physiopathology of Obesity and Nutrition (CIBERObsn), Instituto de Salud Carlos III (ISCIII), Madrid, Spain, ⁶CAP Via Olímpica, Parc Sanitari Pere Virgili, Barcelona, Spain, ⁷Rheumatology Services, Hospital del Mar, Barcelona, Spain

The effect of immunosuppressant treatments on the incidence of coronavirus disease (COVID-19) remains largely unknown. We studied the association between the pre-exposure to disease-modifying antirheumatic drugs (DMARDs) that decrease immunological responses and the incidence of COVID-19 to explore the possible effects of these treatments in early manifestations of the disease. For this purpose, we performed a cross-sectional study including 2,494 patients with immunomediated inflammatory diseases (IMIDs) recruited at the outpatient Rheumatology, Dermatology and Gastroenterology services of Hospital del Mar. The primary outcome was the clinical diagnosis of COVID-19 performed by a physician at the hospital or at the primary care center, from the March 1–29, 2020. Multivariable Poisson regression models were fitted to estimate COVID-19 relative risk (RR) adjusted by comorbidities. We revealed that biological (RR = 0.46, CI 95% = 0.31–0.67) and synthetic (RR = 0.62, CI 95% = 0.43–0.91) DMARDs used in IMIDs diminished the incidence of COVID-19. Striking sex differences were revealed with anti-TNF α compounds (RR = 0.50, CI 95% = 0.33–0.75) with higher effects in women (RR = 0.33, CI 95% = 0.17–0.647). Treatment with low glucocorticoid doses also revealed sex differences decreasing the incidence of COVID-19 predominantly in women (RR = 0.72, CI 95% = 0.42–1.22). Our results report a decreased incidence of COVID-19 in patients receiving specific DMARDs with different immunodepressor mechanisms with striking sex differences. These results underline the interest of repurposing specific DMARDs for the possibility of minimizing the severity of disease progression in the early stages of COVID-19.

Keywords: biological therapy, tumor necrosis factor inhibitor, cross-sectional study, relative risk, disease modifying antirheumatic drugs (DMARDs), gender, glucocorticoids

INTRODUCTION

Since December 2019, cases of severe acute respiratory syndrome coronavirus 2 (SARS-CoV-2) infection leading to a novel disease called COVID-19 were initially identified in China. SARS-CoV-2 infection causes respiratory symptoms that range from mild forms of presentation to more serious ones that can risk patients' lives, causing pneumonia, and damage to other organs, particularly the immune and blood system (Chen et al., 2020; Huang et al., 2020; Wang et al., 2020). This disease has rapidly expanded to multiple countries leading to a pandemic situation in March 2020 now affecting 7,360,239 individuals worldwide, with a global mortality of 416,201 deaths on June 11th. The situation has been dramatic in some European countries during the last months, such as Spain with 242,280 cases and 27,136 deaths (Dong et al., 2020). This official mortality numbers only reflect the casualties occurring in the hospitals, not in nursing homes or at home, and considering the low availability of accurate COVID-19 diagnostic tests, the current situation in Spain could unfortunately be worse. Furthermore, some patients are asymptomatic (Mizumoto et al., 2020; Nishiura et al., 2020) and the current prevalence reflects a possible underdiagnosis of the infection that has facilitated the disease expansion.

Immunomediated inflammatory diseases (IMIDs) are a group of unrelated and highly diverse conditions, such as rheumatoid arthritis and psoriasis, that share a common pathogenesis pathway, i.e., an immune dysregulation leading to an imbalance in inflammatory mediators. Treatments to relieve IMIDs are namely disease modifying antirheumatic drugs (DMARDs), subdivided into two main subgroups: synthetic (sDMARDs) and biological (bDMARDs). Both groups are aimed to decrease the hyperactivity of the immune system: bDMARDs are monoclonal antibodies presenting a much higher affinity and selectivity to their targets (mainly pro-inflammatory IL $_6$ and TNF α), while sDMARDs have a less selective immunosuppressant effect, except for Jak-inhibitors.

On the other side, evidence suggests that the hyperactivation of the immune response is of paramount relevance in COVID-19 progression. The accumulated knowledge about the pathophysiology of this disease reveals a crucial involvement of different molecules of the main inflammatory pathways, including interleukins 1, 6, and 8 (IL-1, IL-6, IL-8) and tumor necrosis factor alpha (TNF α). Drugs inhibiting some of these pathways have been used in the routine management of COVID-19, although results from clinical trials are still required to corroborate their effectiveness (Zhong et al., 2020). Clear examples are anti-IL-6 compounds for patients with severe forms of COVID-19 (Fu et al., 2020; Zhang et al., 2020; Zhou et al., 2020) and hydroxychloroquine, widely used and highly questioned (Adhanom Ghebreyesus, 2020; Mehra et al., 2020).

This similar physiopathology, as well as the mechanism of action of the drugs used for IMID management, has focused the attention on the study of patients suffering from IMID as a population of particular interest in the study of COVID-19 (Gianfrancesco et al., 2020a; Gianfrancesco et al., 2020b;

Favalli et al., 2020; Michelena et al., 2020; Monti et al., 2020; Salvarani et al., 2020). Patients with an autoimmune disease might be at higher risk of developing severe infections, as these medications are immunosuppressants (Memoli et al., 2014). However, this assumption has not been confirmed for SARS-CoV-2 infection, as several studies describe that the COVID-19 incidence in IMID patients is similar to the general population (Memoli et al., 2014; Favalli et al., 2020; Michelena et al., 2020; Salvarani et al., 2020). Some studies have focused on the effect of IMID treatment on COVID-19 severity in terms of hospitalization and death. Thus, systemic glucocorticoid pretreatment was reported to represent a risk factor for severe COVID-19 (OR, 6.9; 95% CI, 2.3–20.5) in patients with inflammatory bowel disease, while anti-TNF α treatment presents no association (Brenner et al., 2020). On the other hand, the COVID-19 Global Rheumatology Alliance studied the demographic and clinical factors associated with COVID-19 hospitalization in rheumatic patients and found that a ≥ 10 mg/day glucocorticoid dose was associated with a higher odds of hospitalization (OR 2.05, 95% CI 1.06–3.96), whereas anti-TNF α present a decreased incidence or hospitalizations (OR 0.40, 95% CI 0.19–0.81). No association were observed neither with DMARDs nor antimalarial use (Gianfrancesco et al., 2020a; Gianfrancesco et al., 2020b). Similar results were reported in patients using immunomodulatory therapy, regardless of the underlying disease. Indeed, a trend to a higher incidence of hospitalization was observed with chronic glucocorticoid treatment < 10 mg/day in these patients, while anti-TNF α use was associated with a reduced odd of hospitalization (Winthrop et al., 2020).

These studies generally use age-standardized rates, so they tackle the problem of comparing populations with different age structures. However, such populations may also differ considering their distribution of associated comorbidities and treatments for these comorbidities, which could influence the results. Furthermore, the majority of studies evaluated the effect of the treatment on developing severe symptoms, with limited data considering also mild to moderate symptoms. In that context, there is a need to study the COVID-19 incidence in IMID patients and the potential effect of immunosuppressants controlling for the influence of the different distribution of risk factors in order to evaluate the possibility of repurposing possible new drugs for COVID-19 therapy.

METHODS

Study Design and Population

This is a cross-sectional study aimed to evaluate the effect of different DMARDs on the accumulated incidence of COVID-19 during March 2020 in patients with IMIDs living in Barcelona (Spain). The studied population was composed of 1) patients with IMIDs taking bDMARDs (exposed patients) and 2) patients with IMIDs or other musculoskeletal diseases that were not taking bDMARDs (unexposed patients). All patients had been visited at the outpatient Rheumatology,

Dermatology and Gastroenterology services of Hospital del Mar (referral hospital from Barcelona) from September 2019 to March 2020.

The exclusion criteria were <18 years old, previous death not related with SARS-CoV-2 infection and patients tested negative for SARS-CoV-2 or without follow up at the primary care center during the studied period. The study was undertaken according to Good Clinical Practice guidelines and the Declaration of Helsinki. The research ethics review committee of Parc de Salut Mar approved the protocol (2020/9,246).

Data Collection

A comprehensive review of the medical history of eligible patients was carried out using the registry of the Catalan national health system (eCAP). This register of the health system of Catalonia is a computerized medical history program that collects the health status of each of the patients and all entries to the public primary care system are recorded in this register. In turn, this database is fed by other information systems of the public network so that it contains continuously updated information on all consultations to hospitals, emergency services, pharmacy, death certifiers and any other relevant clinical information. The Hospital del Mar also has its own program of computerized medical record called IMASIS. Both database platforms were consulted for reviewing the medical histories and both are interconnected online. The immediate updating of the data in these platforms avoids any type of information loss. A clinical history revision of the included patients was performed from the 1st to March 29, 2020, focusing mainly at patient's consulting disease, comorbidities and the treatments being currently followed by them (**Supplementary Tables S1, S2**). Briefly, diabetes, pulmonary disease, cardiovascular (CV) disease and chronic kidney disease were registered. In the case of arterial hypertension (AHT) and transplantation, they were only recorded if patients were receiving treatment with specific drugs for those comorbidities. Finally, cancer was recorded only if the patient had an active process or was following a treatment for a previous cancer, during the studied period.

The primary outcome was the clinical diagnosis of COVID-19 performed by a physician at the hospital or at the primary care center, from the 1st to March 29, 2020. In some patients, the diagnosis was complemented with a positive SARS-CoV-2 test, but in most of them it was based on clinical criteria following the Spanish health authorities' recommendations: fever (defined as axillary temperature $>37^{\circ}\text{C}$) together with shortness of breath and/or cough. If only fever was present, it was also considered as COVID-19 diagnosis if it appeared together with at least two of the following symptoms: anosmia, ageusia, rhinorrhea, diarrhea of one week of evolution, pharyngitis, odynophagia or arthromyalgia.

Statistical Analysis

To evaluate the associations between different treatments and the diagnosis of COVID-19, Poisson regression models with robust variance estimation were used to estimate relative risk (RR) and 95% confidence intervals (CI 95%). Models were adjusted by sex, age, diabetes, pulmonary disease, CV disease, chronic kidney

disease, and active cancer or treatment. Model 1 aimed to estimate the association between treatments grouped by drug type 1) bDMARDs; 2) sDMARDs; 3) glucocorticoids; 4) chronic nonsteroidal anti-inflammatory drugs (NSAIDs) and 5) anti-hypertensive drugs. Then, associations between COVID-19 symptoms were estimated by each individual treatment (with >100 exposed patients; reference category = "unexposed"; Model 2). Finally, as anti-TNF α treatments were the major group of bDMARDs, the effect of each anti-TNF α drug was estimated separately in model 3. Model three also included the effect of anti-IL17 and anti-IL23 (-12), but anti-IL6 could not be analyzed as a separate group as there were not COVID-19 symptoms reported among individuals exposed to IL-6 antagonists. Interactions between different drug types were also tested (model 4). Finally, the main treatment indications for anti-TNF α , together with the studied comorbidities (sex, age, CV disease, diabetes, pulmonary disease, kidney disease and cancer) were used to create a matched dataset with propensity score matching based on the nearest neighbor method (Ho et al., 2011). Propensity score is the probability of exposure conditional upon confounders, estimated by logistic regression. Therefore, each treated individual was matched with an untreated individual whose propensity score was closest to that of the treated subject. Statistical analyses were performed using R (R Foundation for Statistical Computing, Vienna, Austria) version 3.5.2.

RESULTS

A total of 2,544 individuals were examined for eligibility and 2,494 fulfilled inclusion/exclusion criteria and were finally included in the analysis, 902 (36.2%) men and 1,592 (63.8%) women.

Tables 1, 2 show the description of the comorbidities and treatments followed by studied population. The mean age (SD) was 58.7 (15.7) and the most prevalent underlying pathologies were spondyloarthritis (32.6%), rheumatoid arthritis (21.6%) and osteoarthritis (25.1%). Almost half of individuals had at least one of the following comorbidities: hypertension (34%), diabetes (12.1%), pulmonary disease (14%), CV disease (11%), chronic kidney disease (5%), active cancer or treatment (3%) and post-transplant (0.3%). In terms of treatments, 45% of individuals were taking bDMARDs (59% in men and 36% in women), primarily anti-TNF α (30% in total; 42% in men and 24% in women). A third of the population were exposed to sDMARDs, being methotrexate, leflunomide and chloroquine/hydroxychloroquine the most prevalent ones (22%, 5% and 5%, respectively). Glucocorticoid consumption in women was twice that in men (26% vs 13%) but, in both cases, doses of glucocorticoids higher than 10 mg/day were unusual ($<4\%$). NSAIDs and anti-hypertensive drugs were taken by the 20% and 27% of individuals, respectively. A 15.8% of the population (18.4% in women and 11.2% in men) did not take any of the registered treatments (**Supplementary Table S3**).

In the cohort of individuals exposed to bDMARDs, the presence of the main comorbidities (hypertension, pulmonary

TABLE 1 | Characteristics of the study population [N (%)].

Characteristic	All (N = 2,494)	Women (N = 1,592)	Men (N = 902)
Age [mean (SD)]	58.7 (15.7)	60.6 (15.5)	55.5 (15.6)
Primary diagnosis			
spondyloarthritis	812 (32.6%)	359 (22.6%)	453 (50.2%)
Rheumatoid arthritis	538 (21.6%)	424 (26.6%)	114 (12.6%)
Osteoarthritis	627 (25.1%)	480 (30.2%)	147 (16.3%)
Systemic autoimmune rheumatic diseases	165 (6.62%)	149 (9.36%)	16 (1.77%)
Vasculitis	59 (2.37%)	37 (2.32%)	22 (2.44%)
Other rheumatic diseases	38 (1.52%)	26 (1.63%)	12 (1.33%)
Juvenile arthritis	7 (0.28%)	4 (0.25%)	3 (0.33%)
Dermatological diseases	208 (8.34%)	82 (5.15%)	126 (14.0%)
Other	40 (1.60%)	31 (1.95%)	9 (1.00%)
Coexisting conditions			
Hypertension	858 (34.4%)	553 (34.7%)	305 (33.8%)
Diabetes	302 (12.1%)	174 (10.9%)	128 (14.2%)
Pulmonary disease	364 (14.6%)	241 (15.1%)	123 (13.6%)
CV Disease	290 (11.6%)	179 (11.2%)	111 (12.3%)
Chronic kidney disease	129 (5.17%)	76 (4.77%)	53 (5.88%)
Cancer or active treatment	70 (2.81%)	47 (2.95%)	23 (2.55%)
History of organ transplantation	8 (0.32%)	7 (0.44%)	1 (0.11%)
Any of these conditions	1,223 (49.0%)	797 (50.1%)	426 (47.2%)

disease and CV disease) was lower than in the cohort of individuals unexposed to bDMARDs. Also, their mean age (SD) was 52.2 (14.7) years, while in the cohort of unexposed to bDMARDs their mean age was 64 (15.4) years (see **Supplementary Table 4** for further details).

The total number of patients with COVID-19 diagnosis was 156. As shown in **Tables 3, 4**, those presenting clinical diagnosis of COVID-19 had less spondyloarthritis, rheumatoid arthritis or dermatological diseases, and higher osteoarthritis. The proportion of diabetics in the group of individuals with COVID-19 was 20.5%, while in the group without symptoms was 11.5%. In the case of pulmonary disease, these percentages were 22.4% and 14.1%, respectively. The proportion of patients taking bDMARDs and sDMARDs was lower in the group with COVID-19 diagnosis. Among those with a clinical diagnosis of COVID-19, 32 were confirmed by a SARS-CoV-2 test and the remaining 124 had not been tested. There were 26 individuals (8 men and 18 women) hospitalized and there were 4 deaths due to COVID-19.

Adjusted associations between different exposure variables (clinical characteristics and treatments) and COVID-19 symptoms are shown in **Tables 5, 6**. This analysis allows to control the parameters that could be playing a role in the diagnosis of COVID-19, such as sex, age, comorbidities, or treatments. Diabetes and pulmonary disease were associated with COVID-19 diagnosis, with overall RR_{adj} of 1.64 (CI 95% 1.09, 2.47) and 1.47 (CI 95% 1.02, 2.13). Regarding treatments, all bDMARDs presented an RR of 0.46 (CI 95% 0.31, 0.67) and all sDMARDs presented an RR of 0.62 (CI 95% 0.43, 0.91). Specifically, TNF- α antagonists presented RR of 0.50 (CI 95% 0.33, 0.75) in the whole population. This effect was even higher in women (RR = 0.33; CI 95% 0.17, 0.64), while in men the RR was 0.76 (CI 95% 0.41, 1.43), and given the risk difference ranging from 0.41 to 1.43, a substantial positive association was reasonably compatible with our data. All types of TNF- α

antagonists (adalimumab, certolizumab, etanercept, golimumab and infliximab) showed RR estimates <1, although the differences were only statistically significant for adalimumab (RR = 0.53, CI 95% 0.31, 0.93) and etanercept (RR = 0.37, CI 95% 0.16, 0.88). The RR of anti-IL17 was 0.20 (CI 95% 0.03–1.38) and for anti-IL23 (12) was 0.80 (CI 95% 0.39, 1.65). Methotrexate and chloroquine/hydroxychloroquine presented a RR of 0.71 (CI 95% 0.46, 1.08) and 0.76 (CI 95% 0.36, 1.62), respectively. The RR of leflunomide was 0.66 (CI 95% 0.28, 1.58) in the whole population, with higher relative risk reduction in men (RR = 0.36; CI 95% 0.07, 1.75) than in women (RR = 0.81; CI 95% 0.29, 2.87). Glucocorticoids at doses of ≤ 10 mg/day also showed a relative risk reduction in women (RR = 0.72, CI 95% 0.42, 1.22). **Figure 1** represents the adjusted RR for presenting COVID-19 symptoms according to the exposure to different treatments in men and women. The interactions between most prevalent combinations of treatments (bDMARDs + sDMARDs; bDMARDs + anti-hypertensive drugs; bDMARDs + chronic NSAIDs; sDMARDs + glucocorticoids) were included in Model 4 (**Supplementary Table S6**) and our results were most compatible with no important effects, except for the interaction between bDMARDs and cDMARDs (RR = 4.3; CI 95% 2.00, 9.25).

Finally, the crude RR using propensity score matching for the exposure to anti-TNF α was 0.80 (CI 95% 0.50, 1.30) and the adjusted RR (by anti-inflammatory ILs, methotrexate, leflunomide, chloroquine/hydroxychloroquine, glucocorticoids, ACE inhibitors, ARBs, NSAIDs) was 0.69 (CI 95% 0.38, 1.23). A description of the matched dataset is included in **Supplementary Table S7**.

DISCUSSION

Our cross-sectional study reveals that the DMARDs treatments commonly used in IMIDs are not associated with an increase in

TABLE 2 | Characteristics of the study population [N (%)].

	All (N = 2,494)	Women (N = 1,592)	Men (N = 902)
Treatments followed			
Biologic DMARDs¹	1,112 (44.6%)	579 (36.4%)	533 (59.1%)
Any TNF α antagonist	768 (30.8%)	388 (24.4%)	380 (42.1%)
Adalimumab	367 (14.7%)	163 (10.2%)	204 (22.6%)
Etanercept	183 (7.34%)	105 (6.60%)	78 (8.65%)
Infliximab	120 (4.81%)	60 (3.77%)	60 (6.65%)
Golimumab	65 (2.61%)	35 (2.20%)	30 (3.33%)
Certolizumab	33 (1.32%)	25 (1.57%)	8 (0.89%)
Any pro-inflammatory ILs antagonists	279 (11.2%)	136 (8.54%)	143 (15.9%)
IL-6 antagonists	52 (2.09%)	42 (2.64%)	10 (1.11%)
Tocilizumab	46 (1.84%)	37 (2.32%)	9 (1.00%)
Sarilumab	6 (0.24%)	5 (0.31%)	1 (0.11%)
IL-17 antagonists	69 (2.73%)	26 (1.61%)	43 (4.76%)
Brodalumab	2 (0.07%)	1 (0.04%)	1 (0.11%)
Secukinumab	51 (2.04%)	22 (1.38%)	29 (3.22%)
Ixekizumab	16 (0.64%)	3 (0.19%)	13 (1.44%)
IL-23 (12) antagonists	158 (6.31%)	68 (4.26%)	90 (9.99%)
Ustekinumab	155 (6.21%)	67 (4.21%)	88 (9.76%)
Guselkumab	3 (0.12%)	1 (0.04%)	2 (0.22%)
Any T lymphocyte antagonist	29 (1.16%)	22 (1.38%)	7 (0.78%)
Any B lymphocyte antagonist	42 (1.68%)	36 (2.26%)	6 (0.67%)
Vedolizumab	3 (0.12%)	2 (0.13%)	1 (0.11%)
Synthetic DMARDs²	850 (34.1%)	583 (36.6%)	267 (29.6%)
Methotrexate	538 (21.6%)	366 (23.0%)	172 (19.1%)
Leflunomide	116 (4.65%)	86 (5.40%)	30 (3.33%)
Chloroquine or hydroxychloroquine	115 (4.61%)	105 (6.60%)	10 (1.11%)
Azathioprine	80 (3.21%)	52 (3.27%)	28 (3.10%)
JAK inhibitors	41 (1.64%)	32 (2.01%)	9 (1.00%)
Apremilast	52 (2.09%)	20 (1.26%)	32 (3.55%)
Sulfasalazine	10 (0.40%)	7 (0.44%)	3 (0.33%)
Mycophenolate	19 (0.76%)	17 (1.07%)	2 (0.22%)
Tacrolimus	24 (0.96%)	17 (1.07%)	7 (0.78%)
Cyclosporine	3 (0.12%)	2 (0.13%)	1 (0.11%)
Dose of glucocorticoids			
≤ 10 mg/d	441 (17.7%)	347 (21.8%)	94 (10.4%)
> 10 mg/d	86 (3.45%)	62 (3.89%)	24 (2.66%)
Anti-hypertensive drugs³	684 (27.4%)	428 (26.9%)	256 (28.4%)
ACE inhibitors	397 (15.9%)	237 (14.9%)	160 (17.7%)
ARBs	293 (11.7%)	194 (12.2%)	99 (10.9%)
Chronic NSAIDs	496 (20.0%)	345 (21.7%)	153 (17.0%)

CV = cardiovascular; DMARDs = disease modifying anti-rheumatic drugs; JAK = Janus kinase; IL = interleukin; TNF = tumor necrosis factor; NSAIDs = non-steroid anti-inflammatory drugs.

ACE = angiotensin-converting enzyme; ARBs = angiotensin II receptor blockers.

¹Biologic DMARDs include TNF antagonists, pro-inflammatory ILs antagonists, vedolizumab and T and B lymphocyte antagonists.

²Synthetic DMARDs include methotrexate, JAK inhibitors, sulfasalazine, mycophenolate, tacrolimus, azathioprine, cyclosporine, chloroquine or hydroxychloroquine and leflunomide and apremilast.

³Anti-hypertensive drugs include ACE inhibitors and ARBs.

COVID-19 incidence. All the treatments analyzed in our study were not discontinued in our cohorts of patients following the previous recommendations (Gianfrancesco et al., 2020a, Gianfrancesco et al., 2020b; Haberman et al., 2020; Micheleni et al., 2020). It is important to underline that the primary outcome of our study was the manifestation of mild symptoms of COVID-19. Therefore, our results do not provide relevant information about the possible influence of these treatments in the severity of COVID-19, taking into account the low incidence of severe symptoms, hospitalizations and deaths in our cohort or early symptomatic patients. However, several studies have already reported that some IMiD treatments have a protective effect

on the incidence of developing severe symptoms, probably blocking the hyperactivation of the immune response occurring in the COVID-19 progression (Gianfrancesco et al., 2020a, Gianfrancesco et al., 2020b; Winthrop et al., 2020). Interestingly, in our study bDMARDs (RR = 0.46; CI 95% 0.31, 0.67) and sDMARDs (RR = 0.62; CI 95% 0.43, 0.91) treatment diminished the incidence of COVID-19, in agreement with previous preliminary observations (Haberman et al., 2020; Micheleni et al., 2020). Therefore these treatments are also playing a role in the capacity to be infected by SARS-CoV-2 and/or in presenting mild symptoms of COVID-19. At these early stages of the disease, the two comorbidities that significantly enhanced COVID-19 diagnosis

TABLE 3 | Distribution of COVID-19 across categories of study variables.

	All		Women		Men	
	No symptoms (N = 2,338)	Symptoms (N = 156)	No symptoms (N = 1,484)	Symptoms (N = 108)	No symptoms (N = 854)	Symptoms (N = 48)
Age [mean (SD)]	58.5 (15.7)	62.1 (16.2)	60.3 (15.5)	64.8 (15.5)	55.5 (15.5)	56.0 (16.1)
Primary diagnosis						
spondylarthritis	770 (32.9%)	42 (26.9%)	340 (22.9%)	19 (17.6%)	430 (50.4%)	23 (47.9%)
Rheumatoid arthritis	519 (22.2%)	19 (12.2%)	408 (27.5%)	16 (14.8%)	111 (13.0%)	3 (6.25%)
Osteoarthritis	563 (24.1%)	64 (41.0%)	424 (28.6%)	56 (51.9%)	139 (16.3%)	8 (16.7%)
Systemic autoimmune rheumatic diseases	159 (6.80%)	6 (3.85%)	145 (9.77%)	4 (3.70%)	14 (1.64%)	2 (4.17%)
Vasculitis	53 (2.27%)	6 (3.85%)	35 (2.36%)	2 (1.85%)	18 (2.11%)	4 (8.33%)
Other rheumatic diseases	26 (1.1%)	12 (7.69%)	22 (1.48%)	4 (3.70%)	9 (1.05%)	3 (6.25%)
Juvenile arthritis	7 (0.30%)	0 (0.00%)	4 (0.27%)	0 (0.00%)	3 (0.35%)	0 (0.00%)
Dermatological diseases	202 (8.64%)	6 (3.85%)	80 (5.39%)	2 (1.85%)	122 (14.3%)	4 (8.33%)
Other	31 (1.33%)	9 (5.77%)	26 (1.75%)	5 (4.63%)	8 (0.94%)	1 (2.08%)
Coexisting conditions						
Hypertension	788 (33.7%)	70 (44.9%)	505 (34.0%)	49 (44.4%)	283 (33.1%)	22 (45.8%)
Diabetes	270 (11.5%)	32 (20.5%)	152 (10.2%)	22 (20.4%)	118 (13.8%)	10 (20.8%)
Pulmonary disease	329 (14.1%)	35 (22.4%)	216 (14.6%)	25 (23.1%)	113 (13.2%)	10 (20.8%)
CV Disease	265 (11.3%)	25 (16.0%)	161 (10.8%)	18 (16.7%)	104 (12.2%)	7 (14.6%)
Chronic kidney disease	117 (5.00%)	12 (7.69%)	70 (4.72%)	6 (5.56%)	47 (5.50%)	6 (12.5%)
Cancer or active treatment	84 (2.74%)	6 (3.85%)	43 (2.90%)	4 (3.70%)	21 (2.46%)	2 (4.17%)
History of organ transplantation	7 (0.30%)	1 (0.64%)	6 (0.40%)	1 (0.93%)	1 (0.12%)	0 (0.00%)
Any of these conditions	1,122 (48.0%)	101 (64.7%)	728 (49.1%)	69 (63.9%)	394 (46.1%)	32 (66.7%)

in these group of patients were diabetes (RR = 1.64; CI 95% 1.09, 2.47) and pulmonary disease (RR = 1.47; CI 95% 1.02, 2.13). A large number of patients treated with bDMARDs (1,153) and sDMARDs (850 patients, 283 also receiving bDMARDs) has been included in our cohort. Therefore, the global decrease in the incidence of COVID-19 on patients treated with DMARDs has influenced the RR estimated for compounds that are supposed to not modify COVID-19 progression.

The protective effects of the anti-TNF α treatment on the incidence of COVID-19 symptoms reported in our study (RR = 0.50; CI 95% 0.33, 0.75) fully agree with the comments recently published about the urgent need of clinical trials of anti-TNF α therapy for COVID-19 (Feldmann et al., 2020; Robinson et al., 2020). Indeed, previous studies have reported that rheumatic patients treated with anti-TNF α present a decreased incidence of hospitalizations (OR 0.40, 95% CI 0.19–0.81) (Gianfrancesco et al., 2020a; Gianfrancesco et al., 2020b) and this protective effect was also observed in anti-TNF α treated patients regardless of the underlying disease (Winthrop et al., 2020). Our findings corroborate these protective effects considering the incidence of mild symptoms as the primary output of the study. Therefore, anti-TNF α treatment may have protective effects in the incidence of COVID-19 symptoms (our study), but also in the progression to severe manifestations of this disease (Gianfrancesco et al., 2020a, Gianfrancesco et al., 2020b; Winthrop et al., 2020). All together, these studies underlie the urgent need of clinical trials to obtain additional evidences of the possible efficacy of anti-TNF α treatment on COVID-19 (Robinson et al., 2020). Anti-TNF α therapy has been proposed to be initiated as early as is practicable in hospitalized patients

with COVID-19 in order to obtain the possible optimal beneficial effects (Feldmann et al., 2020).

Although the studied population was not sex-balanced (1,592 women vs. 902 men) our analyses stratified by sex also revealed potential sex differences in the effects of several immunomodulatory compounds on the incidence of COVID-19 mild symptoms. Indeed, anti-TNF α compounds showed a decreased COVID-19 incidence that was higher in women (RR = 0.33; CI 95% 0.17, 0.64) than in men (RR = 0.76; CI 95% 0.41, 1.43). Although a possible sex influence in the therapeutic effects of anti-TNF α compounds is controversial, a positive female sex influence was already reported in the prognosis of ulcerative colitis in patients treated with infliximab, an anti-TNF α monoclonal antibody (Nasuno et al., 2017). Sex differences were also revealed in our study in the effects of glucocorticoids. Taken into account the high variability of the doses of glucocorticoids used in these patients (Ruiz-Inatorza et al., 2012) and the differential effects depending on dose exposure (Meng et al., 2020), we have stratified glucocorticoid treatment in low (≤ 10 mg of prednisone or equivalent) and high doses (> 10 mg). Low glucocorticoids doses decreased COVID-19 incidence in women (RR = 0.72; CI 95% 0.42, 1.22), whereas high doses seemed to produce the opposite effect (RR = 1.62; CI 95% 0.75, 3.52).

Considering the high availability and the safety profile of low doses of glucocorticoids, this result could be of potential interest to further evaluate the possible benefits of using such low doses in women in early periods of SARS-CoV-2 infection to prevent progression of the disease. In contrast, the effects of leflunomide treatment were more clearly revealed in men (RR = 0.36; CI 95% 0.07, 1.75) than in women (RR = 0.81; CI 95% 0.29, 2.27). In line with our results, a significant clinical effect of leflunomide,

TABLE 4 | Distribution of COVID-19 across categories of study variables.

	All		Women		Men	
	No symptoms (N = 2,338)	Symptoms (N = 156)	No symptoms (N = 1,484)	Symptoms (N = 108)	No symptoms (N = 854)	Symptoms (N = 48)
Treatments followed	—	—	—	—	—	—
Biologic DMARDs¹	1,070 (45.8%)	42 (26.9%)	560 (37.7%)	19 (17.6%)	510 (59.7%)	23 (47.9%)
Any TNF α antagonist	739 (31.5%)	29 (18.5%)	378 (25.5%)	10 (9.26%)	361 (42.3%)	19 (39.6%)
adalimumab	353 (15.1%)	14 (8.97%)	159 (10.7%)	4 (3.70%)	194 (22.7%)	10 (20.8%)
Etanercept	178 (7.61%)	5 (3.21%)	104 (7.01%)	1 (0.93%)	74 (8.67%)	4 (8.33%)
Infliximab	114 (4.88%)	6 (3.85%)	57 (3.84%)	5 (4.62%)	57 (6.67%)	3 (6.25%)
golimumab	63 (2.69%)	2 (1.28%)	34 (2.29%)	1 (0.93%)	29 (3.40%)	1 (2.08%)
certolizumab	31 (1.33%)	2 (1.28%)	24 (1.62%)	1 (0.93%)	7 (0.82%)	1 (2.08%)
All pro-inflammatory ILs antagonists	269 (11.5%)	10 (6.41%)	130 (8.76%)	6 (5.56%)	139 (16.3%)	4 (8.33%)
IL-6 antagonists	52 (2.22%)	0 (0.00%)	42 (2.83%)	0 (0.00%)	10 (1.17%)	0 (0.00%)
IL-17 antagonists	68 (2.91%)	1 (0.64%)	26 (1.75%)	0 (0.00%)	42 (4.92%)	1 (2.08%)
IL-12/23 antagonists	149 (6.37%)	9 (5.77%)	62 (4.18%)	6 (5.56%)	87 (10.2%)	3 (6.25%)
T lymphocyte antagonists	27 (1.15%)	2 (1.28%)	20 (1.35%)	2 (1.85%)	7 (0.82%)	0 (0.00%)
B lymphocyte antagonists	42 (1.80%)	0 (0.00%)	36 (2.43%)	0 (0.00%)	6 (0.70%)	0 (0.00%)
vedolizumab	2 (0.09%)	1 (0.64%)	1 (0.07%)	1 (0.93%)	1 (0.12%)	0 (0.00%)
Synthetic DMARDs²	807 (34.5%)	43 (27.6%)	553 (37.3%)	30 (27.8%)	254 (29.7%)	13 (27.1%)
Methotrexate	510 (21.8%)	28 (17.9%)	348 (23.5%)	18 (16.7%)	162 (19.0%)	10 (20.8%)
Leflunomide	111 (4.75%)	5 (3.21%)	82 (5.53%)	4 (3.70%)	29 (3.40%)	1 (2.08%)
Apremilast	51 (2.18%)	1 (0.64%)	19 (1.28%)	1 (0.93%)	32 (3.76%)	0 (0.00%)
Chloroquine or hydroxychloroquine	108 (4.62%)	7 (4.49%)	99 (6.67%)	6 (5.56%)	9 (1.05%)	1 (2.08%)
JAK inhibitors	39 (1.67%)	2 (1.28%)	30 (2.02%)	2 (1.85%)	9 (1.05%)	0 (0.00%)
Sulfasalazine	9 (0.38%)	1 (0.64%)	7 (0.47%)	0 (0.00%)	2 (0.23%)	1 (2.08%)
Mycophenolate	18 (0.77%)	1 (0.64%)	16 (1.08%)	1 (0.93%)	2 (0.23%)	0 (0.00%)
Tacrolimus	22 (0.94%)	2 (1.28%)	15 (1.01%)	2 (1.85%)	7 (0.82%)	0 (0.00%)
Azathioprine	77 (3.29%)	3 (1.92%)	50 (3.37%)	2 (1.85%)	27 (3.16%)	1 (2.08%)
Cyclosporine	3 (0.13%)	0 (0.00%)	2 (0.13%)	0 (0.00%)	1 (0.12%)	0 (0.00%)
Glucocorticoids	—	—	—	—	—	—
≤ 10 mg/d	415 (17.8%)	26 (16.7%)	330 (22.2%)	17 (15.7%)	85 (9.95%)	9 (18.8%)
> 10 mg/d	77 (3.29%)	9 (5.77%)	55 (3.71%)	7 (6.48%)	22 (2.58%)	2 (4.17%)
Anti-hypertensive drugs³	631 (27.0%)	53 (34.0%)	391 (26.3%)	37 (34.3%)	240 (28.1%)	16 (33.3%)
ACE inhibitors	375 (16.0%)	22 (14.1%)	221 (14.9%)	16 (14.8%)	154 (18.0%)	6 (12.5%)
ARBs	260 (11.1%)	33 (21.2%)	172 (11.6%)	22 (20.4%)	88 (10.3%)	11 (22.9%)
Chronic NSAIDs	461 (19.7%)	37 (23.7%)	320 (21.6%)	25 (23.1%)	141 (16.5%)	12 (25.0%)
COVID-19 status	—	—	—	—	—	—
SARS-CoV-2 test	—	—	—	—	—	—
Not tested	0 (0.00%)	122 (78.21%)	0 (0.00%)	87 (80.56%)	0 (0.00%)	35 (72.92%)
Positive	0 (0.00%)	34 (21.79%)	0 (0.00%)	21 (19.44%)	0 (0.00%)	13 (27.08%)
Hospitalization due to COVID-19	0 (0.00%)	26 (16.67%)	0 (0.00%)	18 (16.7%)	0 (0.00%)	8 (16.67%)
Deaths due to COVID-19	0 (0.00%)	4 (2.56%)	0 (0.00%)	2 (1.85%)	0 (0.00%)	2 (4.17%)

CV = cardiovascular; DMARDs = disease modifying anti-rheumatic drugs; JAK = Janus kinase; IL = interleukin; TNF = tumor necrosis factor; NSAIDs = non-steroid anti-inflammatory drugs; ACE = angiotensin-converting enzyme; ARBs = angiotensin II receptor blockers.

¹Biologic DMARDs include anti-TNF α , pro-inflammatory ILs antagonists, vedolizumab and T and B lymphocyte antagonists.

²Synthetic DMARDs include methotrexate, JAK inhibitors, sulfasalazine, mycophenolate, tacrolimus, cyclosporine, chloroquine or hydroxychloroquine, leflunomide and Apremilast.

³Anti-hypertensive drugs include ACE inhibitors and ARBs.

particularly in male rheumatoid arthritis patients, has been reported. This could be explained by the synergistic effect of testosterone and leflunomide on proinflammatory cytokine production (Cutolo et al., 2009).

In the case of pre-exposure to anti-IL-17 and anti-IL-23, we observed a reduced COVID-19 incidence (RR = 0.2, CI 95% 0.03, 1.38; and RR = 0.8; CI 95% 0.39, 1.65, respectively). It has been reported that patients infected with SARS-CoV-2 presented elevated IL-17 serum levels (Liu et al., 2020), which are significantly correlated with disease severity (Pacha et al., 2020; Schett et al., 2020). Due to its high capacity to promote the production of a vast amount of pro-inflammatory cytokines

and chemokines, some authors have described that IL-17 and, therefore, the T helper 17 (TH¹⁷) response, play a role in COVID-19 hyperinflammation (Wu and Yang, 2020). Taking into account that IL-23 participates in stabilization of TH¹⁷ cells, our results support the idea (Liu et al., 2020) that targeting this axis could have a positive effect in controlling the cytokine storm.

However, our cohort includes limited number of patients treated with two important groups of immunomodulatory compounds, IL-6 (52 patients) and B lymphocyte antagonists (42 patients). Interestingly, none of these 94 patients showed COVID-19 symptoms, which agrees with the reported efficacy of the IL-6 antagonists tocilizumab (Xu et al., 2020) and sarilumab

TABLE 5 | Adjusted Relative Risk* (aRR) with 95% confidence intervals (CI 95%) of COVID-19 according to the presence of several comorbidities and treatments, stratified by sex.

Clinical characteristics	Model 1 ^a , aRR (CI 95%)				Model 2 ^b , aRR (CI 95%)				Model 3 ^c , aRR (CI 95%)			
	All		Men		All		Men		All		Men	
	Women	Men	Women	Men	Women	Men	Women	Men	Women	Men	Women	Men
Women	1.12 (0.8, 1.57)	—	1.12 (0.8, 1.56)	—	1.12 (0.8, 1.57)	—	1.12 (0.8, 1.57)	—	1.01 (0.99, 1.02)	—	1.01 (0.99, 1.02)	—
Age (years-old)	1 (0.99, 1.01)	—	1 (0.99, 1.01)	—	1 (0.99, 1.01)	—	1 (0.99, 1.01)	—	1 (0.99, 1.01)	—	1 (0.99, 1.01)	—
CA Disease	1.02 (0.75, 2.1)	0.99 (0.97, 1.01)	1.02 (0.75, 2.1)	0.99 (0.97, 1.01)	1.02 (0.75, 2.1)	0.99 (0.97, 1.01)	1.02 (0.75, 2.1)	0.99 (0.97, 1.01)	1.02 (0.75, 2.1)	0.99 (0.97, 1.01)	1.02 (0.75, 2.1)	0.99 (0.97, 1.01)
Cardiovascular disease	1.24 (0.72, 2.14)	0.98 (0.33, 1.98)	1.23 (0.74, 2.08)	0.98 (0.34, 2.08)	1.23 (0.74, 2.08)	0.98 (0.34, 2.08)	1.23 (0.74, 2.08)	0.98 (0.34, 2.08)	1.23 (0.74, 2.08)	0.98 (0.34, 2.08)	1.23 (0.74, 2.08)	0.98 (0.34, 2.08)
Pulmonary disease	1.47 (1.02, 2.13)	1.33 (0.66, 2.72)	1.42 (0.98, 2.05)	1.29 (0.62, 2.82)	1.47 (0.94, 2.27)	1.29 (0.62, 2.82)	1.44 (0.99, 2.08)	1.44 (0.99, 2.08)	1.47 (0.94, 2.27)	1.29 (0.62, 2.82)	1.44 (0.99, 2.08)	1.44 (0.99, 2.08)
Kidney disease	1.21 (0.85, 2.25)	0.87 (0.38, 1.98)	1.19 (0.64, 2.21)	0.83 (0.39, 2.06)	1.21 (0.85, 2.25)	0.83 (0.39, 2.06)	1.21 (0.85, 2.25)	0.83 (0.39, 2.06)	1.21 (0.85, 2.25)	0.83 (0.39, 2.06)	1.21 (0.85, 2.25)	0.83 (0.39, 2.06)
Active cancer or treatment	1.15 (0.52, 2.58)	1.05 (0.38, 2.88)	1.43 (0.39, 5.24)	1.44 (0.36, 5.72)	1.05 (0.38, 2.88)	1.44 (0.36, 5.72)	1.13 (0.5, 2.55)	1.06 (0.39, 2.87)	1.06 (0.39, 2.87)	1.13 (0.5, 2.55)	1.06 (0.39, 2.87)	1.44 (0.36, 5.72)

(unpublished observations) in COVID-19 treatment. The three families of monoclonal antibodies approved to treat rheumatoid arthritis are directed against IL-6, B lymphocyte surface protein CD20 and TNF α , three targets of potential interest for further investigation in COVID-19 treatment. IL-6, TNF α and B lymphocytes have been reported to play a crucial role in the inflammatory cascade taking place days before the manifestation of the most severe forms of SARS-CoV-2 infection (Zhou et al., 2020), as well as in the physiopathological processes leading to rheumatoid arthritis (Ceribelli et al., 2020).

In spite of the decrease incidence of COVID-19 with bDMARDs and sDMARDs treatments, those patients receiving a combination of both groups of compounds (n = 298) show enhanced incidence of COVID-19 (RR = 4.3; CI 95% 2.00, 9.25). The strong immunosuppression that should result by the combination of these treatments and the severity of the diseases targeted by these drug combinations may explain this paradoxical effect. Indeed, previous studies have reported that more patients experienced infectious adverse events when increasing doses of synthetic DMARDs were combined with anti-TNF α compounds (Burmester et al., 2015; Honkila et al., 2019). In addition, the main reason for combining both treatments is related to the lack of efficacy in these particular patients (Van Vollenhoven et al., 2012), which could also have influenced our results.

Some limitations of this study must be addressed. The indications for each treatment not only depend on the underlying pathology, but also on the specific clinical manifestations of each patient, and some of the indications are risk factors of COVID-19 (Sawalha et al., 2020). Given the heterogeneity of the studied treatments and underlying pathologies, it is difficult to analyze all the factors that could cause confounding by indication. However, RR estimates of COVID-19 diagnosis after propensity score matching with some of the covariates that predict receiving anti-TNF α were not substantially different than RR estimates in the unmatched sample (Supplementary Table S7). The slightly different RRs found with this treatment matching the above mention covariates suggest that some of these IMID may represent an increased risk for COVID-19. Indeed, these particular comorbidities have been reported to increase COVID-19 susceptibility and severity (Sawalha et al., 2020). Furthermore, patients receiving these immunomodulatory treatments have an enhanced propensity to bacterial infection (Chiu and Chen, 2020) that could eventually provide manifestations similar to COVID-19. In spite of this possible bias that would impair the results obtained with these treatments, we have obtained promising RRs with these compounds that suggest significant protective effects on COVID-19. Furthermore, our study was focused on the early stages of COVID-19 pandemic in Spain, and the number of confirmed SARS-CoV-2 testing in our setting was limited due to the scarcity of COVID-19 tests in Spain that, for ethical reasons, were mainly reserved to patients showing more severe disease symptoms. Therefore, clinical COVID-19 diagnosis was used as the primary outcome. Consequently, the effect of the treatment

TABLE 6 | Adjusted Relative Risk* (aRR) with 95% confidence intervals (CI 95%) of COVID-19 according to the presence of several

	Model 1 ^a : aRR (CI 95%)			Model 2 ^b : aRR (CI 95%)			Model 3 ^c : aRR (CI 95%)		
	All	Women	Men	All	Women	Men	All	Women	Men
Treatments followed	—	—	—	—	—	—	—	—	—
Biologic DMARDs^d	—	—	—	—	—	—	—	—	—
TNF- α antagonists	0.48 (0.31, 0.67)	0.41 (0.24, 0.69)	0.56 (0.3, 1.03)	0.50 (0.33, 0.76)	0.33 (0.17, 0.64)	0.76 (0.41, 1.43)	—	—	—
Abatacept	—	—	—	—	—	—	0.53 (0.31, 0.92)	0.32 (0.12, 0.86)	0.91 (0.58, 1.79)
Certolizumab	—	—	—	—	—	—	0.66 (0.32, 3.34)	0.08 (0.08, 4.07)	1.69 (0.34, 8.2)
Etanercept	—	—	—	—	—	—	0.37 (0.16, 0.88)	0.13 (0.02, 0.89)	0.71 (0.27, 1.9)
Guselkumab	—	—	—	—	—	—	0.46 (0.12, 1.81)	0.42 (0.05, 2.96)	0.56 (0.07, 4.28)
Infliximab	—	—	—	—	—	—	0.71 (0.31, 1.64)	0.7 (0.22, 2.23)	0.81 (0.24, 2.71)
Anti-p-Interleukin 1 β (IL-12/17.23)	—	—	—	0.47 (0.24, 0.92)	0.57 (0.24, 1.30)	0.44 (0.15, 1.22)	—	—	—
Ani-IL17	—	—	—	—	—	—	0.3 (0.01, 1.38)	NA	0.37 (0.05, 2.38)
Ani-IL23 (I2)	—	—	—	—	—	—	0.3 (0.02, 1.08)	1.19 (0.5, 2.82)	0.57 (0.16, 2)
Synthetic DMARDs^e	0.62 (0.43, 0.91)	0.66 (0.43, 1.07)	0.59 (0.31, 1.15)	—	—	—	—	—	—
Methotrexate	—	—	—	0.71 (0.48, 1.06)	0.7 (0.42, 1.10)	0.91 (0.4, 1.86)	0.74 (0.48, 1.12)	0.74 (0.44, 1.26)	0.86 (0.47, 1.72)
Leflunomide	—	—	—	0.66 (0.38, 1.14)	0.81 (0.29, 2.27)	0.56 (0.07, 1.79)	0.66 (0.27, 1.57)	0.8 (0.28, 2.23)	0.36 (0.07, 1.79)
Chondroine/hydroxychloroquine	—	—	—	0.76 (0.36, 1.62)	0.79 (0.32, 1.78)	1.2 (0.21, 6.78)	0.81 (0.38, 1.71)	0.79 (0.34, 1.86)	1.27 (0.29, 7.16)
Glucocorticoids	—	—	—	—	—	—	—	—	—
<10 mg/day	0.94 (0.61, 1.43)	0.72 (0.42, 1.22)	2.06 (1.01, 4.21)	0.57 (0.37, 1.33)	0.67 (0.4, 1.12)	2.05 (0.97, 4.3)	0.84 (0.55, 1.28)	0.65 (0.36, 1.1)	1.94 (0.93, 4.04)
>10 mg/day	1.76 (0.90, 3.45)	1.62 (0.75, 3.52)	2.20 (1.03, 4.26)	1.69 (0.87, 3.27)	1.61 (0.75, 3.43)	1.76 (0.43, 7.38)	1.7 (0.86, 3.3)	1.71 (0.8, 3.68)	1.78 (0.43, 7.34)
ACE-inhibitors ^f	1.02 (0.75, 1.32)	1.04 (0.7, 1.54)	1.11 (0.56, 2.21)	—	—	—	—	—	—
ARBs	—	—	—	0.81 (0.51, 1.28)	0.85 (0.52, 1.44)	0.73 (0.31, 1.71)	0.8 (0.51, 1.27)	0.84 (0.5, 1.43)	0.72 (0.3, 1.68)
Chronic NSAIDs	1.22 (0.85, 1.79)	1.14 (0.74, 1.74)	1.37 (0.71, 2.67)	1.55 (1.03, 2.33)	1.33 (0.84, 2.17)	2.07 (0.94, 4.58)	1.59 (1.06, 2.39)	1.36 (0.65, 2.18)	2.11 (0.95, 4.88)
Chronic NSAIDs	—	—	—	1.2 (0.84, 1.71)	1.15 (0.73, 1.7)	1.23 (0.67, 2.43)	1.21 (0.88, 1.72)	1.13 (0.74, 1.72)	1.31 (0.67, 2.58)

*Reference categories for clinical characteristics are individuals without that comorbidity. Reference categories for treatments are unexposed individuals.

^aModel 1 contains the following explanatory or exposure variables: sex, age, CV diseases, pulmonary diseases, kidney diseases, active cancer or treatment, TNF- α antagonists, IL-12/17/23 antagonists, synthetic DMARDs, glucocorticoids, anti-hypertensive drugs and chronic NSAIDs.

^bModel 2 contains the following explanatory or exposure variables: sex, age, CV diseases, pulmonary diseases, kidney diseases, active cancer or treatment, TNF- α antagonists, IL-12/17/23 antagonists, methotrexate, leflunomide, chondroine/hydroxychloroquine, glucocorticoids, ACE-inhibitors, ARBs and chronic NSAIDs.

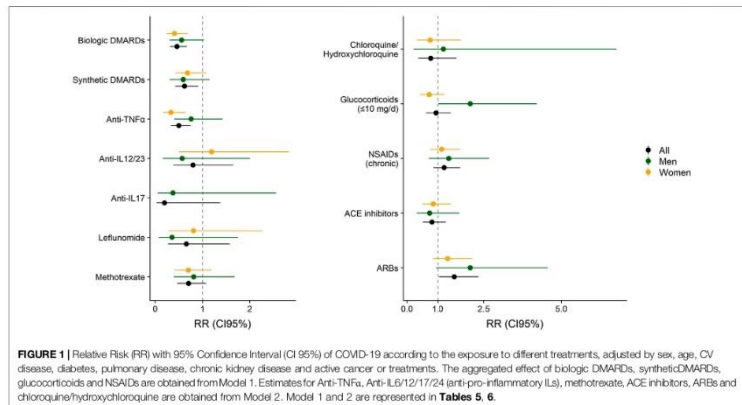
^cModel 3 contains the following explanatory or exposure variables: sex, age, CV diseases, pulmonary diseases, kidney diseases, active cancer or treatment, abatacept, certolizumab, etanercept, guselkumab, infliximab, anti-IL-17, anti-IL-12/23, methotrexate, leflunomide, chondroine/hydroxychloroquine, glucocorticoids, ACE-inhibitors, ARBs and chronic NSAIDs.

CV = cardiovascular; DMARDs = disease modifying anti-rheumatic drugs; JAK = Janus kinase; IL = Interleukin; TNF = tumor necrosis factor; NSAIDs = non-steroid anti-inflammatory drugs; ACE = angiotensin-converting enzyme; ARBs = angiotensin II receptor blockers; NA = number of observations or exposed individuals.

^dBiologic DMARDs include TNF- α antagonists, anti-inflammatory IL-1 antagonists, vedolizumab and T and B lymphocyte antagonists.

^eSynthetic DMARDs include methotrexate, JAK inhibitors, sulfasalazine, mycophenolate, tacrolimus, azathioprine, cyclosporine, chloroquine or hydroxychloroquine, leflunomide and Apremilast.

^fAnti-hypertensive drugs include ACE-inhibitors and ARBs.



could play a role both in the risk to acquire the infection, and/or the risk of being asymptomatic. Finally, it is also important to underline that the clinical symptoms of COVID-19 were recorded from 14 days before the COVID-19 alarm was announced in Spain (March 16th) when patients could be supposed to protect themselves more if they are at risk. Therefore, this potential self-protection would not represent any important bias for the interpretation of our results considering the time schedule of our symptoms recording.

In summary, all these results suggest that bDMARDs and sDMARDs should be continued for IMIDs treatment in COVID-19 patients. The decreased incidence of COVID-19 in patients treated with anti-TNF α and anti-proinflammatory ILs compounds underline the potential interest of these medications for further studies to open novel possible therapeutic strategies to avoid serious COVID-19 manifestations.

DATA AVAILABILITY STATEMENT

The raw data supporting the conclusions of this article will be made available by the authors, without undue reservation, to any qualified researcher.

ETHICS STATEMENT

The Committee of Parc de Salut Mar approved the protocol (2020/9246); IMIM (Hospital del Mar Medical Research

Institute), PRBB, c/ Dr. Aiguader, 88, 08003 Barcelona. The ethics committee waived the requirement of written informed consent for participation.

COVIDMAR STUDY GROUP MEMBERS

The Covidmar Study Group members are: Hospital del Mar, Barcelona: Selene Labrada, Miguel Mejia-Torres (Rheumatology Service) and Irene Carrión-Barberà, Carolina Pérez-García, Fabiola Ojeda, Tarek Carlos Salman-Monte, Josep Blanch-Rubió (Rheumatology Service and IMIM-Hospital del Mar Medical Research Institute) collected data and provided care for study patients; IMIM-Hospital del Mar Medical Research Institute: Luciano Polino, Laura Triginer, Anna Ribes (Cell Research on Inflammation and Cartilage Research Group, Inflammatory and Cardiovascular Processes Program) collected data; Maria-Victòria Puig (Integrative Pharmacology and Systems Neuroscience Research Group, Neurosciences Research Program and IMIM-Hospital del Mar Medical Research Institute); contributed to analysis design; Parc Sanitari Pere Virgili, Barcelona: Maria Teresa Martí Vila, Maria Luisa Perez Miras (CAP Vila Olímpica) collected data; Universitat Pompeu Fabra, Barcelona: Beltrán Álvarez-Pérez, Araceli Bergadà-Martínez, Pablo Calvé Alba Calvet-Pavón, Mireia Carcolé, Laura Domingo-Rodríguez, Alejandra Escudero-Lara, Lorena Galera-López, Jolita Jančytė, Marta Linares-López, Sara Martínez-Torres, Antonio Ortega-Álvarez, Andrés Ozaita, Sheila Piedra-Barrull, Dulce Real-Muñoz, Maria Sanchis-Ollé, Clara Seira Oriach, Miquel-Àngel Serra, Anna Vázquez-Oliver (Laboratory of Neuropharmacology,

Department of Experimental and Health Sciences and IMIM-Hospital del Mar Medical Research Institute) collected data.

AUTHOR CONTRIBUTIONS

NS-D participated in selection of statistical tests/analyses, performed the statistical analyses, computations and related computer work, and participated in writing the manuscript. LT was involved in conceptualizing the research idea, setting-up the research design, making the primary interpretation of the statistical analyses and participated in writing the manuscript. JL-O was involved in conceptualizing the research idea, setting-up the research design, making the primary interpretation of the statistical analyses and participated in writing the manuscript. EM-G contributed to the statistical analyses and revised the manuscript. PN contributed to the statistical analyses and revised the manuscript. RT contributed to the statistical analyses and revised the manuscript. AG was responsible for patient cohort data collection. RM was involved in conceptualizing the research idea, creating the research design, making the final interpretation of the statistical analysis, and writing the first draft and revision of the manuscript. JM was involved in conceptualizing the research idea, creating the research design, making the final interpretation of the statistical analysis, and writing the first draft and revision of the manuscript. Covidmar Study Group participated in collecting data and provided care for study patients.

REFERENCES

- Adhanom Ghebreyesus, T. (2020). WHO Director-General's opening remarks at the media briefing on COVID-19. Geneva, Switzerland: World Health Organization, 4. Available at: <https://www.who.int/dg/speeches/detail/who-director-general-s-opening-remarks-at-the-media-briefing-on-covid-19-11-march-2020>.
- Bennar, E. J., Ungaro, R. C., Geary, R. B., Kaplan, G. G., Kissous-Hunt, M., Lewis, J. D., et al. (2020). Corticosteroids, but not TNF antagonists, are associated with adverse COVID-19 outcomes in patients with inflammatory bowel disease: results from an international registry. *Gastroenterology* 159, 481–491.e3. doi:10.1053/j.gastro.2020.05.032
- Burnester, G. R., Kivitz, A. J., Kupper, H., Arulmani, U., Florentinus, S., Goss, S. L., et al. (2015). Efficacy and safety of ascending methotrexate dose in combination with adalimumab: the randomised CONCERTO trial. *Ann. Rheum. Dis.* 74, 1037–1044. doi:10.1136/annrheumdis-2013-204769
- Ceribelli, A., Motta, F., De Santis, M., Ansari, A. A., Ridgway, W. M., Gershwin, M. E., et al. (2020). Recommendations for coronavirus infection in rheumatic diseases treated with biologic therapy. *J. Autoimmun.* 109, 102442. doi:10.1016/j.jaut.2020.102442
- Chen, N., Zhou, M., Dong, X., Qu, J., Gong, F., Han, Y., et al. (2020). Epidemiological and clinical characteristics of 99 cases of 2019 novel coronavirus pneumonia in Wuhan, China: a descriptive study. *Lancet* 395, 507–513. doi:10.1016/S0140-6736(20)30211-7
- Chiu, Y. M., and Chen, D. Y. (2020). Infection risk in patients undergoing treatment for inflammatory arthritis: non-biologics versus biologics. *Expert Rev. Clin. Immunol.* 16, 207–228. doi:10.1080/1744666X.2019.1705785
- Catoto, M., Montagna, P., Brizzolaro, R., Sulli, A., Seriola, B., Villaggio, B., et al. (2009). Sex hormones modulate the effects of Lefunomide on cytokine production by cultures of differentiated monocyte/macrophages and

FUNDING

“Ministerio de Ciencia, Innovación y Universidades” (#AEI-SAF2017-84060-R FEDER to RM, #DPI2016-80283-C2-2-R), “Ministerio de Sanidad, Servicios Sociales e Igualdad” (#RD16/0017/0020 and #PNSD-20171068 to RM, #PI18/00059 to TCS-M) and “Generalitat de Catalunya” (#2017-SGR-669 and #ICREA-Acadèmia 2015 to RM, #2017-SGR-138 to RdIT). NSD is recipient of predoctoral fellowship #2019-DI-47 from the DIUE-AGAUR of the “Generalitat de Catalunya.” The submitted work was supported by the Hospital del Mar.

ACKNOWLEDGMENTS

We thank all patients who participated in the study, Gemma Vilagut (PhD) for her guidance and support on the statistical analysis and Mónica Gratacós (PhD) for translating the clinical protocol into English, for English language support and proofreading of the manuscript.

SUPPLEMENTARY MATERIAL

The Supplementary Material for this article can be found online at: <https://www.frontiersin.org/articles/10.3389/fphar.2020.583260/full#supplementary-material>.

- synovial macrophages from rheumatoid arthritis patients. *J. Autoimmun.* 32, 254–260. doi:10.1016/j.jaut.2009.02.016
- Dong, E., Du, H., and Gardner, L. (2020). An interactive web-based dashboard to track COVID-19 in real time. *Lancet Infect. Dis.* 20, 533–534. doi:10.1016/S1473-3099(20)30120-1
- Favalli, E. G., Monti, S., Ingegnoli, F., Balduzzi, S., Caporali, R., and Montecucco, C. (2020). Incidence of COVID-19 in patients with rheumatic diseases treated with targeted immunosuppressive drugs: what can we learn from observational data? *Arthritis Rheum.* 72, 1600–1606. doi:10.1002/art.41388
- Feldmann, M., Maini, R. N., Woody, J. N., Hodgate, S. T., Winter, G., Rowland, M., et al. (2020). Trials of anti-tumour necrosis factor therapy for COVID-19 are urgently needed. *Lancet* 395, 1407–1409. doi:10.1016/S0140-6736(20)30858-8
- Fu, B., Xu, X., and Wei, H. (2020). Why tocilizumab could be an effective treatment for severe COVID-19? *J. Transl. Med.* 18, 164. doi:10.1186/s12967-020-02339-3
- Gianfrancesco, M. A., Hrych, K. L., Gossec, L., Strangfeld, A., Carmona, L., Mateus, E. F., et al. (2020a). Rheumatic disease and COVID-19: initial data from the COVID-19 global rheumatology alliance provider registries. *Lancet Rheum.* 2, e250–e253. doi:10.1016/S2665-9913(20)30095-3
- Gianfrancesco, M., Hrych, K. L., Hrych, K. L., Al-Adely, S., Al-Adely, S., Carmona, L., et al. (2020b). Characteristics associated with hospitalisation for COVID-19 in people with rheumatic disease: data from the COVID-19 global rheumatology alliance physician-reported registry. *Ann. Rheum. Dis.* 79, 859–866. doi:10.1136/annrheumdis-2020-217871
- Haberman, R., Axelrad, J., Chen, A., Castillo, R., Yan, D., Izmirlir, P., et al. (2020). COVID-19 in immune-mediated inflammatory diseases—case series from New York. *N. Engl. J. Med.* 383, 85–88. doi:10.1056/nejmc2009567
- Ho, D. E., Imai, K., King, G., and Stuart, E. A. (2011). Matchit: nonparametric preprocessing for parametric causal inference. *J. Stat. Software* 42, 1–28. doi:10.18637/jss.v042.i08
- Honkila, M., Niinimäki, R., Taskinen, M., Kuismin, O., Kettunen, K., Saarela, J., et al. (2019). A nearly fatal primary Epstein-Barr virus infection associated with

- low NK-cell counts in a patient receiving azathioprine: a case report and review of literature. *BMC Infect. Dis.* 19, 404. doi:10.1186/s12879-019-4022-3
- Huang, C., Wang, Y., Li, X., Ren, L., Zhao, J., Hu, Y., et al. (2020). Clinical features of patients infected with 2019 novel coronavirus in Wuhan, China. *Lancet* 395, 497–506. doi:10.1016/S0140-6736(20)30183-5
- Liu, Y., Yang, Y., Zhang, C., Huang, F., Wang, F., Yuan, J., et al. (2020). Clinical and biochemical indexes from 2019-nCoV infected patients linked to viral loads and lung injury. *Sci. China Life Sci.* 63, 364–374. doi:10.1007/s11427-020-1643-8
- Mehra, M. R., Ruschitzka, F., and Patel, A. N. (2020). Retraction—hydroxychloroquine or chloroquine with or without a macrolide for treatment of COVID-19: a multinational registry analysis. *Lancet* 20, 1–10. doi:10.1016/S0140-6736(20)31324-6
- Memoli, M. J., Athota, R., Reed, S., Czajkowski, A., Bristol, T., Proudfoot, K., et al. (2014). The natural history of influenza infection in the severely immunocompromised vs nonimmunocompromised hosts. *Clin. Infect. Dis.* 58, 214–224. doi:10.1093/cid/cit725
- Meng, J., Xiao, G., Zhang, J., He, X., Ou, M., Bi, J., et al. (2020). Renin-angiotensin system inhibitors improve the clinical outcomes of COVID-19 patients with hypertension. *Emerg. Microb. Infect.* 9, 757–760. doi:10.1080/22221751.2020.1746200
- Michielena, X., Borelli, H., López-Corbeto, M., López-Laxanta, M., Moreno, E., Pascual-Pastor, M., et al. (2020). Incidence of COVID-19 in a cohort of adult and paediatric patients with rheumatic diseases treated with targeted biologic and synthetic disease-modifying anti-rheumatic drugs. *Semin. Arthritis Rheum.* 50, 564–570. doi:10.1016/j.semarthrit.2020.05.001
- Mizumoto, K., Kagaya, K., Zarebski, A., and Chowell, G. (2020). Estimating the asymptomatic proportion of coronavirus disease 2019 (COVID-19) cases on board the Diamond Princess cruise ship, Yokohama, Japan, 2020. *Eurosurveill* 25, 2000180. doi:10.2807/1560-7917.ES.2020.25.10.2000180
- Monti, S., Balduzzi, S., Dehine, P., Belli, E., Quadrelli, V. S., and Montecucco, C. (2020). Clinical course of COVID-19 in a series of patients with chronic arthritis treated with immunosuppressive targeted therapies. *Ann. Rheum. Dis.* 79, 667–668. doi:10.1136/annrheumdis-2020-217424
- Nasuno, M., Miyakawa, M., Tanaka, H., and Motoya, S. (2017). Short- and long-term outcomes of infliximab treatment for steroid-refractory ulcerative colitis and related prognostic factors: a single-center retrospective study. *Digestion* 95, 67–71. doi:10.1159/000452439
- Nishitani, H., Kobayashi, T., Miyama, T., Suzuki, A., Jung, S. M., Hayashi, K., et al. (2020). Estimation of the asymptomatic ratio of novel coronavirus infections (COVID-19). *Int. J. Infect. Dis.* 94, 154–155. doi:10.1016/j.ijid.2020.03.020
- Pacha, O., Sallman, M. A., and Evans, S. E. (2020). COVID-19: a case for inhibiting IL-17? *Nat. Rev. Immunol.* 20, 345–346. doi:10.1038/s41577-020-0328-z
- Robinson, P. C., Richards, D., Tanner, H. L., and Feldmann, M. (2020). Accumulating evidence suggests anti-TNF therapy needs to be given trial priority in COVID-19 treatment. *Lancet Rheumatol.* 9913, 19–21. doi:10.1016/S2665-9913(20)30309-X
- Ruiz-Inostroza, G., Danza, A., and Khamishta, M. (2012). Glucocorticoid use and abuse in SLE. *Rheumatol. (Oxford)* 51, 1145–1153. doi:10.1093/rheumatology/ker410
- Salvarani, C., Bajocchi, G., Mancuso, P., Galli, E., Muratore, F., Botardi, L., et al. (2020). Susceptibility and severity of COVID-19 in patients treated with bDMARDs and tDMARDs: a population-based study. *Ann. Rheum. Dis.* 79, 986–988. doi:10.1136/annrheumdis-2020-217903
- Sawalha, A. H., Zhao, M., Coit, P., and Lu, Q. (2020). Epigenetic dysregulation of ACE2 and interferon-regulated genes might suggest increased COVID-19 susceptibility and severity in lupus patients. *Clin. Immunol.* 215, 108410. doi:10.1016/j.clim.2020.108410
- Sdett, G., Stichlerling, M., and Neurath, M. F. (2020). COVID-19: risk for cytokine targeting in chronic inflammatory diseases? *Nat. Rev. Immunol.* 20, 271–272. doi:10.1038/s41577-020-0312-7
- Van Vollenhoven, R. F., Geborek, P., Forslind, K., Albertsson, K., Ernsten, S., Petersson, I. F., et al. (2012). Conventional combination treatment versus biological treatment in methotrexate-refractory early rheumatoid arthritis: 2 year follow-up of the randomised, non-blinded, parallel-group swefot trial. *Lancet* 379, 1712–1720. doi:10.1016/S0140-6736(12)60027-0
- Wang, D., Hu, B., Hu, C., Zhu, F., Liu, X., Zhang, J., et al. (2020). Clinical characteristics of 138 hospitalized patients with 2019 novel coronavirus-infected pneumonia in wuhan, China. *JAMA* 323, 1061–1069. doi:10.1001/jama.2020.1585
- Winthrop, K. L., Brunton, A. E., Beckmann, S., Polgreen, P., Baddley, J., Saag, K. G., et al. (2020). SARS CoV-2 infection among patients using immunomodulatory therapies. *Ann. Rheum. Dis. annrheumdis-2020-218580*. doi:10.1136/annrheumdis-2020-218580
- Wu, D. and Yang, X. O. (2020). TH17 responses in cytokine storm of COVID-19: an emerging target of JAK2 inhibitor Fedratinib. *J. Microbiol. Immunol. Infect.* 3, 368–370. doi:10.1016/j.jmii.2020.03.005
- Xu, X., Han, M., Li, T., Sun, W., Wang, D., Fu, B., et al. (2020). Effective treatment of severe COVID-19 patients with tocilizumab. *Proc. Natl. Acad. Sci. USA* 117, 10970–10975. doi:10.1073/pnas.2005615117
- Zhang, W., Zhao, Y., Zhang, F., Wang, Q., Li, T., Liu, Z., et al. (2020). The use of anti-inflammatory drugs in the treatment of people with severe coronavirus disease 2019 (COVID-19): the experience of clinical immunologists from China. *Clin. Immunol.* 214, 108393. doi:10.1016/j.clim.2020.108393
- Zhong, J., Tang, J., Ye, C., and Dong, L. (2020). The immunology of COVID-19: is immune modulation an option for treatment? *Lancet Rheumatol.* 2, e428–e436. doi:10.1016/S2665-9913(20)30120-X
- Zhou, F., Yu, T., Du, R., Fan, G., Liu, Y., Liu, Z., et al. (2020). Clinical course and risk factors for mortality of adult inpatients with COVID-19 in Wuhan, China: a retrospective cohort study. *Lancet* 395, 1054–1062. doi:10.1016/S0140-6736(20)30566-3

Conflict of Interest: AG has received research grants or consulting fees from AstraZeneca and Bioberica S.A.U., RM has received research grants or consulting fees from Actis, Almirall, Boehringer Ingelheim, BrainCo, Esteve, Ferrer, GlaxoSmithKline, Grünenthal, GW Pharmaceuticals, Janus, Lundbeck, Pharmaleads, Phytoplant, Rhodes, Sanofi, Spherium, Union de Pharmacologie Scientifique Appliquée, Ujohjñ, and Uriach; JM has received grants or consulting fees from Procure Health Iberia S.L, Esteve, Labbra, Bioberica S.A.U, Grunenthal Pharma S.A, Pfizer, OPKO Health Spain S.L.U and Roche Pharma S.A.

The remaining authors declare that the research was conducted in the absence of any commercial or financial relationships that could be construed as a potential conflict of interest.

Copyright © 2020 Sokdevi-Domenach, Tio, Llorente-Ouaindia, Martín-García, Nebot, de la Torre, Gurt, Maldonado and Monfort. This is an open-access article distributed under the terms of the Creative Commons Attribution License (CC BY). The use, distribution or reproduction in other forums is permitted, provided the original author(s) and the copyright owner(s) are credited and that the original publication in this journal is cited, in accordance with accepted academic practice. No use, distribution or reproduction is permitted which does not comply with these terms.

Influence of anti-osteoporosis treatments on the incidence of COVID-19 in patients with non-inflammatory rheumatic conditions

Josep Blanch-Rubió^{1,2,*}, Natalia Soldevila-Domenech^{3,7,*}, Laura Tío², Jone Llorente-Onaindia², Manuel Ciriá-Recasens^{1,2}, Luciano Polino², Alba Gurt⁵, Rafael de la Torre^{3,6,7}, Rafael Maldonado^{2,4,8}, Jordi Monfort^{1,2,8}, and the Covidmar Study Group[#]

¹Rheumatology Service, Hospital del Mar, Passeig Marítim, Barcelona 08003, Spain

²IMIM (Hospital del Mar Medical Research Institute), PRBB, Barcelona 08003, Spain

³Integrative Pharmacology and Systems Neuroscience Research Group, Neurosciences Research Program, IMIM-Institut Hospital del Mar d'Investigacions Mèdiques, PRBB, Barcelona 08003, Spain

⁴Laboratory of Neuropharmacology, Department of Experimental and Health Sciences, Universitat Pompeu Fabra, PRBB, Barcelona 08003, Spain

⁵CAP Vila Olímpica, Parc Sanitari Pere Virgili, Barcelona 08003, Spain

⁶Spanish Biomedical Research Centre in Physiopathology of Obesity and Nutrition (CIBERObn), Instituto de Salud Carlos III (ISCIII), Madrid 28029, Spain

⁷Department of Experimental and Health Sciences, Universitat Pompeu Fabra, PRBB, Barcelona 08003, Spain

*Equal contribution

⁸Equally supervised this work

[#]A list of authors and their affiliations appears in Acknowledgments

Correspondence to: Rafael Maldonado; email: rafael.maldonado@upf.edu

Keywords: denosumab, zoledronate, calcium, vitamin D, anti-resorptive drugs, COVID-19

Received: July 21, 2020

Accepted: September 9, 2020

Published: October 20, 2020

Copyright: © 2020 Blanch-Rubió et al. This is an open access article distributed under the terms of the [Creative Commons Attribution License](https://creativecommons.org/licenses/by/3.0/) (CC BY 3.0), which permits unrestricted use, distribution, and reproduction in any medium, provided the original author and source are credited.

ABSTRACT

Coronavirus disease 19 (COVID-19) is currently a global pandemic that affects patients with other pathologies. Here, we investigated the influence of treatments for osteoporosis and other non-inflammatory rheumatic conditions, such as osteoarthritis and fibromyalgia, on COVID-19 incidence. To this end, we conducted a cross-sectional study of 2,102 patients being treated at the Rheumatology Service of Hospital del Mar (Barcelona, Spain). In our cohort, COVID-19 cumulative incidence from March 1 to May 3, 2020 was compared to population estimates for the same city. We used Poisson regression models to determine the adjusted relative risk ratios for COVID-19 associated with different treatments and comorbidities. Denosumab, zoledronate and calcium were negatively associated with COVID-19 incidence. Some analgesics, particularly pregabalin and most of the studied antidepressants, were positively associated with COVID-19 incidence, whereas duloxetine presented a negative association. Oral bisphosphonates, vitamin D, thiazide diuretics, anti-hypertensive drugs and chronic non-steroidal anti-inflammatory drugs had no effect on COVID-19 incidence in the studied population. Our results provide novel evidence to support the maintenance of the main anti-osteoporosis treatments in COVID-19 patients, which may be of particular relevance to elderly patients affected by the SARS-CoV-2 pandemic.

INTRODUCTION

Infections by SARS-CoV-2, a novel coronavirus that emerged in China in late 2019 [1], and the disease that it

causes, COVID-19, became a global pandemic on March 11th, 2020 [2]. By July 19th, 2020, COVID-19 had infected 14,348,475 people and caused 603,167 deaths worldwide [3]. The incidence of COVID-19 is

heterogeneous within different countries. In Spain, the area of Barcelona (Catalonia, Spain) has suffered one of the highest rates of incidence and deaths in Europe, mostly between March and April of 2020 [4].

COVID-19 initially has a viral phase with symptoms that include fever, dry cough, anosmia/ageusia, odynophagia and diarrhea, among others. Approximately seven days after this initial phase, some patients develop a systemic pro-inflammatory state and progress to more severe symptoms, such as dyspnea, shortness of breath, pulmonary infiltrates and hypoxemia. The progression of the disease has been associated with a hyper inflammatory response with high levels of inflammatory markers and pro-inflammatory cytokines, sometimes accompanying a pro-coagulation state. Patients following this evolution sometimes become seriously ill, often requiring admission to Intensive Care Units, and some ultimately may die [5].

The innate and acquired immune responses play a crucial role in the progression of the disease. The immune system seems to be dysregulated in severe forms of COVID-19, probably due to abnormal responses by monocytes, macrophage, and/or dendritic cells [6]. Some disease-modifying, anti-rheumatic drugs used in the treatment of immune-mediated inflammatory diseases may have a protective effect, such as the IL6 antagonists tocilizumab and sarilumab [7], which are currently off-label used to treat patients. Our team (article under revision) and other researchers [8–10] have also shown that some of these anti-rheumatic treatments reduce COVID-19 incidence.

Among the diseases treated by rheumatology, osteoporosis is an age-related chronic disease that affects tens of millions people worldwide, requiring long-term treatment [11]. It is a global chronic pandemic causing enormous morbidity, mortality and economic burdens [12]. The possible effects of anti-osteoporosis pharmacologic treatments in the clinical expression and incidence of COVID-19 remain unknown. Nonetheless, the most prominent organizations for rheumatology and bone studies, such as the American College of Rheumatology (ACR) [13], the European League Against Rheumatism (EULAR) [14], the American Society for Bone and Mineral Research (ASBMR) [15], and the International Osteoporosis Foundation (IOF) [16], currently do not recommend discontinuing the administration of rheumatologic drugs to treat COVID-19 due to their likely neutral effects. However, such recommendations are based on expert opinions and, to our knowledge, no data are available regarding the safety of using such drugs to treat COVID-19.

Determining whether anti-osteoporosis treatments are safe for COVID-19 patients and whether they influence COVID-19 incidence and its clinical expression could positively impact patient prognosis. These questions apply to all anti-osteoporosis compounds including denosumab, a fully human monoclonal antibody against RANK-L, that inhibits osteoclastogenesis. Denosumab is widely used to treat osteoporosis, but also to prevent skeletal-related events in advanced malignancies with bone metastasis [17]. The RANKL/RANK system participates in processes related to the immune system, including lymph-node development, lymphocyte differentiation, dendritic cell survival and T- cell activation, and tolerance induction [18]. Furthermore, osteoprotegerin, a natural decoy with similar effects to those of denosumab on RANK-L, may elicit beneficial effects to patients suffering from viral infections [19]. Therefore, denosumab may modulate the immune response associated to viral infections, such as SARS-CoV-2.

Non-inflammatory rheumatic conditions such as osteoporosis, osteoarthritis and fibromyalgia are all characterized by a high incidence of chronic pain and are mainly treated with classical non-steroidal anti-inflammatory drugs (NSAIDs) and opioids, but also with gabapentinoids and two particular antidepressant drugs, duloxetine and amitriptyline. In addition to chronic pain, these pathological conditions often present co-morbid emotional disorders that are treated with antidepressants. However, there is no data on the potential effects of these drugs on COVID-19 incidence.

Here, in order to elucidate the possible effects of anti-osteoporosis drugs (anti-resorptives, calcium and vitamin D) and associated treatments (analgesics and antidepressants) on COVID-19 incidence and clinical expression, we carried out a cross-sectional study of the cumulative incidence of COVID-19 in rheumatic patients suffering from non-inflammatory conditions and living in the influence area of a referral hospital in Barcelona, Spain.

RESULTS

A total of 2,498 individuals were examined for eligibility and 2,102 fulfilled the inclusion criteria and were included in the analysis, 80.5% of which were women. Table 1 shows the description of the studied population and the distribution of COVID-19 across studied variables. The mean age was 66.4 years (SD, 13.3) and 63.7% of the population had osteoarthritis, 43.5% osteoporosis and 27.2% fibromyalgia. The most prevalent coexisting conditions were hypertension (42.4%), pulmonary disease (15.0%), cardiovascular (CV) disease (14.9%) and diabetes (12.6%). Regarding

Table 1. Characteristics of the study population and distribution of confirmed or hsCOVID-19 cases.

Characteristic	All population (N=2102)	Confirmed or hsCOVID-19	
		No (N=1993)	Yes (N=109)
Men	409 (19.5%)	388 (19.5%)	21 (19.3%)
Women	1693 (80.5%)	1605 (80.5%)	88 (80.7%)
Age [mean (SD)]	66.4 (13.3)	66.5 (13.3)	65.7 (13.2)
Non-inflammatory rheumatic diagnosis¹			
Osteoarthritis	1340 (63.7%)	1263 (63.4%)	77 (70.6%)
Osteoporosis	914 (43.5%)	880 (44.2%)	34 (31.2%)
Fibromyalgia	571 (27.2%)	539 (27.0%)	32 (29.4%)
Coexisting conditions			
Diabetes	264 (12.6%)	245 (12.3%)	19 (17.4%)
Hypertension	892 (42.4%)	845 (42.4%)	47 (43.1%)
Pulmonary disease	315 (15.0%)	290 (14.6%)	25 (22.9%)
CV disease	314 (14.9%)	286 (14.4%)	28 (25.7%)
Cancer or active treatment	121 (5.76%)	115 (5.77%)	6 (5.50%)
Chronic kidney disease	114 (5.42%)	104 (5.22%)	10 (9.17%)
History of organ transplantation	9 (0.43%)	6 (0.30%)	3 (2.75%)
Any of these comorbidities	1232 (58.6%)	1159 (58.2%)	73 (67.0%)
Treatments followed			
Denosumab	264 (12.6%)	256 (12.8%)	8 (7.34%)
Intravenous Zoledronate	179 (8.52%)	173 (8.68%)	6 (5.50%)
Oral bisphosphonates	143 (6.80%)	136 (6.82%)	7 (6.42%)
Teriparatide	25 (1.19%)	25 (1.25%)	0 (0.00%)
Calcium	490 (23.3%)	474 (23.8%)	16 (14.7%)
Vitamin D	1303 (62.0%)	1241 (62.3%)	62 (56.9%)
Thiazide diuretics	262 (12.5%)	248 (12.4%)	14 (12.8%)
SERMs	11 (0.52%)	11 (0.55%)	0 (0.00%)
Analgesics	1220 (58.0%)	1154 (57.9%)	66 (60.6%)
Gabapentin	164 (7.80%)	153 (7.68%)	11 (10.1%)
Pregabalin	146 (6.95%)	134 (6.72%)	12 (11.0%)
Opioids	546 (26.0%)	510 (25.6%)	36 (33.0%)
Other Analgesics	959 (45.6%)	906 (45.5%)	53 (48.6%)
Antidepressants	657 (31.3%)	612 (30.7%)	45 (41.3%)
Tricyclic antidepressants	124 (5.90%)	116 (5.82%)	8 (7.34%)
Amitriptyline	102 (4.85%)	94 (4.72%)	8 (7.34%)
Others	22 (1.05%)	22 (1.10%)	0 (0.00%)
Dual-action antidepressants	277 (13.2%)	260 (13.0%)	17 (15.6%)
Duloxetine	207 (9.85%)	198 (9.93%)	9 (8.26%)
Venlafaxine	60 (2.85%)	53 (2.66%)	7 (6.42%)
Others	10 (0.48%)	9 (0.45%)	1 (0.92%)
SSRIs antidepressants	333 (15.8%)	307 (15.4%)	26 (23.9%)
Reboxetine	2 (0.10%)	2 (0.10%)	0 (0.00%)
Trazodone	33 (1.57%)	31 (1.56%)	2 (1.83%)
Glucocorticoids	60 (2.85%)	53 (2.66%)	7 (6.42%)
Inhaled Glucocorticoids	189 (8.99%)	172 (8.63%)	17 (15.6%)
Anti-hypertensive drugs	646 (30.7%)	610 (30.6%)	36 (33.0%)
ACE inhibitors	363 (17.3%)	344 (17.3%)	19 (17.4%)
ARBs	290 (13.8%)	273 (13.7%)	17 (15.6%)
Chronic NSAIDs	318 (15.1%)	301 (15.1%)	17 (15.6%)
Synthetic DMARDs	30 (1.43%)	26 (1.30%)	4 (3.67%)
Biologic DMARDs	1 (0.05%)	1 (0.05%)	0 (0.00%)

COVID-19 status			
Grade of hsCOVID-19 symptomatology			
Mild	63 (3.00%)	NA	63 (57.8%)
Moderate	16 (0.76%)	NA	16 (14.7%)
Severe	30 (1.43%)	NA	30 (27.5%)
COVID-19 Evolution:			
Home	71 (3.38%)	NA	71 (65.1%)
Hospitalization	25 (1.19%)	NA	25 (22.9%)
NIV	3 (0.14%)	NA	3 (2.75%)
ICU	1 (0.05%)	NA	1 (0.92%)
Death	9 (0.43%)	NA	9 (8.26%)
Positive SARS-CoV-2 test (PCR)	38 (1.81%)	NA	38 (34.9%)
Radiography:			
Pathologic unilateral	13 (0.62%)	NA	13 (11.9%)
Pathologic bilateral	23 (1.09%)	NA	23 (21.1%)
COVID-19 diagnosed by PCR or radiography	48 (2.28%)	NA	48 (44.0%)

¹Some individuals have more than one diagnosis.

ACE = angiotensin-converting enzyme. ARBs = angiotensin II receptor blockers. CV = cardiovascular disease. DMARDs = disease modifying anti-rheumatic drugs. hsCOVID-19 = highly suspected COVID-19 cases. ICU = intensive care unit. NA = not applicable. NIV = non-invasive ventilation. NSAIDs = non-steroid anti-inflammatory drugs. PCR = polymerase chain reaction. SERMs = selective estrogen receptor modulator. SD = standard deviation. SSRIs = selective serotonin reuptake inhibitors.

treatments, 62% were treated with vitamin D, 23.3% with calcium, 12.6% with denosumab, and 8.5% with intravenous zoledronate. More than a half of the population was exposed to analgesics and almost a third to antidepressants, mainly serotonin reuptake inhibitors (SSRIs) (15.8%) and dual-action antidepressants (13.2%).

A total of 109 individuals had COVID-19 diagnosis (hereafter, COVID-19-positive or "COVID-19+" patients), representing 5.19% of the individuals included. They presented a higher prevalence of diabetes, CV disease, pulmonary disease and chronic kidney disease than those not diagnosed with COVID-19 (hereafter, COVID-19-negative "COVID-19-" patients). In terms of treatments, the exposure to denosumab, intravenous zoledronate, vitamin D, and selective estrogen receptor modulators (SERMs) was lower for COVID-19+ than for COVID-19- patients, whereas antidepressant treatment was more frequent in COVID-19-positive individuals.

As shown in Table 2, the age-standardized cumulative incidence rate in our population was 4.68% (CI95% 3.78-5.59%), being slightly higher than that in the general population of Barcelona (3.69%; CI95% 3.66-3.73%). However, when stratifying by the presence of osteoporosis, osteoarthritis and fibromyalgia, patients with osteoporosis presented lower rates (2.98%, CI95% 1.88-4.08) than the general population, whereas patients with osteoarthritis (4.58%, CI95% 3.46-5.70) and fibromyalgia (4.45%, CI95% 2.76-6.14) showed slightly higher rates.

Adjusted associations between different exposure variables (clinical characteristics and treatments) and COVID-19 diagnosis are shown in Table 3. CV disease was the comorbidity showing the highest RR of COVID-19 (RR=1.84; CI95%1.17-2.87), followed by chronic kidney disease, diabetes and pulmonary disease. Patients suffering from cancer or in active cancer treatment did not show an increased RR for COVID-19 diagnosis. Regarding treatments, the RR for COVID-19 was 0.58 (CI95%0.28-1.22) for denosumab, 0.62 (CI95%0.27-1.41) for intravenous zoledronate and 0.64 (CI95%0.37-1.12) for calcium. No association between COVID-19 and oral bisphosphonates, vitamin D or thiazide diuretics was found. Analgesics, particularly pregabalin (RR=1.55; CI95%0.86-2.79), gabapentin (RR=1.39; CI95%0.75-2.58) and opioids (RR=1.25; CI95%0.85-1.83) showed an increased RR for COVID-19. In the case of antidepressants, SSRIs presented an RR of 1.54 (CI95%1.00-2.36). The tricyclic antidepressant amitriptyline presented an RR of 1.38 (CI95% 0.7, 2.71) and the RR of all dual-action antidepressants together was 1.22 (CI95% 0.72, 2.08). In sharp contrast, the RR of the dual-action antidepressant duloxetine was 0.68 (CI95% 0.34-1.34). Figure 1 summarizes the adjusted RR for the incidence of COVID-19 according to the exposure to the most prevalent studied treatments.

Finally, the RR estimates using propensity score matching for the exposure to denosumab, intravenous zoledronate and calcium are included in Supplementary Table 3. The resulting RR estimates were almost equivalent to the unmatched database, with values of

Table 2. Crude and age-adjusted cumulative incidence rates of confirmed or hsCOVID-19 cases in our cohort and in the population of Barcelona (reference population) registered from March 1st to May 3rd, 2020, stratified by the diagnosis of osteoporosis, osteoarthritis and fibromyalgia.

Age group (years)	Incidence rate of confirmed or hsCOVID-19 cases in Barcelona	Confirmed or hsCOVID-19 cases in our cohort							
		All population		Population with osteoporosis		Population with osteoarthritis		Population with fibromyalgia	
		Crude cumulative incidence rate	Age-adjusted cumulative incidence rate	Crude cumulative incidence rate	Age-adjusted cumulative incidence rate	Crude cumulative incidence rate	Age-adjusted cumulative incidence rate	Crude cumulative incidence rate	Age-adjusted cumulative incidence rate
20-29	4818 / 195194 (2.47%)	0 / 0 (0%)	0%	0 / 0 (0%)	0%	0 / 0 (0%)	0%	0 / 0 (0%)	0%
30-39	6628 / 250517 (2.65%)	2 / 44 (4.55%)	0.84%	0 / 5 (0%)	0%	0 / 10 (0%)	0%	2 / 31 (6.45%)	1.19%
40-49	7515 / 255707 (2.94%)	11 / 172 (6.40%)	1.20%	1 / 20 (5.00%)	0.94%	5 / 61 (8.20%)	1.54%	6 / 116 (5.17%)	0.97%
50-59	7807 / 218163 (3.58%)	28 / 409 (6.85%)	1.10%	6 / 110 (5.45%)	0.87%	18 / 220 (8.18%)	1.31%	15 / 206 (7.21%)	1.15%
60-69	5061 / 177078 (2.86%)	26 / 545 (4.77%)	0.62%	8 / 234 (3.42%)	0.44%	20 / 371 (5.39%)	0.70%	6 / 147 (4.08%)	0.53%
70-79	5147 / 143113 (3.60%)	23 / 545 (4.22%)	0.44%	8 / 295 (2.71%)	0.28%	19 / 391 (4.86%)	0.51%	3 / 52 (5.77%)	0.61%
80-89	8581 / 97289 (8.82%)	15 / 327 (4.59%)	0.33%	7 / 208 (3.37%)	0.24%	12 / 252 (4.76%)	0.34%	0 / 10 (0%)	0%
90 +	4795 / 25924 (18.5%)	4 / 47 (8.51%)	0.16%	4 / 38 (10.53%)	0.20%	3 / 32 (9.38%)	0.18%	0 / 1 (0%)	0%
All	3.69%	5.19%	4.68%	3.72%	2.98%	5.75%	5.60%	4.45%	
(CI95%)	(3.66-3.73%)	(4.24-6.13%)	(3.78-5.59%)	(2.49-4.95%)	(1.88-4.08%)	(4.5-6.99%)	(3.46-5.70%)	(1.71-9.50%)	(2.76-6.14%)

hsCOVID-19 = highly suspected COVID-19.

CI95% = 95% confidence intervals.

Table 3. Adjusted Relative Risk (aRR) with 95% confidence intervals (CI95%) of confirmed or hsCOVID-19 according to the presence of several comorbidities and treatments.

	N (All = 2102)	Model 1 - aRR (CI95%)	Model 2 - aRR (CI95%)
Women	1693	1.12 (0.71, 1.76)	1.11 (0.7, 1.76)
Age		0.99 (0.98, 1.01)	0.99 (0.98, 1.01)
Comorbidities			
CV disease	314	1.84 (1.17, 2.87)	1.86 (1.19, 2.91)
Diabetes	264	1.2 (0.71, 2.03)	1.19 (0.7, 2.03)
Pulmonary disease	315	1.36 (0.76, 2.45)	1.34 (0.73, 2.46)
Chronic kidney disease	114	1.58 (0.82, 3.07)	1.56 (0.8, 3.03)
Cancer or active treatment	121	1.06 (0.46, 2.46)	1.06 (0.45, 2.47)
Treatments followed			
Denosumab	264	0.58 (0.28, 1.22)	0.59 (0.28, 1.23)
Intravenous Zoledronate	179	0.62 (0.27, 1.41)	0.61 (0.27, 1.38)
Oral bisphosphonates	143	0.97 (0.45, 2.08)	0.97 (0.46, 2.06)
Calcium	490	0.64 (0.37, 1.12)	0.64 (0.37, 1.11)
Vitamin D	1303	0.92 (0.63, 1.36)	0.91 (0.62, 1.34)
Thiazide diuretics	262	0.95 (0.54, 1.67)	0.94 (0.53, 1.66)
Analgesics	1220	0.92 (0.61, 1.38)	
Gabapentin	164		1.39 (0.75, 2.58)
Pregabalin	146		1.55 (0.86, 2.79)
Opioids	546		1.25 (0.85, 1.83)
Other Analgesics	959		0.94 (0.64, 1.37)
Dual-action antidepressants	277	1.22 (0.72, 2.08)	
Duloxetine	207		0.68 (0.34, 1.34)
Tricyclic antidepressants	124	1.06 (0.54, 2.08)	
Amitriptyline	102		1.38 (0.7, 2.71)

SSRIs antidepressants	333	1.54 (1, 2.36)	1.39 (0.9, 2.14)
Inhaled Glucocorticoids	189	1.42 (0.73, 2.77)	1.39 (0.7, 2.74)
Anti-hypertensive drugs	646	1.06 (0.7, 1.6)	
ACE inhibitors	363		0.98 (0.58, 1.65)
ARBs	290		1.05 (0.62, 1.76)
Chronic NSAIDs	318	0.94 (0.57, 1.56)	0.95 (0.58, 1.55)

ACE = angiotensin-converting enzyme. ARBs = angiotensin II receptor blockers. CV = cardiovascular disease. hsCOVID-19 = highly suspected COVID-19 cases. NSAIDs = non-steroid anti-inflammatory drugs. SSRIs = selective serotonin reuptake inhibitors.

0.73 (CI95% 0.30- 1.78) for denosumab, 0.55 (CI95% 0.20-1.44) for intravenous zoledronate and 0.72 (CI95% 0.39-1.37) for calcium. The adjusted RRs by the other treatments did not differ from the crude ones: 0.87 (CI95% 0.30-2.52) for denosumab, 0.43 (CI95% 0.37-1.35) for intravenous zoledronate and 0.67 (CI 95% 0.36-1.27) for calcium.

DISCUSSION

The present study reveals that the main treatments currently used for osteoporosis are not associated with an increase in COVID-19 incidence. All the treatments analyzed in our study were continued after the presentation of COVID-19 symptoms following the

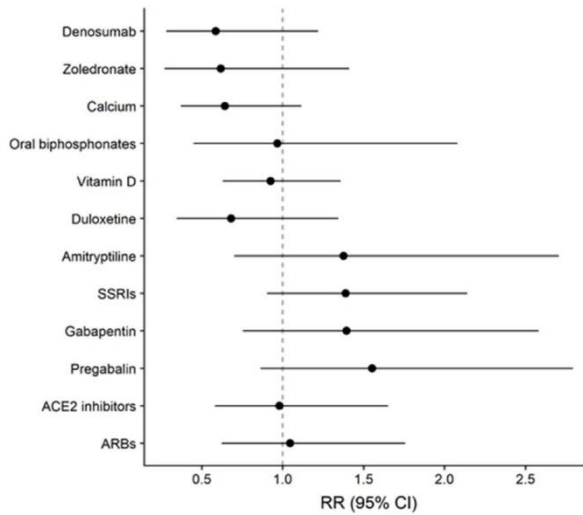


Figure 1. Relative Risk (RR) with 95% Confidence Interval (CI95%) of COVID-19 diagnosis according to the exposure to different treatments, adjusted by sex, age, CV disease, diabetes, pulmonary disease, chronic kidney disease and active cancer or treatments. The effect of Denosumab Zoledronate, Calcium, Oral bisphosphonates and Vitamin D were obtained from Model 1. Estimates for Duloxetine, SSRIs, Gabapentin, Pregabalin, ACE inhibitors and ARBs were obtained from Model 2.

recommendations of multiple international rheumatology [13, 14] and bone field organizations [15, 16]. Interestingly, the exposure to two anti-resorptive drugs, denosumab (RR=0.58; CI95% 0.28, 1.22) and intravenous zoledronate (RR=0.62; CI95% 0.27, 1.41), was associated with a 40% decreased risk of COVID-19. Recent relevant studies underline the high predictive value of the RR points estimate in these Poisson regression models, which often present high confidence interval ranges [20, 21].

The anti-osteoporosis target of denosumab is the RANK/RANKL system involved in the inhibition of osteoclastogenesis. The RANK/RANK-L system also participates in immune responses, including lymph-node development, lymphocyte differentiation, dendritic cell survival and T-cell activation [18]. Denosumab prevents RANK-L from binding to RANK receptor, thereby inhibiting osteoclast differentiation. RANK-L inhibition by denosumab modifies immune cell profiles and decreases the activity of pro-inflammatory cytokines [22]. This decrease in the inflammatory responses might elicit beneficial effects during viral infections, as previously reported with other RANK-L inhibitors [19], and could explain the decreased incidence of COVID-19 cases among patients treated with denosumab. Indeed, COVID-19 progression has been associated with a hyperactivity of pro-inflammatory cytokines [5] and a dysregulation of the immune system related to an abnormal monocytes/macrophage/dendritic cells response [6], which could be attenuated by denosumab treatment.

In contrast to denosumab, bisphosphonates bind to hydroxyapatite crystals and inhibit mature osteoclast function through induction of apoptotic pathways or blockade of cytoskeletal assembly by inhibition of lipid modification of associated proteins [23]. The exposure to intravenous zoledronate, but not to other oral bisphosphonates, showed a negative association with the incidence of COVID-19. The higher potency of intravenous zoledronate in comparison to any other oral bisphosphonate used in this study [24] may explain the differential result obtained with both groups of bisphosphonates. Intravenous zoledronate treatment reduces mortality after hip fracture [25], which may be related to decreased risk of CV disease, general health status improvement, fracture prevention, improved regulation of the immune system and a reduced incidence of pneumonia [26, 27]. Interestingly, zoledronate may make dendritic cells and their precursors less susceptible to SARS-CoV-2 infection, which could explain the beneficial effects here reported on COVID-19 incidence [28]. Indeed, zoledronate inhibits the prenylation of small GTPases [29, 30], which may hinder endosomal exocytosis in the dendritic

cells required for the advance of SARS-CoV-2 infection. These protective effects on dendritic cells and their precursors may lead to immune-stimulation of T cell expansion and enhanced activity of natural killer cells, crucial mechanisms to prevent the progression of SARS-CoV-2 infection in the lung [31].

In the present study, patients treated with calcium supplements also presented a decreased risk of COVID-19 (RR=0.64, CI95% 0.37, 1.12). In agreement, recent studies have reported reduced COVID-19 mortality in patients treated with calcium [32]. A decrease in total and ionized calcium blood levels has been reported in COVID-19 patients [33]. Changes in calcium levels in COVID-19 patients may be due to alterations in intestinal absorption, imbalance in regulatory mechanism involving parathyroid hormone and vitamin D, or to a direct effect caused by SARS-CoV-2 [33]. However, our results are compatible with no relevant effect of vitamin D on COVID-19 incidence (RR=0.97, CI95% 0.45, 2.08). A possible mechanism that may explain the beneficial effects of calcium in COVID-19 found in our study could be related to the action of calcium, through a specific calcium-based signal, on the generation of two immune cell types: T follicular helper cells and T follicular regulatory cells. These T cells promote an appropriate immune response against infectious agents, such as viruses [33, 34]. Accordingly, calcium supplements may counteract the decreased serum levels of calcium promoted by SARS-CoV-2 infection, which may lead to an improvement of the immune cell response and attenuate the probability of infection progression.

In agreement with the protective effects shown by the exposure to the main anti-osteoporosis treatments, age-adjusted cumulative incidence of COVID-19 in osteoporosis patients was lower (RR=2.98%, CI95% 1.88, 4.08) than in all the patients included in this study (RR=4.68%, CI95% 3.78-5.59%). This decrease was not observed with other non-inflammatory rheumatic conditions analyzed in our study. The comorbidity that produced the highest positive association with COVID-19 incidence in non-inflammatory rheumatic conditions was CV disease (RR=1.84, CI95% 1.17, 2.87.), although other co-morbidities, such as chronic kidney disease (RR=1.58, CI95% 0.82, 3.07) also substantially enhanced this incidence, as expected.

In our study, the exposure to different antidepressant drugs produced various effects on COVID-19 incidence. Interestingly, the dual acting serotonin/norepinephrine inhibitor duloxetine decreased the incidence of COVID-19 (RR=0.68, CI95% 0.34, 1.34). Antidepressant drugs have been postulated to modulate immune responses by modifying the serotonin/norepinephrine equilibrium.

which modifies the balance of the different T cell populations involved in the release of cytokines [35]. Antidepressants that change this serotonin/norepinephrine balance, such as the dual inhibitor duloxetine, may facilitate the maintenance or restoration of an appropriate T cells equilibrium and cytokine production [35]. However, amitriptyline, a tricyclic antidepressant that also has this dual serotonin/norepinephrine inhibitory effect, showed a different profile than duloxetine on the incidence of COVID-19. Both antidepressants have a completely different activity on other receptors [36], including antagonist activity of duloxetine on sigma-1 receptors [37], a mechanism postulated as a target of interest for re-purposing compounds for COVID-19 treatment [38]. Interestingly, SSRIs cause bone loss by a mechanism that counteracts local anti-resorption [39], in contrast to anti-osteoporosis medications that decrease COVID-19 incidence in our study. Also, opposite to anti-osteoporosis medications, patients taking SSRIs presented a 50% enhanced risk of COVID-19 (RR=1.54, CI95% 1.0, 2.36).

Our results suggest a positive association between the exposure to gabapentinoids and COVID-19 incidence. This increased risk was mainly revealed after pregabalin exposure (RR=1.55, CI95% 0.86, 2.79), an anti-epileptic drug mainly used in our population for chronic pain treatment. Pregabalin predominantly blocks the alpha2-delta subunit of voltage-gated calcium channels [40] and decreases immune responses under chronic pain conditions [41]. However, chronic pregabalin administration in HIV patients increased T cell levels in blood suggesting a possible activation of the immune response under this particular condition [42]. Moreover, SARS-CoV-2 binds to angiotensin-converting-enzyme-2 (ACE2) receptors and pregabalin has been reported to decrease these receptors in animal models [43]. When the amount of ACE2 is reduced due to the virus occupancy, individuals could be more susceptible to severe COVID-19 illness because enough ACE2 is still available for viral entry, whereas this decreased ACE2 availability facilitates angiotensin II-mediated injury. This pathophysiological mechanism associated to reduced ACE2 expression may promote inflammation, cell death and organ failure, mainly in the heart and lungs [44]. This mechanism may also contribute to the increased risk of COVID-19 we observed here among patients treated with pregabalin.

Our results from the two groups of anti-hypertensive drugs analyzed, ACE2 inhibitors and angiotensin II receptor blockers (ARBs), are compatible with no effect on the incidence of COVID-19. These results are in agreement with a recent meta-analysis showing that the use of these anti-hypertensive drugs in patients with

COVID-19 does not increase the risk of SARS-CoV-2 infection and COVID-19 severity, being these treatments associated with a decreased risk of mortality [45]. Therefore, all these results suggest that treatment with ACE2 and ARBs should be continued in COVID-19 patients who are taking these anti-hypertensive medications.

Some limitations of this study must be addressed. Osteoporosis grade and related comorbidities may have biased the risk estimates in our study. To control for the potential effect of confounding by indication, RRs of COVID-19 were also estimated after propensity score matching with the main available covariates that predict receiving denosumab, zoledronate or calcium treatment and the RRs obtained were also negatively associated with COVID-19. The similar results obtained with denosumab, zoledronate and calcium using both analyses suggest that the effects of these anti-osteoporosis medications on COVID-19 were not due to the presence of osteoporosis or underlying comorbidities. Furthermore, the data in this cross-sectional study were collected from a large number of patients. Thus, data have been collected by different researchers and some data may have been missed or slight differences in classification criteria may have been applied. Notwithstanding, all of the researchers were expert clinicians or medical researchers, and several meetings were held among them to unify classification criteria and to review clinical records. Also due to the cross-sectional design of the study, the degree of severity of some patients may have changed throughout the survey and these changes may not have been assessed. Additionally, our study cohort included patients from a tertiary hospital that were probably suffering from more severe forms of non-inflammatory rheumatic conditions in comparison with patients in primary or secondary care settings, which may introduce bias. However, all the anti-osteoporosis medications were uniformly covered by the public health insurance system in Spain, thus avoiding biases related medication costs. Finally, some asymptomatic patients may not have been registered due to the low availability of tests for SARS-Cov-2 in our country in the early stages of the pandemic.

In summary, our results reveal that chronic treatment with some of the main anti-osteoporosis drugs currently available, anti-resorptives, calcium and vitamin D, are not associated with increased risk of COVID-19. In contrast, a decreased incidence of COVID-19 was revealed with two anti-resorptives drugs, denosumab and zoledronate, as well as with calcium treatment. Some of the pain treatments used in these non-inflammatory rheumatic conditions may influence COVID-19 outcomes, since the incidence of COVID-19

was decreased in patients treated with duloxetine and increased in those taking pregabalin. In conclusion, our data are consistent with a lack of direct relationship between osteoporosis therapies and COVID-19 incidence, providing scientific evidence in support of the recently-published guidelines by the ACR, EULAR, ASBMR and IOF [13–16] to maintain anti-osteoporosis treatments for COVID-19 patients, which were based solely on expert opinions.

MATERIALS AND METHODS

Study design, and population

A cross-sectional study was performed at the Rheumatology Service of Hospital del Mar (Barcelona, Spain) that includes patients diagnosed with osteoporosis, osteoarthritis and/or fibromyalgia. Patients receiving care at the outpatient Rheumatology Service for the last six months were eligible. The exclusion criteria were <18 years old, previous death not related with SARS-CoV-2 infection, presence of immune-mediated inflammatory disease, a negative SARS-CoV-2 test, or failing to follow up at the primary care center during the studied period.

Outcomes

Hospital and primary care clinical history revision have been performed and the patient data included in this study were collected from March 1st to May 31st, 2020, the period of the highest COVID-19 incidence in Spain. The primary outcome was the presence of COVID-19 diagnosis, although other related variables were also recorded, including PCR results, lung radiography, symptomatology and evolution. At the time of revision, demographic and clinical data were also collected, with a particular focus on comorbidities (Supplementary Table 1) and medical drug prescriptions (Supplementary Table 2).

Statistical analysis

Cumulative incidence was adjusted for age by direct standardization using a COVID-19 epidemiological database (RSAcovid19) generated by the Department of Health of the Government of Catalonia [39]. This database contains daily cumulative positive cases and daily cumulative suspicious cases activated by the epidemiological surveillance service. For this analysis, we selected positive or suspicious cases registered from March 1st to May 31st, 2020 in the city of Barcelona, which was the reference population for direct standardization [40]. The RSAcovid19 database considers as positive the cases that tested positive in a diagnostic test (PCR, rapid test, or ELISA

test), and those confirmed by an epidemiologist as a positive case while they consider as “suspicious cases” those who had symptoms classified by a health professional as a possible case, but without a diagnostic test.

To evaluate the associations between different treatments (with >100 exposed patients; reference category: unexposed) and the presence of COVID-19, Poisson regression models with robust variance estimation were used to estimate RR and 95% confidence intervals (CI95%). Models were adjusted by sex, age, diabetes, pulmonary disease, cardiovascular disease, chronic kidney disease, and active cancer or treatment. Model 1 included the following treatments: denosumab, oral/intravenous bisphosphonates, calcium, vitamin D, thiazide diuretics, analgesics, antidepressants (dual action vs tricyclic vs SSRIs), inhaled glucocorticoids, anti-hypertensive drugs and NSAIDs. Model 2 included the specific effect of the analgesics gabapentin, pregabalin, opioids and others; the dual-action antidepressant duloxetine; the tricyclic antidepressant amitriptyline; and two types of anti-hypertensive drugs: ACE2 inhibitors and ARBs; together with denosumab, oral/intravenous bisphosphonates, calcium, vitamin D, thiazide diuretics, inhaled glucocorticoids and chronic NSAIDs.

Finally, the presence of osteoporosis, together with the studied comorbidities (sex, age, cardiovascular disease, diabetes, pulmonary disease, kidney disease and cancer) were used to calculate the probability of treatment assignment for denosumab, bisphosphonates and calcium with propensity score matching based on the nearest neighbor method [41]. Therefore, each treated individual was matched with an untreated individual whose propensity score was closest to that of the treated subject. Statistical analyses were performed using R (R Foundation for Statistical Computing, Vienna, Austria) version 3.5.2.

Ethics statement

All research in this study was conducted in accordance with the ethical standards of the Declaration of Helsinki and according to national and international guidelines. The observational study was approved by the Parc de Salut Mar Ethical Committee on Clinical Studies (ref. 2020/9246) before it started, and was monitored by the Clinical Trial Unit of Rheumatology Service at Hospital del Mar. Due to the nature of the study (all the data are completely anonymous), the importance of expedited results, and their implication for treatment of patients during the SARS-COV-2 pandemic, we did not obtain informed consent from the participants.

Abbreviations

ARBs: angiotensin II receptor blockers; ACE: angiotensin-converting-enzyme; CI: confidence interval; COVID-19: Coronavirus disease 19; CV: cardiovascular; NSAIDs: non-steroidal anti-inflammatory drugs; SERMs: selective estrogen receptor modulators; SSRIs: serotonin reuptake inhibitors.

AUTHOR CONTRIBUTIONS

J.B.R. was involved in conceptualizing the research idea, creating the research design, making the final interpretation of the statistical analyses, and writing the first draft and revision of the manuscript. N.S.D. participated in selection of statistical tests/analyses, performed the statistical analyses, computations and related computer work, and participated in writing the manuscript. L.T. was involved in conceptualizing the research idea, setting-up the research design, making the primary interpretation of the statistical analyses and participated in writing the manuscript. J.L.O. was involved in conceptualizing the research idea, setting-up the research design, making the primary interpretation of the statistical analyses and participated in writing the manuscript. M.C.R., L.P. and A.G. were responsible for patient cohort data collection. R.D.L.T. contributed to the statistical analyses and revised the manuscript. R.M. and J.M. were involved in conceptualizing the research idea, creating the research design, making the final interpretation of the statistical analysis, and writing the first draft and revision of the manuscript.

ACKNOWLEDGMENTS

We thank all patients who participated in the study, Gemma Vilagut (PhD) for her guidance and support on the statistical analysis and Mónica Gratacós (PhD) for translating the clinical protocol into English, for English language support and proofreading of the manuscript. The Covidmar Study Group members are: Hospital del Mar, Barcelona: Selene Labrada, Miguel Mejía-Torres, Francisco Vilchez Oya, Antonio Meraz Ostiz, Helena Sirera Perelló (Rheumatology Service) and Irene Carrión-Barberá, Carolina Pérez-García, Fabiola Ojeda, Tarek Carlos Salman-Monte, Josep Blanch-Rubió, Anna Pros Simón, Emma Beltrán Catalán, Pedro Benito Ruiz (Rheumatology Service & IMIM-Hospital del Mar Medical Research Institute) collected data and provided care for study patients; IMIM-Hospital del Mar Medical Research Institute: Luciano Polino, Laura Triginer, Anna Ribes (Cell Research on Inflammation and Cartilage Research Group, Inflammatory and Cardiovascular Processes Program) collected data; Maria-Victòria Puig (Integrative Pharmacology and Systems Neuroscience Research Group, Neurosciences

Research Program & IMIM-Hospital del Mar Medical Research Institute); contributed to analysis design; Parc Sanitari Pere Virgili, Barcelona: Maria Teresa Martí Vila, Maria Luisa Perez Miras (CAP Vila Olímpica) collected data; Universitat Pompeu Fabra, Barcelona: Araceli Bergadà-Martínez, Cecília Teresa Brambilla-Pisoni, Pablo Calvé- Pérez, Alba Calvet-Pavón, Laura Domingo-Rodríguez, Lorena Galera-López, Jolita Jančytė, Marta Linares-López, Elena Martín-García, Antonio Ortega-Álvaro, Pilar Ortiz-Tebe, Sheila Piedra-Barrull, Dulce Real-Muñoz, Maria Sanchis-Ollé, Eric Senabre-Marchán, Miquel-Àngel Serra, Anna Vázquez-Oliver (Laboratory of Neuropharmacology, Department of Experimental and Health Sciences & IMIM-Hospital del Mar Medical Research Institute) collected data.

CONFLICTS OF INTEREST

All authors have completed the ICMJE uniform disclosure form at www.icmje.org/doi_disclosure.pdf, and declare: NSD has received funding from Centro de Información Cerveza y Salud (CICS); AG has received research grants or consulting fees from Astrazeneca and Bioiberica S.A.U.; RM has received research grants or consulting fees from Aelis, Almirall, Boehringer Ingelheim, BrainCo, Esteve, Ferrer, GlaxoSmithKline, Grünenthal, GW Pharmaceuticals, Janus, Lundbeck, Pharmaleads, Phytoplant, Rhodes, Sanofi, Spherium, Union de Pharmacologie Scientifique Appliquée, Upjohn, and Uriach; JM has received grants or consulting fees from Procure Health Iberia S.L., Esteve, Labhra, Bioibérica S.A.U., Grunenthal Pharma S.A., Pfizer, OPKO Health Spain S.L.U and Roche Pharma S.A. MCR has received grants or consulting fees from Gedeon-Richter Ibérica, Gebro Pharma, Amgen S.A., Laboratorio Stada S.L., Lilly España S.A., Faes, Fidia, Theramex, Grunenthal; JBR has received grants or consulting fees from Amgen S.A., Laboratorio Stada S.L., Gedeon-Richter Ibérica, Lilly España, S.A., Pfizer, Gebro Pharma, and UCB Pharma S.A.; LP has received grants from Lilly España, SA y Celgene España S.L.; LT, JL-O and R.D.L.T. declare no competing interests.

FUNDING

This study was supported by Hospital del Mar. Authors funding includes “Ministerio de Ciencia, Innovación y Universidades” (#AEI-SAF2017-84060-R FEDER to R.M., #DPI2016-80283-C2-2-R), “Ministerio de Sanidad, Servicios Sociales e Igualdad” (#RD16/0017/0020 & #PNSD-20171068 to R.M., #PI18/00059 to TCS-M) and “Generalitat de Catalunya” (#2017-SGR-669 & #ICREA- Acadèmia 2015 to R.M., #2017-SGR-138 to R.D.L.T.). N.S.D. is recipient of predoctoral fellowship #2019-DI-47 from the DIUE-AGAUR of the “Generalitat de Catalunya”.

REFERENCES

1. Huang C, Wang Y, Li X, Ren L, Zhao J, Hu Y, Zhang L, Fan G, Xu J, Gu X, Cheng Z, Yu T, Xia J, et al. Clinical features of patients infected with 2019 novel coronavirus in Wuhan, China. *Lancet*. 2020; 395:497–506. [https://doi.org/10.1016/S0140-6736\(20\)30183-5](https://doi.org/10.1016/S0140-6736(20)30183-5) PMID:31986264
2. World Health Organization. World Health Organization. Coronavirus disease 2019 (COVID-19) [Internet]. Situation Report, 32. 2020. <https://www.who.int/docs/default-source/coronaviruse/situation-reports/20200505covid-19-sitrep-106.pdf?sfvrsn=47090f63>
3. Johns Hopkins Coronavirus Resource Center. COVID-19 dashboard by the Center for Systems Science and Engineering at Johns Hopkins University [Internet]. Johns Hopkins Coronavirus Resource Center. 2020. <https://coronavirus.jhu.edu/map.html>
4. Agencia de Salut Pública de Barcelona. Dades diàries de la infecció per coronavirus SARS Cov- 2 (COVID-19) a Barcelona [Internet]. 2020. <https://www.aspb.cat/docs/COVID19aldiaBCN/>
5. Cao Z, Li T, Liang L, Wang H, Wei F, Meng S, Cai M, Zhang Y, Xu H, Zhang J, Jin R. Clinical characteristics of coronavirus disease 2019 patients in Beijing, China. *PLoS One*. 2020; 15:e0234764. <https://doi.org/10.1371/journal.pone.0234764> PMID:32555674
6. Merad M, Martin JC. Pathological inflammation in patients with COVID-19: a key role for monocytes and macrophages. *Nat Rev Immunol*. 2020; 20:355–62. <https://doi.org/10.1038/s41577-020-0331-4> PMID:32376901
7. Khan F, Fabbri L, Stewart I, Robinson K, Smyth AR, Jenkins G. A systematic review of Anakinra, Tocilizumab, Sarilumab and Siltuximab for coronavirus-related infections. *medRxiv* [Internet]. 2020. <https://www.medrxiv.org/content/10.1101/2020.04.23.20076612v1?%253fcollection=3.20076612v1?%253fcollection=> <https://doi.org/10.1101/2020.04.23.20076612>
8. Gianfrancesco M, Hyrich KL, Al-Adely S, Carmona L, Danila MI, Gossec L, Izadi Z, Jacobsohn L, Katz P, Lawson-Tovey S, Mateus EF, Rush S, Schmajuk G, et al, and COVID-19 Global Rheumatology Alliance. Characteristics associated with hospitalisation for COVID-19 in people with rheumatic disease: data from the COVID-19 global rheumatology alliance physician-reported registry. *Ann Rheum Dis*. 2020; 79:859–66. <https://doi.org/10.1136/annrheumdis-2020-217871> PMID:32471903
9. Haberman R, Axelrad J, Chen A, Castillo R, Yan D, Izmirly P, Neimann A, Adhikari S, Hudesman D, Scher JU. Covid-19 in immune-mediated inflammatory diseases - case series from New York. *N Engl J Med*. 2020; 383:85–88. <https://doi.org/10.1056/NEJMc2009567> PMID:32348641
10. Michelena X, Borrell H, López-Corbeto M, López-Lasanta M, Moreno E, Pascual-Pastor M, Erra A, Serrat M, Espartal E, Antón S, Añez GA, Caparrós-Ruiz R, Pluma A, et al. Incidence of COVID-19 in a cohort of adult and paediatric patients with rheumatic diseases treated with targeted biologic and synthetic disease-modifying anti-rheumatic drugs. *Semin Arthritis Rheum*. 2020; 50:564–70. <https://doi.org/10.1016/j.semarthrit.2020.05.001> PMID:32425260
11. Consensus development conference: diagnosis, prophylaxis, and treatment of osteoporosis. *Am J Med*. 1993; 94:646–50. [https://doi.org/10.1016/0002-9343\(93\)90218-e](https://doi.org/10.1016/0002-9343(93)90218-e) PMID:8506892
12. Kanis JA, Cooper C, Rizzoli R, Reginster JY, and Scientific Advisory Board of the European Society for Clinical and Economic Aspects of Osteoporosis and Osteoarthritis (ESCEO) and the Committees of Scientific Advisors and National Societies of the International Osteoporosis Foundation (IOF). Executive summary of the European guidance for the diagnosis and management of osteoporosis in postmenopausal women. *Calcif Tissue Int*. 2019; 104:235–38. <https://doi.org/10.1007/s00223-018-00512-x> PMID:30796490
13. American College of Rheumatology COVID-19 Guidance Task Force. COVID-19 Clinical Guidance for Patients with Rheumatic Diseases. *Am Coll Rheumatol*. 2020; 1–2.
14. Landewé RB, Machado PM, Kroon F, Bijlsma HW, Burmester GR, Carmona L, Combe B, Gali M, Gossec L, Iagnocco A, Isaacs JD, Mariette X, McInnes I, et al. EULAR provisional recommendations for the management of rheumatic and musculoskeletal diseases in the context of SARS-CoV-2. *Ann Rheum Dis*. 2020; 79:851–58. <https://doi.org/10.1136/annrheumdis-2020-217877> PMID:32503854
15. ASBMR webinar panel on treating patients with osteoporosis during the COVID-19 pandemic [Internet]. 2020. <https://www.asbmr.org/education-detail?cid=b92753f3-0a28-4f37-9a58-6ded595a7b40#.XqfFwy-ZM>
16. Yu EW, Tsourdi E, Clarke BL, Bauer DC, Drake MT. Osteoporosis management in the era of COVID-19. *J Bone Miner Res*. 2020; 35:1009–13. <https://doi.org/10.1002/jbmr.4049> PMID:32406536

17. Xgeva (Denosumab). European Medicines Agency [Internet]. <https://www.ema.europa.eu/en/medicines/human/EPAR/xgeva>
18. Cheng ML, Fong L. Effects of RANKL-targeted therapy in immunity and cancer. *Front Oncol*. 2014; 3:329. <https://doi.org/10.3389/fonc.2013.00329> PMID:24432249
19. Kobayashi-Sakamoto M, Tamai R, Kiyoura Y. Beyond bone remodeling—emerging functions of osteoprotegerin in host defense and microbial infection. *Integr Mol Med*. 2015; 2:384–90. <https://doi.org/10.15761/IMM.1000173>
20. Wasserstein RL, Schirm AL, Lazar NA. Moving to a World Beyond “p < 0.05.” *Am Stat* [Internet]. Taylor & Francis; 2019; 73:1–19. <https://doi.org/10.1080/00031305.2019.1583913>
21. Amrhein V, Greenland S, McShane B. Scientists rise up against statistical significance. *Nature*. 2019; 567:305–307. <https://doi.org/10.1038/d41586-019-00857-9> PMID:30894741
22. Chiu YG, Ritchlin CT. Denosumab: targeting the RANKL pathway to treat rheumatoid arthritis. *Expert Opin Biol Ther*. 2017; 17:119–28. <https://doi.org/10.1080/14712598.2017.1263614> PMID:27871200
23. Baron R, Ferrari S, Russell RG. Denosumab and bisphosphonates: different mechanisms of action and effects. *Bone*. 2011; 48:677–92. <https://doi.org/10.1016/j.bone.2010.11.020> PMID:21145999
24. Cremers S, Drake MT, Ebetino FH, Bilezikian JP, Russell RG. Pharmacology of bisphosphonates. *Br J Clin Pharmacol*. 2019; 85:1052–62. <https://doi.org/10.1111/bcp.13867> PMID:30650219
25. Lyles KW, Colón-Emeric CS, Magaziner JS, Adachi JD, Pieper CF, Mautalen C, Hylndstrup L, Recknor C, Nordsletten L, Moore KA, Lavecchia C, Zhang J, Mesenbrink P, et al, and HORIZON Recurrent Fracture Trial. Zoledronic acid and clinical fractures and mortality after hip fracture. *N Engl J Med*. 2007; 357:1799–809. <https://doi.org/10.1056/NEJMoa074941> PMID:17878149
26. Colón-Emeric CS, Mesenbrink P, Lyles KW, Pieper CF, Boonen S, Delmas P, Eriksen EF, Magaziner J. Potential mediators of the mortality reduction with zoledronic acid after hip fracture. *J Bone Miner Res*. 2010; 25:91–97. <https://doi.org/10.1359/jbmr.090704> PMID:19580467
27. Bergman J, Nordström A, Hommel A, Kivipelto M, Nordström P. Bisphosphonates and mortality: confounding in observational studies? *Osteoporos Int*. 2019; 30:1973–82. <https://doi.org/10.1007/s00198-019-05097-1> PMID:31367949
28. Brufsky A, Marti JL, Nasrazadani A, Lotze MT. Boning up: amino-bisphosphonates as immunostimulants and endosomal disruptors of dendritic cell in SARS-CoV-2 infection. *J Transl Med*. 2020; 18:261. <https://doi.org/10.1186/s12967-020-02433-6> PMID:32600410
29. Okamoto S, Jiang Y, Kawamura K, Shingyoji M, Tada Y, Sekine I, Takiguchi Y, Tatsumi K, Kobayashi H, Shimada H, Hiroshima K, Tagawa M. Zoledronic acid induces apoptosis and s-phase arrest in mesothelioma through inhibiting rab family proteins and topoisomerase II actions. *Cell Death Dis*. 2014; 5:e1517. <https://doi.org/10.1038/cddis.2014.475> PMID:25393473
30. Coxon FP, Helfrich MH, Van't Hof R, Sebti S, Ralston SH, Hamilton A, Rogers MJ. Protein geranylgeranylation is required for osteoclast formation, function, and survival: inhibition by bisphosphonates and GGTI-298. *J Bone Miner Res*. 2000; 15:1467–76. <https://doi.org/10.1359/jbmr.2000.15.8.1467> PMID:10934645
31. Poccia F, Agrati C, Castilietti C, Bordini L, Gioia C, Horejsh D, Ippolito G, Chan PK, Hui DS, Sung JJ, Capobianchi MR, Malkovsky M. Anti-severe acute respiratory syndrome coronavirus immune responses: the role played by V gamma 9 delta 2 T cells. *J Infect Dis*. 2006; 193:1244–49. <https://doi.org/10.1086/502975> PMID:16586361
32. El-Kurdi B, Khatua B, Rood C, Snozek C, Carlin-Ceba R, Singh VP, and Lipotoxicity in COVID-19 Study Group. Mortality from coronavirus disease 2019 increases with unsaturated fat and may be reduced by early calcium and albumin supplementation. *Gastroenterology*. 2020; 159:1015–18.e4. <https://doi.org/10.1053/j.gastro.2020.05.057> PMID:32470338
33. Cappellini F, Brivio R, Casati M, Cavallero A, Contro E, Brambilla P. Low levels of total and ionized calcium in blood of COVID-19 patients. *Clin Chem Lab Med*. 2020; 58:e171–73. <https://doi.org/10.1515/cclm-2020-0611> PMID:32459190
34. Vaeth M, Eckstein M, Shaw PJ, Kozhaya L, Yang J, Berberich-Siebelt F, Clancy R, Unutmaz D, Feske S. Store-operated Ca²⁺ entry in follicular T cells controls humoral immune responses and autoimmunity. *Immunity*. 2016; 44:1350–64.

- <https://doi.org/10.1016/j.immuni.2016.04.013>
PMID:27261277
35. Martino M, Rocchi G, Escelsior A, Fornaro M. Immunomodulation mechanism of antidepressants: interactions between serotonin/norepinephrine balance and Th1/Th2 balance. *Curr Neuropharmacol.* 2012; 10:97–123.
<https://doi.org/10.2174/157015912800604542>
PMID:23204981
 36. Brunton LL. Goodman and Gilman's: The Pharmacological Basis of Therapeutics. 13th ed. 2018.
 37. Buschmann HH, Hernandez JMV. Use of compounds binding to the sigma receptor for the treatment of metabolic syndrome. *Spain; EP 1 787 679 A1*, 2007.
 38. Gordon DE, Jang GM, Bouhaddou M, Xu J, Obernier K, White KM, O'Meara MJ, Rezelj VV, Guo JZ, Swaney DL, Tummino TA, Hüttenhain R, Kaake RM, et al. A SARS-CoV-2 protein interaction map reveals targets for drug repurposing. *Nature.* 2020; 583:459–68.
<https://doi.org/10.1038/s41586-020-2286-9>
PMID:32353859
 39. Ortuño MJ, Robinson ST, Subramanyam P, Paone R, Huang YY, Guo XE, Colecraft HM, Mann JJ, Ducey P. Serotonin-reuptake inhibitors act centrally to cause bone loss in mice by counteracting a local anti-resorptive effect. *Nat Med.* 2016; 22:1170–79.
<https://doi.org/10.1038/nm.4166> PMID:27595322
 40. Taylor CP, Angelotti T, Fauman E. Pharmacology and mechanism of action of pregabalin: the calcium channel alpha2-delta (alpha2-delta) subunit as a target for antiepileptic drug discovery. *Epilepsy Res.* 2007; 73:137–50.
<https://doi.org/10.1016/j.eplepsyres.2006.09.008>
PMID:17126531
 41. Abu-Rish EY, Mansour AT, Mansour HT, Dahabiyeh LA, Aleidi SM, Bustanji Y. Pregabalin inhibits in vivo and in vitro cytokine secretion and attenuates spleen inflammation in Lipopolysaccharide/Concanavalin A - induced murine models of inflammation. *Sci Rep.* 2020; 10:4007.
<https://doi.org/10.1038/s41598-020-61006-1>
PMID:32132609
 42. Lee K, Vivithanaporn P, Siemieniuk RA, Krentz HB, Maingat F, Gill MJ, Power C. Clinical outcomes and immune benefits of anti-epileptic drug therapy in HIV/AIDS. *BMC Neurol.* 2010; 10:44.
<https://doi.org/10.1186/1471-2377-10-44>
PMID:20565780
 43. Awwad ZM, El-Ganainy SO, ElMallah AI, Khedr SM, Khattab MM, El-Khatib AS. Assessment of pregabalin-induced cardiotoxicity in rats: mechanistic role of angiotensin 1-7. *Cardiovasc Toxicol.* 2020; 20:301–11.
<https://doi.org/10.1007/s12012-019-09553-6>
PMID:31720995
 44. Santos RA, Sampaio WO, Alzamora AC, Motta-Santos D, Alenina N, Bader M, Campagnole-Santos MJ. The ACE2/Angiotensin-(1-7)/MAS axis of the renin-angiotensin system: focus on angiotensin-(1-7). *Physiol Rev.* 2018; 98:505–53.
<https://doi.org/10.1152/physrev.00023.2016>
PMID:29351514
 45. Zhang X, Yu J, Pan LY, Jiang HY. ACEI/ARB use and risk of infection or severity or mortality of COVID-19: A systematic review and meta-analysis. *Pharmacol Res.* 2020; 158.
<https://doi.org/10.1016/j.phrs.2020.104927>
PMID:32422341

SUPPLEMENTARY MATERIALS

Supplementary Tables

Supplementary Table 1. Definition of the comorbidities registered.

Comorbidities	Definition
AHT	Diagnosis of arterial hypertension in actual treatment with antihypertensive drugs.
Diabetes	Diagnosis of diabetes, treated with diet, oral drugs or insulin administration.
Pulmonary disease	Any disease affecting respiratory system functionality and treated with any of the related drugs. Patients suffering from asthma, Chronic obstructive pulmonary disease (COPD), Pulmonary fibrosis, Obstructive sleep apnea syndrome (OSAS) and interstitial lung disease were specifically registered.
CV disease	Diagnosis of cardiovascular disease
Chronic kidney disease	Chronic kidney disease diagnosis, in any of the stages.
Active cancer or treatment	Patients in a cancer process or in treatment for a previous cancer, along the period studied (1 st to the 29 th of March)
Tissue or organ transplantation	Any transplantation throughout the patient's life, in actual treatment.

Supplementary Table 2. List of types of treatments registered and drugs belonging to each type.

Type of treatment	Drugs included	
Analgesics	NSAIDs	
	Opioids	
	Pregabalin	
	Gabapentin	
	Other analgesics	
Antidepressants	Dual Acting	Duloxetine Venlafaxine Others
	Tricyclic	Amitriptyline Other
	Selective serotonin reuptake inhibitors (SSRIs)	
	Reboxetine	
	Other antidepressants	
Antiresorptive Agents	Bisphosphonates	Oral Intravenous
	Denosumab	
	Selective estrogen receptor modulator (SERM)	
Anabolic Agents	Teriparatide	
Supplements for osteoporosis	Calcium	
	Vitamin D (in any of its forms or metabolites)	
	Thiazides diuretics	
Corticoids	Any type of oral corticoid (all converted to prednisone dose)	
	Any type of inhaled corticoids	
Antihypertensive drugs	Angiotensin-converting enzyme (Enalapril, Ramipril, Lisinopril, ...)	
	Angiotensin II Receptor Blockers (Losartan, Valsartan, Candesartan...)	

Supplementary Table 3. Relative risk (RR) and 95% confidence interval (95% CI) of hsCOVID-19 after propensity score matching.

Sample size	Denosumab			Intravenous Zoledronate			Calcium			
		control	treated		control	treated		control	treated	
N All	1838	264		N All	1923	179		N All	1612	490
N matched	264	264		N matched	179	179		N matched	490	490
N unmatched	1574	0		N unmatched	1744	0		N unmatched	1122	0
COVID-19 (matched data)	Yes	11	8	Yes	11	6		Yes	22	16
	No	253	256	No	168	173		No	468	474
Crude RR (95%CI)	0.73 (0.30-1.78)			0.55 (0.20-1.44)			0.72 (0.39-1.37)			
Adjusted RR (95%CI)*	0.87 (0.30-2.52)			0.43 (0.14-1.35)			0.67 (0.36-1.27)			
Summary of balance for matched data	Means Treated	Means Control	Mean Diff	Means Treated	Means Control	Mean Diff	Means Treated	Means Control	Mean Diff	
Osteoporosis	0.97	0.97	0.00	0.92	0.92	0.00	0.77	0.77	0.00	
Women	0.86	0.86	-0.01	0.77	0.80	-0.03	0.85	0.88	-0.02	
Age	74.05	73.29	0.76	71.61	71.69	-0.08	71.34	71.57	-0.22	
CV disease	0.17	0.13	0.04	0.18	0.17	0.02	0.17	0.16	0.01	
Diabetes	0.12	0.10	0.02	0.18	0.17	0.01	0.10	0.12	-0.02	
Pulmonary disease	0.20	0.21	-0.01	0.19	0.17	0.02	0.16	0.14	0.01	
Renal disease	0.11	0.09	0.01	0.08	0.04	0.03	0.07	0.06	0.01	
Cancer	0.09	0.08	0.02	0.15	0.15	0.01	0.08	0.08	0.00	

CV= cardiovascular.

*RR for denosumab is adjusted by the exposure to calcium, bisphosphonates, vitamin D, thiazide, analgesics, dual antidepressants, tricyclic antidepressants, SSRI antidepressants (selective serotonin reuptake inhibitors), glucocorticoids, anti-hypertensive drugs and NSAIDs. RR for intravenous zoledronate is adjusted by the exposure to denosumab, oral bisphosphonates, calcium, vitamin D, thiazide, analgesics, dual antidepressants, tricyclic antidepressants, SSRI antidepressants, glucocorticoids, anti-hypertensive drugs and NSAIDs. RR for calcium is adjusted by the exposure to denosumab, bisphosphonates, vitamin D, thiazide, analgesics, dual antidepressants, tricyclic antidepressants, SSRI antidepressants, glucocorticoids, anti-hypertensive drugs and NSAIDs.